University of Southampton

Faculty of Engineering and Physical Sciences

School of Chemistry

Coordination Chemistry and Properties of the Trivalent Group 13 and Divalent Group 14 Metal Triflates with a Range of Neutral Donor Ligands

by

Kelsey R Cairns

Thesis for the degree of Doctor of Philosophy

December 2023

University of Southampton

Abstract

Faculty of Engineering and Physical Sciences

School of Chemistry

Doctor of Philosophy

Coordination Chemistry and Properties of the Trivalent Group 13 and Divalent Group 14 metal Triflates with a Range of Neutral Donating Ligands

by

Kelsey R Cairns

Although commonly used within organic chemistry as a leaving group, the main group chemistry of the weakly coordinating anion triflate $[SO_3CF_3]^-$ (OTf) is limited, with a few known coordination complexes incorporating this anion. The work of this thesis is focused on the synthesis of complexes of Group 13 and 14 metal triflates with the coordination of a range of different donor ligands with varying hardness, donor strength and denticity. Each of the novel complexes synthesised here are characterised by IR and NMR spectroscopy (^1H, $^{13}C\{^1H\}$, $^{19}F\{^1H\}$, $^{31}P\{^1H\}$ and ^{27}Al, ^{71}Ga, ^{119}Sn and ^{207}Pb where applicable) and microanalysis; with structural information being gathered by single crystal X-ray diffraction whenever possible. This began with reaction of the Group 13 metal triflates $M(OTf)_3$ (M = Al, Ga, In) and coordination of the hetroaromatic imine ligands bipy (2,2'-bipyridine), terpy (2,2';6',2"-terpyridine) and phen (1,10-phenanthroline). Each ligand was successfully coordinated with terpy producing a set of neutral complexes *cis*-$[M(OTf)_3(terpy)]$, while the bidenate ligands produced cationic complexes $[M(OTf)_2(bidentate)_2][OTf]$. The reaction of harder oxygen donor ligands OPR_3 (R = Me, Ph), pyNO and $dppmO_2$ were also observed to produce octahedral complexes. The complexes produced from both ligand sets showed displacement of the triflate anion by one or more water ligands, producing di- or tricationic species, with crystal structures showing water ligands becoming involved in H-bonding arrays. This behaviour lead to the formation of a 24-membered pseudomacrocyclic ring with four H-bonded triflate anions bridging four coordinated *meridianal* water ligands in $[In(OTf)_2(OPPh_3)_4][In(OH_2)_4(OPPh_3)_2][OTf]_4$. Following on from previous alkylstibine work in the Reid group, a series of Group 13 metal chloride complexes were synthesised with alkyl-stibine, -arsine and -phosphine ligands. These complexes were reacted with TMSOTf (trimethylsilyl trifluoromethanesulfonate), among other abstraction agents, in an attempt to produce cationic species. The divalent Group 14 metal triflates $M(OTf)_2$ (M = Sn, Pb) were also probed using a range of soft pnictine ligands, following from a previously published report on coordination of these ligands to $M(SbF_6)_2$ (M = Sn, Pb). Expanding on this study, harder oxygen donor ligands were including OPR_3 (R = Me, Ph), pyNO and $dppmO_2$ exploring the geometry and spectroscopic properties of these complexes. Throughout coordination to the divalent Group 14 metal triflates, a preference for oligomerisation was observed with repeated formation of triflate bridges being observed. Reaction of three equivalents of $OPMe_3$ with $Sn(OTf)_2$ produced a hexameric metallocyclic array containing large solvent voids through the structure. Attempts to produce an analogous species using the structurally related $[SO_3F]^-$ anion was ultimately unsuccessful however, use of $Pb(OTf)_2$ produced a bridged dimer species $[\{Pb(OTf)(OPMe_3)_3\}_2(\mu\text{-}OTf)_2]$.

Table of Contents

Table of Tables

Table of Tables

Table of Figures

Table of Figures

Table of Figures

Table of Schemes

List of Accompanying Materials

All the CIF files of single crystal X-ray structures described in this thesis as well as spectroscopic and computational data are to be found at the following DOI:

https://doi.org/10.5258/SOTON/D2732

Research Thesis: Declaration of Authorship

Print name: Kelsey R Cairns

Title of thesis: Coordination Chemistry and Properties of the Trivalent Group 13 and Divalent Group 14 Metal Triflates with a Range of Neutral Donating Ligands

I declare that this thesis and the work presented in it are my own and has been generated by me as the result of my own original research.

I confirm that:

1. This work was done wholly or mainly while in candidature for a research degree at this University;
2. Where any part of this thesis has previously been submitted for a degree or any other qualification at this University or any other institution, this has been clearly stated;
3. Where I have consulted the published work of others, this is always clearly attributed;
4. Where I have quoted from the work of others, the source is always given. With the exception of such quotations, this thesis is entirely my own work;
5. I have acknowledged all main sources of help;
6. Where the thesis is based on work done by myself jointly with others, I have made clear exactly what was done by others and what I have contributed myself;
7. Parts of this work have been published as:-

   "Synthesis, properties and structures of gallium(III) and indium(III) halide complexes with neutral pnictine coordination" – K. R. Cairns, V. K. Greenacre, L. A. Grose, W. Levason, G. Reid and F. Robinson, *J. Organomet. Chem.*, 2020, **912**, 121176.

   "Heterocyclic nitrogen donor complexes of aluminium, gallium and indium with weakly coordinating triflate anions" – K. R. Cairns, W. Levason, G. Reid and W. Zhang, *Polyhedron*, 2021, **207**, 115367.

   "Mono- and di-phosphine oxide complexes of aluminium, gallium and indium with weakly coordinating triflate anions – Synthesis, structures and properties" – K. R. Cairns, W. Levason, G. Reid and W. Zhang, *Polyhedron*, 2021, **210**, 115529.

   "Synthesis, spectroscopic and structural properties of Sn(II) and Pb(II) triflate complexes with soft phosphine and arsine coordination" – K. R. Cairns, R. P. King, R. D. Bannister, W. Levason and G. Reid, *Dalton Trans.*, 2023, **2**, 2293–2308.

   "Self-assembly of $[Sn(OPMe_3)_3(CF_3SO_3)_2]_6$ metallocyclic Sn(II) hexamer stacks with CF_3-lined channel interiors" – K. R. Cairns, R. P. King, W. Levason and G. Reid, *CrystEngComm*, 2022, **24**, 6137–6140.

Signature: ..... Date:.....

Acknowledgements

I'd like to first thank Prof. Gill Reid for her guidance and support through a tumultuous 4 years of PhD study, for keeping me grounded and on the right path as well as keeping me on my toes, all while being incredibly busy yourself! I'd also like to thank my second supervisor, Prof. Bill Leveson, who's almost encyclopaedic knowledge of the literature of the last 30+ years is beyond impressive and was an invaluable resource to be so close to.

Thank you to Dr Rob Bannister, Dr Mark Light and Dr Wenjian Zhang for help with solving and refining some of the more challenging crystal structures I obtained, and to the whole of the NCS for keeping my favourite machines ticking all year round. To Dr Alice Oakley for her assistance in taking BET measurements and Dr Fred Robinson for SEM and GIXRD surface measurements of my samples.

Throughout my time in Southampton I had the pleasure of sharing a lab space with Dr Victoria Greenacre, Dr Rhys King, Dr Danielle Runacres and Miss (for now) Charley Bryant-Gardner as well as the past members of the Reid Group. Thank you Vicki for keeping the lab functional, to Rhys for carrying out DFT calculations for me, to Daniie for keeping the microanalysis samples flying out the door and to Charley for never turning down an offer of a trip to the shop. You all helped to make my time in the lab so fun and memorable. Although we may have only finished 1 crossword in 4 years, you all happily answered my questions, no matter how off topic or dim they seemed.

Although not in Southampton, I'd like to thank Tom, Stuart, Scott and Aaron; whether we spoke daily, weekly or monthly, you guys always helped to distract and distress, get me smiling again and setting my sights back on the prize.

And last but not least, I'd like to thank my Mum. Safe to say 2019 – now has tested us both but we've survived it together and are moving forward to bigger and better things. Thank you for always being a place to escape to, for giving me a voice of reason and listening to my rants every now and again.

It's over guys. I made it!

Definitions and Abbreviations

MeCN	Acetonitrile
R	Alkyl or aryl group
Å	10^{-10} m (Angström)
θ	Angle
Bipy	2,2'-bipyridine
4,4'-Bipy	4,4'-bipyridine
d(M-X)	Bond distance of M and X
$[BAr^F]^-$	Tetrakis[3,5-bis(trifluoromethyl)phenyl]borate anion
δ	Chemical shift (ppm)
18-crown-6	1,4,7,10,13,16-Hexaoxacyclooctadecane
15-crown-5	1,4,7,10,13-Pentaoxacyclopentadecane
12-crown-4	1,4,7,10-Tetraoxacyclododecane
J	Coupling constant
Cp	Cyclopentadienyl
Cp*	Pentamethylcyclopentadienyl
Cy	Cyclohexyl
2,2,2-crypt	4,7,13,16,21,24-hexaoxa-1,10-diazabicyclo[8.8.8]hexacosane
Me_4cyclam	1,4,8,11-tetramethyl-1,4,8,11-tetraazacyclotetradecane
Me_4cyclen	1,4,7,10-tetramethyl-1,4,7,10-tetraazacyclododecane
Δδ	Change in chemical shift
˚C	Degrees Celsius
DFT	Density functional theory
DMSO	Dimethylsulfoxide
Dioxane	1,4-dioxacyclohexane
d	Doublet
Dmpe	*bis*(dimethylphosphino)ethane

Definitions and Abbreviations

Depe	*bis*(diethylphosphino)ethane
E	Donor atom
$dppmO_2$	Bis-(diphenylphosphino)methane Oxide
efg	Electric field gradient
Et	Ethyl
En	ethylenediamine
Edta	ethylenediaminetetraacetic acid
fac	Facial
R^F	Fluorinated alkyl group
v	Frequency
X	Halide
HSAB	Hard-Soft Acid-Base theory
Hz	Hertz
HOMO	Highest occupied molecular orbital
IR	Infrared
^{i}Pr	Isopropyl
K	Kelvin
L	Generic ligand
LUMO	Lowest unoccupied molecular orbital
M	Metal
mer	meridional
Me	Methyl
m	Multiplet
^{n}Bu	*n*-butyl
NBO	Natural bond order
NMR	Nuclear magnetic resonance
o-	Ortho
ppm	Parts per million

Ph	Phenyl
π	Pi symmetry oribital
Phen	1,10-phenanthroline
OPR_3	General phosphine oxide
$\{^1H\}$	proton decoupled
py	Pyridine
pyNO	Pyridine *N*-oxide
q	Quartet
quint	Quintet
σ	Sigma symmetry orbital
s	Singlet
[24]aneS_8	1,4,7,10,13,16,19,22-octathiacyclotetrcosane
Me_3tacn	1,4,7-trimethyl-1,4,7-triazacyclononane
Terpy	2,2';6',2"-terpyridine
3c-4e	Three centre four electron bond
THF	Tetrahydrofuran
OTf	Triflate ($CF_3SO_3^-$)
t	Triplet
^{t}Bu	Tertiary butyl
XRD	X-ray diffraction

Chapter 1 – Introduction

The work of this thesis explores and develops the coordination chemistry of metals in group 13 and 14, describing the synthesis of a range of complexes involving the weakly coordinating trifluoromethanesulfonate anion, $[OTf]^-$. These complexes were formed with ligands containing differing donor atoms including oxygen, heteroaromatic imines as well as a range of pnictine ligands, ER_3 (E = P, As, Sb; R = Me, Et, Ph). The aim was to observe how these complexes would differ from the well-established field of the main group metal halides. This chapter covers the general background chemistry of the work carried out in this thesis, with the introduction to each chapter giving a more detailed background work relevant to that chapter.

1.1 Hard-Soft Acid-Base Theory

Since its introduction, hard-soft acid-base theory (HSAB) has become fundamental within inorganic and coordination chemistry. It makes use of the Lewis definition of acids and bases; a Lewis acid is a species that can accept a pair of non-bonding electrons, while a Lewis base is a substance that can donate a pair of electrons, with these roles being detailed in Figrure 1.1.[1] HSAB theory states that, in a like with like manner, hard acids preferentially bond to hard bases and soft acids preferentially bond to soft bases.[2]

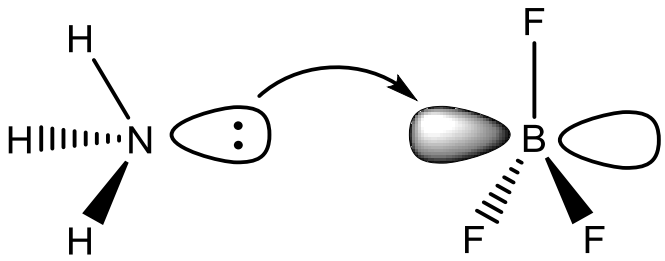

Figure 1.1 - A simple acid/base reaction of an electron rich Lewis base, NH_3 and an electron poor Lewis acid, BF_3 to form an acid-base complex.[3]

The characteristics of a hard acid/base are to have a small atomic or ionic radii and are in a high oxidation state, commonly being charged species.[4] This means that the size : charge ratio is high and the electron orbitals are not polarisable, leading to a preference for electrostatic bonding. Some examples of hard bases include fluoride ions (hardest), oxygen donors (such as water and alcohols), as well as some amines. Hard acids include both the alkali and alkali earth metals, many of the medium and high oxidation state early transition metals and *f*-block ions. In contrast, soft acids and bases are commonly in low oxidation states with larger and more diffuse orbitals which allow for greater polarisation, with examples including later transition metals such as Pd^{2+} and

Au^+. This polarisability allows for the formation of more covalent like bonding. Soft bases include many of the ligands containing later p-block elements that can behave as donor species including chalcogenoethers (R_2S, R_2Se), phosphine and arsine ligands as well as the heavier halides Br^- and I^-. Although these properties are well known and studied, a definitive scale of HSAB theory has not been determined, despite attempts.[5] The thiocyanate anion SCN^- is an example of an ambidentate species that can act as a ligand and has been shown to bind through the soft sulfur base with soft acids such as Pt^{2+} and through the hard nitrogen base when forming complexes with harder acids such as Co^{3+}.[6] The descriptors of 'hard' and 'soft' have no bearing on the strength of the acid/base, and only the types of bonding or reactivity they are likely to display. This theory is useful for describing the bonding of these reagents, however, there are examples of complexes formed with a mismatch of hard/soft acid/bases such as the bonding of a thioether macrocycle (soft base) to a sodium cation (hard acid).[7] The $[BAr^F]^-$ (tetrakis[3,5-bis(trifluoromethyl)phenyl]borate) salt of sodium was also employed as a source of 'naked' Na^+ in the reaction with the azamacrocycles, Me_3-tacn (1,4,7-trimethyl-1,4,7-triazacyclononane) or Me_4-cyclam (1,4,8,11-tetramethyl-1,4,8,11-tetraazacyclotetradecane) to give a distorted octahedral sandwich cation $[Na(Me_3\text{-tacn})_2]^+$ and distorted five-coordinate cation $[Na(THF)(Me_4\text{-cyclam})]^+$, respectively. Following on from these reactions, the softer [24]aneS_8 (1,4,7,10,13,16,19,22-octathiacyclotetracosane) ligand was coordinated to Na^+ and crystallisation revealed the first structural example of homoleptic coordination of a thioether macrocycle to a Group 1 metal, with this structure shown in Figure 1.2.[8]

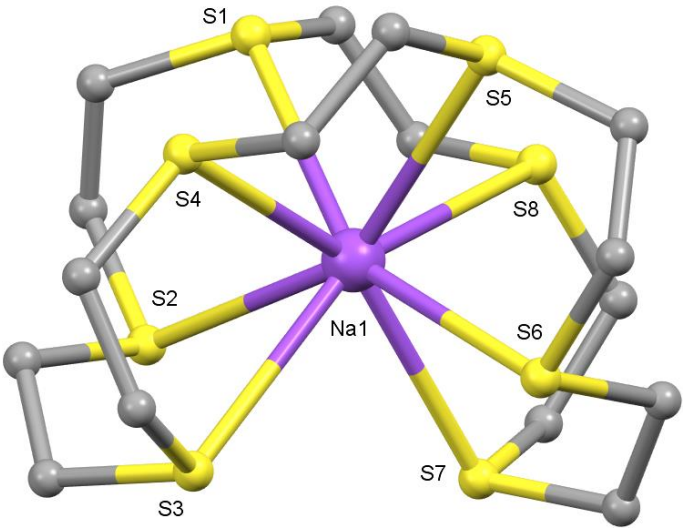

Figure 1.2 - Crystal structure of $[Na([24]aneS_8)]^+$ cation. Redrawn from Ref[8].

These complexes of mismatched acids and bases are much less stable due to the size difference in the overlapping orbitals. The synthesis requires careful reagent selection, the $[BAr^F]^-$ salt is known to be non-coordinating and thus will not compete with the macrocyclic ligand for binding to Na^+.

1.2 – Ligand Types

1.2.1 Neutral Phosphine and Arsine Ligands

Since their discovery in 1847, phosphines and their development in organophosphorus chemistry has shown them as a key class of ligands in organometallic and inorganic chemistry.[9] Chapters 4 and 5 are primarily focused on the coordination of neutral phosphine and arsine ligands to the main group metals from Group 13 and 14. Neutral phosphines (PR_3) and arsines (AsR_3) are found commonly throughout inorganic chemistry due to their extreme versatility and customisability through tuning of both steric and electronic properties of the substituents. Additionally, the use of phosphine ligands allows for the use of $^{31}P\{^1H\}$ NMR (nuclear magnetic resonance) spectroscopy, a very useful tool to probe the change in environment of the donor atom of the ligand species. Phosphine and arsine ligands are generally considered to be sigma donor-pi acceptor ligands, although, with the p-block acceptors studied in this thesis, only sigma donation is possible due to the lack of d-orbitalswith further discussion of this with Fig 1.4. As observed in the lighter congeners (NR_3), phosphine ligands can undergo pyramidal inversion, however with a much higher energy barrier and so this is rarely seen, with the R-group substituents having a large effect on this process.[10,11] Through substitution of one or all of the three R-groups, these ligands can have their steric and electronic properties finely tuned. Incorporation of large and bulky R-groups such as ^{i}Pr, ^{t}Bu or aryl rings causes unfavourable steric interactions and can prevent or weaken the coordination to a metal centre. Phosphines, especially those with alkyl R-groups, are readily oxidised by O_2 in the air and can be pyrophoric, making handling challenging.[12] While aryl phosphines show some stability in air, the alkyl phosphines require an inert atmosphere to be maintained throughout the reaction to prevent the formation of the unwanted phosphine oxide. Similarly, alkyl arsine ligands with a low molecular weight are also toxic and air sensitive.[13] Due to this, all of the reactions described in this thesis were performed under inert conditions, unless otherwise stated.

Quantifying the steric properties of a phosphine (or arsine) ligand is usually by its ‘cone angle’, θ, which is commonly measured from the crystallographic structure of a complex. When no such data is available, this angle is calculated from: the point of a cylindrical cone at a distance of 2.28 Å (idealised M-P bond length, originally from d(Ni-P)) away from the phosphorus atom to the outer edges of the van der Waals radii of the present R-groups (including the H atoms on R), a diagram of this is shown in Figure 1.3.[14]

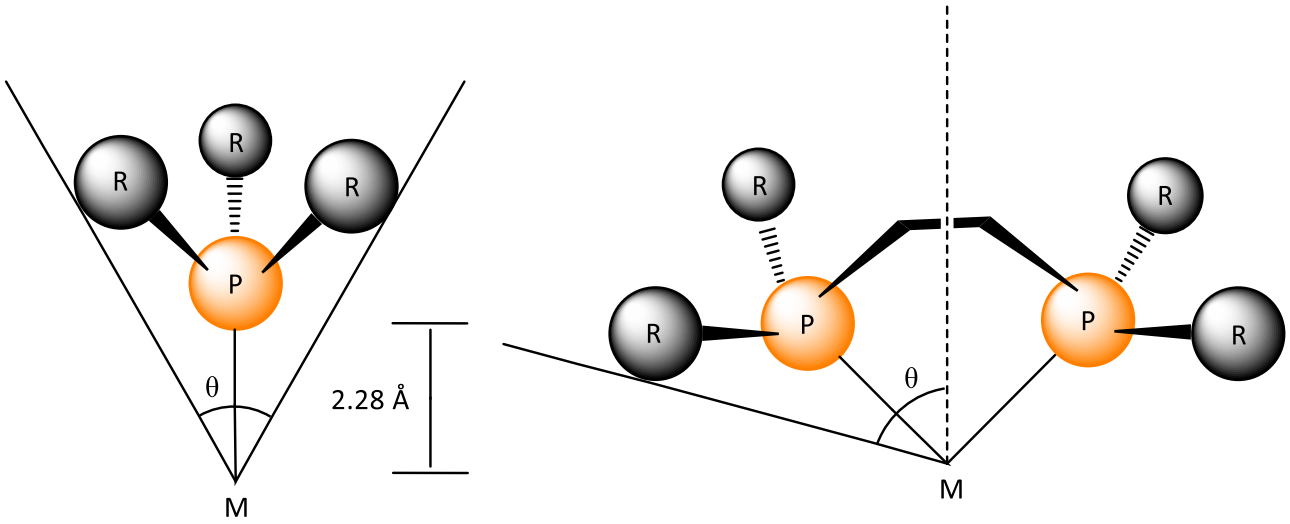

Figure 1.3 - Model of the Tolman cone angle (θ) for both mono- and bidentate phosphine ligands.[15]

A cone with a larger angle will be representative of a phosphine with R-groups with greater steric bulk. For example, PMe_3 is measured to have a cone angle of 118°, while the bulkier aryl PPh_3 has an angle of 145°.[16] This increased steric bulk of the aryl R-groups makes them more resistant to oxidation in air and thus slightly easier to use, however, they are also weaker σ-donors than alkyl phosphines. The measure of steric bulk by Tolman's cone angle has been extended to include bidentate phosphines such as $Me_2P(CH_2)_2PMe_2$ (dmpe) by calculating the outer edge of non-bridging substituents and the bisector of the P-M-P angle, where dmpe is found to have θ = 107°.[17] Use of the Tolman cone angle model does come with limitations as it generally underestimates the steric demands of phosphine ligands. This arises when a crystallographic M-P distance is not known and the 2.28 Å distance is used, this value was set from the average Ni-P distance in a range of nickel complexes.[14] This can introduce errors of as much as 25° in monodentate cases and more for bidentate pnictine ligands. In more recent years, the exact cone angles have been revealed through the optimisation of the structure of phosphorus ligands in metal complexes by DFT calculations.[18]

When phosphine ligands are used to coordinate a transition metal, the bonding of the phosphine is described using the σ-donor π-acceptor model. The phosphorus(III) atom donates the lone pair of electrons into a suitable empty *d*-orbital on the transition metal, forming a standard single bond σ-interaction.[16] Simultaneously, when the metal is electron rich there is back-donation of electrons from a filled metal *d*-orbital to the σ*-orbital of the P-C bond, causing a π-interaction between the metal and the pnictine ligand; there is also lengthening of the P-C bonds of the ligand due to this back bonding.[19]

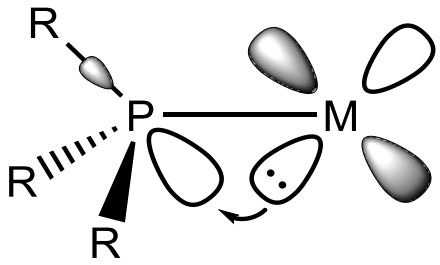

Figure 1.4 - Diagram showing the orbitals involved in M-P π back-bonding.

When phosphine ligands coordinate to the *p*-block metals, this model cannot be applied, due to the lack of *d*-orbitals at the correct energy to partake in back-bonding. The n*d*-orbitals contain no electrons and are too high in energy, while the (n-1) *d*-orbitals are found in the core orbitals and too low in energy and thus neither are capable of forming significant overlaps with the phosphine orbitals. Bonds between phosphine ligands (as well as other pnictine donors) and p-block Lewis acids are therefore primarily formed from σ-donation of the lone pair of the pnictine. Consiquently, electron donating substituents (such as methyl groups) can improve the bonding of these ligands by increasing the σ-donor ability; making alkyl pnictines stronger σ-donors than the aryl pnictines with the main group metals.

Many of the inorganic complexes synthesised in this thesis, as well as throughout inorganic chemistry as a whole, are hypervalent. When the octet rule is broken and more than 8 valence electrons are found around the central metal atom the complex is known as hypervalent.[20] Higher coordination numbers will yield hypervalent molecules and in these cases, the 3-centre-4-electron (3c-4e$^-$) bonding model is used to describe the bonding, with this being shown below in Figure 1.5.

This model details the overlap of the filled *p*-orbitals of two ligands, L, with an n*p*-orbital of a metal to form a linear L-M-L unit, forming three molecular orbitals. The donation of two electron pairs fills the bonding and non-bonding orbitals while the higher energy anti-bonding orbital remains empty. In an octahedral complex, each of the three orthogonal *p*-orbitals of the metal centre are used to form the three 3c-4e$^-$ bonds.

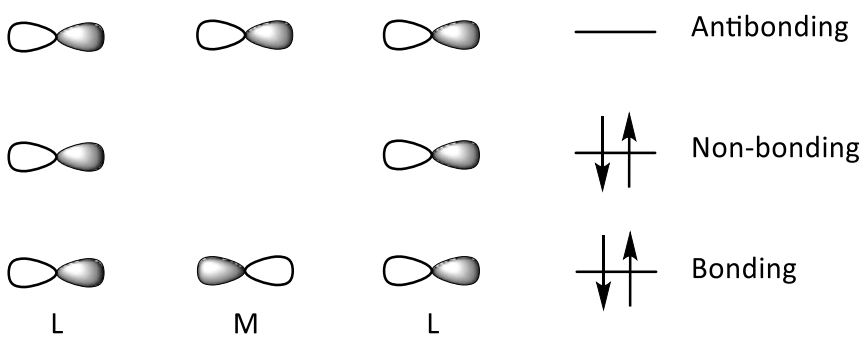

Figure 1.5 - 3-centre-4-electron bonding model (M = metal; L = 2e$^-$ donor ligand).[21]

Traversing down the Group 14 pnictine donors (N-Bi), the separation energy between the n*s*- and n*p*-orbitals increases, meaning the mixing of orbitals is less favourable.[21,22] This means that the lone pair of electrons on the heavier donor ligands (As, Sb) will have a higher *s*-character and is thus less available for bonding. The orbitals becoming more diffuse down the group, means that the later pnictine ligands are weaker σ-donors and therefore show a weaker binding in complexes of the main group metals. Despite this, a recent publication by the Reid group highlighted a group of newly synthesised Group 13 halide complexes formulated as $[MX_3(SbR_3)]$ (M = B, Al, Ga, In; X = Cl, Br, I; R = Et, ^{i}Pr).[23] In the case of bismuthine ligands, structural examples are rare, with a small number of examples of coordination using bulky R groups such as BiR_3 (R = ^{i}Pr, $SiMe_3$).[24–26] The presence of the large R-groups on both the metal and bismuthine ligand provides steric bulk to stabilise the weaker M-Bi bond protecting this from attack of incoming species, allowing for the synthesis of $[MR_3(BiR'_3)]$ (M = Al, Ga; R = Me, Et, ^{t}Bu; R' = $SiMe_3$, ^{i}Pr).

These complexes are best represented by the molecular orbital bonding diagram of a σ-bond, demonstrating the orbital overlap of the lone pair of ligand X and the acceptor orbital of M, as illustrated in Figure 1.6. The overlap of these orbitals produces two molecular orbitals with the donated electrons being found in the lower energy σ-orbital while the higher energy σ*-orbital remains empty. The low energy σ-orbital is polarised towards the incoming electronegative ligand while the antibonding orbital is polarised towards the metal and can then accept electron density from another donor species. The energy and size of each of these molecular orbitals depends on the electronegative and size of the atomic orbitals of M and X. If a second donor species Y donates into the M-X σ*-orbital, the Y-M-X unit should be close to linear due to the directionality of the σ and σ*-orbitals.

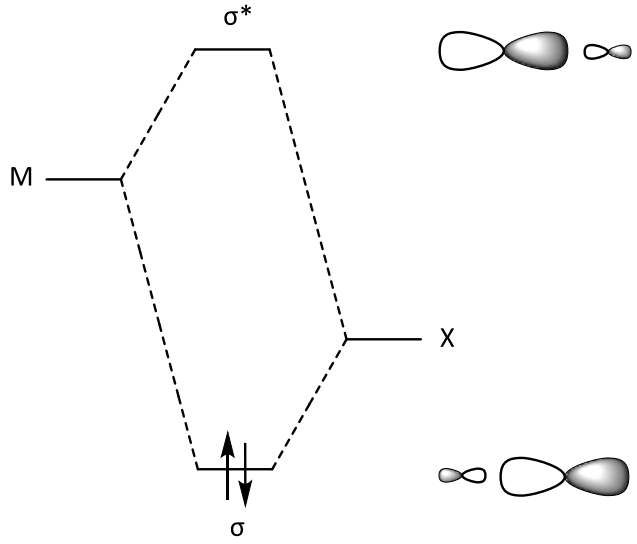

Figure 1.6 - Molecular bonding diagram of an M-X σ bond.

The diagrams in Figure 1.5 and 1.6 are suited for the coordination of up to six ligands in an octahedral geometry and currently there are no satisfactorily detailed models for coordination

numbers >6. There are many examples of main group metal centres with coordination numbers higher than this with large Lewis acidic centres such as Pb(II) commonly taking up higher coordination numbers.

The work in this thesis makes use of not only monodentate phosphines, but bi-, tri- and tetradentate ligands with the majority of these being commercially available. The monodentate ligand PEt_3 was synthesised prior to use, *via* a Grignard preparation adapted from the synthesis of $SbEt_3$, with the full details described in Chapter 4.[23] The bidentate ligand, *o*-$C_6H_4(PMe_2)_2$, and tridentate $MeC(CH_2PPh_2)_3$ were also synthesised in house by Dr Wenjian Zhang, Dr Danielle Runacres or Dr Rhys King. The synthesis of the bidentate, *o*-$C_6H_4(PMe_2)_2$, is shown in Scheme 1.1 following a procedure reported by Harris and co-workers, starting form the commercially available *o*-$C_6H_4(P(O)(OMe)_2)_2$.[27] This involved the reduction of the phosphonate using $LiAlH_4$, before the sequential addition of the methyl R-groups.

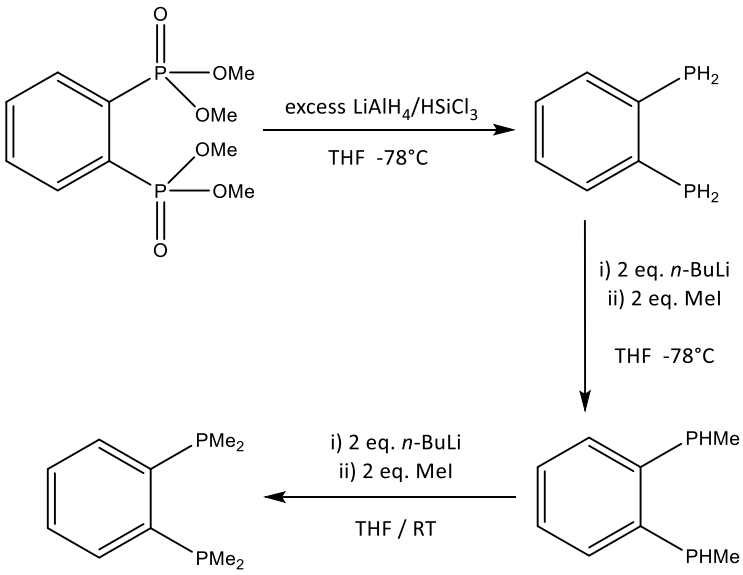

Scheme 1.1 - Synthesis of *o*-$C_6H_4(PMe_2)_2$.[27]

Many polydentate phosphine ligands are synthesised through the formation of sodium diphenylphosphide and followed by reaction with the corresponding haloalkanes. Scheme 1.2 shows this reaction in the case of the tripodal tridentate phosphine, $MeC(CH_2PPh_2)_3$.[28]

$$PPh_3 + Na \xrightarrow[NH_3\ (l)]{} NaPPh_2 \xrightarrow[THF\ (reflux)]{^1/_3\ MeC(CH_2Cl)_3} MeC(CH_2PPh_2)_3$$

Scheme 1.2 - Synthesis of $MeC(CH_2PPh_2)_3$.[28]

1.2.2 Imine Ligands

The nitrogen donor ligand, pyridine, is a Lewis basic heteroaromatic imine that has been commonly used throughout coordination chemistry. Linking of these pyridine rings forms many

structural isomers, of which two are commonly used for coordination. The ligand 4,4'-bipy (4,4'-bipyridine) is shown in Figure 1.7 and is preorganised as a bridging ligand with the pyridine rings being joined at the 4 position, *anti* to the nitrogen donor. Depending on the stoichiometry used, reactions of 4,4'-bipy with different metal centres has produced a range of infinite coordination polymers as well as 2-D and 3-D coordination networks such as MOFs (metal organic frameworks).[36–38] The other isomer formed is 2,2'-bipy (2,2'-bipyridine), which is preorganised for chelation to a central metal as a 5-membered ring and from herein, references to 'bipy' will be implying the use of 2,2'-bipyridine. Due to its structural similarity, 1,10-phen (1,10-phenanthroline) is often used as a comparison to 2,2'-bipy with many complexes of both analogues having been produced with similar structure and properties being observed, the structures of both ligands are shown in Figure 1.7.[39] 2,2'-bipy is able to rotate around the central C-C bond into two conformations with only one of these allowing for chelation; the conformer with both nitrogen donors opposing each other is the energetically favourable conformer of 2,2'-bipy itself.[40] With the conformational rigidity of the back-bone, 1,10-phen cannot rotate and thus the nitrogen donors are locked in the chelating conformation which, makes phen bind to the metal centre more strongly than the analogous 2,2'-bipy complex. However, the additional dissociation of the aromatic electrons within the extra complete aromatic ring lowers the electron density remaining at the nitrogen atoms for donation, making 1,10-phen a slightly weaker σ-donor.[41]

The homoleptic *tris*-bipy complexes such as $[Ru(bipy)_3]^{3+}$ are known to have excellent photochemical activity due to the ability to absorb light at room temperature, with homoleptic octahedral diimine complexes known for a range of metals.[42] Due to the extended aromatic systems of these pyridine-type ligands, reports have detailed a range of molecular species with photo-electronic properties such as metal-to-ligand charge transfer and phosphorescence. The lability of the monodentate pyridine ligand means the formation of the homoleptic $[M(py)_6]^Y$ (M = transition metal, main group, lanthanide) are rare,[43] unlike the *tris*-bipy complexes, which are known for a wide range of metals, shown in Scheme 1.3. The chelation of these bidentate ligands increases their binding affinity for the metal centre more than that of two analogous monodentate species due to the entropic gain in the use of fewer bidentate ligands.

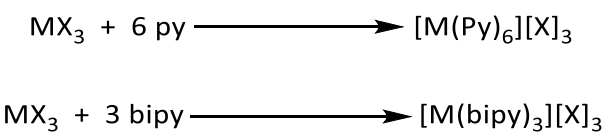

Scheme 1.3 - Reactions of M(III) with the imine ligands pyridine and bipy to form the homoleptic complex.

Similarly to the bidentate ligands, the tridentate ligand terpy (2,2':6',2"-terpyridine) has also been used extensively to explore the effect of changes to the aromatic region of the ligand and how it may affect the photochemical properties, along with the coordinating properties of tridentate nitrogen donors.[44] These nitrogen donors have been used with the Group 14 metals (M = Ge, Sn) to form cationic species, *via* halide abstraction from $[MCl_2(bipy)_2]$ (M = Ge, Sn; X = Cl) using varying equivalents of TMSOTf (trimethylsiliyl trifluoromethanesulfonate) to produce the cationic species $[MCl_{2-n}(bipy)_2][OTf]_n$ (M = Ge, Sn; X = Cl; n = 1, 2).[45]

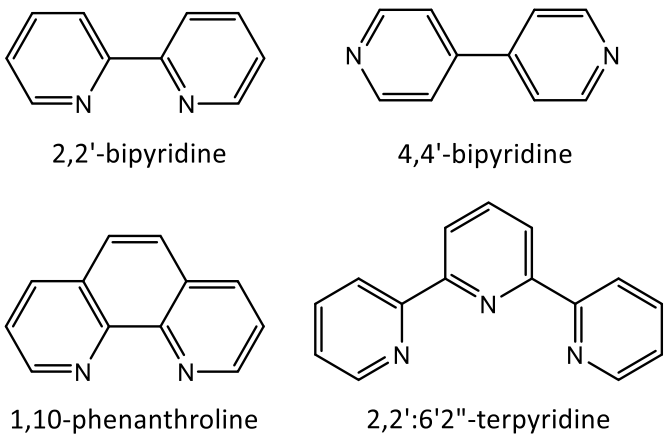

Figure 1.7 - Structurally related polypyridyl imine ligands.

1.3 – Group 13

Group 13 contains the elements B-Tl with the electronic ground state configuration of ns^2np^1 meaning that commonly these elements are found in the 3+ oxidation state.[46] The triel metal halides MX_3 (M = B, Al, Ga, In; X = F, Cl, Br, I) are all readily available for purchase, forming 3 bonds through sp^2 hybridised bonds to the halides with an empty p-orbital found perpendicular upon the central metal atom. The empty p-orbital can accept electron density from a Lewis basic donor and thus the Group 13 trihalides are often perceived as quintessential Lewis acids. A number of studies have been carried out on these compounds exploring how Lewis acidity changes down the group and with the change in halide.[47,48] Measurement of this Lewis acidity of boron centres can be carried out using ^{31}P NMR spectroscopy, deriving from the measured resonance of $OPEt_3$ in varying solvents.[49] Of these metal halides, MF_3 (M = Al, Ga, In) is unique, being found as an inert F-bridged polymer that is unreactive towards water (or other potential ligands). The trihydrates, $MF_3.3H_2O$, are still poorly soluble in water, however, they do have a higher reactivity towards coordination of other ligands.[49] The chemistry of these fluorides has been reviewed,[50,51] with the progress in the coordination of these hydrate salts being advanced by the use of hydrothermal synthesis. This method was successful in coordination of the imine ligands 2,2'-bipy, 1,10-phen and terpy.[52] The hydrothermal route was a direct method for coordination to the $MF_3{\cdot}3H_2O$

species, whereas previously, the analogous chloride species required reacting with fluorinating agents such as $[NMe_4]F$ or KF.[53]

In the case of Tl and In, the inert lone pair effect stabilises the +1 oxidation state, giving ions which are isoelectronic to the M(I) alkali metals.[54] The coordination products of the monohalides MX (M = B, Al, Ga, In; X = F, Cl, Br, I) are known for each of the metalloid elements in Group 13, however, the stability of these compounds greatly decreases up the group. Only InX and TlX (X = Cl, Br) are stable under standard conditions with MX (M = Al, Ga) the products are metastable species. These compounds are also isoelectronic with simple diatomic molecules such as N_2 or CO making them relatively poor Lewis acids, but good Lewis bases, with examples of them acting as both bridging and terminal ligands.[55] Due to the lone pair of electrons, (which is located in the ns^2 valence shell) these species can act as a σ-donor as well as having accessible orbitals for π back-bonding from the metal being coordinated. Until recently, the monohalide field of Group 13 was uncharted but has gained interest since the finding of a reliable method for synthesis of MX (M = B, Al, Ga, In; X = F, Cl, Br, I).[56] The work of this thesis is focused on synthesis of M(III) complexes, without the formation of M(I) products.

Donation of a single lone pair of electrons from a ligand (L = NH_3, OPR_3, PR_3 etc) into the vacant p-orbital of the Group 13 metal halide MX_3, results in the formation of new bond, producing complexes $[MX_3(L)]$ (M = Al, Ga, In; X = Cl, Br, I), as is demonstrated in Figure 1.1. The reaction with a single equivalents of monodentate ligand forms complexes predominantly form in a tetrahedral geometry, with the reduction of magnitude of the X-M-X bond angles being partially dictated by the steric bulk of incoming ligand. Reactions forming complexes of $[MX_3(L)]$ have been shown for each of the M(III) halide compounds down the group with a range of different donor types including imines[57,58], ethers,[59,60] phosphine oxides,[61,62] phosphines[63] as well as other soft donor ligands.[21,64,65]

When two molar equivalents of a monodentate ligand are reacted with MX_3, the complex produced is commonly $[MX_3(L)_2]$ in a trigonal bipyramidal geometry where the incoming donors are found axially.[66,67] These complexes display hypervalency, with 10 electrons being located around the metal centre from 5 covalent bonds. As demonstrated in Figure 1.5 above, this is achieved from the formation of 3 sp^2 hybridised orbitals bonding equatorially and the new ligands forming a 3c-4e^- bonding system. The formation of these trigonal bipyramidal structures has been shown to be possible with a range of both hard and soft donor species, with a range pnictine (P, As, Sb) complexes having been reported in the geometry same shown in Scheme 1.6.[23,68] As discussed earlier in Section 1.2.3, bidentate ligands such as 4'4"-bipyridine, which act as bridging ligands between metal centres, and are known to produce coordination polymers with the Group 13 metal halides.[57,58] Addition of further equivalents of ligand can produce complexes in

octahedral geometry with a six coordinate metal centre. This has been shown to be possible with 3 equivalents of pyridine with the *tris*-pyridyl complex taking up a *mer*-arrangement, the seemingly preferred geometry with monodentate coordination. [62,69] The *fac* arrangement is more commonly seen with polydentate ligand species such as macrocycles, but has is also seen in the complex *fac*-$[InX_3(DMSO)_3]$.[62] This is in contrast to the *tris*-$OPPh_3$ and *tris*-THF complexes, which are both *mer* in arrangement, which is shown in Scheme 1.4.

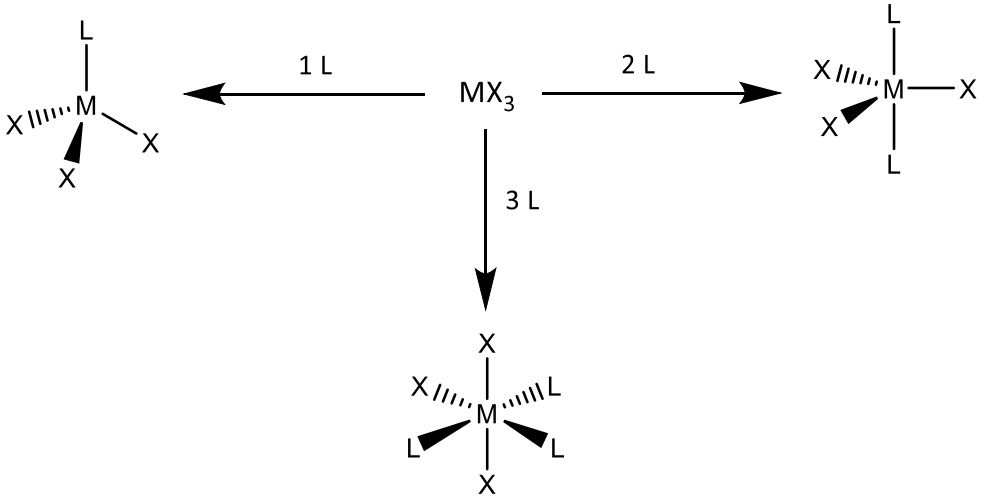

Scheme 1.4 - Commonly observed bonding modes of MX_3 (M = Al, Ga, In) with coordination of monodentate ligand species (L).

The coordination of a single equivalent of the hard bidentate nitrogen donor ethylenedianime (*en*) to MX_3 (M = Al, Ga; X = Cl, Br, I) produced the octahedral complexes $[MX_2(en)_2][MX_4]$.[70] The metal trihalide has lost a halide to allow for the coordination of the bidentate *en* ligand, with this free halide transferring to a second molecule of MX_3 to form a halometalate $[MX_4]^-$ counter anion, in a process known as 'self-ionisation'. This is in direct contrast to the behaviour of the Group 13 organometallic MR_3 or metal hydrides MH_3, which have been repeatedly reported to form bridged dimer species $[X_3M(L\text{-}L)MX_3]$.[71–73] Coordination of the methylated diamine analogue, tmeda (tetramethylethylenediamine), with InI_3 was found to contrast this behaviour and instead produced the 5-coordinate complex $[InI_3(tmeda)]$ in a distorted trigonal bipyramidal geometry, as a result of the larger In(III) radius.[74] This behaviour was then mirrored with coordination of the soft *ortho*-phenylene diphosphine ligand, *o*-$C_6H_4(PPh_2)_2$, to form $[InI_3\{o\text{-}C_6H_4(PPh_2)_2]$, which adopts the same geometry.[75]

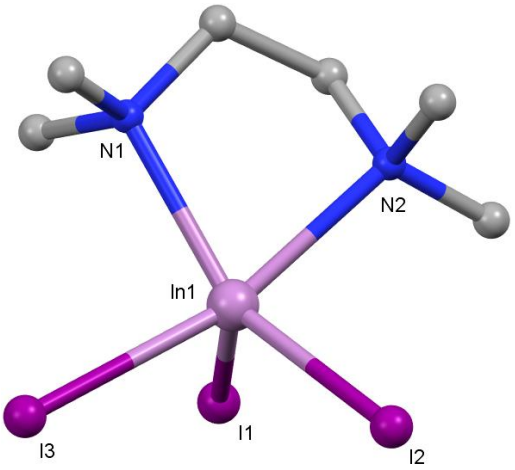

Figure 1.8 - Crystal structure of [InI_3(tmeda)] showing atomic numbering scheme. Redrawn from Ref[74] with H-atoms omitted for clarity.

Reaction of the lighter Group 13 halides MX_3 (M = B, Al, Ga, In; X = Cl, Br) with soft donor bidentate ligands, like phosphine, has been shown to produce a range of different types of complexes. The rigid, *o*-phenylene based ligand *o*-$C_6H_4(PR_2)_2$ (R = Me, Ph) produced both the chelate product [MCl_2{*o*-$C_6H_4(PPh_2)_2$}][MCl_4] as well as the *bis*-chelate product [MX_2{*o*-$C_6H_4(PMe_2)_2$}$_2$][MX_4] (M = Al, Ga, In; X = Cl, Br), with both types of structures shown in Scheme 1.5.[63,76,77] The bulkier Ph-substituted phosphine is a weaker donor and appeared to show a preference for coordination of a single ligand, whereas the smaller, stronger donor methyl-substituted phosphine tends to produce distorted octahedral metal cations with two bidentate diphosphines. The arsine analogue of this ligand, *o*-$C_6H_4(AsMe_2)_2$, was shown to have a preference for coordination of a single equivalent, as reported with both In(III) and Ga(III).[78] This is directly contrasted by the coordination of the harder bipyridyl ligand, which was shown to produce the *cis* isomer [$GaCl_2(bipy)_2$][$GaCl_4$], with more discussion of these complexes in Chapter 3.1.[79] The bridged dimer complexes [{$InCl_2$(*o*-C_6H_4{EMe_2}$_2$)}$_2$(μ^2-Cl)$_2$] (E = P, As) were produced for both E = P or As, however these rearranged to the *bis*-chelate species, [$InCl_2$(*o*-C_6H_4{EMe_2}$_2$)$_2$][InX_4], upon standing in CH_2Cl_2.[77]

The flexible ethylene backboned ligands with soft phosphine donors, $R_2P(CH_2)_2PR_2$, were also shown to produce the auto-ionised *bis*-chelate product [MX_2{κ^2-$R_2P(CH_2)_2PR_2$}$_2$][MX_4],[63,78] as well as acting as a bridging ligand between two metal centres to form [$(MX_3)_2${$R_2P(CH_2)_2PR_2$}] (M = Ga, In; X = Cl, Br, I; R = Et, Ph).[76] These latter complexes were formed with two tetrahedral metal centres and no evidence of a $[MX_4]^-$ anion. Making use of other soft donors such as the chalcogenoethers showed similar trends, with bridging complexes [$(MX_3)_2${$MeE(CH_2)_2EMe$}] (M = Al, Ga, In; X = Cl, Br; E = S, Se) being synthesised from the 2:1 reaction.[80,81] Further exploration with ligands of Group 16 ligands and the Group 13 metal halides showed that the *bis*-chelate product could be produced with both S and Se donor ligands in the form [InX_2{$RE(CH_2)_2ER$}][InX_4]

(X = Cl, Br; E = S, Se).[82] These ligands also show the formation of a halide-bridged species [{$InCl_2$(*o*-C_6H_4{$SeR}_2$)}$_2$(μ^2-Cl)$_2$] (R = Me, ^{n}Bu) which, unlike the pnictine donor (P, As) analogues, was found to be stable under standard conditions. Whereas coordination of the pnictine donors *o*-C_6H_4{ER_2}$_2$ (E = P, As) were found to chelate the Group 13 metal halides, *o*-C_6H_4{SR}$_2$ was found to bridge metal centres, producing bimetallic complexes [(MCl_3)$_2${μ-*o*-C_6H_4(SR)$_2$}] (M = Al, Ga; R = Me, Et).

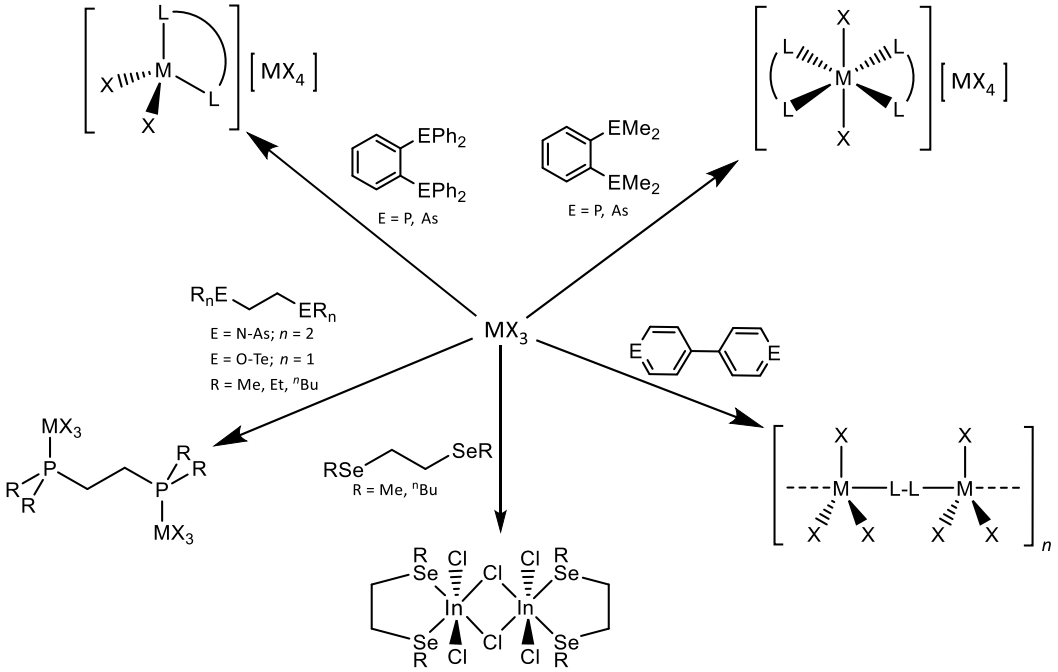

Scheme 1.5 - Primary binding modes for the coordination of bidentate ligand species (L-L).

When looking past the coordination of bidentate species, ligands with higher denticity, such as the tripodal tridentate species, MeC{CH_2PR_2}$_3$, are discussed in Chapter 5.

The macrocyclic nitrogen donor ligands, such as 1,4,7-trimethyl-1,4,7-triazacyclononane (Me_3tacn), have been shown to successfully coordinate to the Group 13 metal halides. These complexes are formulated as [MX_3(Me_3tacn)] (M = Al, Ga, In; X = F, Cl, Br) in a *fac* arrangement and have been the recent subject of research in the Reid group due to their prospects for application in PET imaging.[51,53]

1.4 – Group 14

The elements of Group 14 (C-Pb) are found in an electronic ground state configuration of n*s*^{2}n*p*^{2} which means they commonly form ions in the +2 and +4 oxidation state, depending on where in the group they are found.[83,84] Examples of these elements outside of their standard oxidation states are known, however are much more rare.[85] The lighter tetrels (C-Ge) have their chemistry dominated by the +4 oxidation state, while tin can switch between Sn(II) and Sn(IV) and is known to have a rich chemistry in both oxidation states. Other than strong oxidising agents such as PbO_2

or $Pb(OAc)_4$, the heavier metallic element Pb is found predominantly in the 2+ oxidation state, due to the stabilisation of the inert lone pair.[86] An example of this instability is the strong fluorinating agent PbF_4, which has been used to fluorinate alkene species.[87] In contrast, organolead (IV) compounds (PbR_4) have a much greater stability than inorganic lead compounds, an affect attributed to the lower electronegativity of the organic substituents, stabilising the positive charge at lead.[88] Although less common, there are examples of E(II) (E = C, Si, Ge) stabilised through manipulation of the ligands to increase steric bulk and withdraw some electron density from Group 14 ion.[85,89–92]

As Group 14 descends (excluding the anomalous first row C), there is a gradual increase in the covalent radii measured for each element. In contrast, the van der Waals radii are found to increase down the group with Pb being anomalously small, being measured as 2.02 Å due to the f-block contraction.[93] These have been tabulated below in Table 1.1 along with the sum of the van der Waals radii of both the respective metal and oxygen atoms. In many cases, the bonding distances from M(II) to a neutral or anionic ligand is highly variable, which can make it difficult to determine the coordination number. An upper limit for coordination distance is for the the bond distance to be within the sum of the van der Waals (vdW) radii; significant interactions in the work described in this thesis have been given the upper limit of 0.3 Å below this vdW sum.

Table 1.1 - The covalent[94] and van der Waals[95] radii of Group 14 metals Ge-Pb.

	Covalent radii / Å	Van der Waals radii / Å	Sum of M + O Van der Waals radii / Å
Ge	1.20	2.11	3.63
Sn	1.39	2.17	3.69
Pb	1.49	2.02	3.54

The Lewis acidity of the Sn(II) and Pb(II) metal centres, as well as their sizes, mean that complexes of these divalent metals occur with a range of both neutral and anionic ligand species, with coordination numbers of up to 12 being reported for Pb(II).[89,96] The large majority of the reported complexes contain the harder O and N donor ligands.[97–99] Complexation of oxygen donor crown ether macrocycles (of varying ring-size) to MX_2 produced a range of products including a 10-coordinate sandwich complex $[Sn\{[15]crown\text{-}5\}_2][OTf]_2$ with this structure being shown in Figure 1.9a.[100] Pb(II) has been observed in an 11-coordinate environment as part of a macrocyclic system as $[Pb(NO_3)_3\{benzo\text{-}15\text{-}crown\text{-}5\}]^-$. While 12 coordinate Pb(II) has been reported in the cation $[Pb(NO_3)_6]^{4-}$, with each nitrate anion being found binding in a κ^2 binding mode.[101,102] As well as the first row N and O donors, there are examples with softer donors such as S, Se, P and As, with

further examples and details on macrocyclic coordination to MX_2 (M = Sn, Pb) in Chapters 5 and 6.[90,103]

The observed geometries of the divalent Group 14 metals (Sn, Pb) are dependent on the nature of the ns^2 electrons and whether they are stereochemically active. The stereochemical activity of the lone pair can be partially dictated by the coordination number of the complex, with low coordination numbers manifesting in a hemidirected lone pair.[104] The directionality of the lone pair is presented structurally as a void in the distribution of bonds from the metal centre, where a hemidirected complex contains a void in the distribution of the bonds. This is highlighted in the geometry of the crystal structures shown in Figure 1.9.

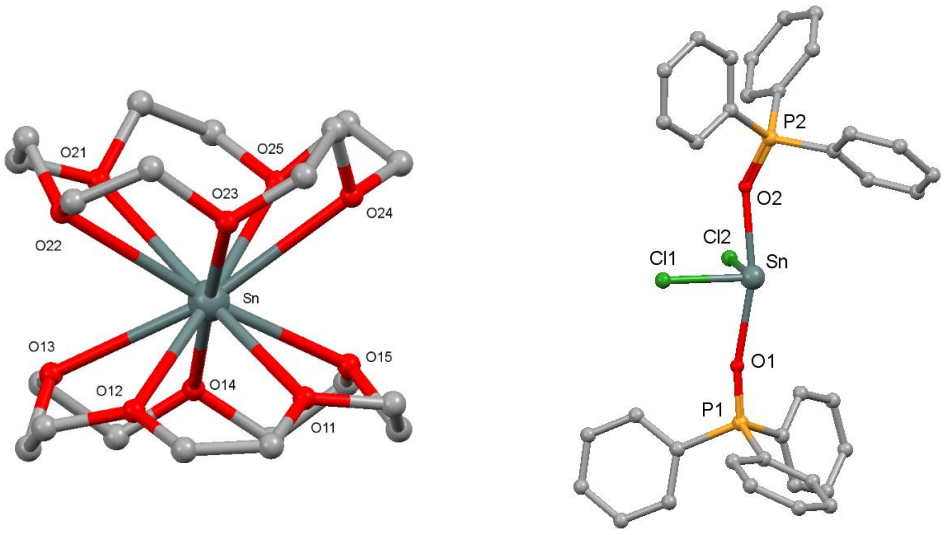

(a) (b)

Figure 1.9 - Crystal structures of (a) $[Sn\{[15]crown5\}_2][OTf]_2$ and (b) $[SnCl_2(OPPh_3)_2]$ are examples of holo and hemidirected complexes, where the lone pair of electons is stereochemically active (b). Redrawn from Ref[100] and Ref [106] with H-atoms and anions omitted for clarity.

Comparing the structures in Figure 1.9, it can be seen that in (a) the crown ether coordination is symmetrical above and below the Sn(II) cation, with no evidence for a void, whereas the $OPPh_3$ complex (b) has a clear void in the equatorial plane. Low coordinate complexes (CN = 2-5) of these divalent metals, such as 1.9(b) are often found to contain a stereochemically active lone pair. [106] Many of the complexes with stereochemically active lone pairs also form bridging interactions through longer secondary bonds.

Three coordinate species, such as $[Ge(PMe_3)_3]^{2+}$, commonly take up a tripodal geometry and examples are known with many different donor atoms, including halides, phosphorus, arsenic, sulphur and oxygen.[90,107,108] The four-coordinate species reported in the literature, especially with halide ligands, often take up a disphenoidal geometry, similar to $[SnCl_2(OPPh_3)_2]$ shown above in Figure 1.9(b).[105] This geometry has also been observed with the coordination of the tripodal arsine

ligand $MeC(CH_2ER_2)_3$ (E = P, R = Ph; E = As, R = Me) to germanium, in the presence of TMSOTF, forming $[Ge(MeC(CH_2AsMe_2)_3][OTf]_2$[90]

Complexes with higher coordination numbers (≥ 8) were found to be primarily homodirected with the n*s* lone pair of electrons being found in the spherically symmetric *n*s orbital. When the electrons are located in this core orbital, the ligand bond lengths are found to be slightly longer, due to repulsion from the additional electrons in the highly shielding *s*-type orbital, as seen in $[Sn([15]\text{-crown5})_2]^{2+}$ in Figure 1.9(a). In structures with coordination numbers of 6-8, both holo- and hemidirected geometries have been reported. Over various studies it has been shown that the geometry of Sn(II) and Pb(II) coordination complexes is often irregular and cannot be readily described. The variety in coordination number, stereochemical activity of the lone pair and variable bond distances can give rise to unusual geometries and make description and rationalisation of the bonding of these complexes difficult.[104]

1.5 – Anion Types

A large amount of work dedicated to the coordination chemistry of Groups 13 and 14 makes use of the halide as a simple, monoatomic anion in the crystalline salts MX_n (n = 1-6). These anions have been shown to bond with both ionic and covalent bonding, with the inorganic halides showing graduation from ionic to covalent bonding. The higher the electronegativity of the halogen gives an indication of a more ionic type of bonding and thus changing the properties and bonding exhibited by the complexes.[109] As a ligand with the p-block metals, the halides are coordinating anions. Commonly, the halides remain in the primary coordination sphere of the complex of interest, with other neutral ligands filling the coordination sphere. In some cases, a single halide is lost upon coordination of the neutral ligand, with the free halide then reacting with another molecule of metal halide starting material *via* auto-ionisation to form a halometalate anion. An example of this type of reaction is shown in Scheme 1.6.

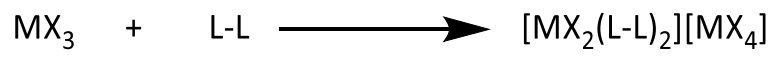

Scheme 1.6 – Coordination of a bidentate ligand, showing auto-ionisation to form a cationic complex and a corresponding halometalate anion

The term “non-coordinating anion” was used historically to describe a complex in which a halide had been replaced with polyatomic anion such as tetrafluoroborate $[BF_4]^-$, perchlorate $[ClO_4]^-$ or hexafluorometallate $[MF_6]^-$ (M = P-Sb). The $CF_3SO_3^-$ triflate anion (OTf^-) has also been described as a ‘non-coordinating anion’. This will be discussed further later. Each of these anions provides slightly different properties such as charge density, resonance structures, and coordinative

strength. With the more recent developments in X-ray crystallography, it is now evidently clear that “non-coordinating anions” is a misnomer, with a more accurate description that they are “weakly coordinating anions”.[110, 111, 112] This term better describes their behaviour when all other donor competition (H_2O, coordinating solvents, *etc.*) are removed from the system. Structural studies have shown examples of coordination of each of the common “weakly coordinating anions” to a range of different metal acceptors across the periodic table.

The fluoroanions, such as $[BF_4]^-$, $[PF_6]^-$ and $[SbF_6]^-$, are known to have increased coordination towards the most electrophilic metal ions, early transition metals in a low oxidation states such as $[M(Cp)_2]^{2+}$ (M = Zr, Ti, Hf). Reaction of $[TiF_2(Cp)_2]^{2+}$ with $[MF_6]^-$ (M = P, As, Sb) has been shown to cause coordination of both anions through a single Ti-F-M bridge per anion.[113] These anions have also been shown to coordinate through 2 or 3 of the fluoride atoms in complexes.[114,115]

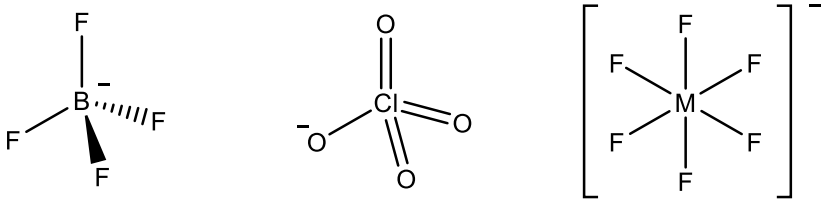

Figure 1.10 - Examples of weakly coordinating anions used in early inorganic research.

Each of these anions has its negative charge stabilised (or distributed) throughout the molecule by conjugation or the strong inductive power of multiple electronegative fluorine atoms. The innate stability of these anions when free in solution gives them high lability when coordinated to the p-block elements and thus can readily create vacant sites in the primary coordination sphere of the metal centre,[116] allowing other ligand species can then be coordinated to produce more complex species or be used for activation of a substrate in catalysis.

Due to the change in the electronic properties of these coordinated anions in comparison with the free anion in solution, IR spectroscopy has been found to a powerful tool when exploring these weakly coordinated anions. In the case of the perchlorate anion $[ClO_4]^-$, for example, a series of complexes $NiL_n(ClO_4)_2$ (L = MeCN; n = 2, 4, 6), where the symmetry exhibited by the complex changed from T_d to C_{3v} and C_{2v}, could be observed by IR spectrometry.[117] This change was characterised as the change in bonding from the anion, from the discrete ion (T_d), to monodentate and bidentate coordination, with these different interactions shown in Figure 1.11.[118]

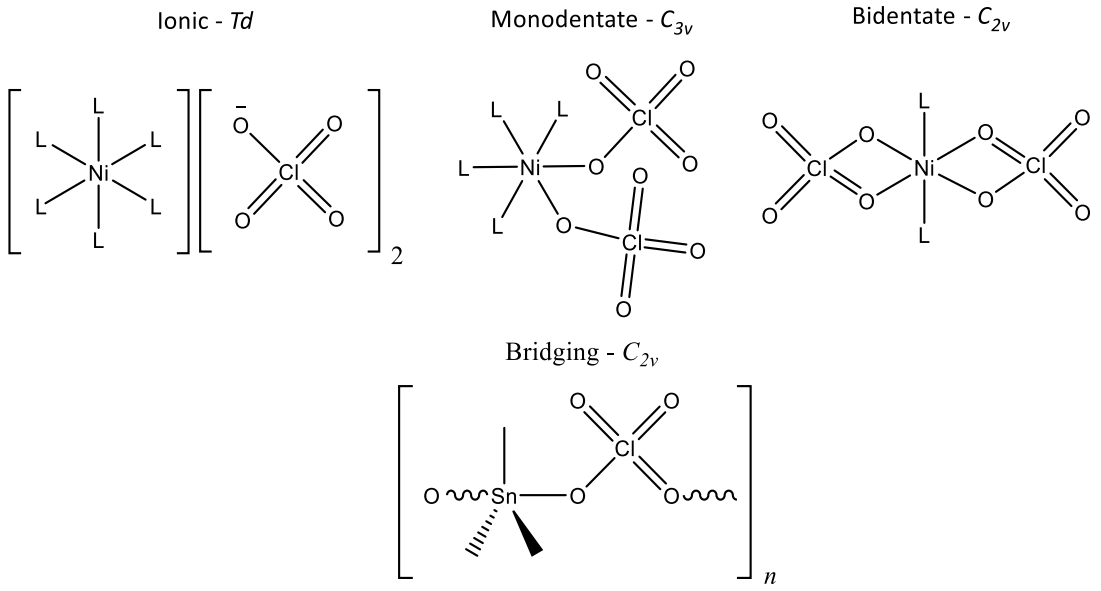

Figure 1.11 - Different binding modes of ClO_4^-.[117]

Another commonly used anion is $[BPh_4]^-$, which has the anionic charge delocalised over the four aryl groups. However, coordination through these phenyl rings has also been shown, for example structural analysis of $[Cu(CO)(\kappa^2\text{-en})(BPh_4)]$ showed a 5-coordinate Cu(I) metal centre of which, two of these bonds were long-contacts to the phenyl rings of the $[BPh_4]^-$ anion.[119] To combat this coordination, fluorine (or fluorine containing groups *e.g.* CF_3) was incorporated into the aromatic system, allowing for a more diffuse and delocalised negative charge. As well as this, $[BPh_4]^-$ was prone to undergoing hydrolysis with cleavage of a phenyl ring.[112] This lead to the development of the weakly coordinating anion *tetrakis*-[3,5-*bis*(trifluoromethyl)phenyl]borate anion ($[BAr^F]^-$), first synthesised by Kobayashi *et al* and shown in Figure 1.12.[120] This was a major development as it allowed for better study of highly electrophilic species as well as giving a route to the 'naked' cations. These anions have been used extensively throughout inorganic chemistry to stabilise cationic species, including p-block complexes. This development greatly lowered the coordinative ability of the tetra-aryl borate anion, although there are some rare cases where both the perfluorinated aryl and 3,5-trifluoromethyl substituted borate anions have been shown to bind through a fluoride.[121–123]

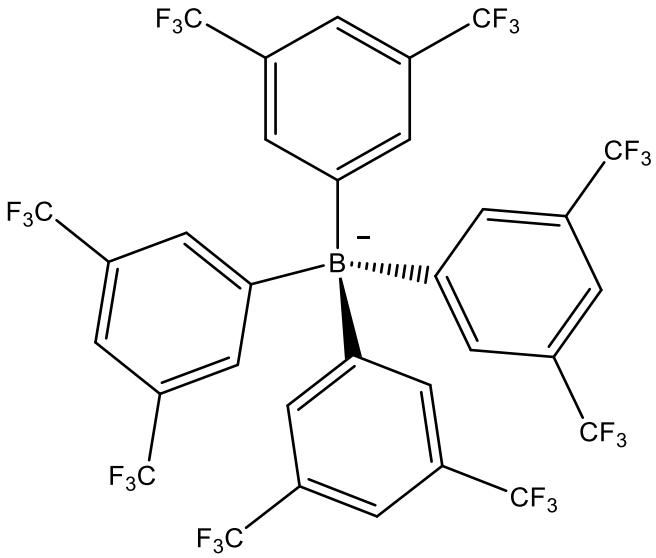

Figure 1.12 - Structure of *tetrakis*-[3,5-*bis*-trifluoromethyl)phenyl] borate anion $[BAr^F]^-$.

The trifluoromethanesulfonate ($[OTf]^-$) anion is the highly stable conjugate base of the super acid triflic acid and has also been shown to have good activity as an organic catalyst.[124,125] This stability arises from the resonance of the negative charge over the three oxygen atoms as well as the strongly electron withdrawing CF_3 group increasing the electropositive nature at the sulphur atom. In organic chemistry it is an excellent leaving group, with alkyltriflates being stored under inert conditions to eliminate nucleophilic attack from atmospheric water.[126] The metal halide salts have been observed to undergo hydrolysis, greatly increasing the catalytic loading required, while the metal triflates have been shown to have good stability in aqueous conditions thus remaining active.[124]

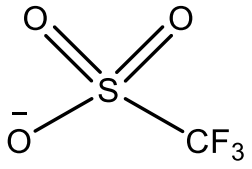

Figure 1.13 – Structure of trifluoromethanesulfonate anion $[OTf]^-$.

Within inorganic chemistry, the triflate anion is a weakly coordinating anion known to have higher aqueous stability than $[BF_4]^-$ without the redox potential associated with the perchlorate anion.[127] As was shown in Figure 1.11 for $[ClO_4]^-$, triflate can coordinate in a monodentate, bidentate and bridged manner. Primarily, monodentate coordination through a single oxygen atom is observed with the triflate anion however, bridging interactions of metal centres through coordination of different oxygen atoms is also known throughout the periodic table.[128,129] Bidentate coordination of triflate is known, but is however less commonly observed in the literature.[111] Although utilised frequently throughout organic and inorganic chemistry, the coordination chemistry of the metal triflates (especially of the main group) with neutral ligands is a relatively unexplored field and a focus of this thesis is to synthesise and explore the properties of novel coordination complexes of

Group 13 and 14 triflates, where the weak coordination of the triflate means that cationic complexes might be expected through easy displacement of the weakly bound triflate groups.

1.6 – Analytical Techniques

Throughout the work carried out in this thesis, the synthesis was accompanied by characterisation of the resulting products using a variety of both solid and solution-state analytical techniques. It is important to use this variety of techniques to understand the structure of both the solid-state and nature of the compound in solution, especially with the use of weakly coordinating anions, where the solution NMR spectroscopic data may not be representative of the solid-state structure due to the dissociation of the weakly coordinated anion in solution.

1.6.1 Microanalysis

Elemental analysis is a solid-state technique which explores the elemental composition (C, H and N) of a sample and is used to determine the percentage of each element present in the bulk product. By comparing the experimentally determined percentages in the synthesised compound with the calculated value of the pure compound, this technique can be used to confirm the synthesis of the expected compound as well as the bulk purity. Through complete combustion of the sample, the mass fractions of the target atoms in the sample will be calculated from the resulting CO_2, H_2O and N_2. In addition to other techniques, this can be used to identify the presence of impurities as well as any lattice solvent present in the bulk solid. In this work, elemental analyses measurements were outsourced to Medac Ltd., and usually conducted in duplicate. Typically, analyses within +/-0.4% of the expected value would be considered good evidence of purity.

1.6.2 Infrared Spectroscopy

IR (Infrared) spectroscopy was used to identify the presence of specific bonds in a complex such as P=O, M-X (where present) as well as if water was present. Throughout this work IR spectra were collected as Nujol mulls using CsI disks to allow for analysis of air and moisture sensitive samples over a range of 4000 – 200 cm^{-1}. The Nujol oil protects samples from interaction with air while the CsI plates do not show any significant absorption above 200 cm^{-1} and therefore allow for observation of vibrations to lower wavenumbers than standard FT-IR experiments without interference. The metal halide stretching vibrations are commonly found between 200 and 600 cm^{-1} and using this technique of IR spectroscopy allows for collection of this key data, primarily of relevance in Chapter 4. The bonds present in the molecule have quantised vibrational energy

levels, which when irradiated with the correct energy can cause a vibrational excitation to a higher vibrational energy level. The specific vibrational mode of a given molecule will causes small changes in the geometry, in some cases this will change the electric dipole, in which case this vibrational mode is IR active.[130] Group theory can be used to identify if the fundamental vibrational mode of a given bond type in a molecule while the symmetry of that vibrational mode can be used to say if a vibration will be IR or Raman active.

The frequency of a vibration is inversely proportional to the square of the reduced mass of the atoms present and the root of the strength of the bond according to Hooke's Law, shown below.

$$\tilde{\nu} = \frac{1}{2\pi c}\sqrt{\frac{\kappa}{\mu}}$$

Hooke's Law – (ν = Frequency, κ = bond strength, μ = reduced mass)

The 'fingerprint' region (*ca.* 1500-200 cm^{-1}) of the IR spectrum is where the majority of the key absorbance bands are found with functional groups such as P=O (~1100 cm^{-1}) being well defined in the literature.[131] Upon coordination, these typically shift to lower wavenumber. The triflate anion has been well studied by IR spectroscopy with many of the stronger C-F and S=O absorbance bands being found between 1000-1400 cm^{-1}.[127] With several triflate vibrational modes in this range, as well as the characteristic P=O absorbance(s) (when present), unequivocal assignment was not possible in some cases.

IR spectroscopy was also used to identify the presence of solvents present in the complex or starting materials, especially water, with strong O-H absorbances being observed at 3500-3300 cm^{-1} for the stretching mode and ~1650 cm^{-1} for the H-O-H bending mode.

1.6.3 Single Crystal X-ray Diffraction

Single crystal X-ray diffraction (SCXRD) allows for the determination of the solid-state structure showing the positions of atoms and ions in a complex with any present solvents, as well as both inter- and intramolecular interactions observed within the species. This is a very powerful technique, especially in the field of main group inorganic chemistry, where labile ligand species can dissociate or rearrange in solution and make the assignment of speciation difficult. However, single crystal X-ray diffraction unambiguously confirms the structure of a complex in the solid-state. From this data, the bond lengths and angles can be calculated to a high level of accuracy, which allows for data about the types of bonding being observed (single, double, bridging *etc.*). The definition of a crystal is a 3D array of repeating units forming a crystal lattice, with the smallest single repeat unit being the unit cell of the crystal. This unit cell will contain all of the

symmetry elements present, with each unit cell being related through translation along the the *x*, *y*, and *z* axis.[132] This unit cell can be made up of smaller units which contain the structural information of the molecule linked by symmetry operations and is known as the asymmetric unit. The unit cells are defined by the three cell lengths (*a, b* and *c*) and three angles (*α, β and γ*) described in Table 1.2.

Table 1.2 - Unit cell parameters of the 7 crystal systems.[133]

Crystal System	Unit Cell Lengths	Unit Cell Angles
Cubic	$a = b = c$	$\alpha = \beta = \gamma = 90$
Hexagonal	$a = b \neq c$	$\alpha = \beta = 90,\ \gamma = 120$
Tetragonal	$a = b \neq c$	$\alpha = \beta = \gamma = 90$
Rhombohedral	$a = b = c$	$\alpha = \beta = \gamma \neq 90$
Orthorhombic	$a \neq b \neq c$	$\alpha = \beta = \gamma = 90$
Monoclinic	$a \neq b \neq c$	$\alpha = \gamma = 90, \beta \neq 90$
Triclinic	$a \neq b \neq c$	$\alpha \neq \beta \neq \gamma \neq 90$

A single crystal diffraction experiment involves firing monochromatic X-rays at a crystal in a random orientation, where incident rays hit a crystal at an incident angle, θ, and if diffracted, will be reflected at an equal angle of reflection. For an X-ray to be diffracted it must satisfy Bragg's Law shown below, which is used to calculate the number of whole wavelengths that will produce constructive (in-phase) interference and produce a spot on the detector.

$$n\lambda = 2d_{hkl}sin\theta$$

The Bragg Equation (*n* = whole number integer, λ = wavelength of X-ray, d = d-spacing of crystal planes, θ = angle of incident)

For a single measurement, the incident angle will remain constant while the d-spacing of Miller atomic planes within the crystal will remain constant as it is a property unique to the crystal. The wavelength of light, λ, will be dependent on the X-ray source of the diffractometer (e.g. molybdenum, silver or copper) being used and will be unchanged. Therefore, at a single incident angle only a small number of X-rays will satisfy Bragg's Law, be diffracted and produce a detected spot. Measurements are then taken from a wide range of different incident angles as the crystal is rotated in all orientations to collect a large number of unique reflections at the detector. Throughout the experiment, the crystal is often cooled to 100 K using N_2 gas which will minimise

the thermal atomic motion (bond vibration, bending, stretching) increasing the precision of the measurements. This will help to lower the size of ellipsoids drawn in the Oak Ridge Thermal Ellipsoid Plots (ORTEP) graphical representation of the molecule, due to the lowering of thermal motion of each atom. It will also help to limit the degradation of the crystal from radiation damage and reaction with air.

Once a complete data set has been collected, the 2D detector images can be used to calculate the unit cell parameters and thus the crystal system present. Each spot on the detector corresponds to a reflection and will be measured for its intensity (amplitude), however its phase is lost known as the phase problem. Every reflection contains structural information about the whole unit cell and the summation of the Furiour Transform can be used to produce a diffraction pattern.

$$|F(hkl)| = \sum_{j} f_j(\theta) \cdot \exp\left(-\frac{8\pi^2 U_j sin^2\theta}{\lambda^2}\right) \cdot \exp[2\pi i\left(hx_j + ky_j + lz_j\right)]$$

1 **2** **3** **4** **5**

Fourier Transform (1 = Diffracted wave in *hkl* direction, 2 = sum of individual atoms, 3 + 4 = scattering of X-rays by atoms, 5 = position of each atom)

To gain insight to the crystal structure, the structural factors are required and can be obtained through the Reverse Fourier transform of this diffraction pattern. This requires summation of all values of *h*, *k*, and *l* as each contains information about the whole structure.

$$\rho(xyz) = \frac{1}{V}\sum_{h,k,l} |F(hkl)| \cdot \exp[i\Phi(hkl)] \cdot \exp[-2\pi i(hx + ky + lz)]$$

1 **2** **3** **4** **5**

Reverse Fourier Transform – (1 = electron density, 2 = sum of diffracted beams, 3 = reflection amplitudes, 4 = intrinsic wave phase 5 = phase shift at each geometric position)

Using the calculated elctron densities, Patterson Synthesis or Direct Methods can be used to infer the positions of atoms in the unit cell. Both are are methods to solve the phase problem; Patterson Synthesis uses Fourier transforms of the intensities, rather than structural factors to produce a map with peaks at the interatomic distance vectors while the peak hight is proportional to the electons of those atoms.The direct methods seek to estimate the phases of the waves from the magnitude of the scattering density and is the commonly used method for solving small molecular structures (< 1000 atoms). A position of higher electron density suggesting the

presence of a heavier atom due to the higher number of electrons found in the core and valence electron orbitals, with H-atoms being located last or added at a standard distance.

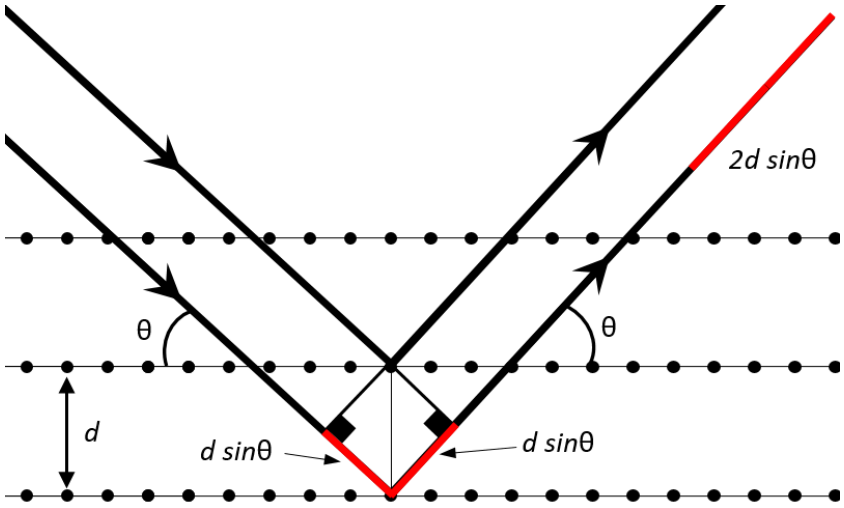

Figure 1.14 - Illustration of Bragg's Law

This technique requires the growth of single crystals of a complex to a suitable size and quality for diffraction, this can be achieved through a range of techniques. Throughout this thesis, crystallisations were achieved through either slow evaporation of solvent, layering of two miscible solvents or vapour diffusion of a solvent into a solution of compound. Due to the use of only a single crystal, the structure observed may not be representative of the bulk solid or the species present in solution. Coupling the information gained through X-ray diffraction with the data from other techniques and chemical knowledge can allow for confident assignment of the structure.

Disorder in a crystal structure arises when the energy difference between two different geometries or orientations is very low. This introduces the possibility for variation in atomic sites as well as partially occupied atomic sites, where an atom is found in more than one location in a structure; commonly in this work it was found to be the rotation of $-CF_3$ groups in the triflate anions and the $[BAr^F]^-$ salts.

1.6.4 Multinuclear NMR Spectroscopy

NMR spectroscopy was an invaluable tool for obtaining solution-state data on synthesised complexes, giving information about the environment in which the specific nuclei is found. Throughout the experimental section of this work the chemical shift, multiplicity and coupling constants are provided for analysis at the conditions attempted. In each case, a combination of the analysis of multiple NMR active nuclei in parallel can give complimentary data and allow for further elucidation of the behaviour in the solution-state, and allow for additional conclusions to

be drawn. More dynamic systems required variable temperature NMR spectroscopy at (208 – 298 K) to allow for the resolution of coupling and satellite couplings in the soft donor complexes in Chapter 5.

Table 1.3 - Selected nuclear properties of NMR nuclei analysed in this work.[134]

Nuclei	Spin (*I*)	Relative Abundance (%)	Receptivity Relative to ^{13}C	Quadrupole Moment (10^{-28} m^2)	Reference
^{1}H	1/2	99.9	5.67×10^3	–	Residual solvent
^{13}C	1/2	1.1	1.00	–	Residual solvent
^{19}F	1/2	100	4.73×10^3	–	$CFCl_3$
^{27}Al	5/2	100	1.17×10^3	0.14	$Al(NO_3)_3$ (*aq)*
^{31}P	1/2	100	3.77×10^2	–	H_3PO_4 (*aq*)
^{71}Ga	3/2	30.8	3.35×10^2	0.11	$Ga(NO_3)_3$ (*aq*)
^{115}In	9/2	95.7	1.98×10^3	0.81	$In(NO_3)_3$ (*aq*)
^{119}Sn	1/2	8.6	25.7	–	Me_4Sn
^{121}Sb	5/2	57.3	–	-0.28	$KSbCl_6$ (*aq*)
^{207}Pb	1/2	22.6	11.9	–	$Pb(NO_3)_2$ (*aq*)

The spin of a nucleus is constantly trying to align itself with the applied magnetic field (the lowest energy state) and those with spin of $I = ½$ and can remain in this low-energy state. There is a constantly changing electric field gradient (efg) caused by asymmetry in the surrounding electrons of the atom and thus the shape, when averaged, is spherical. When irradiated and excited to a higher energy state, the nuclei of $I = ½$ can undergo relaxation through the efficient mechanisms of spin-spin or spin-lattice coupling.

In nuclei where $I > ½$, the distribution of charge in the nucleus is permanently asymmetric and the nucleus has a quadrupole moment, meaning these nuclei are not spherical. This can couple with the electric field gradient of the electrons and provide an effective relaxation pathway by which to release the excess energy and relax to the ground state. The efficiency of this pathway means it will likely dominate in these systems and thus cause increased line broadening, masking satellites and nuclear coupling and in extreme cases, the entire resonance. This relaxation pathway can also affect nuclei nearby, causing broadening in these resonances of nearby nuclei. The symmetry of a molecule will have an effect on the electric field gradient, with higher symmetry lowering its impact which results in sharper and better resolved couplings due to slower relaxation times. An example of these affects is in the use of ^{121}Sb NMR spectroscopy which produces a sharp resonance for the highly symmetric $[SbCl_6]^-$ anion, making it a perfect reference material.[135] As shown in Table 1.3, ^{121}Sb nucleus has a high quadrupole moment and so only molecules with near-

zero electric field gradients (highly symmetric) will be observed; complexes with lower than cubic symmetry produce extremely broad resonances.

$^{31}P\{^{1}H]$ NMR spectroscopy was ubiquitous in this work, with the favourable properties being highlighted in Table 1.3 above. Commonly being involved in the coordination of the ligand species, changes in the nuclear environment of phosphines and phosphine oxides upon coordination to the Lewis acid could be clearly observed, with chemical shifts observed to high frequency of the uncoordinated form. As well as this, coupling to NMR active metal nuclei with a spin of $I = 1/2$ (^{119}Sn and ^{207}Pb) produced satellite peaks which could be used to aid in confirmation of coordination to the metal. The splitting of these peaks would be equal to the splitting observed in the respective metal NMR spectra. As well as differences upon coordination, distinguishing between free phosphine, phosphine oxide and protonated phosphine was easy due to the large shifts between each of these groups of compounds. A sample suspected of containing protonated ligand could quickly be analysed by both ^{31}P and $^{31}P\{^{1}H\}$ NMR spectroscopy where the coupling to the proton would cause splitting of that resonance in the ^{1}H coupled spectrum. Although the ^{75}As nucleus is NMR active with a spin of $I = 3/2$, it has a large quadrupole moment of $Q = 0.29 \times 10^{-28}$ m^2 and this causes broadening of the signal to the point that these resonances were not observed.

1.6.4.1 **Tin NMR Spectroscopy**

Tin is found to have 10 stable nuclei, the most of any atom and of these, three (^{115}Sn, ^{117}Sn and ^{119}Sn) are NMR active with $I = ½$. The NMR active nucleus with the highest abundance is ^{119}Sn (8.59%) and because of this it has a slightly higher sensitivity than ^{117}Sn, making it the preferred isotope for analysis of tin compounds.[136] ^{115}Sn NMR spectroscopy is rare due to a low abundance of only 0.35% and a sensitivity twenty times lower than $^{117/119}Sn$ NMR spectroscopy. With a standard reference of neat $SnMe_4$, ^{119}Sn NMR spectroscopy has an approximate range of >2500 ppm. Analysis of NMR-active nuclei bonded directly to the tin metal centre, commonly $^{31}P\{^{1}H\}$ NMR spectroscopy in this work, also contained satellite resonances corresponding to couplings to both the $^{117/119}Sn$ nuclei. In well resolved NMR spectra, these satellites could be individually identified and the difference in their coupling constants equal to the ratio of the magnetogyric ratios for the ^{119}Sn and ^{117}Sn nuclei. In some spectra individual satellites could not be identified and so an averaged $^{117/119}Sn$ coupling is reported. These satellite coupling constants ranged from 1000 - 2000 Hz in the complexes formed in this work.

1.6.4.2 **Lead NMR Spectroscopy**

In contrast to tin, lead has only 4 stable isotopes and of these, only ^{207}Pb is NMR active with a spin of $I = ½$ and a relative abundance of 22.1%. This medium sensitivity nuclei has a vast expected

range of ~16000 ppm with a standard reference of neat $PbMe_4$.[137] NMR spectroscopy of the ^{31}P nuclei directly coordinated to the Pb(II) in the phosphine complexes showed ^{207}Pb satellites and was useful in confirming coordination of ligands. However, due to the lability of these complexes and the lower sensitivity of ^{207}Pb NMR spectroscopy, ^{207}Pb NMR resonances were not observed under the conditions explored.

1.7 – Aims

This project will primarily focus on the development of the coordination chemistry of the trivalent Group 13 ions and divalent Group 14 ions with the weakly coordinating trifluoromethanesulfonate anion. The overall aim of this work is to generate discrete cationic or polycationic species to further expand the fundamental coordination chemistry in this area.

Chapter 2 explores coordination of the heteroaromatic imine ligands 2,2'-bipyridine, 1,10-phenanthroline and 2,2';6',2"-terpyridine to the Group 13 metal triflates, while Chapter 3 focusses on with coordination of oxygen donor ligands including the monodentate ligands OPR_3 (R = Me, Ph) and pyridine N-oxide, as well as the bidentate phosphine oxide, $dppmO_2$. These ligands, with differing donor strengths and denticities, have been selected to explore any changes to the geometry and spectroscopic properties in complexes containing triflate anions compared to the known halide complexes.

Previous work within the group exploring the coordination of alkylstibine ligands to the Group 13 metal trihalides will be developed further in Chapter 4, alongside the use of alkylphosphine and arsine ligands. These complexes may be potential precursors towards the deposition of III-V semiconductor materials, and thus a selection of the novel stibine complexes will be tested towards thin film deposition *via* LPCVD. Halide abstraction using TMSOTf is also explored as a possible route to produce the corresponding cationic species.

The coordination of the divalent Group 14 metal triflates, $M(OTf)_2$ (M = Sn, Pb), will then be explored, focussing on coordination of a range of soft polydentate phosphine and arsine ligands in Chapter 5 and harder oxygen donor ligands (mainly OPR_3) in Chapter 6. Chapter 7 focusses on the formation and characterisation of an unusual and unexpected hexameric metallocyclic array, formulated as $[Sn(OTf)_2(OPMe_3)_3]_6$. This will also explore the attempts at formation of similar species using related metal or anions.

1.8 – References

1 G. N. Lewis, *Valence and the Structure of Atoms and Molecules*, The Chemical Catalog Company, Inc., New York, 1923.
2 R. G. Pearson, *J. Am. Chem. Soc.*, 1963, **85**, 3533–3539.
3 R. G. Pearson, *J. Chem. Educ.*, 1968, **45**, 581.
4 P. Atkins, T. Overton, J. Rourke, M. Weller, F. Armstrong and M. Hagerman, *Shriver and Atkins' Inorganic Chemistry*, Oxford University Press, Oxford, Fifth., 2010.
5 R. G. Parr and R. G. Pearson, *J. Am. Chem. Soc.*, 1983, **105**, 7512–7516.
6 R. Loos, S. Kobayashi and H. Mayr, *J. Am. Chem. Soc.*, 2003, **125**, 14126–14132.
7 M. Everett, A. Jolleys, W. Levason, D. Pugh and G. Reid, *Chem. Commun.*, 2014, **50**, 5843.
8 M. J. D. Champion, J. M. Dyke, W. Levason, M. E. Light, D. Pugh, H. Bhakhoa, L. Rhyman, P. Ramasami and G. Reid, *Inorg. Chem.*, 2015, **54**, 2497–2499.
9 L. J. Thenard, *Comptes Rendus l'Academie des Sci.*, 1847, 892.
10 K. Mislow and R. D. Baechler, *J. Am. Chem. Soc.*, 1971, **93**, 773–774.
11 G. W. Bowling, Newcastle University, 2019.
12 A. J. Kendall and D. R. Tyler, *Dalton Trans.*, 2015, **44**, 12473–12483.
13 N. C. Norman, *Chemistry of Arsenic, Antimony and Bismuth*, Blackie Academic & Professional, London, 1998.
14 J. Jover and J. Cirera, *Dalton Trans.*, 2019, **48**, 15036–15048.
15 C. A. Tolman, *Chem. Rev.*, 1977, **77**, 313–348.
16 P. B. Dias, M. E. M. de Piedade and J. A. M. Simões, *Coord. Chem. Rev.*, 1994, **135**–**136**, 737–807.
17 C. A. Tolman, W. C. Seidel and L. W. Gosser, *J. Am. Chem. Soc.*, 1974, **96**, 53–60.
18 J. A. Bilbrey, A. H. Kazez, J. Locklin and W. D. Allen, *J. Comput. Chem.*, 2013, **34**, 1189–1197.
19 A. G. Orpen and N. G. Connelly, *Organometallics*, 1990, **9**, 1206–1210.
20 R. H. Crabtree, *Chem. Soc. Rev.*, 2017, **46**, 1720–1729.
21 J. Burt, W. Levason and G. Reid, *Coord. Chem. Rev.*, 2014, **260**, 65–115.
22 W. Levason and G. Reid, *Coord. Chem. Rev.*, 2006, **250**, 2565–2594.
23 V. K. Greenacre, W. Levason and G. Reid, *Organometallics*, 2018, **37**, 2123–2135.
24 A. Kuczkowski, S. Schulz and M. Nieger, *Eur. J. Inorg. Chem.*, 2001, **2001**, 2605–2611.
25 A. Kuczkowski, F. Thomas, S. Schulz and M. Nieger, *Organometallics*, 2000, **19**, 5758–5762.
26 A. Kuczkowski, S. Fahrenholz, S. Schulz and M. Nieger, *Organometallics*, 2004, **23**, 3615–3621.
27 E. P. Kyba, S. T. Liu and R. L. Harris, *Organometallics*, 1983, **2**, 1877–1879.
28 W. Hewertson and H. R. Watson, *J. Chem. Soc.*, 1962, 1490.
29 R. P. Messmer, *J. Am. Chem. Soc.*, 1991, **113**, 433–440.
30 F. R. Hartley and S. Patai, *The Chemistry of Organophosphorus Compounds Vol II: Phosphine Oxides, Sulphides, Selenides and Tellurides*, Wiley, Cranfield, 1992.
31 A. E. Reed and P. v. R. Schleyer, *J. Am. Chem. Soc.*, 1990, **112**, 1434–1445.
32 D. B. Chesnut, *J. Am. Chem. Soc.*, 1998, **120**, 10504–10510.
33 M. J. Petersson, W. A. Loughlin and I. D. Jenkins, *Chem. Commun.*, 2008, 4493.
34 A. R. J. Genge, University of Southampton, 1998.
35 W. Levason, R. Patel and G. Reid, *J. Organomet. Chem.*, 2003, **688**, 280–282.
36 J. Darriet, W. Massa, J. Pebler and R. Stief, *Solid State Sci.*, 2002, **4**, 1499–1508.
37 S. P. Petrosyants and A. B. Ilyukhin, *Russ. J. Inorg. Chem.*, 2010, **55**, 30–33.
38 S. A. Bourne and L. J. Moitsheki, *J. Chem. Crystallogr.*, 2007, **37**, 359–367.
39 T. P. Gerasimova and S. A. Katsyuba, *Dalton Trans.*, 2013, **42**, 1787–1797.
40 S. T. Howard, *J. Am. Chem. Soc.*, 1996, **118**, 10269–10274.
41 Q. Teng and H. V. Huynh, *Dalton Trans.*, 2017, **46**, 614–627.
42 V. Balzani and A. Juris, *Coord. Chem. Rev.*, 2001, **211**, 97–115.
43 J. L. Templeton, *J. Am. Chem. Soc.*, 1979, **101**, 4906–4917.
44 G. S. Papaefstathiou, A. Sofetis, C. P. Raptopoulou, A. Terzis, G. A. Spyroulias and T. F.

Zafiropoulos, *J. Mol. Struct.*, 2007, **837**, 5–14.
45 P. A. Gray, K. D. Krause, N. Burford and B. O. Patrick, *Dalton Trans.*, 2017, **46**, 8363–8366.
46 A. J. Downs, *Chemistry of Aluminium, Gallium, Indium and Thallium*, Springer Netherlands, New York, 1st edn., 1993.
47 B. D. Rowsell, R. J. Gillespie and G. L. Heard, *Inorg. Chem.*, 1999, **38**, 4659–4662.
48 A. Y. Timoshkin, M. Bodensteiner, T. N. Sevastianova, A. S. Lisovenko, E. I. Davydova, M. Scheer, C. Graßl and A. V. Butlak, *Inorg. Chem.*, 2012, **51**, 11602–11611.
49 M. A. Beckett, G. C. Strickland, J. R. Holland and K. Sukumar Varma, *Polymer (Guildf).*, 1996, **37**, 4629–4631.
50 R. Bhalla, J. Burt, A. L. Hector, W. Levason, S. K. Luthra, G. McRobbie, F. M. Monzittu and G. Reid, *Polyhedron*, 2016, **106**, 65–74.
51 W. Levason, F. M. Monzittu and G. Reid, *Coord. Chem. Rev.*, 2019, **391**, 90–130.
52 S. L. Benjamin, W. Levason and G. Reid, *Chem. Soc. Rev.*, 2013, **42**, 1460–1499.
53 R. Bhalla, W. Levason, S. K. Luthra, G. McRobbie, F. M. Monzittu, J. Palmer, G. Reid, G. Sanderson and W. Zhang, *Dalton Trans.*, 2015, **44**, 9569–9580.
54 R. Bhalla, C. Darby, W. Levason, S. K. Luthra, G. McRobbie, G. Reid, G. Sanderson and W. Zhang, *Chem. Sci.*, 2014, **5**, 381–391.
55 J. A. J. Pardoe and A. J. Downs, *Chem. Rev.*, 2007, **107**, 2–45.
56 D. Vidovic and S. Aldridge, *Chem. Sci.*, 2011, **2**, 601.
57 C. Dohmeier, D. Loos and H. Schnöckel, *Angew. Chemie Int. Ed. English*, 1996, **35**, 129–149.
58 T. N. Sevastianova, M. Bodensteiner, A. F. Maulieva, E. I. Davydova, A. V. Virovets, E. V. Peresypkina, G. Balázs, C. Graßl, M. Seidl, M. Scheer, G. Frenking, E. A. Berezovskaya, I. V. Kazakov, O. V. Khoroshilova and A. Y. Timoshkin, *Dalton Trans.*, 2015, **44**, 20648–20658.
59 N. Y. Gugin, A. Virovets, E. Peresypkina, E. I. Davydova and A. Y. Timoshkin, *CrystEngComm*, 2020, **22**, 4531–4543.
60 J. Derouault and M. T. Forel, *Inorg. Chem.*, 1977, **16**, 3207–3213.
61 A. Abedi, N. Safari, V. Amani and H. R. Khavasi, *J. Coord. Chem.*, 2012, **65**, 325–338.
62 N. Burford, B. W. Royan, R. E. V. H. v. H. Spence, T. S. Cameron, A. Linden and R. D. Rogers, *J. Chem. Soc. Dalton. Trans.*, 1990, 1521.
63 W. T. Robinson, C. J. Wilkins and Z. Zeying, *J. Chem. Soc., Dalton. Trans.*, 1990, 219–227.
64 J. Burt, W. Levason, M. E. Light and G. Reid, *Dalton Trans.*, 2014, **43**, 14600–14611.
65 W. T. Robinson, C. J. Wilkins and Z. Zeying, *J. Chem. Soc. Dalton. Trans.*, 1988, 2187.
66 W. Levason and C. A. McAuliffe, *Coord. Chem. Rev.*, 1976, **19**, 173–185.
67 L. M. Engelhardt, P. C. Junk, C. L. Raston, B. W. Skelton and A. H. White, *J. Chem. Soc. Dalton. Trans.*, 1996, 3297.
68 A. H. Cowley, M. C. Cushner, R. E. Davis and P. E. Riley, *Inorg. Chem.*, 1981, **20**, 1179–1181.
69 F. Cheng, H. L. Codgbrook, A. L. Hector, W. Levason, G. Reid, M. Webster and W. Zhang, *Polyhedron*, 2007, **26**, 4147–4155.
70 J. A. J. Pardoe, A. R. Cowley, A. J. Downs and T. M. Greene, *Acta Crystallogr. Sect. C Cryst. Struct. Commun.*, 2005, **61**, m200–m202.
71 C. Trinh, M. Bodensteiner, A. V. Virovets, E. V. Peresypkina, M. Scheer, S. M. Matveev and A. Y. Timoshkin, *Polyhedron*, 2010, **29**, 414–424.
72 J. L. Atwood, S. G. Bott, F. M. Elms, C. Jones and C. L. Raston, *Inorg. Chem.*, 1991, **30**, 3792–3793.
73 D. O'Hare, J. S. Foord, T. C. M. Page and T. J. Whitaker, *J. Chem. Soc. Chem. Commun.*, 1991, 1445.
74 J. J. Byers, W. T. Pennington and G. H. Robinson, *Acta Crystallogr. Sect. C Cryst. Struct. Commun.*, 1992, **48**, 2023–2025.
75 S. Chitsaz, T. Breyhan, J. Pauls and B. Neumüller, *Z. Anorg. Allgem. Chem.*, 2002, **628**, 956.
76 M. Sigl, A. Schier and H. Schmidbaur, *Eur. J. Inorg. Chem.*, 1998, **1998**, 203–210.
77 F. Cheng, A. L. Hector, W. Levason, G. Reid, M. Webster and W. Zhang, *Inorg. Chem.*, 2007, **46**, 7215–7223.
78 F. Cheng, S. I. Friend, A. L. Hector, W. Levason, G. Reid, M. Webster and W. Zhang, *Inorg. Chem.*, 2008, **47**, 9691–9700.

79 P. A. Gray, J. W. Saville, K. D. Krause, N. Burford, R. McDonald and M. J. Ferguson, *Can. J. Chem.*, 2017, **95**, 346–350.
80 R. Restivo and G. J. Palenik, *J. Chem. Soc., Dalton. Trans.*, 1972, 341–344.
81 C. Gurnani, M. Jura, W. Levason, R. Ratnani, G. Reid and M. Webster, *Dalton Trans.*, 2009, 1611.
82 K. George, C. H. (Kees) de Groot, C. Gurnani, A. L. Hector, R. Huang, M. Jura, W. Levason and G. Reid, *Chem. Mater.*, 2013, **25**, 1829–1836.
83 C. Gurnani, W. Levason, R. Ratnani, G. Reid and M. Webster, *Dalton Trans.*, 2008, 6274.
84 J. A. McCleverty and T. J. Meyer, *Comprehensive Coordination Chemistry II*, Elsevier Science S.A., Oxford, 2nd edn., 2004.
85 N. N. Greenwood and A. Earnshaw, *Chemistry of the Elements*, Butterworth-Heinemann, Oxfird, 2nd edn., 1997.
86 W. D. Woodul, E. Carter, R. Müller, A. F. Richards, A. Stasch, M. Kaupp, D. M. Murphy, M. Driess and C. Jones, *J. Am. Chem. Soc.*, 2011, **133**, 10074–10077.
87 N. V. Sidgwick, *Electronic Theory of Valence*, The Clarendon Press, Oxford, 1927.
88 E. R. Bissell and D. B. Fields, *J. Org. Chem.*, 1964, **29**, 1591–1593.
89 M. Kaupp and P. v. R. Schleyer, *J. Am. Chem. Soc.*, 1993, **115**, 1061–1073.
90 V. S. V. S. N. Swamy, S. Pal, S. Khan and S. S. Sen, *Dalton Trans.*, 2015, **44**, 12903–12923.
91 R. P. King, V. K. Greenacre, W. Levason, J. M. Dyke and G. Reid, *Inorg. Chem.*, 2021, **60**, 12100–12108.
92 K. R. Cairns, R. P. King, R. D. Bannister, W. Levason and G. Reid, *Dalton Trans.*, 2023, **2**, 2293–2308.
93 H. Fang, Z. Wang and X. Fu, *Coord. Chem. Rev.*, 2017, **344**, 214–237.
94 S. C. Bart, *Inorg. Chem.*, , DOI:10.1021/acs.inorgchem.3c00440.
95 B. Cordero, V. Gómez, A. E. Platero-Prats, M. Revés, J. Echeverría, E. Cremades, F. Barragán and S. Alvarez, *Dalton Trans.*, 2008, 2832–2838.
96 M. Mantina, A. C. Chamberlin, R. Valero, C. J. Cramer and D. G. Truhlar, *J. Phys. Chem. A*, 2009, **113**, 5806–5812.
97 K. Izod, *Coord. Chem. Rev.*, 2012, **256**, 2972–2993.
98 F. Cheng, A. L. Hector, W. Levason, G. Reid, M. Webster and W. Zhang, *Angew. Chemie Int. Ed.*, 2009, **48**, 5152–5154.
99 P. A. Gray, K. D. Krause, N. Burford and B. O. Patrick, *Dalton Trans.*, 2017, **46**, 8363–8366.
100 C. Gurnani, A. L. Hector, E. Jager, W. Levason, D. Pugh and G. Reid, *Dalton Trans.*, 2013, **42**, 8364–8374.
101 R. Bandyopadhyay, B. F. T. Cooper, A. J. Rossini, R. W. Schurko and C. L. B. Macdonald, *J. Organomet. Chem.*, 2010, **695**, 1012–1018.
102 R. E. Cramer, K. A. Mitchell, A. Y. Hirazumi and S. L. Smith, *J. Chem. Soc. Dalton. Trans.*, 1994, 563.
103 R. D. Rogers and A. H. Bond, *Inorg. Chim. Acta*, 1992, **192**, 163–171.
104 P. Farina, T. Latter, W. Levason and G. Reid, *Dalton Trans.*, 2013, **42**, 4714–4724.
105 L. Shimoni-Livny, J. P. Glusker and C. W. Bock, *Inorg. Chem.*, 1998, **37**, 1853–1867.
106 R. L. Davidovich, V. Stavila, D. V. Marinin, E. I. Voit and K. H. Whitmire, *Coord. Chem. Rev.*, 2009, **253**, 1316–1352.
107 M. Ozaki, Y. Katsuki, J. Liu, T. Handa, R. Nishikubo, S. Yakumaru, Y. Hashikawa, Y. Murata, T. Saito, Y. Shimakawa, Y. Kanemitsu, A. Saeki and A. Wakamiya, *ACS Omega*, 2017, **2**, 7016–7021.
108 P. G. Harrison, B. J. Haylett and T. J. King, *Inorg. Chim. Acta*, 1983, **75**, 259–264.
109 R. Selvaraju, K. Panchanatheswaran and V. Parthasarathi, *Acta Crystallogr. Sect. C Cryst. Struct. Commun.*, 1998, **54**, 905–906.
110 M. A. Busch, in *Encyclopedia of Physical Science and Technology*, Elsevier, 2003, pp. 197–222.
111 S. H. Strauss, *Chem. Rev.*, 1993, **93**, 927–942.
112 G. A. Lawrance, *Chem. Rev.*, 1986, **86**, 17–33.
113 I. Krossing and I. Raabe, *Angew. Chemie Int. Ed.*, 2004, **43**, 2066–2090.

114 P. Gowik, T. Klapötke and U. Thewalt, *J. Organomet. Chem.*, 1990, **385**, 345–350.
115 H. Zhou, C. Wang, Y. Liu, X. Fan, K. Yang, W. Wei, Y. Tang and Y. Tan, *Chem. – An Asian J.*, 2019, **14**, 3946–3952.
116 J. H. N. Buttery, Effendy, S. Mutrofin, N. C. Plackett, B. W. Skelton, C. R. Whitaker and A. H. White, *Z. Anorg. Allgem. Chem.*, 2006, **632**, 1809–1828.
117 M. R. Rosenthal, *J. Chem. Educ.*, 1973, **50**, 331.
118 A. E. Wickenden and R. A. Krause, *Inorg. Chem.*, 1965, **4**, 404–407.
119 R. J. O. H. C. Clark, *Inorg. Chem.*, 1963, **2**, 740–744.
120 M. Pasquali, C. Floriani and A. Gaetani-Manfredotti, *Inorg. Chem.*, 1980, **19**, 1191–1197.
121 H. Nishida, N. Takada, M. Yoshimura, T. Sonoda and H. Kobayashi, *Bull. Chem. Soc. Jpn.*, 1984, **57**, 2600–2604.
122 T. M. Douglas, E. Molinos, S. K. Brayshaw and A. S. Weller, *Organometallics*, 2007, **26**, 463–465.
123 M. W. Bouwkamp, P. H. M. Budzelaar, J. Gercama, I. Del Hierro Morales, J. de Wolf, A. Meetsma, S. I. Troyanov, J. H. Teuben and B. Hessen, *J. Am. Chem. Soc.*, 2005, **127**, 14310–14319.
124 X. Li, M. Nishiura, K. Mori, T. Mashiko and Z. Hou, *Chem. Commun.*, 2007, 4137.
125 G. K. S. Prakash, T. Mathew, C. Panja, S. Alconcel, H. Vaghoo, C. Do and G. A. Olah, *Proc. Natl. Acad. Sci. U. S. A.*, 2007, **104**, 3703–3706.
126 G. A. Olah, O. Farooq, S. M. F. Farnia and J. A. Olah, *J. Am. Chem. Soc.*, 1988, **110**, 2560–2565.
127 B. Dhakal, L. Bohé and D. Crich, *J. Org. Chem.*, 2017, **82**, 9263–9269.
128 D. H. Johnston and D. F. Shriver, *Inorg. Chem.*, 1993, **32**, 1045–1047.
129 J. Ramírez, A.-M. Stadler, L. Brelot and J.-M. Lehn, *Tetrahedron*, 2008, **64**, 8402–8410.
130 R. A. Sanders, R. Frech and M. A. Khan, *J. Phys. Chem. B*, 2003, **107**, 8310–8315.
131 K. Nakamoto, *Infrared and Raman Spectra of Inorganic and Coordination Compounds, Part A: Theory and Applications in Inorganic Chemistry*, A John Wiley & Sons Inc., Publications, 6th edn., 2009.
132 L. W. Daasch and D. C. Smith, *J. Chem. Phys.*, 1951, **19**, 22–25.
133 C. Giacovazzo, H. L. Monaco, G. Artioli, D. Viterbo, M. Milanesio, G. Gilli, P. Gilli, G. Zanotti, G. Ferraris and M. Catti, *Fundamentals of Crystallography*, Oxford University Press, Oxford, Third., 2011.
134 D. W. Bennett, *Understanding Single-Crystal X-Ray Crystallography*, Wiley-VCH, Weinheim, 1st edn., 2010.
135 J. Mason, *Multinuclear NMR*, Plenum Press, New York, 1st edn., 1987.
136 R. G. Kidd and R. W. Matthews, *J. Inorg. Nucl. Chem.*, 1975, **37**, 661–663.
137 B. Wrackmeyer, in *Annual Reports on NMR Spectroscopy*, 1999, vol. 38, pp. 203–264.
138 B. Wrackmeyer, in *Annual Reports on NMR Spectroscopy*, 2002, pp. 1–37.

Chapter 2 – Heterocyclic Nitrogen Donor Complexes of Aluminium, Gallium and Indium with Weakly Coordinating Triflate Anions

The work in this chapter begins to explore the coordination chemistry of the Group 13 metal triflates with the reactions of the polypyridyl ligands 2,2'-bipyridine, 1,10-phenanthroline and 2,2';6'2''-terpyridine. The triflate complexes synthesised here will be compared to the coordination produces of the more commonly studied halide complexes.

2.1 – Introduction and Literature Review

Due to the less developed technology in fields such as single crystal X-ray diffraction and multinuclear NMR spectroscopy during the initial period of research, experiments were primarily guided by IR and Raman spectroscopy. These compounds were often sensitive to atmospheric oxygen or water in solution producing degradation products, or undergoing ligand displacement with even weakly coordinating solvents due to the inherent lability of the p-block, thus requiring inert atmosphere techniques throughout. The first reported imine complex of gallium(III) being structurally characterised as a distorted octahedron was the cation of $[GaCl_2(bipy)_2][GaCl_4]$, which was found to be in a *cis* geometry, with this structure shown in Figure 2.1. This *cis* geometry was an unexpected finding as only one Ga-Cl band was observed in IR spectroscopic studies, suggesting a *trans* geometry.[1–3]

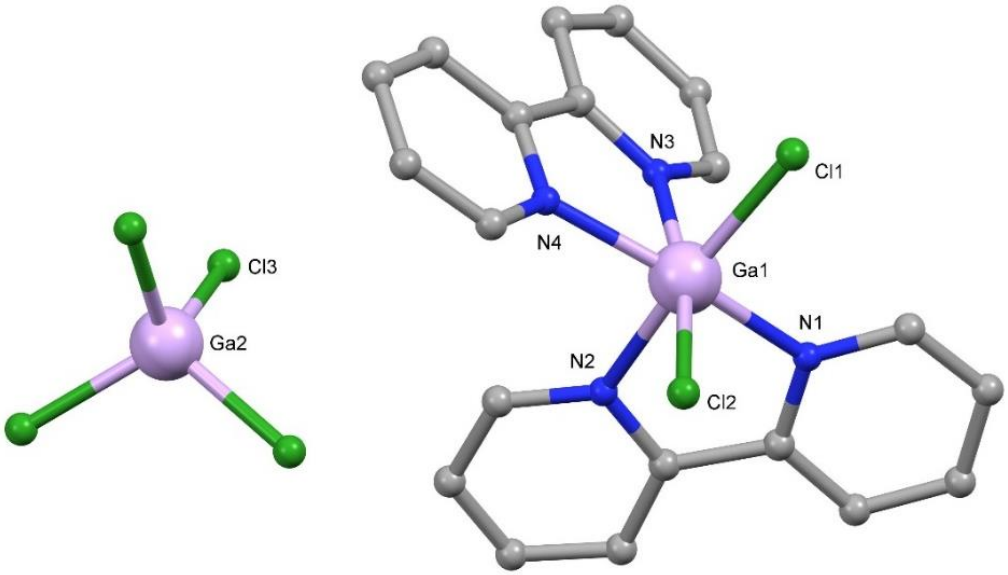

Figure 2.1 – Crystal structure of $[GaCl_2(bipy)_2][GaCl_4]$ showing atomic numbering scheme. Redrawn from Ref[4] with H-atoms omitted for clarity.

This report noted that the Ga-Cl bonds of the cation were 2.264(2) Å, significantly increased from the average bond in the tetrachloro gallate anion at 2.166(3) Å. This suggested an increase in bond radius as coordination number is increased which is as expected. It was also observed that the differences in bond length for the Ga-Cl and Ga-N did not match the difference in ionic radii and suggested the Ga-Cl bond may be influenced by the ligand *trans* to the chloride.[5] This effect was investigated with the production of $[GaCl_3(terpy)]$ which, which would allow a direct comparison of the effect of changing the species coordinated *trans* to the chloride ligands. It showed a significantly longer Ga-Cl bond in those *trans* to an N donor as opposed to *trans* to another Cl anion. The pre-organised nature of the poly-pyridine type ligands restricts the bonding angle that can be achieved, distorting the octahedron formed upon coordination. The addition of a third coordinating pyridinyl arm in terpy does not significantly change the N-Ga-N angle with 77.2(1)° being observed in $[GaCl_2(bipy)_2]^+$ and 77.32(6) and 77.44(6)° in $[GaCl_3(terpy)]$. The Ga-N bond lengths in the *bis*-bipy complex $[GaCl_2(bipy)_2]^+$ were found to be 2.095(4) and 2.111(4) Å, which closely match the Ga-$N_{(outer)}$ bonds at 2.115(6) and 2.110(6) Å of $[GaCl_3(terpy)]$, with the Ga-$N_{(inner)}$ bond distance reported as 2.034(7) Å. Kennard *et al* produced crystal structures of Fe(III) and Ga(III) complexes by coordination of ethylenediaminetetraacetic acid (EDTA) to the respective metal hydroxide to produce $[M(\kappa^3\text{-H.EDTA}).H_2O]$ (M = Fe, Ga).[6] The Ga-N bond lengths of this complex were reported to be 2.182(5) and 2.097(6) Å. These values suggest an expected Ga-N bond length to be around 2.1 Å under these conditions. The 1:1 reaction of $GaCl_3$ and pyridine produces a molecular tetrahedron $[GaCl_3(py)]$ with a shorter Ga-N bond length, likely due to the steric freedom of being in a tetrahedral geometry.[7] The more restricted $[GaCl_2(py)_4][GaCl_4]$ contains Ga-N bond lengths of 2.07-2.12 Å, within the range expected.

The intrinsic geometry of terpy causes complexation to form into the *mer* isomer exclusively. However, to allow for chelation of all three nitrogen donors, the central M-N bond is contracted, allowing for better orbital overlap of the outer two nitrogen donors. A follow up publication to the report of $[GaCl_3(terpy)]$ by Carty *et al* produced a more complete set of these Group 13 terpy complexes with a range of heavier halides and Group 13 metals, including indium and thallium.[8] This gave both spectroscopic and structural information on the complexes $[MX_3(terpy)]$ (M = Al, Ga, In, Tl; X = Cl, Br) and $[MI_3(terpy)]$ (M = Ga, In). Each of these complexes was produced by the equimolar reaction of terpy with the corresponding metal(III) halide in acetonitrile. It was noted that there was no significant increase in Ga-N bond length in the solid state, as would be expected with the lower Lewis acidity of $GaCl_3$ and $GaBr_3$. Research into this finding was studied further by Timoshkin who found that in the solid state, monodentate ligands with a range of donors (N, P, As, O) produced a masking effect of the Lewis acidity trends generally observed.[9] This effect was

later proven with polydentate ligands with the same observation upon comparison of the bond lengths of [$GaCl_3$(terpy)] and [$GaBr_3$(terpy)].[10]

The formation of complexes containing heavier metal(III) fluorides MF_3 (M = Al, Ga, In) had not been achieved until more recently, within the last 15 years, due to the starting material being found as an inert fluoride bridged polymer. The hydrates for all three metals $MF_3 \cdot 3H_2O$ are known and are more reactive towards coordination of other ligands, however they have poor solubility in both water and common organic solvents, hindering the progress of research in this area.[11,12] The aluminium fluoride hydrates are found to crystallise in three reliable forms and are formed through the reaction of elemental aluminium powder with HF under reflux conditions. The crystal structure of the nonahydrate $AlF_3 \cdot 9H_2O$ form is a lattice of [$AlF_3(H_2O)_3$] encapsulated by a six hydrogen bonded water molecules into hexameric cluster network.[13] Two crystallographic polymorphs have been found for the trihydrate, the α being a molecular species of [$AlF_3(OH_2)_3$] while the β-form is a polymeric bridged species [$\{AlF_2(OH_2)_2(\mu\text{-}F)\}_n$]$\cdot n H_2O$.[14,15] The structure of the gallium analogue is crystallographically unclear, but the indium analogue is a fluoride bridged polymer sharing the F1 atom down the *c*-axis. Two bound water molecules and the remaining two fluoride atoms are disordered in the equatorial positions with the final water taking up position as lattice water, forming hydrogen bonds to the infinite chains.[16]

Even with the increased reactivity of the hydrate species, forcing reaction conditions were required to form coordination products. The ammoniates of the gallium and indium fluorides called for the reaction of the $MF_3 \cdot 3H_2O$ with liquid ammonia and microanalysis of the products correlated to the formation of $MF_3 \cdot 3NH_3$ (M = Ga, In).[17] These products were shown to partially hydrolyse to the hydroxides, which were observed by the appearance of peaks matching the X-ray diffraction data for $M(OH)_3$. The reaction of the gallium (III) fluoride hydrate in a prolonged reflux in THF, followed by recrystallization from pyridine produces [$GaF_3(py)_3$] in the *mer*-geometry.[18] Hydrothermal preparations of Group 13 metal fluoride complexes with nitrogen donors were reported for with polydentate ligands such as isomers of bipyridine as well as macrocyclic ligands such as Me_3-tacn (Me_3-tacn = 1,4,7-trimethyl-1,4,7-triazacyclononane) and its derivatives. Reaction of $MF_3 \cdot 3H_2O$ (M = Ga, In) with 4,4'-bipyridyl in aqueous HF at 180°C produced polymeric species *trans*-[MF_3(bipy)] where 4,4'-bipyridyl bridge between two metal centres containing 4 equatorial fluoride anions each.[19]

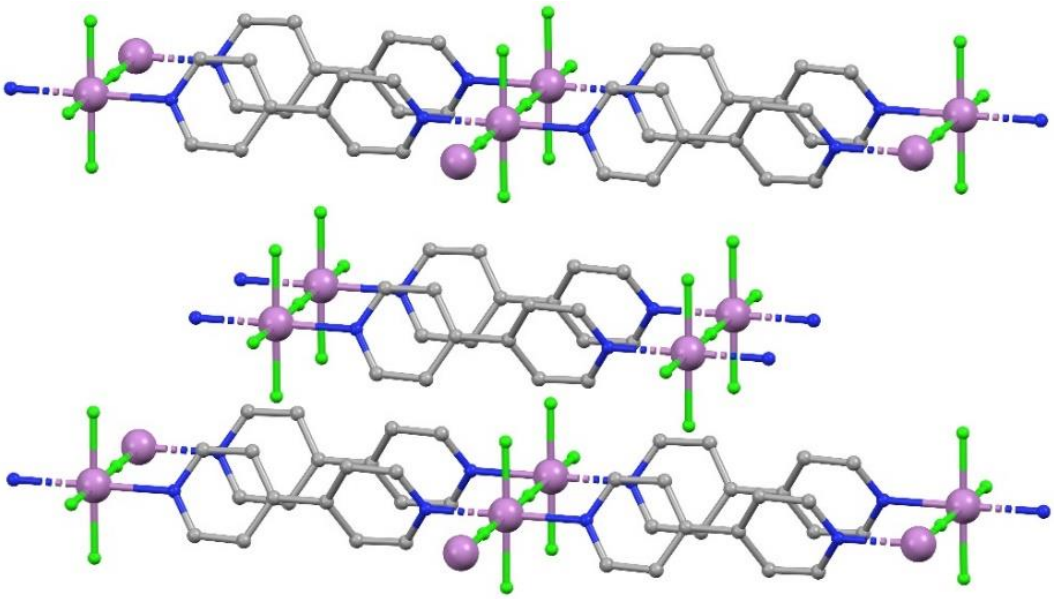

Figure 2.2 - Chain crystal structure of the polymeric [MF_3(4,4'-bipy)] with hydrogens omitted for clarity. Redrawn from Ref[19] In = Pink, F = Green, N = Blue, C = Grey.

These chains connected by fluoride bridges between metal centres result in the octahedral metal centre being coordinated by two *trans* nitrogen bridging ligands, two bridging and two terminal fluorides per metal centre, isostructural to [MF_3(4,4'bipy)] (M = Mn, V).[20,21] The structure of the heteroleptic fluoride bidentate nitrogen donor complexes were reported to form from aqueous HF conditions to form [$InF_3(H_2O)$(diimine)] (L = 2,2'-bipyridyl, 1,10-phenanthroline).[22] Complexes of these types were replicated through a hydrothermal synthesis using various imine ligands at 180°C for 15 h, producing isostructural [$MF_3(OH_2)$(diimine)] complexes, as well as [MF_3(terpy)] (M = Al, Ga, In).[23] These species, as discussed earlier, exhibit a *trans* influence with a significant shortening (by 0.06 Å) of the In-$F_{trans N}$ bond when compared with the two In-$F_{trans F}$. The gallium-centred species also had Ga-N bond lengths close to the 2.1 Å previously observed in similar complexes with heavier halides. An equimolar amount of [NH_4][PF_6] was added to a solution of [GaF_3(terpy)] in H_2O-MeCN and allowed to slowly evaporate, producing orange crystals suitable for single crystal X-ray diffraction. This complex shows the dissociation of one fluoride followed by dimerization to form [{Ga(terpy)F}$_2$(μ-F)$_2$][PF_6]$_2$·4H_2O, shown below.

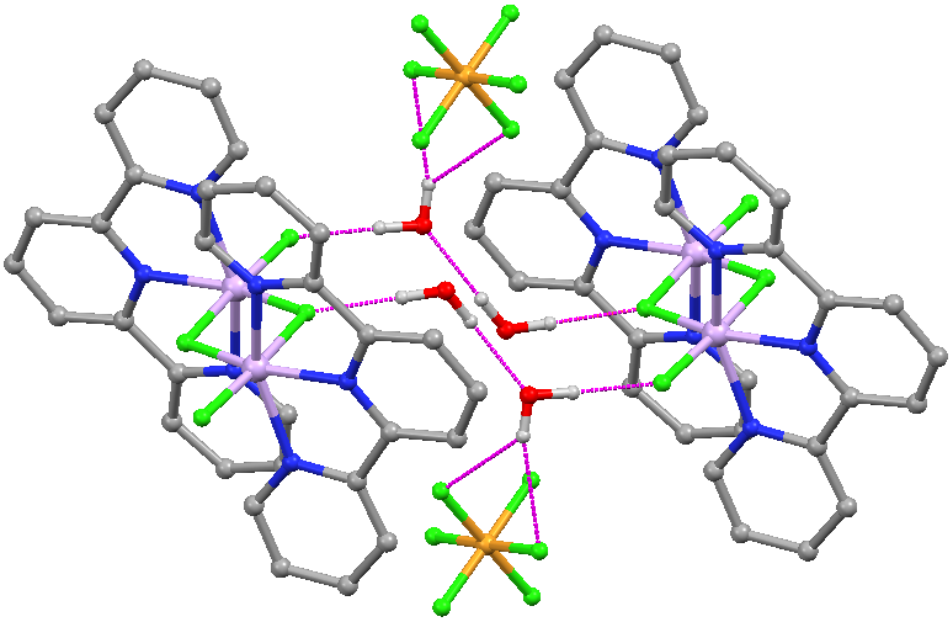

Figure 2.3 - Crystal structure of $[\{GaF(terpy)\}_2(\mu\text{-}F)_2][PF_6]_2{\cdot}4H_2O$, redrawn from Ref[23]. Ga = Pink, F = Green, P = Orange, N = Blue, O = Red, C = Grey, H = White

The bond lengths and angles change very little throughout this dimerization. There are extensive hydrogen bonds present between the lattice water, metal cation and PF_6 anion, likely giving some additional stability to this complex. The hydrothermal synthesis was highly effective with each of the three neutral imines being coordinated to each of the three metal centres in high yields. An alternative method was attempted to produce these species which involved the Cl-F halide exchange of a chloride starting material (e.g. $[GaCl_3(terpy)]$) and worked successfully. Both $[NBu_4]F$ and [K(2.2.2-crypt)F] reacted with the starting material in anhydrous MeCN solutions to give a species that spectroscopically matched that produced by the hydrothermal method. This fluoride exchange had been proven to work on complexes of this type with the formation of $[MF_3(L)]$ (L = Me_3-tacn, $BzMe_2$-tacn; M = Al, Ga, In) from the corresponding chloride.[24] These macrocyclic compounds were able to be produced *via* both a direct hydrothermal synthesis and through halogen exchange, the latter of which using much milder conditions making it more practical for applications in late stage ^{18}F-radiolabelling in medicinal imaging agents. A final synthetic route that was probed was to first produce the molecular solvate species of the form $[MF_3(OH_2)_2(DMSO)]$ (M = Al, Ga, In) from the MF_3 hydrate starting material by dissolving in hot solvent. In the case of M = In, a higher temperature was required and lower yield obtained.[25] Reactions left under reflux conditions for longer reaction times showed no signs of further displacement of the coordinate water with DMSO. This was found to be reactive to a number of neutral donating ligand types; pyNO, Me_3-tacn, 2,2'-bipy, pyridine and PMDTA (N,N,N',N'',N''-pentamethyldiethylenetriamine). The reactions of bipy and Me_3-tacn with $[GaF_3(OH_2)_2(DMSO)]$ produced the same complexes as the hydrothermal synthesis with displacement of the DMSO being achieved. Each of these reactions proceeded in common lab solvents (CH_2Cl_2 and MeOH) at

room temperature, a far milder set of conditions. Hydrothermal synthesis using PMDTA caused cleavage of the ligand species in to 1,1,4-trimethylpiperazinium cation, whereas under these mild conditions coordination is achieved to give crystals of the zwitterionic $[GaF_4(PMDTAH)]\cdot 2H_2O$. Complexes of the Group 13 metals which are halide free are far less common throughout the literature, with only a few reports of weakly coordinating anions such as nitrates. Coordination of the same imine ligands (bipy and phen) to Group 13 metal nitrates was reported by Junk *et al* in 2006. This showed the structure of of $[In(O_2N\mathit{O})_2(ON\mathit{O}_2)(bipy)_2]$, the structurally related bridged species $[\{In(phen)_2\}(\mu\text{-}OH)_2][NO_2]_4\cdot 4H_2O\cdot MeNO_2$ and $[\{In(en)_2\}(\mu\text{-}OH)_2][NO_2]_4$ as well as the gallium centred species $[\{Ga(bipy)_2\}(\mu\text{-}OH)_2][NO_2]_4$ in the two distinct forms, the tetra and pentahydrate.[26]

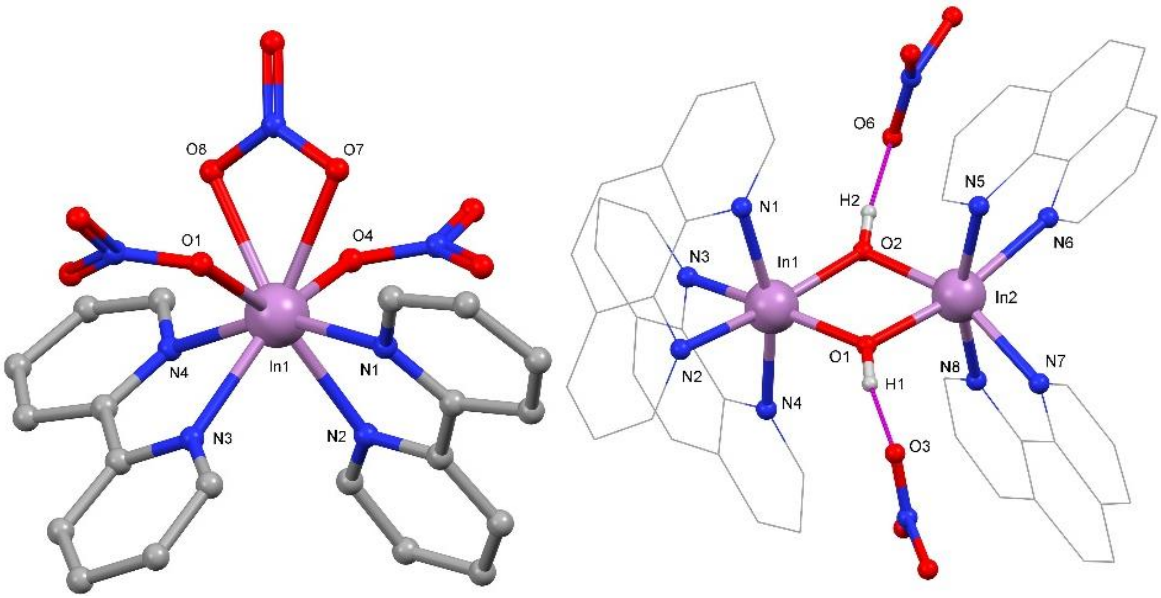

(a) (b)

Figure 2.4 – Crystal structures of $[In(\kappa^1\text{-}NO_3)_2(\kappa^2\text{-}NO_3)(bipy)_2]$ (a) and the bridged species $[\{In(phen)_2\}_2(u\text{-}OH)_2][NO_3]_4$ (b) showing atomic numbering scheme. Redrawn from Ref[27] with H-atoms omitted for clarity, unless involved in H-bonding.

Hydroxide bridged species of these types, isomorphous to those mentioned above had been produced with bismuth(III) nitrate as well as lanthanide metals in the 3+ oxidation state which were observed to have a high coordination number.[28] Both reports of coordination of polydentate imine donor ligands with the Group 13 metals and indium in particular, have shown the dissociation of one of the coordinated anions, allowing for dimerization and the formation of an $In(\mu\text{-}OR)_2In$ (R = H, Me) core; an uncommon structural motif in the literature of Group 13. Bridged species such as these have been explored further and have shown to be able to adopt a number of coordination numbers ranging from 5-8, depending on the coordinating species and strength of the donor atoms present.[27] Many of the hydroxide bridges form hydrogen bonds to the nearby anions, stabilising the complex further. Upon changing of solvent from acetonitrile to methanol, it was noted that the hydroxide bridges can be substituted for methoxy bridges. More recently, research into OLEDs has lead Yang *et al* to produce another of these $In(\mu\text{-}OH)_2In$ centred dimers

being coordinated by a tetradentate Schiff base ligand, shown in Figure 2.5.[29] This ligand, N,N'-bis(2-pyridinylmethylene)cyclohexane-1,2-diimine, is highly preorganised to metal coordination and types such as these are prevalent. These hydroxide bridges were shown to form hydrogen bonds to methanol which also forms an additional hydrogen bond to the non-coordinated nitrate anion.

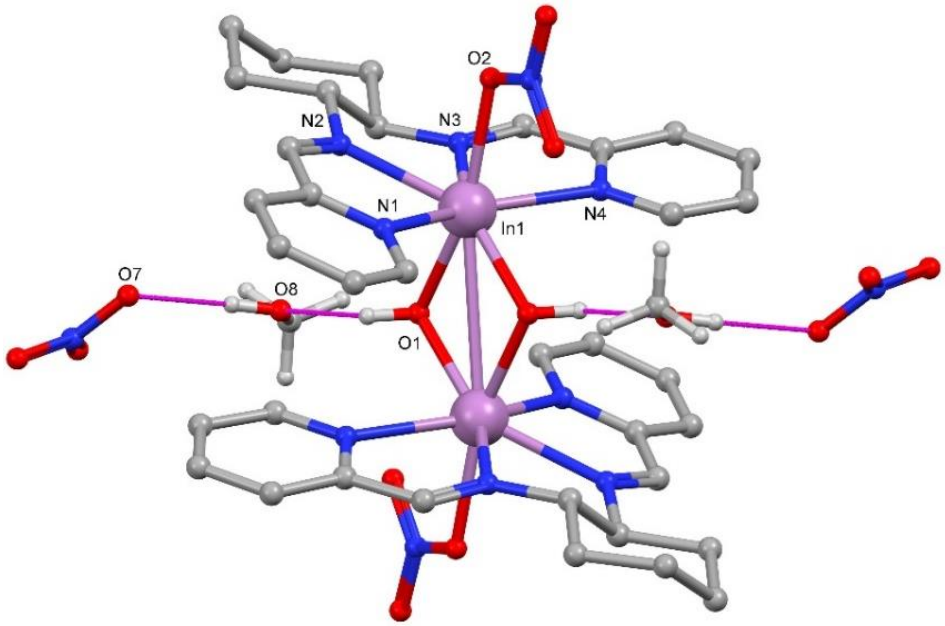

Figure 2.5 – Crystal structure of hydroxide bridged dimer [{$In(NO)_3(L)$}$_2$(μ^2-OH)] showing the atomic numbering scheme. H-atoms omitted for clarity, unless involved in H-bonding.[29]

2.2 – Results and Discussion

As mentioned in Chapter 1.5, trifluoromethanesulfonate or triflate is a weakly coordinating anion derived from a sulphite $[SO_3]^{2-}$ group containing an electron withdrawing $–CF_3$ group. This, along with the resonance structures of the sulphite, produces a more electropositive charge density at the sulphur atom and stabilising the anionic charge. The stability provided makes $[OTf]^-$ an excellent leaving group within both organic and inorganic chemistry, with the latter making use of its properties to provide 'vacant' sites on metal centres. This has made it a candidate for Heck and Sizuki coupling reactions, both of which require the loss of a leaving group, which triflate replaces the need for a halogen.[30] Despite this, the coordination chemistry to the triflate salts have been rare and often being through the displacement of another anion with triflate, or as a small amount of side product from a catalytic reaction.[31,32] Due to the stability of the triflate anion, it is expected that it will display a higher level of lability than a halide and thus allow for the formation of cationic complexes. These complexes would be related to the self-ionised products discussed in Chapter 1.3 and 1.4, in which a halide had been removed from the primary coordination sphere of the metal and formed a halometalate anion. In the triflate case, the free anion would act as the counter ion, without the need for formation of the halometalate.

Although the coordination chemistry of the Group 13 triflates is lacking, compounds have been produced as side products from the development of these Lewis acids for catalysis.[33] As a result of this work, a crystal structure of $[Ga(OTf)_3(THF)_3]$ was reported by Linti and Seifert[32] as one of a range of products from the reaction of GaCp* (Cp* = 1,2,3,4,5-pentamethylcyclopentadiene) and triflic acid, although no other characterisation data were reported for this complex. The metal triflate starting material was procured as 'anhydrous' $M(OTf)_3$ (M = Al, Ga, In) but IR spectroscopy revealed the presence of varying amounts of water associated.

Heating the samples to 120°C *in vacuo* for 12 h did not remove of all of the water of the sample, with an unknown amount of water still present in the IR spectrum. Hence, it is important to note that trace water was present in all of the reactions described below and so the amount of ligand used will be in slight excess. In an attempt to combat this, THF was added with the hope of forming $[Ga(OTf)_3(THF)_3]$ which could then be used as a dry source of $Ga(OTf)_3$ in further synthesis. This involved treatment of the $M(OTf)_3$ with either excess and stoichiometric ratios (1:3 ratio of $M(OTf)_3$: THF in dichloromethane). Both reactions appeared to cause polymerisation of THF after only a short time in solution, producing sticky oils and films rather than precipitates upon concentration or complete removal of the excess solvent. Ring opening of THF is known to be catalysed by metal ions from both the *p*-block and *d*-block and is achieved through activation and thus weakening of the C-O bond.[34] This was not pursued further, and instead, the $M(OTf)_3$

reagents that had been heated *in vacuo*, but still retained small amounts of water (IR evidence), were used for the subsequent chemistry.

Due to the lack of Group 13 triflate complexes reported previously in the literature, bi- and tri-dentate imine ligands were selected to start exploring the coordination and any differences exhibited with the incorporation of the triflate anion. After showing that the hydrated metal fluorides $MF_3 \cdot H_2O$ could only be coordinated with imine ligands through a hydrothermal route,[23] attempts to coordinate these ligands to the metal triflates, followed by anionic exchange may give a mild route to coordinated fluoride complexes. The ligands in Figure 2.6, terpy (2,2′:6′,2′′-terpyridyl), bipy (2,2′-bipyridyl) and phen (1,10-phenanthroline) were each reacted in a 1:1 ratio with three metal triflates, as illustrated in Schemes 2.1 and 2.2 and described in the experimental section of this chapter.

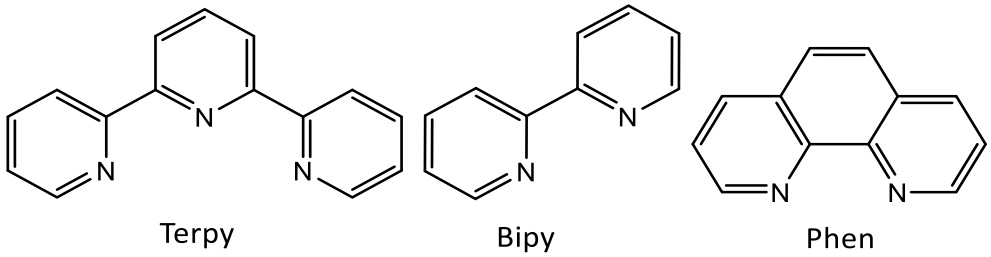

Figure 2.6 - Neutral imine ligand species for coordination to metal triflates.

2.2.1 Terpy Complexes

The reaction of $M(OTf)_3$ (M = Al, Ga, In) with terpy in a 1:1 molar ratio in anhydrous CH_2Cl_2 gave the $[M(OTf)_3(terpy)]$ complexes, each isolated as a white powder in moderate to good yields, as shown in Scheme 2.1.

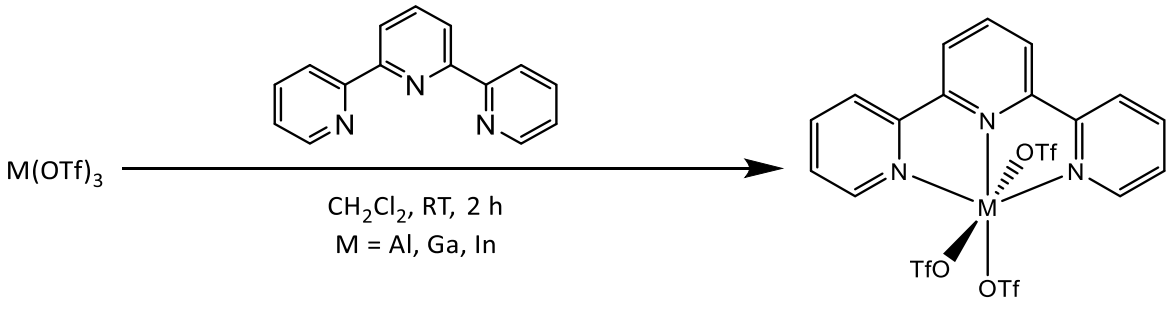

Scheme 2.1 - Reaction scheme of Group 13 metal triflates with 2,2′:6′,2′′-terpyridyl.

The complexes of the corresponding metal halides, *mer*-$[MX_3(terpy)]$ M = Al, Ga, In; X = Cl, Br, I), were fully characterised previously by Carty,[3] with crystal structures showing the expected *mer*-isomer. In more recent years, the corresponding fluorides, *mer*-$[MF_3(terpy)] \cdot 3H_2O$, have been produced from hydrothermal reactions of $MF_3 \cdot 3H_2O$ and terpy in water at 180°C.[23]

Crystals of [In(OTf)$_3$(terpy)] were grown by the slow evaporation of CH_2Cl_2 solutions of the complex and were shown to adopt the expected octahedral geometry in a distorted *mer*-isomer, shown in Figure 2.7. A selection of the bond lengths and angles are detailed in Table 2.1 The coordination sphere consists of the κ^3-coordination of the terpy ligand and the monodentate coordination of three triflate anions. The octahedral geometry is distorted by the restricted bite angle of terpy, with <N–In–N ~74° for adjacent N atoms, similar to other Group 13 complexes containing this ligand.[5]

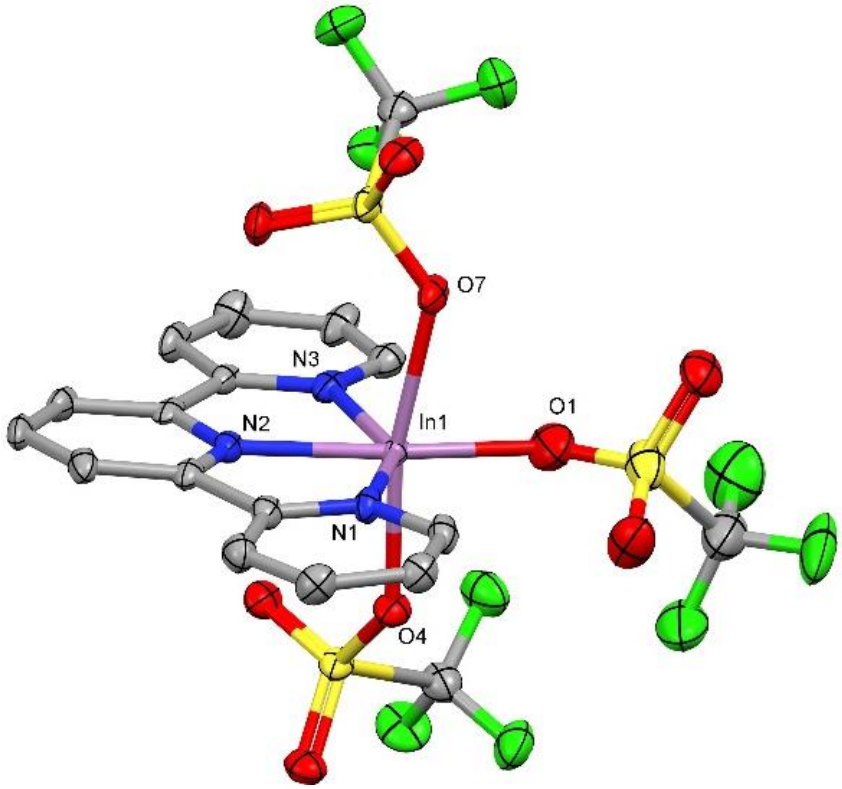

Figure 2.7 - Crystal structure of ***1*** *mer*-[In(OTf)$_3$(terpy)] showing the atomic numbering scheme. Ellipsoids are drawn to 50% probability with H-atoms omitted for clarity.

Table 2.1 - Selected bond lengths and angles for [In(OTf)$_3$(terpy)].

Bond Lengths / Å		Bond Angles / °	
In1 – N1	2.247(6)	N1 – In1 – N2	73.9(2)
In1 – N2	2.176(5)	N2 – In1 – N3	74.2(2)
In1 – N3	2.227(5)	N2 – In1 – O4	93.31(18)
In1 – O1	2.144(6)	N2 – In1 – O7	98.44(18)
In1 – O4	2.160(4)	O1 – In1 – N1	118.9(2)
In1 – O7	2.202(5)	O1 – In1 – N3	93.1(2)

As observed in the previous results, the central In-N bond distance is shorter than the outer two metal–donor distances by ~0.05 Å at 2.176(5) Å, while the In–N bond distances of the pyridyl arms are 2.227(5) and 2.247(6) Å, in a similar range (2.220-2.350 Å) to complexes containing In–N bonds.[35] There is no *trans* directing effect on the triflate anions from the terpy ligand with the In-O bond distances ranging from 2.144(6) – 2.202(5) Å. Furthermore, there is no evidence of long intermolecular contacts in the system.

The $[M(OTf)_3(terpy)]$ (M = Al, Ga, In) complexes were found to be poorly soluble in weakly coordinating solvents, e.g. CH_2Cl_2, but readily dissolve in slightly more strongly donating solvents like MeCN and for this reason CD_3CN was chosen as the NMR solvent. The ^{1}H and $^{13}C\{^{1}H\}$ NMR spectra each show an high frequency shift to the aromatic resonances of the free ligand, indicating a change in electronic environment caused by coordination to the electron rich metal centre. Some of these spectra show broad resonances with loss of proton couplings upon reaction, again suggesting coordination of the terpy to the quadrupolar ^{27}Al, $^{69/71}Ga$ and ^{115}In nuclei. Some samples, including those that had been left in CD_3CN solution for some time, showed the generation of a very broad peak at high frequency (12-15 ppm), thought to correspond to small amounts of the protonated form of terpy being formed. This side product is likely formed by the presence of trace amounts of water in the metal triflate (as seen earlier in IR spectra of the $M(OTf)_3$ starting material) or adventitious water while standing in solution. The ^{1}H aromatic resonances for this protonated species were also shifted to high frequency from free terpy, and $[M(OTf)_3(terpy)]$ (M = Al, Ga, In). The protonated salt [terpyH][OTf] was also observed through single crystal X-ray diffraction experiments on crystals grown from the NMR solutions of these complexes. The $^{19}F\{^{1}H\}$ NMR spectra of these complexes revealed a single very sharp resonance at δ = -79.4, attributed to the $-CF_3$ of the anionic $[OTf]^-$. That this resonance does not change throughout the study of these complexes suggests that the triflate anions are readily displaced by MeCN in solution and the resonance corresponds to the free anion. Qualitative conductance experiments were run showing that solutions of these complexes were highly conducting, however calibration and thus quantitative results were not possible at this time. Although attempted, none of these terpy complexes exhibited a metal NMR resonance, likely due to the fast relaxation of their quadrupolar nuclei (^{27}Al I = 5/2, ^{71}Ga I = 3/2, ^{115}In I = 9/2) in the relatively low symmetry coordination environments present. This is supported by the findings of $[MF_3(terpy)].3H_2O$ with only the ^{27}Al NMR being observed in this study.[23] The much higher lability of the triflate anions compared to coordinated fluoride has likely lowered the symmetry of the complex, when in solution, and the ^{27}Al NMR resonance is not observed for $[Al(OTf)_3(terpy)]$.

As mentioned in Chapter 1.6.2, the triflate anion has been well studied *via* IR spectrascopy with each of the different absorbance bands being assigned.[36] Many of the anions stronger

absorbance's such the C-F and S=O are found between 1000-1400 cm^{-1} along with many of the neutral ligands and so assignment of them is difficult and not attempted here.[36,37] Although the crystal structure shows [In(OTf)$_3$(terpy)], this may not be representative of the bulk solid. It is unknown if the solid-state structure of the other Group 13 metals matches that of [In(OTf)$_3$(terpy)], meaning it is unknown if there are coordinated or ionic triflates in the IR spectra.

A sample of *mer*-[In(OTf)$_3$(terpy)] was left in a CH_2Cl_2 solution for several weeks, forming a small number of crystals suitable for single crystal X-ray diffraction. Single crystal X-ray analysis showed a centrosymmetric hydroxy-bridged dimer, [{In(OTf)(terpy)}$_2$(μ-OH)$_2$][OTf]$_2$ which is shown in Figure 2.8. A selection of bond lengths and angles of this complex have been detailed in Table 2.2. Similar hydroxy-bridged dimers containing a [M(μ^2-OH)$_2$M] (M = Al, Ga, In) core have previously been observed in the literature with bipy, phen and terpy ligands.[4] This behaviour was also illustrated in Figure 2.4, where each hydroxyl bridge forms hydrogen bonds to methanol and then a nitrate anion.[29]

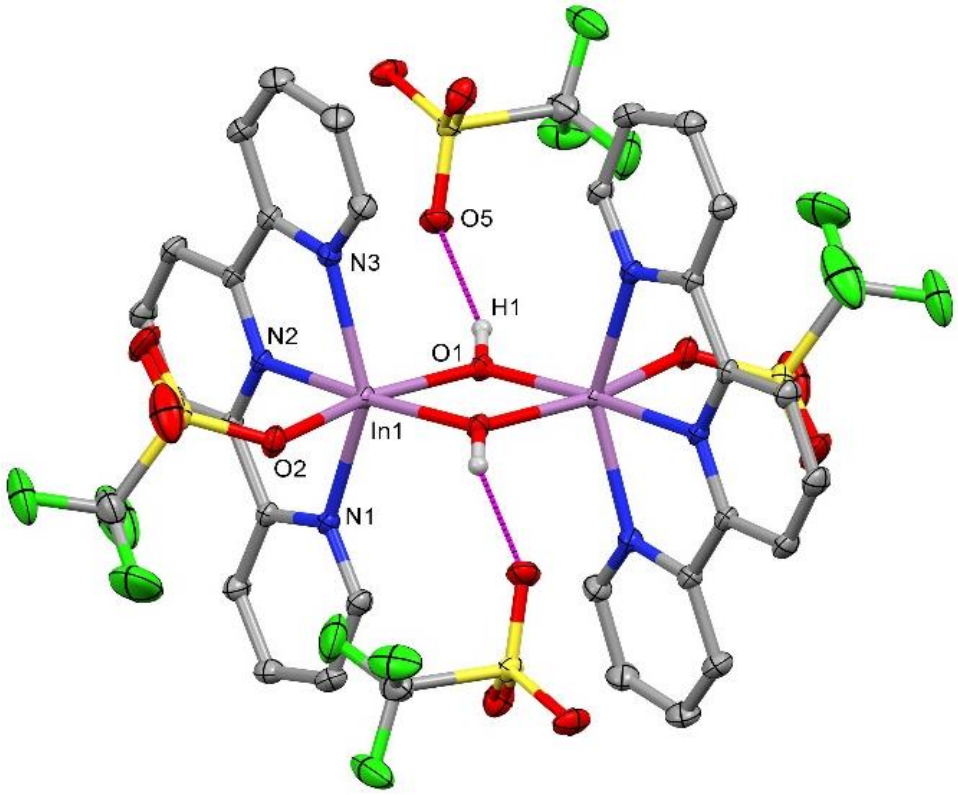

Figure 2.8 - Crystal structure of ***2*** [{In(OTf)(terpy)}$_2$(μ-OH)$_2$][OTf]$_2$ showing the atomic numbering scheme. Ellipsoids are shown at 50% probability with anions and H-atoms and omitted for clarity, unless involved in H-bonding.

Table 2.2 - Selected bond lengths and angles for $[\{In(OTf)(terpy)\}_2(u\text{-}OH)_2][OTf]_2$

Bond Lengths / Å		Bond Angles / °	
In1 – N1	2.2396(12)	N1 – In1 – N2	73.39(4)
In1 – N2	2.1951(12)	N2 – In1 – N3	73.41(5)
In1 – N3	2.2463(13)	N2 – In1 – O2	93.31(18)
In1 – O1	2.0669(11)	O1 – In1 – O1’	75.98(5)
In – O1’	2.1482(11)	O1 – In1 – O2	89.47(4)
In1 – O2	2.1945(12)	O1 – In1 – N1	94.54(4)
O1 … O5	2.743(2)	O1 – In1 – N3	94.24(4)
H1 … O5	2.0031(2)		

The structure of $[\{In(OTf)(terpy)\}_2(\mu\text{-}OH)_2][OTf]_2$ revealed each metal centre to be coordinated by a κ^3-terpy, a single triflate anion and two hydroxyl bridges to give a total coordination number of 6 in a highly distorted octahedron. Each of these hydroxyl bridges is forming a single hydrogen bond to an ionic triflate anion with the H1···O5 hydrogen bonding distance measured at 2.00(4) Å. The In_2O_2 core contains In-O_{OH} bonds at 2.0669(11) and 2.1482(11) Å, 0.05 Å shorter than the In-O_{OTf} bonds observed in both the parent and bridged species12. The In-N bond distances and bite angle of the terpy ligand are not significantly changed from the parent complex $[In(OTf)_3(terpy)]$. This complex $[\{In(OTf)(terpy)\}_2(u\text{-}OH)_2][OTf]_2$ is likely formed through the partial hydrolysis of $[In(OTf)_3(terpy)]$ by small amounts of residual water retained from the metal precursor.

2.2.2 Bipy Complexes

The reaction of $M(OTf)_3$ with two molar equivalents of bipy in CH_2Cl_2 gave very pale pink powders of $[Al(OTf)_2(bipy)_2][OTf]$ and $[Ga(OTf)_2(bipy)_2][OTf]$, or white $[In(OTf)(H_2O)(bipy)_2][OTf]_2$ shown in Scheme 2.2. Each of these complexes was identified by a combination of microanalysis, IR and NMR spectroscopy. The structures $[Ga(OTf)_2(bipy)_2][OTf]$ and $[In(OTf)(H_2O)(bipy)_2][OTf]_2$ were confirmed by single crystal X-ray analyses of crystals formed by layering *n*-hexane on to a CH_2Cl_2 solution of the complex and leaving, undisturbed for 72 h.

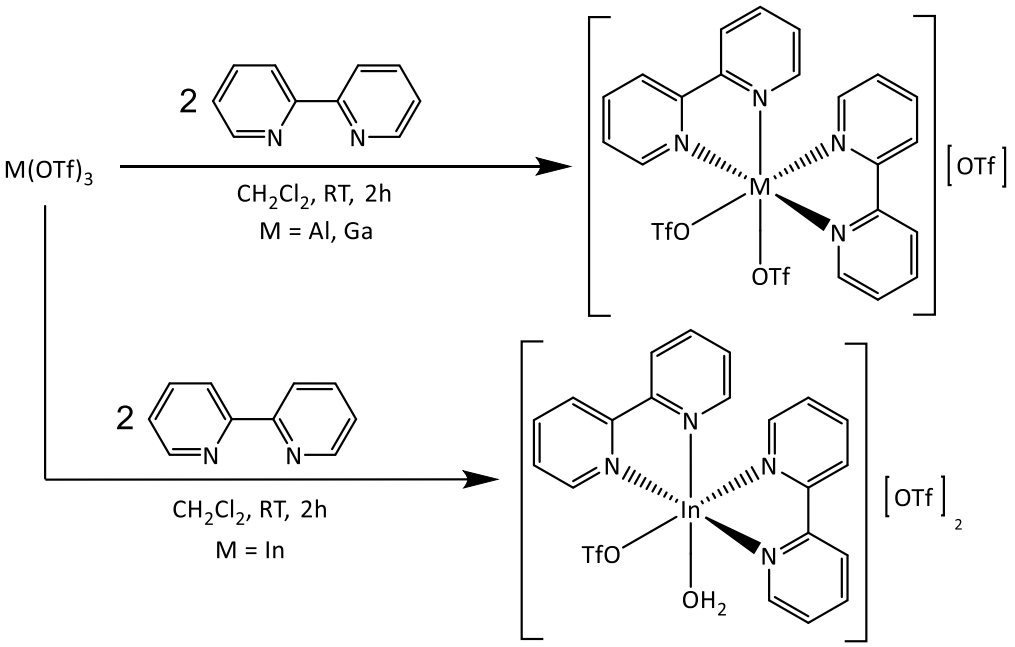

Scheme 2.2 - Reactions of the Group 13 metal triflates with 2,2'-bipyridyl.

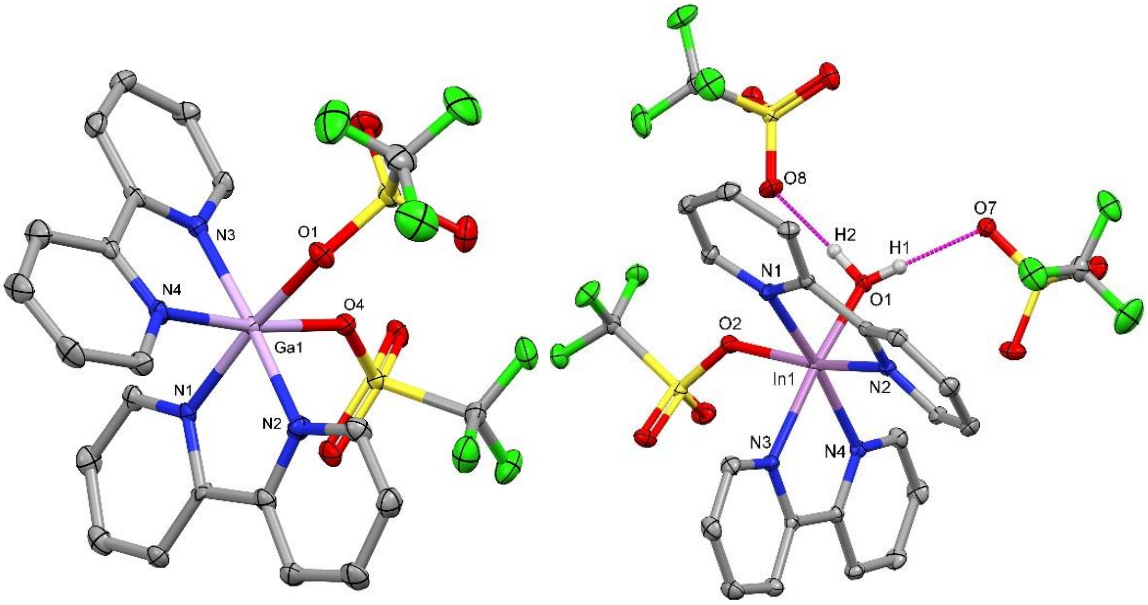

(a) (b)

Figure 2.9 - Crystal structures of (a) ***3*** $[Ga(OTf)_2(bipy)_2][OTf]$ and (b) ***4*** $[In(OTf)(OH_2)(bipy)_2][OTf]_2$ showing the atomic numbering scheme. Ellipsoids are drawn at 50% probability with anions and H-atoms omitted for clarity, unless involved in hydrogen bonding.

Table 2.3 - Selected bond lengths and angles for $[Ga(OTf)_2(bipy)][OTf]$ and $In(OTf)(OH_2)(bipy)][OTf]_2$.

Bond Lengths / Å			Bond Angles / °	
$[Ga(OTf)_2(bipy)_2]$	Ga1 – N1	2.032(6)	N1 – Ga1 – N2	80.8(3)
	Ga1 – N2	2.026(6)	N1 – Ga1 – O4	94.1(2)
	Ga1 – N3	2.011(6)	N2 – Ga1 – O1	90.6(2)
	Ga1 – N4	2.065(6)	N3 – Ga1 – N4	80.8(2)
	Ga1 – O1	2.000(5)	N3 – Ga1 – O4	93.1(2)
	Ga1 – O4	2.031(5)	N4 – Ga1 – O1	94.1(2)
			O1 – Ga1 – O4	88.1(2)
$[In(OTf)(OH_2)(bipy)_2][OTf]_2$	In1 – N1	2.2202(13)	N1 – In1 – N2	75.55(5)
	In1 – N2	2.2146(13)	N3 – In1 – N4	74.30(5)
	In1 – N3	2.2292(11)	N2 – In1 – O1	100.24(5)
	In1 – N4	2.2293(13)	N2 – In1 – N3	86.81(5)
	In1 – O1	2.1326(12)	N3 – In1 – O2	94.47(5)
	In – O2	2.1789(11)	N4 – In1 – N2	102.35(5)
	O1 … O7	2.650(2)	O1 – In1 – N1	94.47(5)
	H1 … O7	1.87(3)	O1 – In1 – O2	82.01(5)
	O1 … O8	2.604(1)		
	H2 … O8	1.76(2)		

The structure of $[Ga(OTf)_2(bipy)_2][OTf]$ in Figure 2.9a reveals a *cis*-octahedral monocation, distorted by the small chelate bite angle of the neutral bipy ligand (<N—Ga—N = 80.8°), taken from Table 2.3. The Ga-N bond distances range from 2.011(6) - 2.065(6) Å, which is typical for previously observed Ga-bipy species, for example, the Ga-N distances for $[GaF_3(bipy)(OH_2)]$ observed as 2.093(2) and 2.064(3) Å.[23] The structure of $[In(OTf)(H_2O)(bipy)_2][OTf]_2$ in Figure 2.9b was obtained from a very small crystal, and the metrical data should be interpreted in that light. It was also revealed to contain a *cis*-octahedral cation, however, one of the triflate anions being replaced by a molecule of water in the primary coordination sphere. This coordinated water then forms hydrogen bonds to the remaining two triflate counter anions, in the same fashion as the methanol in Figure 2.5. The In-O_{OTf} distance of $[In(OTf)(H_2O)(bipy)_2][OTf]_2$ was 2.1789(11) Å, which is comparable to In-O_{OTf} bonds observed in $[In(OTf)_3(terpy)]$, with these values taken from Table

2.3. The In-O_{OTf} distances of both of these complexes were found to be longer than the In-O_{OH2}, likely due to the anionic charge and additional steric size of the triflate anion. Both sets of In-N bonds are comparable to those observed in previous studies of In-bipy complexes,[27] ranging from 2.2146(13) - 2.2293(13) Å as well as the In-$N_{(terpy)}$ distance in $[In(OTf)_3(terpy)]$ discussed earlier. Regardless of which type of oxygen donor ligand is located *trans*, there is little effect on the In-N bond distances.

As was observed in the terpy complexes above, each of the bipy resonances observed in the ^{1}H and $^{13}C\{^{1}H\}$ NMR spectra showed a high frequency shift from the free bipy. There was no evidence for any protonated bipy in the ^{1}H or $^{13}C\{^{1}H\}$ NMR spectra. Both $[M(OTf)_2(bipy)_2][OTf]$ (M = Al, Ga) and $[In(OTf)(OH_2)(bipy)_2][OTf]$ gave a sharp singlet at δ = -79.4 in the $^{19}F\{^{1}H\}$ NMR spectrum while in CD_3CN, again suggesting the dissociation of each $[OTf]^-$ from the complexes with $[M(CD_3CN)_2(bipy)_2]^{3+}$ likely being present in solution. In contrast to the $[Al(OTf)_3(terpy)]$ which did not show a ^{27}Al NMR resonance, $[Al(OTf)_2(bipy)_2][OTf]$ exhibits a single sharp resonance in the ^{27}Al NMR spectrum at δ +12.8. This is within the known characteristic range for of six-coordinate aluminium species,[38] corroborating the theory that the trication $[M(bipy)_2(MeCN)_2]^{3+}$ is the likely species in solution. Although attempted, there were no resonances observed under ^{71}Ga or ^{115}In NMR spectroscopy of the respective metal complexes.[23]

2.2.3 Phen Complexes

As discussed in Chapter 1.2.3, complexes of 2,2'bipy are often compared with coordination of the more rigid but structurally related 1,10-phen ligands. The reactions of $M(OTf)_3$ (M = Al, In) with phen in a 1:2 molar ratio were carried out in CH_2Cl_2 and afforded compounds identified as $[Al(OTf)_2(phen)_2][OTf]$ and $[In(H_2O)_2(phen)_2][OTf]_3$ and is shown in Scheme 2.3. Although attempted repeatedly, synthesis of the gallium analogue was unsuccessful, with mixtures of products being obtained from each reaction, evident from ^{1}H NMR spectroscopy.

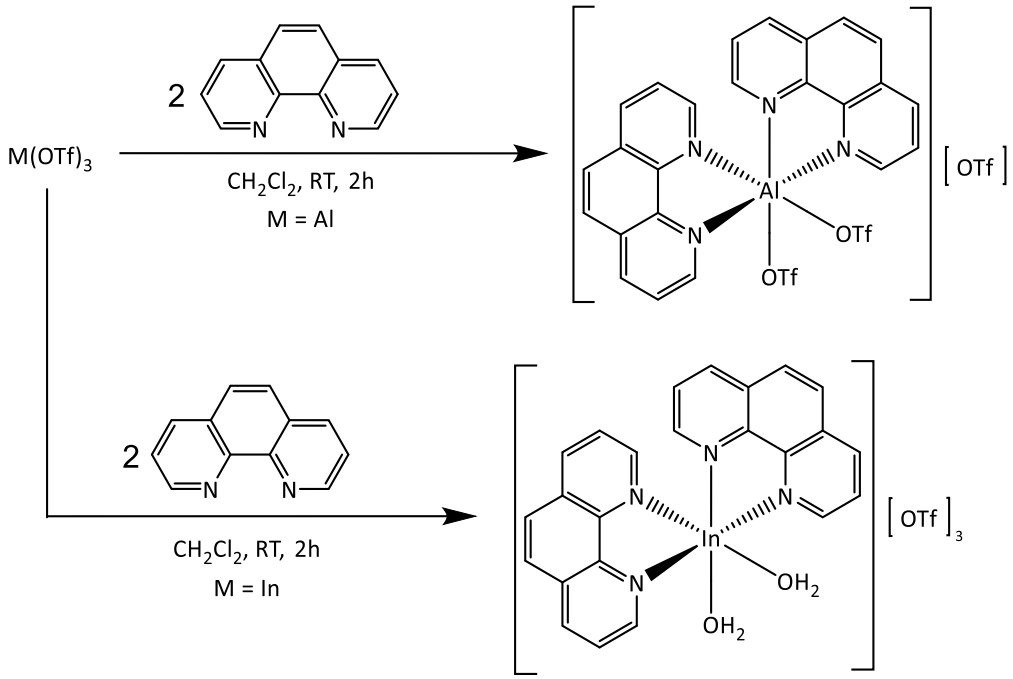

Scheme 2.3 - Reactions of the Group 13 metal triflates with 1,10-phenanthroline.

Protonated phen was identified by the presence of a high frequency resonance at 12-15 ppm in the ^{1}H NMR spectra, similar to that observed with protonated terpy in the discussion above. The other species in the mixture are presumed to be the 1:1 and 1:2 Ga : phen species, $[Ga(OTf)_3(OH_2)(phen)]$ and $[Ga(OTf)_2(phen)_2][OTf]$, as well as residual free ligand. Despite being unable to isolate a pure bulk sample, a few crystals suitable for X-ray diffraction were grown from one of these mixtures by slow evaporation of a CH_2Cl_2 solution, identified as *cis*-$[Ga(H_2O)_2(phen)_2][OTf]_3$, which dimerised to form the H-bonded bridged dimer shown in Figure 2.10. The data collected for this crystal revealed a centrosymmetric dimer despite rather weak data, and hence the overall structure quality is rather modest, with R1 = 8.9%.

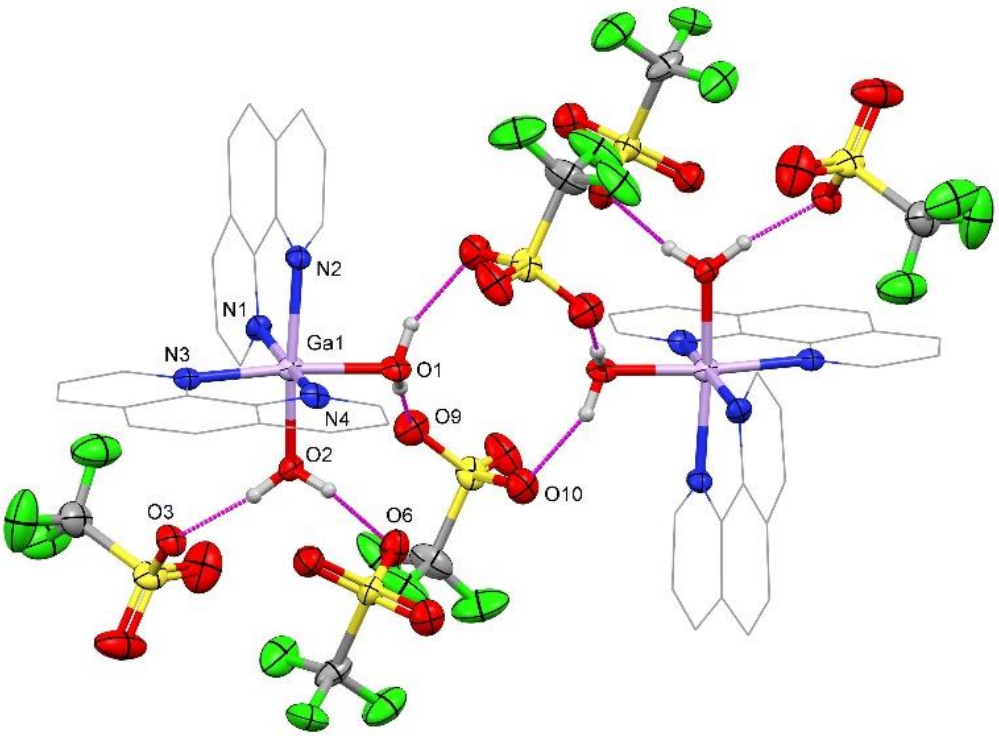

Figure 2.10 – Crystal structure of ***5*** $[\{Ga(OH_2)_2(phen)_2\}_2][OTf]_6$ showing the atom numbering scheme. Ellipsoids are drawn at 50% probability with H-atoms omitted for clarity, unless involved in hydrogen bonding.

Table 2.4 - Selected bond lengths and angles of $[\{Ga(OH_2)_2(phen)_2\}_2][OTf]_6$.

Bond Lengths / Å		Bond Angles / °	
Ga1 – N1	2.054(5)	N1 – Ga1 – N2	73.39(4)
Ga1 – N2	2.085(6)	N2 – Ga1 – N3	73.41(5)
Ga1 – N3	2.060(5)	N2 – Ga1 – O2	93.31(18)
Ga1 – N4	2.035(5)	N2 – Ga1 – N3	94.7(2)
Ga1 – O1	2.002(5)	N3 – Ga1 – O2	92.0(2)
Ga1 – O2	1.949(5)	N4 – Ga1 – O1	92.5(2)
O1 … O9	2.646(7)	O1 – Ga1 – O2	84.8(2)
H1a … O9	1.745	O1 – Ga1 – N1	92.4(2)
O1 … O10	2.612(1)		
H1b … O10	1.876		
O2 … O6	2.649(8)		
H2a … O6	1.806		
O2 … O3	2.596(7)		
H2b … O3	1.76(5)		

As was observed with the other imine complexes in this chapter of work, the coordination of the phen ligand produced a highly distorted octahedron where two *cis*-coordination sites are taken up by aquo ligands, displacing the weakly coordinated triflate anion. Each of these water ligands is seen to exhibit similar behaviour to that observed in $[In(OTf)(OH_2)(bipy)_2][OTf]_2$ by forming significant H-bonding interactions to the triflate anions. The coordinated H_2O ligand is shown to produce significant H-bonding interactions to the triflate anions, similar to the behaviour observed in $[\{GaF(terpy)\}_2(\mu\text{-}F)_2][PF_6]_2 \cdot 4H_2O$ in Figure 2.3. These hydrogen bonds lead to the assembly of a weakly associated binuclear dimer species where two triflate anions bridge between coordinated water molecules. These H-bonds were measured to be slightly shorter than those observed above in $[In(OTf)(OH_2)(bipy)_2][OTf]_2$, instead ranging from 1.75 – 1.88 Å.

Analysis of the successfully isolated products $[Al(OTf)_2(phen)_2][OTf]$ and $[In(H_2O)_2(phen)_2][OTf]_3$ by ^1H and $^{13}C\{^1H\}$ NMR spectroscopy, showed a high frequency shift for the aromatic resonances of each complex when compared to free phen, suggesting successful coordination. The ^1H NMR spectrum of $[In(OH_2)_2(phen)_2][OTf]_3$ revealed a significant water peak and this was backed up by the presence of O-H stretches in the IR spectrum. This, along with the crystal structure observed for the analogous gallium complex, suggests that substitution of the triflate with water has occurred in both the gallium and indium complexes but not the aluminium. When microanalysis was undertaken, each of these complexes matched its calculated formula $[M(OTf)_{(3-n)}(H_2O)_{(n-1)}(phen)_2][OTf]_n$ (n = 1-3) within 0.4%. The $^{19}F\{^1H\}$ NMR spectra for each of these complexes in CD_3CN was near identical, exhibiting a sharp singlet resonances at δ = –79.4. As was the result with the bipy complexes, metal NMR was attempted for each of these complexes with only ^{27}Al NMR spectrum of $[Al(OTf)_2(phen)_2][OTf]$ being seen to produce a resonance. This was a broad resonance at +12.3 ppm, similar to that observed in the $[Al(OTf)_2(bipy)_2][OTf]$, which is known to be typical for a six-coordinate aluminium species, likely corresponding to $[Al(phen)_2(MeCN)_2]^{3+}$ in solution.[39]

2.3 – Conclusion

The Group 13 metal triflates react with tridentate or bidentate ligands in a 1:1 or 1:2 ratio respectively and produce complexes containing $[M(OTf)_3(terpy)]$ or $[M(OTf)_2(bidentate)_2]^+$ (L = bipy, phen) cores. The remaining coordination sites were observed to be filled with triflate anions and/or water ligands, giving M(III) (M = Al, Ga, In) complexes with a six-coordinate octahedral geometry. The complexes containing coordinated water ligands displayed significant H-bonding interactions to the free triflate anions. The H-bonding of these water ligands to the triflate anions were observed as both terminal and bridging interactions, with $[\{Ga(OH_2)_2(bipy)_2\}_2][OTf]_6$ showing bridging through two H-bonded triflate anions. Future work could explore substitution of the weakly coordinating triflate by more strongly coordinating anions such as F^-. The ability to introduce fluoride to a preformed metal complex is relevant for the development of metal-based ^{18}F PET imaging agents, which due to the relatively short half-life of ^{18}F, requires that it is introduced at the final stage of synthesis.

2.4 – Experimental

For supplier and purification of reagents and solvents, instrument specifications and NMR solvent references see Appendix A. Although the Group 13 metal triflates were purchased as 'anhydrous' materials, IR spectroscopy revealed residual water after attempts to dry them by heating *in vacuo*.

2.4.1 Complex Preparation

2.4.1.1 **Mer-[In(OTf)$_3$(terpy)]**

In(OTf)$_3$ (112 mg, 0.20 mmol) was dissolved in CH_2Cl_2 (10 mL) before addition of 2,2':6',2''-terpyridine (47 mg, 0.20 mmol) and stirred for 2 h. The solution was concentrated before addition of *n*-hexane (5 mL) resulted in a white precipitate, the solid was removed from the CH_2Cl_2 solution by filtration before being dried *in vacuo,* resulting in a white solid. Yield: 108 mg, 68%. Required for $C_{18}H_{11}F_9InN_3O_9S_3$ (795.29): C, 27.2; H, 1.4; N, 5.3. Found: C, 27.1; H, 1.4; N, 5.7%. ^{1}H NMR (295 K, CD_3CN): δ = 9.07 (d, [2H], Ar-H), 8.78 (m, [4H], Ar-H), 8.72 (m, [H], Ar-H), 8.57 (td, [2H], Ar-H), 8.11 [ddd, [2H], Ar-H). $^{13}C\{^1H\}$ NMR (295 K, CD_3CN): δ = 150.19, 148.10, 147.24, 145.97, 145.39, 130.16, 125.63, 125.59.$^{19}F\{^1H\}$ NMR (295 K, CD_3CN): δ = -79.23 (s).

2.4.1.2 ***Mer*-[Ga(OTf)$_3$(terpy)]**

Ga(OTf)$_3$ (130 mg, 0.25 mmol) was dissolved in CH_2Cl_2 (10 mL) before addition of 2,2':6',2''-terpyridine (58 mg, 0.25 mmol) and stirred for 2 h. Some white solid was removed from a pink solution by filtration and the removal of solvent from the filtrate resulted in a white solid. This was dried *in vacuo*. Yield: 128 mg, 68%. Required for $C_{18}H_{11}F_9GaN_3O_9S_3$ (750.20): C, 28.8; H, 1.5; N, 5.6. Found: C, 22.5; H, 1.8; N, 4.4%. ^{1}H NMR (295 K, CD_3CN): δ = 8.81 (m, [2H], Ar-H), 8.66 (dt, [2H], Ar-H), 8.48 (d, [2H], Ar-H), 8.35 (td, [2H], Ar-H), 8.23 (dd, [H], Ar-H) 7.78 (m, [2H], Ar-H). $^{13}C\{^1H\}$ NMR (295 K, CD_3CN): δ = 151.84, 151.59, 147.19, 143.60, 141.62, δ 127.47, 124.65, 124.11.$^{19}F\{^1H\}$ NMR (295 K, CD_3CN): δ = -79.40 (s). ^{71}Ga NMR (295 K, CD_3CN): not observed.

2.4.1.3 ***Mer*-[Al(OTf)$_3$(terpy)]**

Al(OTf)$_3$ (95 mg, 0.2 mmol) was dissolved in CH_2Cl_2 (10 mL) before addition of 2,2':6',2''-terpyridine (47 mg, 0.2 mmol) and stirred for 2 h. A white solid was removed by filtration from a pink solution. The filtrate was taken to dryness producing a pale pink solid which was dried *in vacuo*. Yield: 95 mg, 67%. Required for $C_{18}H_{11}F_9AlN_3O_9S_3$ (707.46): C, 30.6; H, 1.6; N, 5.9. Found: C, 30.4; H, 1.7; N, 5.9%. ^{1}H NMR (295 K, CD_3CN): δ = 8.99 (br d, [2H], Ar-H), 8.78 (d, [2H], Ar-H), 8.59 (m, [4H], Ar-H), 8.39 (dd, [H], Ar-H), 8.03 (br t, [2H], Ar-H). $^{13}C\{^1H\}$ NMR (295K, CD_3CN): δ =

148.99, 147.22, 146.87, 143.14, 142.38, 129.25, 126.44, 125.82. $^{19}F\{^{1}H\}$ NMR (295 K, CD_3CN): δ = -79.39 (s). Al NMR (295 K, CD_3CN): not observed.

2.4.1.4 **[In(OTf)(H_2O)(bipy)$_2$][OTf]$_2$**

$In(OTf)_3$ (56 mg, 0.1 mmol) was dissolved in CH_2Cl_2 (5 mL) before addition of 2,2'-bipyridine (31 mg, 0.2 mmol) and stirred for 2 h. The solution was concentrated before addition of *n*-hexane (5mL) resulted in a white precipitate, the solid was removed from the CH_2Cl_2 solution by filtration before being dried *in vacuo,* resulting in a white solid. Yield: 74 mg, 82%. Required for $C_{23}H_{18}F_9InN_4O_{10}S_3$ (892.41): C, 31.0; H, 2.0; N, 6.3. Found: C, 31.6; H, 1.3; N, 5.7%. ^{1}H NMR: (295 K, CD_3CN): δ = 8.78 (d, [H], Ar-H), 8.58-8.53 (m, [2H], Ar-H), 7.98 (m, [H], Ar-H). $^{13}C\{^{1}H\}$ NMR (295 K, CD_3CN): δ = 149.77, 147.64, 146.28, 130.38, 125.86. $^{19}F\{^{1}H\}$ NMR (295 K, CD_3CN): δ = -79.43 (s).

2.4.1.5 **[Ga(OTf)$_2$(bipy)$_2$][OTf]**

$Ga(OTf)_3$ (130 mg, 0.25 mmol) was dissolved in CH_2Cl_2 (10 mL) before addition of 2,2'-bipyridine (78 mg, 0.50 mmol) and stirred for 2 h. A white solid was removed by filtration from the pink solution before the removal of solvent *in vacuo* resulted in a pink solid. Yield: 141 mg, 68%. Required for $C_{23}H_{16}F_9GaN_4O_9S_3.CH_2Cl_2$ (914.23): C, 31.5; H, 2.0; N, 6.1. Found: C, 31.6; H, 1.3; N, 5.7%. ^{1}H NMR (295 K, CD_3CN): δ = 8.81 (d, [H, Ar-H]), 8.48 (m, [H], Ar-H), 8.37 (td, [H], Ar-H), 7.84 (m, [H], Ar-H). $^{13}C\{^{1}H\}$ NMR (295 K, CD_3CN): δ = 147.96, 147.08, 143.90, 128.07, 123.91. $^{19}F\{^{1}H\}$ NMR (295 K, CD_3CN): δ = -79.43 (s).

2.4.1.6 **[Al(OTf)$_2$(bipy)$_2$][OTf]**

$Al(OTf)_3$ (95 mg, 0.2 mmol) was dissolved in CH_2Cl_2 (10 mL) before addition of 2,2'-bipyridine (63 mg, 0.4 mmol) and stirred for 2 h. A white solid was removed from a pink solution before the removal of solvent resulted in a pink solid, which was dried *in vacuo*. Yield: 141 mg, 83%. Required for $C_{23}H_{16}AlF_9N_4O_9S_3.CH_2Cl_2$. (871.49): C, 33.1; H, 2.1; N, 6.4. Found: C, 33.7; H, 2.8; N, 6.9%. H NMR (295 K, CD_3CN): δ = 8.84 (m, [H], Ar-H), 8.49 (m, [2H], Ar-H), 8.43 (m, [H], Ar-H), 7.89 (m, [H], Ar-H) $^{13}C\{^{1}H\}$ NMR (295 K, CD_3CN): δ = 147.42, 147.09, 144.82, 128.69, 124.60. $^{19}F\{^{1}H\}$ NMR (295 K, CD_3CN): δ = -79.34 (s). Al NMR (295K, CD_3CN): δ = +12.8 (s).

2.4.1.7 **[In(OTf)$_2$(phen)$_2$][OTf]**

$In(OTf)_3$ (56 mg, 0.1 mmol) was dissolved in CH_2Cl_2 (5 mL) before addition of 1,10-phenanthroline (36 mg, 0.2 mmol) and stirred for 2 h. The solution was concentrated before addition of *n*-hexane (5 mL) resulted in a white precipitate, the solid was removed from the CH_2Cl_2 solution by filtration before being dried *in vacuo,* resulting in a white solid. Yield: 72

mg, 78%. Required for $C_{27}H_{20}F_9InN_4O_{11}S_3$ (958.47): C, 33.8; H, 2.1; N, 5.9. Found: C, 34.1; H, 2.9; N, 5.9%. ^{1}H NMR (295 K, CD_3CN): δ = 9.11 (m, [H], Ar-H), 8.96 (m, [H], Ar-H), 8.41 (s, [H], Ar-H), 8.23 (m, [H], Ar-H) $^{13}C\{^1H\}$ NMR (295 K, CD_3CN): δ = 151.07, 145.10, 138.54, 131.30, 129.16, 128.04. $^{19}F\{^1H\}$ NMR (295 K, CD_3CN): δ = -79.34 (s).

2.4.1.8 **$[Al(OTf)_2(phen)_2][OTf]$**

$Al(OTf)_3$ (95 mg, 0.2 mmol) was dissolved in CH_2Cl_2 (5 mL) before addition of 1,10-phenanthroline (72 mg, 0.4 mmol) and stirred for 2 h. The solution was concentrated before addition of *n*-hexane (5mL) resulted in a white precipitate, the solid was removed from the CH_2Cl_2 solution by filtration before being dried *in vacuo,* resulting in a white solid. Yield: 103 mg, 62%. Required for $C_{27}H_{16}AlF_9O_9N_4S_3.0.5CH_2Cl_2$ (877.10): C, 37.7; H 2.0; N, 6.4. Found: C, 37.3; H, 2.7; N, 6.5%. H NMR (295 K, CD_3CN): δ = 9.20 (m, [H], Ar-H), 8.96 (m, [H], Ar-H), 8.27 (s, [H], Ar-H), 8.16 (m, [H], Ar-H]). $^{13}C\{^1H\}$ NMR (295 K, CD_3CN): δ = 148.21, 143.48, 138.54, 131.09, 128.70, 126.92. $^{19}F\{^1H\}$ NMR (295 K, CD_3CN): δ = -79.4 (s). Al NMR (295 K, CD_3CN): δ = +12.3 (s).

2.5 – References

1 R. Restivo and G. J. Palenik, *J. Chem. Soc. D Chem. Commun.*, 1969, 867.
2 R. Restivo and G. J. Palenik, *J. Chem. Soc., Dalton. Trans.*, 1972, 341–344.
3 A. J. Carty, *Can. J. Chem.*, 1968, **46**, 3779–3784.
4 G. S. Papaefstathiou, A. Sofetis, C. P. Raptopoulou, A. Terzis, G. A. Spyroulias and T. F. Zafiropoulos, *J. Mol. Struct.*, 2007, **837**, 5–14.
5 G. Beran, A. J. Carty, H. A. Patel and G. J. Palenik, *J. Chem. Soc. D Chem. Commun.*, 1970, **74**, 222–223.
6 C. H. L. Kennard, *Inorg. Chim. Acta*, 1967, **1**, 347–354.
7 T. N. Sevastianova, E. I. Davydova, I. V. Kazakov and A. Y. Timoshkin, *Russ. Chem. Bull.*, 2015, **64**, 2523–2535.
8 G. Beran, K. Dymock, H. A. Patel, A. J. Carty and P. M. Boorman, *Inorg. Chem.*, 1972, **11**, 896–898.
9 A. Y. Timoshkin, M. Bodensteiner, T. N. Sevastianova, A. S. Lisovenko, E. I. Davydova, M. Scheer, C. Graßl and A. V. Butlak, *Inorg. Chem.*, 2012, **51**, 11602–11611.
10 I. V. Kazakov, M. Bodensteiner and A. Y. Timoshkin, *Acta Crystallogr. Sect. C Struct. Chem.*, 2014, **70**, 312–314.
11 A. J. Downs, *Chemistry of Aluminium, Gallium, Indium and Thallium*, Springer Netherlands, New York, 1st edn., 1993.
12 S. L. Benjamin, W. Levason and G. Reid, *Chem. Soc. Rev.*, 2013, **42**, 1460–1499.
13 A. B. Ilyukhin and S. P. Petrosyants, *Crystallogr. Reports*, 2002, **47**, 574–576.
14 W. F. Ehret and F. J. Frere, *J. Am. Chem. Soc.*, 1945, **67**, 64–68.
15 E. Kemnitz, U. Groß, S. Rüdiger, G. Scholz, D. Heidemann, S. I. Troyanov, I. V. Morosov and M.-H. Lemée-Cailleau, *Solid State Sci.*, 2006, **8**, 1443–1452.
16 P. Bukovec and V. Kaučič, *Inorg. Nucl. Chem. Lett.*, 1978, **14**, 79–81.
17 S. A. Polyshchuk, S. P. Kozerenko and Y. V. Gagarinsky, *J. Less Common Met.*, 1972, **27**, 45–50.
18 S. Petricek, A. Demsar, L. Golic, P. Bukovec and J. V. Brencic, *Acta Chim. Slov.*, 1997, **44**, 317–325.
19 S. P. Petrosyants and A. B. Ilyukhin, *Russ. J. Inorg. Chem.*, 2010, **55**, 30–33.
20 D. W. Aldous, R. J. Goff, J. P. Attfield and P. Lightfoot, *Inorg. Chem.*, 2007, **46**, 1277–1282.
21 J. Darriet, W. Massa, J. Pebler and R. Stief, *Solid State Sci.*, 2002, **4**, 1499–1508.
22 S. P. Petrosyants and A. B. Ilyukhin, *Russ. J. Inorg. Chem.*, 2011, **56**, 2047–2069.
23 R. Bhalla, W. Levason, S. K. Luthra, G. McRobbie, F. M. Monzittu, J. Palmer, G. Reid, G. Sanderson and W. Zhang, *Dalton Trans.*, 2015, **44**, 9569–9580.
24 R. Bhalla, C. Darby, W. Levason, S. K. Luthra, G. McRobbie, G. Reid, G. Sanderson and W. Zhang, *Chem. Sci.*, 2014, **5**, 381–391.
25 R. Bhalla, J. Burt, A. L. Hector, W. Levason, S. K. Luthra, G. McRobbie, F. M. Monzittu and G. Reid, *Polyhedron*, 2016, **106**, 65–74.
26 P. C. Junk, B. W. Skelton and A. H. White, *Aust. J. Chem.*, 2006, **59**, 147.
27 A. S. Delbari, A. S. Shahvelayati, V. Jodaian and V. Amani, *J. Iran. Chem. Soc.*, 2015, **12**, 223–232.
28 L. J. Barbour, S. J. Belfield, P. C. Junk and M. K. Smith, *Aust. J. Chem.*, 1998, **51**, 337.
29 S. Chen, R. Fan, X. Wang and Y. Yang, *Inorg. Chem. Commun.*, 2014, **44**, 101–106.
30 I. P. Beletskaya and A. V. Cheprakov, *Chem. Rev.*, 2000, **100**, 3009–3066.
31 A. D. K. Todd, W. L. McClennan and J. D. Masuda, *RSC Adv.*, 2016, **6**, 69270–69276.
32 G. Linti and A. Seifert, *Z. Anorg. Allgem. Chem.*, 2008, **634**, 1312–1320.
33 X. Han and J. Wu, *Org. Lett.*, 2010, **12**, 5780–5782.
34 W. Gruszka and J. A. Garden, *Nat. Commun.*, 2021, **12**, 3252.
35 R. W. H. Small and I. J. Worrall, *Acta Crystallogr. Sect. B Struct. Crystallogr. Cryst. Chem.*, 1982, **38**, 932–934.
36 D. H. Johnston and D. F. Shriver, *Inorg. Chem.*, 1993, **32**, 1045–1047.

37 G. A. Lawrance, *Chem. Rev.*, 1986, **86**, 17–33.
38 J. Mason, *Multinuclear NMR*, Plenum Press, New York, 1st edn., 1987.
39 M. Haouas, F. Taulelle and C. Martineau, *Prog. Nucl. Magn. Reson. Spectrosc.*, 2016, **94**–**95**, 11–36.

Chapter 3 – Synthesis, structure and properties of mono- and di-phosphine oxide complexes of aluminium, gallium and indium with weakly coordinating triflate anions.

This chapter continues to explore the Group 13 metal triflates and their coordination complexes, this time moving to oxygen donor ligands including OPR_3 (R = Me, Ph), pyNO and the bidentate $dppmO_2$. These have a range of donor strength, denticity and steric bulk, to further explore the effect of the weakly coordinating triflate anion on the coordination geometry.

3.1 – Introduction

The previous chapter explored the coordination of neutral nitrogen donor ligands to the Group 13 metal triflates, probing the change in coordination properties when moving from the well-studied halide complexes to a weakly coordinating anionic system. It was shown that the nitrogen donor ligands readily coordinated to the metal triflate centre to produce octahedral complexes with displacement of the triflate to form *bis*-bipy/phen complexes.[1] Using the tridentate nitrogen donor, complexes of $[M(OTf)_3(terpy)]$ (M = Al, Ga, In) were synthesised while the bidentate ligands bipy and phen produced $[M(OTf)_2(bidentate)_2][OTf]$. It was found in a number of the complexes synthesised that the weakly coordinating triflate anion was substituted by trace amounts of water, introduced to the reaction through the wet metal halide starting materials. When this occurred, the water ligand became involved in H-bonding to the triflate anions with $[\{Ga(OH_2)_2(phen)_2\}_2][OTf]_6$ forming a weakly associated dimer through triflate bridging water ligands, shown structurally in Figure 2.9. It is thought that use of anhydrous starting materials would have produced neutral complexes with coordinated triflate anions. Primarily, coordination to the Group 13 halides produces neutral complex due to the strong binding of the halide anion. Displacement of a halide is known, with coordination of bidentate ligands causing self-ionisation to produce cationic species such as $[MX_2(bidentate)]^+$ and the corresponding halometalate anion $[MX_4]^-$. To achieve coordination of nitrogen donors such as bipy, phen and terpy to the Group 13 metal halides harsh hydrothermal conditions were required due to the lack of reactivity as in inert polymeric species. Although Cl^-/F^- halide exchange of $[MX_3(R_3\text{-tacn})]$ (M = Al, Ga, In; X = Cl, Br; R = Me, $BzMe_2$),[2] the production halide abstraction and replacement with weakly coordinating anions is lesser known. Using a starting material that incorporated a weakly coordinating anion such as triflate, allowed for the exploration of how this may change the chemistry observed upon

reaction. Substitution of a labile triflate anion would lower the energy required to break the strong M-F bonds and may allow for new routes to the fluoride complexes, using less harsh synthetic conditions.

Both neutral and cationic complexes of the metal triflates were synthesised with the different polypyridyl ligands, with coordination of the nitrogen donor ligands confirmed by NMR spectroscopy. A number of structural examples were produced by crystallography of crystals grown that showed the retention or displacement of the triflate anion. The mono, di and tri-cationic species were more readily produced using the triflate starting material with trace water being enough to produce the aquo-complex. Analysis *via* $^{19}F\{^{1}H\}$ spectroscopy consistently produced a single sharp resonance at -79.4 ppm (in CD_3CN), suggesting that in solution the complex dissociates, giving a single resonance of ionic triflate. This may also give some explanation as to why these complexes are more readily soluable in stronger donating solvents such as MeCN, with the true nature of the complex in solution being rapid exchange of $[M(MeCN)_2(bidenate)_2]^{3+}$ (M = Al, Ga, In).

Exploration of the literature on the Group 13 triflates is limited, so much of the comparison is to that of a metal halides and the nitrogen donor complexes produced in the previous chapter. Early studies into the coordination of oxygen donor ligands to the non-transition metal halides was undertaken in the early 1960s and explored the change in P=O stretching frequency of complexes with a change in acceptor molecule.[3] The change in Lewis acidity of the metal halide selected gave a change in the observed P=O stretching frequency upon coordination, giving a negative shift to lower wavenumbers than the starting material at 1190 cm^{-1}.[4] This reported the production of $[AlCl_3(OPPh_3)]$, $[GaCl_3(OPPh_3)]$ and $[InCl_3(OPPh_3)_2]$ and showed an averaged shift of ~ -34 cm^{-1}. Using VSEPR and the vibrational spectroscopy collected, it was suggested that these complexes formed with a tetrahedral geometry.[5,6] It was not until later, in 1990, that the crystal structure for $[GaCl_3(OPPh_3)]$ was reported and shown in Figure 3.1.

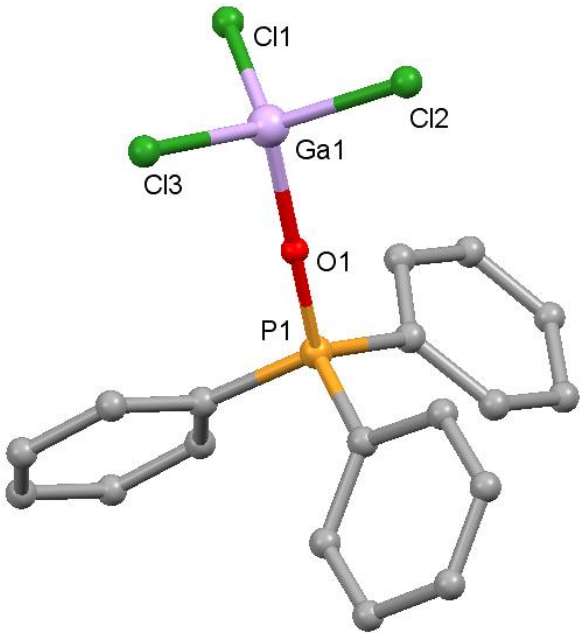

Figure 3.1 - Crystal structure of $[GaCl_3(OPPh_3)]$ showing the atomic numbering scheme. Redrawn from Ref[7] with H-atoms omitted for clarity.

The complexes $[MCl_3(OPPh_3)]$ (M = Al, Ga) and $[AlBr_3(OPPh_3)]$ are isostructural, with each noted to have a uniquely linear M-O-P angle when compared to corresponding BF_3 adducts, which has an angle of 134.5(2)°.[7,8] Structures of complexes formulated as $[MX_3(OPR_3)]$ are commonly seen in the P-1 space group, however, those with this linearized bond were reported in R-3. The P=O-M framework of the complex is found to lay on a crystallographic three-fold axis, with oxygen disorder that was not possible to resolve satisfactorily. A comparative study between the harder, oxygen donating phosphine oxide ligands and the softer phosphine and arsine donors to a GaX_3 was undertaken. This showed that coordination of the harder oxygen donor is preferential, suggesting that $GaCl_3$ is a rather hard Lewis acid.[9]

Comparing the coordination of $OPMe_3$ to the different gallium halides GaX_3 (X = Cl, Br, I), the chemical shift of the $^{31}P\{^1H\}$ resonance falls as the group is descended: Cl > Br > I. Each reaction was carried out in CH_2Cl_2 and in a 1:1 molar ratio between $OPMe_3$ and GaX_3 (X = Cl, Br, I) with spectroscopic analysis suggesting the formation of $[GaX_3(OPMe_3)]$. Although the spectroscopy of $[GaI_3(OPMe_3)]$ gave no evidence of a halometalate anion, layering a CH_2Cl_2 solution with *n*-hexane produced a small number of crystals which were shown to correspond to the ionic species $[GaI_2(OPMe_3)_2][GaI_4]$ with the structure redrawn in Figure 3.2. This structure revealed coordination of two phosphine oxides to form the cation $[GaI_2(OPMe_3)_2]^+$ with the monocationic halometalate anion.

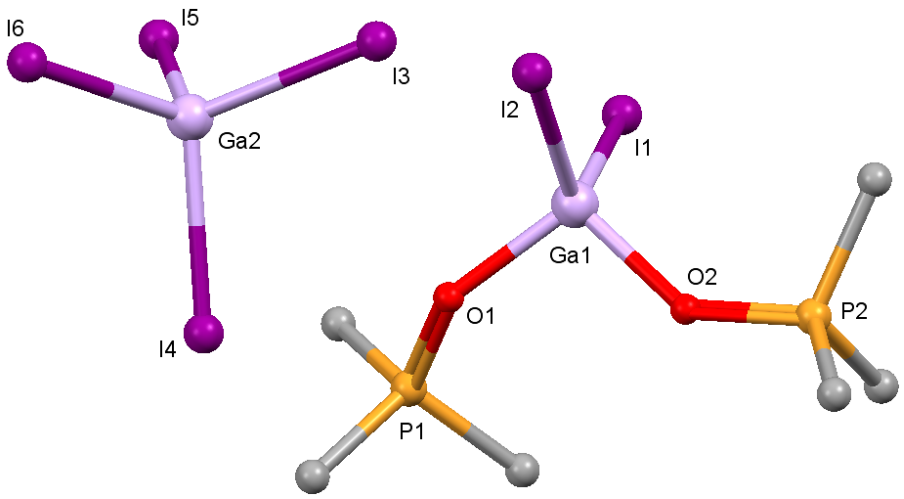

Figure 3.2 - Crystal structure of $[GaI_2(OPMe_3)_2][GaI_4]$ showing the atomic numbering scheme. Redrawn from Ref[9] with H atoms omitted for clarity.

Robinson *et al* went on to report the synthesis of a series of complexes of $InCl_3$ with coordination of two or three equivalents of $OPMe_3$ ligand.[10] Using IR spectroscopy and X-ray crystallography, it was shown that the *tris* product *mer*-$[InCl_3(OPMe_3)_3]$ takes up an octahedral geometry. Addition of only two equivalents of $OPMe_3$ produced a product that did not crystallise and IR spectroscopy showed the presence of $[InCl_4]^-$ suggesting self-ionisation to form $[InCl_2(OPMe_3)_4][InCl_4]$.

However, repeating of this reaction using MeOH as a solvent produced crystals of an octahedral complex *fac*-$[InCl_3(OPMe_3)_2(MeOH)]$. This methanol could be reversibly substituted for water through exposure of the sample to atmospheric oxygen when crystallising. When the methanol was not present, the product reverted back to the ionic product above. Further addition of $OPMe_3$ to this sample with water or methanol reproduced the *tris* product $[InCl_3(OPMe_3)_3]$ in the octahedral geometry. When using the phenyl substituted $OPPh_3$ in a 3:1 reaction with $InCl_3$ an ionic product was formed giving striated crystals unsuitable for crystallography.

A structural study on the complexes of the indium(III) halides with trimethylphosphine and arsine sulphides was later carried out by Robinson, to compare the use of the hard oxygen donors with the softer sulphur donors.[11] Reaction of InX_3 (X = Cl, Br) with $SEMe_3$ (E = P, As) in a 1:2 ratio produced a series of complexes $[InX_3(SEMe_3)_2]$ (X = Cl, Br; E = P, As) where a trigonal bipyramidal geometry was taken up, as seen in Figure 3.3. These complexes were synthesised in dry acetone and crystallised as isomorphic solids in the $P2_1/n$. Crystallisation of these samples while open to atmospheric moisture was found to produce the hydrated complex $[InCl_3(OH_2)(SAsMe_3)_2]$, an octahedral species with water filling the vacant coordination site.

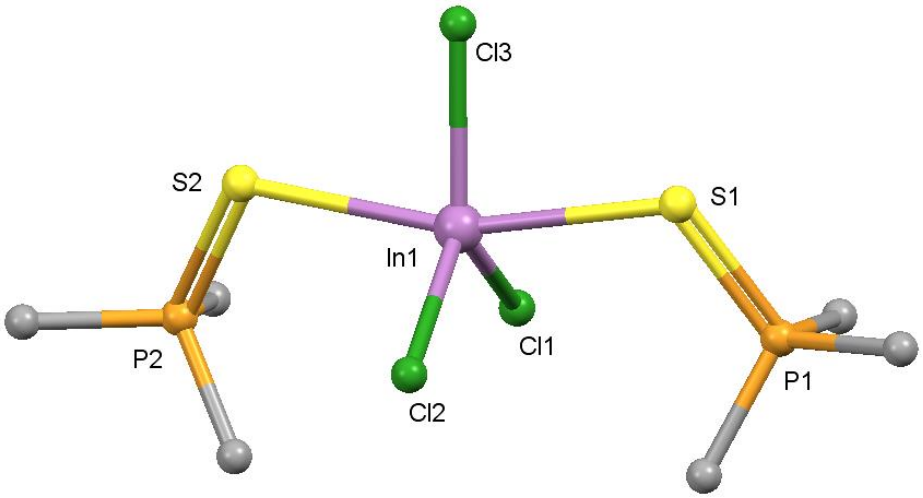

Figure 3.3 - Crystal structure of $[InCl_3(SPMe_3)_2]$ showing the atomic numbering scheme. Redrawn from Ref[11] with the H-atoms omitted for clarity.

There was a decrease in In-S bond length from 2.607 Å to 2.598 Å upon coordination of the water to $[InCl_3(SAsMe_3)_2]$, a very slight strengthening of these In-S bonds with coordination of the water molecule, likely to do with more electron density being available around the metal centre. The presence of water in the complex was observed by its characteristic peaks in the IR spectrum at 3380 and 1620 cm^{-1}. This change was reversible with the addition of a dehydrating agent triethoxymethane (tem) solution causing the water to be removed, reforming the initial compound. Although less common, this trigonal bipyramidal structure was also observed for $[InCl_3(THF)_2]$, formed through the stoichiometric reaction of $InCl_3$ and THF.[11] Later, it was observed that use of excess THF gave the *mer*-$[InCl_3(THF)_3]$ in a good yield.[12]

As aforementioned in Chapter 1, the later elements of the group have a higher stability in the +1 oxidation state due to the inert lone pair effect and are also a softer Lewis acids. The coordination chemistry of thallium is more limited than that of the ligher metals, however despite these factors, coordination of both phosphine and the harder phosphine oxides have been achieved.[13] Reaction of $TlBr_3$ with two equivalents of $OPPh_3$ gave needle crystals that upon analysis showed the five coordinate structure $[TlBr_3(OPPh_3)_2]$.[14] The same geometry was also shown in the mixed halide complex $[TlCl_2I(OPPh_3)_2]$; in each case the phosphine oxide ligands were found *trans* with the central halides maintaining a near to 120° equatorial angle.[15]

Coordination of trimethyl- or triphenylphosphine oxides has not been observed to the inert metal fluorides, even under hydrothermal conditions. Treatment of the hydrated metal fluoride $MF_3{\cdot}3H_2O$ (M = Al, Ga, In) with dimethyl sulfoxide (DMSO) at +70°C substituted one of the aquo ligands for DMSO, with no evidence of further substitution after prolonged reflux. This solvated material had greatly increased reactivity, allowing for the coordination of Me_3tacn and bipy at room temperature, which previously required hydrothermal synthesis. Although this solvate complex $[MF_3(OH_2)_2(DMSO)]$ did not react with OPR_3 (R = Me, Ph), it did undergo substitution of

the solvent with pyridine *N*-oxide (pyNO) to produce the products $[GaF_3(OH_2)_2(pyNO)]\cdot pyNO\cdot H_2O$ and $[AlF_3(OH_2)_2(pyNO)]$.[16] This suggested a stronger donor than the commonly used phosphine oxides and this strength allowed access to different chemistry by displacement of DMSO, something which OPR_3 (R = Me, Ph) was not capable under the conditions explored. Pyridine *N*-oxide is another neutral oxygen donor ligand comparable to OPR_3 (shown in Figure 3.4), both of which are oxygen donor ligands where the coordinating atom is bonded to a pnictine atom.

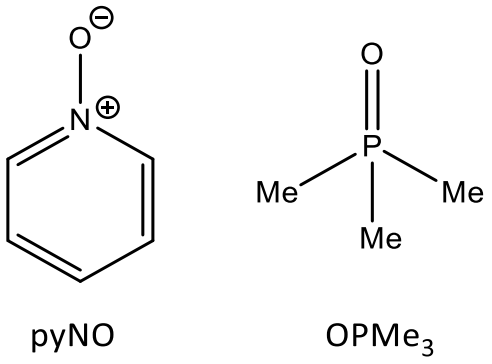

Figure 3.4 - Structures of pyNO and $OPMe_3$, the two monodentate ligands utilised in this chapter of work.

It is hoped that the increased donor strength coupled with the lability of the triflate anion may open the door for new chemistry, differing from that shown by $OPMe_3$ under the same conditions. The examples of coordination of pyridine *N*-oxide are limited within Group 13, primarily focused on the heavier elements of the group to help stabilise these when in low-valent oxidation states. The molecular thallium(III) halide complexes that have been synthesised with pyridine *N*-oxide have been shown to adopt the trigonal bipyramid as expected, being shown with a range of substituted pyNO derivatives.[17–19] When the oxidised form of 4,4'-bipyridine is reacted with salts of the late main group metals (Tl, Pb), coordination polymers can be formed and due to the extended π–systems have promising properties for luminescence and low-energy emissions.

The bidentate phosphine oxide ligand *o*-$C_6H_4(CH_2P(O)Ph_2)_2$ was studied by reaction with 2 equivalents of $GaBr_3$ to produce the bridged species $[(GaBr_3)_2\{o\text{-}C_6H_4(CH_2P(O)Ph_2)_2\}]$ with 2 tetrahedral metal centres, the structure of which has been redrawn in Figure 3.5.[9] In this case, the ligand acts as a bridging species between two gallium(III) metal centres with no evidence of chelating coordination to a single metal. The strongly bound halides are not displaced by the weaker coordinating ability of the bulky phenylene backed ligand. As was discussed in Chapter 1.2.2, the aryl phosphine ligands are weaker σ-donors than alkyl analogues. Coordination of this ligand to the single metal centre would form a destabilising 9-membered chelate ring, coupled with the steric bulk of the phenyl rings lowers the stability of this conformer. These factors, on top of the strength of the M-X bond cause bridging behaviour to be observed instead of chelation.

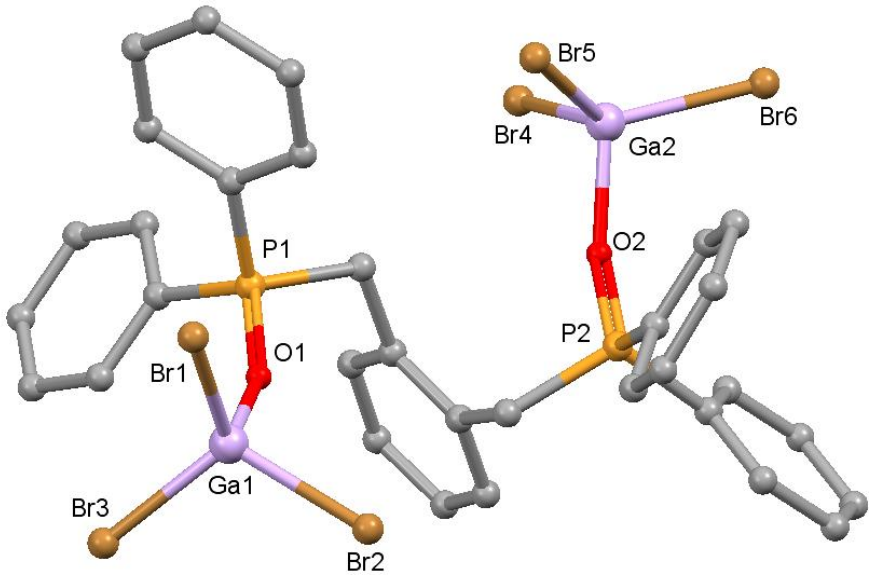

Figure 3.5 – Crystal structure of $[(GaBr_3)_2\{o\text{-}C_6H_4(CH_2P(O)Ph_2)_2\}]$ showing the atomic numbering scheme. Redrawn from Ref[9] with H-atoms omitted for clarity.

Interestingly, coordination of the softer phosphine ligand *bis*-(dimethylphosphino)ethane (dmpe) to GaX_3 (X = Cl, Br) or $AlCl_3$ produced $[MCl_2(dmpe)_2][MCl_4]$ (M = Al, Ga)[20,21] The increased donor strength due to the alkyl R-groups and smaller steric bulk allows for the stability of chelation to overcome the M-X bond strength and produce the cationic species. This would also form a 5-membered chelate ring upon coordination, known for being a relatively stable in the envelope conformation.

Another neutral bidentate phosphine oxide ligand previously explored with the $AlCl_3$ was *bis*-(diphenylphosphino)methane dioxide ($dppmO_2$), exhibiting the same bridging behaviour to produce $[(AlCl_3)_2\{\mu^2\text{-}dppmO_2\}]$. As was observed in Figure 3.5, two tetrahedral metal centres were found with the $dppmO_2$ bridging the two with a bend at the central carbon to minimised destabilising interactions of the phenyl R-groups.[22] Commonly, due to the chelate effect, $dppmO_2$ is shown to form a 6-membered chelate ring with the metal, take up a chair/boat geometry and limit destabilising intramolecular interactions.

More recently, $dppmO_2$ has been used to explore the effect of denticity on the bonding and how it could be compared with the monodentate OPR_3 ligands previously explored and the limits of coordination numbers.[23,24] This has been utilised with transition metal as well as lanthanide chemistry due to their affinity to this type of oxygen donor however, the research in the *p*-block is limited with only 3 examples of Group 13 coordination.[25] There is a low number of main group complexes that incorporate $dppmO_2$ however, the reaction of $dppmO_2$ with $TlCl_3$ produced a self-ionised, co-crystallised complex $[TlCl_2(dppmO_2)][TlCl_4]$ in an octahedral geometry equatorial dppmO2 ligands.[26] A few years later a similar reaction took $[Tl(C_6F_5)_2Cl]$ and produced a *trans* octahedron $[Tl(C_6F_5)(dppmO_2)_2][Tl(C_6F_5)_2Cl_2]$ again, co-crystallised with a tetrahedral mixed

thallate counter ion.[27] Both of these were crystallised in the *trans* geometry with regards to the coordinated anions and a tetrahedral thallate anion with no evidence of a 'free' anion being present. $DppmO_2$ has also been reacted with gallium(III) nitrate in a 3:1 ratio to produce a mononuclear homoleptic octahedral Ga(III) centre encapsulated in a shell of three bidentate ligands; $[Ga(dppmO_2)_3][NO_3]_3$.[28] This cation has no association with the nitrate anions with the whole complex being encapsulated in a 'shell' of ligand backbone with no additional coordination sites. Upon comparison of the Ga-O bond distances from the trication $[Ga(dppmO_2)_3]^{3+}$ with those found in $[(GaBr_3)_2\{o\text{-}C_6H_4(CH_2P(O)Ph_2)_2\}]$, it was found that bridged species contained shorter Ga-O bond lengths than the *tris*-tricationic species. This is likely due to the steric bulk the additional ligands coordinated to a single metal centre; producing destabilising interactions within the complex.

This chapter explores the coordination of neutral oxygen donor ligands to the Group 13 metal triflates to investigate how this changes when moving away from strongly coordinating anions such as halides and how this affects the nature of the complexes formed. This will include the monodentate donors OPR_3 (R = Me, Ph) and pyNO as well as the bidentate ligand $dppmO_2$ to explore denticity, donor strength and steric bulk. Coordination to the halides has previously produced neutral complexes with retention of the halide anions $[MX_3(OPR_3)]$ or displacement of a halide to form cation $[MX_2(L)_2]^+$ and the corresponding halometalate anion. It is hoped that the lability of the triflate anion will allow for displacement and thus further ligands to be added to the metal centre in the form of new cationic species, as was observed with the coordination of $dppmO_2$ to $Ga(NO_3)_3$. Incorporation of labile anions could allow for later addition of additional ligand equivalents or a different, secondary ligand to produce complexes with mixed ligand species. Here, only simple donors have been explored to get an understanding of how the Group 13 triflate reacts and the geometry/bonding that can be achieved. Formation of both neutral compounds $[M(OTf)_3(terpy)]$ and cationic species $[M(OTf)_2(L)][OTf]$ (L = bipy, phen) in the previous chapter suggested that these complexes synthesised with O donors may also take up a octahedral geometry. Using the same wet starting material will likely manifest as the primary coordination sphere being filled with a mixture of triflate, adventitious water or a donor solvent (MeCN) as was seen in a number of the imine complexes.

3.2 – Results and Discussion

As was described in Chapter 1.2.2, Bis-(diphenylphosphino)methane dioxide ($dppmO_2$) is not commercially available and so was synthesised prior to use *via* Scheme 3.1. This was synthesised using a modified procedure described by Levason, which described oxidation of aryl-phosphines by catalytic oxidation using tin(IV) iodide as a catalyst.[29]

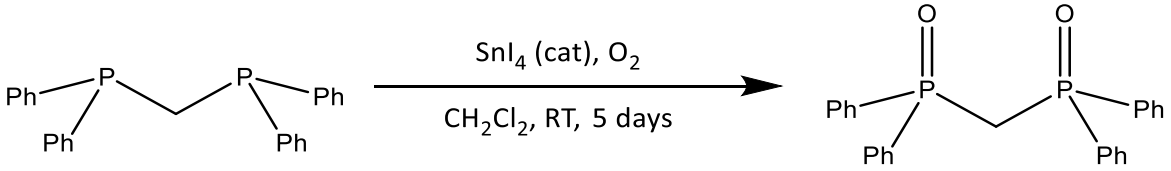

Scheme 3.1 - Oxidation of dppm using atmospheric O_2 with a SnI_4 catalyst, as reported by Levason.[29]

The reported the oxidation of PPh_3, o-$C_6H_4(PPh_2)_2$ and $Ph_2PCH_2CH_2PPh_2$ with atmospheric dioxygen using catalytic amounts of SnI_4 in dichloromethane over a period of 5 days. This method avoids the potential hazards associated with using H_2O_2 to perform this oxidation and gives a cleaner route to the final oxidised product. The reaction was deemed complete by $^{31}P\{^1H\}$ NMR analysis of the crude product, showing a shift in the resonance from -22.7 to 25.3 ppm. The report described purification of the product by recrystallization from ice cold ethanol, however, in the case of oxidation of $dppmO_2$ it was found that recrystallization from acetone gave a cleaner product. This method produced large crystals of $dppmO_2$ in a high yield with no detectable catalyst remaining in the bulk solid. Upon NMR analysis of the product, it was deemed 'clean' by ^1H and $^{31}P\{^1H\}$ NMR and free of unreacted starting material while IR spectroscopy showed no remaining tin(IV) iodide catalyst. In Figure 3.6 is shown the ^1H and $^{31}P\{^1H\}$ NMR spectra of the freshly produced $dppmO_2$, free from dppm starting material. After synthesis, the $dppmO_2$ was then reacted with $M(OTf)_3$ in both a 2:1 and 3:1 molar ratio with crystal structures being obtained for both $[M(dppmO_2)_3][OTf]_3$ (M = Al, Ga), shown in Scheme 3.2.

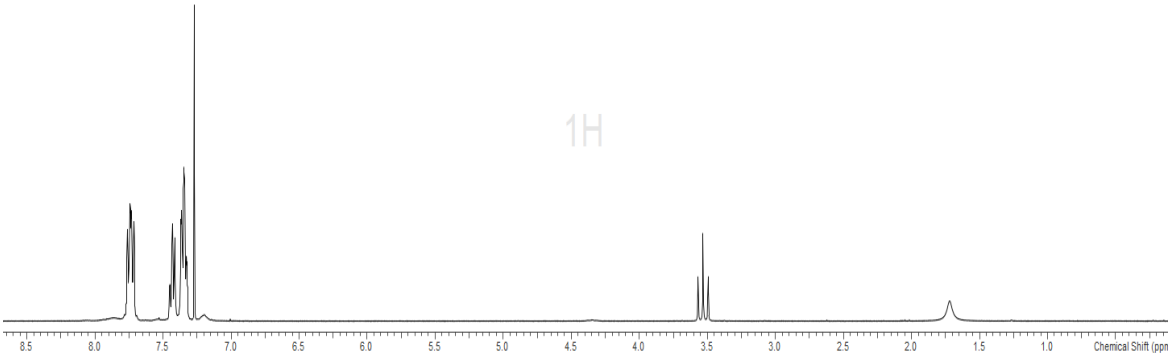

(a)

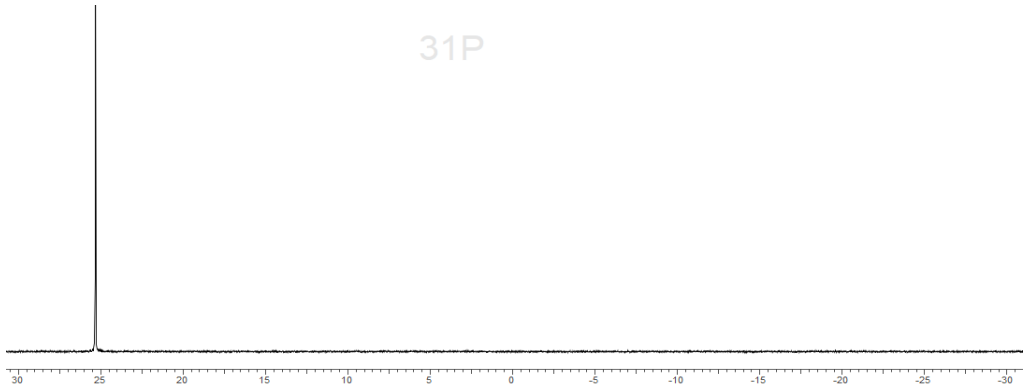

(b)

Figure 3.6 – (a) ^{1}H with the methylene bridge protons at and 3.45 ppm (dppm = 2.95 ppm) and (b) $^{31}P\{^{1}H\}$ NMR spectrum of $dppmO_2$ with a resonance at 25.3 (dppm = -22.7 ppm).

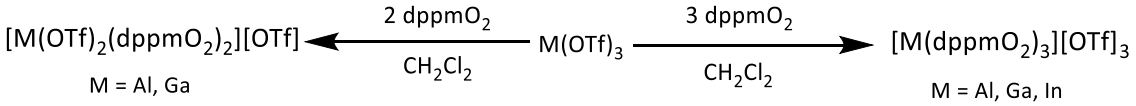

Scheme 3.2 - Reaction scheme for the formation of complexes involving $dppmO_2$.

The reaction of $M(OTf)_3$ (M = Al, Ga, In) with two molar equivalents of $dppmO_2$ yielded white powders in high yield. Analysis of these by both ^{1}H and $^{31}P\{^{1}H\}$ NMR spectroscopy showed the complexes $[M(OTf)_2(dppmO_2)_2][OTf]$ (M = Al, Ga) to only contain a single product with a single sharp resonance observed in both NMR spectra. The indium analogue however, was shown to produce mixtures of products each time the reaction was repeated. These could be mixtures of the *mono-, bis* and *tris* products but identification was never attempted. In both the Ga and Al case, a single sharp resonance was observed in the $^{31}P\{^{1}H\}$ at a higher frequency than free $dppmO_2$, found at 25.3 ppm.[30] As well as this single phosphorus resonance, the ^{1}H NMR spectrum shows the methylene bridge protons between the phosphorus centres which appears as a sharp triplet resonance at 3.53 ppm for the free ligand. This methylene resonance undergoes a high frequency shift upon coordination of the ligand and appears at 4.25 ppm in $[Ga(OTf)_2(dppmO_2)_2][OTf]$. A comparison of both the methylene ^{1}H and $^{31}P\{^{1}H\}$ NMR resonances for this series of $dppmO_2$ complexes is shown in Table 3.1. Microanalysis of both *bis* complexes matched the formulation of $[M(OTf)_2(dppmO_2)_2][OTf]$ (M = Al, Ga) had been synthesised.[31]

Table 3.1 - Table showing a comparison of the metal NMR, $^{31}P\{^{1}H\}$ and ^{1}H NMR resonances of the methylene bridge of $dppmO_2$ complexes produced.

Compound	Methylene Bridge ^{1}H NMR Shift / ppm	$^{31}P\{^{1}H\}$ NMR Shift / ppm	$^{27}Al/^{71}Ga$ NMR Shift / ppm
$dppmO_2$	3.48	25.33	-
$[Al(dppmO_2)_3][OTf]_3$	4.15	44.20	-9.30
$[Al(OTf)_2(dppmO_2)_2][OTf]$	4.17	42.72	-8.27
$[Ga(dppmO_2)_3][OTf]_3$	4.27	46.29	-43.4 (br)
$[Ga(OTf)_2(dppmO_2)_2][OTf]$	4.25	44.82	Not Observed
$[In(dppmO_2)_3][OTf]_3$	4.52	48.01	Not Observed

Attempts to crystallise $[Al(OTf)_2(dppmO_2)_2][OTf]_2$ through layering a chloroform solution of the complex with *n*-hexane, produced the *tris*-$dppmO_2$ coordinated tri-cationic species $[Al(dppmO2)_3][OTf]_3$ shown in Figure 3.7(a). Repeating this method using the gallium complex produced the isomorphous crystal structure shown in Figure 3.7(b). In attempt to produce crystals of the *bis*-product differing solvent systems such as layering of *n*-hexane to a CH_2Cl_2 solution and slow vapour diffusion of Et_2O into an MeCN solution was tried. Each of these attempts was shown to only produce the *tris*-chelate complex with the structure of $[M(OTf)_2(dppmO_2)][OTf]$ unknown at this time. In transition metals, *bis*-chelate complexes of $dppmO_2$ have been shown to take up both *cis* and *trans* conformers, with the electronics of the metal centre and the availability of the *d*-orbital for bonding dictating the final conformation.

These complexes were in a near perfect octahedral geometry with bond angles around the metal differing by < 2°, coordinated by three molecules of $dppmO_2$. The three triflate anions were dissociated from the metal and free from coordination with the closes triflate contact being 6.636(2) Å, significantly over the sum of the van der Waals radii. Depending on the solvent system used, at least one molecule was co-crystallised with these complexes. These structures are also isomorphous to the *tris*-$dppmO_2$ trication $[Ga(dppmO_2)_3]^{3+}$ had previously been synthesised using the nitrate salt by Tunik *et al*.[28]

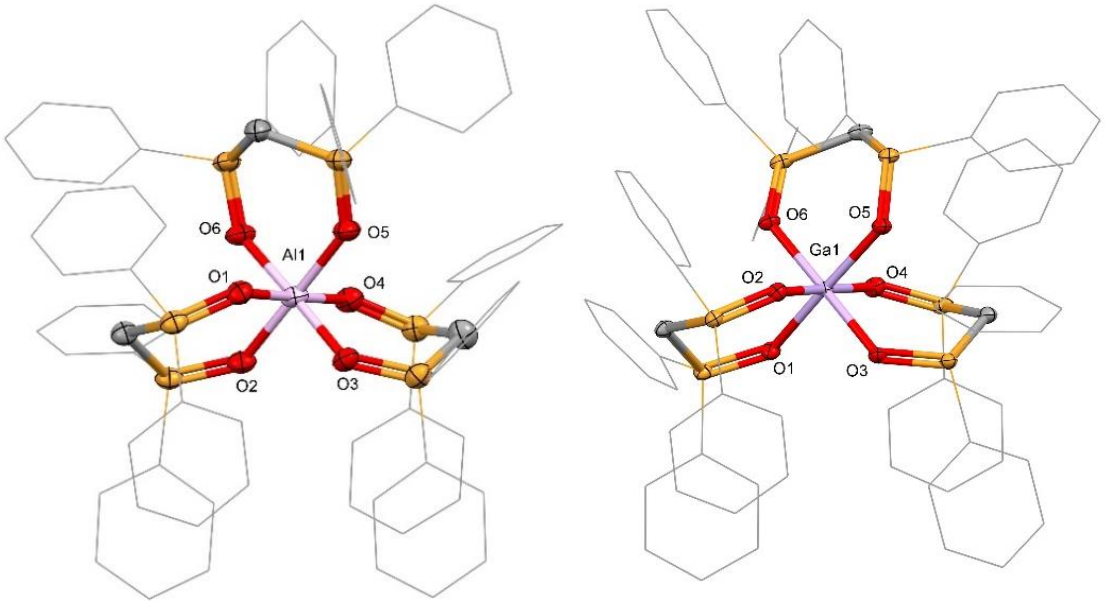

(a) (b)

Figure 3.7 - Crystal structures (a) ***6*** $[Al(dppmO_2)_3][OTf]_3$ and (b) ***7*** $[Ga(dppmO_2)_3][OTf]_3$ showing the atom numbering schemes. Ellipsoids shown at 50% probability with H-atoms, anions and lattice solvent molecules omitted for clarity.

Table 3.2 - Selected bond lengths and angles for $[Al(dppmO_2)_3]$ and $[Ga(dppmO_2)_3]$.

Bond Lengths / Å			Bond Angles / °	
$[Al(dppmO_2)_3][OTf]$	Al1 – O1	1.915(2)	O1 – Al1 – O2	91.0(1)
	Al1 – O2	1.870(2)	O2 – Al1 – O3	90.9(1)
	Al1 – O3	1.866(2)	O3 – Al1 – O4	91.1(1)
	Al1 – O4	1.903(2)	O4 – Al1 – O5	91.0(1)
	Al1 – O5	1.889(2)	O5 – Al2 – O6	91.7(1)
	Al1 – O6	1.881(2)	P – C – P	110.99(2) – 113.3(2)
	P – O	1.509(2) – 1.512(2)	Al – O – P	134.2(1) – 137.8(1)
$[Ga(dppmO_2)_3][OTf]$	Ga1 – O1	1.937(1)	O1 – Ga1 – O2	92.63(6)
	Ga1 – O2	1.946(1)	O2 – Ga1 – O3	87.32(6)
	Ga1 – O3	1.957(1)	O3 – Ga1 – O4	90.74(6)
	Ga1 – O4	1.964(1)	O4 – Ga1 – O5	88.21(6)
	Ga1 – O5	1.968(1)	O5 – Ga2 – O6	90.51(6)
	Ga1 – O6	1.964(1)	P – C – P	112.7(1) – 113.5(1)
	P – O	1.516(1) – 1.527(1)	Ga – O – P	131.61(9) – 136.10(9)

Following this, the reaction of three equivalents of $dppmO_2$ with $M(OTf)_3$ (M = Al, Ga, In) was attempted under the same conditions and produced a white solid that was spectroscopically different from the respective $[M(OTf)_2(dppmO_2)_2][OTf]$ complexes. Again, a single $^{31}P\{^1H\}$ NMR resonance was observed at a slightly higher frequency than the *bis*-product. Similarly, the ^1H NMR spectrum shows the methylene bridge resonance has shifted to a higher frequency than the *bis*-product, with the NMR resonances for this series shown in as can be seen in Table 3.1. Due to the additional high frequency shift, it was thought that these complexes correspond to the expected tricationic complexes $[M(dppmO_2)_3][OTf]_3$. $^{31}P\{^1H\}$ and ^1H NMR spectroscopy of the *tris*-chelate complexes $[M(dppmO_2)_3][OTf]$ (M = Al, Ga, In) produced here show shifts at a higher frequency than the free ligand and the *bis*-chelate, which has been highlighted in the table above. Both the *bis*-complexes $[M(OTf)_2(dppmO_2)_2][OTf]$ produced $^{31}P\{^1H\}$ NMR resonances at roughly 2 ppm lower than the respective *tris*-complex $[M(dppmO_2)_3][OTf]_3$. There also appears to be a shift to higher frequency when descending the pniticine metals with $[In(dppmO_2)_3][OTf]_3$ producing the highest frequency $^{31}P\{^1H\}$ resonance at 48.01. Comparison of $[Ga(dppmO_2)_3][OTf]_3$ with the previously synthesised nitrate analogue showed an almost identical $^{31}P\{^1H\}$ resonance.[28] This was also the case with the protons of the methylene bridge. Each of the three metals being explored are NMR active so, due to the high symmetry of the complexes, collection of the respective metal NMR was attempted for each complex $[M(dppmO_2)_3][OTf]_3$ (M = Al, Ga, In). Resonances were produced by the aluminium and gallium complexes but despite using a high number of scans, the indium complex did not produce a resonance. The ^{27}Al NMR spectrum of $[Al(dppmO_2)_3][OTf]_3$ contained a single sharp resonance at -9.30 ppm, a negative shift of ~20 ppm from the complexes of nitrogen donors $[Al(OTf)_2(bipy)_2][OTf]$ in Chapter 2. This chemical shift is within the expected range for a six-coordinate Al metal centre with oxygen donors.[32] The previously synthesised $[Ga(dppmO_2)_3][NO_3]_3$ was reported with a ^{71}Ga NMR resonance at -41 ppm, the ^{71}Ga NMR spectrum of the triflate salt was found slightly more negative at -43 ppm.[28] The ^{71}Ga resonance for $[Ga(dppmO_2)_3][OTf]$ was weak and broad (3500 Hz) even after ~6000 scans, broadened by the relaxation of the quadrupolar nuclei. Of the *bis*-$dppmO_2$ complexes, only $[Al(OTf)_2(dppmO_2)][OTf]$ produced a resonance with a single sharp peak being observed at -8.72 ppm, shifted slightly to a higher frequency than $[Al(dppmO_2)_3][OTf]_3$. In Chapter 2, $[Al(OTf)_2(bipy)_2][OTf]$ was also seen as the only metal NMR obtained, with the other nuclei showing no resonance after extended scans. The imine complex produced a resonance at 12.8 ppm, mirroring the *tris*-complexes discussed above with the oxygen donors producing a resonance ~20 ppm more negative. Attempts at ^{71}Ga NMR spectroscopy of $[Ga(OTf)_2(dppmO_2)_2][OTf]$ failed to produce a resonance at room temperature with variable temperature NMR was not explored at this time. There is a significant drop in the symmetry moving from the *tris*-$dppmO_2$ complex to the *bis*-complex this is likely broadens the resonance to a point that it is no longer resolved.

IR spectroscopy was used to probe the P=O bond of the $dppmO_2$ ligand, within each of the three $[M(dppmO_2)_3][OTf]_3$ (M = Al, Ga, In) complexes synthesised and how coordination to each metal affected the bonds vibrational frequency. It also revealed that each of these complexes were isolated free of the water that was associated with the metal triflate starting materials. The for each of the *tris*-$dppmO_2$ complexes was observed as a single peak at 1121, 1132 and 1137 cm^{-1} for the Al, Ga and In complexes respectively. As the group is descended, a smaller shift was observed from to free ligand. The IR spectra allowed for tracking of the P=O absorption band to a low wavenumber than free ligand (1162 cm^{-1}) being observed for each complex suggesting coordination had been achieved in each case. Comparison of these values observed for each *tris* complex with the spectra for the isolated *bis* $dppmO_2$-complex of Al and Ga show no significant shift in the absorption band, being within the 4 cm^{-1} instrument resolution.

Once coordination of bidentate phosphine oxide had been achieved, attempts to form neutral *tris* complexes using monodentate phosphine oxide species, $[M(OTf)_3(OPR_3)_3]$ were undertaken. As discussed in the introduction to this chapter, previous literature reported the synthesis of both $[InCl_3(OPMe_3)_2$ and $[InCl_3(OPMe_3)_3]$ with only the latter being structurally characterised.[10] The solid state nature of $[InCl_3(OPMe_3)_2]$ is unknown but does show evidence of $[InCl_4]^-$ in the IR spectrum. Complexes of the other Group 13 metals with phosphine oxide ligands has not been reported.

The reaction of the Group 13 metal triflates $M(OTf)_3$ (M = Al, Ga, In) with three molar equivalents of OPR_3 (R = Me, Ph)in CH_2Cl_2 for two hours afforded high yields of white $[M(OTf)_3(OPR_3)_3]$. $^{31}P\{^1H\}$ NMR spectroscopy of each of these complexes showed a single resonance in each spectra, shifted to a high frequency from the respective free ligand ($OPMe_3$ = 38.5 ppm; $OPPh_3$ = 27.5 ppm).[33] The complexes of the stronger trimethyl donor ligand ranged from 60.87 – 66.62 ppm with a higher chemical shift as Group 13 was descended (Al-In). The same pattern was observed for the complexes of triphenylphosphine $[M(OTf)_3(OPPh_3)_3]$, ranging from 42.48 – 45.87 ppm. Microanalysis of these complexes matched their calculated values within 0.4%, with some being formulated to include residual CH_2Cl_2 solvent. This was confirmed by the presence of small amounts of CH_2Cl_2 in the ^1H NMR spectra of a number of these complexes. The ^1H NMR spectra of these complexes also showed a high frequency shift of the ligand resonances and aided in identifying the presence of a single species when $OPMe_3$ was the coordinating ligand. Upon coordination of the OPR_3 ligands, the IR spectra showed a shift of the P=O stretching band to lower wavenumbers, as expected for coordination of a phosphine oxide ligand, and suggested that there was no unreacted ligand remaining in the isolated product. Commonly IR spectroscopy could be used to infer structural information however due to the presence of a number absorbance bands in the region of 1000-1400 cm^{-1} including, the S-O and C-F bands of the triflate

anion,[34] so the P=O stretching frequency were tentatively assigned. The triphenylphosphine complex $[M(OTf)_3(OPPh_3)_3]$ (M = Al, Ga, In) were assigned with ν(P=O) at 1156, 1143 and 1145 cm^{-1} going down the group respectively. The presence of water in the starting metal triflates was maintained throughout reaction and was present in the products as a broad absorption at ~3300 and a sharper absorption at ~1600.[35]

Attempts to crystals of the phosphine oxide complexes $[M(OTf)_3(OPR_3)_3]$ through a number of different crystallisation methods generally did not produce good quality crystalline solids, with commonly powders being precipitating. A small number of crystals were grown through the slow evaporation of a CH_2Cl_2 from solution of $[In(OTf)_3(OPPh_3)_3]$. These crystals were of a good quality and so analysed single crystal X-ray diffraction to reveal a co-crystallised species *trans*-$[In(OTf)_2(OPPh_3)_4][In(OH_2)_4(OPPh_3)_2][OTf]_4{\cdot}2CH_2Cl_2$, the structure of which is shown in Figure 3.8.

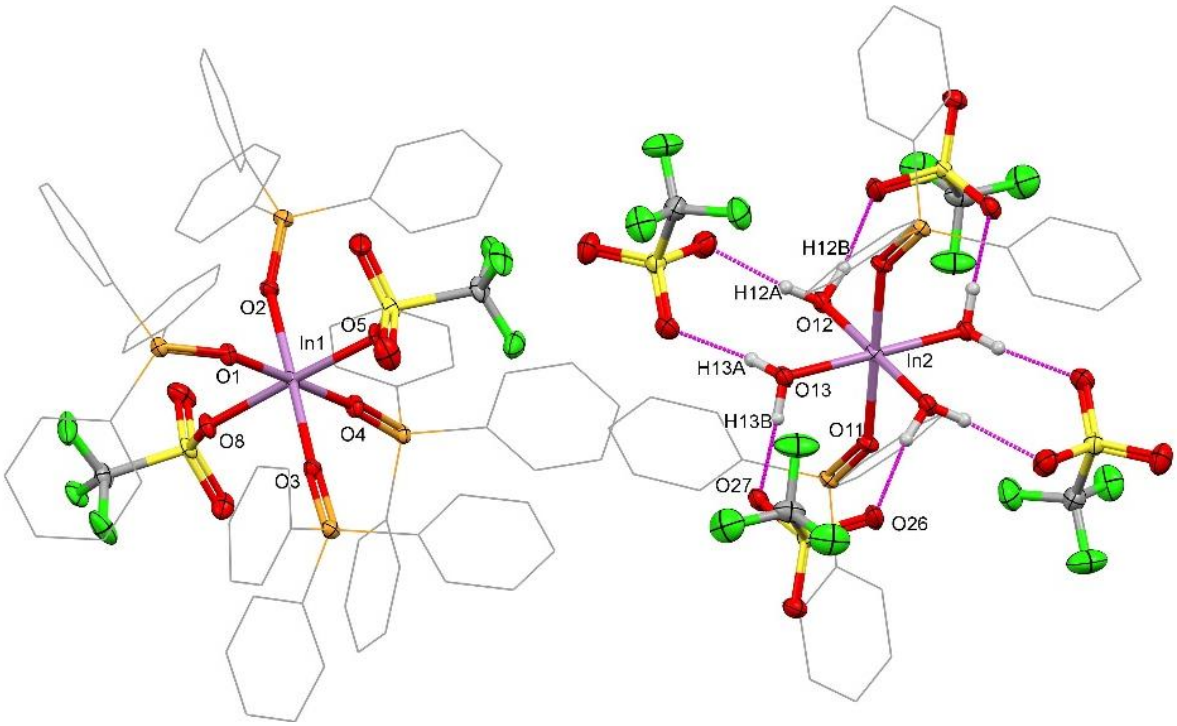

Figure 3.8 - Crystal structure of co-crystallised species ***8*** *trans*-$[In(OTf)_2(OPPh_3)_4][In(OH_2)_4(OPPh_3)_2][OTf]_4$ showing the atom numbering schemes. Ellipsoids shown at 50% probability with H-atoms are omitted for clarity, unless involved in H-bonding.

Table 3.1 - Selected bond lengths and H-bonding contact distances for the co-crystallised species *trans*-$[In(OTf)_2(OPPh_3)_4][In(OH_2)_4(OPPh_3)_2][OTf]_4$.

Bond Lengths / Å		Hydrogen Bonding Contact Distances / Å	
In1 – O1	2.1113(19)	O12 – O20	2.675(3)
In1 – O2	2.1154(19)	H12B – O20	1.862
In1 – O3	2.1139(19)	O12 – O26	2.641(3)
In1 – O4	2.1059(19)	H12B – O23	1.796
In1 – 05	2.1695(18)	O13 – O21	2.643(3)
In1 – O8	2.1695(18)	H13A – O21	1.834
In2 – O11	2.1009(18)	O13 – O21	2649(3)
In2 – O12	2.1553(19)	H13B – O21	1.866
In2 – O13	2.1487(18)		
P – O (In1)	1.507(2) – 1.518(2)		
P – O (In2)	1.515(2)		

This co-crystallised species still followed the expected 3:1 formulation of the stoichiometry being made up of one cationic indium centred species and one anionic. The cationic complex $[In(OTf)_2(OPPh_3)_4]^+$ takes up the a *trans* conformation with the $OPPh_3$ ligands found equatorially and two triflate anions in the axial positions. The second species in this co-crystallised structure is the tetra-aquo species $[In(OH_2)_4(OPPh_3)_2]^{3+}$, with each of the water ligands being involved in two hydrogen bonds to the triflate anions. As shown in Figure 3.8, the triflateanions are involved in H-bonds with two different water ligands of the tricationic complex forming a pseudo 24-membered macrocyclic ring, bonding equatorially through the oxygen donors of each of the 4 water molecules. The association of the triflate anions with this single cation of the co-crystallised species could be formulated as an $[In\{(OH_2)_4(OTf)_4\}(OPPh_3)_2]^-$ anion, instead of showing the triflate anions as purely ionic. The H-bonding between the aquo ligands and the oxygen donor atoms of the triflate anions undoubtedly contributes significantly to the overall stability of the complexes, and therefore provides a driving force for their formation/crystallisation, as opposed to retention of the coordinated triflate. Due to the lability of the *p*-block metals, the NMR spectra do not reflect the crystalline solid as displayed above in Figure 3.8.

Attempts to synthesise the complexes of $In(OTf)_3$ with 4 and 5 equivalents of $OPMe_3$ were carried out following the same procedure as the *tris*-complexes, reacting in CH_2Cl_2 for 2 hours. Analysis *via* ^1H and $^{31}P\{^1H\}$ NMR spectroscopy repeatedly showed these reactions produced mixtures of a major product (targeted ratio) and minor amounts of other complexes (± 1 $OPMe_3$) i.e. the $^{31}P\{^1H\}$

NMR spectrum of $[In(OTf)(Me_3PO)_5]^{2+}$ also contains a small amount of $[In(Me_3PO)_6]^{3+}$. The $^{31}P\{^1H\}$ NMR spectra of each reaction from 3:1 to 6:1 are shown in Figure 3.9 with each colour corresponding to a different equivalents of $OPMe_3$. This was also seen in the ^1H NMR spectra of these reactions, with both the major and minor products observed as sharp doublets, shifted to a higher frequency than that of the free ligand. Each of the doublets were measured to have a splitting frequency of ~13.5 Hz which is typical of a $^2J_{P-H}$ coupling, with little variation.

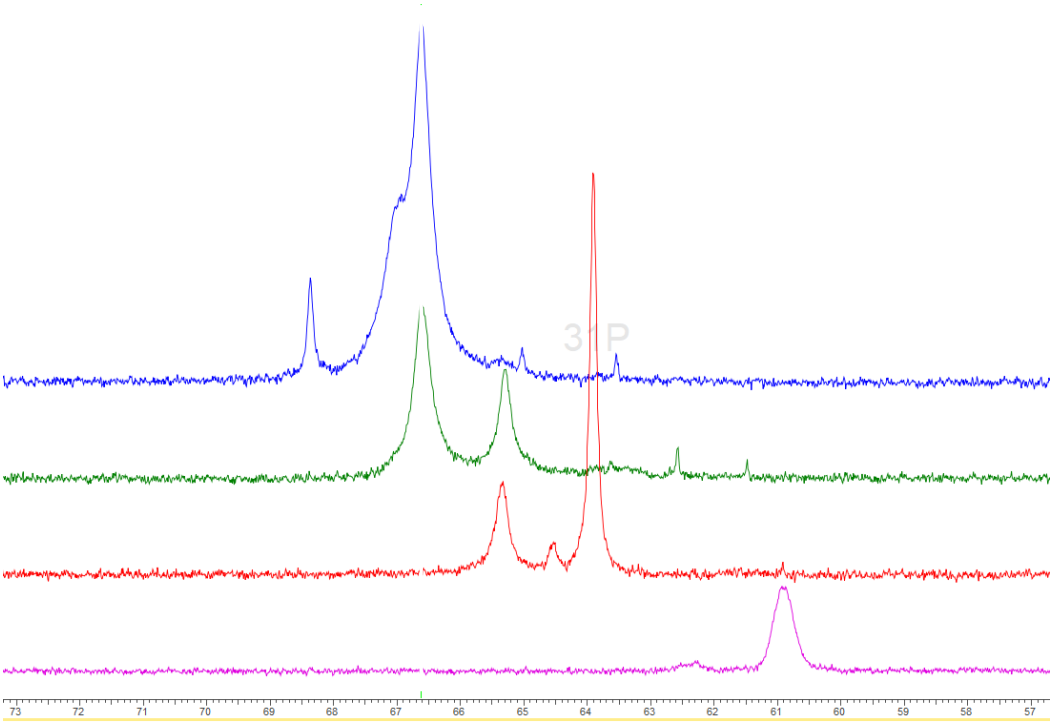

Figure 3.9 – Stacked $^{31}P\{^1H\}$ NMR spectra from the reactions of $In(OTf)_3$ with varying molar ratios of $OPMe_3$. (Blue = 3:1, Green = 4:1, Red = 5:1, Purple = 6:1). Peak assigned to the target complex by coloured *.

Although mixtures were observed with formation of the 4:1 and 5:1 complexes, $[In(OPMe_3)_6][OTf]$ was synthesised as a single species with relative ease, as can be seen by the $^{31}P\{^1H\}$ NMR spectrum (purple) in Figure 3.9. The reaction of $InCl_3$ with six molar equivalents of $OPMe_3$ was carried out in CH_2Cl_2 and precipitated a white powder that, upon microanalysis, was confirmed as $[In(OPMe_3)_6][OTf]_3$. The $^{31}P\{^1H\}$ NMR spectrum produced a single resonance at 60.9 ppm and the addition of further equivalents of $OPMe_3$ produced a sharp second resonance at 39.9 ppm, corresponding to free $OPMe_3$ remaining in solution. This suggests that the lability and ligand exchange rate of the $OPMe_3$ ligands is slow on the NMR timescale, lowering the broadening observed for each peak. The $^{19}F\{^1H\}$ NMR for each of these complexes in CD_3CN was found, unsurprisingly at -79.4 ppm, as has been previously discussed in Chapter 2, likely due to displacement of the triflate in solution by the donating CD_3CN solvent. Attempts were made at the analysis of these compounds *via* ^{115}In NMR spectroscopy with only the *hexaakis*-$[In(OPMe_3)_6][OTf]_3$ complex producing a resonance at -93.73 ppm. This is likely due to the quadrupolar nature of the indium metal centre, with the complexes containing fewer $OPMe_3$

ligands having a lower symmetry than the O_h symmetry of $[In(OPMe_3)_6][OTf]_3$. Although tentative in assignment, with the help of Prof William Levason, the P=O stretching frequencies were assigned ranging from 1103 cm^{-1} in $[In(OTf)_3(OPMe_3)_3]$ to 1112 cm^{-1} in the *hexakis*-$[In(OPMe_3)_6][OTf]_3$. This shows a small increase in wavenumbers with the increase in $OPMe_3$ coordination.

The product of the 4:1 reaction of indium triflate with trimethylphosphine oxide was sent for microanalysis with the weights matching the cationic formula $[In(OTf)_2(OPMe_3)_4][OTf].H_2O$. A number of colourless crystals of a good quality for X-ray diffraction were grown through the layering of a CH_2Cl_2 solution of the $[In(OTf)_2(OPMe_3)_4][OTf]\cdot H_2O$ with *n*-hexane and gave the structure shown in Figure 3.10. A second structure was obtained from crystals grown through slow evaporation of CH_2Cl_2 to give a 2nd polymorph of $[In(OTf)_2(OPMe_3)_4][In(OH_2)_2(OPMe_3)_4][OTf]_4$ with a slightly different arrangement in the crystal, being shown in Figure 3.11. Selected bond lengths and angles of both polymorphs are provided in Table 3.4. Both polymorphs contained the same two species, the first of these a *trans*-$[In(OTf)_2(OPMe_3)_4]^+$ cation, co-crystallised with *trans*-$[In(OH_2)_2(OPMe_3)_4]^{3+}$ trication with four non-coordianted triflate anions. Both of these polymorphs were grown in the P-1 space group with differing unit cell parameters, these being found in the Crystallographic Parameter tables in Appendix B. As was observed above with the co-crystallised *tris*-compound $[In(OTf)_2(OPPh_3)_4][In(OH_2)_4(OPPh_3)][OTf]_4$, the coordinated water molecules form H-bonds to the free triflate anions. The metal complex could be alternatively described as a salt with $[In\{(OH_2)(OTf)_2\}_2(OPMe_3)_4)]^-$ acting as the anion. The H-bonding between the coordinated water molecules and the ionic triflate likely cause significant stabilisation of the complex and likely contribute to the driving force of crystallisation of these structures. When comparing these two polymorphs, the atomic positions of the metals differed within the unit cell. The *trans*-$[In(OTf)_2(OPMe_3)_4]^+$ cation were located on the vertices of the unit cell in polymorph 1, whereas were on both the vertices and edges in polymorph 2. The aquo-complex $[In(OH_2)_2(OPMe_3)_4]^{3+}$ species (and the H-bonded triflates) is located completely within the unit cell of polymorph 1, while is found as a centrosymmetric half cation shared over two faces of the unit cell in polymorph 2.

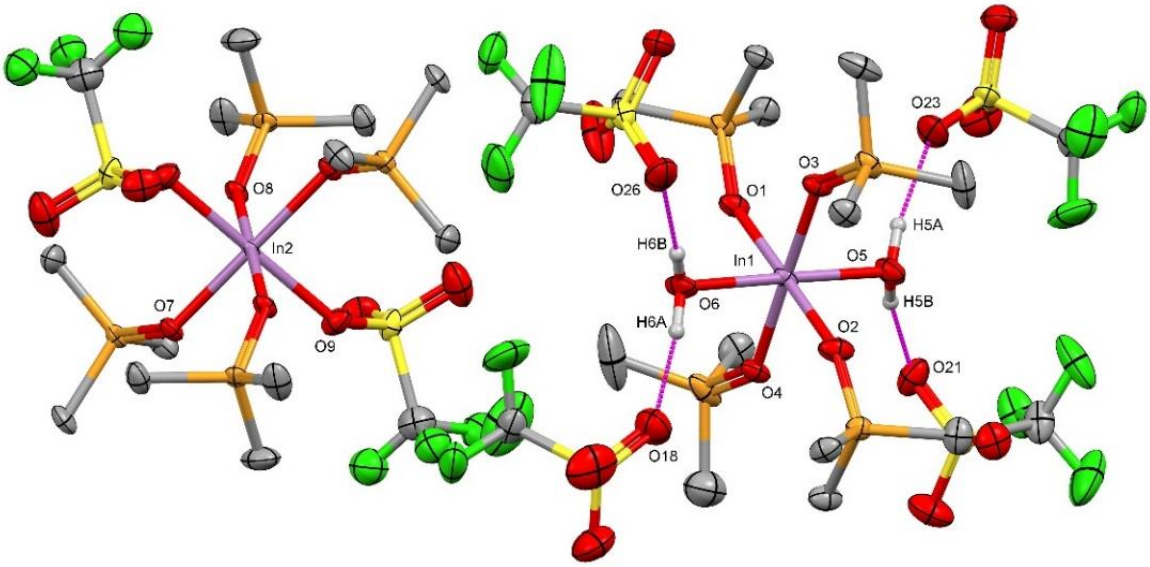

Figure 3.10 - Crystal structure of ***9*** polymorph 1 of *trans*-$[In(OTf)_2(OPMe_3)_4][In(OH_2)_2(OPMe_3)_4][OTf]_4$ showing the atom numbering schemes. Ellipsoids shown at 50% probability with H-atoms are omitted for clarity, unless involved in H-bonding.

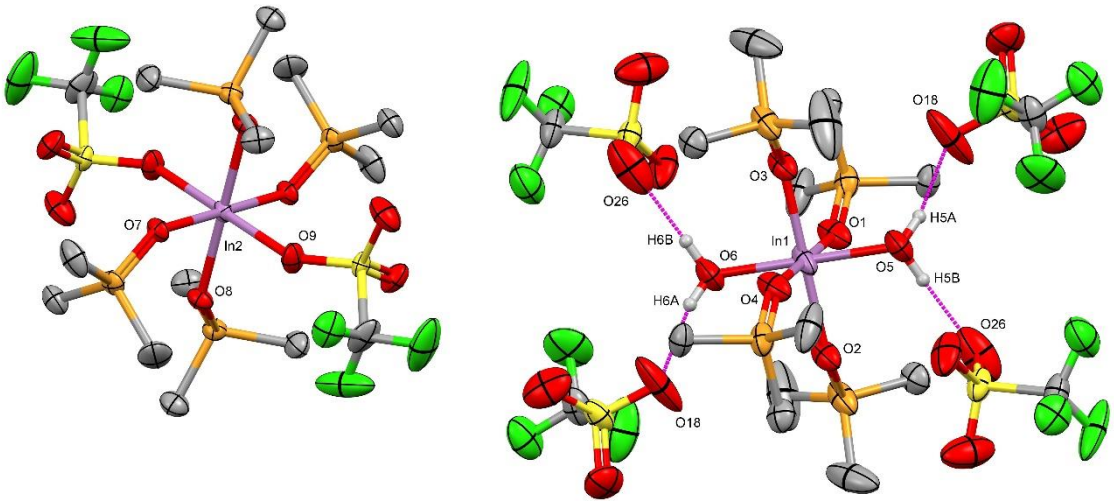

Figure 3.11 - Crystal structure of ***10*** polymorph 2 of *trans*-$[In(OTf)_2(OPMe_3)_4][In(OH_2)_2(OPMe_3)_4][OTf]_4$ showing the atom numbering schemes. Ellipsoids shown at 50% probability and H-atoms are omitted for clarity, unless involved in H-bonding.

Table 3.2 - Table of bond lengths and H-bonding contact distances for polymorphs 1 and 2 of *trans*-$[In(OTf)_2(OPMe_3)_4][InOH_2)_2(OPMe_3)_4][OTf]_4$.

Bond Lengths / Å				Hydrogen Bonding Contact Distances / Å			
Polymorph 1		Polymorph 2		Polymorph 1		Polymorph 2	
In1 – O1	2.120(3)	In1 – O1	2.118(3)	O5 – O21	2.702(6)	O5 – O26	2.837(8)
In1 – O2	2.114(3)	In1 – O2	2.102(3)	H5B – O21	1.823	H5B – O26	1.964
In1 – O3	2.102(3)	In1 – O3	2.108(4)	O5 – O23	2.669(6)	O5 – O18	2.675(7)
In1 – O4	2.102(3)	In1 – O4	2.117(3)	H5A – O23	1.798	H5A – O18	1.843
In1 – 05	2.153(4)	In1 – 05	2.164(4)	O6 – O18	2.671(6)	O6 – O18	2.675(7)
In1 – O6	2.155(4)	In1 – O6	2.165(3)	H6A – O18	1.792	H6A – O18	1.843
In2 – O7	2.101	In2 – O7	2.099(2)	O6 – O26	2.941(7)	O6 – O26	2.837(8)
In2 – O8	2.100	In2 – O8	2.101(3)	H6B – O26	2.033	H6B – O26	1.964
In2 – O9	2.164	In2 – O9	2.165(3)				
P – O (In1)	1.515(4) – 1.519(3)	P – O (In1)	1.514(5) – 1.516(4)				
P – O (In2)	1.518(4) – 1.524(3)	P – O (In2)	1.521(3) – 1.522(3)				

The reaction of 5:1 molar ratio of trimethylphosphine oxide and $In(OTf)_3$ in CH_2Cl_2 for two hours yielded a white solid that microanalysis confirmed to match the calculated formation of $[In(OTf)(OPMe_3)_5][OTf]_2$. While crystallisation attempts were unsuccessful crystals of this indium centred *pentakis*-species, a few crystals of the Ga(III) complex, $[Ga(OPMe_3)_5(MeCN)][OTf]_3$, from a solution containing a few mg of $Ga(OTf)_3$ layered with a solution of four equivalents of $OPMe_3$ in MeCN with the slow vapour diffusion of Et_2O, this structure is shown in Figure 3.12.

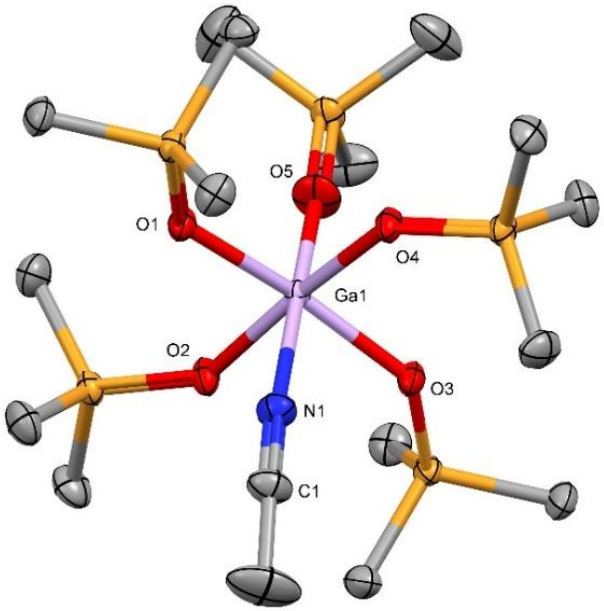

Figure 3.12 – Crystal structure of ***11*** $[Ga(OPMe_3)_5(MeCN)][OTf]_3$ showing the atom numbering scheme. Ellipsoids shown at 50% probability with H-atoms and triflate anions omitted for clarity.

Table 3.5 - Selected bond lengths and angles of $[Ga(OPMe_3)_5(MeCN)][OTf]_3$.

Bond Lengths / Å		Bond Angles / °	
Ga 1 – N1	2.198(2)	N1 – Ga1 – O1	86.62(7)
Ga 1 – O1	1.933(1)	N1 – Ga1 – O2	84.99(7)
Ga 1 – O2	1.921(1)	N1 – Ga1 – O3	84.24(7)
Ga 1 – O3	1.931(1)	N1 – Ga1 – O4	87.47(7)
Ga 1 – 04	1.929(1)	N1 – Ga1 – O5	178.37(8)
Ga 1 – O5	1.899(2)	O1 – Ga1 – O5	94.60(7)
N1 – C1	1.141(3)	O2 – Ga1 – O5	94.92(7)
P – O	1.5007(16) - 1.5254(14)	O3 – Ga1 – O5	94.56(7)
		O4 – Ga1 – O5	93.61(7)
		Ga1 – N1 – C1	163.53(2)
		Ga1 – O5 – P5	176.2(1)

X-ray diffraction revealed this complex to be formulated as tricationic $[Ga(OPMe_3)_5(MeCN)][OTf]_3$ in a near perfect octahedral geometry, with only small angular variations from 90° around the metal centre. This complex shows that coordination of all five $OPMe_3$ ligands were successfully coordinated with the remaining triflate being displaced by the coordinating solvent MeCN. It had been hypothesised that, in solution the labile triflate anions would dissociate from the complex, being rapidly exchanged with other donor species present (MeCN, H_2O). The $^{19}F\{^1H\}$ NMR spectra

has been observed as consistently at -79.4 ppm (in CD_3CN) which supports this hypothesis, however until now displacement by acetonitrile had not been observed in the solid-state. This structure confirms that the MeCN solvent can outcompete the triflate anions for coordination at Ga(III) metal centre in the solid-state.

The $OPMe_3$ ligand located *trans* to the acetonitrile is unique when compared other $OPMe_3$ ligands with a close to linear Ga-O=P coordination angle of 176.2°(1). The equatorial $OPMe_3$ ligands showed angles ranging from 133.75°(9) – 138.6°(1), significantly more bent. The trimethyl-groups of the equatorial ligands are thought cause destabilising interactions which forces linearization of the $OPMe_3$ ligand *trans* to acetonitrile. It was also noted that this $OPMe_3$ ligand had significantly more disorder associated with it that was modelled in this crystal structure as a rotation of the PMe_3 group. This crystal structure is not representative of the bulk solid as there is no evidence of MeCN in the IR spectrum or microanalysis.

The complex produced by reaction of $In(OTf)_3$ with six equivalents of trimethylphosphine oxide was confirmed as $[In(OPMe_3)_6][OTf]_3$ by microanalysis. This was isolated as a single species and fully characterised by multinuclear NMR spectroscopy. Crystallisation attempts for this *hexakis* complex from a number of solvent systems were explored with a CH_2Cl_2 solution layered with *n*-hexane producing a few small crystals that Dr Mark Light helped to identify as a modulated structure, making refinement of the structure very difficult. With the help of Dr Light, a highly constrained model of the crystal structure shown in Figure 3.13.

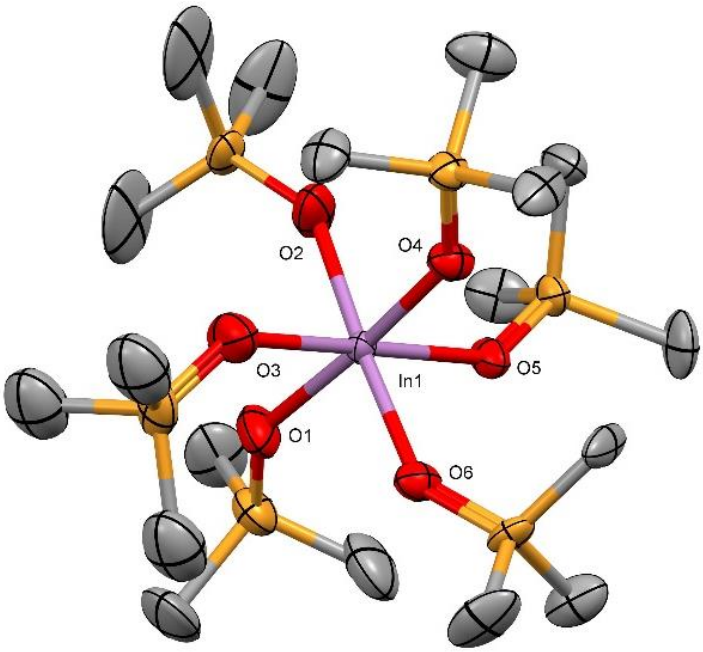

Figure 3.13 - Crystal structure of $[In(OPMe_3)_6][OTf]_3$ showing atomic numbering scheme. Ellipsoids at 50% probability and H-atoms and anions omitted for clarity.

The challenging nature of this crystal lead to a highly constrained and poorly refined model with an R1 of ~15%, so the exact bond lengths and angles are not reliable, however, the general structure can be seen as the tricationic complex $[In(OPMe_3)_6][OTf]_3$. This complex is an octahedral geometry with six $OPMe_3$ ligands coordinated to the In(III) metal centre. This is expected with the structure of the *pentakis*-$[Ga(OPMe_3)_5(MeCN)][OTf]_3$, with the additional equivalents of ligand displacing the final pseudo-vacent MeCN site. Due to the poor quality of the structural model, the bond metrics are unreliable and so are not reported here.

Pyridine *N*-oxide (pyNO) is another oxygen donor ligand that has been used to explore the coordination of the Group 13 metal triflates in comparison to the trialkylphosphine oxide ligands already explored in this chapter. Both are oxidised forms of Group 15 elements N and O, with the differences in their bonding described in Chapter 1.2.3. The higher binding constant of pyNO than $OPMe_3$ may allow for differences in the coordination and thus the complex produced in these reactions. The reactions of pyNO were carried out using the same procedure as the previously described OPR_3 reactions, with a 3:1 molar ratio of ligand : $M(OTf)_3$ (M = Al, Ga, In) in CH_2Cl_2.

The reaction of pyNO with $In(OTf)_3$ produced a white solid in a good yield that microanalysis revealed to match the calculated formulation of *tris*-$[In(OTf)_3(pyNO)_3]$. Analysis *via* ^1H NMR spectroscopy revealed each shift and separation of the aromatic resonances, as demonstrated below by the top and bottom spectra in Figure 3.15. These were separated into the *ortho*, *para* and *meta* protons in a 2:1:2 ratio, with the same pattern seen in the $^{13}C\{^1H\}$ NMR spectra. There is also evidence of the *ortho* protons being broadened with their coupling lost due to the proximity of the quadrupolar indium(III) metal.

Layering of a CH_2Cl_2 solution of *tris*-$[In(OTf)_3(pyNO)_3]$ with *n*-hexane produced crystals of *mer*-$[In(OTf)_3(pyNO)_3]$, matching the formulation suggested by microanalysis, with the structure presented in Figure 3.14. This structure revealed an octahedral complex in the *mer* geometry, with coordination of 3 pyNO ligands and 3 triflate anions with no additional long contacts to the metal centre. This is unlike the $OPMe_3$ complex that produced a bimetallic salt incorporating water as a ligand.

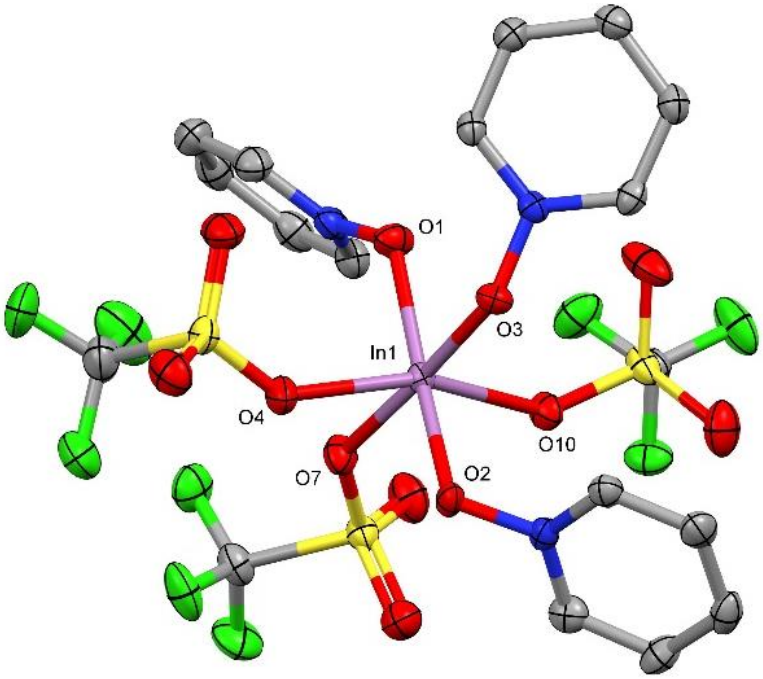

Figure 3.14 – Crystal structure of ***12*** mer-$[In(OTf)_3(PyNO)_3]$ showing the atom numbering scheme. Ellipsoids shown at 50% probability with H-atoms are omitted for clarity.

Table 3.6 - Selected bond lengths and angles for *mer*-$[In(OTf)_3(PyNO)_3]$.

Bond Lengths / Å		Bond Angles / °	
In1 – O1	2.095(3)	O1 – In1 – O3	86.7(1)
In1 – O2	2.105(3)	O2 – In1 – O3	82.9(1)
In1 – O3	2.133(3)	O3 – In1 – O4	96.4(1)
In1 – O4	2.166(3)	O3 – In1 – O10	99.7(1)
In1 – 07	2.168(3)	O7 – In1 – O1	92.1(1)
In1 – O10	2.163(2)	O7 – In1 – O2	98.1(1)
		O7 – In1 – O4	81.5(1)
		O7 – In – O10	82.6(1)

The IR spectrum produced by this complex showed a broad absorption at 1204 cm^{-1}, shifted to a lower frequency from the characteristic peak in the free ligand at 1245 cm^{-1} upon coordination; it was also free from any uncoordinated ligand and water in the final product. This shift is within an expected range, from a study by Tyree it was noted that the absorption band for pyNO coordinated to a *d*-block metal(II) ions (Cu, Ni, Zn, Co) is generally found as part of two groups. The first is found at ~1220 cm^{-1} when pyNO is the only ligand in the coordination sphere of the metal centre, whereas those at ~1205 cm^{-1} have retained one or other coordinated species such as solvent or anions. The crystal structure in Figure 3.14 showed *mer*-$[In(OTf)_3(pyNO)_3]$ where the

pyNO ligands fill the coordination sphere with 3 of the triflate anions, following the pattern observed in the transition metal study. This also suggests that, in the solid structure, this crystal structure is representative of the bulk solid.

The 3:1 reaction of pyNO with $M(OTf)_3$ (M = Al, Ga) repeatedly produced mixtures, by ^1H NMR spectroscopy, regardless of reaction solvent used (CH_2Cl_2 or MeCN). Figure 3.15, is a comparison of free ligand, an example of the mixtures produced by the $M(OTf)_3$ (M = Al, Ga), and the indium complex $[In(OTf)_3(pyNO)_3]$.

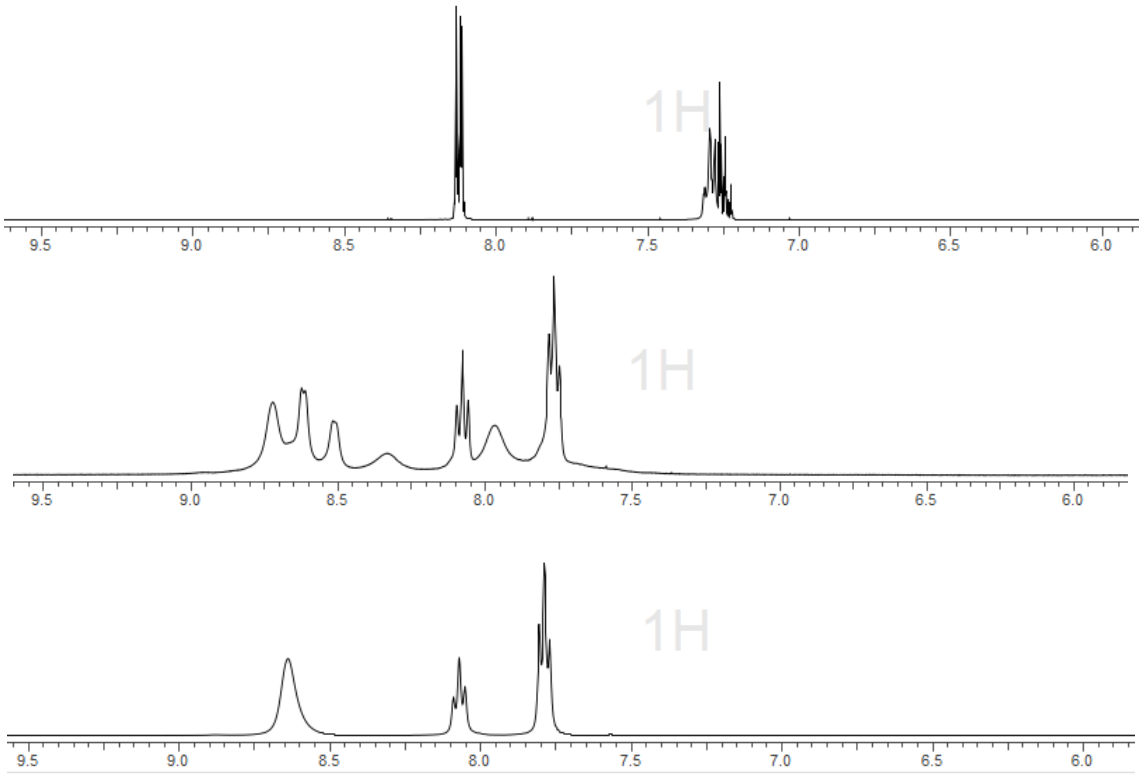

Figure 3.15 - Comparison of free pyNO (top) with the product of the 3:1 reaction with the corrisponding metal triflate (middle: Ga, Bottom: In).

Attempts to crystallise both aluminium and gallium complexes under the same conditions as the indium complex were unsuccessful but the slow vapour diffusion of Et_2O in to an MeCN solution of the complex produced crystals of $[M(OTf)_2(pyNO)_4][OTf]\cdot 0.5MeCN$ (M = Al, Ga). Both of these crystal systems were isostructural in the $P2_1/n$ space group with the asymmetric unit cell containing two disordered octahedral metal cation with two ionic triflate anions and one acetonitrile solvent molecule. The metal cations coordination sphere is made up of two *trans* triflate anions in the axial positions and four pyNO ligands filling the equatorial coordination sites as shown in Figure 3.16. Selected bond lengths and angle of the M = Al and Ga complexes are provided in Table 3.7. NMR spectroscopy of these separated crystals still showed traces of the other species and these crystal structures allowed for the prediction of two species in the ^1H NMR

(*tris* and *tetrakis*) complexes in solution, assignment has not been attempted due to the presence of additional peaks and the uncertainty as to which corresponds to which complex.

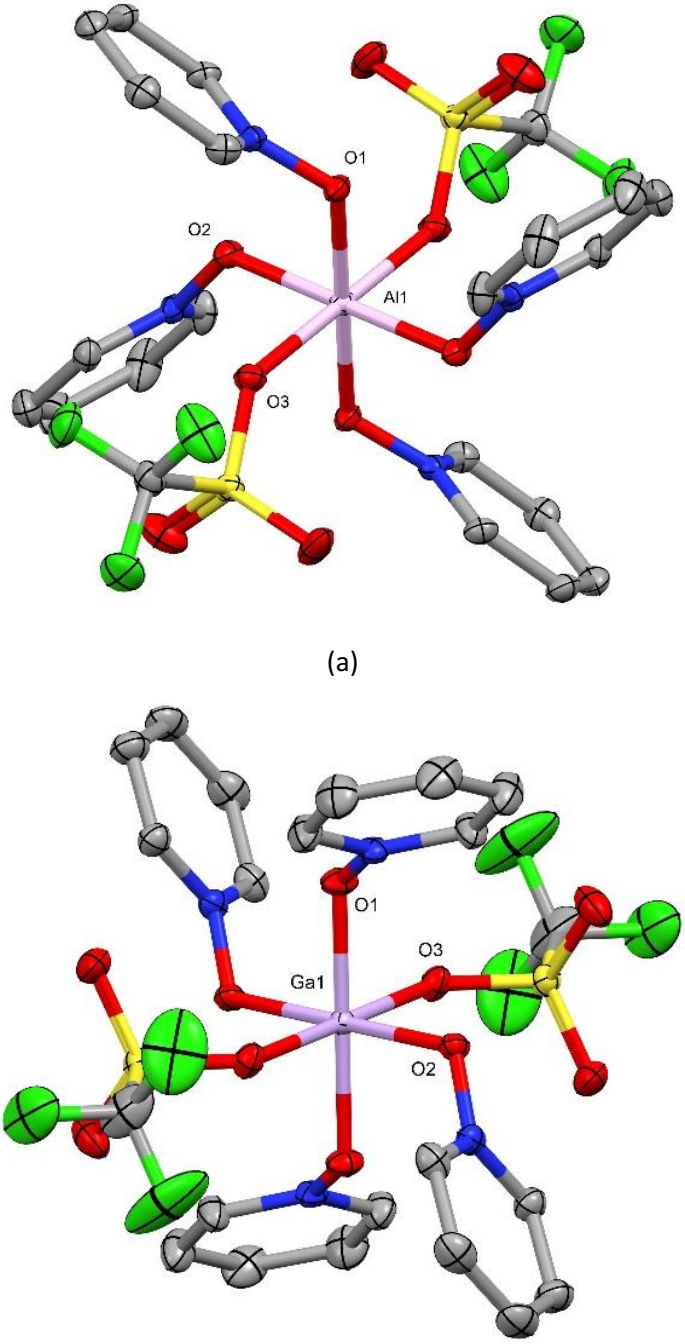

Figure 3.16 – Crystal structures of (a) ***13*** *trans*-$[Al(OTf)_2(pyNO)_4][OTf]$ and (b) ***14*** *trans*-$[Ga(OTf)_2(pyNO)_4][OTf]$. Ellipsoids shown at 50% probability with H-atoms, anions and lattice solvent molecules omitted for clarity.

Table 3.7 - Selected bond lengths and angles for $[Al(OTf)_2(pyNO)_4][OTf]$ and $[Ga(OTf)_2(pyNO)_4][OTf]$.

Bond Lengths / Å			Bond Angles / °	
$[Al(OTf)_2(pyNO)_4][OTf]$	Al1 – O1	1.8613(9)	O1 – Al1 – O2	89.19(4)
	Al1 – O2	1.8615(9)	O1 – Al1 – O3	89.06(4)
	Al1 – O3	1.9571 (10)	O2 – Al1 – O3	91.46(4)
	Al2 – O4	2.065(6)	O5 – Al2 – O6	88.26(4)
	Al2 – O5	2.000(5)	O4 – Al2 – O5	89.06(4)
	Al2 – O6	2.031(5)	O4 – Al2 – O6	88.50(4)
$[Ga(OTf)_2(pyNO)_4][OTf]$	Ga1 – O1	2.2202(13)	O 1– Ga1 – O2	88.98(7)
	Ga1 – O2	2.2146(13)	O1 – Ga1 – O3	91.96(8)
	Ga1 – O3	2.2292(11)	O2 – Ga1 – O3	91.78(7)
	Ga2 – O4	2.2293(13)	O4 – Ga2 – O5	90.75(7)
	Ga2 – O5	2.1326(12)	O4 – Ga2 – O6	91.65(7)
	Ga2 – O6	2.1789(11)	O5 – Ga2 – O6	91.54(8)

3.3 – Conclusion

A range of novel neutral and cationic six-coordinate complexes of the Group 13 metal triflates have been synthesised with mono- and bidentate phosphine oxides as well as pyridine *N*-oxide in varying molar ratios. Three equivalents of the monodentate OPR_3 (R = Me, Ph) and pyNO produce both neutral and cationic complexes. Although spectroscopically characterised, micro analytical results for the product of the of the OPR_3 reactions matched the expected formula $[M(OTf)_3(OPR_3)_3]$ (M = Al, Ga; R = Me, Ph), however, the solid-state structure is unknown. The structure obtained for the *tris*-coordination of $OPPh_3$ to $In(OTf)_3$ was a bimetallic salt $[In(OTf)_2(OPPh_3)_4][In(OH_2)_4(OPPh_3)_2][OTf]_4$ with the four triflate anions part of a H-bonded array with the aquo ligands. This encompassed the species in a 24-membered pseudo-macrocycle giving an alternative formulation as the anionic $[In\{(OH_2)_4(OTf)_4\}(OPPh_3)_2]^-$ species. A series of reactions of $In(OTf)_3$ with $OPMe_3$ in varying ratios produced mixtures in both the 4:1 and 5:1 reactions, showing a second resonance corresponding to the complex with ±1 $OPMe_3$ ligand. The crystal structures of the 4:1 and 5:1 products revealed displacement of the triflate anion by both trace amounts of water and the coordinating solvent MeCN. The crystal structure of $[Ga(OPMe_3)_5(MeCN)][OTf]_3$ revealed that the weakly coordinating MeCN also displaces the triflate anion in these systems.

The Group 13 metal triflates react with $dppmO_2$ to form the *tris*($dppmO_2$) complex, $[M(dppmO_2)_3][OTf]_3$ (M = Al, Ga, In). For gallium and indium, a second spectroscopically unique product was identified as the *bis* product, formulated as $[M(OTf)_2(dppmO_2)_2][OTf]$ but was not structurally characterised. The 3:1 reaction of pyNO and the earlier Group 13 metal triflates (Al, Ga), was shown to produce a mixture of products by ^1H NMR spectroscopy, with separation of the products not being possible. Allowing these products to crystallise produced crystals of *trans*-$[M(OTf)_2(pyNO)_4][OTf]$, likely the second species observed in the ^1H NMR spectroscopy. When attempting the 3:1 reaction was attempted using the heavier $In(OTf)_3$, a single species was identified by ^1H NMR spectroscopy and the results of the microanalysis agreed with the formulation $[In(OTf)_3(pyNO)_3]$. Crystallisation of this product confirmed a *mer*-octahedral geometry in the solid state.

3.4 – Experimental

For supplier and purification of reagents and solvents, instrument specifications and NMR solvent references see Appendix A. Although the Group 13 metal triflates were purchased as 'anhydrous' materials, IR spectroscopy revealed residual water after attempts to dry them by heating *in vacuo*.

3.4.1 Complex Preparation

3.4.1.1 **[Al(dppmO$_2$)$_3$][OTf]$_3$**

$Al(OTf)_3$ (47 mg, 0.1 mmol) was dissolved in CH_2Cl_2 (5 mL) before the addition of $dppmO_2$ (146 mg, 0.35 mmol) and stirring of the solution for 2 h. The solution was concentrated to ca. 50% volume *in vacuo* and the product was precipitated by the addition of n-hexane (5 mL). The white powder was collected by filtration and dried *in vacuo*. Yield: 86 mg, 50%. Required for $C_{78}H_{66}AlF_9O_{15}P_6S_3{\cdot}CH_2Cl_2$ (1723.35): C, 52.5; H, 3.8. Found: 53.0; H, 3.8%. ^{1}H NMR (295 K, CD_3CN): δ = 7.78–7.60 (m, [8H], Ar-H), 7.40–7.23 (m, [12H], Ar-H), 4.08 (t, [2H], $^2J_{PH}$ = 12 Hz, CH_2). $^{19}F\{^1H\}$ NMR (295 K, CD_3CN): δ = −78.6 (s). $^{31}P\{^1H\}$ NMR (295 K, CD_3CN): δ = 44.2 (s). ^{27}Al NMR (295 K, CD_3CN): δ = −9.3. IR (Nujol/cm^{-1}): 1141, ~1120 (sh) (P=O).

3.4.1.2 **[Ga(dppmO$_2$)$_3$][OTf]$_3$**

$Ga(OTf)_3$ (51 mg, 0.1 mmol) was dissolved in CH_2Cl_2 before the addition of $dppmO_2$ (125 mg, 0.3 mmol) and stirring of the solution for 2 h. The solution was concentrated to ca. 50% volume *in vacuo* and the product was precipitated by the addition of n-hexane (5 mL) The white powder was collected by filtration and dried *in vacuo*. Yield: 107 mg, 61%. Required for $C_{78}H_{66}F_9GaO_{15}P_6S_3{\cdot}CH_2Cl_2$ (1851.03): C, 51.3; H, 3.7%. Found: C, 50.2; H, 3.7%. ^{1}H NMR (295 K, CD_3CN): δ = 7.76–7.65 (m, [8H], Ar-H), 7.40–7.30 (m, [12H], Ar-H), 4.27 (t, [2H], $^2J_{PH}$ = 12 Hz, CH_2). $^{19}F\{^1H\}$ NMR (295 K, CD_3CN): δ = –78.7 (s). $^{31}P\{^1H\}$ NMR (295 K, CD_3CN): δ = 46.3 (s). ^{71}Ga NMR (295 K, CD_3CN): δ = −43.4 (br s). IR (Nujol/cm^{-1}): 1160, 1132 (P=O).

3.4.1.3 **[In(dppmO$_2$)$_3$][OTf]$_3$**

$In(OTf)_3$ (56 mg, 0.1 mmol) was dissolved in CH_2Cl_2 before the addition of $dppmO_2$ (146 mg, 0.35 mmol) and stirring of the solution for 2 h. The solution was concentrated to ca. 50% volume *in vacuo* and the product was precipitated by the addition of n-hexane (5 mL) The white powder was collected by filtration and dried *in vacuo*. Yield: 105 mg, 58%. Required for $C_{78}H_{66}F_9InO_{15}P_6S_3{\cdot}CH_2Cl_2$ (1896.12): C, 50.0; H, 3.6. Found: 50.3, 3.9%. ^{1}H NMR (295 K, CD_3CN): δ = 7.53–7.62 (br m, [12H], Ar-H), 7.27 (br s, [8H], Ar-H), 4.52 (t, [2H], $^2J_{PH}$ = 12 Hz, CH_2). $^{19}F\{^1H\}$ NMR

(295 K, CD_3CN): δ = –78.4 (s). $^{31}P\{^1H\}$ NMR (295 K, CD_3CN): δ = 48.0 (s). ^{115}In NMR (CD_3CN): not observed. IR (Nujol/cm^{-1}): 1160 (sh), 1137 (P=O).

3.4.1.4 **$[Ga(OTf)_2(dppmO_2)_2][OTf]$**

$Ga(OTf)_3$ (103 mg, 0.2 mmol) was dissolved in CH_2Cl_2 (10 mL) before the addition of $dppmO_2$ (167 mg, 0.4 mmol) and stirring for 2 h. Removal of the solvent resulted in a white solid, which was washed with n-hexane (2 × 5 mL) and dried *in vacuo*. Yield: 221 mg, 77%. Required for $C_{53}H_{44}F_9GaO_{13}P_4S_3{\cdot}CH_2Cl_2$ (1434.64): C, 45.2; H 3.2. Found: C, 45.1; H, 3.4%. ^1H NMR (295 K, CD_3CN): δ = 7.31–7.77 (m, [20H], Ar-H), 4.25 (t, [2H], $^2J_{PH}$ =13 Hz, CH_2). $^{19}F\{^1H\}$ NMR (295 K, CD_3CN): δ = –79.2 (s). $^{31}P\{^1H\}$ NMR (295 K, CD_3CN): δ = 44.8 (s). ^{71}Ga NMR (295 K, CD_3CN): not observed. IR (Nujol/cm^{-1}): 1163, 1132 (P=O).

3.4.1.5 **$[In(OTf)_3(PyNO)_3]$**

$In(OTf)_3$ (112 mg, 0.2 mmol) was dissolved in CH_2Cl_2 (5 mL) before addition of freshly sublimed pyridine N-oxide (57 mg, 0.6 mmol) and stirred for 2 h. Addition of n-hexane (10 mL) caused the precipitation of a white solid which was collected by filtration and dried *in vacuo*. Crystals suitable for X-ray analysis were grown by slow evaporation of a CH_2Cl_2 solution. Yield: 66 mg, 36%. Required for $C_{18}H_{15}F_9InN_3O_{12}S_3.CH_2Cl_2$ (932.26): C, 24.5; H, 1.8; N, 4.5. Found: 23.9; H, 2.4; N, 4.3%. ^1H NMR (295 K, CD_3CN): δ = 8.64 (br s, [2H], Ar-H), 8.07 (br t, [1H], Ar-H), 7.79 (br t, [2H], Ar-H). $^{13}C\{^1H\}$ NMR (295 K, CD_3CN): δ = 142.44, 139.05, 128.80. $^{19}F\{^1H\}$ NMR (295 K, CD_3CN): δ = –78.3 (s). IR (Nujol/cm^{-1}): 1204 (N-O).

3.4.1.6 **$[Al(OTf)_3(OPPh_3)_3]$**

$Al(OTf)_3$ (95 mg, 0.2 mmol) was dissolved in CH_2Cl_2 (10 mL) before addition of triphenylphosphine oxide (167 mg, 0.6 mmol) and the mixture stirred for 2 h. The solution was concentrated to ca. 50% volume *in vacuo* before addition of n-hexane (10 mL), which caused precipitation of a white solid. This was isolated by filtration before drying *in vacuo*. Yield: 112 mg, 67%. Required for $C_{57}H_{45}AlF_9O_{12}P_3S_3{\cdot}0.5CH_2Cl_2$ (1351.57): C, 51.1; H, 3.4. Found: C, 50.8; H, 3.6%. ^1H NMR (295 K, CD_3CN): δ = 7.67 (t, [3H], 7.40 (br m, [12H], Ar-H). $^{19}F\{^1H\}$ NMR (295 K, CD_3CN): δ = −78.6 (s). $^{31}P\{^1H\}$ NMR (295 K, CD_3CN): δ = 42.5 (s), ^{27}Al NMR (295 K, CD_3CN): not observed. IR (Nujol/cm^{-1}): 1156 (P=O).

3.4.1.7 **$[Ga(OTf)_3(OPPh_3)_3]$**

$Ga(OTf)_3$ (103 mg, 0.2 mmol) was dissolved in CH_2Cl_2 (10 mL) before addition of triphenylphosphine oxide (167 mg, 0.6 mmol) and the mixture stirred for 2 h. Removal of the solvent resulted in a white solid, which was washed with n-hexane (2 × 5 mL) and dried *in vacuo*.

Yield: 215 mg, 80%. Required for $C_{57}H_{45}F_9GaO_{12}P_3S_3 \cdot CH_2Cl_2$ (1436.72): C, 48.5; H 3.3. Found: C, 48.0; H, 4.1%. ^{1}H NMR (295 K, CD_3CN): δ = 7.65 (m, [3H], Ar-H), 7.45 (m, [12H], Ar-H),. ^{19}F{^{1}H} NMR (295 K, CD_3CN): δ =−78.6 (s). ^{31}P{^{1}H} NMR (295 K, CD_3CN): δ = 44.6 (s). ^{71}Ga NMR (295 K, CD_3CN): not observed. IR (Nujol/cm^{-1}): 1143 (P=O).

3.4.1.8 **[In(OTf)$_3$(OPPh$_3$)$_3$]**

$In(OTf)_3$ (112 mg, 0.2 mmol) was dissolved in CH_2Cl_2 (10 mL) before the addition of triphenylphosphine oxide (167 mg, 0.6 mmol) and the mixture stirred for 2 h. Removal of solvent resulted in a white solid, which was washed with n-hexane (2 × 5 mL) and dried *in vacuo*. Yield: 245 mg, 88%. Required for $C_{57}H_{45}F_9InO_{12}P_3S_3 \cdot 0.5CH_2Cl_2$ (1439.34): C, 48.0; H 3.2. Found: C, 48.6; H, 3.6%. ^{1}H NMR (295 K, CD_3CN): δ = 7.65 (m, [3H], Ar-H), 7.50–7.40 (m, [12H], Ar-H). ^{19}F{^{1}H} NMR (295 K, CD_3CN): δ = −78.6 (s). ^{31}P{^{1}H} NMR (295 K, CD_3CN): δ = 45.9 (s). ^{115}In NMR (295 K, CD_3CN): not observed. IR (Nujol/cm^{-1}): 1145 (P=O).

3.4.1.9 **[Al(OTf)$_3$(OPMe$_3$)$_3$]**

$Al(OTf)_3$ (95 mg, 0.2 mmol) was dissolved in CH_2Cl_2 (10 mL) before the addition of trimethylphosphine oxide (55 mg, 0.6 mmol) and stirred for 2 h. Removal of the volatiles *in vacuo*, followed by washing with hexane (2 × 5 mL) and drying *in vacuo* gave a white powdered solid. Yield: 134 mg, 84%. Required for $C_{12}H_{27}AlF_9O_{12}P_3S_3$ (750.4): C, 19.2; H 3.6. Found: C, 18.9; H, 3.5%. ^{1}H NMR (295 K, CD_3CN): δ = 1.72 (d, $^2J_{PH}$ = 12 Hz). ^{13}C{^{1}H} NMR (295 K, CD_3CN): δ = 15.85 (d, $^1J_{PC}$ = 73.5 Hz). ^{19}F{^{1}H} NMR (295 K, CD_3CN): δ = −78.9 (s). ^{31}P{^{1}H} NMR (295 K, CD_3CN): δ = 60.9 (s). ^{27}Al NMR (295 K, CD_3CN): δ = −11.3 (br s). IR (Nujol/cm^{-1}): 1103 vs (P=O).

3.4.1.10 **[Ga(OTf)$_3$(OPMe$_3$)$_3$]**

$Ga(OTf)_3$ (103 mg, 0.2 mmol) was dissolved in CH_2Cl_2 (10 mL) before the addition of trimethylphosphine oxide (55 mg, 0.6 mmol), and stirred for 2 h. Removal of the volatiles *in vacuo* resulted in a white solid, which was washed with n-hexane (2 × 5 mL) and dried *in vacuo*. Yield: 134 mg, 84%. Required for $C_{12}H_{27}F_9GaO_{12}P_3S_3$ (793.16): C, 18.2; H 3.4. Found: C, 18.1; H, 4.0%. ^{1}H NMR (295 K, CD_3CN): δ = 1.75 (d, $^2J_{PH}$ = 12 Hz). ^{13}C{^{1}H} NMR (295 K, CD_3CN): δ = 15.90 (d, $^1J_{PC}$ = 71 Hz). ^{19}F{1H} NMR (295 K, CD_3CN): δ = -78.8 (s). ^{31}P{^{1}H} NMR (295 K, CD_3CN): δ = 65.5 (s). ^{71}Ga NMR (295 K, CD_3CN): not observed. IR (Nujol/cm^{-1}): 1108 s (P=O).

3.4.1.11 **[In(OTf)$_3$(OPMe$_3$)$_3$]**

$In(OTf)_3$ (112 mg, 0.2 mmol) was dissolved in CH_2Cl_2 (10 mL) before the addition of trimethylphosphine oxide (55 mg, 0.6 mmol), and stirred for 2 h. The solution was concentrated to ca. 5 mL *in vacuo*, before the addition of n-hexane (10 mL), which caused precipitation of a

white solid. This was isolated by filtration and dried *in vacuo*. Yield: 113 mg, 71%. Required for $C_{12}H_{27}F_9InO_{12}P_3S_3 \cdot CH_2Cl_2$ (923.19): C, 16.9; H 3.2. Found: C, 16.9; H, 4.4%. ^{1}H NMR (295 K, CD_3CN): δ = 1.71 (d, $^2J_{PH}$ = 16 Hz). $^{13}C\{^1H\}$ NMR (295 K, CD_3CN): δ = 16.73 (d, $^1J_{PC}$ = 72 Hz,). $^{19}F\{^1H\}$ NMR (295 K, CD_3CN): δ = −78.6 (s). $^{31}P\{^1H\}$ NMR (295 K, CD_3CN): δ = 66.6 (s). ^{115}In NMR (295 K, CD_3CN): not observed. IR (Nujol/cm^{-1}): 1104 s (P=O).

3.4.1.12 **$[In(OTf)_2(OPMe_3)_4][OTf] \cdot H_2O$**

$In(OTf)_3$ (112 mg, 0.2 mmol) was dissolved in CH_2Cl_2 (10 mL) before the addition of trimethylphosphine oxide (74 mg, 0.8 mmol) and stirring for 2 h. The solution was concentrated to ca. 5 mL *in vacuo*, before the addition of n-hexane (10 mL) which caused precipitation of a white solid. This was isolated by filtration before drying *in vacuo*. Yield: 102 mg, 53%. Required for $C_{15}H_{40}F_9InO_{15}P_4S_3 \cdot H_2O$ (966.36): C, 18.6; H 4.2. Found: C, 18.6; H, 4.3%. ^{1}H NMR (295 K, CD_3CN): δ = 1.71 (d, 2JPH = 13.7 Hz). $^{13}C\{^1H\}$ NMR (295 K, CD_3CN): δ = 16.75 (d, $^1J_{PC}$ = 70.4 Hz). $^{19}F\{^1H\}$ NMR (295 K, CD_3CN): δ = −78.6 (s). $^{31}P\{^1H\}$ NMR (295 K, CD_3CN): δ = 65.3 (s). IR (Nujol/cm^{-1}): 1106 s (P=O).

3.4.1.13 **$[In(OTf)(OPMe_3)_5][OTf]_2$**

$In(OTf)_3$ (112 mg, 0.2 mmol) was dissolved in CH_2Cl_2 (10 mL) before the addition of trimethylphosphine oxide (92 mg, 1.0 mmol) and stirring for 2 h. After filtering to remove particulates, the filtrate was concentrated to ca. 5 mL *in vacuo* before addition of n-hexane (10 mL), which caused precipitation of a white solid. This was isolated by filtration before drying *in vacuo*. Yield: 100 mg, 49% Required for $C_{18}H_{45}F_9InO_{14}P_5S_3$ (1022.41): C, 21.2; H 4.4. Found: C, 21.8; H, 5.1%. ^{1}H NMR (295 K, CD_3CN): δ = 1.71 (d, $^2J_{PH}$ = 14 Hz). $^{13}C\{^1H\}$ NMR (295 K, CD_3CN): δ = 16.75 (d, $^1J_{PC}$ = 70 Hz). $^{19}F\{^1H\}$ NMR (295 K, CD_3CN): δ =−78.6 (s). $^{31}P\{^1H\}$ NMR (295 K, CD_3CN): δ = 63.9 (s). IR (Nujol/cm^{-1}) 1111 s (P=O).

3.4.1.14 **$[In(OPMe_3)_6][OTf]_3$**

$In(OTf)_3$ (112 mg, 0.2 mmol) was dissolved in CH_2Cl_2 (10 mL) before addition of trimethylphosphine oxide (111 mg, 1.2 mmol) and stirred for 2 h. Concentration of solvent *in vacuo* to ca. 50%, followed by addition of hexane (10 mL) resulted in a white solid which was collected by filtration and dried *in vacuo*. Yield: 148 mg, 66 %. Required for $C_{21}H_{64}F_9InO_{15}P_6S_3$ (1124.56): C, 22.4; H 5.7. Found: C, 22.7; H, 4.9%. ^{1}H NMR (295 K, CD_3CN): δ = 1.70 (d, $^2J_{PH}$ = 13.6 Hz). $^{13}C\{^1H\}$ NMR (295 K, CD_3CN): δ = 17.58 (d, $^1J_{PC}$ = 70.4 Hz). $^{19}F\{^1H\}$ NMR (295 K, CD_3CN): δ = −79.9 (s). $^{31}P\{^1H\}$ NMR (295 K, CD_3CN): δ = 60.9 (s). ^{115}In NMR (295 K, CD_3CN): δ = –93.7 (s). IR (Nujol/cm^{-1}): 1112 s (P=O).

3.4.2 Ligand Synthesis

3.4.2.1 **Bis-(diphenylphosphino)methane Oxide**

Bis-(diphenylphosphino)methane (2.5 g, 6 mmol) was dissolved in CH_2Cl_2 (350 mL) before the addition of SnI_4 (0.15 g, 0.24 mmol) and stirring while open to air for 5 days. After complete oxidation was achieved (observed *via* crude NMR spectroscopy), the solvent was removed *in vacuo* before being recrystallized with cold acetone (5 x 50 mL) yielding a white solid. Yield: 1.650 g, 66 %. ^{1}H NMR (295 K, CD_3Cl): δ = 7.67 (m, 8H, Ar-H), 7.29 (m, 12H, Ar-H), 3.45 (t, 2H, $^{2}J_{PC}$ = 14.7 Hz). $^{31}P\{^{1}H\}$ NMR (295 K, CD_3Cl): δ = 25.33 (s). IR (Nujol/cm^{-1}): 1188, 1169 (P=O).

3.5 – References

1 K. R. Cairns, W. Levason, G. Reid and W. Zhang, *Polyhedron*, 2021, **207**, 115367.
2 R. Bhalla, C. Darby, W. Levason, S. K. Luthra, G. McRobbie, G. Reid, G. Sanderson and W. Zhang, *Chem. Sci.*, 2014, **5**, 381–391.
3 M. J. Frazer, W. Gerrard and R. Twaits, *J. Inorg. Nucl. Chem.*, 1963, **25**, 637–640.
4 A. J. Carty and D. G. Tuck, *J. Chem. Soc. A Inorganic, Phys. Theor.*, 1966, 1081.
5 W. L. Jolly, *Modern Inorganic Chemistry*, McGraw-Hill Book Company, New York, 1984.
6 J. K. Burdett, 1978, pp. 113–146.
7 N. Burford, B. W. Royan, R. E. V. H. v. H. Spence, T. S. Cameron, A. Linden and R. D. Rogers, *J. Chem. Soc. Dalton. Trans.*, 1990, 1521.
8 F. E. Wood, M. M. Olmstead, J. P. Farr and A. L. Balch, *Inorg. Chim. Acta*, 1985, **97**, 77–83.
9 F. Cheng, H. L. Codgbrook, A. L. Hector, W. Levason, G. Reid, M. Webster and W. Zhang, *Polyhedron*, 2007, **26**, 4147–4155.
10 W. T. Robinson, C. J. Wilkins and Z. Zeying, *J. Chem. Soc., Dalton. Trans.*, 1990, 219–227.
11 W. T. Robinson, C. J. Wilkins and Z. Zeying, *J. Chem. Soc. Dalton. Trans.*, 1988, 2187.
12 M. F. Self, A. T. McPhail and R. L. Wells, *Polyhedron*, 1993, **12**, 455–459.
13 R. L. Wells, S. S. Kher, R. A. Baldwin and P. S. White, *Polyhedron*, 1994, **13**, 2731–2735.
14 M. V. Veidis and G. J. Palenik, *J. Chem. Soc. D Chem. Commun.*, 1969, 586b.
15 S. E. Jeffs, R. W. H. Small and I. J. Worrall, *Acta Crystallogr. Sect. C Cryst. Struct. Commun.*, 1984, **40**, 381–383.
16 A. Castiñeiras, M. R. Bermejo, A. Garcia-Deibe and W. Hiller, *Acta Crystallogr. Sect. C Cryst. Struct. Commun.*, 1991, **47**, 1738–1740.
17 R. Bhalla, J. Burt, A. L. Hector, W. Levason, S. K. Luthra, G. McRobbie, F. M. Monzittu and G. Reid, *Polyhedron*, 2016, **106**, 65–74.
18 W. Hiller, M. E. Garcia-Fernandez, M. R. Bermejo and M. V. Castano, *Acta Crystallogr. Sect. C Cryst. Struct. Commun.*, 1986, **42**, 60–62.
19 M. R. Bermejo, A. Castineiras, J. A. Garcia-Vazquez, W. Hiller and J. Strahle, *J. Crystallogr. Spectrosc. Res.*, 1991, **21**, 93–96.
20 E. Gutiérrez-Puebla, A. Vegas and S. García-Blanco, *Acta Crystallogr. Sect. B Struct. Crystallogr. Cryst. Chem.*, 1980, **36**, 145–147.
21 J. Burt, W. Levason, M. E. Light and G. Reid, *Dalton Trans.*, 2014, **43**, 14600–14611.
22 P. A. Gray, J. W. Saville, K. D. Krause, N. Burford, R. McDonald and M. J. Ferguson, *Can. J. Chem.*, 2017, **95**, 346–350.
23 S. A. Sangokoya, B. Lee, M. F. Self, W. T. Pennington and G. H. Robinson, *Polyhedron*, 1989, **8**, 1497–1502.
24 E. A. Pedrick, G. Wu and T. W. Hayton, *Inorg. Chem.*, 2015, **54**, 7038–7044.
25 A. V. Artem'ev, M. P. Davydova, A. S. Berezin, V. K. Brel, V. P. Morgalyuk, I. Y. Bagryanskaya and D. G. Samsonenko, *Dalton Trans.*, 2019, **48**, 16448–16456.
26 R. D. Bannister, W. Levason, G. Reid and W. Zhang, *Polyhedron*, 2017, **133**, 264–269.
27 C. J. Carmalt, L. J. Farrugia and N. C. Norman, *Main Gr. Chem.*, 1996, **1**, 339–344.
28 A. Mendia, E. Cerrada, E. J. Fernandez, A. Laguna and M. Laguna, *J. Organomet. Chem.*, 2002, **663**, 289–296.
29 E. V. Grachova, G. Linti, I. D. Protasova and S. P. Tunik, *Z. Anorg. Allgem. Chem.*, 2009, **635**, 2294–2296.
30 W. Levason, R. Patel and G. Reid, *J. Organomet. Chem.*, 2003, **688**, 280–282.
31 R. D. Bannister, W. Levason and G. Reid, *Chemistry (Easton).*, 2020, **2**, 947–959.
32 K. R. Cairns, W. Levason, G. Reid and W. Zhang, *Polyhedron*, 2021, **210**, 115529.
33 M. Haouas, F. Taulelle and C. Martineau, *Prog. Nucl. Magn. Reson. Spectrosc.*, 2016, **94**–**95**, 11–36.
34 M. A. Guino-o, B. Bustrom, R. A. Tigaa and A. de Bettencourt-Dias, *Inorg. Chim. Acta*, 2017, **464**, 23–30.
35 D. H. Johnston and D. F. Shriver, *Inorg. Chem.*, 1993, **32**, 1045–1047.

36 K. Nakamoto, *Infrared and Raman Spectra of Inorganic and Coordination Compounds, Part A: Theory and Applications in Inorganic Chemistry*, A John Wiley & Sons Inc., Publications, 6th edn., 2009.

Chapter 4 – Synthesis, properties and structures of gallium(III) and indium(III) halide complexes with neutral pnictine coordination

The earlier chapters of this thesis have been exploring the effect of substituting the strongly coordinated halide anion for the weakly coordinating triflate anion, and how this affects the complexes produced. This has required exploration of the literature, much of which is detailed in this introduction to this chapter, where it has been seen that coordination of simple monodentate ligands, in particular arsine donors, in 1:1 and 2:1 ratio dominate the chemistry.

4.1 – Introduction

Complexes of coordinated phosphine ligands are numerous when exploring the chemistry of the d-block, but feature less commonly in the chemistry of the *s*-, *p*- and *f*-block elements. Phosphines, along with the heavier pnictine ligands, are considered soft Lewis bases and therefore, following HSAB discussed in Chapter 1.1, coordination to the softer, low oxidation state *d*-block metals is expected. A comprehensive review of phosphine, arsine and stibine complexes in 1976 highlights the early research done on these systems with a heavy focus on the spectroscopic work due to the lack of structural studies at that time.[1] An updated review on the coordination chemistry of the main group elements with pnictine ligands was published in 2014 and this had a focus on novel reactions, X-ray structural and multinuclear NMR of previously synthesised complexes; both fields that had advanced significantly in that time.[2] Coordination to the boron and aluminium(III) halides are textbook examples of Lewis acids and have been extensively studied with different donating species and anions.

Previous reports on the coordination of softer pnictine ligands to the Group 13 metal halides have shown complexes of InX_3 (X = Cl, Br, I) with a single equivalent of a donor ligand generally taking up a distorted tetrahedral geometry $[InX_3(L)]$ as expected in Group 13.[3,4] The reactions of InX_3 with two molar equivalents of a monodentate ligand have generally produced two types of complex; the first being a self-ionised bimetallic species in the form $[InX_2(L)_4][InX_4]$ (X = Cl, Br). The second complex that is formed has been shown to take up a trigonal bipyramidal geometry formulated as $[InX_3(L)_2]$ (X = Cl, Br, I). The coordination of triphenylphosphine to form $[InCl_3(PPh_3)_2]$ was reported by Veidis and Palenik in 1969 and was the first documented example of an indium complex in the trigonal bipyramidal geometry, with the structure being shown in Figure 4.1. It was noted that the In-P bond lengths were approximately 0.2 Å longer than would be expected for this complex.[5]

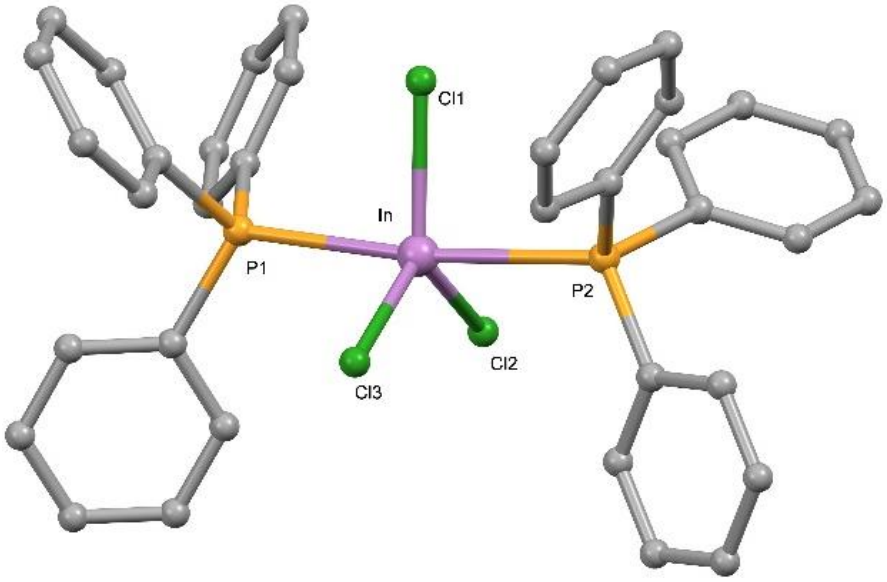

Figure 4.1 – Crystal structure of $[InCl_3(PPh_3)_2]$ showing the atomic numbering scheme. Redrawn from Ref[6] with H-atoms omitted for clarity

Later, synthesis of both $[InCl_3(NMe_3)_2]$ and $[InCl_3(PMe_3)_2]$ were found to adopt the same trigonal bipyramidal geometry with the latter having lengthened In-P bonds when compared with the structure in Figure 4.1, due to the steric bulk of the phenyl rings of the phosphine ligand.[6,7] This is known from the Tolman cone angles of these two ligands, previously mentioned in Chapter 1.2.1.[8] The initial report of the synthesis of $[InCl_3(PMe_3)_2]$ only discussed the ^{1}H NMR spectroscopy with no mention of other NMR techniques being employed. The solid state ^{31}P and ^{115}In NMR spectra were later collected in a separate study, showing two independent ^{31}P resonances at -3.7 and -2.4 ppm giving indication that in the solid state, there are slight differences between the environments of these two phosphines. A study comparing both $[InI_3(PPh_3)]$ and $[InI_3(PPh_3)_2]$ and the resonances produced by these in NMR spectroscopy, revealed a significantly broadened resonance for $[InI_3(PPh_3)_2]$, suggesting dissociation of at least a single equivalence of PPh_3 from $[InI_3(PPh_3)_2]$ in solution.[9] In the same study, the coordination of *bis*-(diphenylphosphino)ethane (dppe) was shown to chelate to form the trigonal bipyramidal $[InI_3(\kappa^2\text{-dppe})]$ where both phosphine donors are found equatorially. The NMR spectrum showed that, in solution, one arm of the phosphine dissociates to a tetrahedral geometry, $[InI_3(\kappa^1\text{-dppe})]$.

Repeating the equimolar reaction of PPh_3 with ethereal indium(III) iodide produced pale yellow crystals that X-ray analysis determined this to be a co-crystallised species $[InI_3(PPh_3)][InI_3(PPh_3)_2]$. Co-crystallisation of both the *mono*- and *bis*-complexes was also observed $[InI_3(AsPh_3)][InI_3(AsPh_3)_2]$ which is the only structure that show the coordination of a monodentate arsine ligand with InX_3 (X = Cl, Br, I).[10] There are no reported structures in the CCDC which show gallium forming complexes of this type $[GaX_3(L_2)]$ in the trigonal bipyramidal geometry with the softer pnictine ligands, with $[GaCl_3(PEt_3)]$ having been synthesised by

Schmidbaur.[11] Other monodentate phosphine and arsine complexes have been synthesised with varying R-groups and halides, all taking the form $[GaX_3(ER_3)]$ in the tetrahedral geometry.[12–14] Higher coordination numbers of gallium have been isolated with *penta*- and *hexa*-coordinate gallium(III) halide complexes have been produced with nitrogen donors. Reaction of $GaCl_3$ with 1,2,3-benzotriazole (Hbta) (ligand shown in Figure 4.2) in a 1:1 and 1:3 molar ratio produced $[GaCl_3(Hbta)]$ and $[GaCl_3(Hbta)_2]$ respectively with the latter being the first example of a $[GaX_3L_2]$ trigonal bipyramidal complex.[15] both the 1,2,3- and 2,1,3- benzothiadiazole ligands were the only Group 15 donor ligands shown to form a trigonal bipyramidal geometry with GaX_3. The only other reported gallium(III) halide complex to take this geometry was $[GaBr_3(THF)_2]$ with coordinated THF solvent molecules in the axial positions produced as a side-product from the synthesis of GaEBr (E = S, Se) in THF.[16,17]

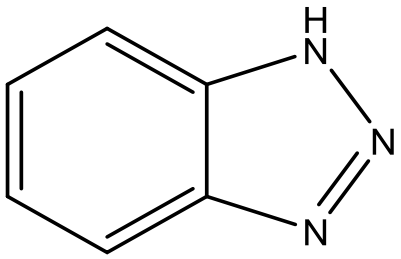

Figure 4.2 - Structure of 1,2,3-benzotriazole (Hbta).

There are currently only two structural examples of trigonal bipyramidal coordination complexes of phosphine ligands to aluminium(III) halides with $[AlCl_3(PMe_3)_2]$ and $[AlI_3(PEt_3)_2]$, with more being found in a tetrahedral geometry.[18,19] These also included a number of complexes with by bidentate phosphines coordinating to two metal centres, both of which take up the tetrahedral geometry.[19,20]

There are very few examples of aluminium halide complexes with heavier pnictine ligands (As, Sb) with each taking up a distorted tetrahedral geometry around the metal centre upon coordination. A study into arsine coordination produced a complete set of aluminium halide complexes from the 1:1 reaction to form $[AlX_3(AsR_3)]$ (X = Cl, Br, I; R = Me, Et, Ph), with X-ray crystal structures being obtained for $[AlX_3(AsPh_3)]$ (X = Cl, I).[21] A range of gallium halide complexes were synthesised with monodentate arsine ligands to produce $[GaX_3(AsMe_3)]$ (X = Cl, Br, I)[12] with a number of other structures showing the coordination with different arsine ligands including $AsPh_3$.[22] There was only a single structural example for the coordination of the soft arsine ligands to InI_3, in the form of $[InI_3(AsPh_3)][InI_3(AsPh_3)_2]$.

Reaction of the Group 13 metal halides with bidentate phosphine ligands such as *o*-$C_6H_4(PR_3)_2$ (R = Ph, Me, $SiMe_3$) shows the difference in the chemistry as the group is descended. There are currently only two complexes of coordination of *o*-$C_6H_4(PR_3)_2$ (R = Me, Ph) with $AlCl_3$ with both

methyl and phenyl R-groups, both taking up $[AlCl_2\{o\text{-}C_6H_4(PR_2)_2\}][AlCl_4]$.[19] The 1:1 reaction between $o\text{-}C_6H_4(PMe_3)_2$ and GaX_3 (X = Cl, Br, I) produces the octahedral cationic species *trans*-$[GaX_2(o\text{-}C_6H_4(PMe_2)_2)_2][GaX_4]$ and analogous species were observed for each of the three halides used. The structure of the cation is shown in Figure 4.3.[12]

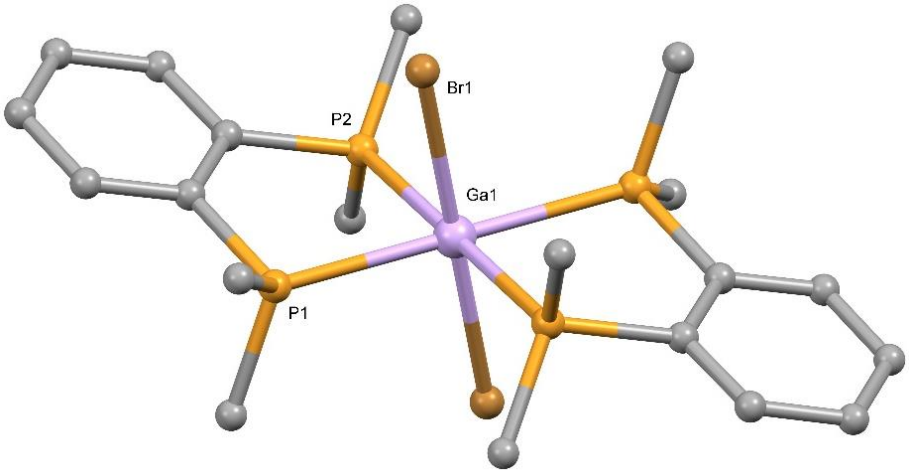

Figure 4.3 – Crystal structure of $[GaBr_2\{o\text{-}C_6H_4(PMe_2)_2\}_2][GaBr_4]$ showing the atomic numbering scheme. Redrawn from Ref[12] with anions, lattice solvent molecules and H-atoms omitted for clarity.

In contrast to the gallium reaction, the 1:1 reaction of $InCl_3$ with $o\text{-}C_6H_4(PMe_2)_2$ produced a centrosymmetric chloride bridged dimer $[\{InCl_2\{o\text{-}C_6H_4(PMe_2)_2\}_2(\mu^2\text{-}Cl)_2]$.[23] Upon dissolving this complex in CH_2Cl_2, the ^{115}In NMR spectrum shows a single resonance at 442 ppm which is characteristic of the $[InCl_4]^-$ anion suggesting that this bridged species undergoes a rearrangement in solution to *trans*-$[InCl_2\{o\text{-}C_6H_4(PMe_2)_2\}_2][InCl_4]$. Repeating this with $InBr_3$ produces the ionic complex $[InBr_2\{o\text{-}C_6H_4(PMe_2)_2\}_2][InBr_4]$ (X = Br, I) in solution, with the presence of $[InX_4]^-$ observed in the solution state ^{115}In NMR spectrum. The iodo-reaction produced an intermediate species $[InI_2\{o\text{-}C_6H_4(PMe_2)_2\}_2][InI_4\{o\text{-}C_6H_4(PMe_2)_2\}]$, with coordination of the phosphine ligand to the halometalate anion. Dissolving this complex in CH_2Cl_2 caused the dissociation of the ligand from the halometalate, producing resonances characteristic of free ligand $\{o\text{-}C_6H_4(PMe_2)_2\}_2$ and $[InI_4]^-$ in the multinuclear NMR spectroscopy.

The equimolar reaction of GaX_3 with the bidentate $o\text{-}C_6H_4(AsMe_2)_2$ differs from that of the phosphine analogue above, producing the distorted tetrahedral species $[GaX_2\{o\text{-}C_6H_4(AsMe_2)_2\}][GaX_4]$ (X = Cl, I) and no evidence of a six-coordinate species being produced.[12] This is one of the few examples where there is a difference in the reaction of these two ligands $o\text{-}C_6H_4(EMe_2)_2$ (E = P, As) with a common metal centre. The reaction of $o\text{-}C_6H_4(AsMe_2)_2$ in a stoichiometric ratio with InX_3 (X = Cl, Br) produces a dimer with two octahedral metal centres joined by bridging chloride anions $[\{InX_2\{o\text{-}C_6H_4(AsMe_2)_2\}_2(\mu^2\text{-}Cl)_2]$ (X = Cl, Br) in the solid state.[23] This underwent a further rearrangement, as was observed for the reactions of $o\text{-}C_6H_4(PMe_2)_2$, to give the ionic complex $[InX_2\{o\text{-}C_6H_4(AsMe_2)_2\}_2][InX_4]$ and another unknown complex. Attempts at

this reaction with InI_3 mirrored that observed with *o*-$C_6H_4(PMe_2)_2$ by forming a complex containing the anion $[InI_4\{o\text{-}C_6H_4(AsMe_2)_2\}]^-$ in solution, the structure of this complex is shown in Figure 4.4.

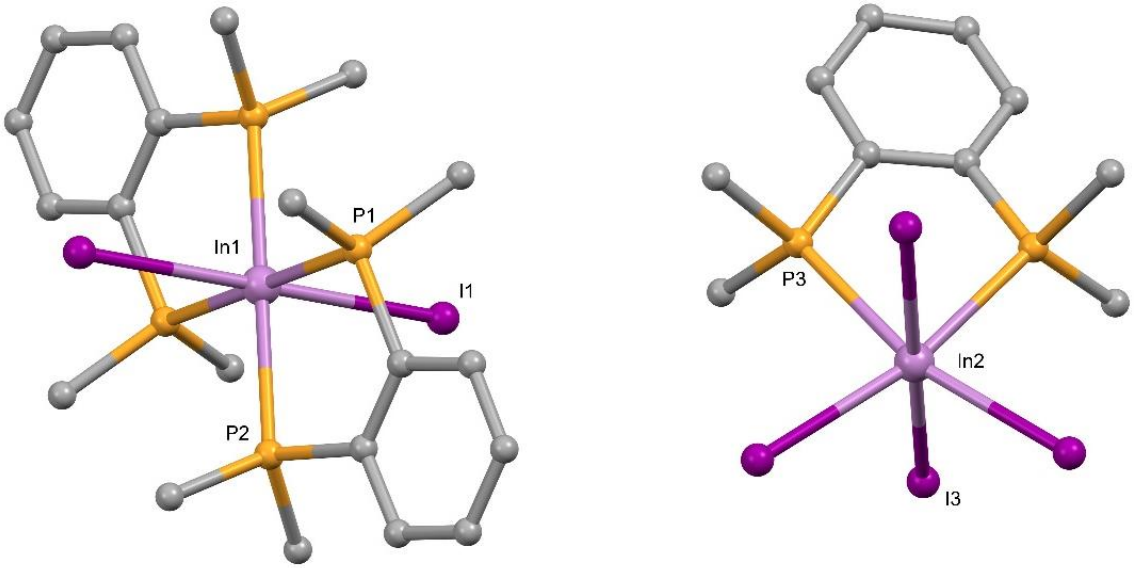

Figure 4.4 - Structure of the co-crystallised $[InI_2\{o\text{-}C_6H_4(PMe_2)_2\}_2][InI_4\{o\text{-}C_6H_4(PMe_2)_2\}]$ showing the atomic numbering scheme. Redrawn from Ref[23] with H-atoms omitted for clarity.

Coordinating stibine ligands to the Group 13 metals is rare, with the majority of structures being reported in a recent publication from the Reid group. This detailed the synthesis of monodentate SbR_3 (R = Et, ^{i}Pr) complexes of the Group 13 metal halides MX_3 (M = Al, Ga, In; X = Cl, Br, I), with their structures revealing complexes formulated as $[MX_3(SbR_3)]$ (M = B, Al, Ga, In; X = Cl, Br, I; R = Me, ^{i}Pr).[24] Each of these reactions was shown to produce a distorted tetrahedral geometry, with this being the commonly observed for monodentate coordination to Group 13 metal halides.[25] The coordination of triphenylstibine to $M(^t Bu)_3$ produced complexes in the same geometry despite the increased steric bulk of both materials.[26] A selection of structures from this publication have been redrawn in Figure 4.5, showing an example of antimony coordination with each of the Group 13 metals.

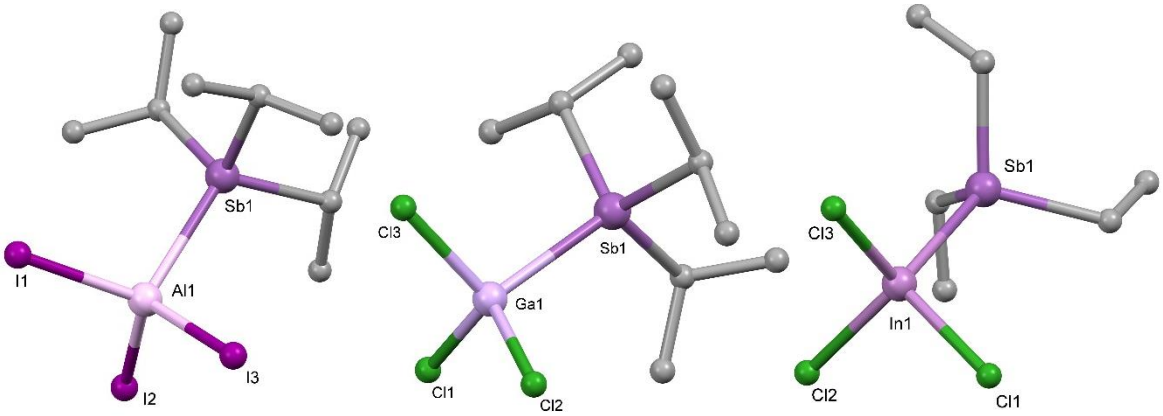

Figure 4.5 - Structures of $[AlI_3(Sb^iPr_3)]$, $[GaCl_3(Sb^iPr)]$ and $[InCl_3(SbEt_3)]$ showing the atomic numbering scheme. Redrawn from Ref[24] with H-atoms and solvent lattice molecules omitted for clarity.

These $[MX_3(SbR_3)]$ (M = B, Al, Ga, In; X = F, Cl, Br, I; R = Et, ^{i}Pr) complexes were very moisture sensitive with colour changes being observed over several days after synthesis, with the stability of the complexes increasing down the group, likely due to the more favourable overlap of similar sized orbitals of the heavier elements. Of these, the boron complexes $[BX_3(SbR_3)]$ (X = F, Cl, Br, I; R = Et, ^{i}Pr) were seen to be particularly unstable, with the fluoride complexes losing BF_3 over a few hours at room temp, unlike $[BF_3(PMe_3)]$ which is stable in the absence of moisture. When left in a CH_2Cl_2 solution, both the boron and aluminium complexes $[MX_3(SbR_3)]$ (M = B, Al; X = Br, I) were seen to undergo halide substitution reactions with the CH_2Cl_2 solvent, to produce the corresponding chloride complex $[MX_{3-n}Cl_n(SbR_3)]$. The increased stability of the gallium and indium complexes meant that any of the halide adducts could be recrystallized from CH_2Cl_2 without reaction, they also showed moderate air stability. Although the five coordinate trigonal bipyramidal geometry is known for indium with many of the soft pnictine ligands, there was no evidence of a *bis*-stibine complex, even though attempted. There was evidence of secondary intermolecular Sb···X contacts in the solid state of $[InCl_3(SbR_3)]$ to form weakly associated dimers through hypervalent interactions of the antimony atom.

As was observed through reaction with the CH_2Cl_2 solvent, the halide anions can be removed from some of these complexes to produce the cationic species. These could contain a weakly coordinating anion (such as triflate) filling the vacant site or alter the structure of the complex for bridging through the remaining halides. Burford had success in this with removal of 1-3 chloride anions using $AlCl_3$ and TMSOTf. The complex $[SnCl_4(PMe_3)_2]$ takes up an octahedral geometry however after reaction of 1-2 equivalents of $AlCl_3$ was shown to produce cationic complexes $[SnCl_{3-n}(PMe_3)_2][AlCl_4]_n$ (n = 1, 2).[27] These two complexes were shown to take up a trigonal bipyramidal and distorted disphenoid respectively. The complex $[SnCl_2(PMe_3)_2][AlCl_4]_2$ also contained short contacts from the metal to the metallate anions, however, no further intermolecular bonding. This work was followed by a report describing synthesis of cationic Ge and Sn with imine ligands,[28] with the scheme of these reactions shown below in Scheme 4.1. This method of abstraction had a driving force for the formation of the stable $[AlCl_4]^-$ anion.

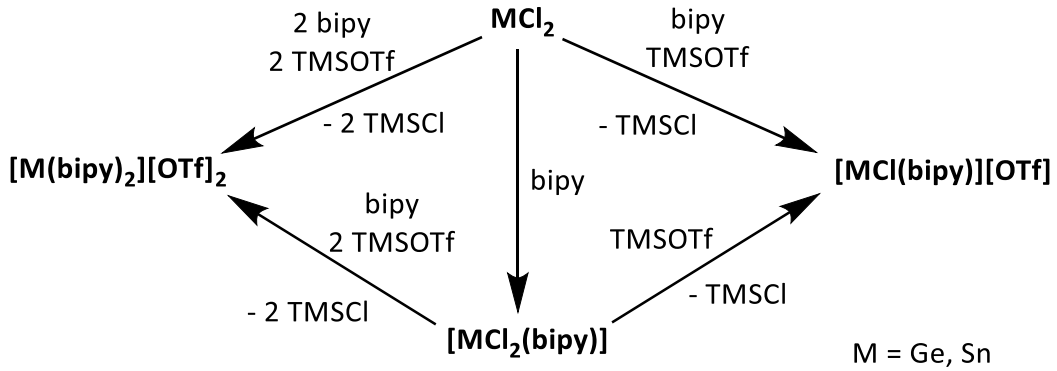

Scheme 4.1 - Reaction schemes for the synthesis of $[MCl_2(bipy)]$, $[MCl(bipy)][OTf]$ and $[M(bipy)_2][OTf]_2$.[28]

Crystal structures of both $[M(bipy)_2][OTf]_2$ showed the dicationic species with long contacts to the anions in solution just within the sum of the van der Waals radii. Of the monocations produced, only [GeCl(bipy)][OTf] was crystallised, with X-ray diffraction revealing the structure to be a weakly associated dimer, bridged through weak interactions of the halides forming a Ge_2Cl_2 core. The driving force for this method was the production and removal *in vacuo* of TMSCl, a volatile product, making the reactions non-reversible. Following on from this, work within the Reid group showed that abstraction of fluoride from complexes of GeF_4 with soft donor ligands (P, As) was also possible using TMSOTf as an abstraction agent. Reaction of *trans*-$[GeF_4(PMe_3)_2]$ with TMSOTf in varying stoichiometric ratios, to produce $[GeF_{4-n}(PMe_3)_2(OTf)_n]$ (n = 1-3) in which the triflate anion was found coordinated to the metal centre after displacing a fluoride.[29] The monocationic complex $[GaF_3(OTf)(PMe_3)_2]$ was found to produce crystals after sitting in CH_2Cl_2 overnight with the structure shown in Figure 4.6.

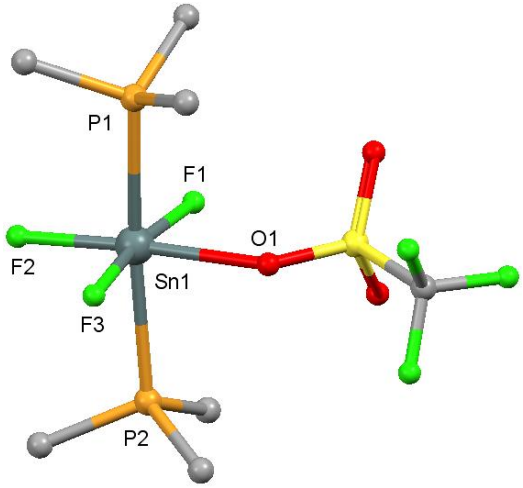

Figure 4.6 - Crystal structure of *trans*-$[SnF_3(OTf)(PMe_3)_3]$ showing the atomic numbering scheme. Redrawn from Ref[29] H-atoms omitted got clarity.

Crystallography showed the dicationic species $[Ge(PMe_3)_3][OTf]_2$ + $[FPMe_3]^+$ and other products, through reductive loss of fluoride. This publication also showed the same behaviour using the bidentate ligands *o*-$C_6H_4(PMe_2)_2$ and $Ph_2P(CH_2)_2PPh_2$. A follow up publication described the abstraction of fluoride from GaF_4 complexes involving a range of other ligands including nitrogen donors such as (MeCN, terpy and azamacrocycles Me_3tacn ad Me_3cyclam) and oxygen donors ($OPPh_3$, $OAsPh_3$).[30] This was shortly followed by a publication detailing the abstraction of fluoride from coordinated SnF_4 complexes with soft donors such as P^iPr_3 and PMe_3, and a range of monodentate oxygen donors (DMSO, py, pyNO, DMF and $OPPh_3$).[31] Each of these complexes was reacted with TMSOTf and an additional equivalents of ligand (L) to produce the corresponding $[SnF_3(L)_3][OTf]$ complex. Reaction of complexes containing later halogens (Cl, Br) showed it was also possible to remove chloride using TMSOTf, producing TMSCl as a volatile product to aid in driving the reaction to completion by removal *in vacuo*. Reactions with the corresponding

bromide complex were unsuccessful, likely due to the less energetically favourable formation of TMSBr. This method was shown to be highly robust method at removal of a halide (F, Cl) from complexes of Group 14 metals, with abstraction being shown with a range of different donors, denticity and coordination numbers.

4.1.1 Low Pressure Chemical Vapor Deposition (LPCVD)

The deposition of Ga_2E_3 (E = Se, Te) through low-pressure chemical vapour deposition (LPCVD) was shown to be possible using substrates with the Ga-E bond pre-incorporated such as $[(GaCl_3)_2\{^nBuE(CH_2)_nEBu^n\}]$ (E = Se, *n* = 2; E = Te, *n* = 3).[32] Figure 4.7 is a simplified diagram showing how LPCVD is carried out inside a furnace to allow for even volatilisation of the precursor. Commonly, these are materials are produced through CVD of dual-sources, using a mixture of MR_3 and SbR_3', with no prior bonding between the metal and donor. These materials are an important class of semiconducting materials with applications across modern electronics and this method of deposition makes use of single source precursors. These precursors are simply synthesised in a 2:1 reaction of $GaCl_3$ with the $^tBuTe(CH_2)Te^tBu$ ligand in CH_2Cl_2, with crystals being grown from the mother liquor overnight. Using the setup illustrated in Figure 4.7, LPCVD experiments were conducted at >750 K with the selenoether materials being deposited as a matt orange film and the telluroethers appearing as a shiny dark grey over the SiO_2 substrate. Details of these materials were then collected through grazing incident X-ray diffraction (GIXRD), energy-dispersive X-ray spectroscopy (EDX), scanning electron microscope (SEM). EDX spectroscopy was able to reveal a 1:1.5 ratio of metal to chalcogen with negligible C or Cl contaminants, giving a good suggestion of successful formation of the target Ga_2E_3 without compromising the chalcogen through the LPCVD process. As well as success with the chalcogenoethers, complexes with soft pnictine donors (P and As) were also shown to act as single source precursors to deposition of GaP and GaAs.[33] The synthesis of the bridged species $[^nBu_2Ga(\mu\text{-}E^tBu_2)_2Ga^nBu_2]$ (E = P, As) was found to give reliable, good quality deposition of GaE (E = P, As). These deposited materials were probed for their composition showing the expected 1:1 ratio but different morphologies between the deposited materials. In the report describing the synthesis of triel stibine complexes $[MX_3(SbR_3)]$ (M = Ga, In; X = Cl, Br, I; R = Et, ^{i}Pr), future work was to use these complexes as precursors to the deposition of thin-films of MSb (M = Ga, In), which are both semiconducting materials.

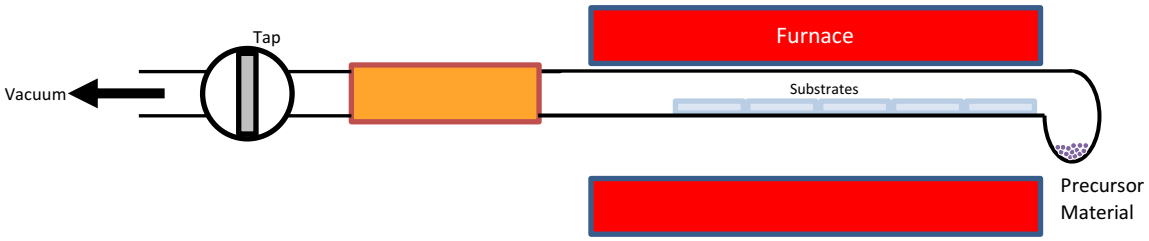

Figure 4.7 - Diagram of an LPCVD experiment.

Following on from the work reported here,[24] and the work of a project student Miss Laura Grose on the further exploration of the trialkylstibines, the work of this chapter focuses on the coordination of the softer pnictine ligands EEt_3 (E = P, As, Sb) to the Group 13 metal chlorides MCl_3 (M = Ga, In). The coordination of arsine ligands has been rarely reported for the triel halides with this chapter both replicating previous results as well as synthesising novel arsine complexes. Once synthesised, these complexes will be tested for their activity towards halide abstraction, following the successful work by abstraction work by Burford *et al*. on Group 14 soft donor complexes. These compounds will also be tested as precursors to the deposition of GaAs and InAs, after the success of this method in the deposition of the triel chalcogenoether complexes.

4.2 – Results and Discussion

4.2.1 Complex Synthesis

Due to the need for β-hydride elimination for the deposition of the target materials (GaAs, GaP), methyl and phenyl ligands are not suitable and so straight chain aliphatic phosphine and arsine ligands are required. The simplest phosphine that can undergo β-hydride elimination during deposition is the ethyl-substituted phosphine, which was synthesised *via* a Grignard type preparation, following an adjusted procedure for the synthesis of triethylstibine.[24] Due to the potentially pyrophoric nature of Grignard reactions, this reaction was carried out under exclusively inert conditions and cooling upon addition to the reaction mixture, preventing thermal runaway. Once a crude product was obtained, the final step was a vacuum transfer to obtain the isolated pure PEt_3 which was characterised by ^{1}H and $^{31}P\{^{1}H\}$ NMR spectroscopy, showing only a single species, matching the literature values of PEt_3.[34] The spectra in Figure 4.8 demonstrates the splitting pattern observed in the ^{1}H NMR spectra, with the methylene protons (upfield) and methyl protons (downfield). This splitting observed here was unexpected, showing a $^{3}J_{PH}$ coupling of the methyl protons but with no evidence of $^{2}J_{PH}$ coupling to the methylene protons.[35]

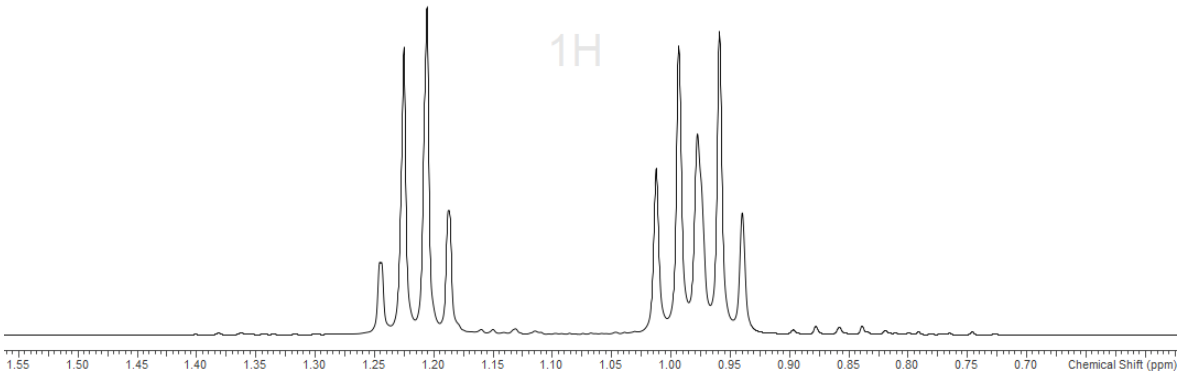

Figure 4.8 - ^{1}H NMR spectra for the freshly synthesised PEt_3.

Knowing that synthesis of $[InCl_3(PMe_3)_2]$ had been completed previously by Wallbridge and co-workers, synthesis of the triethylphosphine analogue was attempted using a modified version of the reported procedure. To a suspension of $InCl_3$ in CH_2Cl_2, PMe_3 was added in a 2:1 molar ratio and allowed to react for two hours, before remaining particulates of $InCl_3$ were filtered away. Concentration of the solution caused the precipitation of a white solid which was characterised by both IR and NMR spectroscopy before being sent for microanalysis. The elemental analysis matched the calculated formulation of $[InCl_3(PEt_3)_2]$ which was corroborated by the NMR spectra, which showed a single species in solution. The coordination of PEt_3 caused a high frequency shift of the alkyl resonances in the ^{1}H NMR spectra as well as inducing changes in the splitting. The methyl protons are found at 1.23 ppm with the resonance splitting unchanged, however, the

methylene protons were shifted to 1.94 ppm and now took up a quintet. The $^{13}C\{^{1}H\}$ NMR spectra showed two resonances, the first as a singlet at a lower frequency corresponding to the methyl carbon, with the methylene carbon producing a second resonance, split into a doublet with a $^{1}J_{PC}$ = 18.34 Hz. When $[InCl_3(PMe_3)_2]$ was first synthesised, only ^{1}H NMR spectroscopy data was discussed but the ^{31}P and ^{115}In NMR spectrum were collected *via* solid state NMR years later.[4] The solid state analysis of $[InCl_3(PMe_3)]$ showed two independent ^{31}P resonances at -3.7 and -2.4 ppm, however, this triethyl analogue appears to contain a single broad resonance in the solution state $^{31}P\{^{1}H\}$ spectrum at 3.54 ppm. Previous studies in the group producing coordination complexes of indium halides in the form $[InX_3(L)_n]$ (n = 1, 2) have observed no resonances in the ^{115}In NMR spectrum and thus was not collected here. Moving from a C_{3v} or D_{3h} point group to a higher symmetry system such *Td* or *Oh* may allow for resolution of an ^{115}In resonance in solution. IR spectroscopy showed that coordination with the PEt_3 ligand caused a shift of the In-Cl stretching frequency from 401 cm^{-1} to 284 cm^{-1}, a significant shift to a lower frequency.

$[InCl_3(PEt_3)_2]$ was crystallised from a CH_2Cl_2 solution by slow evaporation of the solvent under inert conditions with X-ray diffraction experiments revealing the solid state structure $[InCl_3(PEt_3)_2]$ taking up the expected trigonal bipyramidal geometry. The phosphine ligands took up the axial positions with the halides taking up equatorial positons, shown in Figure 4.9 with selected bond lengths and angles provided in Table 4.1. This geometry is consistent with that seen in other trigonal bipyramidal indium complexes, including $[InCl_3(PPh_3)_2]$ which was previously demonstrated in Figure 4.1, and is isostructural to the methyl analogues previously synthesised.

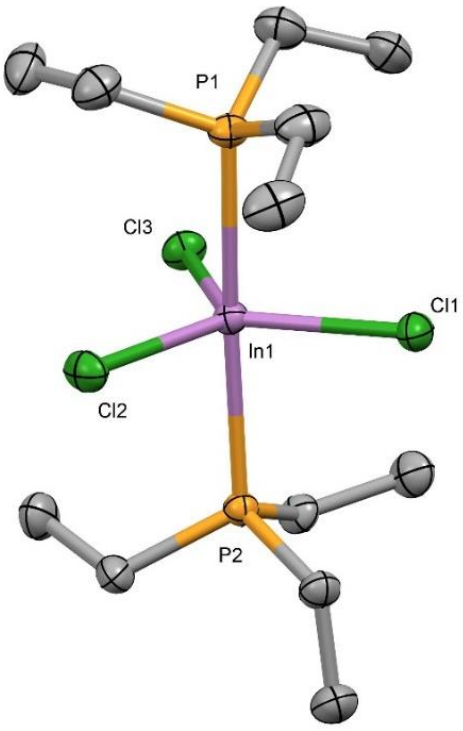

Figure 4.9 - Crystal structure of ***15*** $[InCl_3(PEt_3)_2]$ showing the atomic numbering scheme. Ellipsoids at 50% probability with H-atoms omitted for clarity.

Table 4.1 - Table of selected bond lengths and angles for $[InCl_3(PEt_3)_2]$.

Bond Lengths / Å		Bond Angles / °	
In1 – P1	2.6160(13)	P1 – In1 – P2	176.18(4)
In1 – P2	2.6155(13)	Cl1 – In1 – Cl2	123.02(5)
In1 – Cl1	2.4601(13)	Cl1 – In1 – Cl3	119.99(5)
In1 – Cl2	2.4499(13)	Cl2 – In1 – Cl3	116.14(5)
In1 – Cl3	2.4461(13)	Cl1 – In1 – P1	88.05(4)
		Cl2 – In1 – P1	90.32(4)
		Cl3 – In1 – P1	92.58(4)
		Cl1 – In1 – P2	88.82(4)
		Cl2 – In1 – P2	89.54(4)
		Cl3 – In1 – P2	90.89(4)

The axial phosphine ligands in $[InCl_3(PEt_3)_2]$ are close to linear with a P-In-P bond angle of 176.18°, while the equatorial chlorides displaying minor variations in the Cl-In-Cl angles, but never far from the expected 120° ideal angle. Comparison of the In-P bonds complexes with phosphine ligands with varying R-groups (Me, Et, Ph) is shown in Table 4.2, with a clear increase in the In-P bond length with the increasing steric bulk of the ligand, in the order Me < Et < Ph.

Table 4.2 - Table of In–P bond lengths comparing ligand sterics.

Complex	In – P bond distance / Å		Ref
$[InCl_3(PMe_3)_2]$	2.575(3)	2.576(3)	[6]
$[InCl_3(PEt_3)_2]$	2.6160(13)	2.6155(13)	*This work*
$[InCl_3(PPh_3)_2]$	2.6966(5)	2.7290(5)	[5]

The reaction of $InCl_3$ with a single molar equivalents of $AsEt_3$ under inert conditions produced a white solid in good yield and upon microanalysis, matched the weights of the calculated formulation of $[InCl_3(AsEt_3)]$. Each of the reactions with $InCl_3$ are presented in Scheme 4.1. The ^1H NMR spectroscopy revealed two resonances shifted from free ligand, the first a quartet at 2.22 and the second a triplet 1.40 ppm, corresponding to the methylene and methyl protons respectively. Both resonances observed in the $^{13}C\{^1H\}$ spectrum of $[InCl_3(AsEt_3)]$ were shifted to a higher frequency than those observed for the free ligand. IR spectroscopy of this complex showed two In-Cl vibrational absorbances at 333 and 313 cm^{-1}, as expected from the group theory.

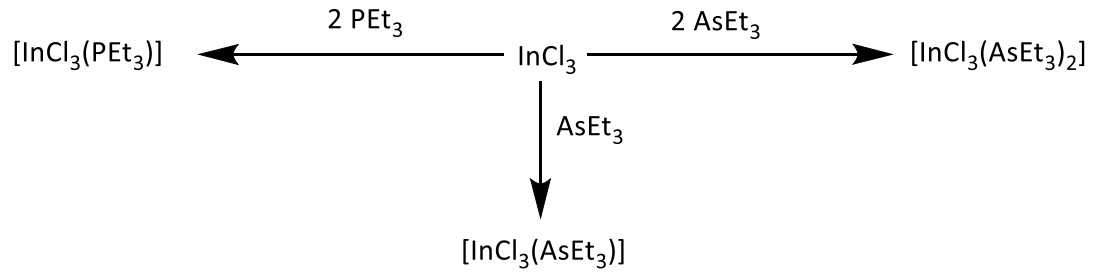

Scheme 4.2 - Reactions of $InCl_3$ with PEt_3 and $AsEt_3$ in 1:1 and 2:1 ratios.

This reaction was then repeated using two molar equivalents of $AsEt_3$ which produced a white solid and confirmed as spectroscopically independent from the first product. The ^{1}H NMR spectrum again showed a high frequency shift from free PEt_3, but at a slightly lower frequency than was observed for $[InCl_3(AsEt_3)]$. A quartet was measured at 1.91 ppm showing a drop of ~0.3 ppm while the triplet was measured at 1.30 ppm, a decrease in frequency of ~0.1 ppm, corresponding to the methylene and methyl protons respectively. IR spectroscopy of this complex showed two absorbance's at 332 and 299 cm^{-1}, where one (299 cm^{-1}) is strong and broad and the other (332 cm^{-1}) is a much weaker shoulder, differing from that observed for $[InCl_3(AsEt_3)]$. Group theory predicts that, for the D_{3h} $[InCl_3(AsEt_3)_2]$ complex, only a single absorbance should be observed, with the second weaker absorbance possible originating from a small amount of the $[InCl_3(AsEt_3)]$ present in the bulk material. There was however, no other spectroscopic evidence for this conclusion. Although attempted for both of these arsine complexes, neither produced a visible ^{115}In resonance even after a high number of scans (10,000+). Previous reports of indium complexes have shown no observable resonances in the chloro-complexes, with the same bromo and iodo analogues found to produce a resonance.[24]

Good quality crystals of both $[InCl_3(AsEt_3)]$ and $[InCl_3(AsEt_3)_2]$ were grown from CH_2Cl_2 solutions when layered with *n*-hexane and the structures of these are shown in Figure 4.10.

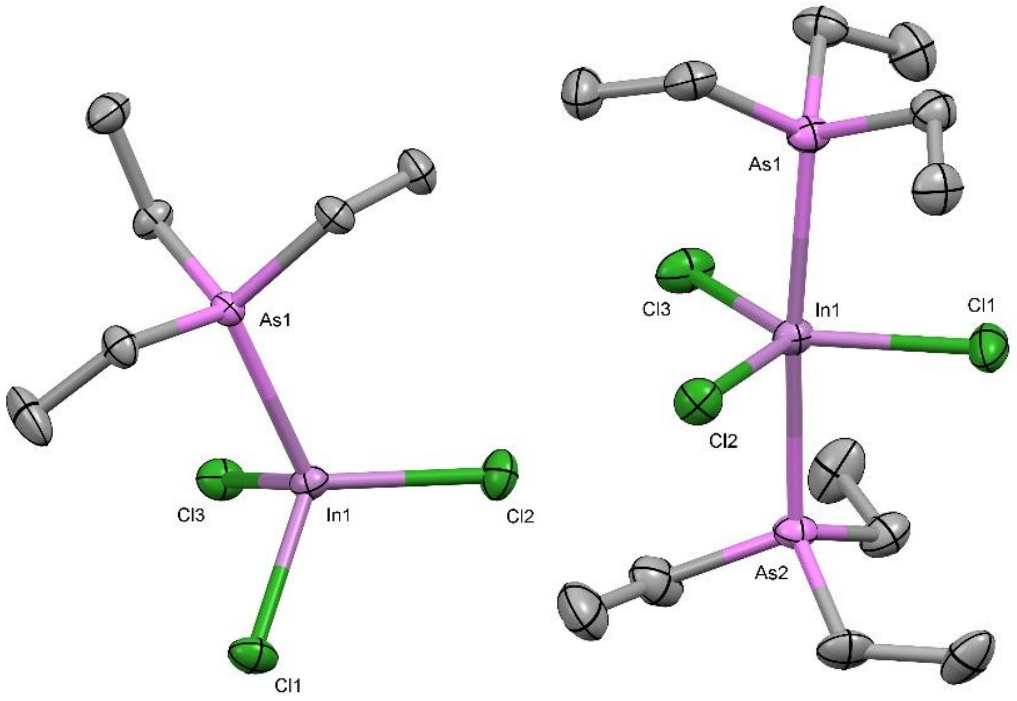

Figure 4.10 - Crystal structures of (a) ***16*** [$InCl_3(AsEt_3)$] and (b) ***17*** [$InCl_3(AsEt_3)_2$] showing the atomic numbering scheme. Ellipsoids at 50% probability with H-atoms are omitted for clarity.

Table 4.3 - Table of selected bond lengths and angles for [$InCl_3(AsMe_3)$] and [$InCl_3(AsMe_3)_2$].

Bond Lengths / Å				**Bond Angles / °**			
[$InCl_3(AsMe_3)$]		[$InCl_3(AsMe_3)_2$]		[$InCl_3(AsMe_3)$]		[$InCl_3(AsMe_3)_2$]	
In1 – As1	2.6051(4)	In1 – As1	2.704(1)	Cl1 – In1 – As1	117.15(2)	As1 – In1 – As2	172.99(3)
In1 – Cl1	2.2766(8)	In1 – As2	2.700(1)	Cl2 – In1 – As1	115.02(2)	Cl1 – In1 – Cl2	117.58(8)
In1 – Cl2	2.3552(9)	In1 – Cl1	2.411(2)	Cl3 – In1 – As1	101.77(2)	Cl1 – In1 – Cl3	125.25(9)
In1 – Cl3	2.3856(9)	In1 – Cl2	2.431(2)	Cl1 – In1 – Cl2	112.50(3)	Cl2 – In1 – Cl3	117.14(8)
		In1 – Cl3	2.427(2)	Cl1 – In1 – Cl3	101.18(3)	Cl1 – In1 – As1	88.80(6)
				Cl2 – In1 – Cl3	106.96(3)	Cl2 – In1 – As1	93.54(6)
						Cl3 – In1 – As1	89.55(6)
						Cl1 – In1 – As2	86.75(6)
						Cl2 – In1 – As2	93.32(6)
						Cl3 – In1 – As2	88.60(6)

These crystal structures revealed both complexes to take up the expected geometry in the solid-state with the 1:1 reaction producing a tetrahedral metal centre and the *bis*-complex found as a *trans*-trigonal bipyramid with the arsine ligands taking up the axial sites. Comparison of the In-As bonds of these complexes shows that coordination of the second equivalents of donor ligand causes bond elongation from 2.6051(4) Å by ~0.1 Å. There is also an increase of ~0.07 Å to each of the In-Cl bonds. This increase and thus weakening of the In-Cl bonds is reflected by the low frequency absorbance band in the IR spectroscopy, at 299 cm^{-1}.

In the report on the synthesis of $[InCl_3(SbR_3)]$ (R = Et, ^{i}Pr), secondary weaker intermolecular In···Cl contacts were identified as bridges between two metal centres, an effect not observed for the *n*-butyl stibine complex.[24] These contacts was also observed in $[InCl_3(AsEt_3)]$ with two 3.2147(9) Å contacts between monomers, a distance within the sum of the van der Waals radii (3.68 Å), forming weakly associated dimers in the solid state.[36] The coordination of arsine ligands to the Group 13 metals found that boron complexes $[BX_3(AsR_3)]$ (X = Ph, C_6F_5; R = Me, Et, Ph) took up a near eclipsed arrangement.[21] The aluminium and gallium complex $[MX_3(AsR_3)]$ (M = Al, Ga; X = Cl, Br, I; R = Me, Et, Ph) took up a staggered arrangement with larger torsion angles, with a selection of these torsion angles detailed in Table 4.4.[21] Comparison to the indium analogue synthesised here shows that this torsion angle is again lowered to take up a staggered arrangement. $[InCl_3(AsEt_3)]$ is found to have a C-As-In-Cl torsion angle of 4.23(13)°; there is likely a decrease in destabilising interactions of the carbon chain of the ligand and the halides due to the increase in M-As distance.

Table 4.4 - Table of X-M-E-C torsion angles with arsine ligands.

Complex	**Smallest Torsion Angle / °**	**Arrangement**	**Ref**
$B(C_6F_5)_3(AsEt_3)$	9.89(13)	Eclipsed	[21]
$AlCl_3(AsPh_3)$	32.58(6)	Staggered	[21]
$AlI_3(AsPh_3)$	38.83(6)	Staggered	[21]
$GaCl_3(AsPh_3)$	29.9(3)	Staggered	[21]
$GaCl_3(AsEt_3)$	38.1(3)	Staggered	*This Work*
$InCl_3(AsEt_3)$	4.23(13)	Eclipsed	*This Work*

The reaction of GaX_3 with some monodentate phosphine and arsines is known, with some being discussed in the introductory section of this chapter. Each of the coordination complexes formed in the 1:1 reaction with these soft donor ligands took up the expected tetrahedral geometry at the metal centre, formulated as $[GaX_3(ER_3)]$ (X = Cl, Br, I; E = P, As; R = Me, Ph).[12–14] The equimolar reaction of PEt_3 with $GaCl_3$ is known to produce $[GaCl_3(PEt_3)]$ and was repeated here, but there has been no report of the 2:1 reaction forming $[GaCl_3(PR_3)_2]$.[11] Attempts at the 2:1 reaction gave the $^{31}P\{^1H\}$ NMR spectrum in Figure 4.11(b), producing a with a very broad resonance at ~-0.5 ppm. Small amounts of a second resonance were observed at 24.73 ppm in $^{31}P\{^1H\}$ NMR spectrum, this had been previously in earlier reactions using PEt_3. This sample was analysed by proton de-coupled ^{31}P NMR spectroscopy, which showed the resonance at being split into a doublet, suggesting protonation of the phosphine had occurred to form the triethylphosphonium cation $[HPEt_3]^+$ *in situ*. ^{71}Ga NMR spectroscopy revealed a major species as a doublet at 273 ppm, with a coupling value of $^1J_{P\text{-}Ga}$ = 980 Hz, as well as a second smaller species, corresponding to $[GaCl_4]^-$, suggesting the impurity be $[HPEt_3][GaCl_4]$.[37] There was a much higher ratio of protonated phosphine:target complex in the 2:1 ratio, suggesting that that is being produced with excess ligand reacting with the adventitious water. Attempts at crystallisation of $[GaCl_3(PEt_3)_2]$ produced small amounts of crystalline material that upon X-ray diffraction showed as $[HPEt_3][GaCl_4]^-$.

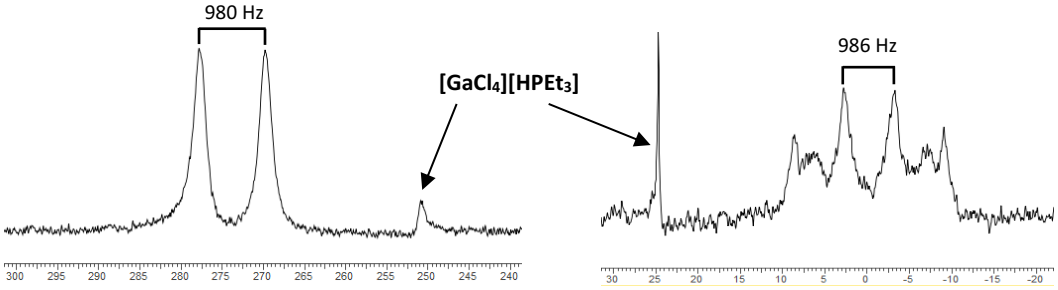

Figure 4.11 – (a) The ^{71}Ga and (b) $^{31}P\{^1H\}$ NMR spectra of $[GaCl_3(PEt_3)]$ labelled with coupling constants as well as the by-product of $[HPEt_3][GaCl_4]$.

In the report detailing the synthesis of $[GaCl_3(PEt_3)]$, the $^{31}P\{^1H\}$ NMR spectrum was described as a broad singlet at -4.6 ppm.[11] After repeating this reaction and collection of a high number of scans (~1000), the resonance was found to be split into a quartet with a coupling constant of 986 Hz, closely matching the coupling observed in the ^{71}Ga NMR spectra. The ^{71}Ga nuclei has a spin of I = 3/2 and thus it would be expected to produce a 1:1:1:1, however appears as a 1:3:3:1. This is distorted by coupling to the NMR active ^{69}Ga nuclei and so the resonances are overlapping at almost identical chemical shift.

The reaction of $AsEt_3$ and $GaCl_3$ was carried out using the same procedure used to form $[GaCl_3(AsMe_3)]$, published by the this group,[12] in an equimolar ratio in Et_2O producing a white solid in a good yield. Microanalysis of this compound confirmed that it matched the calculated

formulation of [$GaCl_3(AsEt_3)$] with no residual solvents present. The coordination of $AsEt_3$ caused the ethyl resonances of the R-groups to shift to a higher frequency than those in the free ligand, suggesting coordination had been successful. The methylene resonance was a quartet at 2.17 ppm, with the methyl protons producing a triplet at 1.37 ppm. When comparing these to the resonances of the complex [$InCl_3(AsEt_3)$] produced earlier in the chapter, the gallium analogue each is found to be at a lower frequency than the indium complex, with the same behaviour being observed in the $^{13}C\{^1H\}$ NMR spectrum.

Due to the absence of phosphorus and other NMR active nuclei, ^{71}Ga NMR was essential for full characterisation and showed a single resonance at 264.5 ppm. This value is consistent with the values seen for [$GaCl_3(AsMe_3)$][12] and [$GaCl_3(AsPh_3)$],[21] showing that the alkyl substituent of the ligand gives little to no change in ^{71}Ga resonance observed. Even comparison to the phosphine donor complex [$GaCl_3(PPh_3)$], which produced a resonance at 273 ppm with only a small change in shift, showing the ligand donor atom has little effect. However, upon comparison of this with the bromide analogue [$GaBr_3(AsMe_3)$] which gave a ^{71}Ga resonance of 147 ppm,[12] suggesting that the metal NMR of these systems is highly dictated by the coordinated halide present on the metal centre.

Crystals of this complex were grown through slow evaporation of a CH_2Cl_2 solution of [$GaCl_3(AsEt_3)$] in a glove box to give good quality crystals for X-ray diffraction. These confirmed the structure as a distorted tetrahedron in a staggered arrangement and is shown in Figure 4.12.

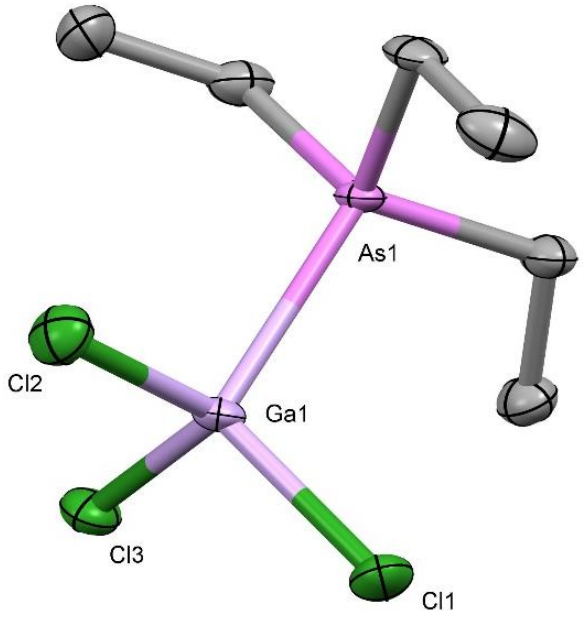

Figure 4.12 - Crystal structure of ***18*** [$GaCl_3(AsEt_3)$] showing the atomic numbering scheme. Ellipsoids at 50% probability with H-atoms omitted for clarity.

Table 4.5 - Selected bond lengths and angles of [$GaCl_3(AsEt_3)$].

Bond Lengths / Å		Bond Angles / °	
Ga1 – As1	2.247(6)	Cl1 – Ga1 – As1	108.43(6)
Ga1 – Cl1	2.176(5)	Cl2 – Ga1 – As1	109.15(6)
Ga1 – Cl2	2.227(5)	Cl3 – Ga1 – As1	106.69(6)
Ga1 – Cl1	2.144(6)	Cl1 – Ga1 – Cl2	111.01(8)
		Cl1 – Ga1 – Cl3	111.91(8)
		Cl2 – Ga1 – Cl3	109.63(8)

To further explore stibine ligands and how a change in R-group affects the coordination and properties of the complex, a short term project undertaken by undergraduate student Miss Laura Grose was set to produce coordination complexes of the trihalides of indium and gallium using Sb^nBu_3. This would be used as a comparison to the previously explored ethyl and *iso*-butyl analogues which had been produced previously in the group as precursors for forming of thin films *via* LPCVD. The reaction of Sb^nBu_3 with GaX_3 or InX_3 (X = Cl, Br or I) in a 1:1 molar ratio in anhydrous CH_2Cl_2 or *n*-hexane gave complexes formulated as: [$GaX_3(Sb^nBu_3)$] and [$InX_3(Sb^nBu_3)$] in good yields as white (X = Cl or Br) or pale-yellow solids (X = I). These were characterised through NMR and IR spectroscopy, microanalysis and X-ray diffraction where possible. Both the ^1H NMR and $^{13}C\{^1H\}$ NMR spectra showed a shift to a higher frequency for each resonance in the butyl chain. The resonance corresponding to the protons of the first carbon (nearest antimony) showing the largest change, a positive shift of 0.5 - 0.7 ppm depending on the metal and halide; this trend was also shown in the $^{13}C\{^1H\}$ NMR spectra. Metal NMR (^{71}Ga, ^{115}In) spectroscopy was attempted for both indium and gallium complexes, with [$GaCl_3(Sb^nBu_3)$] producing a ^{71}Ga NMR resonance at 252.5, slightly lower than that observed for [$GaCl_3(AsR_3)$] complexes discussed earlier. The complex [$InCl_3(Sb^nBu_3)$] did not produce a resonance after a high number of scans, however, analogues with heavier halides did produce a ^{115}In resonance and are shown in Table 4.6. The metal resonances produced in the ^{71}Ga or ^{115}In NMR spectra of [$MX_3(Sb^nBu_3)$] (M = Ga, In; X = Cl, Br, I) is clearly heavily influenced by the halides coordinated to the metal, with large negative shifts being observed when going down Group 17.[24] This influence of the halide on the metal NMR resonance is documented and each of these values fell within the expected range of each metal halide. The ^{71}Ga NMR spectrum of [$GaCl_3(Sb^nBu_3)$] contains a single resonance at 253 ppm while [$GaCl_3(AsEt_3)$] synthesised earlier in the chapter had a resonance of 265 ppm, showing a shift of only 12 ppm. Whereas, when compared with [$GaBr_3(Sb^nBu_3)$] which has a resonance as 116 ppm, a shift of 137 ppm with the change in halide.

Table 4.6 – The IR absorbance bands of the M-X bonds and metal NMR produced by each complex.

Complex	**IR M-X Absorbance Bands / cm^{-1}**	**$^{115}In/^{71}Ga$ NMR Resonance / ppm**
$[GaCl_3(Sb^nBu_3)]$	377, 347	252.5
$[GaBr_3(Sb^nBu_3)]$	276, 221	115.9
$[GaI_3(Sb^nBu_3)]$	230, 209	-236.4
$[InCl_3(Sb^nBu_3)]$	336, 310	Not Observed
$[InBr_3(Sb^nBu_3)]$	214, 211	278.2
$[InI_3(Sb^nBu_3)]$	Not observed (lower than spectrometer range)	-235

The heaviest combination of metal and halide is $[InI_3(Sb^nBu_3)]$, which IR spectroscopy using a Nujol mull and CsI viewing disks could not observe. A report describing the synthesis of $[InI_3(AsPh_3)]$ described the In-I bands at 205 and 152 cm^{-1}, at the edge of the range of spectrometer. Extrapolating the trend set out by the rest of the complexes in Table 4.6, changing from an arsine to a stibine ligand would be expected to drive the absorbance to ~150 cm^{-1}. The increase in halide weight causes a large drop in the frequency of the resonance and is seen for both gallium and indium complexes, with the vibrational absorbances of $[InI_3(Sb^nBu_3)]$ not being observed; located below the observation range of this spectroscopic method. Comparison of the ^{71}Ga resonance for $[GaCl_3(Sb^nBu_3)]$ with that produced by $[GaCl_3(AsEt_3)]$ shows a low frequency shift of ~12 ppm with the change from arsine to stibine donor. This again shows that the nature of the halide has far more of an effect on the metal NMR resonance than the coordinating species.

Crystals of the complexes $[InX_3(Sb^nBu_3)]$ (X = Cl, Br) were grown by the slow evaporation of CH_2Cl_2 over a 72 hours, producing crystals of a good quality for X-ray crystal diffraction. Although forming in different space groups, the complexes are seen to be isostructural with both containing a distorted tetrahedral metal centre, the structures shown in Figure 4.13.

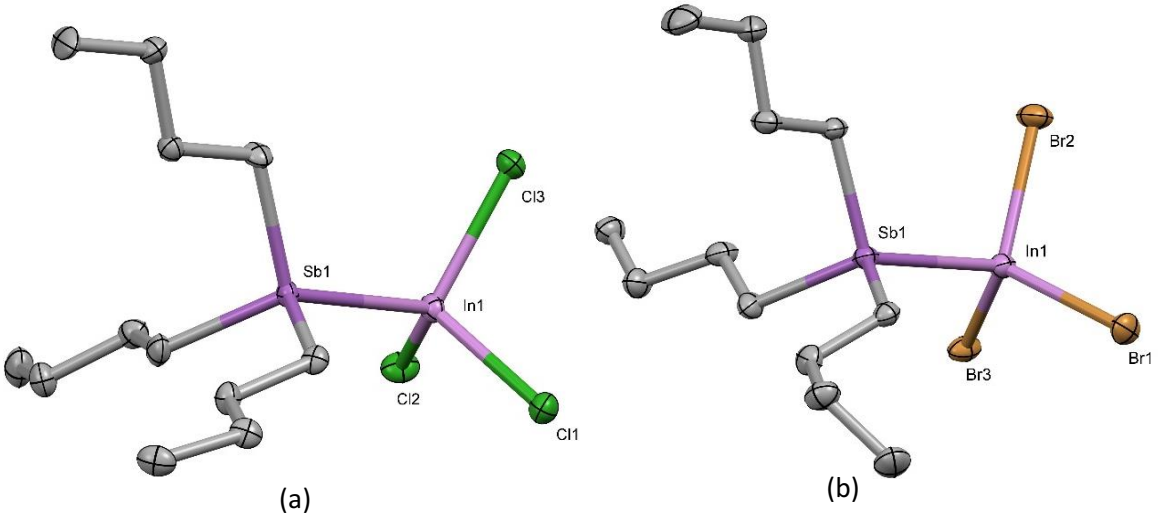

Figure 4.13 - Crystal structure of (a) ***19*** [$InCl_3(Sb^nBu_3)$] and (b) ***20*** [$InBr_3(Sb^nBu_3)$] showing the atomic numbering schemes. Ellipsoids at 50% probability with H-atoms omitted for clarity.

Table 4.7 - Selected bond lengths and angles for [$InCl_3(Sb^nBu_3)$] and [$InBr_3(Sb^nBu_3)$].

Bond Lengths / Å				Bond Angles / °			
[$InCl_3(Sb^nBu_3)$]		[$InBr_3(Sb^nBu_3)$]		[$InCl_3(Sb^nBu_3)$]		[$InBr_3(Sb^nBu_3)$]	
In1 – Sb1	2.7711(7)	In1 – Sb1	2.7789(5)	Cl1 – In1 – Sb1	106.43(5)	Br1 – In1 – Sb1	108.53(2)
In1 – Cl1	2.390(2)	In1 – Br1	2.4922(7)	Cl2 – In1 – Sb1	117.66(5)	Br2 – In1 – Sb1	106.68(2)
In1 – Cl2	2.354(2)	In1 – Br2	2.5030(5)	Cl3 – In1 – Sb1	110.54(5)	Br3 – In1 – Sb1	110.77(2)
In1 – Cl3	2.376(2)	In1 – Br3	2.5047(7)	Cl1 – In1 – Cl2	107.49(7)	Br1 – In1 – Br2	110.28(2)
				Cl1 – In1 – Cl3	103.99(6)	Br1 – In1 – Br3	111.99(2)
				Cl2 – In1 – Cl3	109.73(7)	Br2 – In1 – Br3	108.47(2)

Both of these complexes take up the same tetrahedral geometry at the metal centre showing a slight increase in the In-Sb bond length of 0.007 Å when moving from the chloro- to the bromo-complex. The In-Sb bond lengths of the complexes [$InCl_3(Sb^nBu_3)$] is 2.7711(7) Å, similar to the same bond lengths observed in [$InCl_3(SbR_3)$] (R = Et, ^{i}Pr), at 2.7772(3) and 2.7713(13) Å, respectively.[38] The In-Sb bond length of [$InCl_3(Sb^nBu_3)$] is in the lowest quartile for In-Sb bond lengths with the mean distance of structures on the CCDC being 2.861 Å, a number which includes the distances for both stibine and antimonide coordination with a variety of different anions. As previously discussed, the halide of the complex has a larger effect on the metal-ligand distance than ligand R-groups, with [$InI_3(SbEt_3)$] found to have an increased In-Sb distance of 2.8121(3). This is likely due to the increased ionic radii of the heavier halides causing more destabilising interactions. Coordination of >1 ligand was observed on indium when using the smaller arsine and phosphine ligands producing the trigonal bipyramidal complexes [$InCl_3(EEt_3)_2$] (E = P, As). The

reaction of two molar equivalents of Sb^nBu_3 but was ultimately unsuccessful, with no evidence for the presence of $[InX_3(Sb^nBu_3)_2]$ by spectroscopic analysis.

4.2.2 Halide Abstraction

The introductory section of this chapter explored recent reports of successful halide abstraction reactions from coordination complexes of germanium and tin in both the (II) and (IV) oxidation state using $AlCl_3$ and TMSOTf. The newly synthesised neutral complexes $[MX_3(Sb^nBu_3)]$ (M = Ga, In; X = Cl, Br, I), $[MCl_3(EEt_3)]$ (M = Ga, In; E = P, As) and $[InCl_3(AsEt_3)_2]$ were probed for their activity towards dehalogenation under the same conditions. It was hoped that the reliability and robust nature of this method with the Group 14 metal may be reproduced with the complexes of Group 13 to produce cationic species. The vacant site of these cationic species may allow for later incorporation of differing ligand types and allow for the synthesis of mixed ligands complexes. As well as this, the cationic species will have differing properties to their neutral analogues, including increased Lewis acidity which may increase the functionality of these species.

Initially starting with TMSOTf, due to the success of others in the Reid group, $[GaCl_3(PEt_3)]$ was chosen as the primary complex of study (see Scheme 4.3) due to the additional characterisation techniques available, through $^{31}P\{^1H\}$ and ^{71}Ga NMR spectroscopy. Halide abstraction changes the environment of the metal centre most prominently with this affect being weakener in nuclei further form the metal. Being able to study these nuclei gives further insight into the environment of the metal than the standard characterisation techniques alone. Due to the sensitivity and distance from the metal centre ^1H and $^{13}C\{^1H\}$ NMR spectroscopy and IR spectroscopy may only show small changes. Each of these reactions was carried out on a 0.05 mmol scale in CH_2Cl_2 before drying *in vacuo* to produce sticky oils in each case; these were immediately sent for full NMR characterisation by ^1H, $^{13}C\{^1H\}$, $^{31}P\{^1H\}$ NMR spectroscopy, with $^{19}F\{^1H\}$ NMR spectroscopy being obtained for the triflate and $[BAr^F]^-$ complexes.

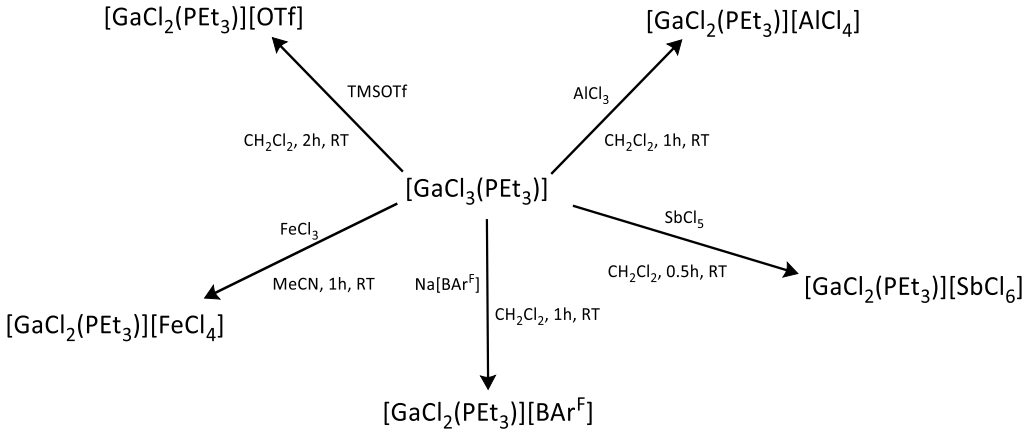

Scheme 4.3 - Reaction schemes for the attempts at halide abstraction of $[GaCl_3(PEt_3)]$ using a variety of dehalogenation agents.

Initial attempts at halide abstraction from $[GaCl_3(PMe_3)]$ used TMSOTf and showed small < 1 ppm changes to both the ^{31}P and ^{71}Ga NMR spectra, while the shape of the resonances were unchanged. Analysis by $^{19}F\{^1H\}$ NMR spectroscopy did show a peak at -77 ppm, in the expected range of ionic triflate, however unknown if this is residual TMSOTf or if a reaction had occurred at the Ga(III) metal centre. Chloride abstraction from $[SnCl_4(PEt_3)_2]$ using TMSOTf to produce the cation $[SnCl_3(PEt_3)_2][OTf]$ showed positive shifts of +20 ppm in the $^{31}P\{^1H\}$ NMR spectrum and +37 ppm in the ^{119}Sn NMR spectrum between the neutral and cationic species. The small changes seen in the NMR spectra for the reaction of $[GaCl_3(PEt_3)]$ with TMSOTf suggest that the reaction has not proceeded, with the resonance observed in the $^{19}F\{^1H\}$ NMR spectra is the presence of small amounts of residual TMSOTf. Although a number of crystallisation techniques were attempted, no crystals were successfully grown for SCXRD.

Reaction of TMSOTf was also attempted with $[GaCl_3(AsEt_3)]$, $[InCl_3(AsEt_3)]$ and $[InCl_3(AsEt_3)_2]$ under the same reaction conditions. The tetrahedral complexes $[MCl_3(AsEt_3)]$ (M = Ga, In) showed no change in the ^1H NMR spectra, after reaction with TMSOTf and were deemed unsuccessful. However, the 1:1 reaction of TMSOTf with the trigonal bipyramidal complex $[InCl_3(AsEt_3)_2]$ gave promising results, with high frequency shifts observed for the proton resonances of the ethyl chain in the ^1H NMR spectrum. The methylene protons showed the largest shift from 1.90 ppm to 2.21 ppm as well as significant broadening of the resonance. This change was not observed in the $^{13}C\{^1H\}$ NMR spectrum, with only minor changes of < 0.1 ppm to a higher frequency. There was generation of a resonance in the $^{19}F\{^1H\}$ NMR spectrum at 77.9 ppm, a value within the range expected for triflate suggesting that the presence of triflate in the end product. Due to the inconclusive nature of the ^1H and $^{13}C\{^1H\}$ NMR spectra and the inability to collect a ^{115}In spectra, the IR spectrum was used to identify changes in the In-Cl stretching frequency. This also showed a change in the In-Cl stretching frequency, with loss of a peak at 299 cm^{-1} and broadening of what was previously shoulder at 332 cm^{-1}. The microanalysis of this product had dropped by ~8% in carbon, much lower than it was calculated to contain if the product corresponded to $[InCl_2(AsEt_3)_2][OTf]$. Unfortunately, crystallisation *via* a number of crystallisation techniques proved unsuccessful with slow evaporation of CH_2Cl_2, layering of *n*-hexane on a CH_2Cl_2 solution and vapour diffusion of Et_2O in to a MeCN solution each failing to produce crystals suitable for diffraction. Although there were significant changes to the NMR spectra of $[InCl_3(AsEt_3)_2]$ the results were deemed unsuccessful. Some data points towards the removal of one equivalents of $AsEt_3$ to give the tetrahedral $[InCl_3(AsEt_3)]$, however, this was never confirmed.

Burford's halide abstraction reactions were reported using $AlCl_3$ as an abstraction agent, due to the favourable formation of the $[AlCl_4]^-$ anion and was shown to be able to form both the cationic and dicationic species $[SnCl_{4-n}(PMe_3)_2][AlCl_4]_n$ (n = 1, 2). Reactions of $AlCl_3$ with $[GaCl_3(PEt_3)]$

repeatedly reproduced spectra matching that of the parent complex, showing changes below the resolution of the machines used. After observing spectroscopic changes in the spectra after the reaction of $[InCl_3(AsEt_3)_2]$ with TMSOTf, this complex was again probed for halide abstraction using $AlCl_3$. This was run as an *in situ* NMR experiment at the same 0.05 mmol in CD_2Cl_2 with the complex fully dissolved before addition of the $AlCl_3$. This again, showed significant shifts in the ^1H NMR spectrum, with the methyl resonances being shifted from 1.91 ppm to 2.53 ppm after reaction, with a similar shift observed for the methylene protons. The small scale of the reaction meant that recovery of the final product was not possible and thus IR spectroscopy and microanalysis could not be pursued further. Due to the higher Lewis acidity of $AlCl_3$ (than $InCl_3$), it is possible that the ligand may have migrated to form $[AlCl_3(AsEt_3)]$. As a comparison, this complex was synthesised ^1H NMR spectroscopy showed highly broadened peaks, not matching those formed in the reaction of $[InCl_3(AsEt_3)_2]$ and $AlCl_3$. However, ^{27}Al NMR spectroscopy showed a single peak at 110 ppm, which is close to the chemical shift produced by $[AlCl_3(AsPh_3)]$ at 104.1 ppm,[21] suggesting this migration may have occurred. Attempts to crystallise the products of the reactions with $AlCl_3$ were unsuccessful *via* a range of pathways.

Following the results of using $AlCl_3$, ferric chloride was employed as an abstraction agent, with the hopes that the lower Lewis acidity when compared to $AlCl_3$ will prevent the migration of the ligand, limiting the formation of $[FeCl_3(EEt_3)]$ (E = P, As). The equimolar reaction of $[GaCl_3(PEt_3)]$ with $FeCl_3$ produced an immediate colour change from yellow to orange, suggesting a reaction had occured. After the removal of residual starting material this was sent for full characterisation by NMR spectroscopy (^1H, $^{13}C\{^1H\}$ $^{31}P\{^1H\}$ and ^{71}Ga). The ^1H NMR spectrum showed significant broadening and loss of couplings of the proton resonances, due to the proximity of the paramagnetic Fe(III) metal centre. The resonances observed in each of the different NMR spectra, with each matching that of the parent complex $[GaCl_3(PEt_3)]$.

The diffuse nature of the anionic charge over the $[BAr^F]^-$ anion means it is less strongly coordinating, with only select examples of coordination through a fluoride being observed, as discussed in Chapter 1.5. Cations produced using $Na[BAr^F]$ are more likely to be observed as "truly cationic" with no additional coordination. Chloride abstraction was then attempted using $Na[BAr^F]$ which would rely on the formation of NaCl, an insoluble salt in the reaction solvent which would drop out of solution as a precipitate, driving the reaction.

Reaction of one molar equivalent of $Na[BAr^F]$ with $[MCl_3(EEt_3)]$ (M = Ga, In; E = P, As) showed no indication of reaction, with no precipitate forming and removal of solvent leaving an oily product. Again, analysis of these products using ^1H, $^{13}C\{^1H\}$ and $^{31}P\{^1H\}$ (where applicable) NMR spectroscopy showed minimal changes, with frequencies observed being within 3 ppm of the

parent complex. For the reaction of the phosphine complexes, evidence of small amounts of phosphonium cation was noted in the ^{1}H NMR spectrum as a doublet of septets forming in solution. This showed the coupling of the proton directly to the phosphorus with a coupling constant of $^{1}J_{PH}$ = 469 Hz, as well as the six methylene protons of the ethyl R-groups. The characteristic phosphonium peak was also identified in the $^{31}P\{^{1}H\}$ NMR spectrum at ~25 ppm, with the proton-coupled ^{31}P NMR spectroscopy showing splitting into a doublet with a constant of $^{1}J_{PH}$ = 456 Hz. This phosphonium species was also crystallised as a side product in a number of cases with the structure solved to be $[GaCl_4][HPEt_3]$ with $GaCl_3$ undergoing self-ionisation to produce the chloro-metalate anion. There was no observation for the formation of the protonated arsine in solution, likely due to it being less Lewis acidic and thus less prone to hydrolysis. Microanalysis of the sticky oils showed a change from the starting material however, unfortunately this did not match the weight of any of the possible cationic species $[GaCl_{3-n}(EEt_3)][BAr^F]_n$ which may suggest only partial halide abstraction or side reactions occurring.

Antimony pentachloride was the final halide abstraction agent employed in this study and was selected due to its high affinity for chloride and driving force to produce the $[SbCl_6]^-$ anion. These reactions were undertaken in a 1:1 molar ratio in CD_3CN as an *in situ* experiment, with a $SbCl_5$ stock solution being made up prior to use due to the small scale. The products of these reactions were immediately sent for $^{31}P\{1H\}$, ^{71}Ga and ^{121}Sb NMR spectroscopy. The ^{121}Sb NMR spectrum showed a single resonance at 0.03 ppm, corresponding to $[SbCl_6]^-$, with $KSbCl_6$ being commonly used as the reference standard for ^{121}Sb NMR spectroscopy. This gave a strong suggestion that chloride has been removed from the complex to form the $[SbCl_6]^-$ anion in solution. The spectrum of the ^{71}Ga NMR analysis shows only a singlet at 251 ppm, shifted from the known spectrum for $GaCl_3$, this along with the loss of coupling observed in $[GaCl_3(PEt_3)]$ suggest a reaction has occurred. The loss of the coupling suggests the loss of PEt_3 in the reaction or the presence of a lower symmetry cation that is not resolved. The $^{31}P\{^{1}H\}$ NMR spectrum had also changed dramatically to show 3 singlet resonances as 112.4, 97.4 and 25.0 ppm with complete removal of the peak observed in the spectrum of $[GaCl_3(PEt_3)]$, this spectra is shown in Figure 4.14.

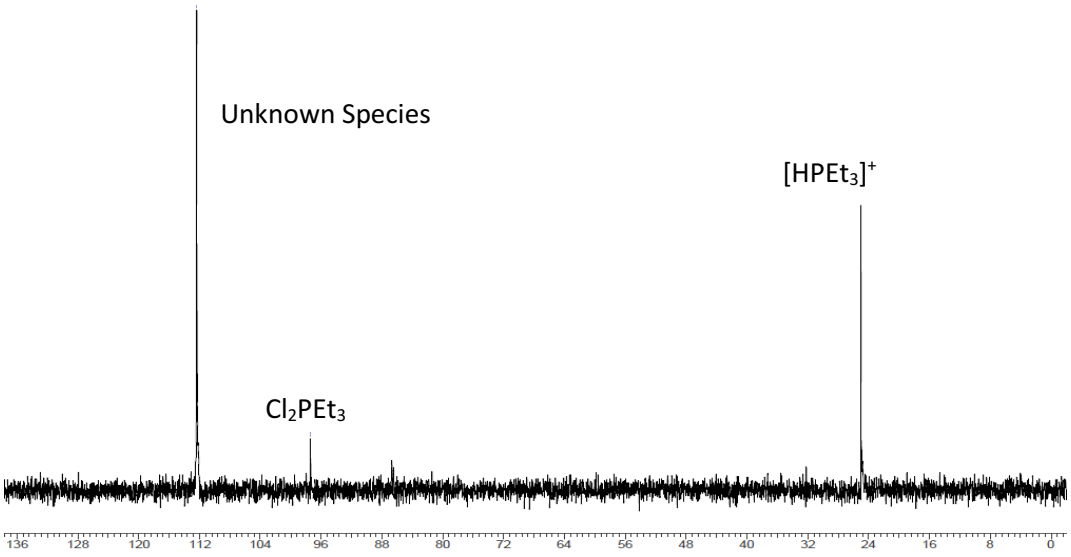

Figure 4.14 - $^{31}P\{^{1}H\}$ NMR spectrum from the in situ reaction of $[GaCl_3(PEt_3)]$ and $SbCl_5$.

The peak at 25.0 ppm corresponds to the previously observed protonated phosphonium cation $[HPEt_3]^+$ and analysis by ^{31}P NMR spectroscopy confirmed this. The second peak, at 97.4 ppm had been previously identified in the Reid group as Cl_2PEt_3, the chlorinated phosphine. The final observed peak has yet to be assigned from the data that has been collected and would require additional information (^{1}H NMR spectra, microanalysis, crystal structure) to be confident in its assignment however, was not completed at this time.

4.2.3 LPCVD Experiments

The chemical vapour deposition of the complexes $[MCl_3(AsEt_3)]$ (M = Ga, In) and $[InCl_3(AsEt_3)_2]$ were attempted following the same procedure reported to deposit Ga_2Te_3 and Ga_2Se_3 *via* LPVCD.[33] The recent success of deposition of GaP and GaAs *via* LPCVD of single source precursors $[^{n}Bu_2Ga(\mu\text{-}E^{t}Bu_2)_2Ga^{n}Bu_2]$ (E = P, As), it was hoped that the newly synthesised complexes would display the same behaviour. The complex containing the M-M bond and the availability of protons on the β-carbon in the precursor, should premote elimination of the organic chains *via* β-hydride elimination. Each of the reactions was carried out under a vacuum of 0.01 mmHg and at 550-650°C and were run until all of the sample had been volatilised in the furnace. For each of the 4-coordinated complexes $[MCl_3(EEt_3)]$ (M = Ga, In; E = P, As) if any deposition was observed, analysis showed it did not match the literature values of the corresponding target material. The reaction of the *penta*-valent complex, $[InCl_3(AsEt_3)_2]$, was found to deposit an orange/brown solid over the quartz substrates at 33-38 cm into the deposition tube after heating to 600°C for 5 minutes. With the help of Dr Fred Robinson, GIXRD and EDX experiments were carried out and produced a powder pattern for the material deposited on the tile, unfortunately this did not match the literature values for InAs.[39]

Additional CVD experiments were run on $[MCl_3(SbR_3)]$ (M = Ga, In; R = Et, ^{n}Bu) to explore the deposition of InSb and GaSb through LPCVD and if the change in donor would aid in the deposition. These experiments were run using the same procedure as the previously experiments, ranging from 450-650°C and were found to leave deposits of black/grey films on select substrates. The attempts at deposition of $[InCl_3(SbEt_3)]$ at 450°C produced a black film on the substrate at 33 cms, which was then analysed by EDX spectroscopy, aided by Dr Fred Robinson. These results revealed that the deposited material was a composite, consisting of a 4:2.5:1 of chlorine : indium : stibine respectively. Increasing the reaction temperature to 500°C produced a grey film that was a 100% match for the deposition of elemental antimony and not the target InSb, with the GIXRD pattern being presented in Figure 4.15.

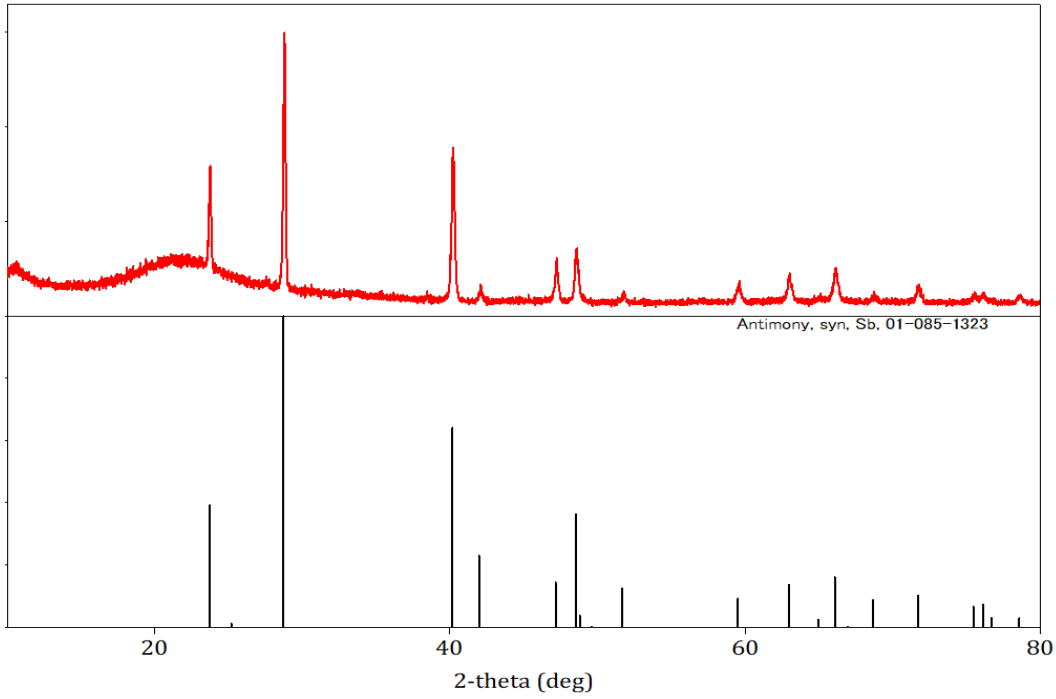

Figure 4.15 - The GIXRD pattern for the deposition of $[InCl_3(SbEt_3)]$ (top) at 500°C and the comparison to the literature pattern for elemental Sb (bottom).[40]

This shows complete loss of all three R-groups from the antimony as ethene, as well as breaking of the In-Sb bond of $[InCl_3(SbEt_3)]$. At temperatures high enough to break Sb-C bonds, it is thought the whole complex is broken down with crystalline antimony being deposited before it is able to be removed fully *in vacuo*. Without EDX measurements on this tile, it is not possible to know if the morphology and composition of the deposits vary across the substrate. Seeing that higher temperatures were causing degradation of the key In-Sb bond in the deposition, attempts at deposition of $[InCl_3(Sb^nBu_3)]$ was tried at 450°C. EDX analysis for this deposition revealed a composition of 4:3 of indium and chlorine however with no evidence of deposition of antimony in any form. Reverting to an increased temperature of 475°C, deposition of a black/gray deposit was achieved that upon EDX analysis, showed the presence of indium, antimony, oxygen and chlorine

in a 1:1:1:1 ratio. GIXRD produced a pattern that was made up of a mixture of at least two phases of elemental antimony as well as indium chloride. This gives an indication that deposition of both antimony and indium from a single source precursor is possible, however chloride is retained through the deposition process. Attempts at deposition of $[InCl_3(Sb^nBu_3)]$ at +600°C and resulted in both EDX and GIXRD demonstrating the presence of 100% antimony deposition only, with no evidence of indium being deposited at this temperature. It appears that temperatures above 500°C cause complete degradation of the parent complex upon volatilisation.

Returning to a gallium complex, LPCVD experiments of $[GaCl_3(SbEt_3)]$ was attempted with the aim to produce GaSb films over a SiO_2 substrate. The deposition procedure of GaP and GaAs using precursors were not replicated with indium analogues and so these may be less able to deposit. The first experiment was attempted at 500°C, gave the most promising results producing a dark grey film across the surface of the substrate. Analysis by EDX spectroscopy demonstrated a 1:1 relationship between gallium and antimony, with the spectrum shown in Figure 4.16.

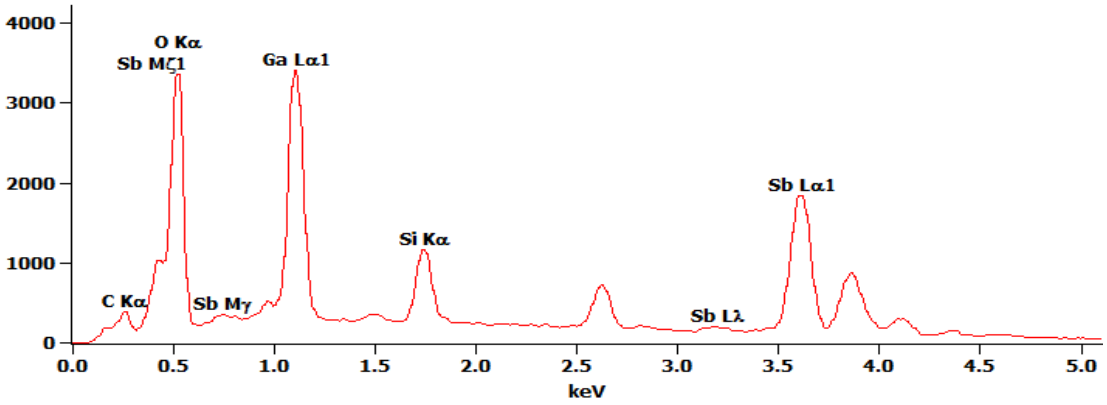

Figure 4.16 - EDX spectrum of the attempted deposition of $[GaCl_3(SbEt_3)]$ showing the 1:1 relationship of Ga and Sb.

Unfortunately, the GIXRD pattern of this deposition showed that this was not a match to the known pattern of PXRD pattern of GaSb, and instead matched deposition of solid antimony and gallium. It was noted that the deposition was not uniform across the tile and so the GIXRD measurements were taken from three different locations across the substrate, with none of them showing the presence of gallium. The GIXRD pattern produced by the deposition is shown to match atleast two phases of antimony but no presence of elemental Ga or GaSb. The discrepancy in evidence for the presence of GaSb in the EDX analysis but not the XRD could be due to the focussing of each technique. EDX spectroscopy is focused on the top few surface layers of deposition, whereas GIXRD penetrates further into the bulk deposition, suggesting that small amounts of GaSb may be found on the surface but not throughout the deposition. GIXRD also focuses on only crystalline deposits of material, it is possible that deposition could be occurring in an amorphous manner, and thus is not observed through this techniques.

4.3 – Conclusion

Following on from previous work in the group, the stibine ligand Sb^nBu_3 was coordinated to InX_3 and GaX_3 (X = Cl, Br) to produce $[MX_3(Sb^nBu_3)]$ (M = Ga, In), shown by X-ray crystal structures in Figure 4.11. The shorter chain, $SbEt_3$, was also found to produce 4-coordinate tetrahedral metal centres, $[MCl_3(SbEt_3)]$, with coordination of a single stibine ligand. Reactions with $GaCl_3$ were shown to produce a tetrahedral complex formulated as $[GaCl_3(EEt_3)]$ (E = P, As, Sb) with each of the three different donor ligands. This was contrasted by the chemistry observed for $InCl_3$, which for the lighter donor ligands, were revealed to take up a trigonal bipyramidal geometry. With use of PEt_3, only the 5-coordinate *bis*-$[InCl_3(PEt_3)_2]$ complex was observed, as had been previously reported with PMe_3. The heavier $AsEt_3$ produced both the tetrahedral 4-coordinate $[InCl_3(AsEt_3)]$ and the 5-coordinate trigonal bipyramidal $[InCl_3(AsEt_3)_2]$ through adjustment of the stoichiometry.

The newly synthesised compounds $[MX_3(ER_3)]$ (M = Ga, In; X = Cl, Br; E = P, As, Sb; R = Et, ^{n}Bu) were seen to be targets to further explore the halide abstraction work initially carried out by Burford on low valent Group 14 compounds such as $[SnCl_4(PMe_3)_2]$.[27] Attempted halide abstraction from $[GaCl_3(PEt_3)]$, $[InCl_3(AsEt_3)]$ and $[InCl_3(AsEt_3)_2]$ were undertaken using equimolar amounts of $AlCl_3$ or TMSOTf. The reaction of $[InCl_3(AsEt_3)_2]$ with these halide abstraction agents were seen as promising, due to a shift in the observed ^1H and $^{13}C\{^1H\}$ NMR resonances; microanalysis data was more consistent with the starting material. The gallium complex $[GaCl_3(PEt_3)]$ was selected for further testing towards halide abstraction using reagents outside of Burford's scope with additional reactions using of $FeCl_3$, $SbCl_5$ and $Na[BAr^F]$.

Low pressure chemical vapour deposition experiments were trialed on a range of the novel compounds produced, including $[InCl_3(AsEt_3)]$, $[InCl_3(AsEt_3)_2]$, $[GaCl_3(SbEt_3)]$ and $[InCl_3(SbR_3)]$ (R = Et, ^{n}Bu) to attempt to deposit InAs, GaSb or InSb respectively; there was no successful deposition from any precursors. The GIXRD analysis of the deposition of $[InCl_3(Sb^nBu)]$ showed two differing crystalline phases of antimony, but with no peaks consistent with formation of crystalline InSb. Although GIXRD analysis of the deposited materials from $[GaCl_3(Sb^nBu_3)]$ didn't match the known pattern for GaSb, the EDX analysis showed the presence of both gallium and antimony in a 1:1 ratio.

4.4 – Experimental

For supplier and purification of reagents and solvents, instrument specifications and NMR solvent references see Appendix A. Both triethylphosphine and triethylstibine were synthesised prior to use with their preparations described here using a modified literature procedure by Taylor *et al*. [41]

4.4.1 Complex Preparation

4.4.1.1 **[$GaCl_3(PEt_3)$]**

Following a reported literature method by Schmidbaur *et al*.[11] $GaCl_3$ (180 mg, 1.0 mmol) was dissolved in Et_2O (15 mL) and to this an ethereal solution of PEt_3 (181 mg, 1.53 mmol – stock of PEt_3 contains Et_2O so requires 1.5 x molar equivalence) was added dropwise at -78°C producing a white precipitate, which dissolved upon warming to ambient temperature and was then stirred for 2 hrs. Removal of the solvent *in vacuo* resulted in white solid which was washed in n-hexane (2 x 10 mL) before drying *in vacuo*. Yield: 207 mg, 70.3%. ^{1}H NMR (295 K, CD_2Cl_2): δ = 2.05 (br quintet, [6H], CH_2), 1.30 (dt, [9H], CH_3, $^3J_{PH}$ = 18.2 Hz, $^3J_{HH}$ = 7.7 Hz). $^{13}C\{^1H\}$ NMR (295 K, CD_2Cl_2): δ = 12.8 (d, CH_2, $^1J_{PC}$ = 30.1 Hz), 7.49 (d, CH_3, $^2J_{PC}$ = 3.67 Hz). $^{31}P\{^1H\}$ (295 K, CD_2Cl_2): δ = 0.2 (br m). $^{71}Ga\{^1H\}$: δ = 274 (d, $^1J_{GaP}$ = 980 Hz). IR (Nujol/cm^{-1}): 375, 350 (Ga-Cl)

4.4.1.2 **[$GaCl_3(AsEt_3)$]**

$GaCl_3$ (210 mg, 1.2 mmol) was dissolved in Et_2O (10 mL) prior to the addition of $AsEt_3$ (195 mg, 1.2 mmol) and the colourless solution was stirred for 3 h, before removing the solvent to leave a white solid, which was dried *in vacuo.* Yield: 339 mg, 84%. Anal. Calcd for $C_6H_{15}AsCl_3Ga$ (338.2): C, 21.3; H, 4.5. Found: C, 21.2; H, 4.3%. ^{1}H NMR: (CD_2Cl_2, 295 K): δ = 2.16 (q, [2H], CH_2, $^3J_{HH}$ = 7.7 Hz), 1.37 (t, [3H], CH_3, $^3J_{HH}$ = 7.7 Hz). $^{13}C\{^1H\}$ NMR (CD_2Cl_2, 295 K): δ = 14.2 (s, CH_2), 9.3 (s, CH_3). ^{71}Ga NMR (CD_2Cl_2, 295 K): δ = 265. IR (Nujol/cm^{-1}): 379, 352 (Ga-Cl).

4.4.1.3 **[$GaCl_3(SbEt_3)$]**

Following a reported literature method by Reid *et al*.[24] $GaCl_3$ (230 mg, 1.30 mmol) was dissolved in Et_2O (10 mL) before $SbEt_3$ (275 mg, 1.30 mmol) was added dropwise and stirred for 3h. Removal of solvent resulted in an off-white solid which was washed with n-hexane (2x10 mL) and dried *in vacuo*. Yield: 427 mg, 85.3%. ^{1}H NMR (295 K, CD_2Cl_2): δ = 2.13 (quartet, [6H], CH_2, $^3J_{HH}$ = 7.8 Hz), δ 1.46 (t, [9H], CH_3, $3J_{HH}$ = 7.8 Hz). $^{13}C\{^1H\}$ NMR (295 K, CD_2Cl_2): δ = 11.1 (s, CH_2), δ 6.93 (s, CH_3). ^{71}Ga NMR (295 K, CD_2Cl_2): δ = 255 (s). IR spectrum (Nujol/cm^{-1}): 373, 353 (Ga-Cl)

4.4.1.4 **[$GaCl_3(Sb^nBu_3)$]**

$GaCl_3$ (285 mg, 1.60 mmol) was suspended in CH_2Cl_2 (10 mL) before addition of Sb^nBu_3 (473 mg, 1.60 mmol) in CH_2Cl_2 and was stirred for 3 h before removal of the solvent afforded a pale-yellow waxy solid, that was dried *in vacuo*. Yield: 653 mg, 88%. Anal. Calcd for $C_{12}H_{27}Cl_3GaSb$ (469.2): C, 30.7; H, 5.8. Found: C, 30.9; H, 5.7%. ^{1}H NMR (CD_2Cl_2, 293 K): δ = 1.98 (t, [2H], $^3J_{HH}$ = 8 Hz), 1.67 (m, [2H]), 1.41 (m, [2H]), 0.94 (t, [3H] $^3J_{HH}$ = 8 Hz). $^{13}C\{^1H\}$NMR (CD_2Cl_2, 293 K): δ = 29.1 (s), 26.5 (s), 14.7 (s), 13.7 (s). ^{71}Ga NMR (CD_2Cl_2, 293 K): δ = 252.5, IR (Nujol/cm^{-1}): 377, 347 (Ga-Cl).

4.4.1.5 **[$InCl_3(PEt_3)_2$]**

$InCl_3$ (55 mg, 0.25 mmol) was suspended in CH_2Cl_2 (15 mL) before the dropwise addition of PEt_3 (60 mg, 0.50 mmol). After 3 hours, the solvent was removed *in vacuo* leaving a white solid which was washed with n-hexane (2 x 5 mL) before being separated and dried *in vacuo*. Yield 86 mg, 74.8%. Anal. Required for $C_{12}H_{30}Cl_3InP_2$ (457.49): C, 31.5; H, 6.7. Found: C, 31.5; H, 6.6%. ^{1}H NMR: (CD_2Cl_2, 295 K) δ = 1.94 (m, [2H], CH_2), 1.23 (dt, [3H], CH_3, $^3J_{PH}$ = 16.3 Hz, $^3J_{HH}$ = 7.8 Hz). $^{13}C\{^1H\}$ NMR: (CD_2Cl_2 295 K): δ = 14.4 (d, CH_2, $^1J_{PC}$ = 18.3 Hz), 8.2 (s, CH_3). $^{31}P\{^1H\}$ NMR: (CD_2Cl_2 295 K): δ = 3.5 (br s). IR (Nujol): 284 (br) cm^{-1} (In-Cl)

4.4.1.6 **[$InCl_3(AsEt_3)$]**

$InCl_3$ (230 mg, 1.04 mmol) was suspended in CH_2Cl_2 (15 mL) before the dropwise addition of one equivalents of $AsEt_3$ (169 mg, 1.04 mmol). The solution stirred for 3 h. then the solvent was removed under partial vacuum, to afford a white solid, which was washed with n-hexane (2 x 5 mL) before being dried *in vacuo*. Yield 362 mg, 90%. Anal. Required for $C_6H_{15}AsCl_3In$ (383.28): C, 18.9; H, 4.0. Found: C, 18.8; H, 3.9%. ^{1}H NMR (CD_2Cl_2, 295 K): δ = 2.23 (q, [2H], CH_2, $^3J_{HH}$ = 7.7 Hz), 1.40 (t, [3H], CH_3, $^3J_{HH}$ = 7.7 Hz). $^{13}C\{^1H\}$ NMR (CD_2Cl_2, 295 K): δ = 15.7 (s, CH_2), 9.9 (s, CH_3). IR (Nujol/cm^{-1}): 323, 313 (In-Cl)

4.4.1.7 **[$InCl_3(AsEt_3)_2$]**

$InCl_3$ (115 mg, 0.52 mmol) was suspended in CH_2Cl_2 (15 mL) before the dropwise addition of two equivalents of $AsEt_3$ (170 mg, 1.04 mmol). After stirring for 3 h, the solvent was removed under partial vacuum, to leave a white solid, which was washed with n-hexane (2 x 5 mL) and dried *in vacuo*. Yield 207 mg, 72%. Anal. Required for $C_{12}H_{30}As_2Cl_3In$ (383.28): C, 26.4; H, 5.7. Found: C, 26.4; H, 5.5%. ^{1}H NMR (CD_2Cl_2, 295 K): δ = 1.91 (quartet, [2H], CH_2, $^3J_{HH}$ = 7.8 Hz), 1.29 (t, [3H], CH_3, $^3J_{HH}$ = 7.8 Hz). $^{13}C\{^1H\}$ NMR (CD_2Cl_2, 295 K): δ = 15.3 (s, CH_2), 9.9 (s, CH_3). IR (Nujol/cm^{-1}): 332, 298 (In-Cl)

4.4.1.8 **[$InCl_3(SbEt_3)$]**

$InCl_3$ (150 mg, 0.68 mmol) was suspended in CH_2Cl_2 (5 mL) before the dropwise addition of $SbEt_3$ (142 mg, 0.678 mmol). After stirring for 3 hours, the solvent was removed *in vacuo* which resulted in a white solid. Yield: 247 mg, 84.5%. ^{1}H NMR (295 K, CD_2Cl_2): δ = 2.25 (quartet, [6H], CH_2, $^3J_{HH}$ = 7.9 Hz), δ 1.50 (t, [9H], CH_3, $^3J_{HH}$ = 7.9 Hz). $^{13}C\{^1H\}$ NMR (295 K, CD_2Cl_2): 10.9 (s, CH_2), 7.5 (S, CH_3). ^{115}In NMR (295 K, CD_2Cl_2): not observed. IR (Nujol/cm^{-1}): 318, 301 (In-Cl).

4.4.1.9 **[$InCl_3(Sb^nBu_3)$]**

$InCl_3$ (478 mg, 2.16 mmol) was dissolved in *n*-hexane (10 mL) before Sb^nBu_3 (473 mg, 1.60 mmol) was added in *n*-hexane was added and stirred for 3 h. The volatiles were removed *in vacuo* before the product was extracted in CH_2Cl_2 (3 mL) and the solvent was removed *in vacuo* yielded a white solid. Yield 489 mg, 44%. Anal. Calcd for $C_{12}H_{27}Cl_3InSb$ (514.3): C, 28.0; H, 5.3. Found: C, 28.2; H, 5.3%. ^{1}H NMR (CD_2Cl_2, 293 K): δ = 2.20 (t, [2H], $^3J_{HH}$ = 8 Hz, CH_2), 1.75 (m, [2H], $^3J_{HH}$ = 8 Hz, CH_2), 1.44 (m, [2H], $^3J_{HH}$ = 8 Hz, CH_2), 0.96 (t, [3H], CH_2). $^{13}C\{^1H\}$ NMR (CH_2Cl_2, 295 K): 29.1 (s, CH_2), 26.5 (s, CH_2), 15.7 (s, CH_2), 13.7 (s, CH_3). ^{115}In NMR (CD_2Cl_2, 293 K): 278.2 (br s). IR (Nujol/cm^{-1}): 336, 310 cm^{-1} (In-Cl).

4.4.2 Ligand Preparation

4.4.2.1 **Triethylstibine**

Using an adapted method from Taylor *et al*.[41] an excess of Mg turnings (8.6 g, 354 mmol) were dried and activated by stirring for 72 h. before Et_2O (250 mL) was added. Bromoethane (23 mL, 310 mmol) was added dropwise at 0 °C before stirring at ambient temperature overnight. The solution was separated from unreacted Mg before an ethereal solution (50mL) of $SbCl_3$ (11.32 g, 50 mmol) was added dropwise at -50 °C before heating to reflux for 1 h. The reaction mixture was quenched with degassed H_2O (75 mL) before the organic layer was separated and dried over $MgSO_4$. Removal of solvent under partial vacuum yielded a colourless oil. Yield: 7.13 g, 68.3%. ^{1}H NMR (295 K, CD_2Cl_2) – δ = 1.36 (q, [6H], CH_2, $^3J_{HH}$ = 7.7 Hz), δ 1.24 (t, [9H], CH_3, $^3J_{HH}$ = 7.7 Hz).

4.4.2.2 **Triethylphosphine**

Using an adapted method from Taylor *et al*.[41] an excess of Mg turnings (8.6 g, 354 mmol) were dried and activated overnight before Et_2O (250 mL) was added. Bromoethane (20 mL, 270 mmol) was added dropwise at 0 °C, allowing the warm to room temperature overnight (16 h) while stirring. The Grignard solution was separated from unreacted Mg and an ethereal solution (50mL) of PBr_3 (7.5 mL, 80 mmol) was added dropwise at -50 °C before heating to reflux for 1 h. The

reaction was slowly quenched with degassed H_2O (75 mL) before separating and drying the ethereal layer over $MgSO_4$. The mixture was concentrated *in vacuo* to approximately 15 mL before the remainder of the solvent was removed by vacuum transfer to afford a colourless solution of Et_3P. ^1H NMR (295 K, CD_2Cl_2): δ = 1.22 (q, [6H], CH_2, $^3J_{HH}$ = 7.42 Hz), δ = 0.98 (dt, [9H], CH_3, $^3J_{HH}$ = 7.8 , 13.3 Hz). $^{31}P\{^1H\}$ NMR: (CD_2Cl_2 295 K): δ = -19.8 (s).

4.5 – References

1 W. Levason and C. A. McAuliffe, *Coord. Chem. Rev.*, 1976, **19**, 173–185.
2 J. Burt, W. Levason and G. Reid, *Coord. Chem. Rev.*, 2014, **260**, 65–115.
3 F. Chen, G. Ma, R. G. Cavell, V. V. Terskikh and R. E. Wasylishen, *Chem. Commun.*, 2008, 5933.
4 F. Chen, G. Ma, G. M. Bernard, R. G. Cavell, R. McDonald, M. J. Ferguson and R. E. Wasylishen, *J. Am. Chem. Soc.*, 2010, **132**, 5479–5493.
5 M. V. Veidis and G. J. Palenik, *J. Chem. Soc. D Chem. Commun.*, 1969, 586b.
6 I. A. Degnan, N. W. Alcock, S. M. Roe and M. G. H. Wallbridge, *Acta Crystallogr. Sect. C Cryst. Struct. Commun.*, 1992, **48**, 995–999.
7 R. Karia, G. R. Willey and M. G. B. Drew, *Acta Crystallogr. Sect. C Cryst. Struct. Commun.*, 1986, **42**, 558–560.
8 J. A. Bilbrey, A. H. Kazez, J. Locklin and W. D. Allen, *J. Comput. Chem.*, 2013, **34**, 1189–1197.
9 M. A. Brown, D. G. Tuck and E. J. Wells, *Can. J. Chem.*, 1996, **74**, 1535–1549.
10 L.-J. J. Baker, L. A. Kloo, C. E. F. Rickard and M. J. Taylor, *J. Organomet. Chem.*, 1997, **545–546**, 249–255.
11 S. Nogai and H. Schmidbaur, *Inorg. Chem.*, 2002, **41**, 4770–4774.
12 F. Cheng, A. L. Hector, W. Levason, G. Reid, M. Webster and W. Zhang, *Inorg. Chem.*, 2007, **46**, 7215–7223.
13 M. A. Brown, J. A. Castro and D. G. Tuck, *Can. J. Chem.*, 1997, **75**, 333–341.
14 J. C. Carter, G. Jugie, R. Enjalbert and J. Galy, *Inorg. Chem.*, 1978, **17**, 1248–1254.
15 G. S. Papaefstathiou, A. Sofetis, C. P. Raptopoulou, A. Terzis, G. A. Spyroulias and T. F. Zafiropoulos, *J. Mol. Struct.*, 2007, **837**, 5–14.
16 S. D. Nogai and H. Schmidbaur, *Dalton Trans.*, 2003, 2488.
17 S. Zanias, G. S. Papaefstathiou, C. P. Raptopoulou, K. T. Papazisis, V. Vala, D. Zambouli, A. H. Kortsaris, D. A. Kyriakidis and T. F. Zafiropoulos, *Bioinorg. Chem. Appl.*, 2010, **2010**, 1–10.
18 A. Ecker and H. Schnöckel, *Z. Anorg. Allgem. Chem.*, 1998, **624**, 813–816.
19 J. Burt, W. Levason, M. E. Light and G. Reid, *Dalton Trans.*, 2014, **43**, 14600–14611.
20 S. A. Sangokoya, B. Lee, M. F. Self, W. T. Pennington and G. H. Robinson, *Polyhedron*, 1989, **8**, 1497–1502.
21 E. Conrad, J. Pickup, N. Burford, R. McDonald and M. J. Ferguson, *Can. J. Chem.*, 2010, **88**, 797–803.
22 L.-J. Baker, C. E. F. Rickard and M. J. Taylor, *J. Organomet. Chem.*, 1994, **464**, C4–C6.
23 F. Cheng, S. I. Friend, A. L. Hector, W. Levason, G. Reid, M. Webster and W. Zhang, *Inorg. Chem.*, 2008, **47**, 9691–9700.
24 V. K. Greenacre, W. Levason and G. Reid, *Organometallics*, 2018, **37**, 2123–2135.
25 S. Schulz, A. Kuczkowski and M. Nieger, *J. Organomet. Chem.*, 2000, **604**, 202–207.
26 A. Heckel, G. Bendt, L. John, C. Wölper and S. Schulz, *Appl. Organomet. Chem.*, 2018, **32**, e4430.
27 E. MacDonald, L. Doyle, S. S. Chitnis, U. Werner-Zwanziger, N. Burford and A. Decken, *Chem. Commun.*, 2012, **48**, 7922.
28 P. A. Gray, K. D. Krause, N. Burford and B. O. Patrick, *Dalton Trans.*, 2017, **46**, 8363–8366.
29 R. P. King, W. Levason and G. Reid, *Dalton Trans.*, 2021, **50**, 17751–17765.
30 M. S. Woodward, R. P. King, R. D. Bannister, J. Grigg, G. McRobbie, W. Levason and G. Reid, *Inorganics*, 2022, **10**, 107.
31 R. P. King, M. S. Woodward, J. Grigg, G. McRobbie, W. Levason and G. Reid, *Dalton Trans.*, 2021, **50**, 14400–14410.
32 K. George, C. H. (Kees) de Groot, C. Gurnani, A. L. Hector, R. Huang, M. Jura, W. Levason and G. Reid, *Chem. Mater.*, 2013, **25**, 1829–1836.
33 F. Cheng, K. George, A. L. Hector, M. Jura, A. Kroner, W. Levason, J. Nesbitt, G. Reid, D. C. Smith and J. W. Wilson, *Chem. Mater.*, 2011, **23**, 5217–5222.

34 N. Muller, P. C. Lauterbur and J. Goldenson, *J. Am. Chem. Soc.*, 1956, **78**, 3557–3561.
35 J. B. Hendrickson, M. L. Maddox, J. J. Sims and H. D. Kaesz, *Tetrahedron*, 1964, **20**, 449–459.
36 M. Mantina, A. C. Chamberlin, R. Valero, C. J. Cramer and D. G. Truhlar, *J. Phys. Chem. A*, 2009, **113**, 5806–5812.
37 F. Cheng, H. L. Codgbrook, A. L. Hector, W. Levason, G. Reid, M. Webster and W. Zhang, *Polyhedron*, 2007, **26**, 4147–4155.
38 K. R. Cairns, V. K. Greenacre, L. A. Grose, W. Levason, G. Reid and F. Robinson, *J. Organomet. Chem.*, 2020, **912**, 121176.
39 A. E. O. Persson, R. Athle, P. Littow, K.-M. Persson, J. Svensson, M. Borg and L.-E. Wernersson, *Appl. Phys. Lett.*, 2020, **116**, 062902.
40 C. S. Barrett, P. Cucka and K. Haefner, *Acta Crystallogr.*, 1963, **16**, 451–453.
41 W. V. Taylor, U. H. Soto, V. M. Lynch and M. J. Rose, *Inorg. Chem.*, 2016, **55**, 3206–3208.
42 M. Brookhart, B. Grant, A. F. Volpe, M. Brookhard, B. Grant and A. F. Volpe Jr, *Organometallics*, 1992, **11**, 3920–3922.

Chapter 5 – Synthesis, spectroscopic and structural properties of Sn(II) and Pb(II) triflate complexes with soft phosphine and arsine coordination

This chapter moves from coordination of the Group 13 metal triflates to the divalent Group 14 metal triflates $M(OTf)_2$ (M = Sn, Pb), with the coordination of a range of soft pnictine donor ligands. Both phosphine and arsine ligands are utilised with a range of different denticities, structures and steric bulk being explored. Previous work by Dean *et al* explored coordination of a similar ligand set to $M(SbF_6)_2$ (M = Sn, Pb) using spectroscopic methods, with the work here additionally exploring the structures observed in the divalent triflate complexes produced.[1,2]

5.1 – Introduction

Chapters 2-5 focused on the chemistry of the Group 13 metals with Chapters 2 and 3 respectively describing the coordination of imine and OPR_3 ligands to $M(OTf)_3$ (M = Al, Ga, In.) From herein, this thesis will focus primarily on the coordination of different ligand species to the Group 14 divalent metal triflates $M(OTf)_2$ (M = Sn, Pb). The coordination chemistry of germanium and particularly tin in both the M(II) and M(IV) oxidation states has been heavily studied, while the chemistry of lead is more limited. Abstraction of a chloride by the phosphine to produce $[R_3PCl][GeCl_3]$ has been previously observed when reacting $GeCl_4$ with soft donors such as phosphines.[3,4] This effect seems to be related to the solvent used, with this occurring in reactions conducted in Et_2O and CH_2Cl_2. When the reaction was carried out using neat PMe_3, the products differed producing *trans*-$[GeCl_4(PMe_3)_2]$, which converts to the ionic product above when dissolved in CH_2Cl_2.[1] The coordination to germanium(IV) halides has been shown to primarily produce six coordinate, octahedral complexes, with both harder *N*- and *O*- donors as well as the softer donor ligands such as the bidentate phosphine ligand, *o*-$C_6H_4(PMe_3)_2$. An example of this octahedral geometry is shown in Figure 5.1 with the complex $[GeF_4\{o\text{-}C_6H_4(PMe_2)_2\}]$.

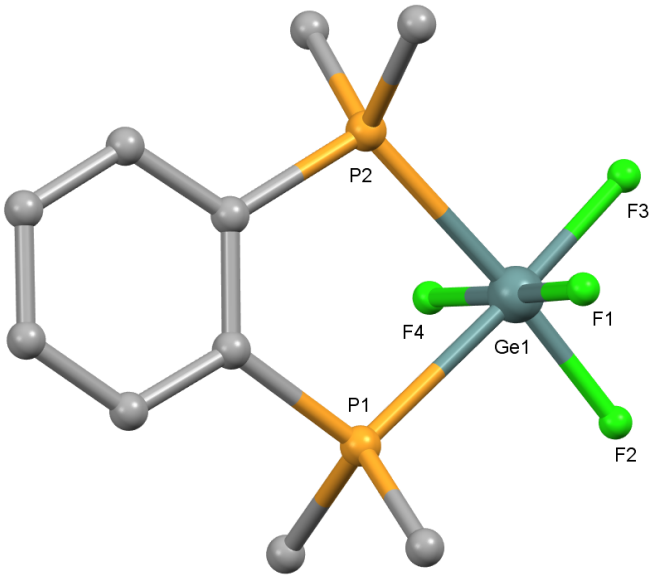

Figure 5.1 – Crystal structure of $[GeF_4(o\text{-}C_6H_4(PMe_2)_2]$ showing the atomic numbering scheme. Redrawn from Ref[5] with H-atoms omitted.

The coordination of Ge(IV) with both phosphines and thioethers has been well established over the past few decades, in particular the chemistry exhibited by GeF_4.[6,7] Throughout this work there have been no reports of coordination products of GeI_4, either as a formal coordination or redox type reactions. Coordination of the heavier arsine and stibine ligands is much more limited than that of the lighter donors, with the molecular complexes of only AsR_3 (R = Me, Et) and *o*-$C_6H_4(AsMe_2)_2$ being previously synthesised.[3,8] In contrast to the chemistry observed for germanium, the chemistry of Sn(IV) has shown that a plethora of complexes can be formed with softer donor species such as *P*, *As*, *S* and *Se* with self-ionisation rarely observed.[9,10] More recent work on Sn(IV) complexes has involved the use of TMSOTf, $Na[BAr^F]$ and $AlCl_3$ as halide abstraction agents to isolate cationic complexes where the halide complexes were reacted stoichiometrically with the abstraction agents.[5,9] It had been shown that phosphine ligands such as PMe_3 do not have the donating power to displace fluoride, therefore, abstraction agents were employed to produce cationic species which could then react further. In Chapter 4, it was shown that this method of halide abstraction was unsuccessful with the Group 13 metal complexes but is versatile within the Group 14 metals, forming cationic species when reacted with various coordinated metal halides. Substitution of the weakly coordinating triflate anion produced crystal structures showing this coordinated to the metal.[5] Starting from $[SnF_4(PMe_3)_2]$, reactions in 1:1, 1:2 and 1:3 ratio produced a set of complexes following the general formula $[SnF_{4-n}(PMe_3)_2(OTf)_n]$, with each being characterised by multinuclear NMR spectroscopy (^1H, $^{19}F\{^1H\}$, $^{31}P\{^1H\}$ and ^{119}Sn) and microanalysis.[5] Of these products, only the product of the 1:1 reaction was successfully crystallised to show $[SnF_3(PMe_3)_2(OTf)]$ where shows the PMe_3 ligands remain to be in a t*rans*

arrangement, while one of the four equatorial fluoride anions is displaced by OTf (Figure 4.6). A selection of examples of halide abstraction using $AlCl_3$ are shown in Figure 5.2.

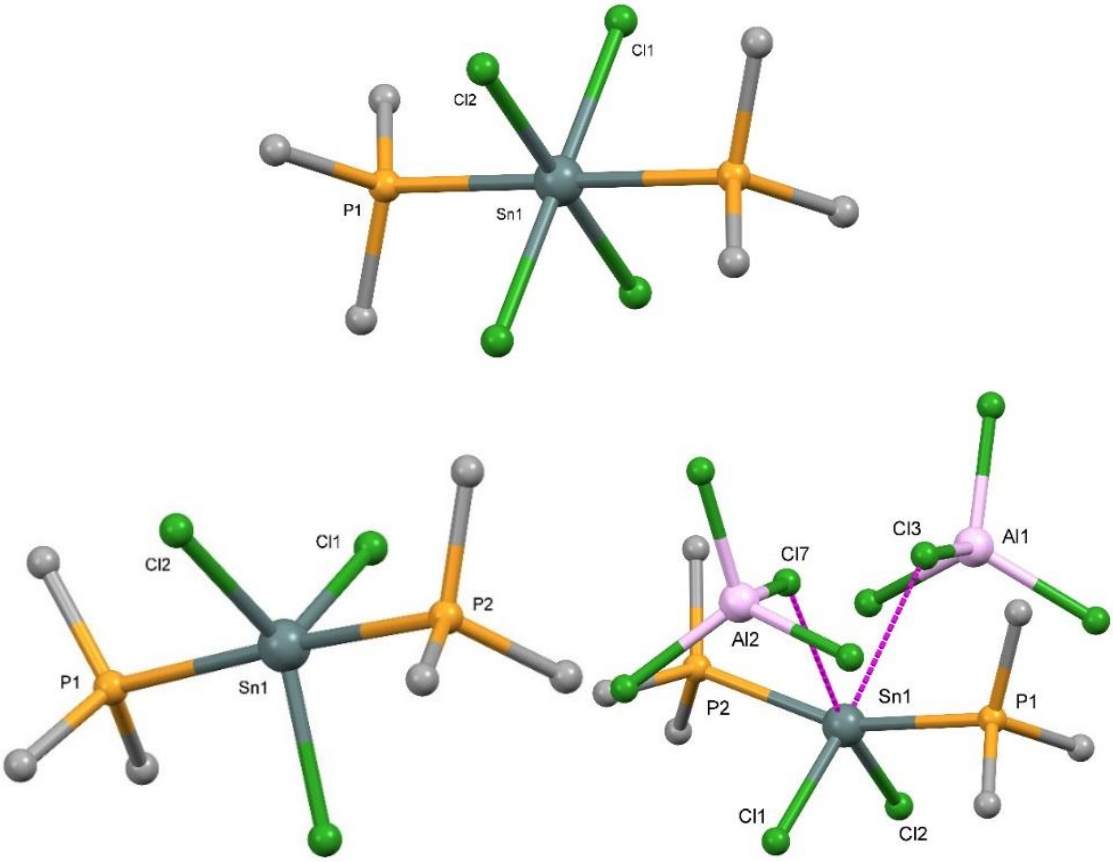

Figure 5.2 - Crystal structure of $[SnCl_4(PMe_3)_2]$, $[SnCl_3(PMe_3)_2][AlCl_4]$, $[SnCl_2(PMe_3)_2][AlCl_4]_2$ showing the atomic numbering schemes. Redrawn from Ref[11] with H-atoms and anions omitted for clarity.

Complexes of lead in the +4 oxidation state are extremely limited due to the prevalence of the +2 oxidation state dominating the examples in the literature. There has been a number of complexes synthesised with Schiff bases,[12,13] with their extended π-systems allowing for a range of redox chemistry and single electron radical exchanges, with properties interesting to the optoelectronics field.[15] A large number of the examples of Pb(IV) in the CCDC are part of clusters of metals or polymeric network/arrays.

Moving away from the M(IV) oxidation state, the M(II) oxidation state has typically received significantly less research, but this has evolved over the past twenty years. Commonly utilising the simple dihalide precursors (GeX_2, SnX_2, PbX_2), where reaction with coordinating ligands produces complexes around a central 3- or 4-coordinate metal core. $[GeCl_2(dioxane)]$ is often used as a soluble source of $GeCl_2$ in solution with dioxane being displaced *via* the incoming ligand, and removed *in vacuo*.[13] In some cases, interactions of the anions to neighbouring molecules can cause oligomerisation through bridging and increase this coordination number to 5 or 6. These halide bridging interactions build di-, oligo- and polymeric structures, with these being commonly observed in the literature.[6] In germanium chemistry, stabalization of the dicationic charge is

required, utilising strongly donating ligands such as carbenes, imines, with the coordination of aza- and oxo- macrocycles being carried out later.[16] The steric bulk and donating strength of the carbene ligand with ^{i}Pr R-groups was able to produce a discrete dicationic species in a trigonal pyramidal geometry.[17] These successes led to a number of Ge(II) cationic species being produced, with a significant number involving oxamacrocycles such as crown ethers, azamacrocycles such as the methylated cyclen and tacn as well as cryptand cages, with these ligand types shown in Figure 5.3. [18–20] The tridentate macrocycles such as [9]aneS_3 and Me_3tacn have been shown to coordinate in a pyramidal geometry with a *fac* arrangement where the other coordinated species (anions, solvents) reside in the opposing hemisphere.[21] Coordination of [9]aneS_3 to M(OTf)$_2$ (M = Ge-Pb) produced *fac*-[M([9]aneS_3)[OTf]$_2$ (M = Ge-Pb) in which the metal centre had a coordination number of 3 with weakly coordinated triflate anions bridging to produce a 1D polymer sheet. [22] This endocyclic coordination directly contrasts the coordination of the same ligands to the GeX_2, as is discussed later in this chapter. Coordination of the cryptand ligands has been reported for both Sn(II) and Pb(II) with a range of anions present.[20,23] In each case, coordination numbers of 8-10 with the metal cation being found encapsulated by the ligand while one or more bonds are maintained to a present anion.[23]

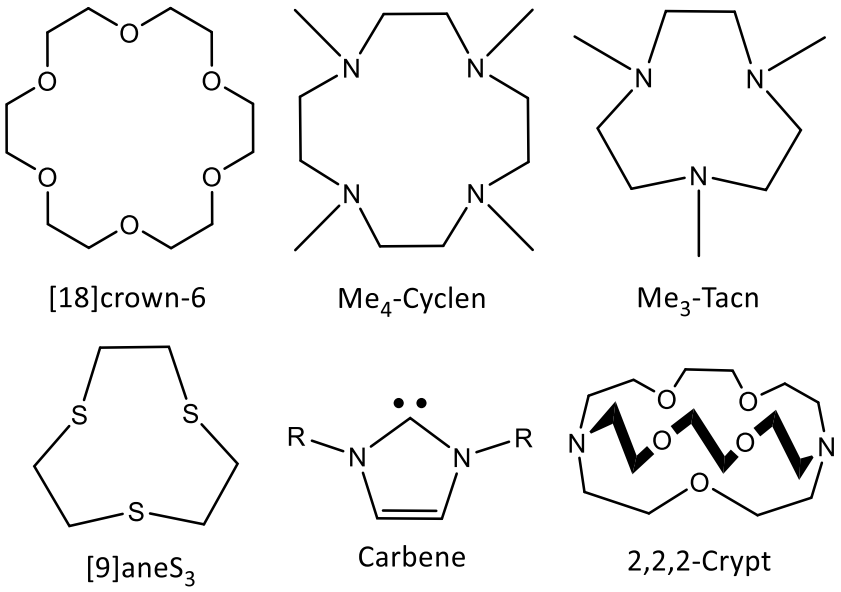

Figure 5.3 - Structures of a range of donor ligands producing Ge(II) cationic species.

Coordination of softer donors was demonstrated with the macrocyclic thioether ligand [9]aneS_3, and its coordination to M(OTf)$_2$ (M = Ge-Pb) producing *fac*-[M([9]aneS_3)[OTf]$_2$ (M = Ge-Pb). in which the metal centre had a coordination number of 5, with two weakly coordinated triflate anions bridging to produce a 1D polymer sheet.[19] Conversely, the reaction of [$GeCl_2$(dioxane)] with the larger thioether macrocycle [14]aneS_4 in both a 1:1 and 2:1 ratio produces complexes exhibiting exocyclic coordination; where the metal central is bonded to 1 donor, outside of the macrocycle.[24] The 1:1 reaction of [14]aneS_4 showed the macrocycle bridging two equivalent $GeCl_2$

metal centres with κ^1-coordination at each forming infinite chains, while the chloride anions also formed bridging interactions with the chains adjacent; this was described as a μ_2-κ^2 binding mode. The 2:1 reaction produced a similar exocyclic coordination of the macrocycle, in this complex however, forming two κ^1-bonds with differing metal centres producing a 2D sheet which were again, formed halide bridges between sheets, being described as μ_4-κ^1 binding. Reaction of $GeBr_2$ with [16]aneS_4 produced [$GeBr_2$([16]aneS_4)], an isostructural crystal structure to the 1:1 product exocyclic product [$GeCl_2$([14]aneS_4)] discussed above.

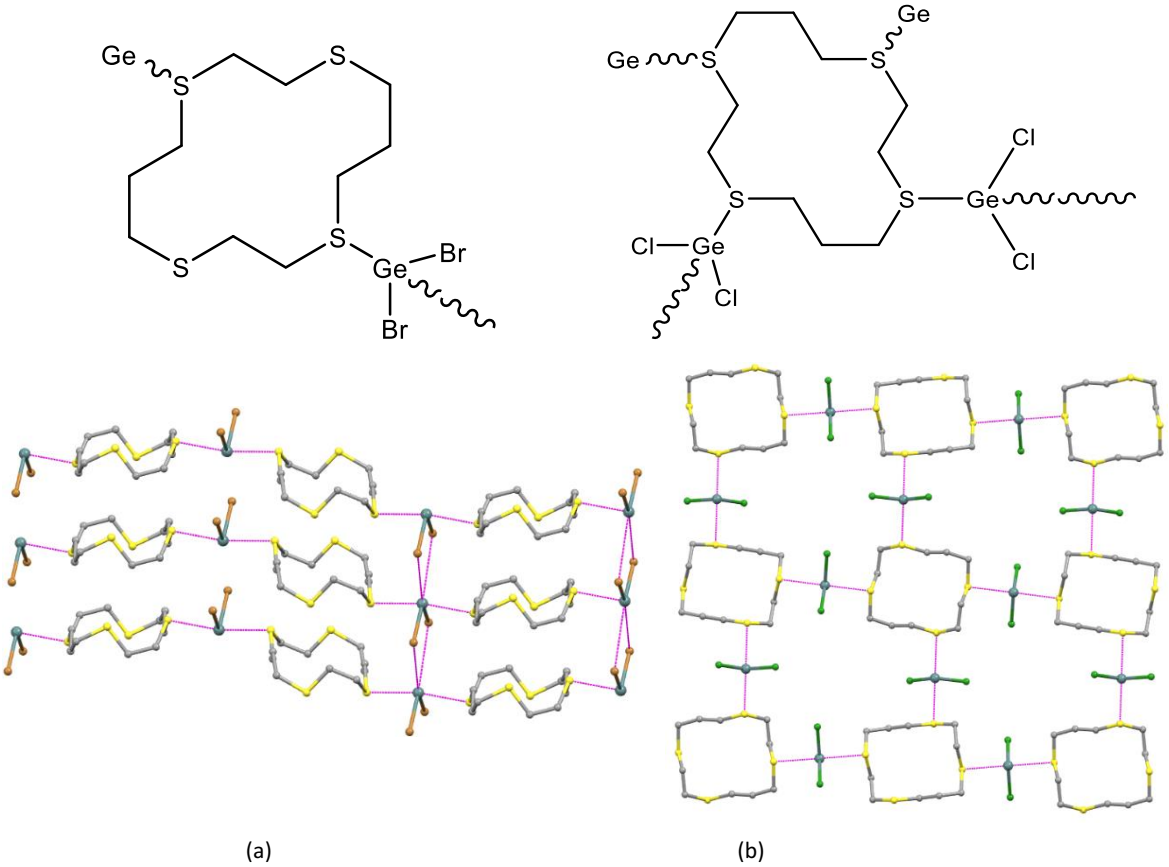

Figure 5.4 - (a) Diagram showing the 3D exocyclic bonding and crystal structure showing the same network in [$GeBr_2${[14]aneS_4). (b) Diagram showing the 2D exocyclic bonding and crystal structure showing the same bonding network in [$(GeCl_2)_2${[14]aneS_4}]. Redrawn from Ref[24] with H-atoms omitted for clarity.

The coordination of the soft pnictine donor ligands ER_3 (E = P, As; R = alkyl, aryl) to any of the Group 14 metals is thus far poorly developed although new examples emerged in the literature over the last few decades.[6] In the case of Ge(II), there are examples of coordination of a number polydentate ligands to each of the halide compounds. Formation of [GeX_2(diphosphine)] (diphosphine = $Me_2PCH_2CH_2PMe_2$ (dmpe), $Et_2PCH_2CH_2PEt_2$ (depe); X = Cl, Br, I) shows a discrete four coordinate metal centre with a near linear GeX_2 core. Unexpectedly, the crystal structure of these complexes were found to be discrete monomers, unlike the previously seen oligomers discussed above.[6] The complexes of [GeX_2(dmpe)] (X = Cl, Br) were found as monomers with no evidence of further interactions however, the iodide analogue was found to form weakly

associated dimers. It has also been shown that reaction of [$GeCl_2$(dioxane)], $Me_2PCH_2CH_2PMe_2$ and TMSOTf in a 1:2:2 ratio forms a unique species $[Ge_2(dmpe)_3][OTf]_4$. This was formulated as $[\{Ge(OTf)(dmpe)\}_2(\mu^2\text{-dmpe})]$, a dimer made up of two Ge(II) metal centres coordinated by a single κ^2-dmpe ligand and single triflate anion, these metal centres were then bridged by a third dmpe ligand.[25] The more rigid *o*-phenylene-based bidentate ligands, *o*-$C_6H_4(PMe_2)_2$ produced weakly associated dimeric complexes, containing a near linear GeX_2 core, forming halide bridges to adjacent molecules.

Substitution of the methyl-groups on the phosphine of this ligand to phenyl-substituents was found to dramatically alter the coordination to each of the germanium halides. The coordination becomes almost exclusively κ^1-coordination with the second donor phosphine being non-coordinating. In the chloride complex, the primary coordinating phosphine was found with a distance of 2.5153(13) Å, with the second, at a distance of 3.1958(15) Å. This asymmetric binding is shown in Figure 5.5.

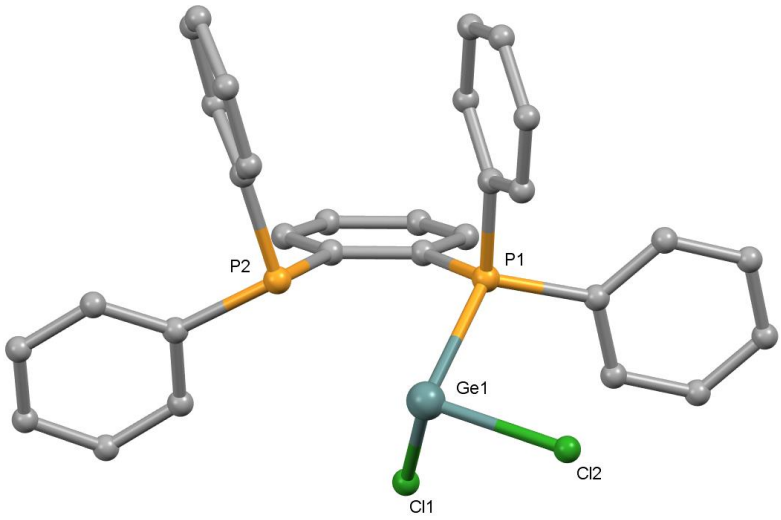

Figure 5.5 - Crystal structure of [$GeCl_2\{o\text{-}C_6H_4(PPh_2)_2\}$] showing the asymmetric coordination. Redrawn from Ref[8] with H-atoms omitted for clarity.

The difference in Ge-P distance observed for the chloride complex was Δd = 0.68 Å and this distance was shown to decrease with the increase in weight of the halide. The analogous bromide complex was measured to have a Δd of 0.59 Å, while the iodide measured Δd = 0.56 Å, showing an increase in the symmetry of this bidentate ligand as the halide weight is increased; this trend was matched with an increase in the P1-Ge1-P2 angle.

Reaction of the bidentate arsine ligand *o*-$C_6H_4(AsMe_2)_2$ with GeI_2 produced the expected 4-coordinate metal centre $[GeI_2\{o\text{-}C_6H_4(AsMe_2)_2\}]$ bridging interactions with neighbouring molecules producing polymeric chains in the solid structure.[8] In contrast to the rest of the bidentate work on Ge(II), reaction of this arsine ligand with [$GeCl_2$(dioxane)] was shown to undergo self-ionisation and form polymeric chains of $[GeCl\{o\text{-}C_6H_4(AsMe_2)_2\}][GeCl_3]$. More recently, halide free, three-

coordinate pyramidal Ge(II) cations were synthesised with triflate anions.[26] These were produced through the reaction of [$GeCl_2$(dioxane)] in the presence of two equivalents of TMSOTf, acting as a halide abstractor, while the addition of donating ligands produced pyramidal complexes. Both of the complexes [$Ge(EMe_3)_3][OTf]_2$ (E = P, As) were shown to take up a similar pyramidal geometry with the same core GeE_3 structure being observed with tripodal tridentate ligands such as $MeC(CH_2PPh_2)_3$, $MeC(CH_2AsMe_2)_3$. The pyramidal structure of the complex $[Ge(PMe_3)_3][OTf]_2$ is illustrated in Figure 5.6, where the directionality of the lone pair can be seen on the opposite face to the coordinated PMe_3 ligands. The crystal structures obtained from this work were then compared to DFT calculations of the optimised electronic structure which were found to be close to that of the measured structure. These calculations included simulation of the frontier HOMO and LUMO orbitals, finding that the HOMO corresponded to the lone pair of electrons, located on the Ge(II) metal centre.[26]

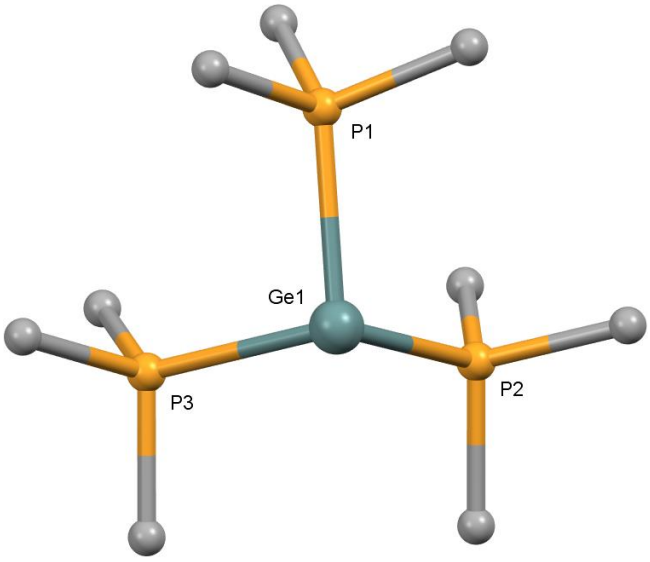

Figure 5.6 - Crystal structure of $[Ge(PMe_3)_3][OTf]_2$ showing the atomic numbering scheme. Redrawn from Ref[26] with H-atoms and anions omitted for clarity.

The study of Sn(II) complexes has received significantly less interest than the corresponding Sn(IV) complexes that have been produced.[6] Reactions of SnF_2 are thus limited, primarily with coordination of *N*- and *O*- donors such as imine ligands (bipy, phen etc), phosphine oxides and oxygen donor solvents (THF, 1,4-dioxane etc). As yet, there are no examples of SnF_2 with coordination of soft pnictine donors such as P and As ligands.[27] Both 1,10-phenanthroline and 2,2'-bipyridine produce complexes formulated as [SnF(L-L)][SnF_4] (L-L = bipy, phen) with a halometalate anion found bridging the metal centres.[28] Comparison of these to the previously synthesised $SnCl_2$ analogues where [$SnCl_2$(bipy)] and [$SnCl_2$(phen)] were shown to form infinite chains through chloride bridges, with additional π-π stacking interactions were also identified in the phenanthroline case.[29] As discussed in Chapter 4, the use of a halide abstraction agent TMSOTf on the bipy complexes of tin would produce the cationic species of [ECl(bipy)][OTf] (E =

Ge, Sn). The halide abstraction was found to break up these chains into weakly associated dimers, bridged by a M_2Cl_2 core, with terminal triflate anions bound to each metal centre. Addition of a second equivalents of abstraction agent and second equivalents of bipy produced the dicationic species $[E(bipy)_2][OTf]_2$.[28] The Sn-O_{OTf} bond distances observed for these species was long, just within the sum of the van der Waals radii and so these were categorised as dicationic species.

Moving to the softer pnictine ligands, a series of $SnCl_2$ complexes was produced by using bidentate ligands such as $R_2P(CH_2)_2PR_2$, *o*-$C_6H_4(PR_2)_2$ and *o*-$C_6H_4(AsR_2)_2$ (R = Me, Ph). As observed for the GeX_2 analogue, the methyl substituted ligands ($Me_2P(CH_2)_2PMe_2$, *o*-$C_6H_4(PMe_2)_2$ and *o*-$C_6H_4(AsMe_2)_2$) were each shown to bind in a chelating mode to produce complexes formulated as $[SnCl_2(L\text{-}L)]$. The metal centres have a coordination sphere made up of P_2Cl_2 where the two halide anions form long-range bridging interactions to another metal centre to form weakly associated dimers. Swapping to the larger phenyl R-group had a significant effect on the coordination observed with the complex [$SnCl_2$(*o*-$C_6H_4(PPh_2)_2$] showing near κ^1-coordination, exactly as the analogous germanium complex displayed in Figure 5.5. The primary Sn-P distance was measured as 2.8293(9) Å whereas, the second was much longer, at 3.285(1) Å. The substitution of methyl to phenyl R-group in the more flexible ethylene-backboned ligand gave the complex $[(SnCl_2)_2\{Ph_2P(CH_2)_2PPh_2\}]$, with ligands bridging two tin metal centres as opposed to chelating a single metal centre. The orientation of the $SnCl_2$ units was such that Sn-Cl bridging interactions were formed to produce infinite chains, which were then cross linked into a 2D sheet. As observed in the Ge(II) analogue, the reaction of the arsine ligand, *o*-$C_6H_4(AsMe_2)_2$, produced the ionic product $[SnCl\{o\text{-}C_6H_4(AsMe_2)_2\}][SnCl_3]$, which was also seen to polymerise through Sn-Cl bridging interactions, with this behaviour shown in Figure 5.7.

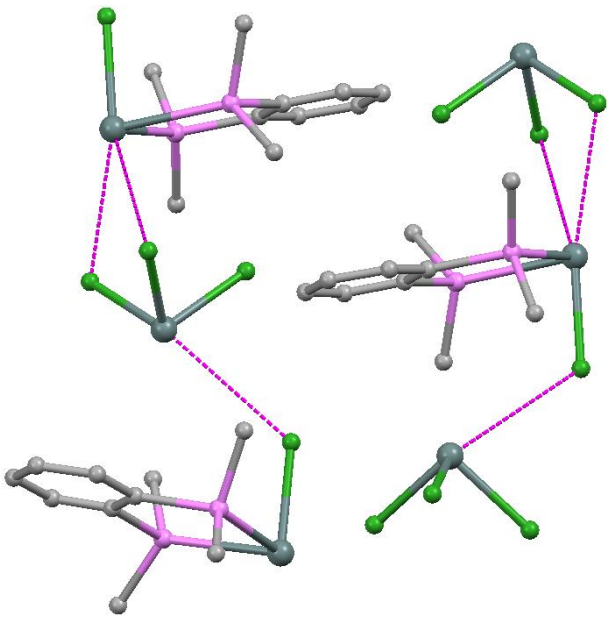

Figure 5.7 - Crystal structure of $[SnCl\{o\text{-}C_6H_4(AsMe_2)_2\}][SnCl_3]$ showing the bridging to form a 2D sheet. Redrawn from Ref with the H-atoms omitted for clarity.

A larger study on the coordination of these polydentate soft donors was undertaken by Dean *et al.* through study of the $^{31}P\{^{1}H\}$ and ^{119}Sn NMR spectroscopy for a series of complexes with $Sn(SbF_6)_2$.[1,2] Ligands explored included $PhP(CH_2CH_2PPh_2)_2$, $MeC(CH_2PPh_2)_3$, $\{Ph_2P(CH_2)_2P(Ph)(CH_2)_2P(Ph)(CH_2)_2PPh_2\}$ and $P(CH_2CH_2PPh_2)_3$, where an excess of ligand was dissolved in $MeNO_2$ along with 1 equivalent of $Sn(SbF_6)_2$ and analysed by multinuclear NMR experiments. These experiments were reported *in situ* and thus none of the products were isolated for further characterisation or structural study through X-ray crystallography, hence the solid-state structures for these complexes are unknown. The splitting of each of the resonances observed in the both the ^{119}Sn metal NMR spectra, together with the corroborating results from the coupling and satellites in the $^{31}P\{^{1}H\}$ NMR spectra strongly suggests that the tri- and tetradentate ligands were only bound through three phosphines in solution. All of the NMR studies were carried out in $MeNO_2$ at room temperature with variable temperature studies only being carried out where resonances were not observed at room temperature. These papers have been key to confirming the spectroscopic data collected, in particular, the ^{119}Sn NMR resonances and an insight into the binding modes of the tri- and tetradentate ligands used in the work of this chapter.

The early study of the coordination chemistry of divalent lead was extremely limited with sporadic and diverse entries exhibiting a range of coordination numbers with little suggestion of a directional lone pair of electrons in the coordination sphere. A series of Pb(II) halide complexes of $[PbX_2(n\text{-}MePy)_m]$ (X = Cl, Br, I; *n* = 3, 4; m = 1, 2)) were coordinated with 1:1 and 1:2 ratios of *n*-methylpyridine to produce a total of six complexes, which were each found to be 6-coordinate at the lead.[31] These complexes were made up of a *trans*-PbX_2L_2 core with an additional two halide bridges forming infinite polymeric chains throughout the crystal. The crystal structures grown using 4-methylpyridine $[PbX_2(4\text{-}MePy)_2]_n$ (X = Cl, Br, I) were confirmed to take up a *trans* arrangement in the solid-state with each of the different halides. When using 3-methylpyridine, the same *trans* geometry was observed the iodo-analogue $[PbI_2(3\text{-}MePy)_2]$ while the chloride and bromide analogues formed the *cis* isomer. The first Pb(II)-P bonds characterised by X-ray crystallography was $Pb[CH(PPh_2)_2]_2$ is shown in Figure 5.8, after the coordination of the anionic ligand $Li[CH(PPh_2)_2]$ to $PbCl_2$, forming a three coordinate Pb(II) complex.[32]

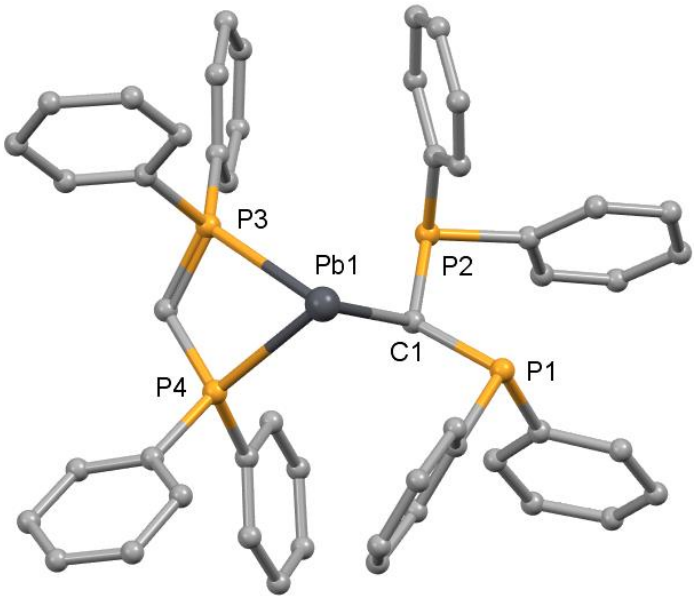

Figure 5.8 - Crystal structure of $[Pb\{C(PPh_2)_2\}_2]$ showing the atomic numbering scheme. Redrawn from Ref[33] with H-atoms omitted for clarity.

The lead is found in a three coordinate environment a first anionic ligand molecule chelating to form two Pb-P bonds and the second forming a Pb-C bond through the methylene carbon. This complex was also synthesised using the same ligand with bulky *tert*-butyl R-group.[34,35] The precursor compound $LiCH(PPh_2)_2$, was also reacted with a number of different metals from both the p- and d-block where coordination was shown by both *C*- and *P*-donors in chelating and bridging modes, or a combination of these, depending on the metal present.[36] Recently, a comparative study explored the changes in coordination between the flexible amine donor ligand, tetramethylethylenediamine (tmeda) and the phosphine donor ligands, dmpe or dppe, with the lead thiolate reagent, $Pb(2,6\text{-}Me_2C_6H_3S)_2$.[37] The amine ligand was shown to produce a dinuclear lead complex, $[Pb(2,6\text{-}Me_2C_6H_3S)(tmeda)][Pb(2,6\text{-}Me_2C_6H_3S)_3]$ with one bridging thiolate ligand. The coordination of the softer phosphine analogue produced $[Pb(dmpe)\{Pb(2,6\text{-}Me_2C_6H_3S)_3\}_2]$, in which the thiolate anion bridges to another molecule of $Pb(2,6\text{-}Me_2C_6H_3S)_2$ to give the structure shown in Figure 5.9.

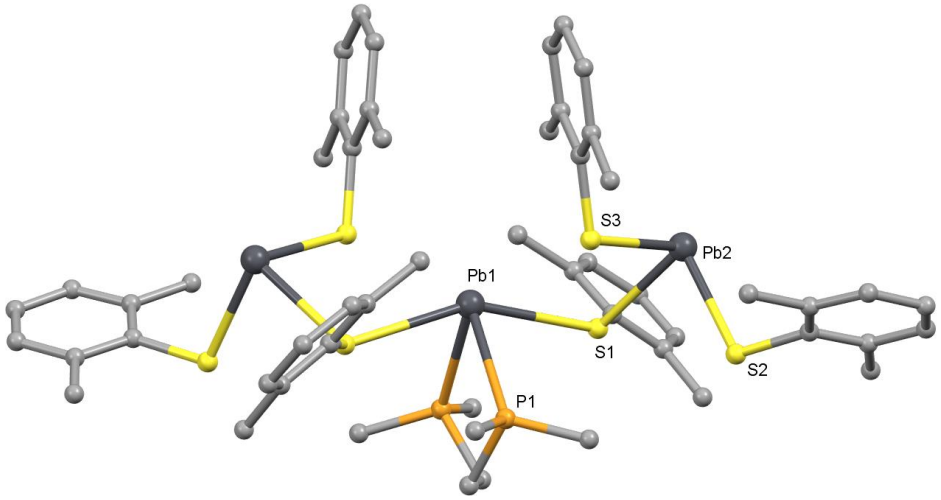

Figure 5.9 - Crystal structure of [Pb(dmpe){Pb(2,6-$Me_2C_6H_3S)_3$}$_2$] showing the atomic numbering scheme. Redrawn from Ref[37] with H-atoms omitted for clarity.

The P_2X_2 (X = anion) core is also observed in many of the PbX_2 complexes with bidentate ligand species. Substituting the methyl R-groups on the phosphine for the larger phenyl groups was shown to change the coordination of these thiolate compounds, taking up the same bridging mode as [$(SnCl_2)_2${$Ph_2P(CH_2)_2PPh_2$}]. This formed a neutral complex [{Pb(2,6-$Me_2C_6H_3S)_3$}$_2${μ^2-$Ph_2P(CH_2)_2PPh_2$}] where both metals retain the anions upon coordination.

Commonly, when exploring the coordination of a metal in a specific oxidation state, the simple halides are used as a starting material as these are commonly the most convenient. In the case of coordination to Pb(II), the lead dihalides are insoluble and intractable due to the their polymeric form and for this reason, many of the known lead(II) complexes are synthesised from other precursors such as $Pb(ClO_4)_2$, $Pb(NO_3)_2$ or salts of fluoroanions $[BF_4]^-$ and $[PF_6]^-$.[27,38] Lead nitrate was a key starting material through the research into coordination of crown ether ligands of varying sizes. Coordination of benzo-[15]crown5 to $Pb(NO_3)_2$ produces the complex [Pb(benzo-[15]crown5)$_2$][$Pb(NO_3)_3$(benzo-[15]crown5)] containing a dicationic Pb(II) sandwich species. The anionic species a Pb(II) metal centre with a coordination number of 11; five bonds from the macrocycle and 6 from three κ^2-nitrate anions, with this being one of the highest coordination numbers observed for Pb(II) with the structure of the anion shown in Figure 5.10.[38]

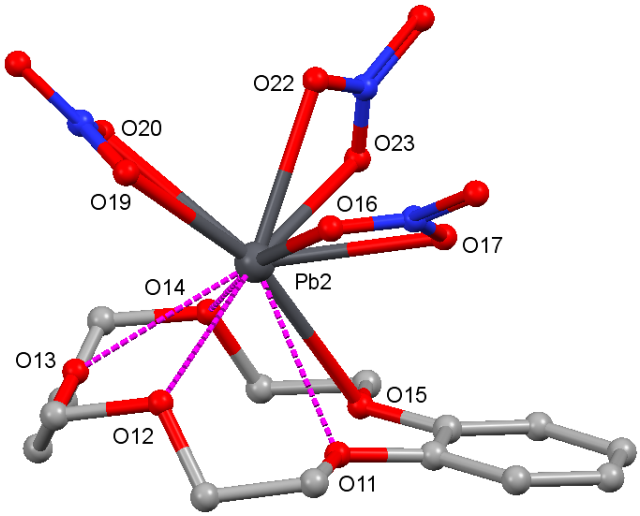

Figure 5.10 - Crystal structure of $[Pb(benzo\text{-}[15]crown5)_2][Pb(NO_3)_3(benzo\text{-}[15]crown5)]$ showing the atomic numbering scheme. Redrawn from Ref[38] with the cation and H-atoms omitted for clarity.

There is a good match between the ionic radius of the Pb(II) cation and the bonding cavity of the [18]crown6 macrocycle giving suggestion that it would fit and allow for good overlap of the donor orbitals. The crystal structure of $[Pb(NO_3)_2([18]crown6)]$ was found to reveal that the Pb(II) was located exactly in the centre of the macrocycle, unlike the smaller [15]crown5.[38] This was shown to have bonds from each of the six oxygen donors of the macrocycle as well as two κ^2-coordinated nitrate anions above and below the plane of the complex, giving the Pb(II) a formal coordination number of 10. Replacement of the nitrate anion with the fluoroanion, $[BF_4]^-$, was shown to form the complex $[\{Pb([18]crown6)(OH_2)(\mu^2\text{-}BF_4)\}_2]$ with both anions forming bridges between the metal centres.[25] Both $[BF_4]^-$ and $[PF_6]^-$ are weakly coordinating anions used to help explore this system by both being more weakly coordinating than the $[ClO_4]^-$ and $[NO_3]^-$ anions, commonly used in Pb(II) chemistry. Mixed donor macrocycles such as $[18]aneO_4S_2$ and $[18]aneO_4Se_2$ were bound to the lead salts PbX_2 (X = $[NO_3]^-$, $[BF_4]^-$, $[PF_6]^-$) and were shown to be coordinated by both the soft and harder donors. These complexes were found with the Pb(II) metal to have a range of coordination numbers, geometries. The differences in donor strength and hardness caused distortion of the ligand, with twisting and puckering of the macrocycle being observed; attempts to coordinate $[18]aneO_4Te_2$ were found to be unsuccessful. The nitrate anions were shown to coordinate in a primarily κ^2-fashion, $[BF_4]^-$ also took up a bidentate coordination, however, $[PF_6]^-$ was shown to bind through two or three of the fluorine atoms. The success of reactions of soft macrocycles with the nitrate and hexafluorophosphate complexes spurred follow up work of the coordination of neutral phosphine ligands. These ligands included many of these explored earlier with SnX_2, $Me_2P(CH_2)_2PMe_2$, *o*-$C_6H_4(PMe_2)_2$ or $Et_2P(CH_2)_2PEt_2$, with the resulting complexes being reminiscent to those observed for the lighter tin analogues. Reaction of $Pb(NO_3)_2$ with the methyl-substituted bidentate phosphines produced $[Pb(NO_3)_2(L\text{-}L)]$ irrespective of the ratios used, where the nitrate anions were κ^2-coordinated in a *trans* arrangement.[39] The third oxygen of each of

these two nitrates is shown to form bridging interactions with adjacent molecules, giving a final coordination number of 8 at the Pb(II), and forming infinite polymeric chains in the solid-state. Reaction of *o*-$C_6H_4(PMe_2)_2$ with $Pb(SiF_6)$ was shown to produce [Pb{*o*-$C_6H_4(PMe_2)_2$}$(H_2O)(SiF_6)$]·H_2O. As expected, the phosphine was shown to chelate to the metal centre with the coordination sphere being filled by a water ligand and the hexafluorosilicate anion. These complexes were also shown to polymerise through a complex array of $[SiF_6]^{2-}$ bridging interactions and H-bonding to form infinite chains.

The work by Dean *et al*. focused on the coordination of polydentate phosphine to $M(SbF_6)_2$ (M = Sn, Pb), with the tin analogues being discussed earlier in this report. This report also described the spectroscopic NMR data about coordination of these ligands to $Pb(SbF_6)_2$ metal centres, including ^{207}Pb NMR spectroscopy.[1,2] As was the case with the tin reactions, these were again performed *in situ* followed by immediate $^{31}P\{^1H\}$ ^{207}Pb NMR spectroscopy in CD_3NO_2. These papers were invaluable for helping the assignment of NMR spectra however, no complexes were isolated in that work and thus no structural information is available.

This chapter focuses on the systematic synthesis, X-ray crystallography and multinuclear NMR spectroscopy of complexes formed by the coordination of polydentate pnictine ligands to the metal triflates $M(OTf)_2$ (M = Sn, Pb). These will be compared to the results of Ge(II) analogues prepared recently in our group as well as with complexes formed with differing anions such as $[SbF_6]^-$, $[NO_3]^-$ and $[SiF_6]^{2-}$. The ligands studied are shown in Figure 5.11, including a range of donor types and donor strengths, denticities and steric bulk.

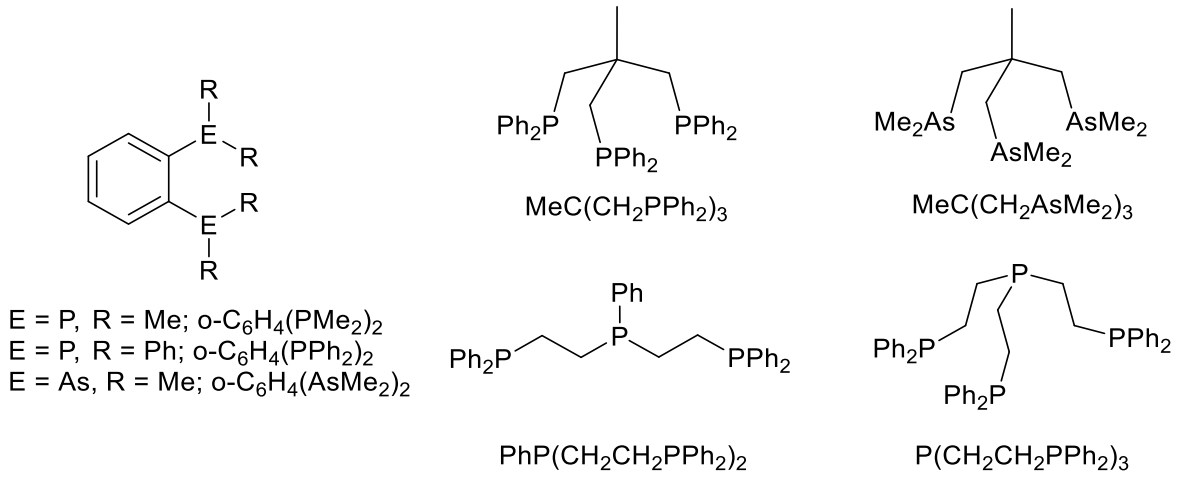

Figure 5.11 - Structures of the ligands used throughout this chapter.

The previous chapters have explored the reactions of the Group 13 metals with Chapter 4 focusing on the non-labile chloride anions and Chapters 2 and 3 being focused on the weakly coordinated triflate anions and the coordination of various neutral imine and *O*-donor ligands. From this, it has been shown that the incorporation of the weakly coordinated triflate anion

changes the observed reactivity when compared to the chemistry of the Group 13 metal halides. The substitution of the triflate anion has been shown successful in the Group 13 systems, with trace amounts of water being enough to produce aquo complexes with hydrogen bonds to the ionic triflate anions. The work with both imine ligands and phosphine oxide ligands produced complexes which had undergone substitution of triflate, something not commonly seen in the halide examples unless undergoing self-ionisation to produce the halometalate anion.

5.2 – Results and Discussion

The results in the previous chapters showed a noticeable difference between the coordination chemistry observed in the Group 13 metal triflates when compared to the analogous metal halides. Following on from the recent publication from this group exploring Ge(II) dications with a range of soft donor ligands and triflate anions,[26] the heavier Sn(II) and Pb(II) metal triflates have been coordinated with a range of soft pnictine ligands to form both neutral and cationic species; literature reports of this chemistry are currently limited.[6,26] $Sn(OTf)_2$ is commercially available, while $Pb(OTf)_2$ required synthesised prior to use, using a modified procedure by Persson and co-workers where PbO was treated with neat trifluoromethanesulfonic acid to produce a white solid.[40] This reaction was attempted but could not be reproduced using commercially available PbO, with retention of the starting material being observed by IR spectroscopy. For this reason the procedure was altered to use the more reactive $PbCO_3$ as a Pb(II) source. After reflux of $PbCO_3$ with neat trifluoromethanesulfonic acid, an off-white/grey solid was isolated and was confirmed as $Pb(OTf)_2$ by the loss of the $[CO_3]^{2-}$ bands and generation of $-CF_3$ and $-SO_3$ bands in the IR spectrum.[41] Although partially soluble in CH_2Cl_2, $Pb(OTf)_2$ was noted to have significantly higher solubility in MeCN and therefore this solvent was used throughout the work involving lead; reactions of $Sn(OTf)_2$ were primarily performed using CH_2Cl_2 as solvent.

Using a similar procedure to King and co-workers,[26] $M(OTf)_2$ (M = Sn, Pb) was first suspended in an organic solvent (CH_2Cl_2, MeCN) before addition of bi- tri- or tetradentate pnictine ligand in a 1:1 molar ratio. Upon addition of the ligand, the majority of the metal salt was drawn into solution and any residual solid was removed *via* filtration after 2 h. The solution was then concentrated *in vacuo* before addition of Et_2O (reactions in CH_3CN) or *n*-hexane (reactions in CH_2Cl_2) caused precipitation of a white solid. Of these, the complexes formed with $MeC(CH_2PPh_2)_3$ were then further reacted with two equivalents $Na[BAr^F]$ in CH_2Cl_2 to produce the dicationic $[BAr^F]^-$ salts. Each of these reactions is shown in Scheme 5.1. Both the $[BAr^F]^-$ and triflate complexes involving the $MeC(CH_2PPh_2)_3$ were confirmed by microanalysis to be the 1:1 product and somewhat stable in air, with the NMR spectra remaining consistant after the sample was left open to air for a number of hours and reanalysed.

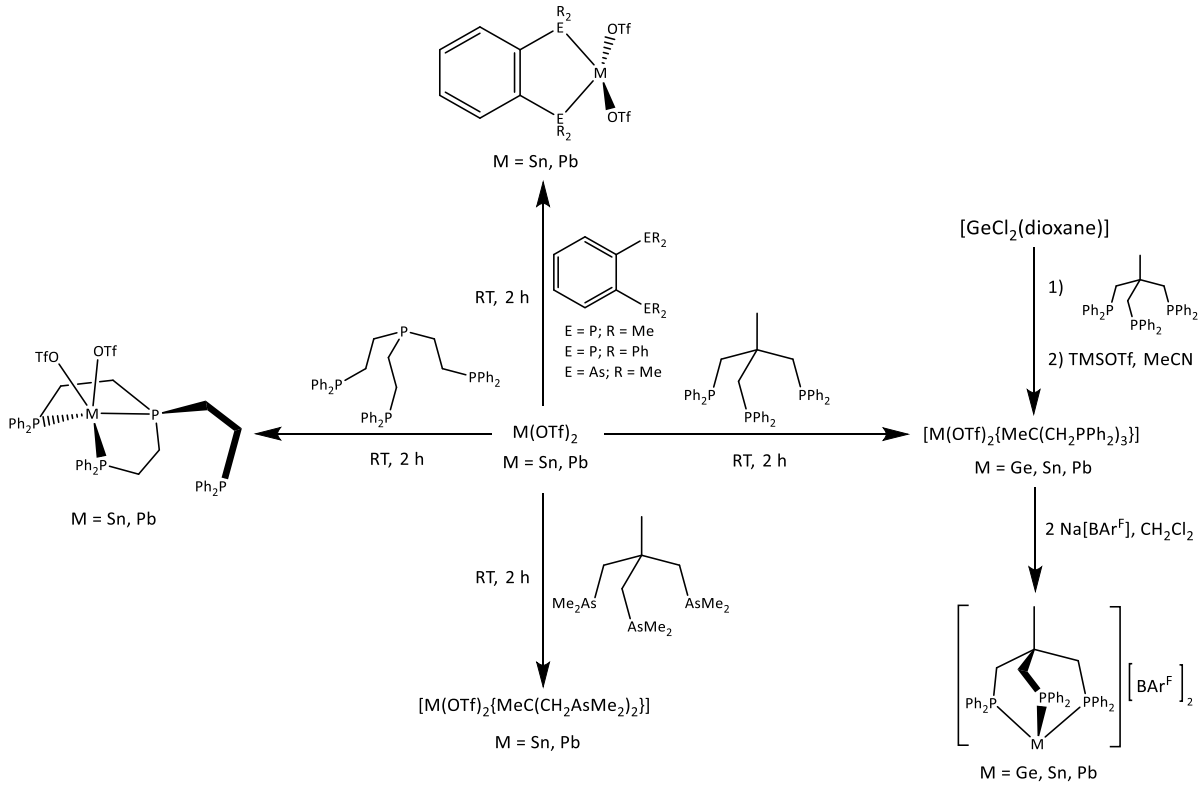

Scheme 5.1 - Reaction scheme for the synthesis of the complexes described in this chapter.

Previous work in the literature shows that complexes of these metals and ligands are likely to dimerise and in some case, form polymeric solids. Throughout the work described here, triflate was observed either as a free anion, a terminally coordinated anion or as a bridging species between metal centres. These different motifs produced complexes with a wide range of M-OTf distances with coordinative interactions becoming weaker as these become longer. The sum of the van der Waals radii of Sn + O is calculated to be 3.69 Å, while Pb + O is slightly shorter at 3.54 Å, and therefore in this work triflate anions located with a distance of > 0.3 Å below these summed distances are being described as significant interactions and therefore included in discussion.[42]

As discussed in the introductory section to this chapter, work carried out by Dean *et al*. reported the spectroscopic data for the $[SbF_6]^-$ salts of Sn and Pb complexes, using a range polydentate pnictine (P, As) ligands with different numbers of donor atoms.[1,2] The reported reactions were carried out *in situ* with complexes never being isolated and thus the true solid-state structures are unknown. Because of this, the X-ray crystal structures of similar complexes were determined throughout this work, the six tin and five lead complexes are discussed first, before the solution NMR spectroscopic data, how this differs and the potential speciation in solution. This work aims to structurally characterise these complexes with the triflate anion as an insight to the solid-state structure and bonding exhibited. These crystallographic disscussions are hoped to display the

formation of dicationic species and is discussed separately to the solution based spectroscopic measurements.

5.2.1 Crystallographic Discussion

The first complexes synthesised used phenylene back-boned bidentate ligands *o*-$C_6H_4(ER_2)_2$ (E = P, R = Me, Ph; E = As, R = Me) which were reacted in a 1:1 ratio to produce a white powder in each case. [$Sn(OTf)_2$(*o*-$C_6H_4(PMe_2)_2$)] with crystals being grown *via* layering of *n*-hexane on to a CH_2Cl_2 solution of the above complex. This crystal structure revealed the geometry to be disphenoidal or trigonal bipyramidal with a vacant equatorial site and can be seen in Figure 5.12(a), a selection of bond lengths and angles are provided in Table 5.1. The asymmetric unit cell there are two molecules with only slight differences, hence only one is shown. Expansion of this structure shows bridging interactions between both triflate anions and neighbouring molecules with these weaker secondary interactions ranging from 2.967(4) – 3.002(4) Å. These form a trimeric assembly with each tin centre being pseudo 6-coordinate and in a highly distorted octahedral geometry as illustrated in Figure 5.12(b).

One of the triflate anions in this crystal structure showed large amounts of disorder, as well as severe disorder in the benzene backbone of the ligand. This disorder, stemming from a small amount of twinning (20%), shows a second crystallographic orientation in which one of the triflate anions is rotated, no longer forming a trimeric array, with the phenylene backbone shifted. With the help of Dr Robert Bannister, both the *o*-phenylene and triflate disorder were modelled successfully in the final CIF file.

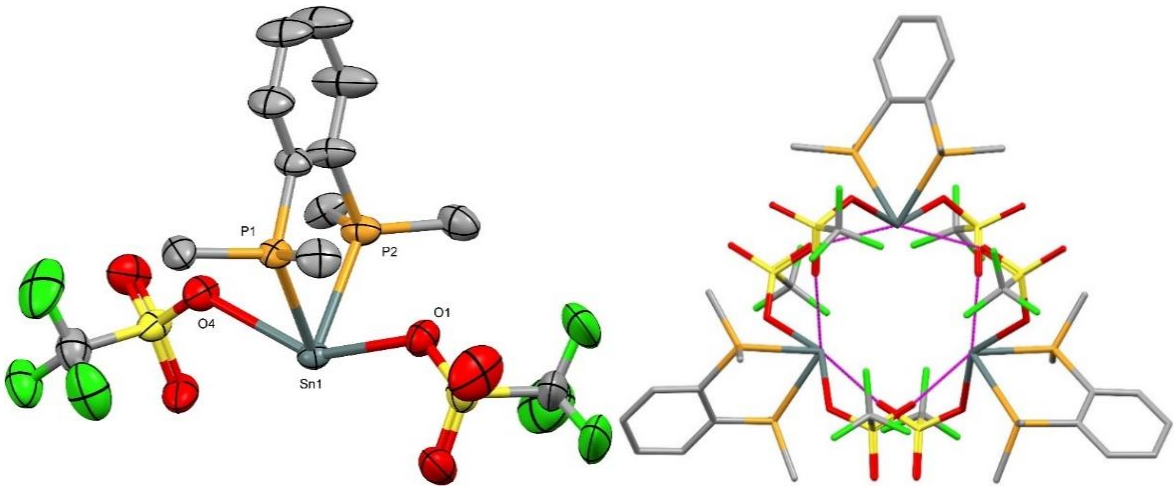

(a) (b)

Figure 5.12 – (a) Crystal structure of ***21*** [$Sn(OTf)_2${*o*-$C_6H_4(PMe_2)_2$}] showing the atom numbering scheme. Ellipsoids are drawn at 50% probability with H-atoms omitted for clarity. There are two crystallographically independent molecules in the cell, only one is shown. (b) The trimeric array of the extended structure.

Table 5.1 - Selected bond lengths and angles of [Sn(OTf)$_2$(*o*-C$_6$H$_4$(PMe$_2$)$_2$)].

Bond Lengths / Å		Bond Angles / °	
Sn1 – P1	2.6723(14)	P1 – Sn1 – P2	75.85(5)
Sn1 – P2	2.6682(15)	P1 – Sn1 – O1	77.890(11)
Sn1 – O1	2.346(4)	P1 – Sn1 – O4	72.74(9)
Sn1 – O4	2.527(4)	P2 – Sn1 – O1	79.14(11)
Sn1'…O3	2.967(4)	P2 – Sn1 – O4	74.50(11)
Sn1'…O8	3.002(4)	O1 – Sn1 – O4	144.36(14)

Comparison of this complex with the chloride analogue, [SnCl$_2${*o*-C$_6$H$_4$(PMe$_2$)$_2$}], show similarities in the core structure with both taking up a disphenoidal geometry andundergoing oligomerisation, however the trimer is unique to triflate. [SnCl$_2${*o*-C$_6$H$_4$(PMe$_2$)$_2$}] forms a weakly associated dimer through chloride bridges with an Cl-Sn-Cl angle of 160.84(9) while [Sn(OTf)$_2${*o*-C$_6$H$_4$(PMe$_2$)$_2$}] shows an O-Sn-O angle of 144.36(14).[28] The Sn-P bond distances of both complexes are comparable with both being found to have Sn-P distances of ~2.65 Å.

Substitution of the methyl R-groups of this ligand for phenyl increases the steric bulk of the ligand as well as lowering the σ-donor strength. The reaction of *o*-C$_6$H$_4$(PPh$_2$)$_2$ with Sn(OTf)$_2$ produced a complexes with a crystal structure in which the metal centre sits in a square-based pyramidal or distorted octahedral geometry with one vacant site. This complex is found to crystallise in to a weakly coordinated dimer through secondary bridging interactions of the triflate anions, shown in Figure 5.13. The coordination sphere of each tin is filled by the diphosphine ligand, a single κ^1-coordinated OTf with a Sn1 – O1 distance of 2.472(3) Å. The two bridging triflates were unsurprisingly found to have longer secondary contacts with a Sn1···O5 distances of 2.751(3) Å, with further bond lengths and angles shown in Table 5.2.

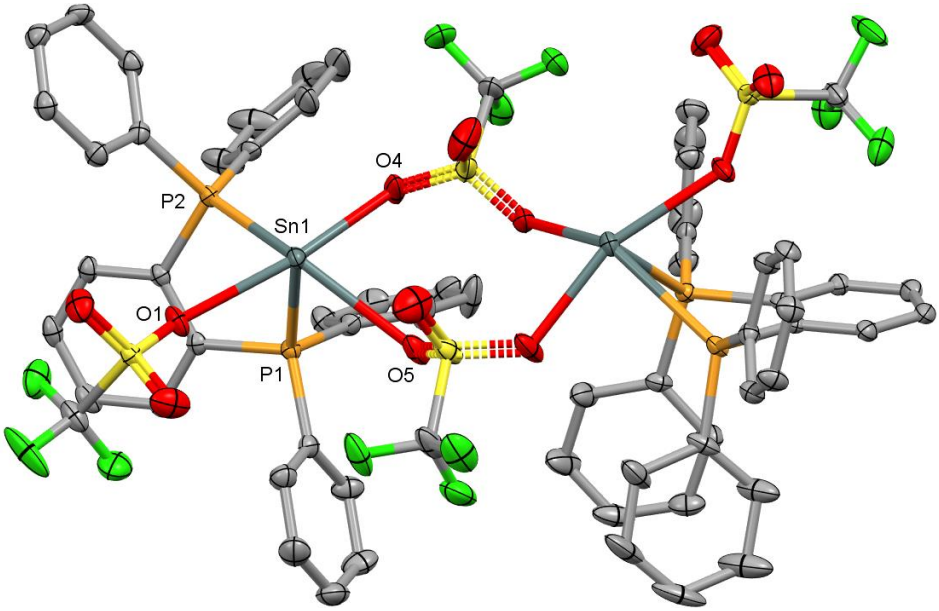

Figure 5.13 – Crystal structure of ***22*** [$Sn(OTf)_2\{o\text{-}C_6H_4(PPh_2)_2\}$] showing the atom numbering scheme. Ellipsoids are drawn at 50% probability with H-atoms omitted for clarity.

Table 5.2 - Selected bond lengths and angles of [$Sn(OTf)_2(o\text{-}C_6H_4(PPh_2)_2)$]

Bond Lengths / Å		Bond Angles / °	
Sn1 – P1	2.7179(10)	P1 – Sn1 – P2	69.80(3)
Sn1 – P2	2.8186(11)	P1 – Sn1 – O1	76.66(7)
Sn1 – O1	2.472(3)	P1 – Sn1 – O4	91.53(10)
Sn1 – O4	2.394(3)	P2 – Sn1 – O1	76.94(8)
Sn1'…O5	2.751(3)	P2 – Sn1 – O4	85.14(8)
Sn1'…O6	3.318(4)	O1 – Sn1 – O4	161.06(11)

The coordination of $o\text{-}C_6H_4(PPh_2)_2$ to $SnCl_2$ produced [$SnCl_2\{o\text{-}C_6H_4(PPh_2)_2\}$], which showing significant asymmetric coordination with Sn-P distances of 2.8293(9) and 3.285(1) Å, in essentially a κ^1-coordination. The Ge(II) analogue shows the same bonding in Figure 5.5.[28] This is a significant contrast to the complex produced here, clearly demonstrating κ^2-coordination with similar Sn-P distances of 2.7179(10) and 2.8186(11) Å. As expected by moving to a weaker donor ligand, the Sn-P bond distances increase with the change in R group from [$Sn(OTf)_2\{o\text{-}C_6H_4(PMe_2)_2\}$] to [$Sn(OTf)_2\{o\text{-}C_6H_4(PPh_2)_2\}$], with an increase of ~0.1 Å. The change in R-group to the bulkier and less donating phenyl substituted phosphine also decreased the P-M-P bite angle from 75.85(5)° (PMe_2) to 69.80(3)° (PPh_2), likely due to more unfavourable interactions being caused by the phenyl R-groups. The difference in packing of these two complexes, with one in a dimer and the other a trimer, may give some explanation as to the large change in this angle, in order to stabilise these altered packing affects.

When moving from the bidentate phosphine ligand *o*-$C_6H_4(PMe_2)_2$ to the arsine analogue *o*-$C_6H_4(AsMe_2)_2$, the resulting crystal structure showed a core structure of $[Sn(OTf)_2\{o\text{-}C_6H_4(AsMe_2)_2\}]$. This complexes was found to take up the same disphenoidal geometry as both phosphine complexes, $[Sn(OTf)_2(o\text{-}C_6H_4(PR_2)_2)]$. When crystallised by vapour diffusion of Et_2O into an acetonitrile solution of $[Sn(OTf)_2\{o\text{-}C_6H_4(AsMe_2)_2\}]$, a polymeric chain structure was observed, *via* long Sn···OTf contacts, similar to the oligomerisation of the earlier phosphines.

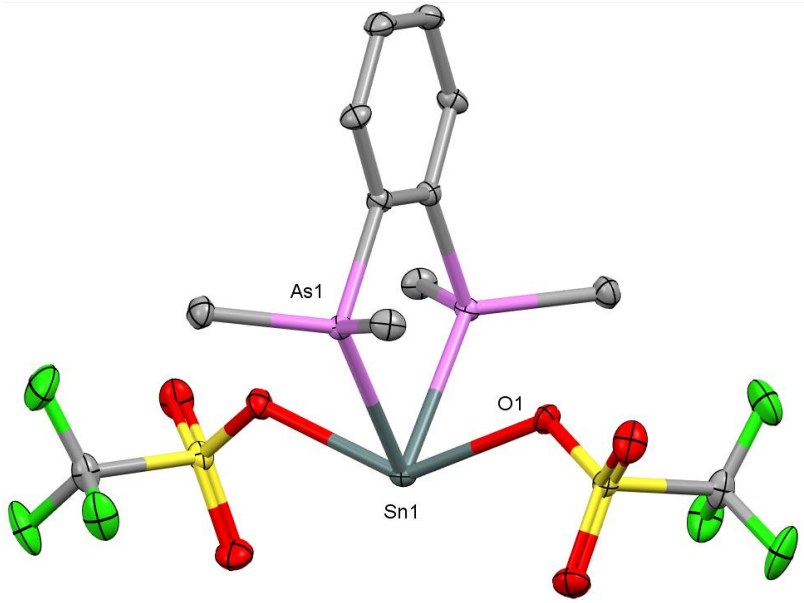

(a)

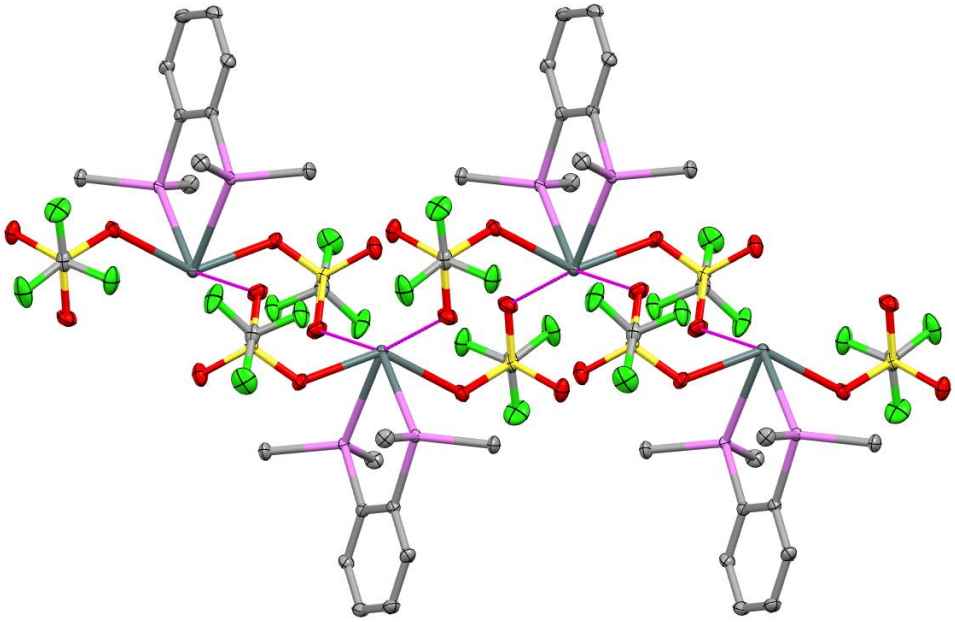

(b)

Figure 5.14 – (a) Crystal structure of ***23*** $[Sn(OTf)_2\{o\text{-}C_6H_4(AsMe_2)_2\}]$ showing the atom numbering scheme. Ellipsoids are drawn at 50% probability with H-atoms omitted for clarity. (b) A section of polymeric chain with bridging OTf groups viewed down the c-axis.

Table 5.3 - Selected bond lengths and angles of $[Sn(OTf)_2(o\text{-}C_6H_4(AsMe_2)_2)]$

Bond Lengths / Å		Bond Angles / °	
Sn1 – As1	2.7585(2)	As1 – Sn1 – As2	76.755(8)
Sn1 – O1	2.4438(12)	As1 – Sn1 – O1	73.75(3)
O2 – Sn1'	3.0094(14)	O1 – Sn1 – O2	137.76(6)

The Sn-As distance was measured to be 2.7585(2) Å, a slight increase from the Sn-P distances observed in earlier complexes, which is expected from the small increase in covalent radii from phosphorus to arsenic (P = 1.80; As = 1.85).[42] Selected bond lengths and angles have been displayed in Table 5.3. Despite this, comparison of the E-Sn-E angle of $[Sn(OTf)_2(o\text{-}C_6H_4(PMe_2)_2)]$ and $[Sn(OTf)_2(o\text{-}C_6H_4(AsMe_2)_2)]$ showed that this value is almost unchanged.

The next ligand employed was $MeC(CH_2PPh_2)_2$, a tridentate phosphine ligand in a tripod geometry with phenyl R-groups, shown in Figure 5.11. This ligand was reacted with $Sn(OTf)_2$ in a 1:1 molar ratio to produce a white solid with solid-state microanalysis consistent with the formulation $[Sn(OTf)_2\{MeC(CH_2PPh_2)_3\}]$ as expected. However, no structure was ever obtained to confirm the geometry at the metal centre. As shown in Scheme 5.1, this product was then reacted with two equivalents of $Na[BAr^F]$ in CH_2Cl_2 in a metathesis reaction to attempt to produce and isolate the dicationic species $[Sn\{MeC(CH_2PPh_2)_3]^{2+}$. Layering a CH_2Cl_2 solution of this complex with *n*-hexane grew a crystal with the structure showing the successful anionic substitution of triflate to produce $[Sn\{MeC(CH_2PPh_2)_3\}][BAr^F]_2$, shown in Figure 5.15.

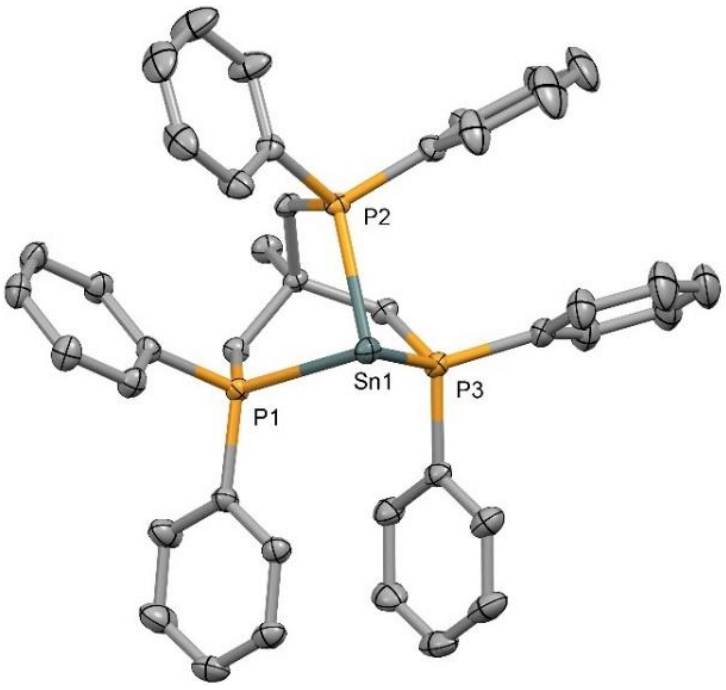

Figure 5.15 – Crystal structure of the cation of ***24*** $[Sn\{MeC(CH_2PPh_2)_3\}][BAr^F]_2$ showing the atom numbering scheme. Ellipsoids drawn at the 50% probability with H-atoms and $[BAr^F]^-$ anions omitted for clarity.

Table 5.4 – Selected bond lengths and angles for $[Sn\{MeC(CH_2PPh_2)_3\}][BAr^F]_2$

Bond Lengths / Å		Bond Angles / °	
Sn1 – P1	2.6438(4)	P1 – Sn1 – P2	69.80(3)
Sn1 – P2	2.6194(4)	P1 – Sn1 – P3	76.66(7)
Sn1 – P3	2.6249(4)	P2 – Sn1 – P3	91.53(10)

The $[BAr^F]^-$ anion was chosen due to its non-coordinating nature and because of the diffuse negative charge over the anion, displaying limited cation-anion interactions to isolate the dication, observed in this structure. The Sn-P bond distances (shown in Table 5.4) of $[Sn\{MeC(CH_2PPh_2)_3\}]^{2+}$ range from 2.6194(4) – 2.6438(4) Å. Comparison of this with the bond distances observed for $[Sn(OTf)_2\{o\text{-}C_6H_4(PPh_2)_2\}]$ with a range of Sn-P distances of 2.7179(10) – 2.8186(11), an increase of over 0.1 - 0.2 Å. The lower coordination number and the higher cationic charge of $[Sn\{MeC(CH_2PPh_2)_3\}]^{2+}$ dication likely allows for tighter binding of the tripodal triphosphine ligand and shortening of the Sn-P bonds. The Ge and Pb analogues of both the triflate and $[BAr^F]^-$ complexes have been synthesised with crystal structures being obtained for both $[BAr^F]$ salts with further discussion later in the chapter.

As well as the tripodal triphosphine ligand $MeC(CH_2PPh_2)_3$, the linear tridentate $PhP(CH_2CH_2PPh_2)_2$ was reacted with $Sn(OTf)_2$ in an equimolar ratio and produced a good amount of powdered white solid. Slow vapour diffusion of Et_2O into an MeCN solution of this solid produced crystals which X-ray diffraction revealed as a highly distorted five-coordinate geometry. This complex was found to be formulated as $[Sn(OTf)\{PhP(CH_2CH_2PPh_2)_2\}][OTf]$, shown in Figure 5.16, where the coordination sphere of the Sn(II) metal centre was made up of P_3 coordination of the phosphine ligand with coordination of one triflate anion.

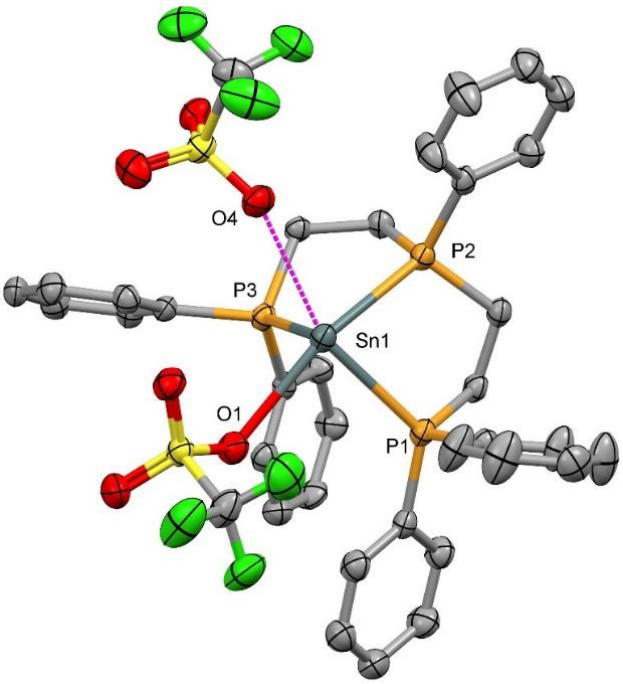

Figure 5.16 - Crystal structure of ***25*** [Sn(OTf){PhP($CH_2CH_2PPh_2$)$_2$}][OTf] showing the atom numbering scheme. Ellipsoids drawn at 50% probability with H-atoms are omitted for clarity.

Table 5.5 - Selected bond lengths and angles for [Sn(OTf){PhP($CH_2CH_2PPh_2$)$_2$}][OTf].

Bond Lengths / Å		Bond Angles / °	
Sn1 – P1	2.6800(12)	P1 – Sn1 – P2	74.52(3)
Sn1 – P2	2.7655(12)	P1 – Sn1 – P3	90.23(4)
Sn1 – P3	2.7627(12)	P2 – Sn1 – P3	72.35(4)
Sn1 – O1	2.623(4)	O1 – Sn1 – O4	115.10(10)
Sn…O4	2.821(4)		

The Sn-P bond distances of [Sn(OTf){PhP($CH_2CH_2PPh_2$)$_2$}][OTf] (shown in Table 5.5) were found to range from 2.6800(12) - 2.7655(12), significantly longer than those observed for the dicationic species $[Sn\{MeC(CH_2PPh_2)_3\}]^{2+}$ discussed above. This primary coordinated triflate anion was located at a Sn-O_{OTf} distance of 2.623(4) Å while the secondary triflate contact was longer with an Sn···O_{OTf} distance of 2.821(4) Å, highlighted in Figure 5.16 in purple.

Substitution of the phenyl ring of the central phosphorus atom of this ligand with an additional –$CH_2CH_2PPh_2$ arm produces the tripodal tetra-phosphine ligand P($CH_2CH_2PPh_2$)$_3$. This ligand was also reacted with Sn(OTf)$_2$ and after crystallisation, was found to coordinated in a similar manner with *P_3O* coordination around the tin metal centre. As observed in the crystal structure of the above [Sn(OTf){PhP($CH_2CH_2PPh_2$)$_2$}][OTf], the tetra-phosphine complex was found to have a

secondary long contact to a second anion with a longer Sn-O_{OTf} distance of 2.968(3) Å, with additional bond lengths and angles provided in Table 5.6.

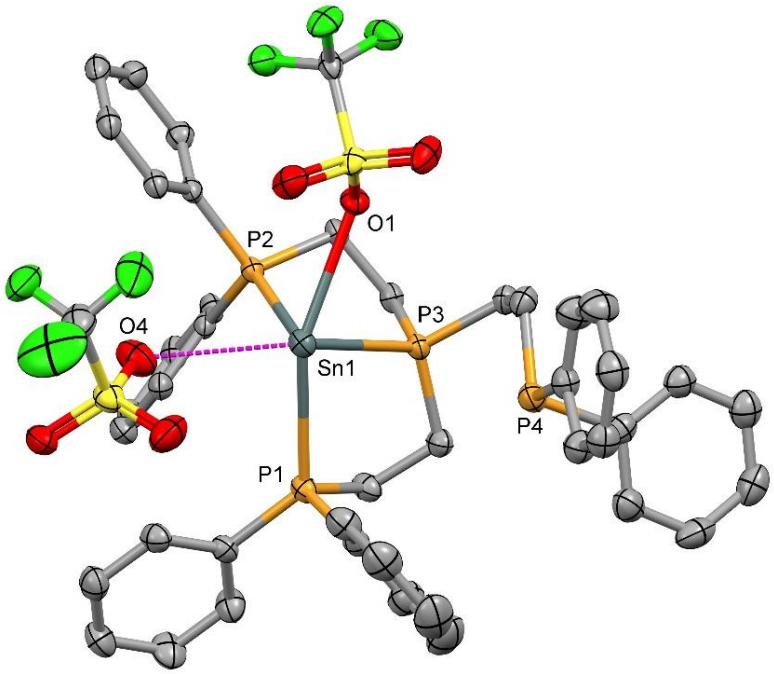

Figure 5.17 – Crystal structure of ***26*** [Sn(OTf){P($CH_2CH_2PPh_2$)$_3$}][OTf] showing the atom numbering scheme. Ellipsoids are drawn at 50% probability with H-atoms omitted for clarity.

Table 5.6 - Selected bond lengths and angles of [Sn(OTf){P($CH_2CH_2PPh_2$)$_3$}][OTf].

Bond Lengths / Å		Bond Angles / °	
Sn1 – P1	2.7085(7)	P1 – Sn1 – P2	96.68(2)
Sn1 – P2	2.7055(7)	P1 – Sn1 – P3	74.31(2)
Sn1 – P3	2.8412(7)	P2 – Sn1 – P3	72.82(2)
Sn1 – O1	2.698(2)	O1 – Sn1 – O4	115.21(7)
Sn…O4	2.968(3)		

In the solid-state, this ligand binds through the central phosphine and two of the side arms with the fourth phosphine arm (-$CH_2CH_2PPh_2$) not involved in coordination with an Sn-P distance of 4.2725(8) Å, well outside the sum of the van der Waals radii of Sn and P (3.97 Å).[42] This is unsurprising as the binding mode of the tridentate PhP($CH_2CH_2PPh_2$)$_2$ and the tetradentate P($CH_2CH_2PPh_2$)$_3$ ligands are very similar, with coordination of a central phosphine with two arms, and so the primary coordination sphere is near consistent.

The equimolar reaction of $Pb(OTf)_2$ with the bidentate ligand *o*-$C_6H_4(PMe_2)$ was seen to produce a white powder in a good yield that produced diffraction quality crystals *via* slow vapour diffusion of Et_2O into an MeCN solution of this product. The structure revealed this complex [$Pb(OTf)_2${*o*-$C_6H_4(PMe_2)_2$}] had a structure analogous with the tin complex [$Sn(OTf)_2${*o*-$C_6H_4(PMe_2)_2$}] discussed

earlier in the chapter, containing the same four-coordinate, P_2O_2 geometry and is shown in Figure 5.18(a).

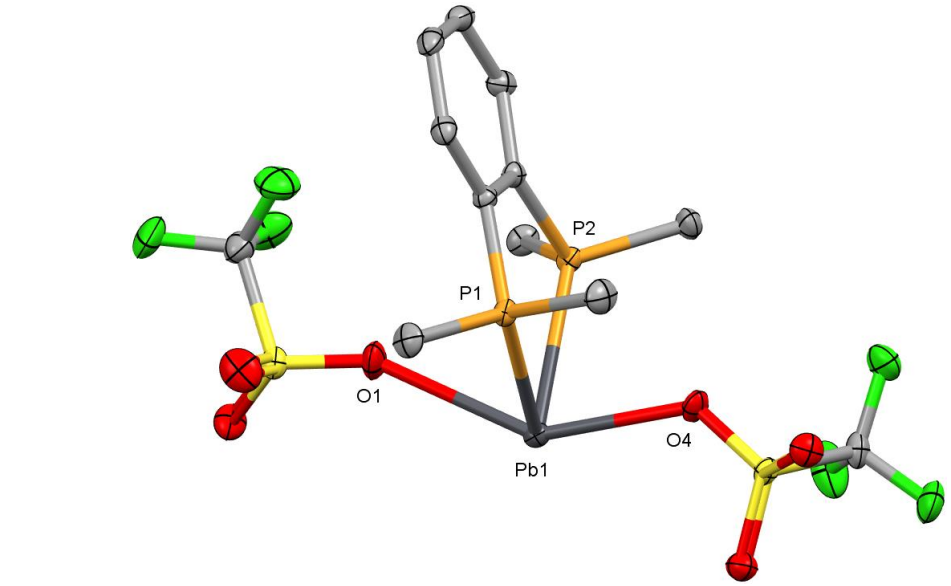

(a)

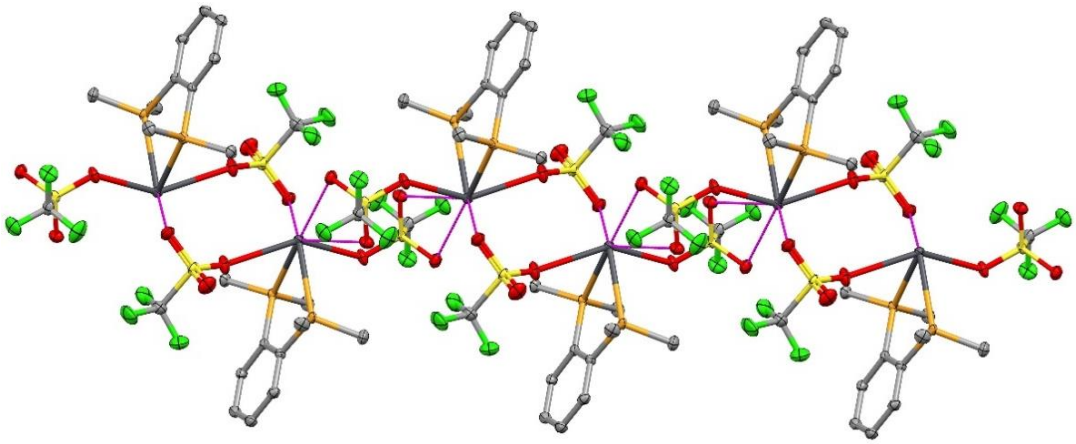

(b)

Figure 5.18 – (a) Crystal structure of ***27*** [Pb(OTf)$_2${*o*-C$_6$H$_4$(PMe$_2$)$_2$}] core showing the atom numbering scheme. Ellipsoids are drawn at 50% probability with H-atoms omitted for clarity (b) A section of the polymeric chain with bridging OTf groups.

Table 5.7 - Selected bond lengths and angles for [Pb(OTf)$_2${o-C$_6$H$_4$(PMe$_2$)$_2$}].

Bond Lengths / Å		Bond Angles / °	
Pb1 – P1	2.7623(6)	P1 – Pb1 – P2	72.28(5)
Pb1 – P2	2.7581(6)	P1 – Pb1 – O1	76.99(5)
Pb1 – O1	2.6740(19)	P1 – Pb1 – O4	79.60(5)
Pb1 – O4	2.4504(19)	O1 – Pb1 – O4	146.26(7)
Pb1 … O3	2.9394(19)		
Pb1 … O5	3.0193(19)		

Unlike the earlier tin analogue, this lead complex does not form a discrete trimer, instead triflate bridging results in the formation of a zig-zag polymer chain, shown in Figure 5.18(b), as was observed for [Sn(OTf)$_2${(*o*-C$_6$H$_4$(AsMe$_2$)$_2$}]. With this polymerisation, the Pb(II) metal centre is in (effectively) a six-coordinate environment with bridging contacts of 2.9394(19) and 3.0193(19) Å. The selected bond lengths and angles are provided in Table 5.7. The ligand backbone is oriented differently to the other phenylene backed complexes synthesised, less perpendicular to disphenoid. Side-by-side comparison of the crystal structures of [Sn(OTf)$_2${*o*-C$_6$H$_4$(PMe$_2$)$_2$}] and [Pb(OTf)$_2${*o*-C$_6$H$_4$(PMe$_2$)$_2$}] show the Pb(II) complex contains an additional triflate oxygen within the sum of the van der Waals radii at 3.26 Å. This triflate anion appears to be rotated, suggesting slight κ^2-coordination character, whereas [Sn(OTf)$_2${*o*-C$_6$H$_4$(PMe$_2$)$_2$}] shows no evidence of this. This long contact however, is only 0.28 Å below the sum of the van der Waals radii (Pb-O = 3.54 Å) and so is not thought of as a significant interaction, although Pb(II) complexes have been shown in higher coordination environments. Comparison of the M-P bond lengths of the this complex with that of the analogous tin complex [Sn(OTf)$_2${*o*-C$_6$H$_4$(PMe$_2$)$_2$}], shows an increase from ~2.67 Å to ~2.76 Å in [Pb(OTf)$_2${*o*-C$_6$H$_4$(PMe$_2$)$_2$}], despite there being a decrease in the sum of the van der Waals radii, (Sn - P = 3.97; Pb – P = 3.82).[42] This is likely due to the decrease in Lewis acidity of the Group 14 metals as the group is descended.

Swapping to the diarsine *o*-C$_6$H$_4$(AsMe$_2$)$_2$ ligand produced the lead(II) triflate complex, [Pb(OTf)$_2${*o*-C$_6$H$_4$(AsMe$_2$)$_2$}], on reaction with Pb(OTf)$_2$. X-ray diffraction revealed this complex takes up the same core structure (*As$_2$O$_2$*) as had been observed in each complex formed from these bidentate ligands. A four-coordinate disphenoidal Pb(II) monomer is found in the asymmetric unit cell with a coordination sphere filled with bidentate coordination of the arsine ligand and two *trans* triflate anions is part of a polymer chain in the solid-state. As was observed in both [Pb(OTf)$_2${*o*-C$_6$H$_4$(PMe$_2$)$_2$}] and [Sn(OTf)$_2$(*o*-C$_6$H$_4$(AsMe$_2$)$_2$)], this complex forms a triflate bridged polymer, both the asymmetric unit cell and a section of polymer are shown in Figure 5.19, with bond lengths and angles provided in Table 5.8.

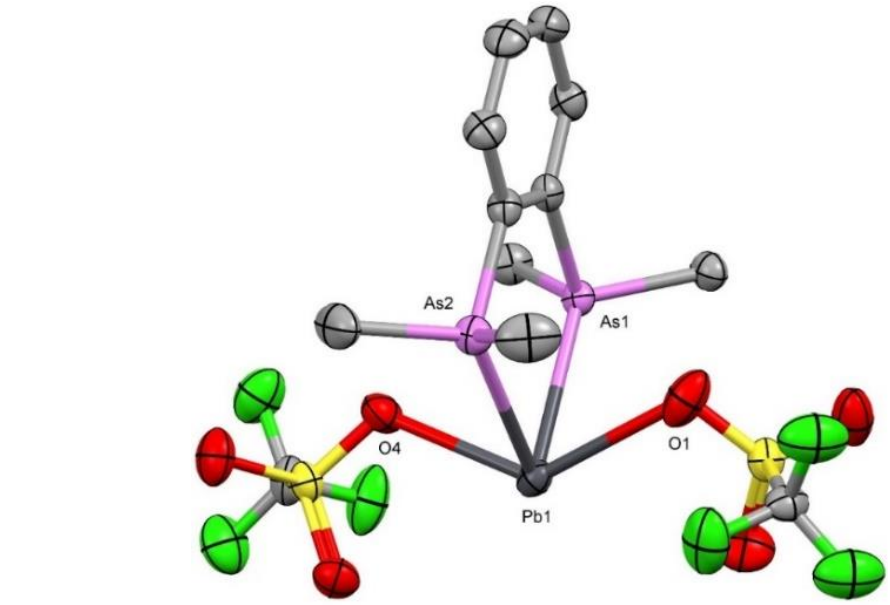

(a)

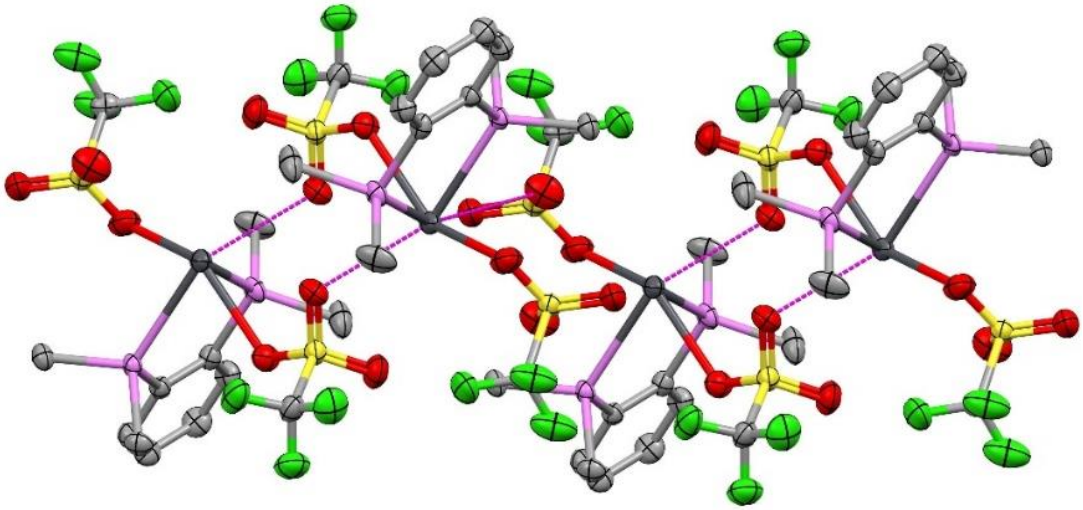

(b)

Figure 5.19 – (a) Crystal structure of ***28*** [$Pb(OTf)_2\{o\text{-}C_6H_4(AsMe_2)_2\}$] core showing the atom numbering scheme. Ellipsoids are drawn at 50% probability with H-atoms omitted for clarity. (b) A section of the polymeric chain with bridging OTf groups.

Table 5.8 - Selected bond lengths and angles for [$Pb(OTf)_2\{o\text{-}C_6H_4(AsMe_2)_2\}$].

Bond Lengths / Å		Bond Angles / °	
Pb1 – As1	2.8675(6)	As1 – Pb1 – As2	73.297(16)
Pb1 – As2	2.8752(6)	As1 – Pb1 – O1	74.98(10)
Pb1 – O1	2.539(4)	As1 – Pb1 – O4	69.56(9)
Pb1 – O4	2.712(5)	As2 – Pb1 – O1	72.57(9)
Pb1 … O5	2.972(5)	As2 – Pb1 – O4	69.84(10)
		O1 – Pb1 – O4	133.97(13)

As was observed for the complex [Pb(OTf)$_2${*o*-C$_6$H$_4$(PMe$_2$)$_2$}], it was noted that the bridging triflate anions had additional oxygen atoms (of triflate anion) within the sum of the van der Waals radii for Pb and O at 3.54 Å.[42] These were located with Pb-O distances of 3.430(6) Å, just within the sum of the van der Waals, so these were not considered significant metal-anion interactions. Upon comparison of this complex [Pb(OTf)$_2${*o*-C$_6$H$_4$(AsMe$_2$)$_2$}] and the tin analogue explored earlier in the chapter [Sn(OTf)$_2${*o*-C$_6$H$_4$(AsMe$_2$)$_2$}], there is a clear lengthening of the M-As bond distance in the lead complex, despite the smaller covalent radius of the Pb atom. Unlike the phosphine complex discussed in Figure 5.18(a), the orientation of the ligand backbone matches the observed structure of the Sn(II) complexes discussed earlier in the chapter.

Reaction of the tetradentate ligand P(CH$_2$CH$_2$PPh$_2$)$_3$ produced a crystal structure isomorphous to that of the tin analogue discussed earlier in the chapter. The same core of *P$_3$O$_2$* coordination made up of two triflate anions with two of the pendent arms and the central phosphine groups coordinating the Pb(II) metal centre while the remaining phosphine arm is uncoordinated. The complex is shown in Figure 5.20 and selected bond lengths and angles found in Table 5.9.

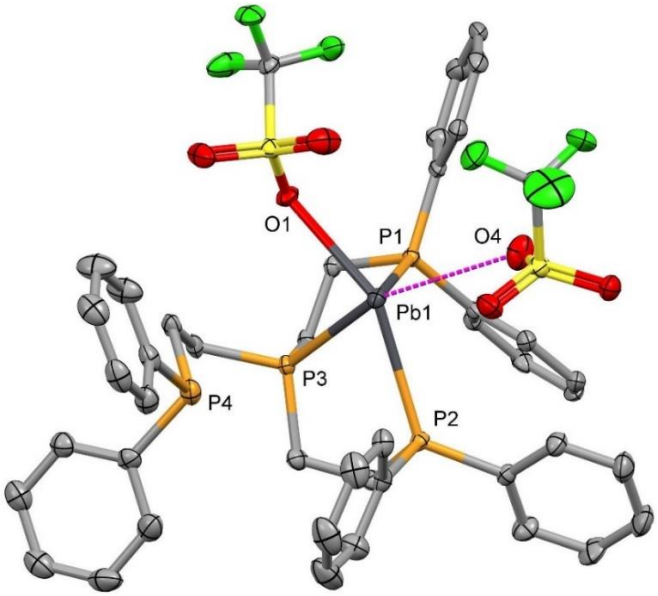

Figure 5.20 – Crystal structure of ***29*** [Pb(OTf){P(CH$_2$CH$_2$PPh$_2$)$_3$}][OTf] showing the atom numbering scheme. Ellipsoids are drawn at 50% probability with H-atoms omitted for clarity.

Table 5.9 - Selected bond lengths and angles for [Pb(OTf){P(CH$_2$CH$_2$PPh$_2$)$_3$}][OTf].

Bond Lengths / Å		Bond Angles / °	
Pb1 – P1	2.7771(8)	P1 – Pb1 – P2	96.20(2)
Pb1 – P2	2.9185(7)	P1 – Pb1 – P3	72.95(2)
Pb1 – P3	2.8021(7)	P2 – Pb1 – P3	70.72(2)
Pb1 – O1	2.7514(19)	O1 – Pb1 – O4	114.67(6)
Pb1…O4	2.951(2)		

The tetradentate ligand again shows coordination of the central phosphine and two of the three pendant arms with the final phosphine arm being uncoordinated with a Pb-P distance of 4.1886(8) Å, a shortening of < 0.1 Å than that measured in the tin analogue. As was observed in the bridging triflates of the bidentate ligand complexes $[Pb(OTf)_2\{o\text{-}C_6H_4(EMe_2)_2\}]$ (E = P, As) discussed above, the second triflate (O4, O5, O6) has a second Pb-O contact within the van der Waals radii with a distance of 3.284(2) Å. The Pb-P distances of this complex range from 2.7771(8) – 2.9185(7) Å, significantly longer than those observed in the complex $[Pb(OTf)_2\{o\text{-}C_6H_4(PMe_2)_2\}]$. The preference to higher coordination number of this metal centre maybe explains this lengthening. Each of the complexes $[M(OTf)_2\{MeC(CH_2PPh_2)_3\}]$ (M = Ge, Sn, Pb) were synthesised and isolated before the salt-exchange reaction with $Na[BAr^F]$, but only the Pb complex crystallised. The structure of the lead triflate complex with the tripodal triphosphine, $[Pb(OTf)_2\{MeC(CH_2PPh_2)_3\}]$ revealed a dimeric unit containing three bridging and a single ionic triflate, better formulated as $[\{Pb\{MeC(CH_2PPh_2)_3\}_2\{\mu\text{-}OTf)_3][OTf]]$ and shown in Figure 5.21 and selected bond lengths and angles found in Table 5.10.

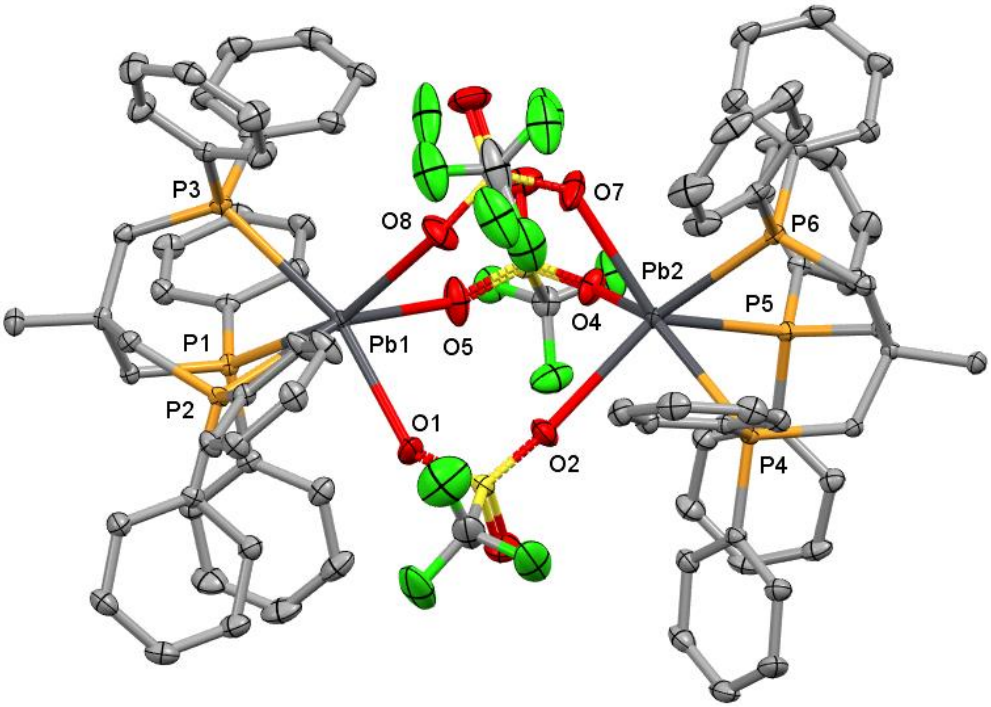

Figure 5.21 – Crystal structure of ***30*** $[\{Pb\{MeC(CH_2PPh_2)_3\}_2\{\mu\text{-}OTf)_3][OTf]]$ showing the atom numbering scheme. Ellipsoids are drawn at 50% probability with H-atoms and free anions omitted for clarity.

Table 5.10 - Selected bond lengths and angles for [{Pb{MeC(CH_2PPh_2)$_3$}$_2$(μ-OTf)$_3$}$_2$][OTf].

Bond Lengths / Å		Bond Angles / °	
Pb1 – P1	2.8277(4)	P1 – Pb1 – P2	71.68(2)
Pb1 – P2	2.8844(4)	P1 – Pb1 – P3	72.80(2)
Pb1 – P3	2.9261(5)	P1 – Pb1 – O1	77.35(2)
Pb1 – O1	2.6542(15)	O1 – Pb1 – O5	85.16(5)
Pb1 – O5	2.7722(15)	O1 – Pb1 – O8	93.03(5)
Pb1 – O8	2.8398(15)	O5 – Pb1 – O8	82.13(5)
Pb2 – P4	2.9075(5)	P4 – Pb2 – P5	73.03(2)
Pb2 – P5	2.8441(5)	P4 – Pb2 – P6	75.12(2)
Pb2 – P6	2.9158(5)	P5 – Pb2 – P6	73.61(2)
P2 – O2	2.7889(14)	O2 – Pb2 – O4	85.16(5)
Pb2 – O4	2.6707(14)	O2 – Pb2 – O7	101.93(5)
Pb2 – O7	2.7375(17)	O4 – Pb2 – O7	80.64(5)

The bridging interactions of the triflate anions and the metal centres of this complex range from 2.6542(15) – 2.8398(15) Å which is comparable to the distances observed for the other bridging anions in the earlier examples. Dr Rhys King synthesised the Ge(II) analogue by reacting $GeCl_2$.dioxane with TMSOTf stepwise, before addition of $MeC(CH_2PPh_2)_3$, for 2h. An oily solid was isolated before characterisation, suggesting [Ge(OTf)$_2${$MeC(CH_2PPh_2)_3$}] had been successfully synthesised, however crystallisation was not achieved.[26] It is unknown if the bridged dimer motif is present in the lighter metal elements of Group 14 as crystals of the Sn(II) and Ge(II) complexes could not be grown, despite use of a range of crystallisation methods.

Reaction of each of these complexes in a 2:1 ratio with Na[BAr^F] produced crystals suitable for X-ray diffraction which revealed the complexes [M{$MeC(CH_2PPh_2)_3$}][BAr^F]$_2$, (M = Ge, Sn, Pb) with the Sn complex being illustrated in Figure 5.15 and Ge and Pb complexes shown in Figure 5.22. Selected bond lengths and angles for both of these complexes can be located in Table 5.11. Each of these complexes, [M{$MeC(CH_2PPh_2)_3$}][BAr^F]$_2$ (M = Ge, Sn, Pb), were found to be isomorphous with the complexes crystallising in a P-1 space group.

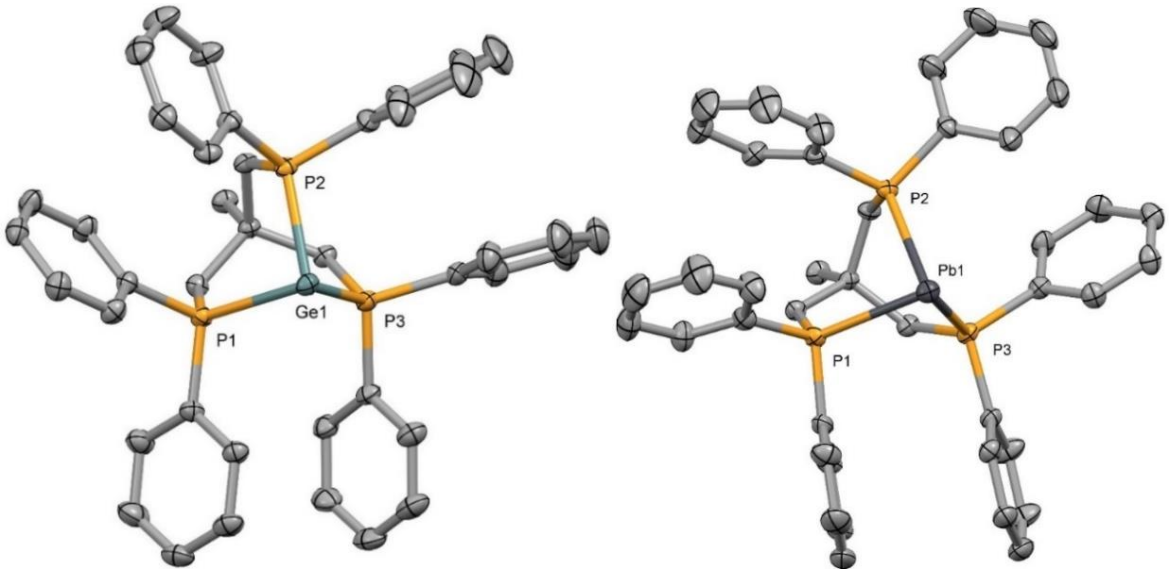

(a) (b)

Figure 5.22 – (a) Crystal structure of ***31*** $[Ge\{MeC(CH_2PPh_2)_3\}][BAr^F]_2$ showing the atom numbering scheme. Ellipsoids are drawn at 50% probability with H-atoms and $[BAr^F]^-$ anions omitted for clarity.
(b) Crystal structure of ***32*** $[Pb\{MeC(CH_2PPh_2)_3\}][BAr^F]_2$ showing the atom numbering scheme. Ellipsoids are drawn at 50% probability with H-atoms and $[BAr^F]^-$ anions omitted for clarity.

Table 5.11 - Table of selected bond lengths and angles for $[Ge\{MeC(CH_2PPh_2)_3\}][BAr^F]_2$and $[Pb\{MeC(CH_2PPh_2)_3\}][BAr^F]_2$.

$[Ge\{MeC(CH_2PPh_2)_3\}][BAr^F]_2$	Bond Lengths / Å		Bond Angles / °	
	Ge1 – P1	2.4239(4)	P1 –Ge1 – P2	86.609(14)
	Ge1 – P2	2.4070(4)	P1 – Ge1 – P3	85.912(15)
	Ge1 – P3	2.4110(5)	P2 – Ge1 – P3	85.412(15)
$[Pb\{MeC(CH_2PPh_2)_3\}][BAr^F]_2$	Bond Lengths / Å		Bond Angles / °	
	Pb1 – P1	2.7360(5)	P1 – Pb1 – P2	80.594(17)
	Pb1 – P2	2.7092(6)	P1 – Pb1 – P3	78.676(17)
	Pb1 – P3	2.7184(7)	P2 – Pb1 – P3	77.868(17)

Comparison of the Pb-P bond lengths in the $[BAr^F]^-$ and $[OTf]^-$ complexes shows significantly longer bonds in the latter of the two complexes. The shortening and strengthening of these bonds upon reaction with $Na[BAr^F]$ is attributed to the lower coordination number, as well as the greater positive charge being found at the dicationic M(II) centre. The shorter bonds present in this $[BAr^F]^-$ species also cause a widening in the P-Pb-P bond angles.

There is a significant increase in the bond distances observed between this ligand and the metal centre, which does not directly follow the change in covalent radii of these metals. The M-P distances and P-M-P angles are tabulated for comparison in Table 5.13. It clearly shows an increase in the M-P distances observed within these three crystal structures and the widening of

the corresponding angles in the order Ge > Sn > Pb. The increase in the M-P bond distance is consistent with the increase in covalent radii of these elements.[43]

Table 5.13 - Comparison of $[M\{MeC(CH_2PPh_2)_3\}][BArF]_2$ (M = Ge, Sn, Pb)

	M = Ge	M = Sn	M = Pb
M – P / Å	Ge1–P1 = 2.4239(4) Ge1–P2 = 2.4070(4) Ge1–P3 = 2.4110(5)	Sn1–P1 = 2.6438(4) Sn1–P2 = 2.6194(4) Sn1–P3 = 2.6249(4)	Pb–P1 = 2.7360(5) Pb1–P2 = 2.7092(6) Pb1–P3 = 2.7184(6)
< P–M–P / °	P1–Ge1–P2 = 86.609(14) P1–Ge1–P3 = 85.912(15) P2–Ge1–P3 = 85.412(15)	P1–Sn1–P2 = 82.120(13) P1–Sn1–P3 = 80.761(14) P2–Sn1–P3 = 80.160(14)	P1–Pb1–P2 = 80.594(17) P1–Pb1–P3 = 78.676(17) P2–Pb1–P3 = 77.868(17)

5.2.2 Spectroscopic Discussion

The crystal structures obtained have been key throughout this work for giving the unequivocal solid-state structure and a basis for the assignment of the observed solution-state NMR and IR spectroscopic data. Multinuclear NMR spectroscopy (^1H, $^{13}C\{^1H\}$, $^{19}F\{^1H\}$, $^{31}P\{^1H\}$ and ^{119}Sn) was used to explore the environments of the different nuclei in each the complexes and how these changed before and after coordination. These were primarily recorded in CD_3CN, however due to the solubility of some of these complexes, additional NMR experiments were run in CD_3NO_2 or CD_2Cl_2. Of the NMR spectra recorded, the information gained *via* $^{31}P\{^1H\}$ and ^{119}Sn NMR spectroscopy was key, giving an insight to the complex and the change of the environment caused by the coordination of the ligand. The ^1H and $^{13}C\{^1H\}$ NMR spectra (values summarised in Experimental Sections) produced by each complex consistently showed a shift to a higher frequency, congruent with that observed for coordinated pnictine ligands in previous work.[26,39] Due to the number of bonds between the C or H atoms and donor atom/metal, the observed changes in chemical shifts are small. As has been seen throughout the work carried out in this thesis thus far, the resonances produced in the the $^{19}F\{^1H\}$ spectra has consistently shown a triflate resonance as a sharp singlet at ~ -79 ppm which has been assigned to ionic triflate in solution. This suggests that in solution the triflate anions are not coordinated and exchanging in solution, on a faster time scale than can be observed by this technique. Those NMR spectra that were run in CD_2Cl_2, showed movement of this resonance to a chemical shift of -79.4 ppm. Although no information is given about the about the coordination of the triflate other than the crystal-structure, compounds containing both free and coordinated triflate in the solid-state have been shown to produce the same resonance. This may also suggest that in solution the triflate

anions are not coordinated and exchanging in solution on a faster time scale than is observed by NMR spectroscopy.

The highly informative $^{31}P\{^{1}H\}$ and ^{119}Sn NMR spectra are summarised with the key data (chemical shifts and couplings) in Table 5.13 with the full spectra described in the Experimental sections and the ESI. As previously discussed, the work by Dean *et al.* described *in situ* NMR experiments on related phosphine complexes $[M(phosphine)][SbF_6]_2$ (M = Sn, Pb).[1,2,44] As part of this work, the complexes $[M\{MeC(CH_2PPh_2)_3\}][SbF_6]_2$ (M = Sn, Pb) were produced with the both the $^{31}P\{^{1}H\}$ and $^{119}Sn/^{207}Pb$ NMR resonances were described. Using $M(OTf)_2$ (M = Sn, Pb) in reaction with $MeC(CH_2PPh_2)_3$ produced the complexes $[M\{MeC(CH_2PPh_2)_3\}][OTf]_2$ with a crystal structure being obtained for the lead analogue, revealing the dimeric structure shown in Figure 5.21. The reaction of these complexes with an equimolar amount of Na[BArF] produced the complexes $[M\{MeC(CH_2PPh_2)_3\}][BArF]_2$ (M = Ge, Sn, Pb), with these shown in Figures 5.15 and 5.22. Comparison of the triflate and $[BAr^F]^-$ complexes with the $[SbF_6]^-$ complexes produced by Dean are shown below in Table 5.13. This highlights that substitution of these weakly coordinating anions causes minimal changes in resonance produced by the complex.

Table 5.13 - Table of NMR data for the three complexes $[Sn\{MeC(CH_2PPh_2)_3\}][X]_2$ (X = $[OTf]^-$, $[SbF_6]^-$ and $[BAr^F]^-$).

Complex	$\delta(^{31}P)$ / ppm	$\delta(^{119}Sn)^b$ / ppm	$^1J_{119SnP}$ / Hz	Ref.
$[Sn(OTf)_2\{MeC(CH_2PPh_2)_3\}]$	−9.4	−834.0	1248	*This work*
$[Sn\{MeC(CH_2PPh_2)_3\}][BAr^F]_2$	−8.9 −6.0 (258 K)	−824.3 −843.7 (258 K)	1246 1252 (258 K)	*This work*
$[Sn\{MeC(CH_2PPh_2)_3\}][SbF_6]_2$	−11.3	−792	1279	[1,2]

The chemical shift exhibited in the ^{119}Sn NMR spectra of the triflate and $[BAr^F]^-$ complexes showed a 10 ppm difference after the substitution of the anion. This is a small changes in the metal NMR spectra and suggests that both the triflate and $[BAr^F]^-$ anions are free from the metal and giving very little influence over the observed resonance, suggesting a dicatonic nature in solution. The complex produced by Dean with the $[SbF_6]^-$ anion was found at a higher frequency shift of -792 ppm, at a less negative chemical shift. This indicates that the $[SbF_6]^-$ anion has more of an affinity for the metal centre and produces a larger influence over the observed resonance. The same pattern is the observed for the $^1J_{SnP}$ coupling constants, with the $[BAr^F]^-$ and triflate showing almost identical values, while the $[SbF_6]^-$ complex with an increase of ± 30 Hz. Again, these small changes in solution suggest that the present anion has dissociated in solution and is thus ionic. These values did show variability with changes in solvent, and for this reason the coordinating

solvent CD_3CN was used primarily. Due to the labile nature of the main group metals, the phosphine exchange and interactions with anions in solution are also responsible for changes in shift and coupling constants. While coordination by $[SbF_6]^-$ is viewed as rare, examples are known in the solid state, and coordinated triflate is well known.[45]

The other tridentate ligand explored was $PhP(CH_2CH_2PPh_2)_2$, which the crystal structure in Figure 5.16. The $^{31}P\{^1H\}$ and ^{119}Sn NMR spectra for the tin complex $[Sn(OTf)\{PhP(CH_2CH_2PPh_2)_2\}][OTf]$ are shown in Figure 5.23, highlighting the $^{117/119}Sn$ coupling satellites exhibited. These spectra appear to be consistent with the coordination observed in the crystal structure.

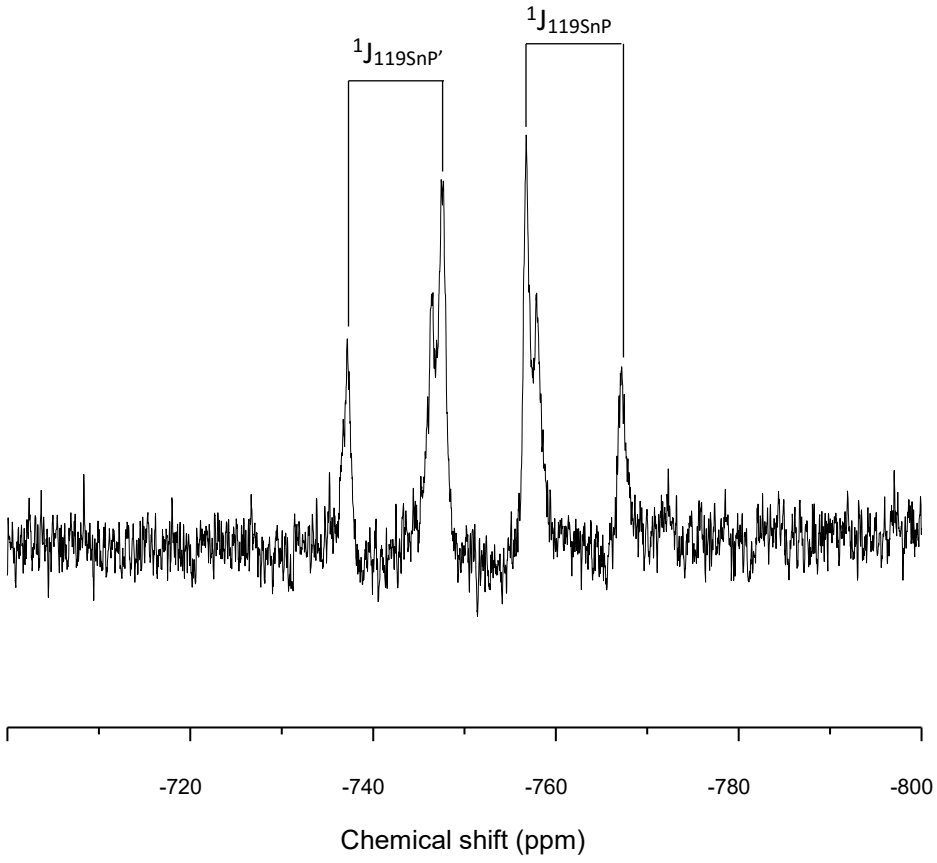

(a)

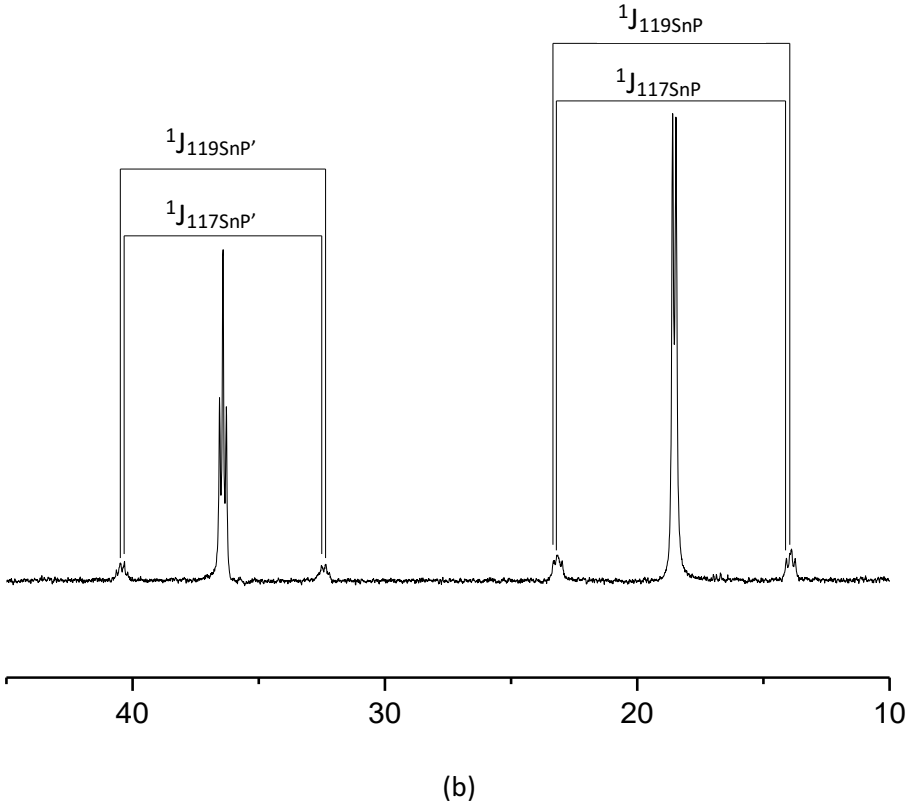

Figure 5.23 – (a) ^{119}Sn NMR spectrum of [Sn(OTf){PhP($CH_2CH_2PPh_2$)$_2$}][OTf] showing the $^1J_{119SnP}$ couplings to the two distinct P atoms; (b) $^{31}P\{^1H\}$ NMR spectrum [Sn(OTf){PhP($CH_2CH_2PPh_2$)$_2$}][OTf] showing the $^1J_{117/119SnP}$.

The crystal structure revealed two phosphine environments in this complex, with both being bonded to the metal centre: the central phosphine and the two the pendent arms with the arms in a near equivalent environment. The $^{31}P\{^1H\}$ NMR spectra containing two resonances at 18.5 and 36.4 ppm, split into a doublet and triplet respectively. The resonances at 36.4 ppm corresponds to the central phosphine, with a coupling constant of 20.9 Hz and an integration of 1. The phosphines of the pendent arms were found as a doublet at 18.5 ppm, with a matching coupling constant and an integration of 2. As can be seen in Figure 5.23(b), the satellite couplings to both $^{117/119}$Sn were observed. The central phosphine resonance showed satellite couplings of $^1J_{117/119SnP}$ = 1266 and 1377 Hz respectively, while the coordinated arms had slightly larger coupling constants, of 1460 and 1549 Hz respectively. The ^{119}Sn NMR spectra showed overlapping triplets, due to the similarity in the couplings to the donating phosphines. These were measured as 1544 and 1386 Hz, closely matching the measured $^1J_{119SnP}$ couplings in the $^{31}P\{^1H\}$ NMR spectra.

The work reported by Dean showed resonances at 24.9 and 47.7 ppm in the $^{31}P\{^1H\}$ NMR spectrum and comparison of these with the resonances of the triflate complex, are at a higher frequency in the $[SbF_6]^-$ salt.[1] The ^{119}Sn NMR spectrum of [Sn{PhC($CH_2CH_2PPh_2$)$_2$}][SbF_6]$_2$ was reported as a doublet of triplets, showing $^1J_{119SnP}$ couplings closely matching those observed in the triflate complex. The resonance observed in the ^{119}Sn NMR spectrum of [Sn(OTf)$_2${PhP(CH_2CH_2PPh-

$_2)_2$}] was found to be more negative than the resonance observed for [Sn{PhP(CH_2CH_2PPh-$_2)_2$}][SbF_6]$_2$. From the crystal structure it is known that the solid-state structure of the triflate complex has coordination of at least one triflate with long contacts to a second. In solution, triflate may have a higher affinity for the dicationic metal complex than the weakly coordinating $[SbF_6]^-$ anion. This could be a factor rising to differences in the resonances observed in both the $^{31}P\{^1H\}$ and ^{119}Sn NMR spectra. The ^{119}Sn satellite coupling constants observed for the $[SbF_6]^-$ complex were measured as 1593 and 1381 Hz, again showing only a small shift from those observed in the triflate complex. The lowering of these satellite couplings could be due to the differences in lability of the anions changing the strength of the binding of the phosphine ligand.

Structurally, the complexes [Sn(OTf){PhP($CH_2CH_2PPh_2)_2$}][OTf] and [Sn(OTf){P($CH_2CH_2PPh_2)_3$}][OTf] were found to contain the same *P_3O* core geometry in the crystal structures shown in Figure 5.16 and 5.17, with the additional pendent –$CH_2CH_2PPh_2$ arm not coordinating to the metal centre. The solution data collected from the $^{31}P\{^1H\}$ and ^{119}Sn NMR spectroscopy produced a resonance pattern suggesting coordination of all four of the phosphines in the tetraphosphine ligand. The $^{31}P\{^1H\}$ NMR spectrum revealed two resonances with the first found as a quartet found at 37.8 with an integral of 1, while the second resonance is found at 5.5 ppm and is split into a doublet with an integral of 3. This data is complimented by the ^{119}Sn NMR spectrum, showing a single resonance being split into a doublet of quartets which are significantly overlapping due to the coupling constants being nearly half at 1485 Hz and 720 Hz. These data are consistent with tetradentate coordination of the ligand in the solution-state, a direct contrast to the structure observed in the solid-state. Low temperature NMR analysis, completed by Dr Rhys King and Dr Danielle Runacres, was conducted at 258 K in CD_3CN. Unfortunately this caused broadening of the responances, resulting in the loss of splitting, suggesting lower temperatures would be required to freeze out of the spectra. It is probable that the rate of exchange between coordinated and free pendent –$CH_2CH_2PPh_2$ groups is still too high for the NMR time scale and would require study at a lower temperature to freeze out this exchange. Running these NMR experiments at lower temperatures could allow for observation of a spectra that matches the crystal structure, however, the lower solubility of these complexes in CD_2Cl_2 at low temperatures caused broadening of these peaks during LT-NMR experiments.

The complexes of tin with coordinated arsine ligands revealed no ^{119}Sn NMR resonances at room temperature (298 K) but upon cooling to 254 K, each complex was seen to produce a broad resonance in the ^{119}Sn NMR spectrum. Comparison of the ^{119}Sn resonances exhibited by the complexes [Sn$(OTf)_2${*o*-$C_6H_4(EMe_2)_2$}] (E = P, As) showed a negative shift from -690 ppm to -886.5 ppm when moving from a phosphine to an arsine donor. A more negative shift was also observed for the coordination of the tripodal triarsine ligand MeC($CH_2AsMe_2)_2$. [Sn$(OTf)_2${MeC($CH_2PPh_2)_2$]

was revealed to have a single ^{119}Sn resonance at -834 ppm at RT, with $[Sn(OTf)_2\{MeC(CH_2AsMe_2)_2\}]$ showing a single broad resonance at -920 ppm. Unfortunately, this complex was never crystallised despite many attempts.

Although the complexes synthesised in this chapter of work were found to not produce a ^{207}Pb NMR resonance, the $^{31}P\{^1H\}$ NMR spectra of $[Pb\{MeC(CH_2PPh_2)_3\})][BAr^F]_2$ revealed ^{207}Pb satellite peaks, shown in Figure 5.24. This spectrum shows the $^{31}P\{^1H\}$ NMR resonance of the dicationic $[Pb\{MeC(CH_2PPh_2)_3\}][BAr^F]_2$ as a singlet at 16.34 ppm, exhibiting ^{207}Pb satellites which were measured at 1777 Hz. Comparison of the $^{31}P\{^1H\}$ NMR spectrum of the triflate complex $[\{Pb(OTf)\{MeC(CH_2PPh_2)_3\}\}_2(\mu^2\text{-}OTf)_3]$, showed a broad and unresolved peak at 11.59 ppm with a width of ~ 3000 Hz. This broadness shows that there is still fast phosphine exchange between the arms of the ligand in solution at a higher rate than the NMR analysis for the Pb(II) metal centre. Both of the complexes $[M\{MeC(CH_2PPh_2)_3\}][BAr^F]_2$ (M = Ge, Sn) produced $^{31}P\{^1H\}$ NMR resonances at -8.9 and -4.3 respectively, as a singlet in each case. The substitution of the triflate anion for $[BAr^F]^-$ shows sharpening of the resonances observed with resolution of the satellite peaks, less coordinating $[BAr^F]^-$ anion likely increasing the symmetry of the complexes.

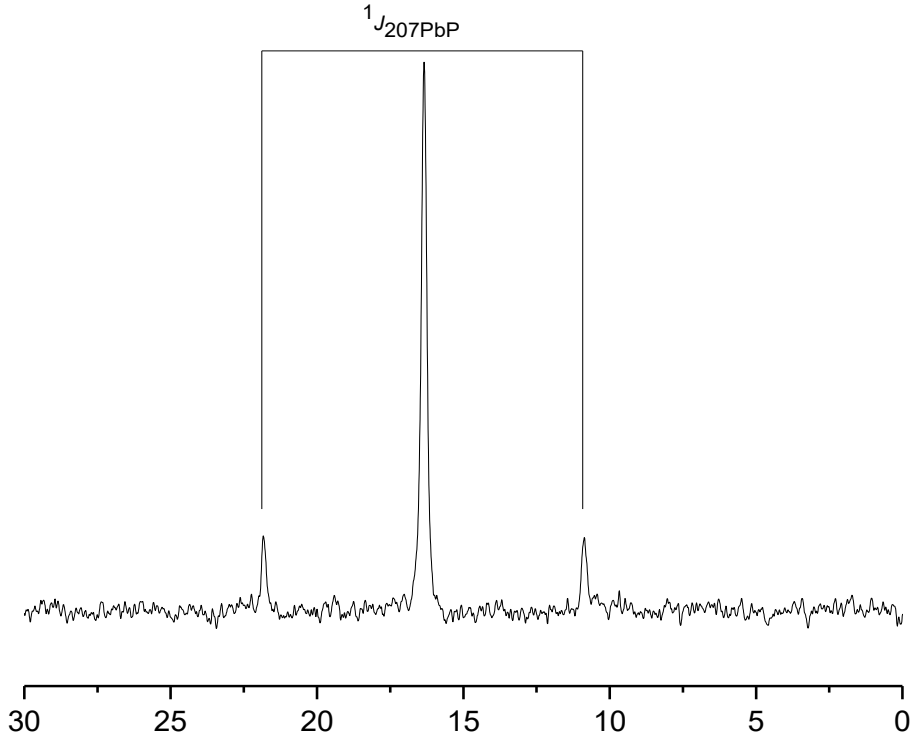

Figure 5.24 - The $^{31}P\{^1H\}$ NMR spectrum of $[Pb\{MeC(CH_2PPh_2)_3\}][BAr^F]_2$ showing the $^1J_{207PbP}$ coupling.

The ^{207}Pb NMR spectra obtained by Dean exhibited resonances at room temperature which was complimented by the resolution of lead satellite peaks in the $^{31}P\{^1H\}$ NMR spectra.[1,2] The NMR studies of the lead complexes produced in this chapter with either $[OTf]^-$ anions did not exhibit ^{207}Pb resonances, even at low temperatures (258 K). The $^{31}P\{^1H\}$ NMR spectra of these complexes showed clear ^{207}Pb satellites which, at low temperature, were found to sharpen and the coupling

constants have been included in Table 5.14. Despite repeating these NMR experiments at variable temperature (258 K) none of the triflate complexes were found to produce ^{207}Pb NMR resonances. The rapid reversible exchange of both the phosphine and triflate anions in solution may explain the absence of a ^{207}Pb resonance. Further cooling, using CD_2Cl_2, may allow for this exchange to be frozen out revealing the ^{207}Pb resonance, however, due to the lower solubility in this solvent was not attempted here. The rapid exchange in solution would be consistent with the structure shown in Figure 5.24, where the weakly coordinated triflate anions are found to both be formally coordinated triflate anions as well as weakly coordinated anions.

Table 5.14 - Selected $^{31}P\{^{1}H\}$ and ^{119}Sn NMR data from the $[OTf]^-$ and $[BAr^F]^-$ complexes produced here with comparison to $[SbF_6]^-$ complexes produced by Dean *et al*.[1,2]

Complex	δ(^{31}P) / ppm	δ(^{119}Sn)[b] / ppm	$^{1}J_{119SnP}$ / Hz	$^{1}J_{207PbP}$ / Hz	Ref.
$[Sn(OTf)_2\{o\text{-}C_6H_4(PMe_2)_2\}]$	18.0	−690	1882	–	*This work*
$[Sn(OTf)_2\{o\text{-}C_6H_4(AsMe_2)_2\}]$	–	−886.5	–	–	*This work*
$[Sn(OTf)_2\{o\text{-}C_6H_4(PPh_2)_2\}]$	19.9 22.7 (258 K)	−809 −1150 (258 K)	1550 1506 (258 K)	–	*This work*
$[Sn(OTf)_2\{MeC(CH_2PPh_2)_3\}]$	−9.4	−834.0	1248	–	*This work*
$[Sn\{MeC(CH_2PPh_2)_3\}][BAr^F]_2$	−8.9 −6.0 (258 K)	−824.3 −843.7 (258 K)	1246 1252 (258 K)	–	*This work*
$[Sn\{MeC(CH_2PPh_2)_3\}][SbF_6]_2$	−11.3	−792	1279	–	*1,2*
$[Sn(OTf)\{PhP(CH_2CH_2PPh_2)_2\}][OTf]$	36.4, 18.5	−751	1549, 1319	–	*This work*
$[Sn\{PhP(CH_2CH_2PPh_2)_2\}][SbF_6]_2$	47.7, 24.9	−686	1593, 1381	–	*1,2*
$[Sn(OTf)_2\{MeC(CH_2AsMe_2)_3\}]$	-	not observed −920 (258 K)	-	–	*This work*
$[Sn(OTf)\{P(CH_2CH_2PPh_2)_3\}][OTf]$	37.8, 5.5	−778.6	720, 1485	–	*This work*
$[Sn\{P(CH_2CH_2PPh_2)_3\}][SbF_6]_2$	36.8, 2.5	−756	702, 1487	–	*1,2*
$[Pb(OTf)_2\{o\text{-}C_6H_4(PMe_2)_2\}]$	74.9	–	–	1777	*This work*
$[\{Pb\{MeC(CH_2PPh_2)_3\}_2\{\mu\text{-}OTf)_3\}][OTf]]$	11.6	–	–	1150	*This work*
$[Pb\{MeC(CH_2PPh_2)_3\}][SbF_6]_2$	13.8	–	–	1786	*1,2*
$[Pb\{MeC(CH_2PPh_2)_3\}][BAr^F]_2$ [c]	15.8	–	–	1777	*This work*
$[Pb(OTf)_2\{P(CH_2CH_2PPh_2)_3\}]$	77.5, 26.1	–	–	437, 1870	*This work*
$[Pb\{P(CH_2CH_2PPh_2)_3\}][SbF_6]_2$	80.1, 27.5	–	–	476, 2136	*1,2*
$[Pb\{PhP(CH_2CH_2PPh_2)_2\}][SbF_6]_2$	90.2, 66.0	–	–	1836, 1863	*1,2*

a. spectra recorded at 298 K in MeCN unless otherwise stated.

5.2.3 DFT Calculations

The complete set of crystal structures of the dicationic complexes, $[M\{MeC(CH_2PPh_2)_3\}]^{2+}$ (M = Ge, Sn, Pb), were also then electronically investigated using DFT calculations by Dr Rhys King, with the procedure being fully described in the Experimental section. DFT calculations for each of the dicationic complexes converged to a structure that had strong correlation with the crystallographic structures which were used as a starting geometry. The finished calculations had no imaginary frequencies, which suggests that the calculated structure is at a point of stability and not corresponding to a transitional state between two geometries. The corroboration data for the structure of the physical crystal structures and optimised structure suggests this is a low-energy state for this complex.

As well as simulation of the crystal structures, the frontier molecular orbitals of these complexes was also calculated with the HOMO and LUMO orbitals shown in Figure 5.25 and 5.26. For each of these tripodal complexes, the HOMO orbital is associated with the lone pair of the group 14 metal(II) centre, clearly visible in the diagram. The structures collected for $[M\{MeC(CH_2PPh_2)_3\}]^{2+}$ (M = Ge, Sn, Pb) showing directionality, suggesting the presence of a homodirected stereochemically active lone pair, being made up of changing *s*- and p_z-character. The key data for the calculations carried out on each complex are shown in Table 5.15 where it can be seen that $[[Ge\{MeC(CH_2PPh_2)_3\}]^{2+}$ had the highest *p*-character at 18.35 % and descending down the group to tin (13.75 %) and lead (8.12 %), following the expected trend for this group. The HOMO-1 and HOMO-2 were found to be approximately degenerate in energy and are associated with the bonding interactions between the lone pairs of the phosphine ligand and the empty p_x/p_y type orbitals located on the central metal centre. The LUMO and LUMO+1 orbitals were found to be degenerate in energy and associated with the empty p_x/p_y orbitals on the central metal atom, with diagrams displaying these orbitals shown in Figure 5.26. The HOMO-LUMO gap was calculated for each of the complexes and was found to follow the same pattern as the *p*-character for the different metal complexes, with germanium having the largest gap of 5.41 eV gap decreasing down the group with the tin (4.81 eV) and lead analogues (4.74 eV).

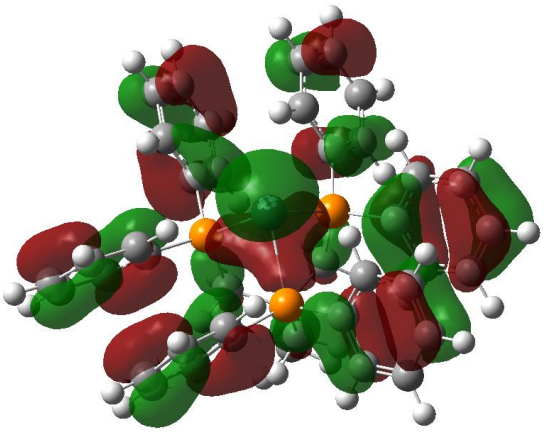

HOMO (-11.917/-11.859/-11.837 eV)

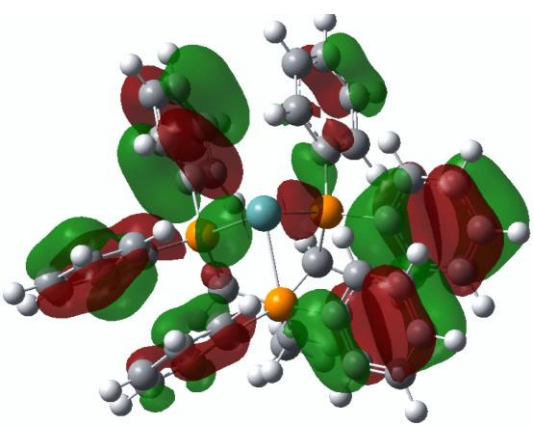

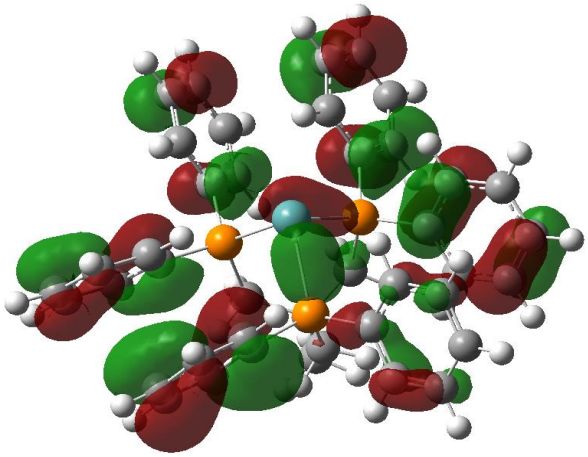

HOMO-1 (-12.063/-12.000/-11.941 eV)

HOMO-2 (-12.064/-12.020/-11.941 eV)

Figure 5.25 - Representations of the HOMO, HOMO-1 and HOMO-2 orbitals for $[Ge\{MeC(CH_2PPh_2)_3\}]^{2+}$ with the orbital energies for each complex shown in brackets (Ge/Sn/Pb).

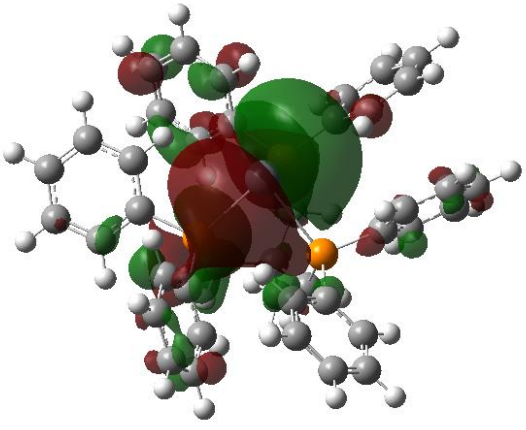

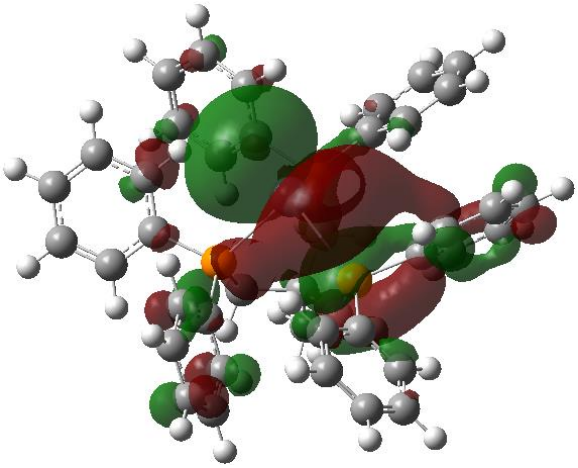

LUMO (-6.747/-7.052/-7.092 eV)

LUMO+1 (-6.746/-7.041/-7.075 eV)

Figure 5.26 - Representations of the LUMO and LUMO+1 orbitals for $[Ge\{MeC(CH_2PPh_2)_3\}]^{2+}$ with the orbital energies of each complex shown in brackets (Ge/Sn/Pb).

The directionality of the HOMO (lone pair) gives overlap with the σ* orbital of one of the P-C bonds of the tripodal phosphine ligand species, leading to lone pair→P-C σ* interactions shown in Figure 5.27. Following the same trend as the % *p*-character for this group, germanium was found to give the strongest of these interactions, calculated to be equal to 34.1 kJ mol^{-1} over the molecule. This decreased to 21.8 kJ mol^{-1} for tin and 15.3 kJ mol^{-1} for lead. These stabilising interactions will partially fill these anti-bonding orbitals, thus weakening (and lengthening) these P-C bonds of the ligand. The calculated P-C bond lengths of the free tripodal phosphine ligand $MeC(CH_2PPh_2)_3$ range from 1.816 – 1.860 Å, comparison of these to the measured P-C bonds of $[Ge\{MeC(CH_2PPh_2)_3\}]^{2+}$ showed a slight shortening, to a range of 1.798 (2) – 1.840(2) Å.

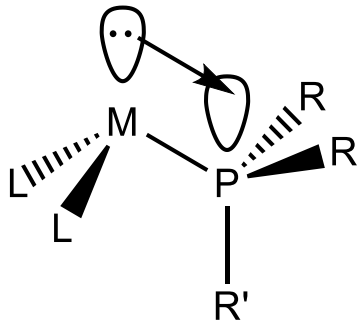

Figure 5.27 - Interaction between the lone pair on the metal and the σ* orbital of the P-C bond.

The NBO calculations also showed the natural charge located at the metal centre for each complex and this, in contrast to the % *p*-character and HOMO-LUMO gap, to decrease down the group. The lead atom of the complex $[Pb\{MeC(CH_2PPh_2)_3\}]^{2+}$ was calculated to have a natural charge of +0.84, with the tin analogue having +0.76 and while the germanium complex was significantly lower at +0.26. Although smaller, these changes were mirrored by the calculated charge located on the phosphines of the ligand, where higher natural charge of +1.11 was located on the phosphorous atom of $[Ge\{MeC(CH_2PPh_2)_3\}]^{2+}$ and only +0.95 in the lead analogue. The higher positive charge located at the Ge(II) metal centre suggests more lone-pair back-donation in to the P-C σ* orbital, manifesting as these P-C bonds being shortened less than Ge(II) analogue.

Table 5.15 - Summary of the orbital character and charge distributions in $[M\{MeC(CH_2PPh_2)_3\}]^{2+}$ determined from the DFT calculations. lp = lone pair

Complex	HOMO-LUMO gap / eV	$\%p_z$ character of lp on M	Charge at M	Charge at P	lp→P-C σ* over molecule / kJ mol^{-1}
$[Ge\{MeC(CH_2PPh_2)_3\}]^{2+}$	5.17	18.35	0.25788	1.11489	34.1
$[Sn\{MeC(CH_2PPh_2)_3\}]^{2+}$	4.81	13.75	0.76107	0.96659	21.8
$[Pb\{MeC(CH_2PPh_2)_3\}]^{2+}$	4.74	8.12	0.84092	0.95483	15.3

5.3 – Conclusions

The preparation and characterisation of a series of Sn(II) and Pb(II) triflate complexes with phosphine and arsine ligands have been described. Structural studies of these complexes confirm the coordination of the soft donor ligands in each case with dimerisation and oligamerisation being commonly observed. Coordination of *o*-$C_6H_4(ER_2)_2$ (E = P, As; R = Me, Ph) showed the formation of polymeric chains of six-coordinate metal centres connected through triflate bridges. The bulkier ligand phenyl analogue, *o*-$C_6H_4(PPh_2)_2$ was reacted with $GeCl_2$ and was shown to coordinate in near κ^1-asymmetric binding. Coordination of the same ligand to $M(OTf)_2$ (M = Sn, Pb) contrasted this, showing symmetric bonding with only small differences in the M-P bond lengths of $[M(OTf)_2(o\text{-}C_4H_6(PPh_2)_2]$.

A series of complexes were synthesised with the tripodal phosphine ligand $Me\{CH_2PPh_2\}_3$ and found to form the complexes $[M(OTf)_2(Me\{CH_2PPh_2\}_3)]$ (M = Ge, Sn, Pb). The lead(II) complex formed with $MeC(CH_2PPh_2)_3$ ligand crystallises as a triply triflate-bridged dimer with a single triphosphine bonded to each metal. The $[M(OTf)_2\{MeC(CH_2PPh_2)_3\}]$ (M = Ge, Sn, Pb) complexes have been reacted with $Na[BAr^F]$ in metathesis reactions to form the analogous $[BAr^F]^-$ salts, which were crystallised to show the dicationic species $[M(Me\{CH_2PPh_2\}_3)][BAr^F]_2$ (M = Ge, Sn, Pb).

The bond lengths and angles of these crystal structures matched closely with the DFT calculations of the optimised structure of each, in the gas phase. The DFT calculations also revealed the HOMO of each complex to be directionally at the metal centre, corresponding to the lone pair of electrons on the metal centre. It also gave insight to the electronics of the metal centres, showing the decline of HOMO-LUMO gap and %p character of the lone pair and increases in the charge ratio found at the metal centre down the Group 14 metals.

5.4 – Experimental

For supplier and purification of reagents and solvents, instrument specifications and NMR solvent references see Appendix A. The diphosphine ligand *o*-$C_6H_4(PMe_2)_2$ was synthesised by Dr Wenjian Zhang and Dr Rhys King using a procedure described by Harris and co-workers.[46] The arsine ligands used in this chapter were synthesised by Dr Wenjian Zhang using a procedure described by Nyholm and co-workers.[47] Na[BAr^F] was synthesised prior to use with the procedure being reported here.

5.4.1 Complex preparations

5.4.1.1 **[Sn(OTf)$_2${o-$C_6H_4(PMe_2)_2$}]**

$Sn(OTf)_2$ (125 mg, 0.3 mmol) was suspended in benzene (10 mL) before addition of *o*-$C_6H_4(PMe_2)_2$ (60 mg, 0.3 mmol), upon which the majority of solid was taken up into solution which was stirred for 2 h. The remaining particulates were removed by filtration, before the addition of Et_2O (10 mL) causing precipitation of a white solid, which was collected by filtration and dried *in vacuo*. Yield: 128 mg, 69 %. Required for $C_{12}H_{16}F_6O_6P_2S_2Sn$ (615.03): C, 24.4; H, 2.6. Found: C, 24.0; H, 3.0 %. ^{1}H NMR (CD_3CN, 295 K): δ = 7.98 (m, [2H], Ar-H), 7.81 (m, [2H], Ar-H), 1.89 (m, [12H], Me). $^{19}F\{^1H\}$ NMR (298 K, CD_3CN): δ = −78.7 (s, OTf). $^{31}P\{^1H\}$ NMR (298 K, CD_3CN): 14.5 (s, $^1J_{117SnP}$ = 1796 Hz, $^1J_{119SnP}$ = 1878 Hz). ^{119}Sn NMR (298 K, CD_3CN): −689.7 (t, $^1J_{119SnP}$ = 1882 Hz).

5.4.1.2 **[Sn(OTf)$_2${o-$C_6H_4(AsMe_2)_2$}]**

$Sn(OTf)_2$ (125 mg, 0.3 mmol) was suspended in CH_2Cl_2 (10 mL) before addition of *o*-$C_6H_4(AsMe_2)_2$ (86 mg, 0.3 mmol), upon which the majority of solid dissolved into solution before stirring for 2 h. The remaining particulates were removed by filtration before the addition of *n*-hexane (10 mL) caused precipitation of a white solid, which was collected by filtration and dried *in vacuo*. Yield: 181 mg, 61 %. Required for $C_{12}H_{16}As_2F_6O_6S_2Sn{\cdot}CH_2Cl_2$: C, 19.8; H, 2.3. Found: C, 20.0; H, 2.5%. ^{1}H NMR (CD_3CN, 298 K): δ = 7.89 (m, [2H], Ar-H), 7.73 (m, [2H], Ar-H), 1.83 (s, [12H], Me). $^{19}F\{^1H\}$ NMR (298 K, CD_3CN): δ = −79.1 (s, OTf). ^{119}Sn NMR (298 K, CD_3CN): not observed; (258 K, CD_3CN): −886.5 (br s).

5.4.1.3 **[Sn(OTf)$_2${MeC(CH_2PPh_2)$_3$)]**

$Sn(OTf)_2$ (83 mg, 0.2 mmol) was partially dissolved in CH_2Cl_2 (10 mL) before addition of $MeC(CH_2PPh_2)_3$ (125 mg, 0.2 mmol), upon which the majority of solid was taken up into solution. The solution was stirred for 2 h. The remaining particulates were removed by filtration, and the

solution was concentrated by 50 % before the addition of *n*-hexane (10 mL) caused precipitation of a white solid which was collected by filtration and dried *in vacuo*. Yield: 177 mg, 61 %. Required for $C_{43}H_{39}F_6O_6P_3S_2Sn{\cdot}0.5CH_2Cl_2$ (1083.99): C, 48.2; H, 3.7. Found: C, 47.9; H, 4.3 %. ^{1}H NMR (CD_3CN, 298 K): δ = 7.41 (m, [18H], Ar-H), 7.24 (m, [12H], Ar-H), 3.12 (br d, $^2J_{PH}$ = 12 Hz, [6H], CH_2), 2.01 (br s, [3H], Me). ^{19}F{^{1}H} NMR (298 K, CD_3CN): δ = −79.2 (s, OTf). ^{31}P{^{1}H} (298 K, CD_3CN): δ = −9.4 (s, $^1J_{117SnP}$ = 1189 Hz, $^1J_{119SnP}$ = 1248 Hz). ^{119}Sn NMR (298 K, CD_3CN): δ = −834.0 (q, $^1J_{119SnP}$ = 1242 Hz).

5.4.1.4 **[Sn{MeC(CH$_2$PPh$_2$)$_3$)][BAr^F]$_2$**

[Sn(OTf)$_2${MeC(CH$_2$PPh$_2$)$_3$}] (25 mg, 0.023 mmol) was suspended in CH_2Cl_2 (3 mL) before addition of Na[BAr^F] (40 mg, 0.046 mmol) in CH_2Cl_2 (5 mL) and stirred for 30 min. Over this time, the solution remained slightly cloudy but the appearance of the solid changed texture and colour over time, suggesting successful reaction. Precipitated NaOTf and any other particulates were removed by filtration before the solution was concentrated by 50 % *in vacuo.* Addition of *n*-hexane caused precipitation of white solid, which was collected by filtration and dried *in vacuo*. Yield: 41 mg, 73 %. Required for $C_{105}H_{63}B_2F_{48}P_3Sn$ (2469.80): C, 51.1; H, 2.6. Found: C, 51.2; H, 2.5 %. ^{1}H NMR (CD_3CN, 298 K): δ = 7.70 (br m, [16H], Ar-H), 7.67 (br m, [8H], Ar-H), 7.39 (br m, [18H] Ar-H) 7.25 (br m, [12H] Ar-H), 3.11 (br d, $^2J_{PH}$ = 12 Hz, [6H], CH_2), 1.99 (br s, [3H], Me). ^{19}F{^{1}H} NMR (298 K, CD_3CN): δ = −63.4 (s, BAr^F). ^{31}P{^{1}H} (298 K, CD_3CN): −8.9 (s, $^1J_{SnP}$ = 1246 Hz); (258 K, CD_3CN): −6.0 (s, $^1J_{119SnP}$ = 1252 Hz, $^1J_{117SnP}$ = 1197 Hz), ^{119}Sn NMR (298 K, CD_3CN): −824.3 (q,$^1J_{SnP}$ = 1260 Hz); (258 K, CD_3CN): −843.7 (q, $^1J_{SnP}$ = 1251 Hz).

5.4.1.5 **[Sn(OTf){PhP(CH$_2$CH$_2$PPh$_2$)$_2$}][OTf]**

Sn(OTf)$_2$ (83 mg, 0.2 mmol) was partially dissolved in CH_2Cl_2 (10 mL) before addition of PhP(CH$_2$CH$_2$PPh$_2$)$_2$ (107 mg, 0.2 mmol); the mixture was stirred for 2 h. Particulates were removed by filtration, and the solution was concentrated by 50 % *in vacuo* before addition of *n*-hexane (10 mL) caused precipitation of a white solid. This was collected by filtration and dried *in vacuo*. Yield: 141 mg, 71 %. Required for $C_{36}H_{33}F_6O_6P_3S_2Sn{\cdot}0.5CH_2Cl_2$ (993.86): C, 44.1; H, 3.5. Found: C, 44.6; H, 2.9 %. ^{1}H NMR (CD_3CN, 298 K): δ = 7.82 (m, [4H], Ar-H), 7.71 (m, [2H], Ar-H), 7.56 (m, [9H], Ar-H), 7.37 (m, [6H], Ar-H), 7.17 (m, [4H], Ar-H), 3.37 (br m, [2H], CH_2), 3.10 (br m, [2H], CH_2), 2.93 (br m, [2H], CH_2) 2.70 (br m, [2H], CH_2). ^{19}F{^{1}H} NMR (298 K, CD_3CN): δ = −79.3 (s, OTf). ^{31}P{^{1}H} (298 K, CD_3CN): 36.4 (t, $^3J_{PP}$ = 21 Hz, [P], $^1J_{117SnP}$ = 1266 Hz, $^1J_{119SnP}$ = 1319 Hz), 18.5 (d, $^3J_{PP}$ = 21 Hz, [2P], $^1J_{117SnP}$ = 1460 Hz, $^1J_{119SnP}$ = 1549). ^{119}Sn NMR (298 K, CD_3CN): −834.0 (dt, $^1J_{SnP}$ = 1544 Hz, $^1J_{SnP}$ = 1386 Hz).

5.4.1.6 **[Sn(OTf)$_2${MeC(CH$_2$AsMe$_2$)$_3$}]**

Sn(OTf)$_2$ (83 mg, 0.2 mmol) was partially dissolved in CH_2Cl_2 (10 mL) before addition of MeC(CH$_2$AsMe$_2$)$_3$ (77 mg, 0.2 mmol), and the mixture then stirred for 2 h. The solution was filtered to remove any remaining solid, concentrated by 50% before addition of *n*-hexane (10 mL) caused precipitation of a white solid which was collected by filtration and dried *in vacuo*. Yield: 77 mg, 42 %. Required for $C_{13}H_{27}As_3F_6O_6S_2Sn{\cdot}CH_2Cl_2$ (885.88): C, 19.0; H, 3.3. Found: C, 18.8; H, 3.5%. ^{1}H NMR (CD_3CN, 298 K): δ = 2.15 (s, [6H], CH_2), 1.58 (s, [18H], Me), 1.24 (s, [3H], Me). ^{19}F{^{1}H} NMR (298 K, CD_3CN): δ = −79.2 (s, OTf). ^{119}Sn NMR (298K, CD_3CN): not observed; (CD_3CN, 258 K): −920 (br).

5.4.1.7 **[Sn(OTf){P(CH$_2$CH$_2$PPh$_2$)$_3$}][OTf]**

Sn(OTf)$_2$ (83 mg, 0.2 mmol) was partially dissolved in CH_2Cl_2 (10 mL) before addition of P(CH$_2$CH$_2$PPh$_2$)$_3$ (134 mg, 0.2 mmol) and the mixture stirred for 2 h. Any residual solid was removed by filtration, the solution was concentrated by 50 % before addition of *n*-hexane (10mL) caused precipitation of a white solid which was collected by filtration and dried *in vacuo*. Yield: 112 mg, 50 %. Required for $C_{44}H_{42}F_6O_6P_4S_2Sn{\cdot}0.5CH_2Cl_2$ (1121.99): C, 47.3; H, 3.8. Found: C, 47.4; H, 3.3 %. ^{1}H NMR (CD_3CN, 298 K): δ = 7.41 (m, [18H], Ar-H), 7.31 (m, [12H], Ar-H), 2.88 (br m, [6H], CH_2), 2.67 (br m, [6H], CH_2). ^{19}F{^{1}H} NMR (298 K, CD_3CN): δ = −79.2 (s, OTf). ^{31}P{^{1}H} (298 K, CD_3CN): 37.8 (br q $^3J_{PP}$ = 39 Hz, [P], $^1J_{PSn}$ = 1426 Hz), 5.5 (br d, $^3J_{PP}$ = 39 Hz, [3P], $^1J_{PSn}$ = 711 Hz); (258 K, CD_3CN): 36.3 (br s, [P], $^1J_{SnP}$ = 1440 Hz), 3.8 (br s, [3P], $^1J_{SnP}$ = 685 Hz); (298 K, CD_2Cl_2): 35.7 (q, $^3J_{PP}$ = 35 Hz, [1P], $^1J_{SnP}$ = 1103 Hz), 7.34 (d, $^3J_{PP}$ = 35 Hz, [3P], $^1J_{PSn}$ = 864 Hz); (208 K, CD_2Cl_2): 33.9 (br s, [P], $^1J_{SnP}$ = 1123 Hz), 4.59 (br s, [3P], $^1J_{PSn}$ = 894 Hz). ^{119}Sn NMR (298 K, CD_3CN): −778.6 (dq, $^1J_{119SnP}$ = 1485 Hz, $^1J_{119SnP}$ = 720 Hz); (258 K, CD_2CN): −796 (dq, $^1J_{119SnP}$ = 732 Hz, $^1J_{119SnP}$ = 1477 Hz).

5.4.1.8 **[Sn(OTf)$_2${o-C$_6$H$_4$(PPh$_2$)$_2$}]**

Sn(OTf)$_2$ (104 mg, 0.25 mmol) was partially dissolved in CH_2Cl_2 (10mL) before addition of *o*-C$_6$H$_4$(PPh$_2$)$_2$ (112 mg, 0.25 mmol) and then stirred for 2 h. The solution was concentrated by 50% before addition of *n*-hexane (10 mL) caused precipitation of a white solid which was collected by filtration and dried *in vacuo*. Yield: 151 mg, 70 %. Required for $C_{32}H_{24}F_6O_6P_2S_2Sn$ (863.31): C, 44.5; H, 2.8. Found: C, 44.2; H, 2.8 %. ^{1}H NMR (CD_3CN, 298 K): δ = 7.78 (br s, [2H], Ar-H), 7.56 (br m, [6H], Ar-H), 7.46 (br s, [16H], Ar-H). ^{19}F{^{1}H} NMR (298 K, CD_3CN): δ = −79.2 (s, OTf). ^{31}P{^{1}H} (298 K, CD_3CN): 19.8 (br s); (CD_3CN, 258 K): 22.7 (s, $^1J_{SnP}$ = 1506 Hz). ^{119}Sn NMR (298 K, CD_3CN): −809 (br s); (CD_3CN, 258 K): −1150 (br t, $^1J_{119SnP}$ = 1550 Hz).

5.4.1.9 **[Pb(OTf)$_2${o-C$_6$H$_4$(PMe$_2$)$_2$}]**

Pb(OTf)$_2$ (151 mg, 0.3 mmol) was partially dissolved in CH_2Cl_2 (10mL) before addition of *o*-$C_6H_4(PMe_2)_2$ (60 mg, 0.3 mmol), and the solution stirred for 2 h, during which the majority of solid dissolved. The solution was filtered before the addition of Et_2O (10 mL) caused precipitation of a white solid which was collected by filtration and dried *in vacuo*. Yield: 128 mg, 69 %. Required for $C_{12}H_{16}F_6O_6P_2PbS_2 \cdot 0.5Et_2O$ (740.58): C, 22.7; H, 2.9. Found: C, 22.6; H, 3.3 %. ^{1}H NMR (CD_3CN, 298 K): δ = 7.92 (m, [2H], Ar-H), 7.75 (m, [2H], Ar-H), 2.00 (br m, [12H], Me). ^{19}F{^{1}H} NMR (298 K, CD_3CN): δ = −79.2 (s, OTf). ^{31}P{^{1}H} (298 K, CD_3CN): δ = 74.9 (s, $^1J_{PbP}$ = 1777 Hz).

5.4.1.10 **[Pb(OTf)$_2${o-C$_6$H$_4$(AsMe$_2$)$_2$}]**

Pb(OTf)$_2$ (126 mg, 0.25 mmol) was suspended in benzene (10mL) and *o*-$C_6H_4(AsMe_2)_2$ (72 mg, 0.25 mmol) and stirring for 2 h. Remaining particulates were removed by filtration before the addition of Et_2O (10 mL) caused precipitation of a white solid which was filtered off and dried *in vacuo*. Yield: 101 mg, 58 %. Required for $C_{12}H_{16}As_2F_6O_6PbS_2$ (791.41): C, 18.2; H, 2.0. Found: C, 18.4; H, 2.4 %. ^{1}H NMR (CD_3CN, 298 K): δ = 7.85 (m, [2H], Ar-H), 7.60 (m, [2H], Ar-H), 1.78 (s, [12H], Me). ^{19}F{^{1}H} NMR (298 K, CD_3CN): δ = −79.1 (s, OTf).

5.4.1.11 **[Pb(OTf)$_2${MeC(CH$_2$PPh$_2$)$_3$}]**

Pb(OTf)$_2$ (101 mg, 0.2 mmol) was dissolved in CH_3CN (10 mL) before the addition of $MeC(CH_2PPh_2)_3$ (125 mg, 0.2 mmol) and the reaction mixture was stirred for 2 h. Remaining particulates were removed by filtration, the solution was concentrated by 50 % causing the precipitation of a white solid which was collected by filtration and dried *in vacuo*. Yield: 115 mg, 55 %. Required for $C_{43}H_{39}F_6O_6P_3PbS_2$ (1130.01): C, 45.7; H, 3.5. Found: C, 45.6; H, 3.8 %. ^{1}H NMR (CD_3CN, 298 K): δ = 7.36 (br m, [18H Ar-H]), 7.27 (m, [12H], Ar-H), 3.04 (br s, [6H], CH_2), 1.65 (br s, [3H], Me). ^{19}F{^{1}H} NMR (298 K, CD_3CN): δ = −79.2 (s, OTf). ^{31}P{^{1}H} (298 K, CD_3CN): δ = 11.6 (s),$^1J_{PbP}$ = 1150 Hz).

5.4.1.12 **[Pb{MeC(CH$_2$PPh$_2$)$_3$}][BAr^F]$_2$**

[Pb(OTf)$_2${MeC(CH$_2$PPh$_2$)$_3$}] (45 mg, 0.04 mmol) was suspended in CH_2Cl_2 (5 mL) before addition of Na[BAr^F] (71 mg, 0.08 mmol) in CH_2Cl_2 (5 mL) stirred for 30 min. Over this time, the solution remained slightly cloudy but any remaining solid had changed texture and colour, suggesting successful reaction. Solids were removed by filtration before the solution was concentrated by 50 %. Addition of *n*-hexane (10 mL) caused precipitation of a white solid which was collected by filtration and dried *in vacuo*. Yield: 50 mg, 49 %. Required for $C_{105}H_{63}B_2F_{48}P_3Pb$ (2558.29): C, 49.3; H, 2.5. Found: C, 49.3; H, 2.0%. ^{1}H NMR (CD_3CN, 298 K): δ = 7.62 (br m, [16H], Ar-H), 7.58 (br s,

[8H], Ar-H), 7.30 (br m, [6H], Ar-H) 7.21 (br m, [24H], Ar-H), 3.05 (br s, [6H], CH_2), 1.66 (br s, [3H], Me). $^{19}F\{^1H\}$ NMR (298 K, CD_3CN): δ = −63.4 (s, BAr^F). $^{31}P\{^1H\}$ (298 K, CD_3CN): 15.5 (br s); (298 K, CD_3NO_2): 15.8 (s), $^1J_{PbP}$ = 1777 Hz).

5.4.1.13 **[Pb(OTf){P(CH$_2$CH$_2$PPh$_2$)$_3$}][OTf]**

$Pb(OTf)_2$ (101 mg, 0.2 mmol) was added to MeCN (10 mL) followed by $P(CH_2CH_2PPh_2)_3$ (134 mg, 0.2 mmol), upon which the majority of solid dissolved; the mixture was stirred for 2 h. Remaining particulates were removed by filtration, and the solution was concentrated to 50 % volume before the addition of *n*-hexane (10 mL), which caused precipitation of a white solid. This was collected by filtration and dried *in vacuo*. Yield: 89 mg, 48 %. Crystals were grown from CH_2Cl_2 solution. Required for $C_{44}H_{39}F_6O_6P_4PbS_2{\cdot}0.3CH_2Cl_2$ (1172.99): C, 44.9; H, 3.6. Found: C, 44.4; H, 4.0 %. ^1H NMR (CD_3CN, 298 K): δ = 7.37 (m, [18H] Ar-H), 7.31 (m, [12H], Ar-H), 2.86 (br m, [6H], CH_2), 2.64 (br m, [6H], CH_2). $^{19}F\{^1H\}$ NMR (298 K, CD_3CN): δ = −79.2 (s, OTf). $^{31}P\{^1H\}$ (298 K, CD_3CN): δ = 77.5 (q, $^1J_{PbP}$ = 437 Hz, $^3J_{PP}$ = 44 Hz, [P]), 26.1 (d,$^1J_{PbP}$ = 1870, $^3J_{PP}$ = 44 Hz, [3P]).

5.4.1.14 **[Pb(OTf)$_2${MeC(CH$_2$AsMe$_2$)$_3$}]**

$Pb(OTf)_2$ (101 mg, 0.2 mmol) was partially dissolved in CH_3CN (10 mL) before addition of *MeC(CH$_2$AsMe$_2$)$_3$* (125 mg, 0.2 mmol), and the mixture then stirred for 2 h. The solution was concentrated by 50 % before addition of Et_2O (10 mL) caused precipitation of a white solid over 10 mins. of stirring and was then collected by filtration and dried *in vacuo*. Yield: 41 mg, 23 %. Required for $C_{13}H_{27}As_3F_6O_6PbS_2$ (889.43): C, 17.6; H, 3.1. Found: C, 17.1; H, 3.1 %. ^1H NMR (CD_3CN, 298 K): δ = 2.21 (s, [6H], CH_2), 1.61 (s, [18H], Me), 1.16 (s, [3H], Me). $^{19}F\{^1H\}$ NMR (298 K, CD_3CN): δ = −79.3 (s, OTf).

5.4.1.15 **[Ge{MeC(CH$_2$PPh$_2$)$_3$}][BAr^F]$_2$**

$[Ge\{MeC(CH_2PPh_2)_3\}][OTf]_2$ (0.050 g, 0.05 mmol) was suspended in CH_2Cl_2 (1 mL), $Na[BAr^F]$ (0.089 g, 0.10 mmol) added, the solution is stirred for ~ 10 minutes forming a colourless solution with a small amount of precipitate (NaOTf). The supernatant was filtered away from the solid and layered with n-hexane (2 mL), after a 24 h, colourless crystals formed which were isolated by filtration and dried in *vacuo*. The crystals were suitable for single crystal X-ray diffraction. Yield: 0.068 mg, 50 %. Required for Required for $C_{105}H_{63}B_2F_{48}P_3Ge$ (2423.59): C, 52.0; H, 2.6. Found: C, 52.3; H, 2.8 %. ^1H NMR (298 K, CD_2Cl_2): δ = 7.73 (m, [16H], Ar-H), 7.56 (s, [8H], Ar) 7.41 (m, [6H], Ar-H), 7.22 (m, [24H], Ar-H), 3.05 (m, [6H], CH_2), 2.15 (q, [3H], $^3J_{PH}$ = 4.0 Hz, Me). $^{19}F\{^1H\}$ NMR (298 K, CD_2Cl_2): δ = –62.8 (s, BAr^F). $^{31}P\{^1H\}$ NMR (298 K, CD_2Cl_2): δ = −4.34 (s).

5.4.2 Reagent Synthesis

5.4.2.1 $Pb(OTf)_2$

Following the procedure by Peerson and co-workers.[40] $Pb(CO_3)_2$ (1000 mg, 3.74 mmol) was reacted with neat triflic acid (134.9 mg, 8.98 mmol) and allowed to reflux for 2 hrs before drying *in vacuo* until a grey solid remained which was stored under inert conditions. Storage of this material in the triflic acid mother liquor produced crystals of $Pb(OTf)_2$ confirming its presence.

5.4.2.2 Sodium Tetrakis-3,5-bis(trifluoromethyl)phenyl borate

Following the procedure by Volpe and co-workers.[48] An excess of Mg turnings (5.1 g, 2.1 mol) was dried and activated overnight before suspension in Et_2O (350 mL). A solution of 3,5-bis(trifluoromethyl)bromobenzene (50 g, 170 mmol) was diluted in Et_2O (100 mL) and a portion of this solution (20 mL) was slowly added to the reaction mixture to initiate the Grignard. The remainder was carefully added over 2 h before heating to reflux for 2 h. The yellow solution was cooled to room temperature over 1 h, before the addition of $NaBF_4$ (3.4 g, 31 mmol). The reaction mixture was then heated to reflux for 48 h. The reaction was carefully quenched with 10% w/w $NaCO_3$ solution (20 mL) before further addition of 10% w/w $NaCO_3$, totalling 1 L. The aqueous layer was washed in Et_2O (4x150 mL) before drying over $MgSO_4$. The solvent was removed to afford a white solid, which was then redissolved in THF and crystallised by layering with n-hexane. Recrystallizations were repeated 3 times to result in an off-white powder. Residual THF was removed by heating to 75 °C under vacuum for 10-12 h. ^{1}H NMR (295 K, CD_2Cl_2): δ = 7.59 (d, [12H], $^3J_{HH}$ = 7.7 Hz, CH). $^{13}C\{^1H\}$ NMR (295 K, CD_2Cl_2): δ = 163.25 (q), 136.2 (s), 130.86 (q), 127.5 (s), 124.8 (s), 118.9 (s). $^{19}F\{^1H\}$ NMR (295 K, CD_2Cl_2): δ = -64.41 (s).

5.4.3 DFT Calculations

The electronic structures of the set of dications, $[M\{MeC(CH_2PPh_2)_3\}]^{2+}$ (M = Ge, Sn, Pb), were investigated using DFT calculations using the Gaussian 16W software package by Dr Rhys King.[18] The density functional used was B3LYP-D3,[19] with the basis set 6-3116G(d) for H, C, P and Ge atoms[20] and the lanl2dz basis set for the Sn and Pb atoms.[21] For M = Ge and Sn the initial geometries were taken from their crystal structures, while for M = Pb the initial geometry chosen was from the optimised structure of M = Sn with the tin atom replaced for lead. Calculations for all structures converged with no imaginary frequencies. The calculated structures were found to be in good agreement with the crystallographically-derived metrics (see Table S2).

5.5 – References

1 P. A. W. Dean, D. D. Phillips and L. Polensek, *Can. J. Chem.*, 1981, **59**, 50–61.
2 P. A. W. Dean, *Can. J. Chem.*, 1983, **61**, 1795–1799.
3 M. F. Davis, W. Levason, G. Reid and M. Webster, *Dalton Trans.*, 2008, 2261–2269.
4 S. M. Godfrey, I. Mushtaq and R. G. Pritchard, *J. Chem. Soc. Dalton. Trans.*, 1999, 1319–1324.
5 R. P. King, W. Levason and G. Reid, *Dalton Trans.*, 2021, **50**, 17751–17765.
6 J. Burt, W. Levason and G. Reid, *Coord. Chem. Rev.*, 2014, **260**, 65–115.
7 M. F. Davis, W. Levason, G. Reid, M. Webster and W. Zhang, *Dalton Trans.*, 2008, **4**, 533–538.
8 F. Cheng, A. L. Hector, W. Levason, G. Reid, M. Webster and W. Zhang, *Inorg. Chem.*, 2010, **49**, 752–760.
9 R. P. King, M. S. Woodward, J. Grigg, G. McRobbie, W. Levason and G. Reid, *Dalton Trans.*, 2021, **50**, 14400–14410.
10 V. K. Greenacre, R. P. King, W. Levason and G. Reid, *Dalton Trans.*, 2019, **48**, 17097–17105.
11 E. MacDonald, L. Doyle, S. S. Chitnis, U. Werner-Zwanziger, N. Burford and A. Decken, *Chem. Commun.*, 2012, **48**, 7922.
12 N. S. Biradar, V. H. Kulkarni and N. N. Sirmokadam, *J. Inorg. Nucl. Chem.*, 1972, **34**, 3651–3657.
13 N. S. Biradar and N. N. Sirmokadam, *J. Inorg. Nucl. Chem.*, 1973, **35**, 3639–3641.
14 A. V. Piskunov, O. Y. Trofimova, G. K. Fukin, S. Y. Ketkov, I. V. Smolyaninov and V. K. Cherkasov, *Dalton Trans.*, 2012, **41**, 10970–10979.
15 S. Nagendran and H. W. Roesky, *Organometallics*, 2008, **27**, 457–492.
16 F. Cheng, J. M. Dyke, F. Ferrante, A. L. Hector, W. Levason, G. Reid, M. Webster and W. Zhang, *Dalton Trans.*, 2010, **39**, 847–856.
17 P. A. Rupar, V. N. Staroverov, P. J. Ragogna and K. M. Baines, *J. Am. Chem. Soc.*, 2007, **129**, 15138–15139.
18 F. Cheng, A. L. Hector, W. Levason, G. Reid, M. Webster and W. Zhang, *Angew. Chemie Int. Ed.*, 2009, **48**, 5152–5154.
19 P. A. Rupar, R. Bandyopadhyay, B. F. T. Cooper, M. R. Stinchcombe, P. J. Ragogna, C. L. B. Macdonald and K. M. Baines, *Angew. Chemie Int. Ed.*, 2009, **48**, 5155–5158.
20 P. A. Rupar, V. N. Staroverov and K. M. Baines, *Science (80-.).*, 2008, **322**, 1360–1363.
21 M. S. Woodward, R. P. King, R. D. Bannister, J. Grigg, G. McRobbie, W. Levason and G. Reid, *Inorganics*, 2022, **10**, 107.
22 R. P. King, J. M. Herniman, W. Levason and G. Reid, *Inorg. Chem.*, 2023, **62**, 853–862.
23 J. C. Avery, M. A. Hanson, R. H. Herber, K. J. Bladek, P. A. Rupar, I. Nowik, Y. Huang and K. M. Baines, *Inorg. Chem.*, 2012, **51**, 7306–7316.
24 F. Cheng, A. L. Hector, W. Levason, G. Reid, M. Webster and W. Zhang, *Chem. Commun.*, 2008, 5508–5510.
25 P. A. Gray, University of Victoria, 2018.
26 R. P. King, V. K. Greenacre, W. Levason, J. M. Dyke and G. Reid, *Inorg. Chem.*, 2021, **60**, 12100–12108.
27 P. Farina, T. Latter, W. Levason and G. Reid, *Dalton Trans.*, 2013, **42**, 4714–4724.
28 C. Gurnani, A. L. Hector, E. Jager, W. Levason, D. Pugh and G. Reid, *Dalton Trans.*, 2013, **42**, 8364–8374.
29 S. J. Archer, K. R. Koch and S. Schmidt, *Inorg. Chim. Acta*, 1987, **126**, 209–218.
30 P. A. Gray, K. D. Krause, N. Burford and B. O. Patrick, *Dalton Trans.*, 2017, **46**, 8363–8366.
31 L. Engelhardt, J. Patrick, C. Whitaker and A. White, *Aust. J. Chem.*, 1987, **40**, 2107.
32 A. L. Balch and D. E. Oram, *Organometallics*, 1986, **5**, 2159–2161.
33 A. L. Balch and D. E. Oram, *Inorg. Chem.*, 1987, **26**, 1906–1912.
34 A. M. Arif, A. H. Cowley, R. A. Jones and J. M. Power, *J. Chem. Soc. Chem. Commun.*, 1986, 1446–1447.

35 A. H. Cowley, D. M. Giolando, R. A. Jones, C. M. Nunn and J. M. Power, *Polyhedron*, 1988, **7**, 1909–1910.

36 A. L. Balch and D. E. Oram, *Phosphorous Sulfur Relat. Elem.*, 1987, **30**, 101–104.

37 A. J. Rossini, A. W. Macgregor, A. S. Smith, G. Schatte, R. W. Schurko and G. G. Briand, *Dalton Trans.*, 2013, **42**, 9533–9546.

38 R. D. Rogers and A. H. Bond, *Inorg. Chim. Acta*, 1992, **192**, 163–171.

39 J. Burt, W. Grantham, W. Levason and G. Reid, *Dalton Trans.*, 2015, **44**, 11533–11541.

40 K. Lyczko, W. Starosta and I. Persson, *Inorg. Chem.*, 2007, **46**, 4402–4410.

41 D. H. Johnston and D. F. Shriver, *Inorg. Chem.*, 1993, **32**, 1045–1047.

42 M. Mantina, A. C. Chamberlin, R. Valero, C. J. Cramer and D. G. Truhlar, *J. Phys. Chem. A*, 2009, **113**, 5806–5812.

43 B. Cordero, V. Gómez, A. E. Platero-Prats, M. Revés, J. Echeverría, E. Cremades, F. Barragán and S. Alvarez, *Dalton Trans.*, 2008, 2832–2838.

44 P. A. W. Dean, *Can. J. Chem.*, 1982, **60**, 2921–2926.

45 S. H. Strauss, *Chem. Rev.*, 1993, **93**, 927–942.

46 E. P. Kyba, S. T. Liu and R. L. Harris, *Organometallics*, 1983, **2**, 1877–1879.

47 R. D. Feltham, A. Kasenally and R. S. S. Nyholm, *J. Organomet. Chem.*, 1967, **7**, 285–288.

48 M. Brookhart, B. Grant, A. F. Volpe, M. Brookhard, B. Grant and A. F. Volpe Jr, *Organometallics*, 1992, **11**, 3920–3922.

Chapter 6 – Synthesis, spectroscopic and structural properties of phosphine oxide complexes of Sn(II) and Pb(II) with weakly coordinating triflate anions

This chapter continues to explore the coordination to the divalent Group 14 metal triflates, moving to harder oxygen donor ligands. Reactions of $M(OTf)_2$ (M = Sn, Pb) with the phosphine oxide ligands OPR_3 (R = Me, Ph) and $dppmO_2$ are demonstrated as well as examples of $OAsPh_3$ and pyNO ligands.

6.1 – Introduction

The earlier chapters of this thesis explored the coordination of a variety of ligands with both *N*- and *O*-donor ligands to the Group 13 metal triflates (M = Al, Ga, In) in an attempt to explore the effect of the weakly coordinating trifluoromethanesulfonate anion on their speciation, structures, geometries and properties. This showed the coordination of different OPR_3 ligands to $M(OTf)_3$ (M = Al, Ga, In), producing octahedral complexes with coordinated OPR_3 in each case.[1] This included a series of indium complexes with coordination of three to six $OPMe_3$ ligands or three $dppmO_2$ ligands, as well as other monodentate *O*-donor ligands. Complexes of the metal triflates have been observed to contain triflate both in the coordinated form and as a free anion. As expected, and as observed from the work in Chapters 2 and 3, this anion is easily displaced by other neutral ligands such as OH_2 or donor solvents like acetonitrile, to produce the corresponding cation.[2] In cases where water was present, the triflate anion would often form hydrogen bonds to the coordinated water, allowing for extended structures such as dimers and tetrameric pseudo-macrocycles, as seen in the complex $[In(OTf)_2(OPPh_3)_4][In(OH_2)_4(OPPh_3)_2][OTf]_4$. Thus, while triflate was observed as a discrete anion, there was additional stabilisation provided by hydrogen bonding in some cases. Chapter 5 focused on the coordination of the soft pnictine ligands to the divalent Group 14 triflates, producing an array of novel complexes.[3] This chapter will continue to explore metal triflates with harder oxygen donor ligands such as OPR_3 and pyNO.

Coordination of phosphine oxides to the Group 14 metals, Ge and Sn, has been dominated by the chemistry of the +4 oxidation state, with few examples of complexes in the 2+ state.[4] Within the published research of the Group 14 metals, structural studies of the coordination of OPR_3 ligands to the metal halides are limited, but a number of examples of both Ge(IV) and Sn(IV) have been

reported.[5] The reaction of GeX_4 (X = Cl, Br) with 4 molar equivalents of $OPMe_3$ produced colourless powders of *cis*-$[GeX_2(OPMe_3)_4][X]_2$ (X = Cl, Br). This was unusual as commonly, coordination of this type would cause self-ionisation of MX_4 with the halometallate anion being more stable than the free halide anion. Using a 2:1 molar ratio of ligand to metal was found to give the self-ionised product, *fac*-$[GeX_3(OPMe_3)_3]_2[GeX_6]$ (X = Cl, Br). The structures of the *tris* complex, *cis*-$[GeCl_3(OPMe_3)_3]_2[GeCl_6]$ is shown in Figure 6.1(a), was found to have a Ge-O bond distance of 1.891(3) Å, with the other Ge-O_{OPMe3} bonds being generated by rotational symmetry in the P-3 space group. Both the chloride and iodide complexes were found to adopt a *cis* geometry, whereas the bromide complex was found in the *trans* arrangement. The *tetrakis* complex, $[GeCl_2(OPMe_3)_4][Cl]_2$ shown in Figure 6.1(b), was found to have distances of 1.886(4) Å and 1.857(4) Å with the latter of these being *trans* to the chloride anions, a slight shortening in this bond distance with the additional equivalent of ligand. Both *cis*-$[GeCl_3(OPMe_3)_3]_2[GeCl_6]$ and $[GeCl_2(OPMe_3)_4][Cl]_2$ take up an octahedral geometry with the crystal structures of both chloro-complexes shown in Figure 6.1.

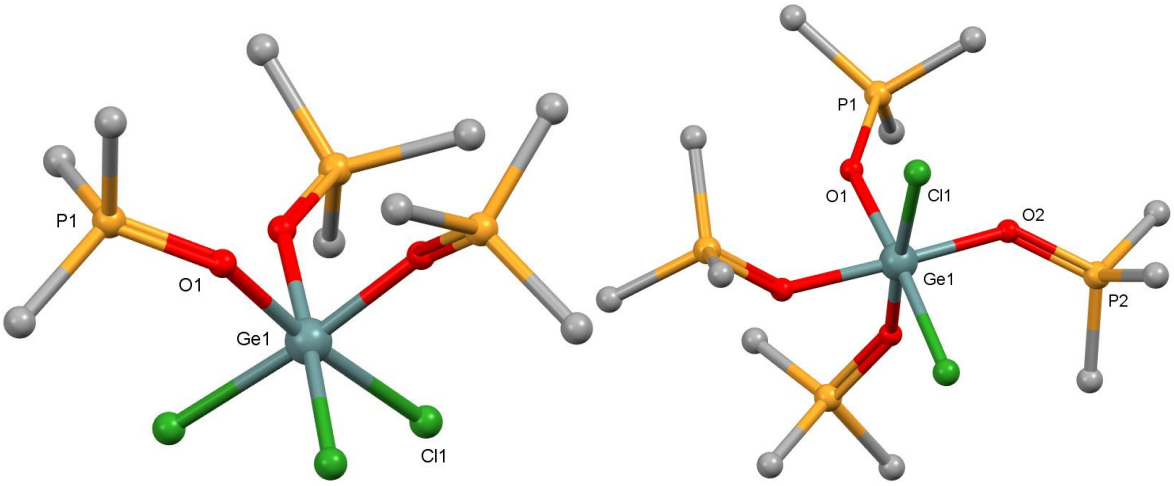

Figure 6.1 - Crystal structures of the cations in (a) $[GeCl_3(OPMe_3)_3]_2[GeCl_6]$ and (b) $[GeCl_2(OPMe_3)_4][Cl]_2$ showing the atom numbering scheme. Redrawn from Ref[5] with anions and H-atoms omitted for clarity.

Reaction of the Sn(IV) halides with two equivalents of $OPPh_3$ produced the octahedral complexes $[SnX_4(OPPh_3)_2]$ (X = Cl, Br, I).[6–8] As well as these halide complexes, some metal fluorides MF_4 (M = Ge, Sn) were coordinated with both mono- and bidentate phosphine oxide ligands. Two equivalents of OER_3 (E = P, As; R = Me, Ph) or a single equivalent of the bidentate ligands, *o*-$C_6H_4(P(O)Ph_2)_2$ or $Ph_2P(O)CH_2P(O)Ph_2$ were found to take up an octahedral geometry when coordinated to the fluoride and chloride.[5,9,10] Recently, the solid state structure of *mer*-$[GeF_3(OPPh_3)_3][OTf]$ was obtained through the reaction of $[GeF_4(MeCN)_2]$, $OPPh_3$ in the presence of TMSOTf, with $^{19}F\{^1H\}$ NMR spectroscopy showing both the *mer* and *fac* geometries present.[11]

Examples of metal(II) complexes are less common, with ligands coordinated to MX_2 (M = Ge, Sn, Pb; X = Cl, Br, I) forming 4- and 5-coordinate neutral complexes of the type $[MX_2(L)_2]$ or $[MX_2(L)_3]$.[12] These were often shown to produce weakly associated oligomers through halide bridges, with many forming discrete dimers, but others adopting infinite coordination polymers.[13] As was described in Chapter 5, complexes of Ge and Sn with softer bidentate ligand species such as *o*-$C_6H_4(EMe_2)_2$ (E = P, As) have been reported produce complexes $[MX_2\{o\text{-}C_6H_6(ER_2)\}]$ (M = Sn, Pb; E = P, As; X = Cl, Br, I) as a four-coordinate product. These species often displayed oligomerisation through weakly associated halide bridges between metal centres to form polymeric or dimeric complexes.

A single structural example of monodentate OPR_3 coordination to tin(II) chloride has been reported for reaction of $OPPh_3$ with $SnCl_2$, producing $[SnCl_2(OPPh_3)_2]$ as distorted disphenoidal, shown in Figure 6.2.[14] This geometry has appeared consistently through the literature examples of complexes of SnX_2 (X = Cl, Br) with many of these structures showing additional long contacts to another metal centre through halide bridges.[13,15]

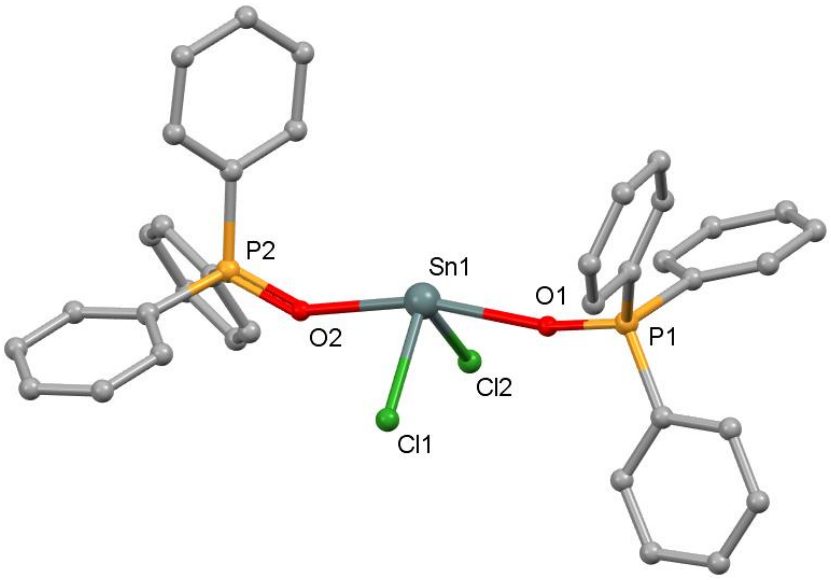

Figure 6.2 - Crystal structure of $[SnCl_2(OPPh_3)_2]$ showing the atom numbering scheme. Redrawn from Ref[14] with H-atoms omitted for clarity.

As seen in Figure 6.2, this discrete four-coordinate complex has the two $OPPh_3$ ligands in the axial positions while the *cis*-chloride ligands being found equatorial. The lone pair of electrons of the Sn(II) is stereochemically active and directional with the orbital in the equatorial plane, categorising this as a hemidirected complex.

In the study of Pb(II) coordination complexes, a precursor used is $Pb(NO_3)_2$ which was used throughout the research of Dr Jennifer Burt and her research into the chemistry of tin(II) and lead(II) complexes.[16] The reports of this work focused on the coordination of phosphine ligands to

MX_2 (M = Sn, Pb; X = $[NO_3]^-$, $[PF_6]^-$, $[BF_4]^-$) with the bidentate ligand dmpe being employed for coordination.[17] When attempting the same reaction with the slight steric increase by substituting methyl for ethyl groups on the phosphine, a few small crystals of $[Pb(NO_3)_2(depeO_2)]$ were isolated, containing the oxidised form of the phosphine ligand. Due to the *in-situ* oxidation of phosphines in the presence of heavy p-block metal halides having been reported previously, it is possible that the Lewis acidic $Pb(NO_3)_2$ precurso catalysed the reaction.[13] The complex $[Pb(NO_3)_2(depeO_2)_2]$, shown in Figure 6.3, contains an 8-coordinate Pb(II) centre with two κ^2-nitrate anions and four bridging $depeO_2$ ligands forming a 2D network.

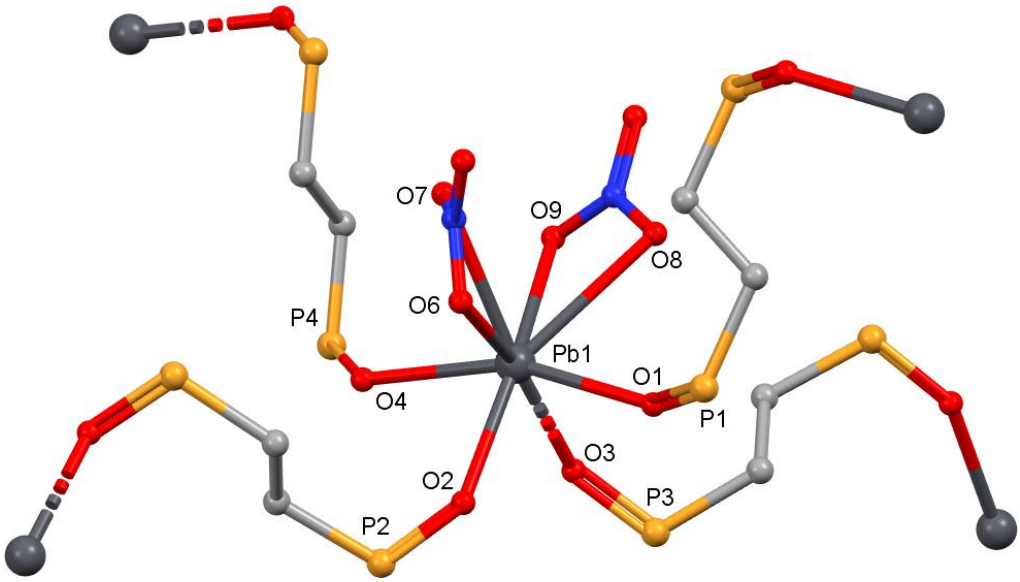

Figure 6.3 - Crystal structure of $[Pb(NO_3)_2(depeO_2)_2]$ showing the atom numbering scheme. Redrawn from Ref[17] with the H-atoms and the ethyl R-groups omitted for clarity.

Previous reports of the coordination of phosphine and phosphine oxide ligands to Sn(II) and Pb(II) were focused on the $[SbF_6]^-$ and $[AsF_6]^-$ anions, primarily exploring these coordination complexes through *in situ* spectroscopic methods.[18,19] These reports was used as a point of reference as to likely ranges for resonances of the triflate complexes could be observed in the multinuclear NMR spectra ($^{31}P\{^1H\}$, ^{119}Sn, ^{207}Pb). This worked employed a range of donor ligands with differing donor atoms, a range denticities and binding modes to probe how these changes affected the metal cation. It was noted that, despite coordination occurring through the oxide, the $^{31}P\{^1H\}$ NMR spectra of these complexes contained well-resolved satellite peaks that aided in confirmation of coordination. Due to the lack of solid-state structural data in these publications, discussion of the possible structures was limited to the splitting and size of the satellite couplings observed in the multinuclear NMR spectra obtained and the surrounding literature.

The halide complexes of Group 14 metals showing coordination of imine[21–23] and pnictine[15] ligands as well as crown ethers[24,25] and cryptands[26,27] have been structurally characterised and reported where possible. Coordination of [18]crown-6 to $SnCl_2$ was found to retain a single

chloride within the primary coordination sphere while the macrocycle of this complex is nearly co-planer in [SnCl{[18]crown-6}][$SnCl_3$], with the structure shown in Figure 6.4.[25] The single chloride is found perpendicular to the plane of the macrocycle with a Sn-Cl bond distance of 2.482(2) Å while the Sn-O bonds ranged from 2.590(6) - 2.8819(7) Å. There is an additional long contact to a chloride of the $[SnCl_3]^-$ anion at 3.655 Å which makes up a weakly associated dimer through halide bridging with a final formulation of [{SnCl([18]crown-6)}$_2$(μ^2-$SnCl_3$)$_2$]. Some of these reactions were also carried out using other tin(II) salts, incorporating the triflate or perchlorate anions. These were introduced either directly, through use of $M(OTf)_2$ starting materials or through salt metathesis using the appropriate acid in the crystallisation step. Addition of perchloric acid to the solution during crystallisation produced crystals with the $[SnCl_3]^-$ anion was substituted by perchlorate, forming [SnCl{[18]crown-6}][ClO_4].

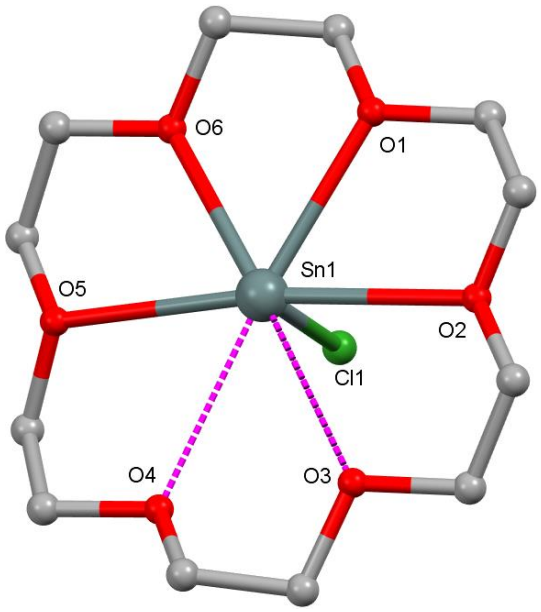

Figure 6.4 - Crystal structure of the cation in [SnCl{[18]crown-6}][$SnCl_3$] showing the atom numbering scheme. Redrawn from Ref[25] with the anion and H-atoms omitted for clarity.

Coordination of the smaller [15]crown-5 macrocycle in a 2:1 ratio with $SnCl_2$ produced a sandwich complex containing a dicationic Sn(II) metal centre with no contacts to the present anions.[28] Attention was also given to the investigation of Sn(II) with differing macrocyclic ligands such as thia- and mixed donor macrocycles.[29] Leading on from the success of the anionic exchange with perchlorate, triflate was also proven to substitute the halometallate anion in solution. As well as exchange, $Sn(OTf)_2$ was used directly as a starting material to produce [Sn(OTf){[18]crown-6}][OTf], as seen in Figure 6.5, where the triflate anions are both located axially. One of these triflates (O11) was bound significantly closer at a distance of 2.282(8) Å, while the other (O21) had an Sn-O distance of 2.596(9), within the sum of the van der Waals radii. The change in anion causes an increase in the Sn-O bond distances, now ranging from 2.464(5) – 3.026(6) Å with both O3 and O4 being found at a distance >3 Å.

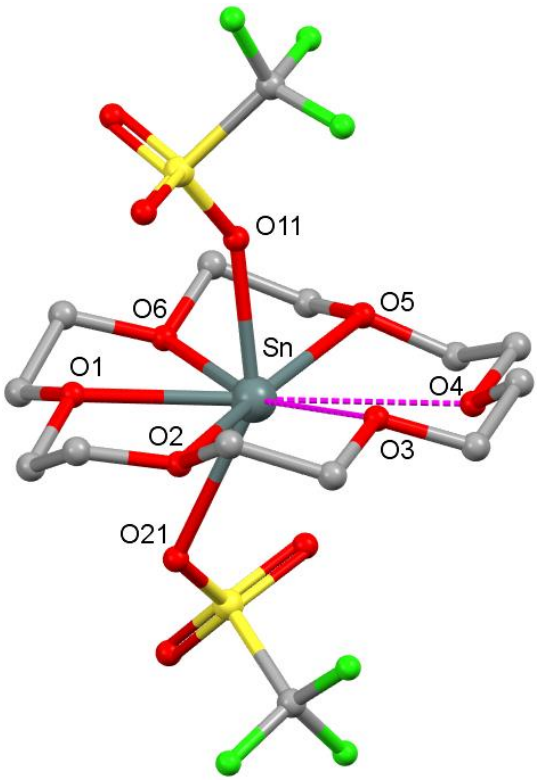

Figure 6.5 - Crystal structure of [Sn(OTf){[18]crown-6}][OTf] redrawn from Ref[24]. H-atoms omitted for clarity.

This work was followed by DFT calculations of the optimised gas phase structures and found that the observed structure of $[Sn(OTf)\{[18]crown\text{-}6\}]^+$ is matched closely to the calculated structure. One significant difference relates to the position of the Sn atom in respect to the plane of the macrocycle. The Sn atom was experimentally determined to be in the plane, although slightly off centre, while the calculated neutral structure showed the Sn atom lying 0.2 Å above the plane of the crown ether, with a corresponding shortened $Sn\text{-}O_{OTf}$ distance (by 0.15 Å).

Due to the structural similarity between $[Sn(OTf)\{[18]crown6\}]^+$ and the isoelectronic $[In(OTf)\{[18]crown\text{-}6\}]^{2+}$, it was thought that the smaller [15]crown-5, when coordinated to $Sn(OTf)_2$ in a 2:1 reactions, may produce a complex analogous to this sandwich. Although this reaction produced very poor crystals, a structure was obtained to adequately confirm the dicationic sandwich complex $[Sn\{[15]crown\text{-}5\}_2][OTf]_2$. The Sn(II) metal was found sandwiched between two macrocyclic ligands with no additional contacts to the triflate anions present; there appears to be no stereochemically-active lone pair of non-bonding electrons. This report also described the coordination of [12]crown-4 to $Sn(OTf)_2$, producing $[Sn\{[12]crown\text{-}4\}_2[OTf]_2$ with a bent sandwich geometry and a single weak-contact to a triflate anion. This bent sandwich structure has been observed before with *bis*-coordination of [12]crown-4 to potassium cations, which cannot have any directional valence electrons. Comparison of these tin complexes with their germanium analogues can highlight the differences between each metal. When coordinating [15]crown-5 to Ge(II), the metal centre was encapsulated in the centre of the macrocycle however

the details of the coordination depended on the anion present. Coordination to $GeCl_2$ caused self-ionisation to form a halometalate anion and a $[GeCl\{[15]crown5\}]^+$ cation with Ge-$O_{macrocycle}$ distances ranging from 2.195(3)-3.237(4), with this large range indicating the presence of a stereochemical lone pair. When two equivalents of TMSOTf were added during the synthesis, TMSCl was lost as a side product with both chloride anions being replaced by triflate with the $[Ge(OTf)\{[15]crown5\}]^+$ cation. The measured Ge-$O_{macrocycle}$ distances of 2.233(5)-2.349(6) Å, showing that the metal was much closer to the centroid of the macrocycle. This vast difference of the Ge-O distances and Ge(II) centrality show how the anion can change the structure of the complex.

Most recently, the Reid group reported the structural diversity that occurs between the divalent $M(OTf)_2$ (M = Ge, Sn, Pb) with varying size of thia-macrocycles.[30] In contrast to the exocyclic coordination complexes of $GeCl_2$ discussed in Chapter 5, the coordination here was shown to be endocyclic with greater ring deformation than observed in the study of crown ethers.

6.2 – Results and Discussion

6.2.1 Coordination to $Sn(OTf)_2$

The previous chapter focused on the coordination of the polydentate soft donor ligands yielding a range of geometries and coordination number (3-7) in complexes of Sn(II) and Pb(II) salts.[3] The complexes formed in that chapter showed a preference for oligomerisation to form dimeric and polymeric complexes through bridging interactions of the triflate anions. Similar behaviour was not observed in Chapter 2 and Chapter 3, which focused on the Group 13 metal triflates. This work was followed by coordination of harder *O*-donors, specifically using phosphine oxide and pyridine *N*-oxide ligands, to further probe the effect of having a weakly coordinated anion in divalent Group 14 metal complexes.

With the help of undergraduate project student, Charlotte Denman, a series of tin(II) complexes with a range of OPR_3 ligands carrying differing donor strength, steric bulk and denticity. The complexes synthesised where then characterised by microanalysis, IR and NMR spectroscopy, with crystal structures being obtained where possible. This began with attempts to vary the $Sn(OTf)_2$: $OPPh_3$ ratios (from 2-4 equivalents of ligand – see Scheme 6.1) to explore the geometry of the complexes formed, expecting that the phosphine oxides would be stronger σ-donor ligand than the soft phosphine and arsine donors in the previous chapter. $Sn(OTf)_2$ only partially dissolves in CH_2Cl_2, however, upon addition of the OPR_3 ligand, the majority of the metal triflate goes into solution over ca. 2 h. Any residual solid was removed by filtration before precipitation from the mother liquor and isolation of the target product. Reaction of $Sn(OTf)_2$ with two equivalents of $OPPh_3$ produced a white solid was then fully characterised by NMR and IR spectroscopy in addition to microanalysis proving consistency throughout the bulk solid.

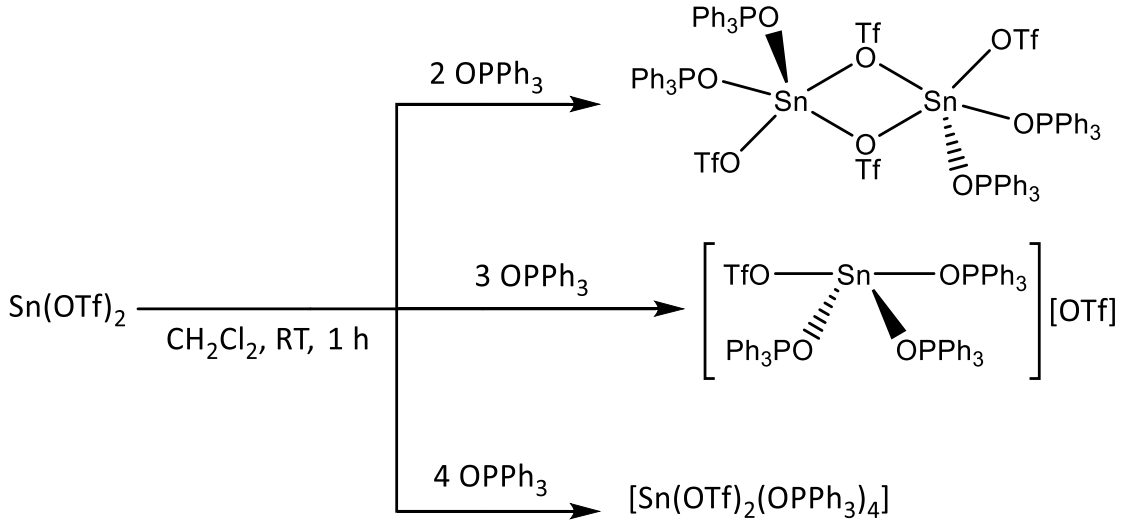

Scheme 6.1. - Reactions of varying ratios of $OPPh_3$ with $Sn(OTf)_2$.

The ^{1}H NMR spectrum of this complex showed minor shifts of the aromatic resonances, but these shifts now overlapped the aromatic protons into two environments with integrals of 3:2. The $^{19}F\{^{1}H\}$ NMR spectrum for this complex $[Sn(OTf)_2(OPPh_3)_2]$ showed a single, very sharp resonance at -79.2 ppm in CD_2Cl_2, within the established range for ionic triflate in CD_2Cl_2, as was observed throughout the work of the previous chapters. Analysis *via* $^{31}P\{^{1}H\}$ NMR spectroscopy, produced a single sharp resonance at 43.9 ppm, showing a significant shift from resonance of the free $OPPh_3$, found at 27.2 ppm in the same solvent (CD_2Cl_2). Work carried out by Dean *et al* synthesised a number of $M(SbF_6)_2$ (M = Sn, Pb) complexes with OPR_3 ligands and reported analysis *via* $^{31}P\{^{1}H\}$ and either ^{119}Sn or ^{207}Pb NMR spectroscopy.[19] He reported both the *bis* and *tris* complexes for each metal (M = Sn, Pb), with $[Sn(SbF_6)_2(OPPh_3)_2]$ producing a $^{31}P\{^{1}H\}$ resonance at 44.8 ppm and a coupling constant of $^{2}J_{119Sn\text{-}P}$ coupling of 229 Hz. The coupling for the $[Sn(OTf)_2(OPPh_3)_2]$ in the present study was $^{2}J_{119Sn\text{-}O\text{-}P}$ = 110.7 Hz, a significant lowering from the value reported by Dean, however these satellites were poorly resolved.[19] A similar coupling constant of 92.8 Hz was measured for the related $dppmO_2$ complex $[Sn(OTf)_2(dppmO_2)]$ which is discussed below. The previously reported chloride analogue $[SnCl_2(OPPh_3)_2]$,[31] shows a single $^{31}P\{^{1}H\}$ NMR resonance at 36.3 ppm, *i.e.* significantly to low frequency of both $[Sn(X)_2(OPPh_3)_2]$ (X = OTf, SbF_6). The higher lability of the weakly coordinated anions $[OTf]^-$ and $[SbF_6]^-$ may account for this difference, as the chlorides are believed to be coordinated. $[Sn(OTf)_2(OPPh_3)_2]$, was found to produce a two stretches at 1085 and 1067 cm^{-1} which have been tentatively assigned as the P=O stretching frequency. This is in agreement with the predicted peaks from the group theory of this complex, from the C_{2v} point group of $[Sn(OTf)_2(OPPh_3)_2]$ in Figure 6.6. This is similar to what was observed by Dean *et al*, with the IR spectrum of $[SnCl_2(OPPh_3)_2]$ showing two P=O stretching vibrations at 1145 and 1115 cm^{-1} .As previously discussed, the presence of the S-O and C-F bonds of the triflate anion produce IR bands in the same region as the P=O stretch and so confident assignment is difficult.

Table 6.1 - Comparison of the NMR and IR spectroscopy data for the *bis*-$OPPh_3$ complexes of Sn(II) with varying anions.

	$^{31}P\{^{1}H\}$ resonance / ppm	P=O stretching frequency / cm^{-1}	Ref
$OPPh_3$	27.2	1190	-
$[SnCl_2(OPPh_3)_2]$	36.3	1145, 1088	14
$[Sn(SbF_6)_2(OPPh_3)_2]$	44.8	not reported	19
$[Sn(OTf)_2(OPPh_3)_2]$	43.9	1085, 1067	*This Work*

Layering of a CH_2Cl_2 solution of $[Sn(OTf)_2(OPPh_3)_2]$ with *n*-hexane produced large single crystals which were analysed *via* single-crystal X-ray diffraction to give the structure shown in Figure 6.6, with selcected bond lengths and angles provided in Table 6.2

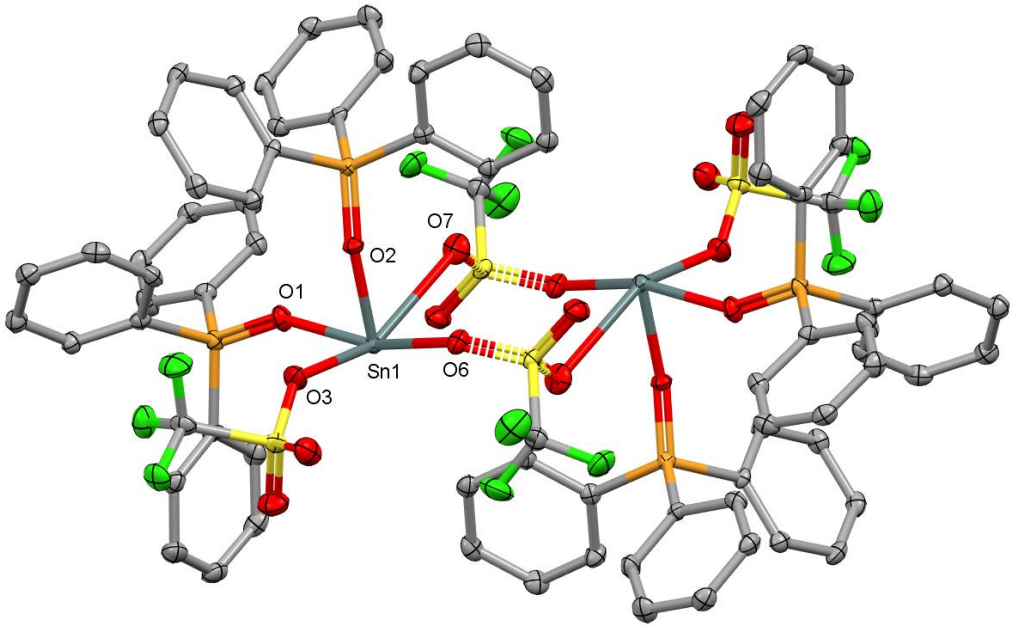

Figure 6.6 - Crystal structure of ***33*** $[\{Sn(OTf)(OPPh_3)_2\}_2(\mu\text{-}OTf)_2]$ showing the atom numbering scheme. Ellipsoids are shown at 50% probability with H-atoms omitted for clarity.

Table 6.2 - Selected bond lengths (Å) and angles (°) for $[\{Sn(OTf)(OPPh_3)_2\}_2(\mu\text{-}OTf)_2]$.

Bond Lengths / Å		Bond Angles / °	
Sn1 – O1	2.2077(16)	O1 – Sn1 – O2	82.94(7)
Sn1 – O2	2.0938(16)	O1 – Sn1 – O3	87.98(7)
Sn1 – O3	2.3215(18)	O2 – Sn1 – O3	80.82(7)
Sn1 – O6	2.6307(18)	O3 – Sn1 – O6	80.21(6)
Sn1 – O7	2.744(2)	O3 – Sn1 – O7	153.10(7)
		O6 – Sn1 – O7	90.65(6)

This crystal structure revealed $[\{Sn(OTf)(OPPh_3)_2\}_2(\mu\text{-}OTf)_2]$ to be a bimetallic dimer bridged by triflate anions, with each metal centre found in a 5-coordinate tetragonal pyramidal geometry, matching that of $[\{Sn(OTf)(o\text{-}C_6H_4(PPh_2)_2)\}_2(\mu\text{-}OTf)_2]$ seen in Chapter 5. The coordination sphere of each metal centre is made up of two $OPPh_3$ ligands, one κ^1-triflate and two symmetrically bridging triflate anions. This leaves a single vacant site on the Sn(II), presumably where the stereochemically active lone pair of electrons is located. The κ^1-triflate had an Sn-O_{OTf} distance of 2.315(18) Å, significantly shorter than the bridging triflates, 2.6307(18) and 2.744(2) Å, respectively. The structure of the chloro-analogue $[SnCl_2(OPPh_3)_2]$,[14] is monomeric with Sn-O_{OPPh3} distances of 2.364(3) and 2.394(3) Å, which are significantly longer than those in the triflate

complex. This could be due to the weaker $[OTf]^-$ coordination causing an increase in Lewis acidity at the metal centre, and hence an increase in the Sn-O_{OPPh3} bond strength.

Increasing the number of ligands coordinated to the metal centre generally increases the metal-donor distances because of the increased steric interactions. The reaction of $Sn(OTf)_2$ with three molar equivalents of $OPPh_3$, with each of these reactions following the conditions highlighted in Scheme 6.1. This produced a white solid in a good yield that microanalysis confirmed as consistent with the formulation of $[Sn(OTf)_2(OPPh_3)_3]$. The ^1H NMR spectrum of this compound was found to show three aromatic multiplets ranging from 7.66 – 7.36 ppm with integrals of 1:2:2, showing a change from the two environments observed in $OPPh_3$ itself. The analysis of this solid by $^{31}P\{^1H\}$ NMR spectroscopy showed a sharp singlet at 42.0 ppm, slightly to low frequency of the *bis*-complex, found at 43.9 ppm. The work by Dean on the complexes of $M(SbF_6)_2$ found the same pattern when moving from the *bis* to *tris* complexes of $OPPh_3$, with a differing chemical shift of $\Delta\delta$ = -0.9 ppm in liquid SO_2, with $[Sn(SbF_6)_2(OPPh_3)_3]$ producing a resonance at 44.1 ppm, with a coupling of $^2J_{119Sn\text{-}OPR3}$ = 201 Hz, whereas, satellite couplings were not evident in the spectrum of $[Sn(OTf)_2(OPPh_3)_3]$. Dean also went on to explore other phosphine oxide ligands, with $[Sn(SbF_6)_2(OPCy_3)_n]$ (n = 2, 3) producing resonances of 75.4 and 72.3 respectively in the $^{31}P\{^1H\}$ NMR spectra.[18] The IR spectrum of $[Sn(OTf)_2(OPPh_3)_3]$ contained a single absorption at 1059 cm^{-1}, tentatively assigned as the P=O stretching frequency.

Layering of a CH_2Cl_2 solution of the complex with *n*-hexane produced a number of plate-like crystals suitable for diffraction. These gave the structure shown in Figure 6.7, and confirmed the coordination of three $OPPh_3$ ligands to the Sn(II) centre. Selected bond lengths and angles for this complex are provided in Table 6.3.

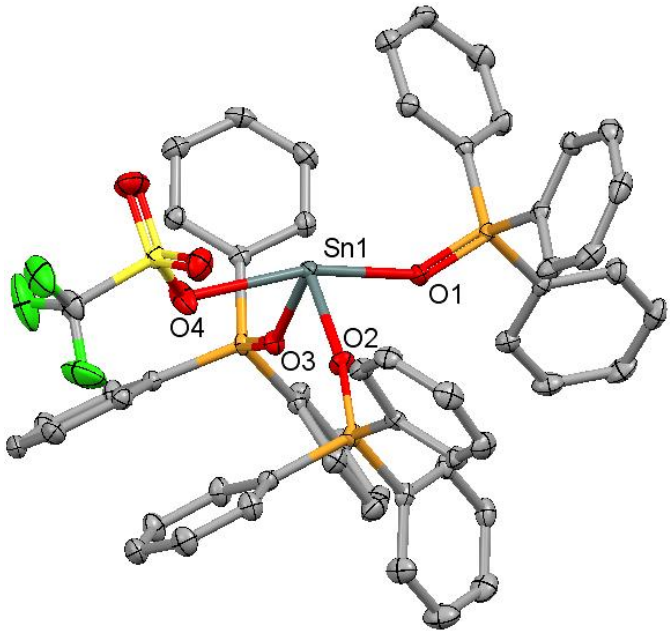

Figure 6.7 – Crystal structure of ***34*** $[Sn(OTf)(OPPh_3)_3][OTf]$ showing the atom numbering scheme. Ellipsoids are shown at 50% probability with H-atoms and anions omitted for clarity.

Table 6.3 - Selected bond lengths (Å) and angles (°) for $[Sn(OTf)(OPPh_3)_3][OTf]$.

Bond Lengths / Å		Bond Angles / °	
Sn1 – O1	2.2566(14)	O1 – Sn1 – O2	84.71(6)
Sn1 – O2	2.0780(15)	O1 – Sn1 – O3	85.89(5)
Sn1 – O3	2.1163(13)	O1 – Sn1 – O4	164.752(5)
Sn1 – O4	2.5054(16)	O2 – Sn1 – O3	84.66(6)
		O2 – Sn1 – O4	86.41(6)
		O3 – Sn1 – O4	80.92(5)

The structure reveals a four-coordinate Sn(II) metal centre into a disphenoidal geometry where the axial components consist of one $OPPh_3$ ligand and a single κ^1-coordinated triflate anion, while the two equatorial sites are filled with $OPPh_3$ ligands. There are no additional contacts to the metal centre from adjacent molecules making this a monomeric monocation. The $Sn\text{-}O_{OPPh3}$ distances for $[Sn(OTf)(OPPh_3)_3][OTf]$ are found within the expected range of 2.05 - 2.26 Å, was observed in the *bis*-complex in Figure 6.7. Of the $OPPh_3$ ligands, the equatorial ligands are found to have a bond angle of O2 – Sn1 – O3 = 84.66(6)°, which is wider than the equivalent angle in the *bis*-complex, O1- Sn1 – O2 = 82.94(7) ° in Table 6.2. Comparison of the $Sn\text{-}O_{OTf}$ distances of this complex and the *bis*-complex in Figure 6.6, showed a shortening to 2.5054(16) Å. The cationic nature of this species would be expected to have increased Lewis acidity and thus could account for the slightly shorter bond with the triflate anion. There was rotational disorder associated with the $-CF_3$ of the free triflate anion in the unit cell which was modelled such that the two positions had occupancies of 45:55; due to it having no interaction with the metal complex, this anion has been omitted from Figure 6.7.

A similar reaction followed with the addition of 4 molar equivalents of $OPPh_3$, aiming to displace a 2nd triflate and produce the homoleptic Sn(II) dicatioic complex. Following the procedure shown in Scheme 6.1, precipitation of the product as a white solid which ^{1}H NMR spectroscopy showed splitting of the aromatic peaks with the same 1:2:2 integral pattern as the *tris* product discussed above. The position of these aromatic peaks appears to change very little upon coordination of additional $OPPh_3$ ligand, likely due to the distance of the aromatic protons to the metal centre. Analysis by $^{31}P\{^1H\}$ NMR spectroscopy produced a single resonance at 39.8 ppm, slightly broadened compared to the *bis* and *tris* species; this resonance showed no satellite coupling. This follows the pattern of increasing the ratio of $OPPh_3$ producing a resonance at a slightly lower frequency. As well as this, the $^{19}F\{^1H\}$ NMR spectroscopy produced a single sharp resonance at -79.2 ppm, the characteristic shift of ionic triflate in CD_2Cl_2. The IR spectrum for this complex produced a single absorption peak at 1059 cm^{-1}, matching that observed for the *tris*-product. Each

of the ^{1}H, $^{19}F\{^{1}H\}$ and $^{31}P\{^{1}H\}$ NMR spectra and the IR spectrum, were very similar to the values produced by the *tris*-complex and thus the formulation as a *tetrakis* complex was unconfirmed. Microanalysis gave a value that closely matched the calculated values for $[Sn(OTf)_2(OPPh_3)_4]$ and significantly was removed from the values calculated for the *tris*-complex, suggesting successful coordination of four $OPPh_3$ ligands.

A few poor quality crystals were grown through the layering of a CH_2Cl_2 solution of this product with *n*-hexane. The crystal structure revealed a highly distorted and disordered octahedral geometry, showing four equatorial $OPPh_3$ ligands, in the *P4/ncc* space group. The metal species was found on a 4-fold rotation axis, which made modelling the disorder extremely difficult. This structure was never completed and has been omitted.

In order to continue to explore the coordination of the phosphine oxide ligands, the R-groups of the ligand species were substituted from phenyl to methyl, increasing the donor power and decreasing the steric demands. The hygroscopic nature of $OPMe_3$ required sublimation under an inert atmosphere prior to use.[32] This was then reacted in a 2:1 ratio with $Sn(OTf)_2$ in CH_2Cl_2 for 2 hours, producing a white solid. The ^{1}H NMR spectrum of this complex showed a doublet at 1.83 ppm, a shift of $\Delta\delta$ = +0.33 ppm to a higher frequency from the $OPMe_3$ itself. This complex also displayed a slightly larger $^{2}J_{P\text{-}H}$ coupling constant of 13.5 Hz than OPMe3 (12.8 Hz). Analysis *via* $^{31}P\{^{1}H\}$ spectroscopy showed a single resonance, shift to a higher frequency of 64.8 ppm than that of $OPMe_3$, with $\Delta\delta$ = +26.2 ppm. This complex was then dissolved in CH_2Cl_2 and this solution was layered with *n*-hexane with large needle like crystal forming after 48 h and diffraction experiments revealing the structure in Figure 6.8. The bond lengths and angles of interest to this complex have been provided in Table 6.4.

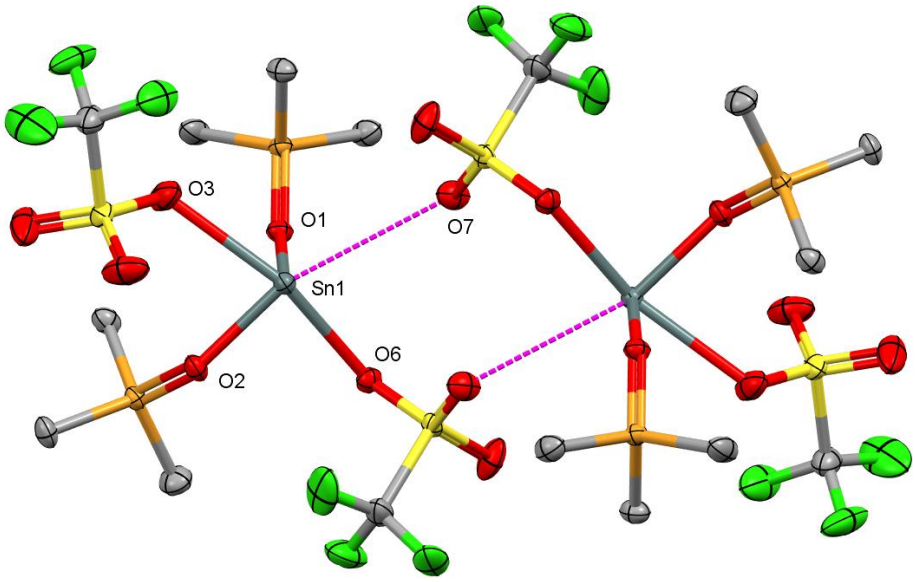

Figure 6.8 - Crystal structure of the weakly associated dimer ***35*** $[\{Sn(OTf)(OPMe_3)_2\}_2(\mu\text{-}OTf)_2]$ showing the atom numbering scheme. Ellipsoids are shown at 50% probability with H-atoms omitted for clarity.

Table 6.4 - Selected bond lengths (Å) and angles (°) of [{Sn(OTf)(OPMe$_3$)$_2$}$_2$(μ-OTf)$_2$]

Bond Lengths / Å		Bond Angles / °	
Sn1 – O1	2.1119(10)	O1 – Sn1 – O2	91.02(4)
Sn1 – O2	2.1038(10)	O1 – Sn1 – O3	78.67(4)
Sn1 – O3	2.4667(13)	O1 – Sn1 – O6	81.74(4)
Sn1 – O6	2.4322(11)	O2 – Sn1 – O3	81.49(5)
Sn1 – O7	3.2198(13)	O3 – Sn1 – O6	153.28(4)
		O3 – Sn1 – O7	116.53(4)
		O6 – Sn1 – O7	73.03(3)

As was observed with the coordination of two equivalents of OPPh$_3$, the structure of the complex [{Sn(OTf)(OPMe$_3$)$_2$}$_2$(μ-OTf)$_2$] was revealed to be a weakly associated dimer formed by association of two 5-coordinate Sn(II) centres. The metal coordination spheres comprises two OPMe$_3$ ligands and one κ^1-coordinated triflate, while the remaining triflates bridge the two metal centres. Comparison of the Sn-O$_{OTf}$ bridging distances of for the OPMe$_3$ and OPPh$_3$ complexes, [{Sn(OTf)(OPR$_3$)$_2$}$_2$(μ-OTf)$_2$] (R = Me, Ph), showed that moving to the methyl R-group weakened this secondary bridging interaction, lengthening the Sn-O$_{OTf}$ from 2.744(2) Å seen in Figure 6.6 to 3.2198(13) Å in Figure 6.8.

The angle between each of the OPR$_3$ ligands of these bridged dimer species shows the OPMe$_3$ complex has a more acute than the same angle in [Sn(OTf)$_2$(OPPh$_3$)$_2$]. The related [SnCl$_2$(OPMe$_3$)$_2$] complex[15] is a neutral monomer, taking up a disphenoidal geometry with one chloride and one OPMe$_3$ ligand axial and one of each equatorial. The Sn-O$_{OPMe3}$ distances for [SnCl$_2$(OPMe$_3$)$_2$] were 2.3043(14) and 2.1275(15) Å, significantly longer than those observed in the newly synthesised [{Sn(OTf)(OPMe$_3$)$_2$}$_2$(μ-OTf)$_2$], again consistent with the increased Lewis acidity resulting from the weaker triflate coordination.

As with the OPPh$_3$ ligand, a series of reactions with differing molar equivalents of OPMe$_3$ were undertaken to explore the effect of having a weakly coordinating anion present. The reaction of 3 molar equivalents of OPMe$_3$ produced a white powder that crystallisation and X-ray diffraction, revealed [Sn(OTf)$_2$(OPMe$_3$)$_3$] as unusual hexameric structure containing a large central void, with the structure of this complex shown in Figure 7.5, as well as bond lengths and angles in Table 7.1. This complex and its characterisation, properties and structure and attempts to produce analogous species are discussed in full in Chapter 7 along with number of synthesised analogues. After successful synthesis of [Sn(OTf)$_2$(OPMe$_3$)$_3$], the reaction of Sn(OTf)$_2$ with 4 molar equivalents of OPMe$_3$ was carried out under analogous conditions, producing a white powder. Microanalysis of this solid revealed a ratio matching that observed for the 3:1 product with additional attempts

producing the same result and so was abandoned. It is known that the hexamer structure is robust due to the same structure being repeatedly obtained from a range of crystallisation techniques.

Moving away from phosphine oxides, the donor ligand was changed to $OAsPh_3$ as to see if this change in the electronicsand thus the donor strength of the ligand would have a significant effect on the nature of the complexes formed. Arsenic has a lower electronegativity as well as a slightly larger ionic radius.[33] These were started with the reaction of $Sn(OTf)_2$ with 2 molar equivalents of $OAsPh_3$ in CH_2Cl_2 and reacted for two hours, during which time the starting material was pulled into solution. Precipitation using *n*-hexane yielded a white solid which was then analysed by NMR spectroscopy. The ^1H NMR spectra showed two significantly broadened aromatic resonances found shifted to a higher frequency than the free ligand.[34] Due to the broadness of these aromatic resonances, the information from splitting is lost. The complex $[Sn(OTf)_2(OAsPh_3)_2]$ showed the same $^{19}F\{^1H\}$ NMR spectrum as with OPR_3 complexes, producing a sharp singlet at -79.4 ppm, characteristic for anionic triflate in CD_3CN.

Using group theory, it is predicted that the IR spectrum should produce 2 absorbance bands for the O=As bond in this C_{2v} complex. However, collection of the IR spectrum showed three absorbances at 865, 852 and 833 cm^{-1}, at lower frequencies than free ligand at 881 cm^{-1}, as shown in Figure 6.10.[35,36] Thus may be a suggestion that the crystal structure in Figure 6.9, may not be representative of the bulk solid. The crystallisation of $[Sn(OTf)_2(OAsPh_3)_2]$ was carried out by layering of a CH_2Cl_2 solution with *n*-hexane produced good quality crystals, with the crystal structure demonstrated Figure 6.9. Selected bond lengths and angles are located in Table 6.5.

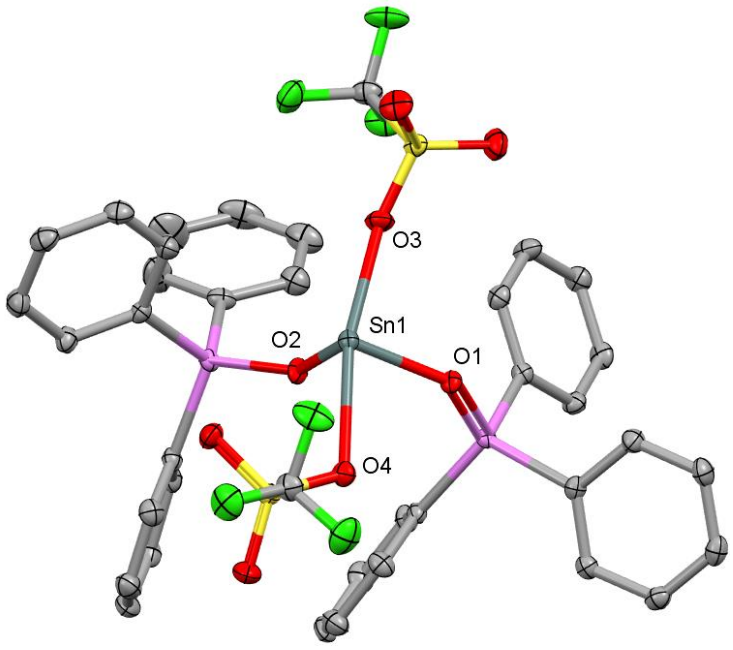

Figure 6.9 - Crystal structure of ***36*** $[Sn(OTf)_2(OAsPh_3)_2]$ showing the atom numbering scheme. Ellipsoids are shown at 50% probability with H-atoms omitted for clarity.

Table 6.5 - Selected bond lengths (Å) and angles (°) for $[Sn(OTf)_2(OAsPh_3)_2]$.

Bond Lengths / Å		Bond Angles / °	
Sn1 – O1	2.0806(15)	O1 – Sn1 – O2	86.68(6)
Sn1 – O2	2.0841(15)	O1 – Sn1 – O3	84.71(6)
Sn1 – O3	2.4755(16)	O1 – Sn1 – O4	80.42(6)
Sn1 – O4	2.4559(16)	O2 – Sn1 – O3	82.42(6)
		O2 – Sn1 – O4	92.33(6)
		O3 – Sn1 – O4	164.50(6)

The structure of $[Sn(OTf)_2(OAsPh_3)_2]$ showed a 4-coordinate disphenoidal geometry, with two triflate anions taking the axial positions while the coordinated $OAsPh_3$ ligands fill the equatorial positions. This is similar to the structure of one of the metal centres of $[\{Sn(OTf)(OPPh_3)_2\}_2(\mu^2\text{-}OTf)]$, but with no suggestion of additional bridging contacts to the Sn(II) centre from adjacent molecules. The $Sn\text{-}O_{OPPh3}$ distances measured in $[\{Sn(OTf)(OPPh_3)_2\}_2(\mu^2\text{-}OTf)]$ were 2.2077(16) and 2.0938(16) Å, showing that changing to the arsine oxide ligands causes a shortening of the $Sn\text{-}O_{OAsPh3}$. This is the first example of $OAsPh_3$ coordinated to Sn(II), with only a single example of coordination to an organotin(IV) previously reported.[37]

Following in the series, $Sn(OTf)_2$ was reacted with three molar equivalents of $OAsPh_3$ in CH_2Cl_2 for 2 hours before precipitation of a white solid in a good yield. The spectroscopic analysis of this complex by ^1H NMR produced a spectrum, unlike the *bis*-complex, displaying two aromatic regions with multiplet splitting shifted from free ligand, differing from that of the $[Sn(OTf)_2(OAsPh_3)_2]$ with a lower frequency, with an integral pattern of 1:4. The $^{13}C\{^1H\}$ NMR spectrum revealed peaks being shifted from that of free ligand when coordinated in the complex $[Sn(OTf)_2(OAsPh_3)_3]$. This technique also showed the presence of a small amount of residual $OAsPh_3$ starting material. The most informative spectroscopic method was IR spectroscopy, showing the shift of the As=O absorbance band with coordination and increase in molar ratio of $OAsPh_3$. Free $OAsPh_3$ has an As=O stretch at 881 cm^{-1} and this peak is shifted to a single broad peak at 824 cm^{-1} in the $[Sn(OTf)_2(OAsPh_3)_3]$ complex, as shown in Figure 6.10.

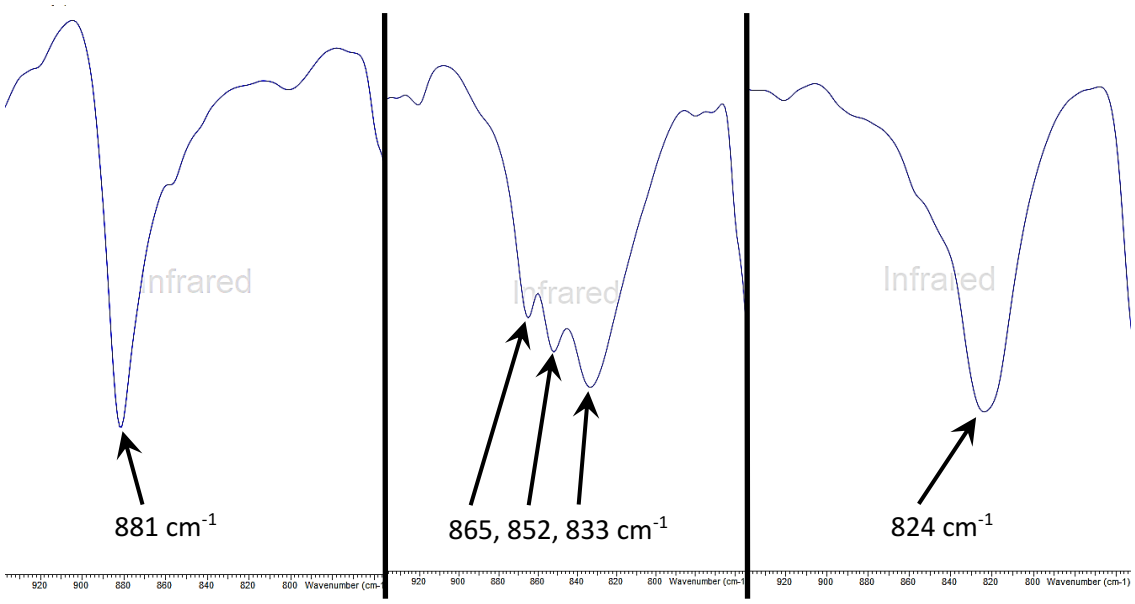

Figure 6.10 - The shift in As-O stretching frequency in $OAsPh_3$ (*left*), $[Sn(OTf)_2(OAsPh_3)_2]$ (*central*) and $[Sn(OTf)_2(OAsPh_3)_3]$ (*right*).

As has been previously discussed, the location of the P=O stretching frequency is generally found between 950 - 1200 cm^{-1}, with free $OPPh_3$ being found at 1190 cm^{-1}.[38] When moving to the $OAsPh_3$ ligand, the As=O stretching frequency is located at 881 cm^{-1} (seen in Figure 6.10),[35,36] a region with fewer peaks and where a more confident assignment of the peaks can be made. Figure 6.10 shows the difference in spectra of the *bis* and *tris*-products, highlighting the shift of the peak with increasing equivalents of ligand. The results of the spectroscopic analysis were corroborated by the results of the microanalysis which closely matched with the calculated formulation of $[Sn(OTf)_2(OAsPh_3)_3]$. Crystallisation was attempted using the same layering technique which was used to grow similar crystal structures earlier in this chapter, unfortunately this unsuccessful. A range of other crystallisation techniques were attempted including slow vapour diffusion of Et_2O into an MeCN solution and storage of a CH_2Cl_2 solution of $[Sn(OTf)_2(OAsPh_3)_3]$ at -18°C, however, none of these were found to induce crystallisation and so the solid-state structure is unknown.

As an additional *O*-donor ligand for comparison to the OPR_3 ligands, pyNO (pyridine *N*-oxide) was also used to give further insight into how changes in the electronics of the ligand can affect the properties and structure of the synthesised complexes. Due to the differences in E=O (E = N, P) bonding of OPR_3 and pyNO, discussed in Chapter 1, it was expected that this may change the composition and geometry of the complexes formed with $M(OTf)_2$ (M = Sn, Pb). The reaction of two molar equivalents of pyNO with $Sn(OTf)_2$ produced a white powder in a moderate yield which ^1H NMR spectroscopy showed as a single species in solution. This spectrum showed three aromatic multiplet resonances at 8.68, 7.97 and 7.74 ppm in a ratio of 2:1:2 (*ortho*, *para*, *meta* respectively), shifted to a higher frequency than free pyNO. These shifts from free ligand were

also accompanied by similar shifts in the $^{13}C\{^{1}H\}$ NMR spectra, with the three carbon environments observed at 141.9, 137.8 and 127.88 ppm. While two of these resonances only shifted 2-3 ppm, the peak at 137.8 ppm had a much larger shift, with a $\Delta\delta$ = 11.62 ppm from free ligand. The elemental analysis of this sample matched the calculated values for $[Sn(OTf)_2(pyNO)_2]$. The IR spectrum displayed bands at 1216 and 1205 cm^{-1} with a medium strength which have been assigned as the N=O stretching frequencies of the coordinated pyNO and is in line with literature reports of this ligand in transition metal complexes.[40]

Layering of a CH_2Cl_2 solution of this complex with *n*-hexane produced a small number of crystals that X-ray crystal diffraction experiments unexpectedly revealed as the *tris*-pyNO complex, $[\{Sn(OTf)(pyNO)_2\}_2(\mu^2\text{-}pyNO)_2][OTf]_2$ as a bridged dimer, shown in Figure 6.11. Selected bond lengths and angles for this complex are provided in Table 6.6.

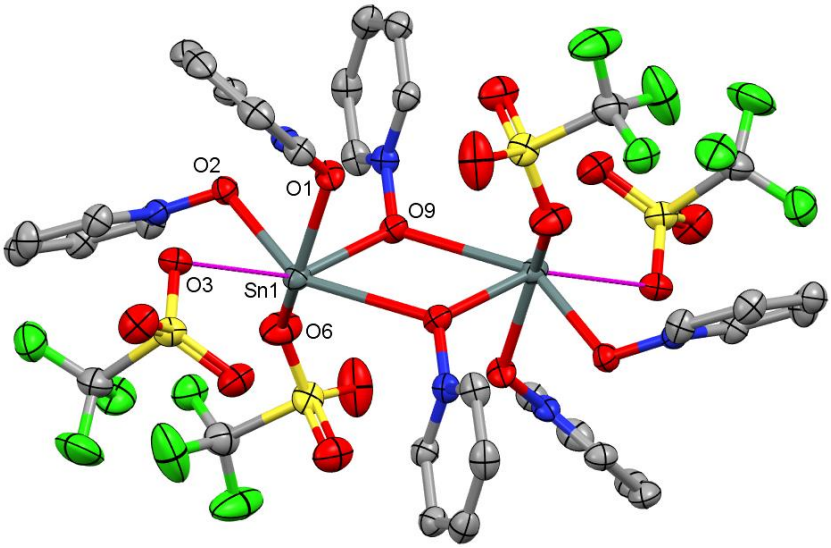

Figure 6.11 - Crystal structure of the dimeric ***37*** $[\{Sn(OTf)_2(pyNO)_2\}_2(\mu\text{-}pyNO)_2]$ showing the atom numbering scheme. Ellipsoids shown at 50% probability with H-atoms omitted for clarity.

Table 6.6 - Selected bond lengths (Å) and angles (°) for $[\{Sn(OTf)_2(pyNO)_2\}_2(\mu\text{-}pyNO)_2]$.

Bond Lengths / Å		Bond Angles / °	
Sn1 – O1	2.1949(17)	O1 – Sn1 – O2	80.52(7)
Sn1 – O2	2.2286(18)	O1 – Sn1 – O3	75.46(6)
Sn1 – O3	3.0109(19)	O1 – Sn1 – O6	141.76(7)
Sn1 – O6	2.691(2)	O1 – Sn1 – O9	75.96(6)
Sn1 – O9	2.2205(18)	O2 – Sn1 – O9	86.12(7)
Sn1 – O9’	2.671(2)	O3 – Sn1 – O6	127.68(6)
		O3 – Sn1 – O9	150.45(6)
		O6 – Sn1 – O9	73.85(7)

The complex contains a planar Sn_2O_2 core where each Sn(II) centre is found in a highly distorted octahedral geometry formed of two bridging pyNO molecules, two κ^1-pyNO ligands and a coordinated triflate anions. A second weakly associated triflate anion was located at a longer Sn-O_{OTf} distance of 3.0109(19) Å, within the sum of the Van der Waals radii (3.52 Å). The bridging pyNO ligands show asymmetry in their binding with a primary Sn-O_{pyNO} distance of 2.2205(18) Å, similar to the κ^1-pyNO ligands. The secondary bridging interaction is significantly longer, at 2.671(2) Å, shown in Table 6.6. Each of the dimers discussed earlier in this chapter, as well as those in Chapter 5, were bridged by the triflate ligands, with this being the first complex bridged by the neutral ligands in this work. The increased electron density associated with the donor atom in the pyNO system *vs* OPR_3 and the need to disperse this between the electron deficient Sn(II) centres could explain this. Previous attempts at coordination of other *N*-oxide ligands, such as $ONMe_3$, have been shown to produce cyclodistannoxane [{$SnR_2(\mu\text{-}O)_2$}] with the same planer Sn_2O_2 core, even with bulky groups surrounding the metal centre.[41,42] The fact that microanalysis on the bulk solid isolated from the pyNO reaction matched the calculated values for the formulation [$Sn(OTf)_2(pyNO)_2$], clearly suggests that the crystal structure of the 3:1 pyNO:Sn product is not representative of the bulk. However, the structure does confirm that coordination of 3 molar equivalents of pyNO is possible.

Therefore the reaction was repeated using 3 molar equivalents of pyNO with $Sn(OTf)_2$ in CH_2Cl_2 yielding a white precipitate that was isolated and characterised. The ^{1}H NMR spectroscopy was very similar to that of the *bis* product discussed above, with three aromatic resonances in a 2:1:2. The highest frequency resonance in *bis*-[$Sn(OTf)_2(pyNO)_2$] was located at 8.68 ppm, while for the *tris*-[$Sn(OTf)_2(pyNO)_3$] it was found at 8.53 ppm. The $^{13}C\{^1H\}$ spectrum of the same sample showed three aromatic resonances, each shifted slightly to a higher frequency than both free ligand and the previously discussed [$Sn(OTf)_2(pyNO)_2$]. Microanalysis was required to ascertain the formulation of this product, gave percentage compositions that closely matched the values calculated for the [$Sn(OTf)_2(pyNO)_3$]. The IR spectrum showed an absorbance band at 1204 cm^{-1}, shifted to a lower frequency than that observed in [$Sn(OTf)_2(pyNO)_2$]. Crystallisation of this compound produced crystals which, upon analysis, matched the unit cell parameters of the crystal structure in Figure 6.11.

After the successful synthesis of a number of different monodentate ligand complexes of $Sn(OTf)_2$, the bidentate $dppmO_2$ ligand was also explored to determine the effect of denticity on the geometry and coordination number it is possible to reach with the Group 14 metal(II) cations. The equimolar reaction of $dppmO_2$ and $Sn(OTf)_2$ over two hours in CH_2Cl_2 produced a white precipitate which was isolated in a good yield. Analysis *via* ^{1}H NMR spectroscopy in CD_2Cl_2 produced a spectrum with a sharp and well resolved triplet at 3.96 ppm corresponding to the protons of the

methylene bridge; with $^{2}J_{PH}$ = 12.96 Hz. There are also three aromatic multiplet resonances with integrations of 8:4:8 as expected. The $^{13}C\{^{1}H\}$ NMR spectrum shows a weakly resolved triplet at 27.6 ppm, corresponding to the methylene carbon of the bridge split by the two adjacent I = ½ phosphorus atoms, with $^{1}J_{PC}$ = 55.0 Hz. This spectrum also showed the corresponding aromatic carbon environments between 125 – 135 ppm with the *ipso* carbon being split by the adjacent phosphorus atom by 127 Hz. The $^{31}P\{^{1}H\}$ NMR spectrum showed a sharp singlet at 40.00 ppm, with unresolved $^{119/117}$Sn satellite coupling of 92.75 Hz, suggesting successful coordination to the Sn(II) metal centre. The IR spectrum of this complex was found to have a single broad band at 1136 cm^{-1} which was assigned to the P=O stretching frequency of the coordinated $dppmO_2$ ligand.

Layering of *n*-hexane on to a CH_2Cl_2 solution of this product produced crystals and analysis by X-ray diffraction confirmed the crystal structure in Figure 6.12 with selected bond lengths and angles found in Table 6.7.

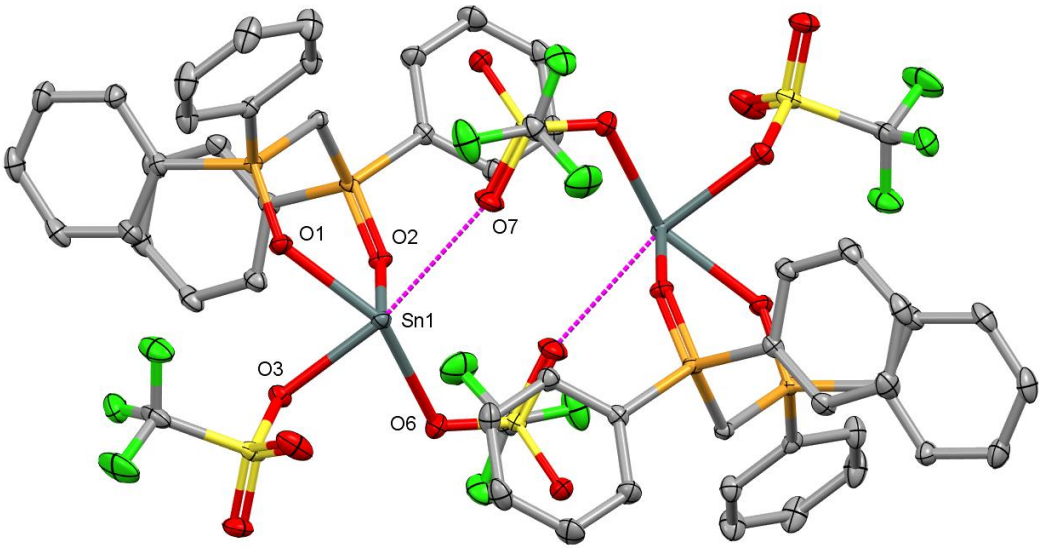

Figure 6.12 - Crystal structure of the weakly associated dimer ***38*** $[\{Sn(OTf)(dppmO_2)\}_2(\mu^2\text{-}OTf)_2]$ showing the atom numbering scheme. Ellipsoids shown at 50% probability with H-atoms omitted for clarity.

Table 6.7 - Selected bond lengths (Å) and angles (°) for $[\{Sn(OTf)(dppmO_2)\}_2(\mu^2\text{-}OTf)_2]$

Bond Lengths / Å		Bond Angles / °	
Sn1 – O1	2.2257(10)	O1 – Sn1 – O2	82.45(4)
Sn1 – O2	2.1368(9)	O1 – Sn1 – O3	78.38(3)
Sn1 – O3	2.3165(10)	O1 – Sn1 – O6	145.86(4)
Sn1 – O6	2.5663(11)	O2 – Sn1 – O3	90.05(4)
Sn1 – O7	2.8235(13)	O3 – Sn1 – O6	72.16(3)
		O3 – Sn1 – O7	163.59(4)
		O6 – Sn1 – O7	109.90(4)

This revealed the complex to take the form of a weakly associated dimer in the solid-state, where each Sn(II) metal centre takes up a distorted octahedral form with one vacant site, presumed to be the location of the lone pair. Similar to the structures of $[\{Sn(OTf)(OPPh_3)_2\}_2(\mu^2\text{-}OTf)_2]$ and $[\{Sn(OTf)(OPMe_3)_2\}_2(\mu^2\text{-}OTf)_2]$, the coordination sphere of each Sn(II) centre is made up of a bidentate $dppmO_2$ ligand, a single κ^1-coordinated triflate anion and two bridging triflate anions. The coordination of the $dppmO_2$ ligand gives an O1–Sn1–O2 bite angle of 82.45. In contrast to Chapter 3, the *tris*-chelate product $[Ga(dppmO_2)_3][OTf]_3$ was found to have O–Ga–O bite angles of 90.51(6) - 92.63(6)°.[1] The Sn-O bond distances involving the $dppmO_2$ are 2.2257(10), 2.1368(9) Å. The Sn-O bond distances and O-Sn-O bond angles for each of the triflate bridged dimers with OPR_3 donors is compared in Table 6.8.

Table 6.8 - The bond distances and bond angles of each of the triflate bridged dimer species.

Complex	$Sn–O_{OPR3}$ Bond distances / Å		O–Sn–O Bond angle / °
$[\{Sn(OTf)(OPPh_3)_2\}_2(\mu^2\text{-}OTf)_2]$	2.2077(16)	2.0938(16)	82.94(7)
$[\{Sn(OTf)(OPMe_3)_2\}_2(\mu^2\text{-}OTf)_2]$	2.1119(10)	2.1038(10)	91.02(4)
$[\{Sn(OTf)(dppmO_2)\}_2(\mu^2\text{-}OTf)_2]$	2.2257(10)	2.1368(9)	82.45(4)

The Sn-O bond distances and angles of $[\{Sn(OTf)(OPPh_3)_2\}_2(\mu^2\text{-}OTf)_2]$ and $[\{Sn(OTf)(dppmO_2)\}_2(\mu^2\text{-}OTf)_2]$ are similar, while the smaller ligand in $[\{Sn(OTf)(OPMe_3)_2\}_2(\mu^2\text{-}OTf)_2]$ leading a significant shortening of the bond lengths and the O-Sn-O angle closer to 90°. Microanalysis of the crystalline material also confirmed the formulation $[Sn(OTf)_2(dppmO_2)]$ for the bulk product.

The crystal structures discussed thus far in this chapter have shown complexes, primarily with a coordination number of four, either forming cationic species with three neutral donor ligands and a single coordinated triflate, or forming a neutral species with two triflates and two neutral donor ligands. The latter were also seen to form an additional longer contact with other nearby molecules, forming bridging interactions and increasing the coordination number to five. Attempts to coordinate two equivalents of $dppmO_2$ were undertaken to see if the *bis*-coordination would form the dicationic $[Sn(dppmO_2)_2]^{2+}$ or if the coordination number could be increased further, with triflate being retained. The reaction was carried out under the same conditions as the equimolar reaction described above, being allowed to react for two hours in CH_2Cl_2 before precipitation of a white solid. Analysis of this solid by ^1H NMR spectroscopy revealed two regions of aromatic protons between 7.64 - 7.52 ppm and 7.35 - 7.29 ppm with integrations of 12:8. There was also a sharply resolved triplet at 4.09 ppm with an integration

value of 2 protons, corresponding to the methylene bridge, with $^{2}J_{PH}$ = 13.33 Hz. The methylene bridge carbon of $[Sn(OTf)_2(dppmO_2)_2]$ is also found in the $^{13}C\{^{1}H\}$ NMR spectrum at 28.13 ppm as a triplet with a splitting of 57.22 Hz, both couplings slightly larger than for $[Sn(OTf)_2(dppmO_2)]$. The aromatic region of the $^{13}C\{^{1}H\}$ NMR spectrum is shown in Figure 6.13.

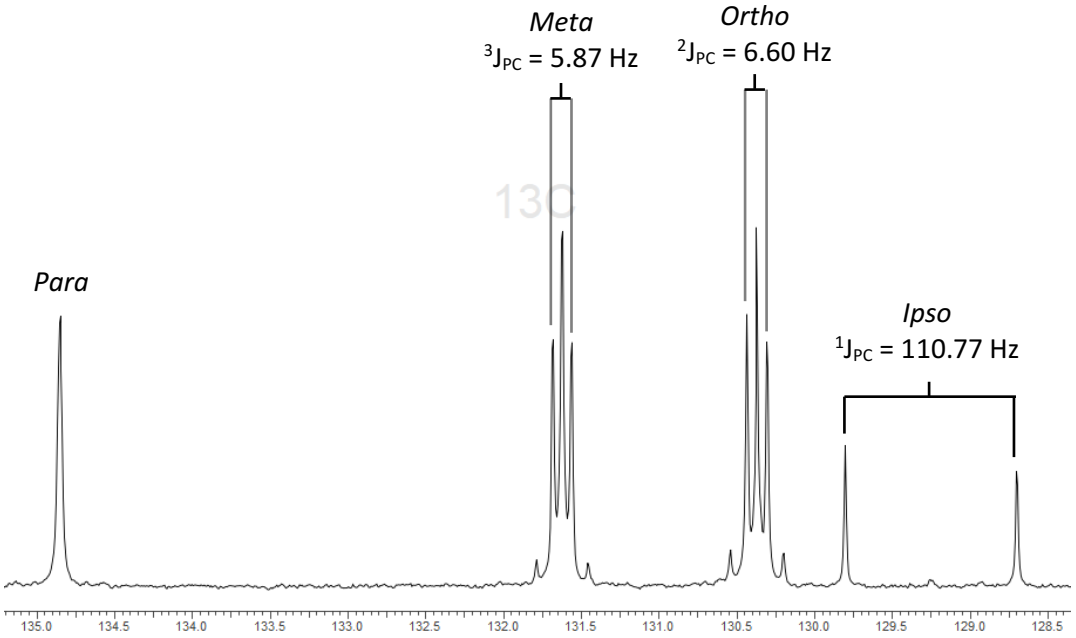

Figure 6.13 - Aromatic region of the $^{13}C\{^{1}H\}$ NMR spectrum for $[Sn(OTf)_2(dppmO_2)_2]$ with each of the carbon environments assigned.

Each of the aromatic regions is highlighted with the assigned protons and the corresponding $^{1}J_{PC}$ coupling constant to the phosphorus atom, decreasing as the distance is increased. The $^{31}P\{^{1}H\}$ NMR spectrum shows a singlet at 35.37 ppm, with no resolved $^{117/119}Sn$ satellites associated with the resonance. This is significantly shifted from the resonance of free ligand at 25.3 ppm, but less than observed for the 1:1 product, $[\{Sn(OTf)(dppmO_2)\}_2(\mu^2\text{-}OTf)_2]$ at 40 ppm. Analysis of this complex by ^{119}Sn NMR spectroscopy produced a weak resonance at -990 ppm after a long acquisition of >50,000 scans.

The IR spectrum of $[Sn(OTf)_2(dppmO_2)_2]$ showed two signals observed at 1141 and 1131 cm^{-1} being assigned as the P=O stretching bands. The results of the microanalysis carried out on this product, strongly suggested that coordination of both ligands has been successful, with results much closer to the calculated values for $[Sn(OTf)_2(dppmO_2)_2]$ or the cationic $[Sn(OTf)(dppmO_2)_2][OTf]$ than observed for $[\{Sn(OTf)(dppmO_2)\}_2(\mu^2\text{-}OTf)_2]$. Crystallisation of this product through layering of a CH_2Cl_2 solution with *n*-hexane resulted in a small number of crystals that produced the crystal structure of the ionic complex $[Sn(OTf)(dppmO_2)_2][OTf]$, shown in Figure 6.14. A selection of bond lengths and angles of interest are displayed in Table 6.9.

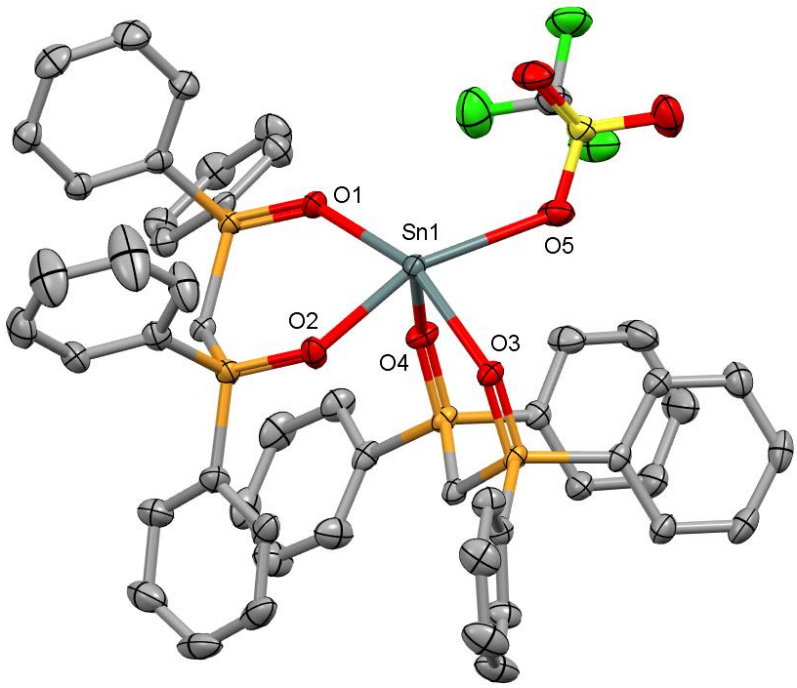

Figure 6.14 - Crystal structure of the cation of ***39*** $[Sn(OTf)(dppmO_2)_2][OTf]$ showing the atom numbering scheme. Ellipsoids shown at 50% probability with the H-atoms and triflate anion omitted for clarity.

Table 6.9 - Selected bond lengths (Å) and angles (°) for $[Sn(OTf)(dppmO_2)_2][OTf]$

Bond Lengths / Å		Bond Angles / °	
Sn1 – O1	2.3090(15)	O1 – Sn1 – O2	82.63(6)
Sn1 – O2	2.2321(17)	O1 – Sn1 – O3	156.06(6)
Sn1 – O3	2.3108(15)	O1 – Sn1 – O5	78.38(3)
Sn1 – O4	2.1683(17)	O2 – Sn1 – O5	157.77(6)
Sn1 – O5	2.7418(18)	O3 – Sn1 – O4	82.06(6)
		O3 – Sn1 – O5	85.53(6)
		O4 – Sn1 – O5	76.71(6).

The structure of $[Sn(OTf)(dppmO_2)_2][OTf]$ confirmed that both $dppmO_2$ ligands are chelated to the tin, and that this product is monocationic. There was no evidence of further bonding or secondary contacts such as bridging to other molecules within the unit cell, or to the discrete triflate anion. The $Sn\text{-}O_{OPR3}$ bond distances are within the range of 2.15 to 2.31 Å, very similar to those observed in $[\{Sn(OTf)(dppmO_2)\}_2(\mu\text{-}OTf)_2]$, with both ligands displaying slight asymmetry between the two oxygen donors of each ligand. O1 and O3 are found to be in a *trans* arrangement in the crystal structure whereas O2 is found *trans* to the coordinated triflate, and O4 is *trans* to a vacant site. The *trans* effect of the OPR_3 group opposing the triflate anion appears to be causing a slight extension in the $Sn\text{-}O_{OTf}$ of the triflate anion. The Sn-O1 and Sn-O3 distances appear to be longer

than many of the other Sn-O_{OPR3} bonds observed in the neutral [Sn(, cationic $[Sn(OTf)(OPPh_3)_3]^+$ or bridged species $[\{Sn(OTf)(OPR_3)_2\}_2(\mu^2\text{-}OTf)_2]$. Although not specifically discussed in many of the *trans* influence series, it is hypothesised that when compared to the phosphine, the phosphine oxide would have an increased effect on the opposing coordinated species. This is attributed to the additional π-orbitals that can interact with the orbitals on the metal, allowing for stronger backbonding and thus more of an influential effect.[43,44] The *trans* influence of the OPR_3 ligands, as well as the packing and steric effects of the different OPR_3 ligands utilised, may explain the variation in bond length observed throughout this chapter. The $dppmO_2$ bite angles in $[Sn(OTf)(dppmO_2)_2][OTf]$ were measured at 82.63(6) and 82.06(6)°, very similar to that seen in $[\{Sn(OTf)(dppmO_2)\}_2(\mu^2\text{-}OTf)]$. This structure was found to crystallise with lattice CH_2Cl_2 molecules which were highly disordered and treated with a solvent mask. Seventy two residual electrons remained over the asymmetric unit cell after modelling of $[Sn(OTf)(dppmO_2)_2][OTf]$. There were two major sites of residual electron density and therefore a mask consisting of two CH_2Cl_2 molecules (84 electrons), was used to treat the heavily disordered solvent molecules.

6.2.2 Coordination to $Pb(OTf)_2$

For comparison to the Sn(II) complexes synthesised above, a number of these reactions were repeated using the heavier $Pb(OTf)_2$ in MeCN starting with reactions of $OPMe_3$, shown in Scheme 6.2. The reactions of $Sn(OTf)_2$ were carried out as a suspension in CH_2Cl_2 with the majority of the metal triflate being pulled into solution upon addition of the phosphine oxide ligand. The solubility of $Pb(OTf)_2$ was noted to be higher in MeCN and hence this was used as the reaction solvent. This first of these reactions was the 3:1 ratio of $OPMe_3$ with $Pb(OTf)_2$ in MeCN, an attempt to produce an analogous complex to the hexameric $[Sn(OTf)_2(OPMe_3)_3]$ array, with this being discussed fully in Chapter 7. The structure of this complex was revealed to be a triflate bridged dimer, similar to the structures observed for the 2:1 reactions of $Sn(OTf)_2$ with OPR_3 (R = Ph, Me), the Pb(II) structure is shown in Figure 7.5.

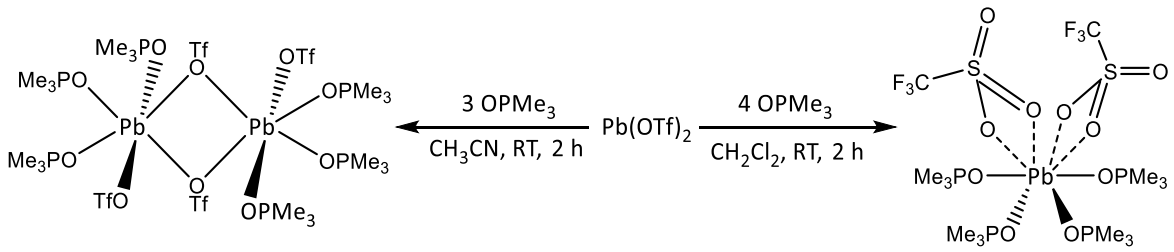

Scheme 6.2 - Reactions of $OPMe_3$ with $Pb(OTf)_2$

Pb(II) is known to more readily form complexes with higher coordination numbers (> 6) than corresponding Sn(II) complexes, with examples being shown in Chapter 5 as well as the wider literature.[17,45] To explore this affect with $Pb(OTf)_2$ as well as the presence of the weakly

coordinating triflate anion a large excess of $OPMe_3$ (6 molar equivalents) was reacted with $Pb(OTf)_2$ in CH_2Cl_2 with the reaction liquor being stored at -18°C over the next 72 hrs. This resulted in small crystals that were analysed by single crystal X-ray diffraction to confirm the formation of $[Pb(OTf)_2(OPMe_3)_4]$ as seen in Figure 6.15. Bond lengths and angles are provided in table 6.10. Partially due to twinning of the crystal, the collected data set had inherent disorder and required the specific expertise of Dr Robert Bannister who assisted with the processing of twinned data and modelling the disordered CH_2Cl_2 solvent molecules.

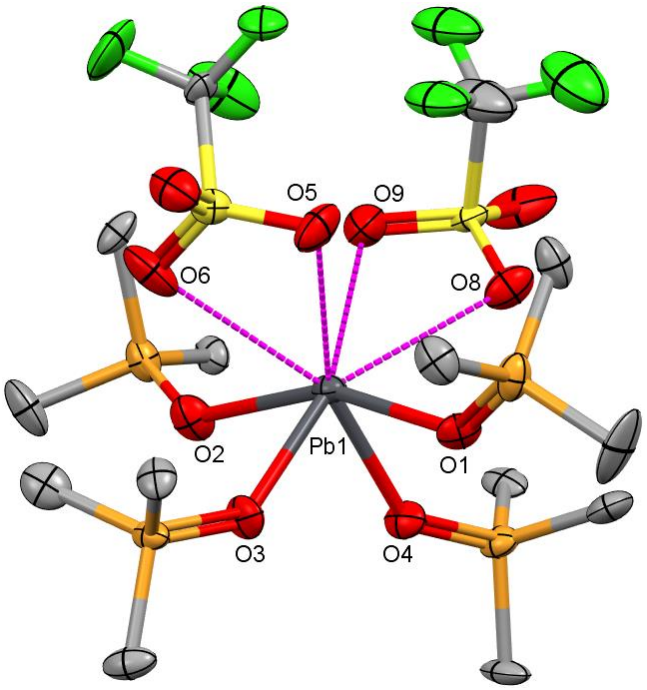

Figure 6.15 - Crystal structure of ***40*** $[Pb(OTf)_2(OPMe_3)_4]$ showing the atom numbering scheme. Ellipsoids shown at 50% probability with H-atoms and solvent molecules omitted for clarity.

Table 6.10 - Selected bond lengths (Å) and angles (°) for $[Pb(OTf)_2(OPMe_3)_4]$

Bond Lengths / Å		Bond Angles / °	
Pb1 – O1	2.466(9)	O1 – Pb1 – O2	157.7(2)
Pb1 – O2	2.502(9)	O1 – Pb1 – O3	82.5(4)
Pb1 – O3	2.344(9)	O1 – Pb1 – O4	80.3(4)
Pb1 – O4	2.348(9)	O2 – Pb1 – O3	80.1(4)
Pb1 – O5	3.025(12)	O2 – Pb1 – O4	83.8(4)
Pb1 – O6	3.172(15)	O3 – Pb1 – O4	83.1(2)
Pb1 – O8	3.020(12)	O5 – Pb1 – O6	46.8(3)
Pb1 – O9	3.085(14)	O8 – Pb1 – O9	44.8(3)

The crystal structure of $[Pb(OTf)_2(OPMe_3)_4]$ confirmed the coordination of four equivalents of $OPMe_3$ in a disphenoidal geometry with two triflate anions weakly coordinated in a κ^2-form, making the coordination number at Pb(II) of 8. This higher coordination number suggests the lone pair of the Pb(II) is stereochemically inactive and thus the complex is holodirected in structure. Table 6.10 shows that the Pb-O_{OPMe3} bond lengths of $[Pb(OTf)_2(OPMe_3)_4]$, with an increase in the M-O bond length compared with the Sn(II) OPR_3 complexes discussed earlier in this chapter. The crystal structure of $[Pb(OTf)_2(OPMe_3)_4]$ shows a slight elongation of the axial bonds, with distances of 2.466(9) and 2.502(9) Å (O1 + O2), when compared to the equatorial Pb-O_{OPMe3} distances 2.344(9) and 2.348(9) Å (O3 + O4)).

As discussed for the crystal structure of $[Sn(OTf)(dppmO_2)_2][OTf]$, the lengthening of the axial Pb-O bonds may be explained by the *trans* influence of the $OPMe_3$ ligand, increasing these distances by 0.1-0.2 Å when compared with the equatorial. Both of the triflate anions in this complex are rotated to allow for weak κ^2-coordination, where both Pb-O_{OTf} distances are ~3 Å. Similar behaviour was observed with the Pb(II) soft donor complexes in Chapter 5. This type of coordination is commonly observed in complexes containing nitrate anions, while triflate analogues of this κ^2-bonding are less common. This behaviour has been more heavily documented to the metals of Group 1 and 2, the earlier transition metals in higher oxidation states as well as both the lanthanide and actinide ions.[46–49] There are few examples of this type of coordination with the main group, with complexes of the later metal complexes of Pb(II) and Bi(III) displaying κ^2-triflate anions.[50–52]

The ^{1}H NMR spectrum of $[Pb(OTf)_2(OPMe_3)_4]$ showed a single sharp doublet at 1.58 ppm, a high frequency shift from free $OPMe_3$, with a coupling constant $^2J_{PH}$ 13.5 Hz. Coordination of the $OPMe_3$ ligand to Pb(II) also showed a high frequency shift from free $OPMe_3$ in the $^{31}P\{^1H\}$ NMR spectrum, with a single resonance observed at 53.6 ppm. Comparison of this to the *tris*-complex $[Pb(OTf)_2(OPMe_3)_3]$ (discussed in Chapter 7), shows that the additional equivalent of ligand gave a small low frequency shift to each resonance in both the ^{1}H and $^{31}P\{^1H\}$ NMR spectra. When looking at the IR spectrum, the strong absorbance peaks at 1115 and 1100 cm^{-1} were tentatively assigned to the P=O bonds of this complex.

Coordination of pyNO to $Sn(OTf)_2$ produced $[\{Sn(OTf)_2(pyNO)_2\}_2(\mu^2\text{-pyNO})]$. Previous reports in the literature of pyNO being used as a ligand for coordination to lead are predominantly focused on Pb(IV), producing polymeric arrays through bridging pyNO ligands.[53–55] The reaction of $Pb(OTf)_2$ with two molar equivalents of pyNO for 2 hrs in CH_2Cl_2 produced $[Pb(OTf)_2(pyNO)_2]$ as a white precipitate which was collected by filtration and stored under inert conditions. The ^{1}H NMR spectrum of free pyNO shows two distinct aromatic regions at 8.11-8.08 ppm and 7.33-7.25 ppm

with integration ratio of 2:3.[56] Upon coordination to $Pb(OTf)_2$, the ^1H NMR spectrum showed a high frequency shift from that of free ligand, as well as separation of the aromatic protons into three regions; 8.42-8.45, 7.81-7.87 and 7.68-7.73 ppm, with an integration pattern of 2:1:2. This is matched by the $^{13}C\{^1H\}$ NMR spectrum showing a high frequency shift as well as an increased separation of the aromatic carbon environments. The IR spectrum of $[Pb(OTf)_2(pyNO)_2]$ showed a strong absorbance band at 1216 cm^{-1} which has been assigned as the N-O stretching frequency of the pyNO. In a paper discussing the donor properties of pyNO with when coordinating to transition metals, the authors classified complexes into two classes of coordination. The first category contained only pyNO ligands in the primary coordination sphere, with the N-O stretching frequency reported ~1220 cm^{-1}, while the second category contained other coordinated anionic ligands in the primary coordination sphere (halide, nitrate, perchlorate etc.), with the infrared stretching frequencies around 1205 cm^{-1}. The structure of the earlier tin complex $[\{Sn(OTf)_2(pyNO)_2\}_2(\mu^2\text{-}pyNO)_2]$ showed a mixed coordination sphere with an IR absorption of 1204 cm^{-1} suggesting that this trend is replicated in the main group. The formulation of $[Pb(OTf)_2(pyNO)_2]$ was confirmed by microanalysis, however, it is unknown at this time if this takes up the neutral form or an ionic formulation in the solid-state. Crystallisation of the lead complex $[Pb(OTf)_2(pyNO)_2]$ was not achieved and thus the solid-state structure is unknown, however, the N-O stretching frequency of this complex suggest the metal centre may be triflate free.

Due to the successful coordination of three equivalents of pyNO to $Sn(OTf)_2$, the analogous reaction was attempted with $Pb(OTf)_2$, using MeCN as the solvent. A white solid product was precipitated from the reaction solution and collected for characterisation. Each of the spectroscopic methods utilised (^1H, $^{13}C\{^1H\}$, $^{19}F\{^1H\}$ NMR and IR) produced data consistent with the formation of the 1:2 complex $[Pb(OTf)_2(pyNO)_2]$, rather than the targeted 1:3. This formulation was also confirmed by microanalysis.

The bidentate $dppmO_2$ ligand was also utilised and see how coordination of this ligand to Pb(II) may differ from the lighter Sn(II) centre. A single molar equivalent of $dppmO_2$ was reacted with $Pb(OTf)_2$ in CH_2Cl_2 for 2 hours before a white precipitate of $[Pb(OTf)_2(dppmO_2)]$ was collected in a moderate yield. This was analysed by ^1H NMR spectroscopy which revealed a sharp triplet at 3.95 ppm with a coupling constant of 13.39 Hz and an integration of 2 protons, corresponding to the methylene bridge. The remaining aromatic protons are split into three aromatic multiplet resonances with an integration ratio of 8:4:8, shifted to higher frequency than the same resonances in the free ligand. These shifts are matched in the $^{13}C\{^1H\}$ NMR spectrum with the methylene carbon displayed as a triplet at 29.66 ppm with a coupling constant of $^1J_{PC}$ = 57.95 Hz. Except for the *para* carbon, which was resolved as a singlet, the remaining aromatic carbon

resonances were displayed as doublets with *ipso* having the largest coupling constant of $^{1}J_{PC}$ of 110.04 Hz. The $^{1}J_{PC}$ couplings of the *ipso* carbon in [Sn(OTf)$_2$(dppmO$_2$)] was 112.97 Hz. Analysis of [Pb(OTf)$_2$(dppmO$_2$)] *via* ^{31}P{^{1}H} NMR spectroscopy revealed a sharp singlet at 33.99 ppm with no ^{207}Pb satellite couplings resolved. The P=O stretches in the IR spectrum of the newly synthesised Pb(II) complex were observed at 1168 and 1147 cm^{-1}. Again, this is similar to that observed in the *bis*-[Sn(OTf)(dppmO$_2$)$_2$][OTf] where two peaks (1141 and 1131 cm^{-1}) were observed.

Microanalysis of this lead(II) product was consistent with [Pb(OTf)$_2$(dppmO$_2$)$_2$], rather than the expected [Pb(OTf)$_2$(dppmO$_2$)]. In order to determine the coordination environment at the metal, crystals suitable for X-ray diffraction were grown from a CH_2Cl_2 solution of complex layered with hexane. The structure of [Pb(OTf)$_2$(dppmO$_2$)$_2$] is shown in Figure 6.16. The bond lengths and angles of interest are shown in Table 6.11

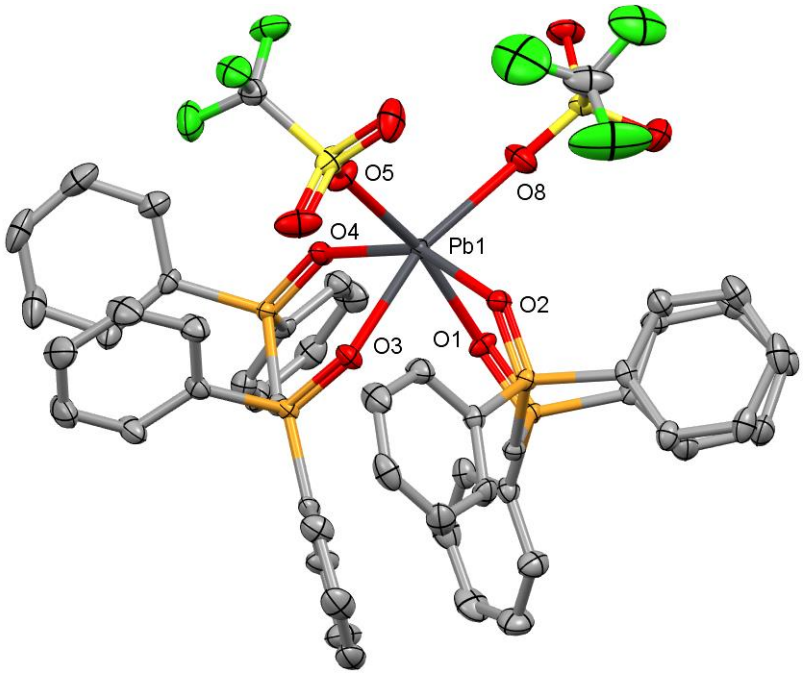

Figure 6.16 - Crystal structure of ***41*** [Pb(OTf)$_2$(dppmO$_2$)$_2$] showing the atom numbering scheme. Ellipsoids shown at 50% probability with H-atoms omitted for clarity.

Table 6.11 - Selected bond lengths (Å) and angles (°) for [Pb(OTf)$_2$(dppmO2$_2$)$_2$].

Bond Lengths / Å		Bond Angles / °	
Sn1 – O1	2.3658(17)	O1 – Sn1 – O2	79.95(6)
Sn1 – O2	2.3977(16)	O3 – Sn1 – O4	79.70(6)
Sn1 – O3	2.3743(16)	O5 – Sn1 – O8	117.91(6)
Sn1 – O4	2.4637(16)		
Sn1 – O5	2.7635(19)		
Sn1 – O8	2.876(2)		

This structure revealed the Pb(II) metal centre to be in a distorted 6-coordinate geometry with two bidentate $dppmO_2$ ligands, as well as two κ^1-triflate anions, in a *cis*-arrangement. The angle between the two triflate anions is 117.91(6)°, which highlights the level of distortion in this complex, being far removed from the ideal 90°. The $dppmO_2$ ligands have bite angles of 79.95(6) and 79.70(6)°, slightly smaller than the ~82° observed in both $[Sn(OTf)(dppmO_2)_2][OTf]$ and $[\{Sn(OTf)(dppmO_2)\}_2(\mu^2\text{-}OTf)_2]$.

6.3 – Conclusion

The work of this chapter moved forward with the study of the Group 14 metal triflates $M(OTf)_2$ (M = Sn, Pb) with use of the harder oxygen donor atoms, using the same ligands as employed in Chapter 3 (OPR_3, $dppmO_2$ and pyNO). A series of reactions were carried with $OPPh_3$ to $Sn(OTf)_2$ with varying molar ratios producing neutral and cationic complexes containing 2-4 $OPPh_3$ ligands. This was followed by reactions of tin triflate with the stronger σ-donor ligand, $OPMe_3$, with complexes being isolated with 2-4 $OPMe_3$ ligands. The 3:1 reaction produced a complex with an unusual extended crystal structure, containing solvent channels through the the *c*-axis with the full characterisation and properties being the focus of Chapter 7. Reactions of the heavier $Pb(OTf)_2$ were limited and focused on attempts to produce complexes with higher coordination numbers. This produced complexes contrasting the analogous Sn(II) structures, with the triflate anions being observed to be bound in a κ^2-fashion.

Coordination of a single equivalent of $dppmO_2$ to $Sn(OTf)_2$ produced $[\{Sn(OTf)(dppmO_2)\}_2(\mu\text{-}OTf)_2]$, taking up a the same triflate bridged dimer motif as the *bis*-phosphine oxide complexes. Reaction of a second equivalents of $dppmO_2$ produced $[Sn(OTf)(dppmO_2)_2][OTf]$ in a square based pyramidal geometry, containing a vacant site with no additional interactions. Repeating these reactions with $Pb(OTf)_2$ produced a neutral complex, $[Pb(OTf)_2(dppmO_2)_2]$, where both triflate anions are coordinated in an octahedral geometry.

The stronger donating pyNO ligand was utilised as a contrast to the OPR_3 (R = Me, Ph) ligands previously used, with both the 2:1 and 3:1 reaction being carried out. Crystallisation of the 2:1 product revealed a bridged dimer complex $[\{Sn(OTf)_2(pyNO)_2\}_2(\mu\text{-}pyNO)_2]$, with no *bis*-coordination complex being observed. In contrast to the triflate bridged dimer, seen for the OPR_3 ligands, this complex was bridged by the pyNO ligands.

6.4 Experimental

For supplier and purification of reagents and solvents, instrument specifications and NMR solvent references see Appendix A.

6.4.1.1 **[Sn(OTf)$_2$(OPPh$_3$)$_2$]**

$Sn(OTf)_2$ (83 mg, 0.2 mmol) was suspended in CH_2Cl_2 (10 mL) before the addition of $OPPh_3$ (111 mg, 0.4 mmol) and stirred for 1 h. Remaining particulates were removed by filtration before the solvent was concentrated by 50% and addition of Et_2O (10 mL). Precipitate evolved after further reduction in solvent level which was collected by filtration and dried *in vacuo*. Yield: 116 mg, 58 %. Required for $C_{38}H_{30}F_6O_8P_2S_2Sn.0.3(C_2H_5)_2O$ (998.12): C, 47.3; H, 3.4. Found C, 47.5; H, 3.3 %. ^{1}H NMR (CD_2Cl_2, 295 K): δ = 7.63 (m, [3H], Ar-H), 7.44 (m, [2H], Ar-H). ^{19}F{^{1}H} NMR (298 K, CD_2Cl_2): δ = −79.3 (s, OTf). ^{31}P{^{1}H} NMR (298 K, CD_2Cl_2): 43.9. IR (Nujol/cm^{-1}): 1085, 1067 (P=O).

6.4.1.2 **[Sn(OTf)(OPPh$_3$)$_3$][OTf]**

$Sn(OTf)_2$ (83 mg, 0.2 mmol) was suspended in CH_2Cl_2 (10 mL) before the addition of $OPPh_3$ (167 mg, 0.6 mmol) and stirred for 1 h. Remaining particulates were removed by filtration before the solvent was concentrated by 50% and addition of Et_2O (10 mL) caused precipitation which was collected by filtration and dried *in vacuo*. Yield: 168 mg, 67 %. Required for $C_{56}H_{45}F_6O_9P_3S_2Sn$ (1251.64): C, 53.7; H, 3.6. Found C, 54.0; H, 3.9 %. ^{1}H NMR (CD_2Cl_2, 295 K): δ = 7.63 (m, [1H], Ar-H), 7.52 (m, [2H], Ar-H), 7.40 (m, [2H], Ar-H). ^{19}F{^{1}H} NMR (298 K, CD_2Cl_2): δ = −79.4 (s, OTf). ^{31}P{^{1}H} NMR (298 K, CD_2Cl_2): 42.0 (s). IR (Nujol/cm^{-1}): 1059 (P=O).

6.4.1.3 **[Sn(OPPh$_3$)$_4$][OTf]$_2$**

$Sn(OTf)_2$ (83 mg, 0.2 mmol) was suspended in CH_2Cl_2 (10 mL) before the addition of $OPPh_3$ (223 mg, 0.8 mmol) and stirred for 1 h. Remaining particulates were removed by filtration before the solvent was concentrated by 50% and addition of Et_2O (10 mL) caused precipitation which was collected by filtration and dried *in vacuo*. Yield: 202 mg, 63 %. Required for $C_{74}H_{60}F_6O_{10}P_4S_2Sn.C_4H_{10}O$ (1604.11): C, 58.4; H, 4.4. Found: C, 58.7; H, 4.4 %. ^{1}H NMR (CD_2Cl_2, 295 K): δ = 7.63 (m, [1H], Ar-H), 7.52 (m, [2H], Ar-H), 7.40 (m, [2H], Ar-H). ^{19}F{^{1}H} NMR (298 K, CD_2Cl_2): δ = −79.4 (s, OTf). ^{31}P{^{1}H} NMR (298 K, CD_2Cl_2): 39.82 (s). IR (Nujol/cm^{-1}): 1059 (P=O).

6.4.1.4 **[Sn(OTf)$_2$(OPMe$_3$)$_2$]**

$Sn(OTf)_2$ (83 mg, 0.2 mmol) was suspended in CH_2Cl_2 (10 mL) before the addition of freshly sublimed $OPMe_3$ (37 mg, 0.4 mmol) and stirring for 1 h. Remaining particulates were removed by filtration before the solvent was concentrated by 50%. This was then layered with *n*-hexane (10 mL) where

crystals were grown, collected by filtration and dried *in vacuo*. Yield 154 mg, 77 %. Required for $C_{38}H_{30}F_6O_8P_2S_2Sn.0.3(C_2H_5)_2O$ (998.12): C, 16.0; H, 3.0. Found C, 15.7; H, 3.4 %. ^{1}H NMR (CD_2Cl_2, 295 K): δ = 1.83 (d, $^2J_{PH}$ = 13.5 Hz, [3H], Me). ^{19}F{^{1}H} NMR (298 K, CD_2Cl_2): δ = −79.4 (s, OTf). ^{31}P{^{1}H} NMR (298 K, CD_2Cl_2): 64.8 (s). IR (Nujol/cm^{-1}): 1063 (P=O).

6.4.1.5 **[Sn(OTf)$_2$(OAsPh$_3$)$_2$]**

$Sn(OTf)_2$ (83 mg, 0.2 mmol) was suspended in CH_2Cl_2 (10 mL) before the addition of $OAsPh_3$ (129 mg, 0.4 mmol) and stirred for 2 h. Remaining particulates were removed by filtration before the solvent was concentrated by 50% and addition of *n*-hexane (10 mL) caused the precipitation of a white solid which was collected by filtration and dried *in vacuo*. Yield: 127 mg, 60 %. Required for $C_{38}H_{30}As_2F_6O_8S_2Sn$ (1061.31): C, 43.00; H, 2.85. Found C, 43.24; H, 3.01 %. ^{1}H NMR (CD_3CN, 295 K): δ = 7.65 (br m, Ar-H). ^{19}F{^{1}H} NMR (298 K, CD_3CN): δ = −79.4 (s, OTf). IR (Nujol/cm^{-1}): 865, 852, 833 (As-O).

6.4.1.6 **[Sn(OTf)$_2$(OAsPh$_3$)$_3$]**

$Sn(OTf)_2$ (83 mg, 0.2 mmol) was suspended in CH_2Cl_2 (10 mL) before the addition of $OAsPh_3$ (193 mg, 0.6 mmol) and stirred for 2 h. Remaining particulates were removed by filtration before the solvent was concentrated by 50% and addition of *n*-hexane (10 mL) caused the precipitation of a white solid which was collected by filtration and dried *in vacuo*. Yield: 137 mg, 46 %. Required for $C_{56}H_{45}As_3F_6O_9S_2Sn.0.5CH_2Cl_2$ (1426.01): C, 47.6; H, 3.3. Found C, 47.6; H, 3.6. ^{1}H NMR (CD_3CN, 295 K): δ = 7.65 (br m, Ar-H).^{19}F{^{1}H} NMR (298 K, CD_3CN): δ = −79.4 (s, OTf). IR (Nujol/cm^{-1}): 824 (As-O).

6.4.1.7 **[Sn(OTf)$_2$(pyNO)$_2$]**

$Sn(OTf)_2$ (83 mg, 0.2 mmol) was suspended in CH_2Cl_2 (10 mL) before the addition of freshly sublimed pyridine N-oxide (38 mg, 0.4 mmol) and stirred for 1 h. Remaining particulates were removed by filtration before the solvent was concentrated by 50% and addition of Et_2O precipitated a white solid which was collected by filtration and dried *in vacuo*. Yield 74 mg, 61 %. Required for $C_{12}H_{10}F_6N_2O_8S_2Sn$ (607.05): C, 23.7; H, 1.7; N, 4.6. Found C, 24.0; H, 2.2; N, 4.7 %. ^{1}H NMR (CD_2Cl_2, 295 K): δ = 8.67 (m, [2H], Ar-H), 7.97 (m, [1H], Ar-H), 7.74 (m, [2H], Ar-H). ^{19}F{^{1}H} NMR (298 K, CD_2Cl_2): δ = −79.1 (s, OTf). IR (Nujol/cm^{-1}): 1216, 1205 (N=O).

6.4.1.8 **[Sn(OTf)$_2$(pyNO)$_3$]**

$Sn(OTf)_2$ (83 mg, 0.2 mmol) was suspended in CH_2Cl_2 (10 mL) before the addition of freshly sublimed pyridine N-oxide (57 mg, 0.6 mmol) and stirred for 1 h. Remaining particulates were removed by filtration before the solvent was concentrated by 50% and addition of Et_2O precipitated a white

solid which was collected by filtration and dried *in vacuo*. Yield 85 mg, 57 %. Required for $C_{17}H_{15}F_6N_3O_9S_2Sn$ (744.61): C, 26.2; H, 2.2; N, 5.6. Found C, 26.2; H, 2.3; N, 5.6. ^{1}H NMR (CD_3CN, 295 K): δ = 8.52 (m, [2H], Ar-H), 8.05 (m, [1H], Ar-H), 7.79 (m, [2H], Ar-H). $^{19}F\{^1H\}$ NMR (298 K, CD_3CN): δ = −79.2 (s, OTf). IR (Nujol/cm^{-1}): 1226, 1214 (N=O).

6.4.1.9 **[Sn(OTf)$_2$(dppmO$_2$)]**

$Sn(OTf)_2$ (83 mg, 0.2 mmol) was suspended in CH_2Cl_2 (10 mL) before the addition of $dppmO_2$ (83 mg, 0.2 mmol) and stirred for 1 h, over this time a yellow solid formed. This was removed from the solution by filtration before the solvent was concentrated by 50% and addition of Et_2O (10 mL) caused precipitation which was collected by filtration and dried *in vacuo*. Yield: 140 mg, 84 %. Required for $C_{27}H_{22}F_6O_8P_2S_2Sn$ (833.19): C, 38.9; H, 2.7. Found: C, 38.9; H, 2.8 % ^{1}H NMR (CD_2Cl_2, 295 K): δ = 7.63 (m, [8H], Ar-H), 7.51 (m, [4H], Ar-H), 7.35 (m, [8H], Ar-H), 3.96 (t, $^2J_{PH}$ = 12.96 Hz, [2H], CH_2). $^{19}F\{^1H\}$ NMR (298 K, CD_2Cl_2): δ = −79.3 (s, OTf). $^{31}P\{^1H\}$ NMR (298 K, CD_2Cl_2): 40.0 (s, $^2J_{SnP}$ = 92.8). IR (Nujol/cm^{-1}): 1136 (P=O).

6.4.1.10 **[Sn(OTf)(dppmO$_2$)$_2$][OTf]**

$Sn(OTf)_2$ (83 mg, 0.2 mmol) was suspended in CH_2Cl_2 (10 mL) before the addition of $dppmO_2$ (166 mg, 0.4 mmol) and stirred for 1 h, over this time a yellow solid formed. This was removed from the solution by filtration before the solvent was concentrated by 50% and addition of Et_2O (10 mL) caused precipitation which was collected by filtration and dried *in vacuo*. Yield: 224 mg, 87 %. Required for $(C_{52}H_{44}F_6O_{10}P_4S_2Sn).0.5CH_2Cl_2$ (1292.09): C, 48.8; H, 3.5. Found: C, 48.7; H, 2.7% ^{1}H NMR (CD_2Cl_2, 295 K): δ = 7.59 (m, [12H], Ar-H), 7.33 (m, [8H], Ar-H), 4.09 (t, $^2J_{PH}$ = 13.33 Hz, [2H], CH_2). $^{19}F\{^1H\}$ NMR (298 K, CD_2Cl_2): δ = −79.3 (s, OTf). $^{31}P\{^1H\}$ NMR (298 K, CD_2Cl_2): 35.4 (s). IR (Nujol/cm^{-1}): 1141, 1131 (P=O).

6.4.1.11 **[Pb(OTf)$_2$(OPMe$_3$)$_4$]**

$Pb(OTf)_2$ (101 mg, 0.2 mmol) was suspended in CH_2Cl_2 (10 mL) before the addition of freshly sublimed $OPMe_3$ (74 mg, 0.4 mmol) and stirring for 2 h. Remaining particulates were removed by filtration before the solvent was concentrated by 50%. This was then layered with *n*-hexane (10 mL) where crystals were grown, collected by filtration and dried *in vacuo*. Yield: 84 mg, 48 %. Required for $C_{14}H_{36}F_6O_{10}P_4S_2Pb$ (873.64): C, 16.0; H, 3.0. Found C, 15.7; H, 3.4. ^{1}H NMR (CD_2Cl_2, 295 K): δ = 1.58 (d, $^2J_{PH}$ = 13.5 Hz, Me). $^{19}F\{^1H\}$ NMR (298 K, CD_2Cl_2): δ = −79.4 (s, OTf). $^{31}P\{^1H\}$ NMR (298 K, CD_2Cl_2): 53.6 (s). IR (Nujol/cm^{-1}): 1115, 1100 (P=O).

6.4.1.12 **[Pb(OTf)$_2$(pyNO)$_2$]**

$Pb(OTf)_2$ (152 mg, 0.3 mmol) was suspended in CH_3CN (20 mL) before the addition of freshly sublimed pyridine N-oxide (57 mg, 0.6 mmol) and stirred for 1 h. Remaining particulates were removed by filtration before the solvent was concentrated by 50% and addition of Et_2O precipitated a white solid which was collected by filtration and dried *in vacuo*. Yield 120 mg, 66 %. Required for $C_{12}H_{10}F_6N_2O_8S_2Pb$ (607.05): C, 20.7; H, 1.5; N, 4.0. Found C, 20.7; H 2.0; N, 3.9. ^{1}H NMR (CD_2Cl_2, 295 K): δ = 8.44 (m, [2H], Ar-H), 7.84 (m, [1H], Ar-H), 7.70 (m, [2H], Ar-H). ^{19}F{^{1}H} NMR (298 K, CD_2Cl_2): δ = −79.3 (s, OTf). IR (Nujol/cm^{-1}): 1216 (N=O).

6.4.1.13 **[Pb(OTf)$_2$(dppmO$_2$)$_2$]**

$Pb(OTf)_2$ (101 mg, 0.2 mmol) was suspended in CH_2Cl_2 (10 mL) before the addition of $dppmO_2$ (83 mg, 0.2 mmol) and stirred for 2 h. Remaining particulates were removed by filtration before the solvent was concentrated by 50%, layered with *n*-hexane and stored at -20°C, causing crystallisation overnight. These were collected by filtration and dried *in vacuo* to give a white solid. Yield 135 mg, 46 %. Required for $C_{52}H_{44}F_6O_{10}P_4S_2Pb.2CH_2Cl_2$ (1507.98): C, 43.0; H, 3.2. Found C, 43.4; H, 3.4. ^{1}H NMR (CD_3CN, 295 K): δ = 7.62 (m, [8H], Ar-H), 7.50 (m, [4H], Ar-H), 7.33 (m, [8H], Ar-H), 3.95 (t, $^2J_{PH}$ = 13.4 Hz, [2H], CH_2). ^{19}F{^{1}H} NMR (298 K, CD_3CN): δ = −79.3 (s, OTf). ^{31}P{^{1}H} NMR (298 K, CD_3CN): 34.0 (s). IR (Nujol/cm^{-1}): 1168, 1147 (P=O).

6.5 – References

1 K. R. Cairns, W. Levason, G. Reid and W. Zhang, *Polyhedron*, 2021, **210**, 115529.
2 K. R. Cairns, W. Levason, G. Reid and W. Zhang, *Polyhedron*, 2021, **207**, 115367.
3 K. R. Cairns, R. P. King, R. D. Bannister, W. Levason and G. Reid, *Dalton Trans.*, 2023, **2**, 2293–2308.
4 J. A. McCleverty and T. J. Meyer, *Comprehensive Coordination Chemistry II*, Elsevier Science S.A., Oxford, 2nd edn., 2004.
5 F. Cheng, M. F. Davis, A. L. Hector, W. Levason, G. Reid, M. Webster and W. Zhang, *Eur. J. Inorg. Chem.*, 2007, **2007**, 2488–2495.
6 Z. L. Kaluski and Y. T. Struchkov, *J. Struct. Chem.*, 1966, **6**, 705–713.
7 T. Szymanska-Buzar, T. Glowiak and I. Czelusniak, *Main Gr. Met. Chem.*, 2001, **24**, 821–822.
8 E. Wlaźlak, W. Macyk, W. Nitek and K. Szaciłowski, *Inorg. Chem.*, 2016, **55**, 5935–5945.
9 K. George, A. L. Hector, W. Levason, G. Reid, G. Sanderson, M. Webster and W. Zhang, *Dalton Trans.*, 2011, **40**, 1584.
10 M. F. Davis, W. Levason, G. Reid and M. Webster, *Polyhedron*, 2006, **25**, 930–936.
11 M. S. Woodward, R. P. King, R. D. Bannister, J. Grigg, G. McRobbie, W. Levason and G. Reid, *Inorganics*, 2022, **10**, 107.
12 F. Cheng, J. M. Dyke, F. Ferrante, A. L. Hector, W. Levason, G. Reid, M. Webster and W. Zhang, *Dalton Trans.*, 2010, **39**, 847–856.
13 J. Burt, W. Levason and G. Reid, *Coord. Chem. Rev.*, 2014, **260**, 65–115.
14 R. Selvaraju, K. Panchanatheswaran and V. Parthasarathi, *Acta Crystallogr. Sect. C Cryst. Struct. Commun.*, 1998, **54**, 905–906.
15 C. Gurnani, A. L. Hector, E. Jager, W. Levason, D. Pugh and G. Reid, *Dalton Trans.*, 2013, **42**, 8364–8374.
16 J. Burt, University of Southampton, 2016.
17 J. Burt, W. Grantham, W. Levason and G. Reid, *Dalton Trans.*, 2015, **44**, 11533–11541.
18 P. A. W. Dean, *Can. J. Chem.*, 1982, **60**, 2921–2926.
19 P. A. W. Dean, D. D. Phillips and L. Polensek, *Can. J. Chem.*, 1981, **59**, 50–61.
20 I. Lange, J. Krahl, P. G. Jones and A. Blaschette, *J. Organomet. Chem.*, 1994, **474**, 97–106.
21 A. P. Singh, H. W. Roesky, E. Carl, D. Stalke, J.-P. Demers and A. Lange, *J. Am. Chem. Soc.*, 2012, **134**, 4998–5003.
22 M. Bouška, L. Dostál, A. Růžička and R. Jambor, *Organometallics*, 2013, **32**, 1995–1999.
23 I. Objartel, H. Ott and D. Stalke, *Z. Anorg. Allgem. Chem.*, 2008, **634**, 2373–2379.
24 R. Bandyopadhyay, B. F. T. Cooper, A. J. Rossini, R. W. Schurko and C. L. B. Macdonald, *J. Organomet. Chem.*, 2010, **695**, 1012–1018.
25 M. G. B. Drew and D. G. Nicholson, *J. Chem. Soc. Dalton. Trans.*, 1986, 1543.
26 P. A. Rupar, V. N. Staroverov and K. M. Baines, *Science (80-.).*, 2008, **322**, 1360–1363.
27 J. C. Avery, M. A. Hanson, R. H. Herber, K. J. Bladek, P. A. Rupar, I. Nowik, Y. Huang and K. M. Baines, *Inorg. Chem.*, 2012, **51**, 7306–7316.
28 E. Hough, D. G. Nicholson and A. K. Vasudevan, *J. Chem. Soc. Dalton. Trans.*, 1989, 2155.
29 C. Beattie, P. Farina, W. Levason and G. Reid, *Dalton Trans.*, 2013, **42**, 15183.
30 R. P. King, J. M. Herniman, W. Levason and G. Reid, *Inorg. Chem.*, 2023, **62**, 853–862.
31 J. D. Donaldson and D. G. Nicholson, *J. Chem. Soc. A*, 1970, 145–150.
32 C. R. Hilliard, N. Bhuvanesh, J. A. Gladysz and J. Blümel, *Dalton Trans.*, 2012, **41**, 1742–1754.
33 M. Rahm, R. Hoffmann and N. W. Ashcroft, *Chem. – A Eur. J.*, 2016, **22**, 14625–14632.
34 K. Grudzień, T. Basak, M. Barbasiewicz, T. M. Wojciechowski and M. Fedoryński, *J. Fluor. Chem.*, 2017, **197**, 106–110.
35 G. B. Deacon and J. H. S. Green, *Spectrochim. Acta Part A Mol. Spectrosc.*, 1969, **25**, 355–364.
36 D. M. L. Goodgame and F. A. Cotton, *J. Chem. Soc.*, 1961, 3735.
37 N. Wee Kong, C. Wei, V. G. Kumar Das and R. J. Butcher, *J. Organomet. Chem.*, 1989, **361**,

53–61.
38 R. R. Shifrina, I. P. Romm, E. N. Gur'yanova and N. A. Rozanel'skaya, *J. Appl. Spectrosc.*, 1981, **34**, 84–88.
39 D. H. Johnston and D. F. Shriver, *Inorg. Chem.*, 1993, **32**, 1045–1047.
40 J. V. Quagliano, J. Fujita, G. Franz, D. J. Phillips, J. A. Walmsley and S. Y. Tyree, *J. Am. Chem. Soc.*, 1961, **83**, 3770–3773.
41 B. P. Johnson, S. Almstätter, F. Dielmann, M. Bodensteiner and M. Scheer, *Z. Anorg. Allgem. Chem.*, 2010, **636**, 1275–1285.
42 M. A. Edelman, P. B. Hitchcock and M. F. Lappert, *J. Chem. Soc., Chem. Commun.*, 1990, 1116–1118.
43 F. Guégan, V. Tognetti, L. Joubert, H. Chermette, D. Luneau and C. Morell, *Phys. Chem. Chem. Phys.*, 2016, **18**, 982–990.
44 B. J. Coe and S. J. Glenwright, *Coord. Chem. Rev.*, 2000, **203**, 5–80.
45 R. D. Rogers and A. H. Bond, *Inorg. Chim. Acta*, 1992, **192**, 163–171.
46 E. A. Pedrick, G. Wu and T. W. Hayton, *Inorg. Chem.*, 2015, **54**, 7038–7044.
47 J.-C. Berthet, M. Nierlich, Y. Miquel, C. Madic and M. Ephritikhine, *Dalton Trans.*, 2005, **3**, 369–379.
48 F. Basuli, U. J. Kilgore, D. Brown, J. C. Huffman and D. J. Mindiola, *Organometallics*, 2004, **23**, 6166–6175.
49 T. Mandai, S. Tsuzuki, K. Ueno, K. Dokko and M. Watanabe, *Phys. Chem. Chem. Phys.*, 2015, **17**, 2838–2849.
50 D. J. Hutchinson, M. P. James, L. R. Hanton and S. C. Moratti, *Inorg. Chem.*, 2014, **53**, 2122–2132.
51 M. B. Kindervater, T. Hynes, K. M. Marczenko and S. S. Chitnis, *Dalton Trans.*, 2020, **49**, 16072–16076.
52 L. Dostál, P. Novák, R. Jambor, A. Růžička, I. Císařová, R. Jirásko and J. Holeček, *Organometallics*, 2007, **26**, 2911–2917.
53 S. A. Bourne and L. J. Moitsheki, *J. Chem. Crystallogr.*, 2007, **37**, 359–367.
54 Y.-H. Zhao, H.-B. Xu, K.-Z. Shao, Y. Xing, Z.-M. Su and J.-F. Ma, *Cryst. Growth Des.*, 2007, **7**, 513–520.
55 Y.-H. Zhao, Z.-M. Su, Y. Wang, Y.-M. Fu, S.-D. Liu and P. Li, *Inorg. Chem. Commun.*, 2007, **10**, 410–414.
56 J. Mendez-Arroyo, J. Barroso-Flores, A. M. Lifschitz, A. A. Sarjeant, C. L. Stern and C. A. Mirkin, *J. Am. Chem. Soc.*, 2014, **136**, 10340–10348.

Chapter 7 – Self-assembly of $[Sn(OPMe_3)_3(CF_3SO_3)_2]_6$ metallocyclic Sn(II) hexamer stacks with CF_3-lined channel interiors.

During the work of the previous chapter, the reaction of three equivalents of $OPMe_3$ with $Sn(OTf)_2$ produced a unique structure in the solid state, with a triflate bridged, hexameric array of complexes made up of $[\{Sn(OTf)_2(OPMe_3)_3]$ units. The full characterisation and properties of this structure are explored here including gas-adsorption and PXRD experiments. This species is the focus of this chapter of work, along with analogous reactions exploring the changes observed when changing the anion or metal, in an attempt to produce a similar structural motif.

7.1 Introduction

The coordination chemistry of OPR_3 and other oxygen donor ligands to Sn(II) halide systems is discussed in Chapter 6, as well as the coordination complexes of these ligands systems containing weakly coordinating anions such as $[BF_4]^-$, $[SiF_6]^{2-}$ or $[SbF_6]^{2-}$.[1–3] These less Lewis basic anions have been shown to lead to a diverse chemistry when compared with the halides, specifically with the formation of highly Lewis acidic *p*-block cations of the Group 14 metals. In recent years, these cations, and routes to their synthesis has been an area of interest within both organic and organometallic chemistry.[4–6] The stabilisation provided by these weakly coordinating anions has facilitated the synthesis of highly reactive species such the homoleptic phosphine complexes $[Ge(PPh_3)_3]^+$ and $[Ag(P_4)_2]^+$.[7,8] Many fluorine comtaning anions such as triflate $[OTf]^-$, fluorous aluminates or bulky fluorinated tetraarylborates, such as $Na[BAr^F]$ are weakly coordinating anions due to the electron withdrawing fluorine atom, removing electron density from a donor atom or better diffusing the electron density over the molecule. The incorporation of these anions is known to alter the properties of complexes synthesised, often introducing sort after properties such as giving better solubility in low-polarity solvents, increased hydrophobicity and the lowering of the dimensionality of MOF/PCP structures.

The triflate anion has more recently been used in work focusing on the developments of cations of Group 14 metals including stabilisation of 'naked' Ge(II) dications. This has been observed encapsulated within a 2.2.2-cryptand,[9] and softer donors such as pnictines and thioether macrocycles.[10] Reaction of the thioether macrocyclic ligands [9]aneS_3 (1,4,7- trithiacyclononane), [12]aneS_4 (1,4,7,10-tetrathiacyclododecane), or [24]aneS_8 to $M(OTf)_2$ (M = Sn, Pb) or $[GeCl_2$.dioxan (in the presence of 2 eq of TMSOTf) produced endocyclic coordination; where the

metal centre is found centrally in the macrocyclic ligand.[10] This directly contrasts the chemistry observed for coordination of these ligands directly to GeX_2, which showed exocyclic coordination.[11] Reaction of [9]andS_3 to each of the metal triflates produced complexes $[M([9]aneS_3)][OTf]_2$ (M = Ge, Sn, Pb). The crystal structures of these complexes revealed κ^3-coordination of the ligand in a tripodal geometry with the triflate anions showing weak coordination to the respective metal centre, with the tin analogue being shown in Figure 7.1. Of this series of metal complexes, the Pb(II) analogue was also shown to form additional interactions to through triflate bridges, giving octahedral metal centres in a 1D-polymer.

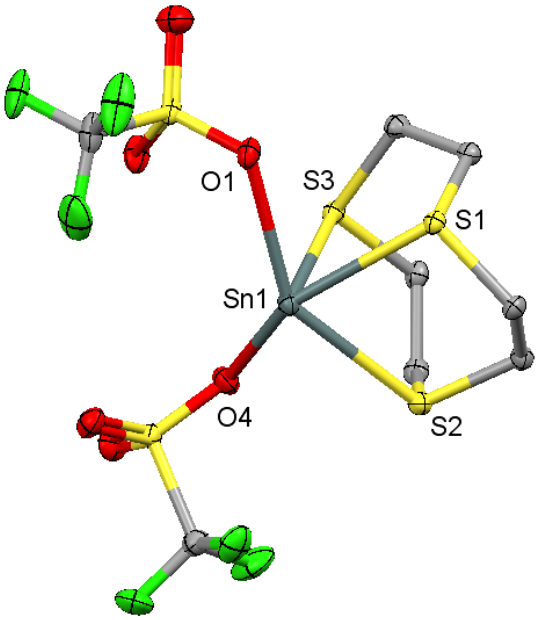

Figure 7.1 - Crystal structure of $[Sn([9]aneS_3)][OTf]_2$ showing the atomic numbering scheme. Redrawn from Ref[10] with H-atoms omitted for clarity.

Halide abstraction from the neutral neutral coordination product was shown to be possible with use of TMSOTf by Burford and co-workers, as discussed in Chapter 6, producing cationic complexes $[MX_{2-n}(L)][OTf]_n$ (n = 1, 2).[12] Adapting this method, recent work in Reid group has explored whether TMSOTf can also be used for the dehalogenation of fluoride from reactive M(IV) (M = Sn, Ge) complexes. As well as exploring complexes containing different halogens, a range of other halide abstractors including $Na[BAr^F]$ and Lewis acidic metal halides such as $AlCl_3$ and $FeCl_3$ were trialled.[13–15] This type of substitution has been used to abstract halides from a metal centre, producing a vacant coordination site which can be subsequently filled by the weakly coordinating anions.[16] The weakly coordinating anions then likely dissociate in solution, allowing for follow-up reactions such as secondary ligand additions to be carried out. The complexes explored generally retained one or more of the original halides present, with the final products being mixed anionic species. Work carried out in previous chapters have explored coordination of soft pnictines and harder phosphine oxides to $M(OTf)_2$ (M = Ge, Sn, Pb), shows that the chemistry exhibited by these complexes differs to the corresponding halide complexes.[17] It has been shown in Chapters 5 and 6

that the chemistry exhibited by the triflate complexes differs to that of the corresponding halide complexes. The use of the triflate starting materials removes the need for halide substitution post-coordination, requiring breaking the strong M-X bond when forming the cationic species. It was hoped that the high lability of these anions would allow for the easy formation of cationic species of the type $[M(OTf)_{2-x}(L)_m][OTf]_x]$. It was shown in Chapters 5 and 6 that the coordination complexes of the Group 14 metal triflates have a preference for forming oligomers.

Substitution of the anions associated with a complex can have a large effect on the properties and structure of a complex, as was shown with the substitution of the $[OTf]^-$ anion for the larger and bulkier $[BAr^F]^-$ anion used in Chapter 5.[17] The anionic substitution cleaved the bridged complex $[\{Pb(MeC(CH_2PPh_2)_3)\}_2(\mu\text{-}OTf)_3][OTf]$ to produce the dicationic complex $[Pb\{MeC(CH_2PPh_2)_3\}][BAr^F]_2$. As was discussed in Chapter 1, the development of the $[BAr^F]^-$ anion was a major advancement in the field of weakly coordinating anions, due to its complete lack of coordinating ability. This allowed for the study of highly reactive species that would otherwise not be formed, such as the successful coordination of [24]aneS_8 to a Na^+ cation, as shown in Figure 7.2.[18] The $[BAr^F]^-$ anion provides no competition, allowing for coordination of the thioether macrocycle, despite the mismatch of hardness. This was after the successful coordination of the harder N-donor azamacrocycles Me_3-tacn and Me_4-cyclam, both of which were carried out using $Na[BAr^F]$ as a starting material, allowing access to a 'naked' Na^+ cation.[19]

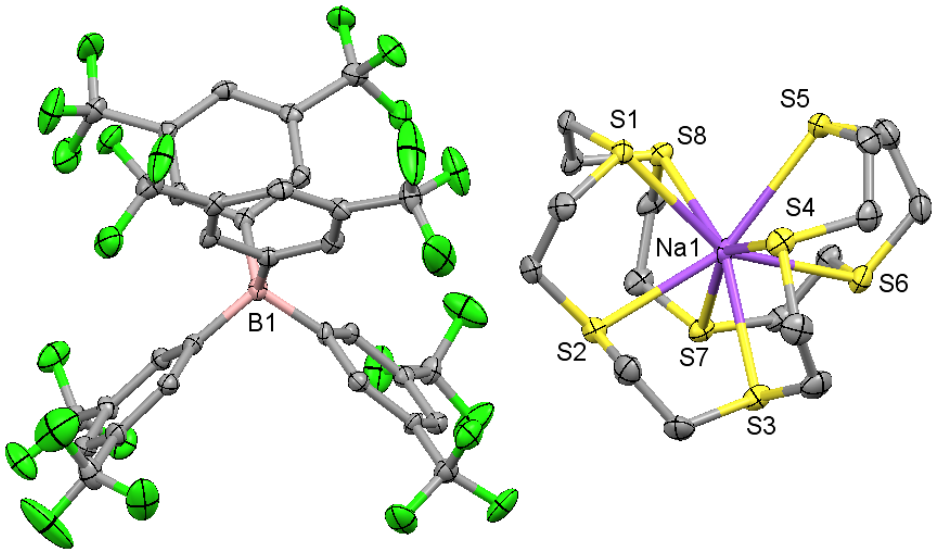

Figure 7.2 - Crystal structure of $[Na\{[24]aneS_8\}][BAr^F]$ showing the atomic numbering scheme. Redrawn from Ref[18] with H-atoms omitted for clarity.

Another important fluoroinorganic anion is the fluorosulfate anion $[SO_3F]^-$, while structurally related to triflate, it is known to have a slightly higher binding strength than triflate.[20,21] This has been previously synthesised by reaction of the corresponding metal(II) fluoride with excess amounts of fluorosulfonic acid, an acid of similar strength acid to trifluoromethanesulfonic acid. It has also been shown that this salt metathesis reaction is possible using other metal halides, which

avoids the production of dangerous HF acid as a side product.[20] This method of production was used for the synthesis of this starting material with further details being discussed later in this chapter.[22] The formation of $Sn(SO_3F)_2$ was confirmed *via* crystallisation of the product, from storage of the mother liquor at -30°C overnight, as well as IR spectroscopy, with $Sn(SO_3F)_2$ having been spectroscopically characterised previously.[23] The crystal structure of $Sn(SO_3F)_2$ had been previously reported, two crystallographically unique tin(II) centres being located in the asymmetric unit cell, each being octahedral in geometry with a network of $[SO_3F]^-$ anion bridges.[24] Research into complexes containing this fluorosulfate anion is very limited, with only a few structural examples containing the fluorosulfate anion, with only two examples of main group elements being found in the CCDC; $[SnMe_2(SO_3F)_2]_x$ and $[SnMe_2(SO_3F)_2(MeCN)_2]$.[25,26]

Throughout this thesis, the triflate containing complexes produced have shown a preference for the formation of additional secondary interactions, with the structures of many complexes showing dimer, oligomer and polymerisation in the solid state. This includes triflate bridging in complexes such as $[M(OTf)_2\{C_6H_4(PR_2)_2\}]$ (M = Sn, Pb; R = Ph, Me) and hydrogen bonding, in the presence of aquo ligands, such as the 24-membered pseudomacrocyclic arrangement adopted in $[[In(OTf)_2(Ph_3PO)_4][In\{(OH_2)_4(OTf)_4\}(Ph_3PO)_2]$.[17,27]

A recent publication in *Science* by Itoh and co-workers*.* described the synthesis of oligoamide nanorings that had a fluorine dense surface leading to high hydrophobicity inside the channels, with an internal diameter of 0.9 - 1.9 nm.[28] These were synthesised by amide-forming condensation reactions using varying ratios of 2,3-difluoroterephthalic acid and a derivative of 3,5-diamino-4-fluorobenzamide with an R-group of $C_{12}H_{25}$. The different ratios produced nanochannel structures with small internal diameters and high fluorine densities on the inner surface being dependent on this ratio, the structure of one of these complexes is shown in Figure 7.3 In each of the complexes synthesised by Itoh and co-workers, there are intramolecular H-bonds between the proton on the newly formed amide bond and fluoride, greatly increasing the stability of the cyclic structure. When modelling the core structure with DFT calculations, they also modelled these H-bonds, with each of the fluorine atoms oriented to the centre of this channel, suggesting these "C–F···H–N" H-bonds determine, at least partially, the conformation formed in the solid state. The hydrogen bonding is illustrated by dotted lines on the structural diagram in Figure 7.3(b).

These nanoring arrays were annealed in pentadecane and subjected to transmission electron microscopy (TEM) which showed that these complexes can form very long nanotubes with uniform diameters. The diameters measured from these TEM images match almost exactly with the external diameters of the DFT calculated structure of the respective complex with the smallest

of these being 5.2 nm (0.9 nm internal diameter). The long nanotube structures suggest a strong drive to form these H-bonded channels in 1D. These nanotubes were then tested for the permeation of water by insertion to vesicles.

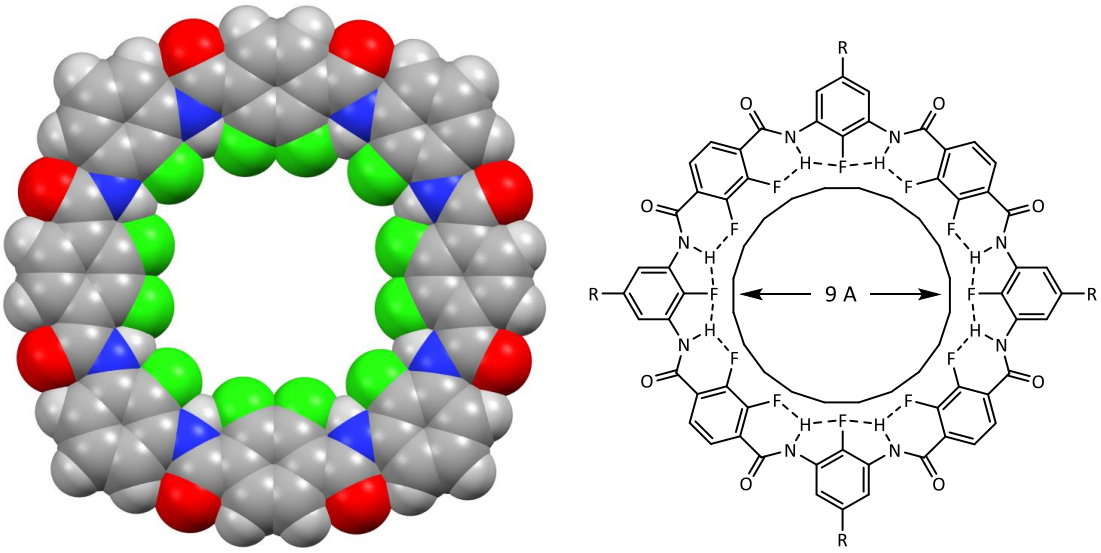

(a) (b)

Figure 7.3 – Space-filling crystal structure (a) and structural diagram (b) of $^{F12}NR_4$ produced by Itoh. Fluorine (green) and the interactions formed through H-bonds to adjacent amide protons. Redrawn from Ref[28].

It was shown that the hydrophobic surface promotes the ultrafast permeation of water through these channels by interrupting H-bonded water clusters and allows for the movement of individual water molecules, increasing the flow-rate, with this behaviour being shown in Figure 7.4. As well as a significant increase to the rate of permeation through the membrane types tested, these fluorous-lined channels also showed selectivity against the transport of dissolved anions and salt through the channel. Using stop-flow fluorescence measurements, the selectivity of these channels was tested with a NaCl solution. Vesicles containing the fluorous-lined channels showed that the water movement of water through the channel was selective, with very little movement of the dissolved ions. The powerful electrostatic barrier provided by the electronegative fluorous atoms at the surface repelled the chloride anions to prevent their transport out of the vesicles.[28]

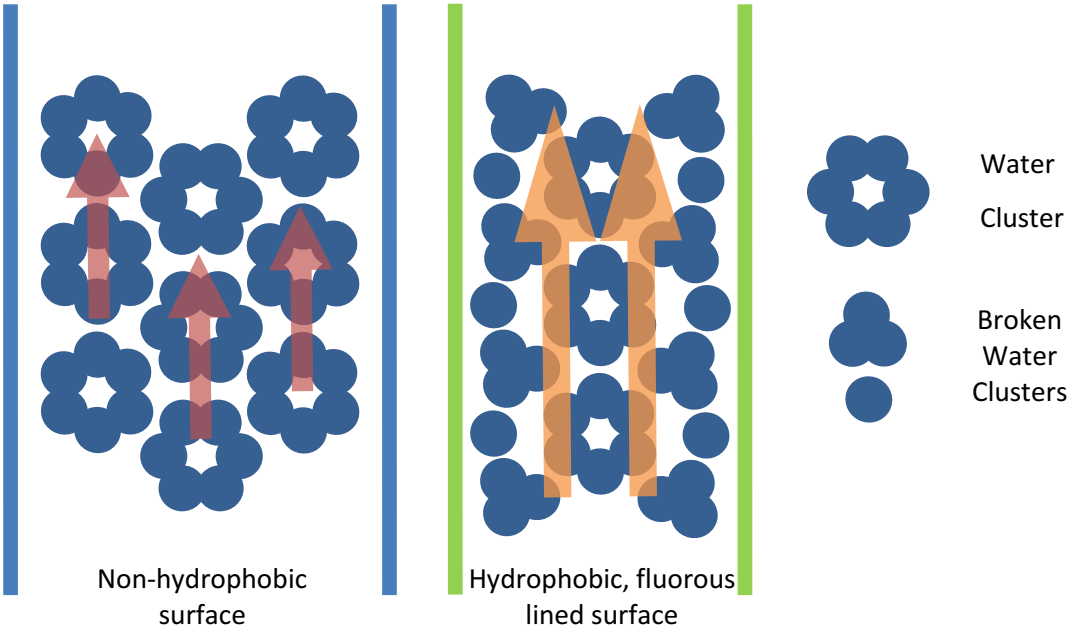

Figure 7.4 - Proposed mechanism for the transport of water through hydrophobic (right) and non-hydrophobic (left) nanochannels. Redrawn from Ref[28].

MOF and PCP type structures can be functionalised at either at the linker molecules, or at the metal centres directly. Organic linkers like those used in the work by Itah and co-workers can be functionalised with the addition of differing R-groups, before the growth of the extended structure. The addition of fluorous groups such as –F, $-CF_3$, $-CH_3$ and $–OCF_3$ can lower the dimensionality of the MOF/PCP formed, increasing the solubility in low-polarity solvents and increasing the hydrophobicity of the surface. This effect is known to increase the selectivity and capacity of the framework towards the adsorption of hydrocarbons as shown by the addition of $-CF_3$ groups to a Ag(I)-based MOF.[29] The high electronegativity and low polarizability of the fluorine atom, it can give MOFs preferential properties and unique characteristics such as chemical stability, hydrophobicity, selective gas absorbency and lower boiling points. Incorporation of fluorine containing substituents, such as fluorinated arenes, trifluoromethyl groups or addition of fluorinated inorganic anions (e.g. $[PF_6]^-$, $[SiF_6]^{2-}$) can not only stabilise the complex but also greatly increase the gas absorbency by acting as adsorption site for gases such as N_2, H_2 or CO. Some of the commonly utilised inorganic species used as linkers in these MOF/PCP type structures are $[AF_6]^{2-}$ (A = Si, Ge, Sn, Ti) which act as a bridging ligand between metals due to the high charge density with a number of compounds formulated as $[M(AF_6)(L)_2]$ (M = Fe - Zn where L is a pyridine derived bridging ligand. The monoanionic building blocks $[PF_6]^-$, $[BF_4]^-$ and $[CF_3SO_3]^-$ all have a lower charge density compared to the dianions discussed above. This is due to the delocalisation of the negative charge over the molecule, leading to weaker intermolecular interactions and thus lower melting points and in some cases, use as ionic liquids.[30] The weaker intermolecular interactions means the bridging ability is also weaker and

leads to the lowering of dimensionality of the formed complexes, commonly producing 2D sheets or 1D nanowires/channels.[31,32] Along with lower dimensionality, the weaker intermolecular bonding causes fluorinated MOF/PCP complexes often have a higher of flexibility than the non-fluorinated analogues. This flexibility can aid in the gas-sorption properties and breathing properties as seen in the MIL-53 system, a breathing MOF, and similar motifs.[33]

The work of this chapter focuses on the synthesis, characterisation and properties of the unique hexameric extended structure observed for $[Sn(OTf)_2(OPMe_3)_3]$. This complex was produced as part of a series of reactions with varying ratios of $OPMe_3$ with $Sn(OTf)_2$. This will include both PXRD and adsorption measurements due to the potential voids associated with the hexameric array of metal centres. It will also explore the synthesis of other, related complexes which may take up the same or similar extended structure including use of other metals(II) from Group 14 and use of the structurally related fluorosulfate anion. Both the spectroscopic and structural properties of these potentially analogous species will be explored.

7.2 Results and Discussion

The reaction of $Sn(OTf)_2$ with three molar equivalents of $OPMe_3$ in CH_2Cl_2 is shown in Scheme 7.1, and readily forms a white solid in a high yield, with microanalysis confirming the empirical formulation to be $[Sn(OTf)_2(OPMe_3)_3]$.[34] Attempts to synthesise complexes of four and five-equivalents of $OPMe_3$ were found to produce the same 1:3 Sn : $OPMe_3$ ratio by micro-analytical and spectroscopic measurements. This gave a suggestion that there was an inherent stability of the $[Sn(OTf)_2(OPMe_3)_3]$ compound compared with other possible complexes with a higher Sn : $OPMe_3$ ratio.

$$Sn(OTf)_2 + 3OPMe_3 \longrightarrow [Sn(OTf)_2(OPMe_3)_3]$$

Scheme 7.1 - Reaction scheme for the synthesis of $[Sn(OTf)_2(OPMe_3)_3]$.

Crystals of $[Sn(OTf)_2(OPMe_3)_3]$, suitable for single crystals X-ray diffraction were grown by both diffusion of *n*-hexane into a CH_2Cl_2 solution. Crystals were also grown through vapour diffusion of $(CH_2)_2O$ into a MeCN solution, with the crystals matching the unit cell parameters and space group of the previous collection, despite the change on solvent. The crystal structure of $[Sn(OTf)_2(OPMe_3)_3]$ shows a pseudo-octahedral geometry at Sn(II) with three $OPMe_3$ ligands in a *facial* arrangement around the tin(II) centre and the other face being occupied by Sn-O contacts to three triflate anions, as shown in Figure 7.5(a). This contrasts the structures of other OPR_3 complexes of Sn(II) observed in the previous two chapters, with these complexes generally taking up a disphenoidal or square-based pyramidal geometry at the metal centre, depending on the coordination number. The $Sn\text{-}O_{OPMe3}$ bond distances of $[Sn(OTf)_2(OPMe_3)_3]$ range from 2.0942(11) - 2.1669(11) Å, similar to the $Sn\text{-}O_{OPPh3}$ distances observed in $[Sn(OTf)(OPPh_3)_3][OTf]$. Of the $Sn\text{-}O_{OTf}$ contacts of $[Sn(OTf)_2(OPMe_3)_3]$, two were bridging interactions measured as 2.858(1) and 3.028(2) Å while the remaining terminal triflate anion had an $Sn\text{-}O_{OTf}$ distance of 3.082(1) Å. In the solid-state, $[Sn(OTf)_2(OPMe_3)_3]$ oligomerises through bridging triflate interactions to form the hexameric metallocyclic array shown in Figure 7.5(b). The hexameric metallocycles are aligned along the crystallographic *c*-axis resulting in the structure containing channels throughout the crystal, shown in purple in Figure 7.6(b).

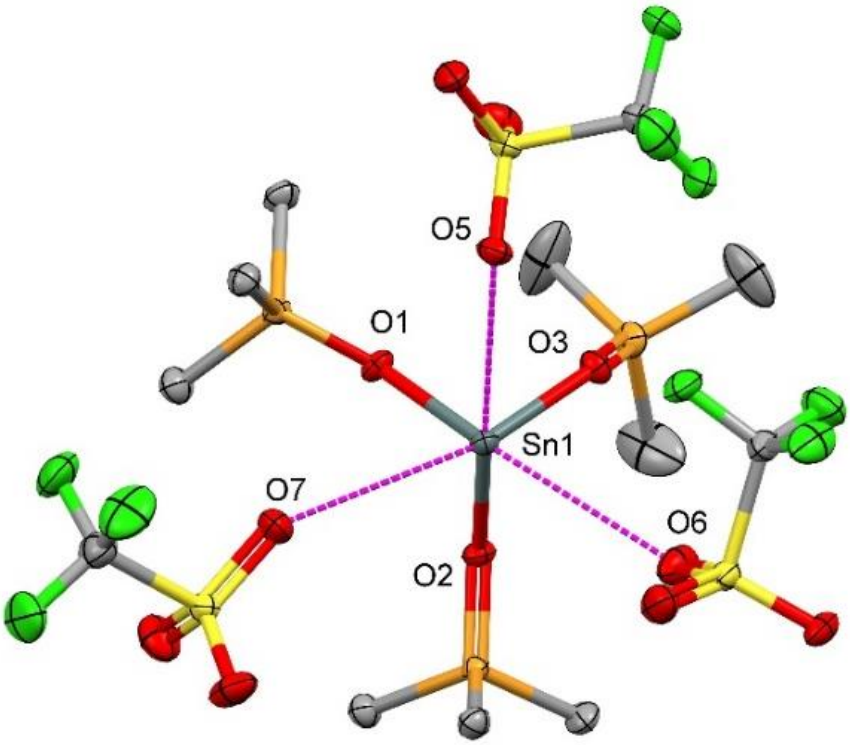

(a)

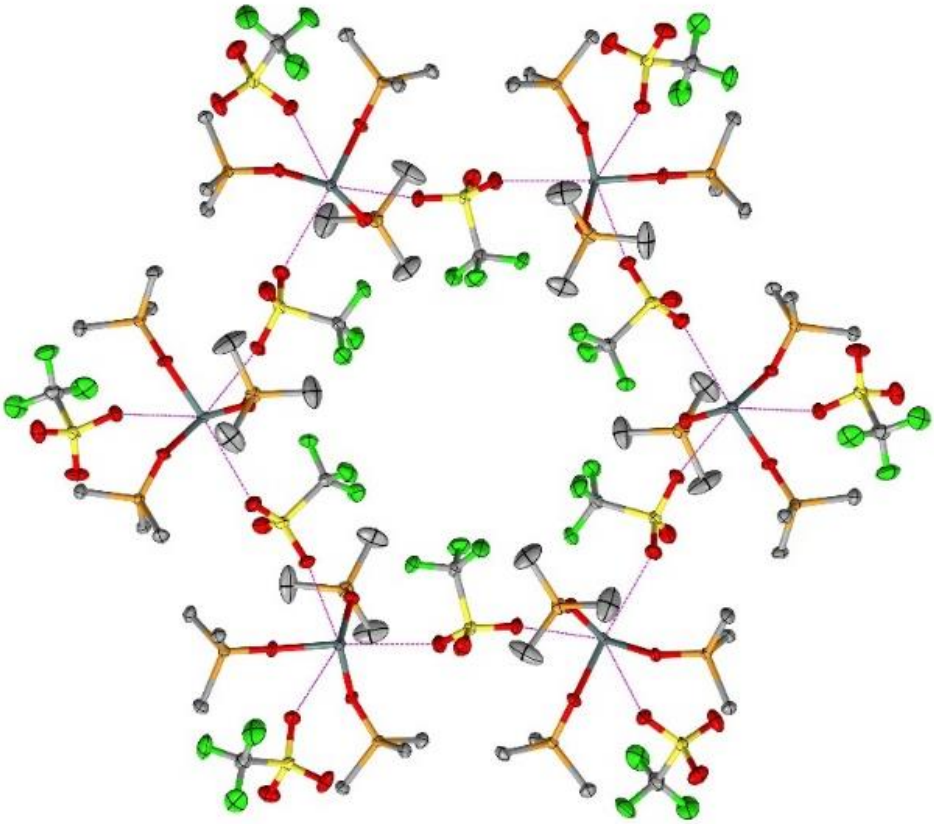

(b)

Figure 7.5 - (a) Crystal structure of a single unit of ***42*** $[Sn(OTf)_2(OPMe_3)_3]$ showing the atomic numbering scheme. Ellipsoids shown at 50% probability with H-atoms omitted for clarity. (b) View down the *c*-axis showing the hexameric assembly of $[Sn(OTf)_2(OPMe_3)_3]_6$ around one pore through triflate bridges.

Table 7.1 - Selection of bond lengths and angles a single tin metal centre in the hexameric array, $[Sn(OTf)_2(OPMe_3)_3]_6$.

Bond Lengths / Å		Bond Angles /	
Sn1 – O1	2.1557(11)	O1 – Sn1 – O2	82.14(5)
Sn1 – O2	2.1669(11)	O1 – Sn1 – O3	85.97(5)
Sn1 – O3	2.0942(11)	O1 – Sn1 – O5	83.74(4)
Sn1 – O5	2.858(1)	O1 – Sn1 – O6	147.43(5)
Sn1 – O6	3.028(2)	O1 – Sn1 – O7	74.26(4)
Sn1 – O7	3.082(1)	O2 – Sn1 – O3	87.49(5)
P1 – O1	1.5137(11)	O2 – Sn1 – O5	160.46(4)
P2 – O2	1.5168(11)	O2 – Sn1 – O6	73.26(4)
P3 – O3	1.5122(11)	O2 – Sn1 – O7	85.09(4)
		O3 – Sn1 – O5	78.08(4)
		O3 – Sn1 – O6	72.19(5)
		O3 – Sn1 – O7	159.64(4)

Residual electron density located inside these channels was calculated to be equal to fifty electrons within each asymmetric unit, corresponding to $0.167[C_6H_{14}]$ per asymmetric unit or one molecule of *n*-hexane per unit cell. A solvent mask of one molecule of *n*-hexane was applied, and the remaining void space was calculated by PLATON to be 256 $Å^3$ or 6.1% of the total unit cell volume. The bridging triflate anions were found to be oriented as such that the $–CF_3$ groups lined each of these channels, producing a hydrophobic surface inside the channels with an F···F distance of 8.019(2) Å across the diameter of the void. Because this measurement would be taken from the centre of the fluorine atom on each side, the accessible size of the pore is smaller due to the radii of the fluorine atom. A more reliable method of diameter measurement would be the F···F distance minus a single fluorine radii (2 x $^1/_2$ the vdV radii) leaving an accessible pore diameter of 6.55 Å. In the side view of the space-filling diagram in Figure 7.6(a), the zig-zag arrangement of the metal centres can be seen, which orients one $OPMe_3$ ligand either above or below the plane of the metallocycle. This $OPMe_3$ ligand (O3 – Figure 7.5(a)) was found to have significant rotational disorder which was modelled through the Olex2 software package, however, the ellipsoids are still enlarged compared with the other two $OPMe_3$ ligands.[35]

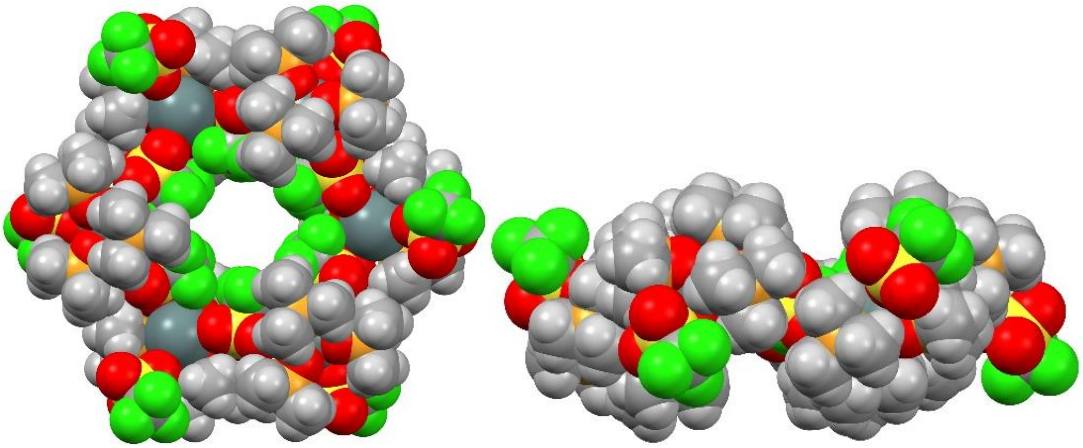

(a)

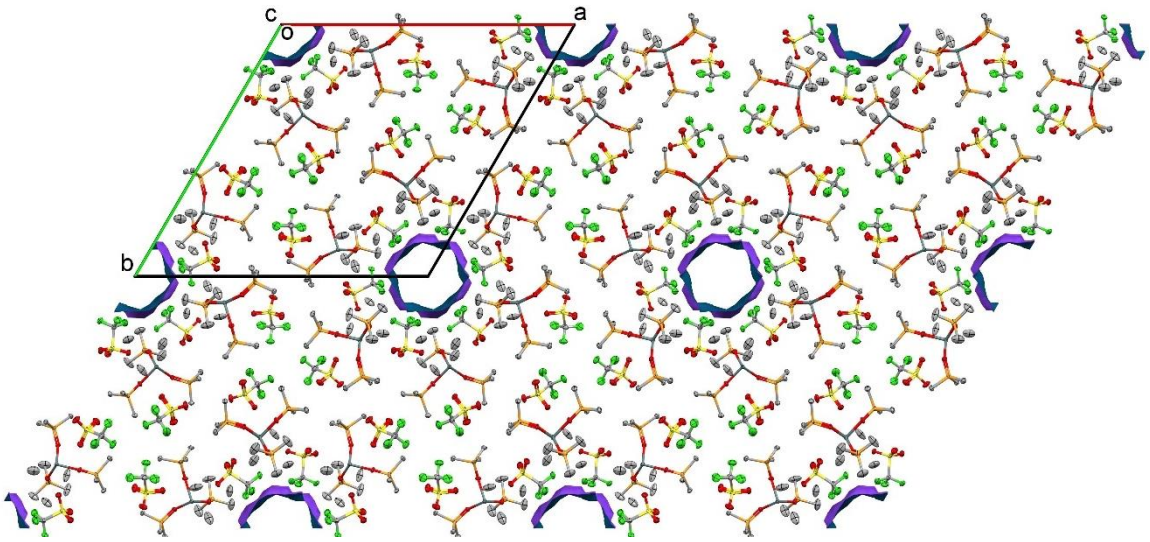

(b)

Figure 7.6 – (a); space-filling diagram of a discrete hexamer – top and edge views. Sn = Dark Gray, P = Orange, F = Green, O = Red, S = Yellow, C = Grey, H = White (b); View down the *c*-axis showing the hydrophobic CF_3-lined channels (marked purple) throughout the extended structure.

Analysis of the $[Sn(OTf)_2(OPMe_3)_3]$ product by ^1H NMR spectroscopy showed a clear shift from the free $OPMe_3$ ligand (1.49 ppm in CD_2Cl_2) to 1.79 ppm, with the $^2J_{HP}$ coupling remaining relatively unchanged at 13 Hz.[36] The $^{19}F\{^1H\}$ NMR spectrum was consistent with the resonances observed in the previous chapter with a single sharp resonance at -79.1 ppm in CH_2Cl_2. Analysis *via* $^{31}P\{^1H\}$ NMR spectroscopy showed only a single phosphorus environment, a sharp resonance being observed at 60.0 ppm. This is a shift of $\Delta\delta$ = 22 ppm from free $OPMe_3$ (found at 38.5 ppm in $CDCl_3$), in line with the shifts observed for the *bis*-complex $[\{Sn(OTf)(OPMe_3)_2\}_2(\mu^2OTf)_2]$ described in Chapter 6. Although requiring a high number of scans (NS = > 50,000), ^{119}Sn NMR spectroscopy of $[Sn(OTf)_2(OPMe_3)_3]$ produced a resonance at –783 ppm. This value is close to those observed for the phosphine and arsine complexes described in Chapter 5,[17] as well as those reported for the $Sn(SbF_6)_2$ complexes produced by Dean and co-workers.[37] Analysis of this product *via* IR

spectroscopy showed peaks at 1085 and 958 cm^{-1} which were assigned as the P=O stretching bands. The appearance of two peaks is in agreement with the number of bands predicted by group theory calculations and with the bands predicted by DFT calculations, carried out by Dr Rhys King.

The full discussion of $[Sn(OTf)(OPPh_3)_3][OTf]$ is found in Chapter 6, however, comparison with $[Sn(OTf)_2(OPMe_3)_3]$ shows a drastic change in solid-state structure, with the structure of the $OPPh_3$ complex previously illustrated in Figure 6.7. This structure shows coordination of three $OPPh_3$ ligands and a single triflate anion in a disphenoidal geometry, with $Sn\text{-}O_{OPPh3}$ distances of 2.0780(15) - 2.2566(14) Å, with these distances from 6.3. These are close to those observed for $[Sn(OTf)_2(OPMe_3)_3]$ which is surprising, due to the changes in both donor strength, steric bulk of the ligand and the packing of the crystal. The $OPPh_3$ complex shows no evidence of oligomerisation through triflate bridges, with the second triflate anion outside the sum of the Van der Waals radii of Sn + O (3.52 Å). Both of these complexes show significant high frequency shifts in the $^{31}P\{^1H\}$ NMR spectra, with $[Sn(OTf)(OPPh_3)_3][OTf]$ showing a smaller Δδ of 15 ppm, which is consistent with the weaker donating power of the $OPPh_3$ ligand.

Although the supramolecular structure of this complex is unexpected, it was readily reproducible from different batches of product, as well as through crystallisation using different solvent systems with no other polymorphs being observed. The powder X-ray diffraction pattern of the bulk solid of $[Sn(OTf)_2(OPMe_3)_3]$ was collected by Sidrah Hussain and Charley Bryant-Gardner, with the pattern shown below alongside the simulated powder pattern (using single crystal data) in Figure 7.7. Comparison of the two PXRD patterns show that, each of the simulated peaks was observed in the collected, with differing reflection intensities being likely due to a preference of a specific crystallite orientation. This is a good suggestion that the single crystal structure is representative of the solid-state structure of the bulk, showing no evidence for other polymorphs, morphologies or impurities. The collected powder pattern shows differences in intensity of reflections which indicated a preference for a specific orientation when packing in to the cell for analysis.

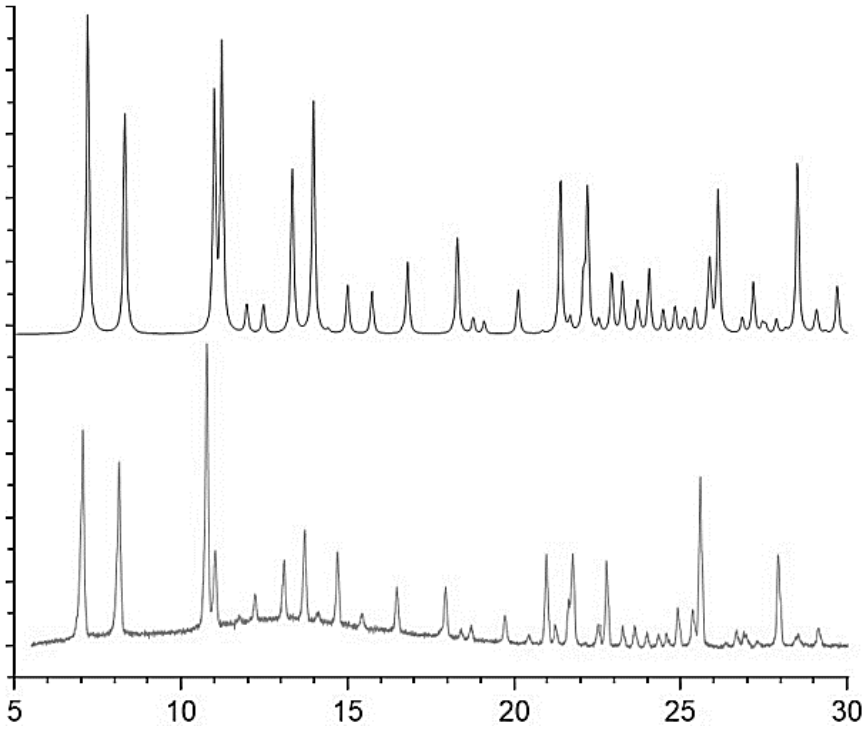

Figure 7.7 - (top): PXRD pattern for $[Sn(OPMe_3)_3(CF_3SO_3)_2]_6$ simulated from the single crystal structure data by Mercury Crystallographic Software; collected at 100 K; (bottom): PXRD pattern recorded from the isolated bulk powder $[Sn(OPMe_3)_3(CF_3SO_3)_2]_6$, collected at 298 K.

Due to the similarity in pore size of $[Sn(OTf)_2(OPMe_3)_3]_6$ with that of Itoh's work discussed in the introduction to this chapter, gas-adsorption experiments were run using Braunauer-Emmett-Teller (BET) surface measurements to explore the accessible surface area. Samples of $[Sn(OTf)_2(OPMe_3)_3]$ were run by Dr Alice Oakley, alongside a control sample of microporous silicon doped AlPO-5 (MP SAPO-5) which has been well studied by BET analysis.[38,39] Each of the samples was heated to 80 °C under vacuum for 12 hours to remove all volatiles within the complex, before N_2 adsorption experiments were run. The analysis showed that under the conditions explored, there was no significant adsorption of N_2 by this complex. One explanation for these results could be that the pores still contain residual hexane solvent that is not being removed through the degassing/drying phase of the experiment. A second interpretation of these results, maybe that the fluorous lining of the channel interfere with the adsorption of N_2 to the surface. Powder XRD was repeated on the sample after BET analysis to observe if exposure to air, heating or drying had altered the structure of the solid. The PXRD pattern was unchanged from the original, confirming that firstly, the attempts at removal of the residual solvent had not removed the crystallinity of the sample, and secondly, these results suggested that this complex is somewhat air stable, with no change in the PXRD after a number of days under an atmosphere of air.

Due to the unexpected hexameric structure of this complex, attempts to probe whether any other divalent Group 14 ions would produce the same supramolecular structure, the corresponding $[M(OTf)_2(OPMe_3)_3]$ (M = Ge, Pb) were also prepared. The germanium analogue was synthesised by

Dr Rhys King, using [$GeCl_2$·(dioxane)] due to the lack of commercially available $Ge(OTf)_2$. *In situ* reaction of [$GeCl_2$·dioxane] with TMSOTf has previously been shown as an entry to synthesis of coordination products of $Ge(OTf)_2$ and thus was utilised here.[40] Initial attempts to produce of [$Ge(OTf)_2(OPMe_3)_3$] in a one-pot reaction resulted in the formation of [$Me_3Si(OPMe_3)$][OTf], a complex previously observed by Burford and co-workers.[41] This was identified by the presence of a peak at 82 ppm in the $^{31}P\{^1H\}$ NMR spectrum and an additional peak at 0.27 ppm in the ^1H NMR spectrum, corresponding to the residual $[Me_3Si]^+$ moiety. To avoid this unwanted side reaction, [$GeCl_2$·dioxane] was first reacted with two molar equivalents of TMSOTf *in situ*. Subsequent drying *in vacuo* gave a white solid free of volatiles such as TMSOTf or TMSCl. This additional separation step was required due to the stronger donor properties of phosphine oxide ligands than the phosphine/arsine ligands explored in previous work with $Ge(OTf)_2$.[40] This solid was then redissolved in MeCN and reacted with 3 equivalents of $OPMe_3$ producing a waxy low melting solid after isolation. This solid showed both NMR spectra and micro-analytical data that was consistent with the formulation of [$Ge(OTf)_2(OPMe_3)_3$]. ^1H NMR spectroscopy of this waxy solid showed a significant shift from free $OPMe_3$, with the ^1H resonance being at a higher chemical shift of 1.82 ppm. There was also a large shift from free $OPMe_3$ in the $^{31}P\{^1H\}$ NMR spectrum of this sample, being located at 62.1 ppm. These values are close to those observed in the analysis of [$Sn(OTf)_2(OPMe_3)_3$], however, due to the complex being a low melting solid, growth of a crystal for X-ray diffraction was not achieved.

Following on from the preparation of both the Ge and Sn complexes, the lead(II) analogue was also synthesised in order to see if this hexameric structure was unique to the synthesis with Sn or replicable with other Group 14 metals. As was the case with the germanium analogue, the inability to purchase $Pb(OTf)_2$ meant initial synthesis of this was undertaken using a procedure by Persson *et al* whereby PbO was reacted with neat trifluoromethanesulfonic acid, as described in Chapter 5.[42] Reaction of $Pb(OTf)_2$ with three equivalents of $OPMe_3$ in MeCN produced a powdered solid and colourless crystals after storage of the mother liquor at -18°C. The ^1H NMR spectrum again showed a significant shift from free $OPMe_3$ to 1.66 ppm ($\Delta\delta = 0.16$), smaller than that observed for the Ge and Sn analogues, with $\Delta\delta = 0.32$ and $\Delta\delta = 0.29$, respectively. As with the other analogous complexes, there was only a single resonance observed in the $^{31}P\{^1H\}$ NMR spectrum at 59.0 ppm, showing slight broadening when compared to the resonances of the other two metal complexes. It is thought that, due to the weaker Lewis acidity of the metals going down Group 14, the $OPMe_3$ ligand is less strongly coordinated.[43] This weakening of coordination would increase the lability of the ligand species thus increasing the broadness of the resonance observed. The Lewis acidity of the metals could also explain the trend seen in the $^{31}P\{^1H\}$ NMR

data in Table 1.2. There is a clear trend to a lower chemical shift in the resonance observed for the $OPMe_3$ ligand species upon coordination to a heavier main group metal nuclei.

Table 7.2 - ^{1}H and $^{31}P\{^{1}H\}$ NMR resonances for the synthesised complexes $[Ge(OTf)_2(OPMe_3)_3]$, $[Sn(OTf)_2(OPMe_3)_3]_6$ and $[\{Pb(OTf)(OPMe_3)_3\}_2(u\text{-}OTf)_2]$.

Complex	δ ^{1}H / ppm	δ $^{31}P\{^{1}H\}$ / ppm
$OPMe_3$	1.50	38.5
$[Ge(OTf)_2(OPMe_3)_3]$	1.82	62.1
$[Sn(OTf)_2(OPMe_3)_3]_6$	1.79	60.0
$[\{Pb(OTf)(OPMe_3)_3\}_2(\mu\text{-}OTf)_2]$	1.66	59.0

The $^{19}F\{^{1}H\}$ NMR resonance for the $-CF_3$ group of the triflate was located at -79.4 ppm, as had been seen for each of the triflate groups in these studies. It is thought that in solution the labile ligands and weakly coordinated anions will dissociate, this explains why there are not multiple resonances for both bridging and κ^1-triflate anions.

Layering a CH_2Cl_2 solution of this complex with *n*-hexane produced colourless crystals of a suitable size for single crystal X-ray diffraction. This structure differs significantly from the Sn hexameric array, and showed the formation of a bridged dimer species $[\{Pb(OTf)(OPMe_3)_3\}_2(\mu\text{-}OTf)_2]$ with two highly distorted, pseudo-octahedral Pb(II) metal centres, this structure is shown in Figure 7.8. Selected bond lengths and angles are provided in Table 7.3. Microanalysis of the bulk solid confirmed that the formulation seen in the crystal structure, $[\{Pb(OTf)(OPMe_3)_3\}_2(\mu\text{-}OTf)_2]$, is likely representative of the bulk solid of the sample.

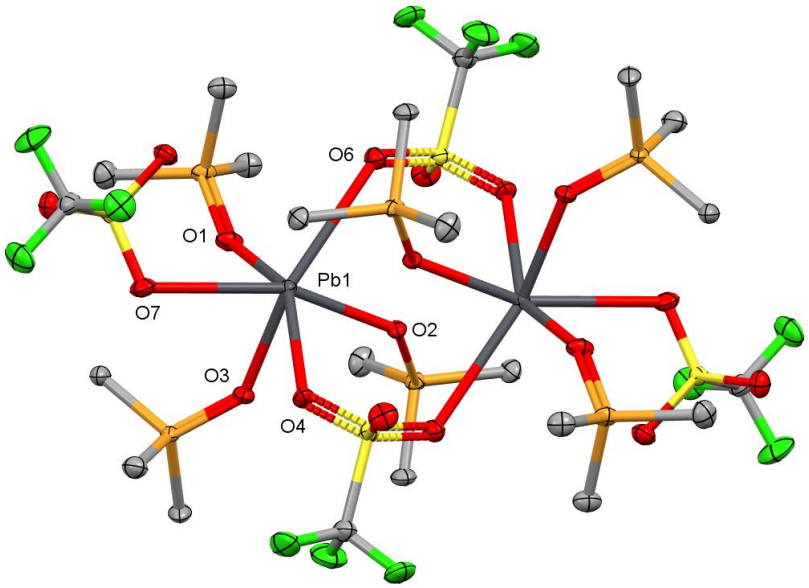

Figure 7.8 - Crystal structure the ***43*** $[\{Pb(OTf)(OPMe_3)_3\}_2(\mu\text{-}OTf)_2]$ dimer with ellipsoids shown at 50% probability and H-atoms omitted for clarity.

Table 7.3 - Selected bond lengths and angles for [{Pb(OTf)(OPMe$_3$)$_3$}$_2$(μ-OTf)$_2$].

Bond Lengths / Å		Bond Angles / °	
Pb1 – O1	2.3628(18)	O1 – Pb1 – O2	97.35(6)
Pb1 – O2	2.3295(17)	O1 – Pb1 – O3	76.97(6)
Pb1 – O3	2.3218(17)	O1 – Pb1 – O6	76.97(6)
Pb1 – O4	2.7325(19)	O1 – Pb1 – O7	87.38(6)
Pb1 – O6	2.889(2)	O2 – Pb1 – O3	80.09(6)
Pb1 – O7	2.888(2)	O2 – Pb1 – O4	72.34(6)
P1 – O1	1.5067(19)	O3 – Pb1 – O6	75.28(6)
P2 – O2	1.5128(17)	O4 – Pb1 – O6	133.09(6)
P3 – O3	1.509(2)	O4 – Pb1 – O7	78.36(6)
		O6 – Pb1 – O7	126.18(5)

The coordination sphere at the metal centres of this complex contain three OPMe$_3$ ligands and one κ^1-coordinated triflate anion, while the remaining coordination sites are occupied by two asymmetrically bridging triflate anions. The two contacts to the bridging triflates are different, with the primary contact (Pb-O4) having a distance of 2.7325(19) Å, while the secondary bridge contact (Pb-O6) is longer at 2.889(2) Å. Each of the primary Pb-O$_{OPMe3}$ bonds is similar in distance, however, one of these ligands appears to be oriented to form a secondary contact. The oxygen of OPMe$_3$ ligand labelled as O2 in Figure 7.8, appears to be oriented to form a bridging interaction with the second metal centre with a Pb-O2 distance of 2.984(2) Å, within the sum of the Van der Waals radii of 3.54 Å.[44] The additional bridging contacts of this OPMe$_3$ ligand distorts the octahedral geometry of the Pb metal centres of this complex, with both being pseudo-seven coordinate.

These discrete dimers show no further intermolecular contacts to other dimers in the crystal, however, they do align to form discrete layers with hydrophobic -CF$_3$ groups being oriented above and below the metal centres in the *bc*-plane, this can be seen in Figure 7.9.

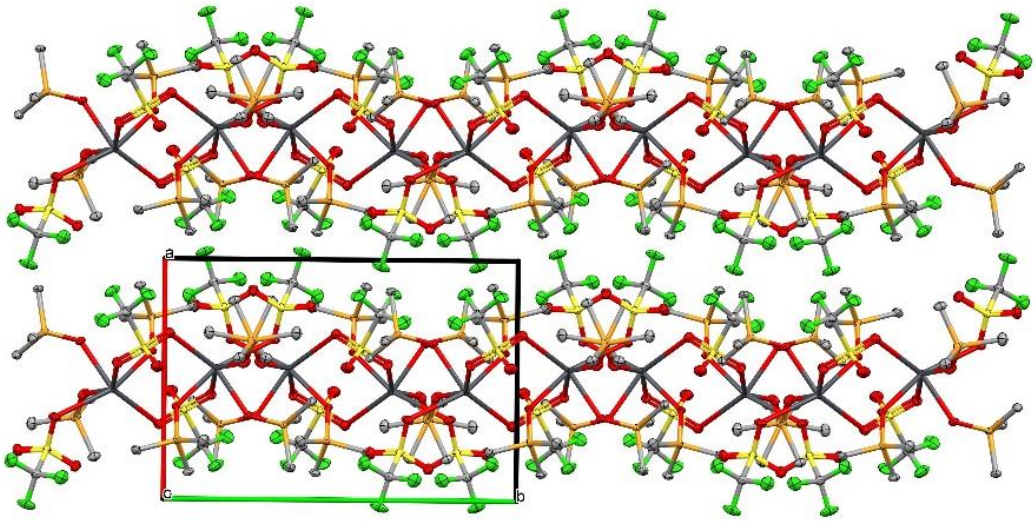

Figure 7.9 - View down the *bc*-plane showing the extended structure of $[\{Pb(OTf)(OPMe_3)_3\}_2(\mu\text{-}OTf)_2]$ with the hydrophobic CF_3 groups aligned above and below the chain of Pb(II) metal centres.

In addition to attempts to produce analogues of the hexameric supramolecular structure with the other Group 14 metals (Ge, Pb), varying the anionic species to the structurally related fluorosulfate anion (SO_3F^-) was attempted as this anion is known to be a less weakly coordinating anion.[45] Synthesis of $Sn(SO_3F)_2$ was completed using the procedure reported by Adams *et al*. by the reaction of fluorosulfonic acid with SnF_2 and gave an off white solid in a good yield, which produced a singlet $^{19}F\{^1H\}$ NMR resonance at 39.3 ppm, this reaction is described in Scheme 7.2.[24] As was described in the procedure, suspension of the retrieved solid in a small amount of fluorosulfonic acid overnight produced crystals of a good quality for diffraction and the unit cell parameters were consistent with those reported.[24] The single crystal X-ray analysis showed a polymeric structure with a single monomer unit with the connectivity to adjacent molecules in the unit cell shown in Figure 7.10. Each tin centre is singly bonded to six different fluorosulfate anions in a distorted octahedral geometry, while the oxygen of each fluorosulfate anion bridges three separate tin metal centres; these additional bonds are shown as dashed bonds. The unit cell parameters of these crystals matched the literature values reported by Adams and co-workers.[24]

$$SnF_2 + HSO_3F \longrightarrow Sn(SO_3F)_2 + 2\,HF$$

Scheme 7.2 - Reaction scheme for the formation of $Sn(SO_3F)_2$

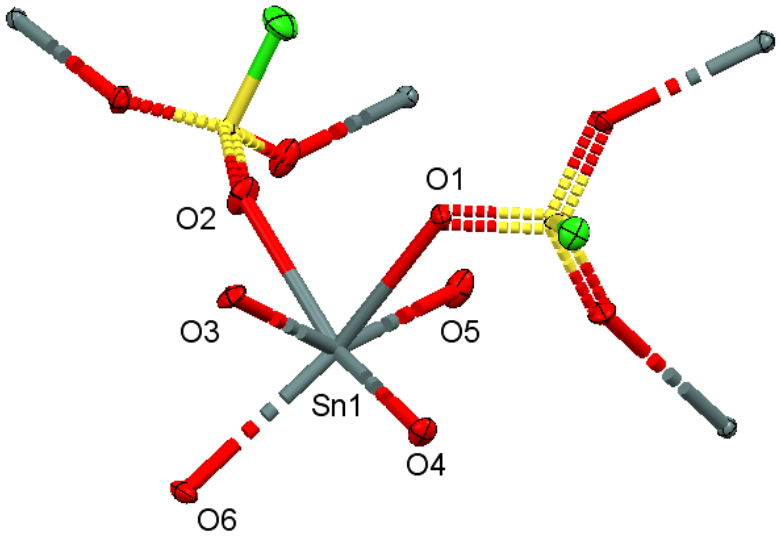

Figure 7.10 – Crystal structure of $Sn(SO_3F)_2$ showing the atomic numbering scheme with ellipsoids shown at 50% probability.

Table 7.4 - Selected bond lengths and angles of $Sn(SO_3F)_2$.

Bond Lengths / Å		Bond Angles / °	
Sn1 – O1	2.3146(15)	O1 – Sn1 – O2	79.26(6)
Sn1 – O2	2.4053(17)	O1 – Sn1 – O5	74.72(5)
Sn1 – O3	2.3239(15)	O1 – Sn1 – O6	145.79(5)
Sn1 – O4	2.4053(17)	O2 – Sn1 – O5	79.18(5)
Sn1 – O5	2.6563(16)	O3 – Sn1 – O4	77.65(5)
Sn1 – O6	2.4159(16)	O5 – Sn1 – O6	139.47(5)

Reaction of $Sn(SO_3F)_2$ with 3 molar equivalents of $OPMe_3$ in MeCN gave a good yield of a white solid that produced a single slightly broadened resonance in the $^{31}P\{^1H\}$ NMR spectrum at 58.4 ppm, a high frequency shift from the free $OPMe_3$ at 38.5 ppm. Comparison of this resonance with that observed for $[Sn(OTf)_2(OPMe_3)_3]$, found at 60.0 ppm, shows only a small difference when substituting the anion. The ^1H NMR spectrum shows the doublet resonance at 1.67 ppm, with $\Delta\delta$ = 0.15 ppm, a smaller shift than was observed in the triflate analogue ($\Delta\delta$ = 0.29 ppm). The $^{19}F\{^1H\}$ NMR resonance of this product was observed at 37.4 ppm with no other peaks observed in solution, within the expected region for fluorosulfate anions.[46]

The microanalysis of this product was low in both carbon and hydrogen, by 8% and 2%, respectively when compared to the anticipated formula of $[Sn(SO_3F)_2(OPMe_3)_3]$. Even with incorporation of appropriate amounts solvents present throughout the synthesis. With no obvious second species being present in solution, meaning that the impurity is not visible by ^1H, $^{19}F\{^1H\}$ or $^{31}P\{^1H\}$ NMR spectroscopy, or is in small enough quantities to not appear in the NMR spectrum. A likely candidate for this is the SnF_2 starting material that remains from synthesis of

the fluorosulfate which had not been reacted and was not removed during the crystallisation. Layering of a CH_2Cl_2 solution of this complex with *n*-hexane produced a few crystals that were analysed by SCXRD and the structure of $[Sn(OPMe_3)_4][SO_3F]_2$ is shown in Figure 7.11, with bond lengths and angles provided in Table 7.5.

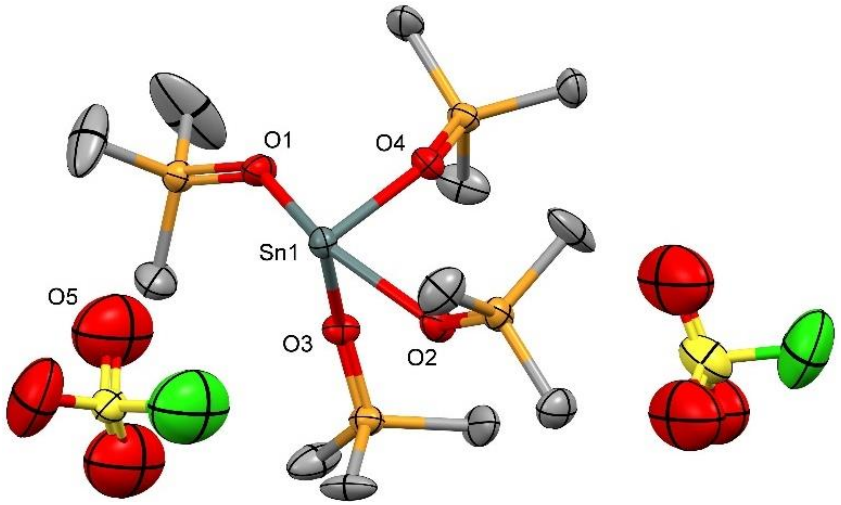

Figure 7.11 - Crystal structure of ***44*** $[Sn(OPMe_3)_4][SO_3F]_2$ drawn with elipsoids at 50% probability. Solvent and H-atoms omitted for clarity.

Table 7.5 - Selected bond lengths and angles for $[Sn(OPMe_3)_4][SO_3F]_2$.

Bond Lengths / Å		Bond Angles / °	
Sn1 – O1	2.285(4)	O1 – Sn1 – O2	97.35(6)
Sn1 – O2	2.344(4)	O1 – Sn1 – O3	76.97(6)
Sn1 – O3	2.113(4)	O1 – Sn1 – O4	76.97(6)
Sn1 – O4	2.129(4)	O2 – Sn1 – O3	87.38(6)
P1 – O1	1.505(4)	O2 – Sn1 – O4	80.09(6)
P2 – O2	1.494(5)	O3 – Sn1 – O4	72.34(6)
P3 – O3	1.523(4)		
P4 – O4	1.521(4)		

The crystal structure produced shows the complex to be $[Sn(OPMe_3)_4][SO_3F]_2$, containing a tin(II) metal centre coordinated by four $OPMe_3$ ligands in a distorted disphenoidal geometry with no additional short contacts. This 4:1 ratio of $OPMe_3$: Sn was unexpected, with no evidence of a mixture of *tris* and *tetrakis* complexes in solution, from the NMR spectrum collected. The presence of SnF_2 in the $Sn(SO_3F)_2$ precursor would result in a higher ligand : metal ratio, meaning the bulk product could be $[Sn(OPMe_3)_4][SO_3F]_2$ as observed by SCXRD.

The shortest distance between the tin(II) centre and a fluorosulfate anion is 3.564(18) Å, which is beyond the sum of the van der Waals radii of 3.54 Å, and hence is indicative of ionic fluorosulfate.[44] The similar electron density of oxygen and fluorine made identification of the fluorine atoms less certain and so the bond lengths were used. The single fluorine atom was modelled with the furthest distance from the sulphur, with the longer bond length of 1.531(10) Å, while the three S=O double bonds are shorter, lying in the range 1.334(15) – 1.427(11) Å. There was a high degree of disorder associated with each of these fluorosulfate anions largely due to rotation of this anion in space which has the effect of increasing the ellipsoids observed in the modelled structure. The observation of this crystal structure, as well as the unmatched microanalysis, suggests that this reaction may produce a mixture of products, of which $[Sn(OPMe_3)_4][SO_3F]_2$ is one which crystallises most readily.

7.3 – Conclusion

This chapter primarily explored the synthesis, characterisation and properties of $[Sn(OTf)_2(OPMe_3)_3]$ which adopts a very unusual hexameric structure bridged by triflate anions. Six pseudo-octahedral tin metal centres, each with a (SnP_3O_3) core, form a hexagonal channel down the *c*-axis with the $-CF_3$ groups of the bridging triflates all being oriented towards the centre of this channel. This directionality of the $-CF_3$ groups gives a surface of electronegative fluorine atoms which, as seen in materials such as Teflon, causes hydrophobicity of the surface. The channels contained residual electron density that matched that of 1/6th of *n*-hexane per asymmetric unit. Measurement of this channel across the diameter revealed an F···F distance of 8.019(2) Å, with the channels taking up 6.1% of the total unit cell volume, which is comparable to the nanorings produced in the report by Itoh and co-workers.[28] BET measurements carried out on this sample, however, revealed limited N_2 adsorption when compared to a known breathable MOF.

In an attempt to explore if this extended structure was unique to $[Sn(OTf)_2(OPMe_3)_3]_6$, analogous reactions were carried out using both Ge(II) and Pb(II) starting materials. Attempts to produce this using $GeCl_2$·dioxane produced a waxy solid, with repeated attempts at crystallisation under varying conditions being unsuccessful. The analogous reaction using $Pb(OTf)_2$ produced a dimeric complex, $[\{Pb(OTf)(OPMe_3)_3\}_2(\mu\text{-}OTf)_2]$, formed in layers with orientation of the $-CF_3$ groups above and below the metal centres in the *bc*-plane.

Changing the anion to the structurally similar fluorosulfate (SO_3F^-) and undertaking the equivalent rection with Sn(II) and $OPMe_3$ in a 1:3 ratio yielded crystals of the tetrakis species, $[Sn(OPMe_3)_4][SO_3F]_2$, with two ionic $[SO_3F]^-$ anions, as opposed to the expected tris-complex.

7.4 – Experimental

7.4.1 Complex Preparation

7.4.1.1 **[Sn(OTf)$_2$(OPMe$_3$)$_3$]**

$Sn(OTf)_2$ (83 mg, 0.2 mmol) was dissolved in CH_2Cl_2 (10 mL) before the addition of $OPMe_3$ (55 mg, 0.6 mmol) and stirred for 2 h. Particulates were removed by filtration and the solution was concentrated by 50% *in vacuo* before addition of Et_2O (5 mL) caused precipitation of a white solid. This was collected by filtration before being dried *in vacuo* with crystals being grown *via* vapour diffusion of Et_2O into a CH_3CN solution. Yield: 101 mg, 73 %. Required for $C_{11}H_{27}F_6O_9P_3S_2Sn$ (693.08): C, 19.1; H, 3.9. Found: 19.3; H, 4.1%. ^{1}H NMR (295 K, CD_2Cl_2): δ = 1.79 (d, ^2J = 13.5 Hz). $^{13}C\{^1H\}$ NMR (295 K, CD_2Cl_2): δ = 17.4 (d, J= 70.0 Hz). $^{19}F\{^1H\}$ NMR (295 K, CD_2Cl_2): δ = –79.1 (s). $^{31}P\{^1H\}$ NMR (CD_2Cl_2, 298 K): δ = +60.0 (s); ^{119}Sn NMR (298 K, CH_2Cl_2): δ = −783 (s). IR spectrum (ν/cm^{-1}): 1085, 958 (P=O).

7.4.1.2 **[Ge(OTf)$_2$(OPMe$_3$)$_3$]**

$GeCl_2$(dioxane) (58 mg, 0.25 mmol) was dissolved in MeCN (2 mL) to which TMSOTf (111 mg, 0.50 mmol) was added as a solution in MeCN (2 mL) and stirred for 1 h. The solution was concentrated to dryness *in vacuo* to yield a white solid before it was dissolved in MeCN (5 mL) and $OPMe_3$ (100 mg, 0.75 mmol) was added as a solution in MeCN, the mixture was stirred for 1 h, the resulting colourless solution was concentrated *in vacuo* to yield an oily residue. This residue was dissolved in CH_2Cl_2 (2 mL) and pentane (15 mL) was added to deposit a waxy white solid which was isolated by filtration and dried *in vacuo*. Yield: 0.072 mg, 44 %. Required for $C_{11}H_{27}F_6O_9P_3S_2Ge$ (646.97): C, 20.4; H, 4.2. Found: C, 20.7; H, 4.4%. ^{1}H NMR (298 K, CD_2Cl_2): δ = 1.82 (d, $^2J_{PH}$ = 13.5 Hz). $^{13}C\{^1H\}$ NMR (298 K, CD_2Cl_2): δ = 17.2 (d, $^1J_{PC}$ = 69.0 Hz). $^{19}F\{^1H\}$ NMR (298 K, CD_2Cl_2): δ = –79.0 (s). $^{31}P\{^1H\}$ NMR (CD_2Cl_2, 298 K): δ = +62.1 (s). IR spectrum (ν/cm^{-1}): 1040, 958 (P=O).

7.4.1.3 **[{Pb(OTf)(OPMe$_3$)$_3$}$_2$(μ-OTf)$_2$]**

$Pb(OTf)_2$ (152 mg, 0.3 mmol) was partially dissolved in CH_2Cl_2 (10 mL) before addition of $OPMe_3$ (83 mg, 0.9 mmol) at which point the ma*j*ority of solid was taken up in solution and was stirred for 2 h. Residual particulates were removed from the solution before it was concentrated by 75%. This was layered with *n*-hexane (5 mL) and stored at -18 °C for 24 h, yielding colourless crystals suitable for single crystal X-ray diffraction. These were collected by filtration and dried *in vacuo*. Yield: 122 mg, 52 %. Required for $C_{22}H_{54}F_{12}O_{18}P_6S_4Pb_2$ (1563.13): C, 16.9; H, 3.5. Found: C, 17.2; H, 3.6%. ^{1}H NMR (CD_2Cl_2, 298 K): δ = 1.66 (d, [3H], $^2J_{PH}$ = 13.7 Hz). $^{13}C\{^1H\}$ NMR (295 K, CD_2Cl_2): δ = 17.3 (d, $^1J_{PC}$ = 70

Hz). $^{19}F\{^{1}H\}$ NMR (CD_2Cl_2, 298 K): δ = –79.4 (s). $^{31}P\{^{1}H\}$ NMR (CD_2Cl_2, 298 K): δ = +59.0 (s). IR spectrum (v/cm^{-1}): 1093, 949s (P=O).

7.4.1.4 **$[Sn(OPMe_3)_4][SO_3F]_2$**

$Sn(SO_3F)_2$ (95 Mg, 0.3 mmol) was dissolved in CH_2Cl_2 (10 mL) before the addition of $OPMe_3$ (111 mg, 1.2 mmol) and stirring for 2 hrs. The solution was then concentrated by *ca* 50% before layering with *n*-hexane produced a white precipitate which was collected and dried *in vacuo*. Yield: 124 mg, 55 %. Required for $SnS_2O_{10}F_2P_4C_{12}H_{36}.CH_3CN$ (726.19): C, 23.2; H, 5.4. Found: C, 23.2; H, 5.7. ^{1}H NMR (CD_3CN, 298 K): 1.67 (d, [3H], $^{2}J_{PH}$ = 13.69 Hz). $^{13}C\{^{1}H\}$ NMR (295 K, CD_3CN): δ = 16.98 (d, $^{1}J_{PC}$ = 70 Hz). $^{19}F\{^{1}H\}$ NMR (CD_3CN, 298 K): δ = 37.4 (s). $^{31}P\{^{1}H\}$ NMR (CD_3CN, 298 K): δ = +58.4 (s) IR spectrum (v/cm^{-1}) 1093, 955 (P=O).

7.4.2 Reagent synthesis

7.4.2.1 **$Sn(SO_3F)_2$**

Using a procedure by Adams *et al*.[24] SnF_2 (1000 mg, 6.38 mmol) was dried *in vacuo* for 4 hrs, before addition of fluorosulfuric acid (1277 mg, 12.76 mmol) and stirring at 60°C for 4 hrs. This solution was stored at 2°C with large colourless crystals being collected by filtration for SCXRD before drying *in vacuo* yielding a white powder. $^{19}F\{^{!}H\}$ NMR (295 K, CD_3CN) δ = 39.25. IR spectrum (v/cm^{-1}) = 1287, 1075, 771, 576, 556.

7.5 – References

1 P. A. W. Dean, D. D. Phillips and L. Polensek, *Can. J. Chem.*, 1981, **59**, 50–61.
2 P. A. W. Dean, *Can. J. Chem.*, 1983, **61**, 1795–1799.
3 J. Burt, W. Grantham, W. Levason and G. Reid, *Dalton Trans.*, 2015, **44**, 11533–11541.
4 S. H. Strauss, *Chem. Rev.*, 1993, **93**, 927–942.
5 I. Krossing and I. Raabe, *Angew. Chemie Int. Ed.*, 2004, **43**, 2066–2090.
6 T. A. Engesser, M. R. Lichtenthaler, M. Schleep and I. Krossing, *Chem. Soc. Rev.*, 2016, **45**, 789–899.
7 J. M. Slattery, A. Higelin, T. Bayer and I. Krossing, *Angew. Chemie Int. Ed.*, 2010, **49**, 3228–3231.
8 I. Krossing, *J. Am. Chem. Soc.*, 2001, **123**, 4603–4604.
9 P. A. Rupar, V. N. Staroverov and K. M. Baines, *Science (80-.).*, 2008, **322**, 1360–1363.
10 R. P. King, J. M. Herniman, W. Levason and G. Reid, *Inorg. Chem.*, 2023, **62**, 853–862.
11 F. Cheng, A. L. Hector, W. Levason, G. Reid, M. Webster and W. Zhang, *Chem. Commun.*, 2008, 5508–5510.
12 P. A. Gray, K. D. Krause, N. Burford and B. O. Patrick, *Dalton Trans.*, 2017, **46**, 8363–8366.
13 R. P. King, M. S. Woodward, J. Grigg, G. McRobbie, W. Levason and G. Reid, *Dalton Trans.*, 2021, **50**, 14400–14410.
14 M. S. Woodward, R. P. King, R. D. Bannister, J. Grigg, G. McRobbie, W. Levason and G. Reid, *Inorganics*, 2022, **10**, 107.
15 V. K. Greenacre, R. P. King, W. Levason and G. Reid, *Dalton Trans.*, 2019, **48**, 17097–17105.
16 M. Bouska, L. Dostál, M. Lutter, B. Glowacki, Z. Ruzickova, D. Beck, R. Jambor and K. Jurkschat, *Inorg. Chem.*, 2015, **54**, 6792–6800.
17 K. R. Cairns, R. P. King, R. D. Bannister, W. Levason and G. Reid, *Dalton Trans.*, 2023, **2**, 2293–2308.
18 M. J. D. Champion, J. M. Dyke, W. Levason, M. E. Light, D. Pugh, H. Bhakhoa, L. Rhyman, P. Ramasami and G. Reid, *Inorg. Chem.*, 2015, **54**, 2497–2499.
19 M. Everett, A. Jolleys, W. Levason, D. Pugh and G. Reid, *Chem. Commun.*, 2014, **50**, 5843.
20 T. Michałowski, P. J. Malinowski and W. Grochala, *J. Fluor. Chem.*, 2016, **189**, 102–118.
21 T. Enomoto, K. Matsumoto and R. Hagiwara, *Dalton Trans.*, 2011, **40**, 12491.
22 N. E. Dixon, G. A. Lawrance, P. A. Lay, A. M. Sargeson and H. Taube, in *Inorganic Syntheses*, ed. R. J. Angelici, Inorganic Syntheses Organization, John Wiley & Sons, 2007, vol. 28, pp. 70–76.
23 T. Birchall, P. A. W. Dean and R. J. Gillespie, *J. Chem. Soc. A Inorganic, Phys. Theor.*, 1971, 1777.
24 D. C. Adams, T. Birchall, R. Faggiani, R. J. Gillespie and J. E. Vekris, *Can. J. Chem.*, 1991, **69**, 2122–2126.
25 O. Hiemisch, D. Henschel, P. G. Jones and A. Blaschette, *Z. Anorg. Allgem. Chem.*, 1997, **623**, 147–150.
26 F. H. Allen, J. A. Lerbscher and J. Trotter, *J. Chem. Soc. A Inorganic, Phys. Theor.*, 1971, 2507.
27 K. R. Cairns, W. Levason, G. Reid and W. Zhang, *Polyhedron*, 2021, **210**, 115529.
28 Y. Itoh, S. Chen, R. Hirahara, T. Konda, T. Aoki, T. Ueda, I. Shimada, J. J. Cannon, C. Shao, J. Shiomi, K. V. Tabata, H. Noji, K. Sato and T. Aida, *Science (80-.).*, 2022, **376**, 738–743.
29 C. Yang, U. Kaipa, Q. Z. Mather, X. Wang, V. Nesterov, A. F. Venero and M. A. Omary, *J. Am. Chem. Soc.*, 2011, **133**, 18094–18097.
30 J. S. Wilkes, *Green Chem.*, 2002, **4**, 73–80.
31 P. Pachfule and R. Banerjee, in *Encyclopedia of Inorganic and Bioinorganic Chemistry*, John Wiley & Sons, Ltd, Chichester, UK, 2014, pp. 1–14.
32 D.-S. Zhang, Z. Chang, Y.-F. Li, Z.-Y. Jiang, Z.-H. Xuan, Y.-H. Zhang, J.-R. Li, Q. Chen, T.-L. Hu and X.-H. Bu, *Sci. Rep.*, 2013, **3**, 3312.
33 C. Serre, F. Millange, C. Thouvenot, M. Noguès, G. Marsolier, D. Louër and G. Férey, *J. Am.*

Chem. Soc., 2002, **124**, 13519–13526.
34 K. R. Cairns, R. P. King, W. Levason and G. Reid, *CrystEngComm*, 2022, **24**, 6137–6140.
35 O. V. Dolomanov, L. J. Bourhis, R. J. Gildea, J. A. K. Howard and H. Puschmann, *J. Appl. Crystallogr.*, 2009, **42**, 339–341.
36 K. Bläsing, R. Labbow, A. Schulz and A. Villinger, *Angew. Chemie Int. Ed.*, 2021, **60**, 13798–13802.
37 P. A. W. Dean, *Can. J. Chem.*, 1982, **60**, 2921–2926.
38 G. Basina, D. AlShami, K. Polychronopoulou, V. Tzitzios, V. Balasubramanian, F. Dawaymeh, G. N. Karanikolos and Y. Al Wahedi, *Surf. Coatings Technol.*, 2018, **353**, 378–386.
39 M. E. Potter, J. Kezina, R. Bounds, M. Carravetta, T. M. Mezza and R. Raja, *Catal. Sci. Technol.*, 2018, **8**, 5155–5164.
40 R. P. King, V. K. Greenacre, W. Levason, J. M. Dyke and G. Reid, *Inorg. Chem.*, 2021, **60**, 12100–12108.
41 A. P. M. Robertson, S. S. Chitnis, S. Chhina, S. H. J. Cortes, B. O. Patrick, H. A. Jenkins and N. Burford, *Can. J. Chem.*, 2016, **94**, 424–429.
42 K. Lyczko, W. Starosta and I. Persson, *Inorg. Chem.*, 2007, **46**, 4402–4410.
43 E. I. Davydova, A. Y. Timoshkin, T. N. Sevastianova, A. V. Suvorov and G. Frenking, *J. Mol. Struct. THEOCHEM*, 2006, **767**, 103–111.
44 M. Mantina, A. C. Chamberlin, R. Valero, C. J. Cramer and D. G. Truhlar, *J. Phys. Chem. A*, 2009, **113**, 5806–5812.
45 G. A. Lawrance, *Chem. Rev.*, 1986, **86**, 17–33.
46 P. Press, G. Britain, T. Use, E. Synthesis, S. Physics, W. Kerr, U. Bridge, S. Thermonitor and M. St, 1975, **37**, 282–283.

Chapter 8 – Conclusions

The chemistry of the Group 13 and 14 metal triflates was previously very limited in its exploration and has been investigated more thoroughly here, through coordination of ligands containing a range of different donor atoms (N, O, P, As, Sb). Many of the known halide complexes lose a single halide to produce and form salts with the halometalate anion $[MX_4]^-$. In many cases, it was observed that the structures of the synthesised complexes differed greatly from those of the corresponding metal halide complex, showing a preference to produce oligomeric structures through triflate bridge motifs.

The Group 13 metal triflates $M(OTf)_3$ (M = Al, Ga, In) were first probed for coordination with a series of heteroaromatic polydentate *N*-donor imine ligands with a range of differing denticity and donor strength. Each of the ligands was shown to produce octahedral complexes $[M(OTf)_3(terpy)]$ and $[M(OTf)_2(bidentate)_2][OTf]$ (bidentate = bipy, phen). The complexes formed with coordination of bidentate ligands were cationic, with displacement of one of the triflate anions producing octahedral species in a *cis* geometry. The harder oxygen donors ligands (OPR_3 (R = Ph, Me), $dpmo_2$, pyNO) also took up this octahedral geometry. With both ligand sets, trace amounts of water or donor solvent during crystallisation was shown to displace the weakly coordinated triflate anion, with aquo ligands foming H-bonds to the free anions. The easy displacement of these anions could allow for further functionalisation of these complexes through anionic exchange. The displacement of the triflate anions was not explored here and could be a worthwhile area of study in the future for the development of cationic complexes of Group 13 metals. Due to the presence of trace amounts of water introduced through the metal triflate starting materials, the study carried out here revealed the ease of displacement by competitive donor species.

Coordination of the soft pnictine donors PEt_3 and $AsEt_3$ to the Group 13 halides contrasted the octahedral geometry dominating the Group 13 triflate complexes, with only 4 and 5-coordinate complexes being produced. Reaction of $InCl_3$ with PEt_3 produced the expected *bis* complex, $[InCl_3(PEt_3)_2]$, with no indication of the formation of the four coordinate $[InCl_3(PEt_3)]$. This was contrasted by the gallium complex, which was shown to produce only the four coordinate $[GaCl_3(PEt_3)]$. Reaction with $InCl_3$ however, was shown to produce both the four and five coordinate products $[InCl_3(AsEt_3)]$ and $[InCl_3(AsEt_3)_2]$. Although ultimately unsuccessful here, further attempts at deposition of these materials using a wider range of methods and experimental conditions may yield these important semiconductor materials.

The remaining chapters of this thesis focused on the coordination of the Group 14 metal triflate $M(OTf)_2$ (M = Sn, Pb) with Chapter 5 continuing the study of the soft pnictine donors. Structural analysis of a range of the newly synthesised triflate complexes revealed a preference for oligomerisation, with many of the complexes showing triflate bridging. The complexes produced from $Pb(OTf)_2$ generally contained higher coordination numbers, with the triflate anions appearing shifting to coordinate in a κ^2-fashion. Analysis *via* ^{119}Sn NMR spectroscopy of these coordination complexes showed resonances similar to those observed for previously reported halide complexes and Dean's reported $Sn(SbF_6)_2$ complexes. The $Pb(OTf)_2$ complexes however, were not observed to produce any resonances *via* ^{207}Pb NMR spectroscopy.

Chapters 6 and 7 focused on the coordination of oxygen donor ligands to the Group 14 metal triflate salts, with a series of both OPR_3 (R = Me, Ph) ligands, in varying molar equivalents, producing both neutral and cationic complexes. Again, triflate bridges were observed on a number of complexes including $[\{Sn(OTf)(OPR_3)_2\}_2(\mu^2\text{-}OTf)_2]$ (R = Me, Ph, $-CH_2P(O)PPh_2$). The 3:1 reaction of $OPMe_3$ and $Sn(OTf)_2$ produced the *tris*-complex $[Sn(OTf)_2(OPMe_3)_3]$ and revealed a unique hexameric metallocyclic containing a large solvent void. BET adsorption experiments carried out by Dr Alice Oakley, however, unfortunately revealed limited gas adsorption when compared to known MOF species. Attempts to replicate this hexameric array in the solid state were undertaken using differing metals and inorganic anions but were ultimately unsuccessful. Additional research into this complex and the bridging behaviour of the triflate anion may possibley aid in the formation of an analogous species.

Anionic substitution of triflate for the $[BAr^F]^-$ anion was shown as successful in Chapter 5, with the formation of the dicationic complexes $[M\{MeC(CH_2PPh_2)_3\}]^{2+}$ (M = Ge, Sn, Pb). Future work in this field could include additional anionic exchange reactions using $Na[BAr^F]$, as well as other weakly coordinating anions, to probe the structure of dicationic complex and how it compares to complexes involving triflate. This could help further understand the affect of triflate on the structure of the complex and how this compares to other weakly coordinating.

Appendix A – General Experimental Details

All reactions in this thesis were carried out under a dry nitrogen atmosphere using standard Schlenk line and glove box techniques throughout, unless otherwise stated. Each of the solvent used were dried and degassed by Dr Victoria Greenacre and Dr Danielle Runacres prior to use. Hexane and and benzene were distilled over Na; CH_2Cl_2 and MeCN were distilled over CaH_2; Et_2O and THF were distilled over Na/benzophenone ketyl, all solvents were subsequently stored over 4 Å molecule sieves. The ligands *o*-$C_6H_4(PMe_2)_2$,[1] *o*-$C_6H_4(AsMe_2)_2$[2] and $CH_3C(CH_2AsMe_2)_3$[2] were prepared by Dr Wenjian Zhang and Dr Rhys King according to the literature procedures, as well as $dppmO_2$[6], PEt_3[4] and $Na[BAr^F]$[5] and were produced by myself with the experimental procedures being found in Chapter 3 and 4 respectively. $AlCl_3$, $Al(OTf)_3$, $GaCl_3$, $Ga(OTf)_3$ $InCl_3$, $In(OTf)_3$, $FeCl_3$, $GeCl_2$.dioxane, 2'2"-bipyridine, 1,10-phenanthroline, 2,2':6'2"-terpyridine, $OPPh_3$, $OPMe_3$ (sublimed prior to use), pyNO (sublimed prior to use), o-$C_6H_4(PPh_2)_2$, $CH_3(CH_2PPh_2)_3$, $PhP(CH_2CH_2PPh_2)_2$, $P(CH_2CH_2PPh_2)_3$ were obtained from Sigma-Aldrich. PMe_3 and $AsEt_3$ were obtained from Strem. Majority of purchased reagents were used as received however, TMSOTf which was distilled prior to use. Each of the metal triflates were purchased with the "anhydrous" formulation however, IR spectroscopy showed varying amount of water which prolonged drying *in vacuo* would not remove completely. Although satisfactory for synthetic use, the unknown amount of retained water means that the metal:ligand ratios may deviate somewhat from those calculated, resulting in a slight excess of ligand.

Infrared spectra were recorded as Nujol mulls between CsI plates using a PerkinElmer Spectrum 100 spectrometer over the range 4000−200 cm^{-1}. All NMR spectroscopy carried out in this body of work was run on a Bruker AVII 400 spectrometer ^{1}H, $^{13}C\{^{1}H\}$,$^{19}F\{^{1}H\}$,$^{31}P\{^{1}H\}$, ^{27}Al, ^{71}Ga, ^{115}In, ^{119}Sn and ^{207}Pb NMR spectra were recorded from CD_3CN or CD_2Cl_2 solutions. The machine was referenced to $SiMe_4$ *via* the residual solvent resonance (^{1}H and ^{13}C), external $CFCl_3$ (^{19}F), 85% H_3PO_4 (^{31}P), $[Al(H_2O)_6]^{3+}$ (^{27}Al), $[Ga(H_2O)_6]^{3+}$ (^{71}Ga), $[In(H_2O)_6]^{3+}$ (^{115}In), $SnMe_4$ (^{119}Sn), $[K][SbCl_6]$ (^{121}Sb), $PbMe_4$ (^{207}Pb) respectively. Low temperature NMR experiments were run by Dr Danielle Runeacres and Dr Rhys King. Microanalytical measurements were performed by either London Metropolitan University or Medac Ltd.

Data collections used a Rigaku AFC12 goniometer equipped with an enhanced sensitivity (HG) Saturn724+ detector mounted at the window of an FR-E+ SuperBright molybdenum (λ = 0.71073 Å) rotating anode generator with HF Varimax optics (100 μm focus) with the crystal held at 100 K, or a Rigaku UG2 goniometer equipped with a Rigaku hybrid pixel array detector (Hypix 6000 HE detector) mounted at the window of an FR-E+ SuperBright molybdenum (λ = 0.71073 Å) or copper, λ = 1.5406 Å, for the three [BArF] salts) rotating anode generator with Arc)Sec VHF

Varimax confocal mirrors (70 μm focus), with the crystal held at 100 K. Structure solution and refinement were performed using SHELX(S/L)97, SHELX2013, or SHELX-2014/7 *via* Olex2.[7–9] Structure solution and refinement was mostly routine, except for -CF_3 rotational disorder of OTf and $[BAr^F]^-$ anions in some cases, details of which are provided in the relevant cif files. In a few cases, poor crystal quality and disorder meant modelling was more complex and help was obtained from Dr Rob Bannister, Dr Mark Light and Dr Wenjian Zhang. Details of the crystallographic parameters are given in each chapter.

Powder X-ray diffraction (XRD) patterns were collected by Charley Bryant-Gardner and Sidrah Hussain using a grazing incidence mode (θ1 = 1°) or in-plane mode (θ1 = 0.5°, 2θχ scan with the detector scanning in the film plane) using a Rigaku SmartLab diffractometer (Cu-Kα, λ = 1.5418 Å) with parallel X-ray beam and a DTex Ultra 250 1D detector. Scanning electron microscopy (SEM) was performed on samples at an accelerating voltage of 10 or 15 kV using a Philips XL30 ESEM. Energy dispersive X-ray spectroscopy (EDX) spectra were obtained coupled to SEM, using a Thermo Scientific NORAN System 7 X-ray Microanalysis System.

N_2 physiorption measurements were performed by Dr Alice Oakley using a Micrometrics gemini 2375 surface area and porosity analyser at liquid nitrogen temperatures (77 K). Samples were degassed overnight under a vacuum at a temperature of 80°C. Surface area measurements and isotherms were determined using Braunauer, Emmett and Teller (BET) model.

Good laboratory practice included the use of PPE, fumehoods and glove boxes at all times, especially when handling volatile and hazardous substances. Residues, washings and unneeded samples containing tin, lead or antimony were treated as hazardous and collected in labelled containers for special disposal. Organophosphorus and arsenic compounds were treated with sodium hypochlorite before disposal. Solvent residues were separated in to chlorinated and non-chlorinated containers for disposal.

A.1 – References

1 E. P. Kyba, S. T. Liu and R. L. Harris, *Organometallics*, 1983, **2**, 1877–1879.

2 R. D. Feltham, A. Kasenally and R. S. Nyholm, *J. Organomet. Chem.*, 1967, **7**, 285–288.

3 W. V. Taylor, U. H. Soto, V. M. Lynch and M. J. Rose, *Inorg. Chem.*, 2016, **55**, 3206–3208.

4 V. K. Greenacre, W. Levason and G. Reid, *Organometallics*, 2018, **37**, 2123–2135.

5 M. Brookhart, B. Grant and A. F. Volpe, *Organometallics*, 1992, **11**, 3920–3922.

6 W. Levason, R. Patel and G. Reid, *J. Organomet. Chem.*, 2003, **688**, 280–282.

7 G. M. Sheldrick, *Acta Crystallogr. Sect. C Struct. Chem.*, 2015, **71**, 3–8.

8 G. M. Sheldrick, *Acta Crystallogr. Sect. A Found. Crystallogr.*, 2008, **64**, 112–122.

9 O. V. Dolomanov, L. J. Bourhis, R. J. Gildea, J. A. K. Howard and H. Puschmann, *J. Appl. Crystallogr.*, 2009, **42**, 339–341.

Appendix B – Crystallographic Tables

B.1 Chapter 2

Compound	**$[In(OTf)_3(terpy)]$**	**$[\{In(OTf)(terpy)\}_2(\mu^2\text{-}OH_2)_2][OTf]_2$**	**$[Ga(OTf)_2(bipy)_2][OTf]$**
Number	**1**	**2**	**3**
Formula	$C_{18}H_{11}F_9InN_3O_9S_3$	$C_{36}H_{24}F_{12}In_2N_6O_{14}S_4$	$C_{23}H_{16}F_9GaN_4O_9S_3$
M	795.30	1326.47	829.30
Crystal system	Triclinic	Triclinic	Triclinic
Space group (no.)	P-1 (2)	P-1 (2)	P-1 (2)
a /Å	8.8580(4)	9.1657(1)	8.3516(3)
b /Å	12.0801(5)	11.4074(1)	9.9145(3)
c /Å	12.8951(6)	12.3845(2)	18.5808(6)
α /°	71.426(4)	100.473(1)	104.726(3)
β /°	79.615(4)	103.266(1)	93.321(3)
γ /°	86.099(4)	106.159(1)	97.344(3)
U /Å^3	1286.47(10)	1168.00(3)	1469.21(8)
Z	2	1	2
μ(Mo-K_α) /mm^{-1}	1.283	1.283	12.67
F(000)	780	652	828
Total number reflns	28216	63854	45445
R_{int}	0.0602	0.0259	0.0935
Unique reflns	5023	7679	5773
No. of params, restraints	397, 12	329, 0	442, 0
GOF	1.186	1.049	1.166
R_1, wR_2 [$I > 2\sigma(I)$][b]	0.0669, 0.1513	0.0259, 0.0695	0.0885, 0.2371
R_1, wR_2 (all data)	0.0695, 0.1526	0.0269, 0.0700	0.0926, 0.2391

Compound	**$[In(OTf)(H_2O)(bipy)_2[OTf]_2.CH_2Cl_2$**	**$[Ga(OH_2)_2(phen)_2][OTf]_3.CH_2Cl_2$**
Number	**4**	**5**
Formula	$C_{23}H_{18}ClF_9InN_4O_{10}S_3$	$C_{27.50}H_{25}ClF_9GaN_4O_{11}S_3$
M	927.86	959.86
Crystal system	Monoclinic	Triclinic
Space group (no.)	C2/c (15)	P-1 (2)
a /Å	37.0587(6)	10.1475(5)
b /Å	8.96670(10)	19.6843(7)
c /Å	26.5744(4)	19.9711(9)
α /°	90.00	114.029(4)
β /°	130.506(2)	103.751(4)
γ /°	90.00	91.840(4)
U /Å^3	6714.17	3501.5(3)
Z	1	4
μ(Mo-K_α) /mm^{-1}	1.079	1.154
F(000)	3700	1932
Total number reflns	35771	45494
R_{int}	0.0208	0.0904
Unique reflns	6594	12314
No. of params, restraints	474, 0	1018, 0
GOF	1.043	1.062
R_1, wR_2 [$I > 2\sigma(I)$][b]	0.0185, 0.0438	0.0791, 0.1757
R_1, wR_2 (all data)	0.0202, 0.0445	0.1221, 0.1964

B.2 - Chapter 3

Compound	**$[Al(dppmO_2)_3][OTf]_3.CH_3CN$**	**$[Ga(dppmO_2)_3][OTf]_3.2CH_2Cl_2$**	**$[In(OTf)_2(Ph_3PO)_4][In(OH_2)_4(Ph_3PO)_2][OTf]_4.2CH_2Cl_2$**
Number	**6**	**7**	**8**
Formula	$C_{80}H_{69}AlF_6O_{15}P_6S_3$	$C_{80}H_{68.50}Cl_6F_9GaO_{15.25}P_6S_3$	$C_{116}H_{102}Cl_4F_{18}In_2O_{28}P_6S_6$
M	1766.61	2009.27	3035.60
Crystal system	Monoclinic	Monoclinic	Triclinic
Space group (no.)	$P2_1/n$ (14)	$P2_1/c$ (14)	P-1 (2)
a /Å	23.2259(3)	27.2588(5)	14.9532(3)
b /Å	21.9395(3)	18.9738(3)	19.3894(5)
c /Å	31.3366(5)	17.3899(3)	23.0722(6)
α /°	90	90.00	99.852(2)
β /°	92.104(1)	103.356(2)	106.775(2)
γ /°	90	90.00	90.8505(19)
U /Å^3	15957.3(4)	8750.8(3)	6295.7(3)
Z	4	4	2
μ(Mo-K_α) /mm^{-1}	0.312	0.760	0.726
F(000)	7273.4	4080	3072
Total number reflns	192869	75171	81740
R_{int}	0.0718	0.0289	0.0570
Unique reflns	41232	22607	24726
No. of params, restraints	2420, 81	1081, 0	1630, 0
GOF	1.019	1.030	1.006
R_1, wR_2 [$I > 2\sigma(I)$][b]	0.0718, 0.1803	0.0401, 0.0965	0.0351, 0.0887
R_1, wR_2 (all data)	0.1017, 0.1803	0.0609, 0.1040	0.0522, 0.0666

Compound	**$[In(OH_2)_2(Me_3PO)_4][In(OTf)_2(Me_3PO)_4][OTf]_4$ – polymorph 1**	**$[In(OH_2)_2(Me_3PO)_4][In(OTf)_2(Me_3PO)_4][OTf]_4$ – polymorph 2**	**$[Ga(MeCN)(Me_3PO)_5][OTf]_3$**
Number	**9**	**10**	**11**
Formula	$C_{30}H_{76}F_{18}In_2O_{28}P_8S_6$	$C_{15}H_{38}F_9InO_{14}P_4S_3$	$C_{20}H_{48}F_9GaNO_{14}P_5S_3$
M	1896.67	948.33	1018.34
Crystal system	Triclinic	Triclinic	Monoclinic
Space group (no.)	P-1 (2)	P-1 (2)	$P2_1/n$ (14)
a /Å	11.2931(2)	9.6477(3)	15.7227(2)
b /Å	18.4641(3)	11.2964(2)	17.5004(2)
c /Å	19.3056(4)	17.6524(4)	15.8907(2)
α /°	110.285(2)	83.7685(16)	90.00
β /°	95.0470(10)	79.394(2)	91.417(1)
γ /°	93.4490(10)	85.0987(18)	90.00
U /Å^3	3743.49(12)	1875.57(7)	4371.05(9)
Z	2	2	4
μ(Mo-K$_\alpha$) /mm^{-1}	1.066	1.064	1.047
F(000)	1912	956	2088.0
Total number reflns	81590	49095	99561
R_{int}	0.0483	0.055	0.0503
Unique reflns	14680	11257	11618
No. of params, restraints	878, 140	514, 29	525, 3
GOF	1.253	1.053	1.056
R_1, wR_2 [$I > 2\sigma(I)$][b]	0.0612, 0.1566	0.056, 0.134	0.0382, 0.0918
R_1, wR_2 (all data)	0.0658, 0.1635	0.081, 0.151	0.0443, 0.0945

Compound	**$[Al(OTf)_2(pyNO)_4][OTf]$**	**$[Ga(OTf)_2(pyNO)_4][OTf]$**	**$[In(OTf)_3(PyNO)_3]$**
Number	**12**	**13**	**14**
Formula	$C_{25}H_{23}AlF_9N_5O_{13}S_3$	$C_{25}H_{23}F_9GaN_5O_{13}S_3$	$C_{18}H_{15}F_9InN_3O_{12}S_3$
M	895.64	938.38	847.33
Crystal system	Monoclinic	Monoclinic	Monoclinic
Space group (no.)	$P2_1/n$ (14)	$P2_1/n$ (14)	$P2_1/c$ (14)
a /Å	11.3920(1)	11.3583(2)	9.6045(2)
b /Å	23.7735(3)	23.7389(2)	27.2680(5)
c /Å	13.2470(2)	13.4302(2)	11.0199(2)
α /°	90	90	90.00
β /°	91.253(1)	91.435(2)	101.931(2)
γ /°	90	90	90.00
U /Å^3	3586.80(8)	3620.10(10)	2823.71(9)
Z	4	4	4
μ(Mo-K_α) /mm^{-1}	0.347	1.048	1.183
F(000)	1816	1888	1672
Total number reflns	80071	45561	50880
R_{int}	0.0330	0.0460	0.0810
Unique reflns	9273	9320	5550
No. of params, restraints	549, 21	509, 0	415, 0
GOF	0.799	1.038	1.108
R_1, wR_2 $[I > 2\sigma(I)]$[b]	0.0330, 0.0893	0.0460, 0.1182	0.0396, 0.0920
R_1, wR_2 (all data)	0.0382, 0.0933	0.0601, 0.1249	0.0442, 0.0946

B.3 - Chapter 4

Compound	**$[InCl_3(PEt_3)_2]$**	**$[GaCl_3(AsEt_3)]$**	**$[InCl_3(AsEt_3)]$**
Number	**15**	**16**	**17**
Formula	$C_{12}H_{30}Cl_3InP_2$	$C_6H_{16}AsCl_3Ga$	$C_6H_{15}AsCl_3In$
M	457.47	339.18	383.27
Crystal system	Monoclinic	Monoclinic	Monoclinic
Space group (no.)	P2/c (13)	$P2_1/c$ (14)	$P2_1/c$ (14)
a /Å	22.9339(4)	13.0066(5)	8.6540(3)
b /Å	7.54410(10)	7.2916(3)	10.8181(3)
c /Å	24.1465(4)	26.7116(9)	13.4378(4)
α /°	90	90	90
β /°	90.534(1)	92.935(3)	90.960(3)
γ /°	90	90	90
U /Å^3	4177.54(11)	2523.98(17)	1257.87(7)
Z	4	8	4
μ(Mo-K_α) /mm^{-1}	1.655	5.354	5.076
F(000)	1856	1336	736
Total number reflns	30015	24027	18879
R_{int}	0.0535	0.0487	0.0404
Unique reflns	8206	7664	3247
No. of params, restraints	337, 0	205, 0	103, 0
GOF	1.177	1.156	1.052
R_1, wR_2 $[I > 2\sigma(I)]^b$	0.0449, 0.1019	0.0783, 0.1882	0.0312, 0.0862
R_1, wR_2 (all data)	0.0461, 0.1025	0.1035, 0.1997	0.338, 0.0878

Compound	**$InCl_3(AsEt_3)_2$]**	**[$InCl_3(Sb^nBu_3)$]**	**[$InBr_3(Sb^nBu_3)$]**
Number	**18**	**19**	**20**
Formula	$C_{12}H_{30}As_2Cl_3In$	$C_{12}H_{27}Cl_3InSb$	$C_{12}H_{27}Br_3InSb$
M	545.37	514.25	647.63
Crystal system	Orthorhombic	Monoclinic	Triclinic
Space group (no.)	$P2_12_12_1$ (19)	$P2_1/c$ (14)	P-1 (2)
a /Å	12.1428(5)	10.4537(7)	10.1205(4)
b /Å	12.8759(5)	9.9956(7)	10.1347(3)
c /Å	13.4300(5)	17.7853(13)	10.6870(3)
α /°	90	90	66.724(3)
β /°	90	91.341(6)	86.703(3)
γ /°	90	90	79.609(3)
U /Å^3	2099.77(14)	1857.9(2)	990.31(6)
Z	4	4	2
μ(Mo-K_α) /mm^{-1}	4.622	3.109	8.564
F(000)	1072	1000	608
Total number reflns	58096	14751	17126
R_{int}	0.1375	0.0677	0.0954
Unique reflns	6972	4795	3869
No. of params, restraints	169, 0	157, 0	157, 0
GOF	1.067	0.915	1.015
R_1, wR_2 [$I > 2\sigma(I)$][b]	0.0668, 0.1550	0.0527, 0.1340	0.0354, 0.0727
R_1, wR_2 (all data)	0.0849, 0.1623	0.1014, 0.1620	0.0412, 0.0772

B.4 - Chapter 5

Compound	**$[Sn(OTf)_2\{o\text{-}C_6H_4(PMe_2)_2\}]$**	**$[Sn(OTf)_2\{o\text{-}C_6H_4(AsMe_2)_2\}]$**	**$[Sn(OTf)\{PhP(CH_2CH_2PPh_2)_2\}][OTf]\cdot Et_2O$**
Number	**21**	**22**	**23**
Formula	$C_{36}H_{48}F_{18}O_{18}P_6S_6Sn_3$	$C_{12}H_{16}As_2F_6O_6S_2Sn$	$C_{40}H_{43}F_6O_7P_3S_2Sn$
M	2215.59	702.92	1025.46
Crystal system	orthorhombic	monoclinic	monoclinic
Space group (no.)	Pnna (52)	C2/c (15)	$P2_1/n$ (14)
a /Å	16.2539(3)	15.8316(5)	15.8064(5)
b /Å	24.0871(5)	14.0437(4)	10.1469(2)
c /Å	20.0157(5)	9.7168(3)	27.2193(6)
α /°	90	90	90
β /°	90	95.863(3)	91.081(2)
γ /°	90	90	90
U /Å^3	7836.3(3)	2149.06(11)	4364.82(19)
Z	4	4	4
μ(Mo-Kα) /mm^{-1}	1.346	4.517	7.232
F(000)	4464	1352	2080
Total number reflns	74108	14822	78496
R_{int}	0.0774	0.0346	0.0791
Unique reflns	10118	3237	8919
No. of params, restraints	490, 468	134, 0	534, 9
GOF	1.042	1.054	1.085
R_1, wR_2 $[I > 2\sigma(I)]^b$	0.0602, 0.1519	0.0203, 0.0453	0.0624, 0.1642
R_1, wR_2 (all data)	0.0959, 0.1674	0.0246, 0.0464	0.0671, 0.1681

Compound	**[Sn(OTf)$_2${*o*-C$_6$H$_4$(PPh$_2$)$_2$}] ·CH$_2$Cl$_2$**	**[Sn(OTf){P(CH$_2$CH$_2$PPh$_2$)$_3$}][OTf]·CH$_2$Cl$_2$ ***	**[Ge{MeC(CH$_2$PPh$_2$)$_3$}] [BAr^F]$_2$. 0.5 CH$_2$Cl$_2$**
Number	**24**	**25**	**26**
Formula	$C_{33}H_{26}Cl_2F_6O_6P_2S_2Sn$	$C_{45}H_{44}Cl_2F_6O_6P_4S_2Sn$	$C_{105.5}H_{64}B_2ClF_{48}GeP_3$
M	948.19	1172.39	2466.13
Crystal system	monoclinic	monoclinic	triclinic
Space group (no.)	$I1_2/a$ (15)	$P2_1/c$ (14)	P-1 (2)
a /Å	26.1551(8)	16.1811(2)	12.73530(10)
b /Å	8.8030(2)	14.49840(10)	16.7939(2)
c /Å	33.6112(9)	21.3672(2)	26.6298(3)
α /°	90	90	79.1070(10)
β /°	107.604(3)	97.9480(10)	89.4620(10)
γ /°	90	90	69.1300(10)
U /Å^3	7376.3(4)	4964.59(9)	5215.47(10)
Z	8	4	2
μ(Mo-Kα) /mm^{-1}	1.112	7.689	0.500
F(000)	3776	2368	2466
Total number reflns	49013	118476	134869
R_{int}	0.0506	0.0657	0.0290
Unique reflns	9513	8946	26892
No. of params, restraints	469, 0	595, 0	1600, 1546
GOF	1.138	1.050	1.016
R_1, wR_2 [I > 2σ(I)][b]	0.0497, 0.1084	0.0379, 0.1045	0.0440, 0.1048
R_1, wR_2 (all data)	0.0646, 0.1126	0.0391, 0.1054	0.0508, 0.1091

Compound	**[Pb(OTf)$_2${*o*-C$_6$H$_4$(PMe$_2$)$_2$}]**	**[Pb(OTf)$_2${*o*-C$_6$H$_4$(AsMe$_2$)$_2$}]**	**[{Pb$_2$(OTf)$_3${MeC(CH$_2$PPh$_2$)$_3$}$_2$}][OTf]·MeCN**
Number	**27**	**28**	**29**
Formula	$C_{12}H_{16}F_6O_6P_2PbS_2$	$C_{12}H_{16}As_2F_6O_6PbS_2$	$C_{88}H_{81}F_{12}NO_{12}P_6Pb_2S_4$
M	703.50	791.40	2300.97
Crystal system	triclinic	monoclinic	orthorhombic
Space group (no.)	P-1 (2)	$P2_1/c$ (14)	Pbca (61)
a /Å	10.4025(2)	10.58200(10)	20.7298(2)
b /Å	10.4520(2)	21.4899(2)	29.4124(2)
c /Å	11.9474(3)	9.72860(10)	29.6444(2)
α /°	105.687(2)	90	90
β /°	106.932(2)	95.1510(10)	90
γ /°	110.441(2)	90	90
U /Å^3	1059.39(4)	2203.41(4)	18074.6(2)
Z	2	4	8
μ(Mo-K$_\alpha$) /mm^{-1}	8.389	20.735	4.005
F(000)	668	1480	9104
Total number reflns	15069	21504	274211
R_{int}	0.0230	0.0280	0.0381
Unique reflns	6025	3966	23338
No. of params, restraints	266, 0	266, 218	1157, 603
GOF	1.035	1.053	1.017
R_1, wR_2 [I > 2σ(I)][b]	0.0192, 0.0419	0.0289, 0.0675	0.0191, 0.426
R_1, wR_2 (all data)	0.0219, 0.0430	0.0294, 0.0678	0.0244, 0.0448

Compound	**[Pb(OTf){P(CH$_2$CH$_2$PPh$_2$)$_3$}][OTf].MeCN**	**[Sn{MeC(CH$_2$PPh$_2$)$_3$}][BAr^F]$_2$.0.5CH$_2$Cl$_2$**	**[Pb{MeC(CH$_2$PPh$_2$)$_3$}][BAr^F]$_2$.0.5CH$_2$Cl$_2$**
Number	**30**	**31**	**32**
Formula	$C_{46}H_{45}F_6NO_6P_4PbS_2$	$C_{105.5}H_{64}B_2ClF_{48}P_3Sn$	$C_{105.5}H_{64}B_2ClF_{48}P_3Pb$
M	1217.02	2512.23	2600.73
Crystal system	monoclinic	triclinic	triclinic
Space group (no.)	$P2_1/c$ (14)	P-1 (2)	P-1 (2)
a /Å	16.3354(5)	12.7643(2)	12.7607(2)
b /Å	14.2959(3)	16.7092(2)	16.7182(2)
c /Å	21.6774(5)	26.6628(3)	26.6413(3)
α /°	90	78.5010(10)	78.0880(10)
β /°	102.940(2)	89.4220(10)	89.0490(10)
γ /°	90	69.6880(10)	69.7810(10)
U /Å^3	4933.7(2)	5215.19(12)	5208.49(12)
Z	4	2	2
μ(Mo-Kα) /mm^{-1}	3.704	0.451	1.826
F(000)	2416	2502	2566
Total number reflns	44954	141657	134409
R_{int}	0.0373	0.0332	0.0408
Unique reflns	11554	31821	26898
No. of params, restraints	604, 0	1572, 1784	1544, 1392
GOF	1.019	1.036	1.028
R_1, wR_2 [I > 2σ(I)][b]	0.0314, 0.0515	0.0443, 0.0987	0.0343, 0.0794
R_1, wR_2 (all data)	0.0470, 0.0546	0.0536, 0.1032	0.0383, 0.0815

B.5 - Chapter 6

Compound	**[{Sn(OTf)(OPPh$_3$)$_2$}$_2$(μ-OTf)$_2$]**	**[Sn(OTf)(OPPh$_3$)$_3$][OTf]**	**[Sn(OTf)$_2$(OPMe$_3$)$_2$]**
Number	**33**	**34**	**35**
Formula	$C_{38}H_{30}F_6O_8P_2S_2Sn$	$C_{56}H_{45}F_6O_9P_3S_2Sn$	$C_8H_{18}F_6O_8P_2S_2Sn$
M	973.437	1251.64	600.97
Crystal system	Monoclinic	Triclinic	Monoclinic
Space group (no.)	$P2_1/n$ (14)	P-1 (2)	$P2_1/c$ (14)
a /Å	10.6878(2)	11.75890(10)	13.19910(10)
b /Å	20.7093(3)	12.5952(2)	11.3597(2)
c /Å	17.6086(3)	19.6439(3)	14.1089(2)
α /°	90	107.9820(10)	90
β /°	106.485(2)	97.8220(10)	94.1720(10)
γ /°	90	97.6570(10)	90
U /Å^3	3800.17(12)	2693.68(7)	2109.85(5)
Z	4	2	4
μ(Mo-K$_\alpha$) /mm^{-1}	0.949	0.719	1.643
F(000)	1952.758	1268	1184
Total number reflns	29496	36483	38142
R_{int}	0.0367	0.0303	0.0255
Unique reflns	9790	10613	5446
No. of params, restraints	514, 0	725, 7	250, 0
GOF	0.8580	0.926	1.050
R_1, wR_2 [I > 2σ(I)][b]	0.0356, 0.1078	0.0281, 0.0623	0.0180, 0.0441
R_1, wR_2 (all data)	0.0460, 0.1226	0.0356, 0.0649	0.0190, 0.0446

Compound	**[Sn(OTf)$_2$(dppmO$_2$)]**	**[Sn(OTf)$_2$(dppmO$_2$)$_2$]**	**[{Sn(OTf)$_2$(pyNO)$_2$}$_2$(μ-pyNO)$_2$]**
Formula	$C_{27}H_{22}F_6O_8P_2S_2Sn$	$C_{52}H_{44}F_6O_{10}P_4S_2Sn$	$C_{18}H_{16}F_6N_3O_8S_2Sn$
Number	**36**	**37**	**38**
M	833.19	1249.56	699.15
Crystal system	Orthorhombic	Monoclinic	Monoclinic
Space group (no.)	Pbca (61)	$P2_1/c$ (14)	$P2_1/n$ (14)
a /Å	15.8728(2)	11.33730(10)	13.02260(10)
b /Å	17.9938(2)	28.1908(3)	14.67460(10)
c /Å	21.7167(2)	18.7751(2)	13.1085(2)
α /°	90	90	90
β /°	90	96.5430(10)	97.1270(10)
γ /°	90	90	90
U /Å^3	6202.55(12)	5961.58(10)	2485.70(5)
Z	8	4	4
μ(Mo-K$_\alpha$) /mm^{-1}	1.146	0.676	10.638
F(000)	3312	2528	1380
Total number reflns	111784	46272	28118
R_{int}	0.0651	0.0376	0.0372
Unique reflns	9948	15373	4674
No. of params, restraints	415, 0	676, 0	343, 0
GOF	1.024	1.043	1.059
R_1, wR_2 [I > 2σ(I)][b]	0.0245, 0.0589	0.0407, 0.0934	0.0265, 0.0669
R_1, wR_2 (all data)	0.0287, 0.0604	0.0534, 0.1005	0.0278, 0.0676

Compound	**$[Sn(OTf)_2(OAsPh_3)_3]$**	**$Pb(OTf)_2(OPMe_3)_4]$.$2CH_2Cl_2$**	**$[Pb(OTf)_2(dppmO_2)_2]$.$2CH_2Cl_2$**
Number	**39**	**40**	**41**
Formula	$C_{38}H_{30}As_2F_6O_8S_2Sn$	$C_{16}H_{40}Cl_4F_6O_{10}P_4PbS_2$	$C_{54}H_{48}Cl_4F_6O_{10}P_4PbS_2$
M	1061.27	1043.47	1507.91
Crystal system	Triclinic	trigonal	Monoclinic
Space group (no.)	P-1 (2)	$P3_221$ (154)	$P2_1/c$ (14)
a /Å	9.9923(2)	11.76685(12)	14.25260(10)
b /Å	10.2393(3)	11.76685(12)	20.83590(10)
c /Å	20.7004(5)	24.5584(3)	20.38590(10)
α /°	85.398(2)	90	90
β /°	88.172(2)	90	96.5270(10)
γ /°	69.258(2)	120	90
U /Å^3	1974.27(9)	2944.77(7)	6014.67(6)
Z	2	3	4
μ(Mo-K_α) /mm^{-1}	2.496	4.906	3.232
F(000)	1048	1536	2992
Total number reflns	44582	77008	65948
R_{int}	0.0414	0.0536	0.0320
Unique reflns	10200	10133	15396
No. of params, restraints	514, 0	401, 226	758, 3
GOF	1.026	1.047	1.013
R_1, wR_2 [I > 2σ(I)][b]	0.0288, 0.0647	0.0308, 0.0761	0.0268, 0.0590
R_1, wR_2 (all data)	0.0380, 0.0675	0.316, 0.0764	0.0340, 0.0618

B.6 - Chapter 7

Compound	**$[Sn(OTf)_2(OPMe_3)_3]_6.C_6H_{14}$**	**$[\{Pb(OTf)(OPMe_3)_3\}_2(\mu\text{-}OTf)_2]$**	**$[Sn(OPMe_3)_4][SO_3F]_2 .CH_2Cl_2$**
Number	42	43	44
Formula	$C_{11}H_{27}F_6O_9P_3S_2Sn.0.167\ C_6H_{14}$	$C_{11}H_{27}F_6O_9P_3PbS_2$	$C_{12}H_{36}F_2O_{10}P_4S_2Sn.CH_2Cl_2$
M	707.40	781.54	770.08
Crystal system	Trigonal	Monoclinic	Monoclinic
Space group (no.)	P-3 (147)	$P2_1/c$ (14)	$P2_1$ (4)
a /Å	24.5947(4)	9.7633(3)	11.5999(3)
b /Å	24.5947(4)	14.2131(4)	11.2204(3)
c /Å	7.88970(10)	18.8859(5)	12.3183(4)
α /°	90	90	90
β /°	90	98.257(2)	98.077(3)
γ /°	120	90	90
U /Å^3	4133.08(14)	2593.57(13)	1587.39(8)
Z	6	4	2
μ(Mo-Kα) /mm^{-1}	1.330	6.931	1.357
F(000)	2126	1512	781.124
Total number reflns	23416	30244	19548
R_{int}	0.023	0.041	0.0482
Unique reflns	6587	6662	7638
No. of params, restraints	311, 3	298, 0	314, 7
GOF	1.043	1.026	1.0267
R_1, wR_2 $[I > 2\sigma(I)]^b$	0.019, 0.048	0.022, 0.043	0.0560, 0.1462
R_1, wR_2 (all data)	0.022, 0.047	0.022, 0.045	0.0646, 0.1514

Common items: T = 100 K; θ(max) = 27.5°; wavelength (Mo-Kα) = 0.71073 Å; b $R_1 = \Sigma||Fo|-|Fc||/\Sigma|Fo|$; $wR_2=[\Sigma w(Fo^2-Fc^2)^2/\Sigma wF_o^4]^{1/2}$